GHENT UNIVERSITY

FACULTY OF SCIENCES

Host-RSV interactions:

a siRNA and proteomics approach

Koen Sedeyn

Thesis submitted in partial fulfillment of the requirements for the degree of Doctor of Science: biochemistry and biotechnology

Academic year 2017-2018

Promoter: Prof. Dr. Xavier Saelens

Co-promoter: Dr. Bert Schepens

Ghent University - Faculty of sciences

Department of Biomedical Molecular Biology

VIB - UGent Center for Medical Biotechnology

VIB-UGENT CENTER FOR MEDICAL BIOTECHNOLOGY

The research described in this thesis has been supported by a doctoral scholarship from the special research fund (BOF) from the University of Ghent, by a FWO-PhD fellowship and by IUAP BELVIR p7/45.

Host-RSV interactions: a siRNA and proteomics approach

Koen Sedeyn

Unit Molecular Virology

Department of Biomedical Molecular Biology, Ghent University

VIB - Center for Medical Biotechnology

Academic year 2017-2018

Promoter: **Prof. Dr. Xavier Saelens[1,2]**

Co-promoter: **Dr. Bert Schepens[1,2]**

Examination board:

Chairman: **Prof. Dr. Rudi Beyaert[2,3]**

Secretary: **Prof. Dr. Geert van Loo[2,3]**

Other members: **Prof. Dr. Sven Eyckerman[1,4]**

Prof. Dr. Peter Delputte[5]

Prof. Dr. Thomas Michiels[6]

[1] VIB - UGent Center for Medical Biotechnology, Ghent, Belgium

[2] Department of Biomedical Molecular Biology, Ghent University, Belgium

[3] VIB- UGent Center for Inflammation research, Ghent, Belgium

[4] Department of Biochemistry, Ghent University, Belgium

[5] Laboratory of Microbiology, Parasitology and Hygiene (LMPH), Faculty of Pharmaceutical, Biomedical and Veterinary Sciences, University of Antwerp, Wilrijk, Belgium

[6] De Duve Institute, Université Catholique de Louvain, Brussels, Belgium

English summary

Respiratory syncytial virus (RSV) is a negative strand RNA virus belonging to the genus *Orthopneumovirus* within the *Pneumoviridae* family. RSV infects the epithelial cells lining the upper and lower respiratory tract in humans. During life, humans are repeatedly infected by RSV, which nearly always leads to mild respiratory symptoms comparable to a common cold. The very young, the immunocompromised and the elderly, however, are at increased risk of developing severe RSV disease. RSV is the most important cause of acute lower respiratory tract disease in infants worldwide with 34 million cases estimated in children below 5 years of age in 2005. Despite the medical significance of RSV infections and more than half a century of research, no approved vaccine or effective antiviral therapy are available. A RSV-neutralizing, humanized mouse monoclonal antibody, Palivizumab, is recommended for prophylactic use in infants at increased risk of developing severe RSV disease. Yet, protection by Palivizumab is only partial and its high cost limits its use to high-risk infants. A better understanding of the complex interplay between RSV and the human host can help in the development of a safe vaccine and effective antiviral drugs.

A first aim of this thesis was to identify phosphorylation-dependent signaling pathways that are activated and possibly exploited by a RSV infection. Therefore we performed two parallel high-throughput screens. First, we investigated the role of each human kinase one-by-one during RSV infection in a human lung epithelial cell line by using a siRNA-mediated knockdown screen. We measured RSV replication by staining RSV plaques formed by multiple rounds of infection and tested a subset of the initial kinase hits in a RSV replication kinetics experiment. Ten primary kinase hits that either increased or decreased both the RSV plaque size and - titer were subsequently tested by different siRNAs. Knockdown of two kinases, IRAK3 and MYLK4, by different siRNAs resulted in a decreased RSV plaque size. Expression at the mRNA level, however, could only be detected for MYLK4 and not for IRAK3. The reduced RSV plaque size upon MYLK4 knockdown was not caused by a reduction of the cell metabolism or by siRNA-dependent induction of type I interferons. MYLK4 knockdown reduced the plaque size of both laboratory and clinical RSV isolates. RSV plaque size reduction, however, could not be rescued by restoring MYLK4 expression. Moreover, RSV plaque size was not reduced in cells presumed to lack MYLK4. Possibly, RSV plaque size reduction upon transfection of MYLK4-targeting siRNAs was caused by sequence-dependent off-target silencing by the siRNAs. Secondly, we performed a phosphoproteomics screen to identify RSV-induced host protein (de)phosphorylations during the entry phase of a RSV infection. We identified 8 RSV-induced phosphorylation events and 13 RSV-induced dephosphorylation events. A selection of these (de)phosphorylation events were validated by electrophoretic mobility shift assays.

A second aim of this thesis was to study the interactomes of the two non-structural (NS) proteins of RSV, which strongly suppress type I and III interferon responses at different steps. Therefore, we used three complementary protein-protein interaction mapping techniques, *i.e.* proximity-based protein biotinylation (BioID), Virotrap and affinity purification. Four candidate NS1 interactors and 15 candidate NS2 interactors were found in 2 of the 3 techniques. We identified several subunits of the proteasome complex to interact with NS1 and NS2. Candidate NS1 interactors of the cleavage and polyadenylation of precursor mRNA pathway identified by BioID were validated by affinity purification.

Nederlandstalige samenvatting

Respiratoir syncytieel virus (RSV) is een negatief-streng RNA virus behorend tot het genus *Orthopneumovirus* in de *Pneumoviridae* familie. RSV infecteert de epitheelcellen die de luchtwegen aflijnen, zowel in de bovenste als in de onderste luchtwegen van de mens. RSV infecties komen herhaaldelijk voor tijdens het leven en veroorzaken zo goed als altijd milde symptomen ter hoogte van de luchtwegen, vergelijkbaar met een klassieke verkoudheid. Zeer jonge kinderen, mensen met een verstoord immuunsysteem en ouderen hebben echter een verhoogd risico om ernstig ziek te worden tijdens een RSV infectie. RSV is de belangrijkste oorzaak van acute infecties van de onderste luchtwegen bij jonge kinderen, met naar schatting 34 miljoen gevallen in kinderen onder de 5 jaar wereldwijd in 2005. Ondanks het medisch belang van RSV infecties en reeds meer dan 50 jaar onderzoek naar dit virus, is er op heden geen veilig vaccin of een doeltreffend antiviraal geneesmiddel beschikbaar. Er is wel een gehumaniseerd muis antilichaam beschikbaar dat het RSV virus neutraliseert, namelijk Palivizumab. Dit antilichaam wordt preventief gebruikt in zeer jonge kinderen met een verhoogd risico voor het ontwikkelen van ernstige ziekte tijdens een RSV infectie. Bescherming door Palivizumab is echter slechts gedeeltelijk en de hoge kostprijs beperkt het gebruik tot kinderen met een verhoogd risico. Een beter begrip van de ingewikkelde wisselwerking tussen RSV en de mens zou kunnen helpen in de ontwikkeling van een veilig vaccin en een doeltreffend geneesmiddel.

Een eerste doelstelling van deze thesis was het identificeren van fosforylatie-afhankelijke signalisatie cascades die geactiveerd en mogelijk gebruikt worden tijdens een RSV infectie. Hiervoor hebben we twee analyses op grote schaal uitgevoerd naast elkaar. Ten eerste hebben we de rol van alle menselijke kinasen onderzocht tijdens een RSV infectie door de expressie van elk kinase uit te schakelen in een luchtweg epitheel cellijn via siRNAs gevolgd door een RSV infectie. Hierbij hebben we de replicatie van RSV gemeten door RSV plaques aan te kleuren. Een selectie van de initieel geïdentificeerde kinasen die de plaque-grootte beïnvloeden werd vervolgens onderzocht in een RSV groei kinetiek. Tien kinasen die zowel de plaque-grootte als de virus titer verhoogden of verlaagden werden vervolgens getest met meerdere siRNAs. Voor twee kinasen, IRAK3 en MYLK4, konden we een verminderde plaque-grootte observeren na het uitschakelen van hun expressie door verschillende siRNAs, wat suggereert dat deze kinasen een belangrijke functie hebben tijdens een RSV infectie. Expressie van boodschapper RNA werd echter enkel gedetecteerd voor MYLK4 en niet voor IRAK3. De verminderde RSV plaque-grootte na uitschakeling van MYLK4 expressie werd niet veroorzaakt door een algemene daling van het metabolisme van de cellen of door de aanmaak van type I interferonen. De plaque-grootte van zowel laboratorium als klinische RSV stammen verminderde na uitschakeling van MYLK4 expressie. Wanneer we de expressie van MYLK4 terug herstelden konden we echter geen herstel zien van de plaque grootte. Bijkomend zagen we geen verminderde RSV plaque-grootte in cellen waarvan we vermoeden dat de expressie van MYLK4 volledig ontbreekt. Bijgevolg zou het kunnen dat de verminderde plaque-grootte na uitschakeling van MYLK4 expressie veroorzaakt werd door siRNA-sequentie afhankelijke ongewenste uitschakeling van andere genen dan MYLK4. Ten tweede hebben we een fosfoproteoom analyse uitgevoerd om RSV-geïnduceerde (de)fosforylaties van

gastheer eiwitten na te gaan tijdens het binnendringen van de gastheercel. Hierbij hebben we 8 RSV-geïnduceerde fosforylaties en 13 RSV-geïnduceerde defosforylaties terug gevonden. Een selectie van deze (de)fosforylaties werd gevalideerd aan de hand van fosforylatie-afhankelijke veranderingen in de migratiesnelheid tijdens elektroforese.

Een tweede doelstelling van deze thesis was het in kaart brengen van eiwit-eiwit interacties van de twee niet-structurele (NS) eiwitten van RSV. Deze eiwitten onderdrukken de aangeboren immuunrespons van de gastheercel op basis van type I en III interferonen sterk op verschillende niveaus. Hiervoor hebben we 3 complementaire technieken gebruikt, namelijk biotinylatie van eiwitten in de nabijheid (BioID), *Virotrap* en affiniteitszuivering. Voor NS1 werden 4 mogelijke interagerende eiwitten teruggevonden en 15 voor NS2 in 2 van deze 3 technieken. Hierbij werden meerdere eiwitten van het proteasoom complex teruggevonden, zowel voor NS1 als voor NS2. Mogelijke eiwit-eiwit interacties tussen NS1 en eiwitten van de “splitsing en polyadenylatie van precursor boodschapper RNA” cascade, die gevonden werden via BioID, werden gevalideerd op basis van affiniteitszuivering.

Table of contents

List of abbreviations

2D-DiGE	2 dimensional-differential gel electrophoresis

A

ACN	Acetonitrile
AMHR2	Anti-Mullerian hormone receptor type 2
AP-1	Activator protein 1
APol	Amphipol
ARP	Actin-related protein
ATM	ataxia-telangiectasia mutated
ATR	ataxia-telangiectasia and rad3 related

B

BCR	BTB-CUL3-RBX1
BDV	Borna disease virus
Bp	Base pairs
BPD	Bronchopulmonary dysplasia

C

CACYBP	Calcyclin-binding protein
CARD	Caspase recruitment domain
CBP	CREB binding protein
CCP110	Centriolar coiled-coil protein 110
cGAS	Cyclic GMP-AMP synthase
CK	Casein kinase
CLT B	Clathrin light chain B
CMV-IE	Cytomegalovirus-Immediate early
CPSF	Cleavage and polyadenylation specificity factor subunit
CREB	Cyclic-AMP responsive element binding protein
CSNK1G1	Casein kinase 1 gamma 1
CSTF	Cleavage stimulation factor subunit
CTL	Cytotoxic T lymphocyte

D

DAG	Diacylglycerol
DDX6	DEAD-box helicase 6
DHFR	Dihydrofolate reductase
DNA	Deoxyribonucleic acid
DOCK7	Dedicator of cytokinesis 7
dpi	Days post infection
DSG2	Desmoglein-2
dsRNA	Double stranded RNA
DTT	Dithiothreitol

E

EBOV	Ebola virus
ECS	Elongin B/C-CUL2/5-SOCS box
EGFP	Enhanced green fluorescent protein
EGFR	Epidermal growth factor receptor
EPHB2	Ephrin receptor B2
ER	Endoplasmic reticulum

F

FA	Formic acid
FACS	Fluorescence activated cell sorting
FC	Fold change
FCS	Fetal Calve serum
Fig	Figure

G

GAP	GTPase activating proteins
GEF	Guanine nucleotide exchange factor
GOI	Gene of interest
GS	Gene specific

H

h	Hours
HAE	Human airway epithelial
HeV	Hendra virus
HIV	Human immunodeficiency virus
hMPV	Human metapneumovirus
HSV	Herpes simplex virus

I

IAV	Influenza A virus
IB	Inclusion bodies
IF	Immunofluorescence
IFIT	Interferon-induced protein with tetratricopeptide repeats
IFITM	Interferon inducible transmembrane protein
IFN	Interferon
IKBKE	Inhibitor of nuclear factor kappa-B kinase subunit epsilon
IPA	Ingenuity pathway analysis
IRAK3	Interleukin-1 receptor-associated kinase 3
IRF	Interferon regulatory factor

J

JNK	c-Jun N-terminal kinase

K

KEA	Kinase enrichment analysis

L

LC-MS/MS	Liquid chromatography-tandem mass spectrometry
LFQ	Label-free quantification
LGP2	Laboratory of genetics and physiology 2

M

MARV	Marburg virus
MAVS	Mitochondrial antiviral signaling protein
MDA5	Melanoma differentiation associated gene 5
MEF	Mouse embryonic fibroblasts
miRNA	MicroRNA
MOI	Multiplicity of infection
mTOR	mechanistic target of rapamycin
MyD88	Myeloid differentiation primary response 88
MYLK4	Myosin light chain kinase 4
MYO5B	Myosin-Vb

N

N	Nucleoprotein
NCL	Nucleolin
ND10	Nuclear domain 10
NiV	Nipah virus
NLR	NOD like receptor
NMMHC	Non-muscle myosin heavy chain
NOD	Nucleotide binding oligomerization domain
NS	Non structural
NSD	NS degradasome
NSFL1C	NSFL1 cofactor p47
NT	Non-Targeting
N-WASP	neural Wiskott-Aldrich syndrome protein

O

OASL	2’-5’-oligoadenylate synthetase like protein
OFD1	Oral-facial-digital syndrome 1 protein
ORF	Open reading frame
OSBPL8	Oxysterol binding protein-like 8

P

PABPN1	polyadenylate-binding nuclear protein 1
PAK1	p21 (CDC42/rac1) activated kinase 1
PAMP	Pathogen associated molecular pattern
PAPOLA	poly (A) polymerase alpha
PBS	Phosphate buffered saline
PCM1	Pericentriolar material 1
PCR	Polymerase chain reaction
PDGFRB	Platelet derived growth factor receptor β
PEI	Polyethyleneimine

PFU	Plaque forming units
PIK3R5	Phosphoinositide-3-kinase regulatory subunit 5
PIV	Parainfluenza virus
PLK	Polo-like kinase
PNKP	Polynucleotide kinase 3'-phosphatase
PP1	Protein phosphatase type 1
PPI	Protein-protein interaction
PPP1R12A	Protein phosphatase 1 regulatory subunit 12A
PRD	Positive regulatory domain
PRKACG	Protein kinase cAMP-activated catalytic subunit γ
PRKC	Protein kinase C
PRKD	Protein kinase D
PRR	Pattern recognition receptor
PSM	Proteasome subunit
PSTPIP1	proline-serine-threonine phosphatase interacting protein 1
PTK2B	protein tyrosine kinase 2 beta
PTOV1	Prostate tumor overexpressed 1

R

RAD23B	RAD23 homolog B
RIG-I	Retinoic acid inducible gene I
RLR	RIG-I like receptor
RNA	Ribonucleic acid
RNAi	RNA interference
RNP	Ribonucleocapsid
RSK	p90 ribosomal S6 kinase
RSV	Respiratory syncytial virus
RT	Room temperature
RT-PCR	Reverse transcription polymerase chain reaction

S

SEM	Standard error of the means
SFTSV	Severe fever with thrombocytopenia syndrome virus
SG	Stress granule
shRNA	Short hairpin RNA
siRNA	Small interfering RNA
SNAP23	Synaptosome-associated Protein 23
ssRNA	Single stranded RNA
Suppl	Supplementary

T

TBK1	TANK binding kinase 1
TetR	Tetracycline repressor
TFA	Trifluoroacetic acid
TICAM1	Toll-like receptor adaptor molecule 1
TLR	Toll-like receptor
TMOD3	Tropomodulin 3
TNF	Tumor necrosis factor

TOM1	Target of myb1 membrane trafficking protein
TRAF3	TNF receptor associated factor 3
TTBK1	Tau tubulin kinase 1
TWB	Tris wash buffer

U

Untr	Untransfected
UTR	Untranslated region

V

VCP	Valosin containing protein
VLP	Virus like particle
VSV	Vesicular stomatitis virus

W

WDR33	WD repeat domain 33
WT	Wild type

Y

Y2H	Yeast-two-hybrid

Z

ZBP1	Z-DNA binding protein 1

Part I: Introduction

Chapter I

Respiratory syncytial virus

1.1 Discovery of RSV

Respiratory syncytial virus was discovered in 1955 as the etiological cause of a respiratory illness in a colony of chimpanzees in Washington D.C. [1]. This virus was initially called the chimpanzee coryza agent (CCA). Serological data from a laboratory worker, that experienced an upper respiratory infection after close contact with the animals and CCA, suggested that CCA was of etiological importance for the disease. Interestingly, analysis of multiple sera from infants to young adults revealed that these contained antibodies directed against CCA, suggesting that humans could also be infected with CCA or a closely related virus. This was confirmed one year later, when Chanock and colleagues isolated two viruses that were indistinguishable from the CCA from infants with severe lower respiratory illness [2]. *In vitro* growth of these viruses on permissive confluent cell monolayers was associated with the formation of syncytial areas, *i.e.* the accumulation of intact nuclei within a homogeneous cytoplasm formed by the loss of cell bounderies. Hence CCA was renamed human respiratory syncytial virus (RSV).

1.2 Epidemiology, risk factors and disease associated with RSV

Throughout life all humans become infected by RSV multiple times. These infections nearly always result in moderate respiratory symptoms with minor discomfort. However, the very young, the immunocompromised and the elderly are at highest risk of developing severe disease upon RSV infection. In temperate climates RSV infections mostly occur during fall, winter and spring season, *e.g.* November until April in the northern hemisphere, whereas RSV seasonality in more tropical climates tends to vary between geographical regions [3, 4]. RSV strains can be subdivided in two serotypes, A and B, with one serotype being dominant over the other per RSV season. This dominance regularly shifts over consecutive RSV seasons. By the age of 2 years, nearly all infants experienced at least one RSV infection [5]. A RSV infection typically initiates at the upper respiratory tract and is characterized by mild clinical symptoms such as coughing, a runny nose and low-grade fever [6]. After a few days, the viral infection can progress to the lower respiratory tract and cause bronchiolitis or pneumonia (inflammation at the bronchioles and alveoli, respectively), characterized by wheezing, more severe coughing and/or breathing difficulties. Typically, severe RSV disease is only observed during primary and not during secondary RSV infections [5]. On a global scale, about 34 million cases of RSV-associated acute lower respiratory tract infections (ALRI) in children below 5 years of age were estimated for 2005 [7]. These RSV-associated ALRI represented about 22% of all ALRI in children below 5 years of age, making RSV the most important cause of lower respiratory tract disease in infants worldwide. It was estimated that in 2005, about 66,000-199,000 children below 5 years of age died due to RSV-associated ALRI, with the vast majority (99%) occurring in developing countries. More or less in line with these mortality numbers, Lozano and colleagues estimated a total of 234,000 deaths in children below 5 years of age due to RSV ALRI in 2010 [8]. In most children RSV infections are cured without medical intervention and only a minority of severe RSV infections demands hospitalization. In industrialized countries hospitalization rates due to RSV typically vary between 10 and 40 per 1,000 infants below 1 year of age and drop to 0.6 to 6 per 1,000 children below 5 years of age depending on the study

population [9-11]. Hospitalization rates in developing countries are much less studied, but two studies from Kenya and South-Africa found a hospitalization rate of 20 and 26.2 per 1,000 infants <6 months of age, respectively [12, 13].

Epidemiological studies have identified several factors that increase the risk of developing severe RSV disease, although the majority of RSV-associated hospitalizations occur in infants that were previously healthy [14]. The most important risk factors include age (very young or very old) at onset of disease, premature birth, bronchopulmonary dysplasia, congenital heart disease and immunodeficiency disorders. In infants, the risk of hospitalization due to severe RSV disease is highest for infants around the age of 2 months and gradually declines with increasing age (Figure (Fig) 1)[15, 16]. The transfer of maternal RSV neutralizing antibodies during the last trimester of the pregnancy provides some protection during the first month of life. A second risk factor is premature birth, which is associated with smaller, less developed lungs, a more immature immune system and an incomplete transfer of maternal antibodies in comparison to infants born at term. Depending on the gestational age, increased hospitalization rates up to 14% have been reported for infants born prematurely as reviewed by Sommer *et al.* [17].

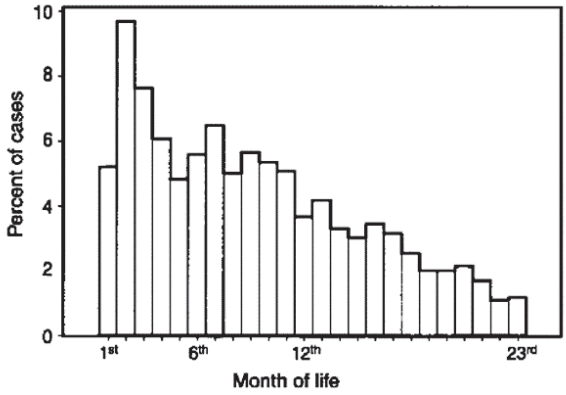

Figure 1: Incidence of RSV-associated hospitalization according to age. On a total of 1,272 cases of RSV-associated hospitalization in infants below 2 years of age, cases were categorized per age (X-axis, in months of life). Figure taken from [15].

Prematurity can necessitate prolonged mechanical ventilation leading to bronchopulmonary dysplasia (BPD, formerly called chronic lung disease), a third risk factor. Although BPD is complex and poorly understood, it is thought that mechanical ventilation can induce a pulmonary inflammatory response, due to oxygen toxicity and mechanically-induced lung injury. Such injury can disturb lung development. The presence of BPD in preterm infants further increases the risk of RSV-associated hospitalization with rates ranging from 12.3% to 24.4% [17]. Congenital heart disease is a fourth risk factor for the development of severe RSV disease with marked higher mortality rates compared to *e.g.* infants with BPD. RSV-associated hospitalization rates in infants with congenital heart disease range from 3.0% to 16.4% [17]. Immunodeficiency disorders and immunosuppression, such as severe combined immune

deficiency syndrome, acquired immune deficiency syndrome and hematopoietic stem cell transplantations represent a last set of major risk factors. RSV-associated hospitalization rates in the immune compromised range from 5.3% to 7.7%, with substantially higher mortality rates [17]. Mortality rates can be as high as 20% in human immunodeficiency virus (HIV) infected children and even up to 80% in bone marrow transplant patients as reported by one study [18, 19].

Although reinfections with RSV in healthy adults are common, those are mostly mild and limited to the upper respiratory tract with symptoms such as *e.g.* coughing, nasal congestion and sore throat among others. In about one-fourth of cases, progression to the lower respiratory tract occurs with tracheobronchitis and wheezing as possible symptoms [20, 21]. RSV-associated hospitalizations in adults are relatively rare and rates were recently estimated as about 2 and 10 per 10,000 adults aged 18-49 years and ≥ 50 years, respectively [22]. The average duration of RSV illness, however, is significantly longer compared to influenza (9,5 days versus 6,8 days, respectively) [20]. A recent retrospective study in adults confirmed that, although much lower in number, RSV-associated hospitalization tends to be more severe compared to influenza-associated hospitalization, as indicated by higher mortality rates, incidence of mechanical ventilation and average length of stay [23]. Apart from the direct medical costs for the treatment of severe RSV infections in adults, societal costs associated with *e.g.* absence from work may also be considerable.

In recent years, the elderly are increasingly recognized as a risk group for severe RSV disease in addition to infants. RSV-associated hospitalization rates are about 3-fold higher in the elderly >65 years old (25.4 per 10,000 persons) compared to adults of 50-64 years old (8.2 per 10,000 persons) [24]. Hospitalization rates in the elderly due to RSV are comparable to human metapneumovirus, a closely related respiratory virus (25.4 and 22.1 per 10,000 persons, respectively). Moreover, these hospitalization rates are about two times higher than those due to influenza (12.3 per 10,000 persons) in a population of which the majority (~72%) had been vaccinated against influenza. Estimates of mortality in the elderly due to RSV, up to 6.8% in RSV-associated hospitalized patients >60 years [23], highlights the importance of this age group for severe RSV disease.

RSV naturally infects the epithelial cells lining the respiratory lumen, with a tropism specific for the ciliated epithelial cells as shown both on primary human airway epithelial cells grown *in vitro* and on post-mortem autopsy lung samples [25-28]. The ciliated epithelial cells are infected only by the apical surface and virus release is also polarized to the apical surface [25, 27]. In contrast, basal cells and goblet cells appear resistant to RSV infection [26, 27]. In the alveoli, both type 1 and type 2 pneumocytes are infected with RSV [26, 28]. Although RSV antigens can sometimes be detected in macrophages, this is thought to be the result of phagocytic activity of macrophages and not due to productive RSV infection [26]. Syncytia can be observed in primary airway epithelial cells, but this is not always the case [26-28]. The histopathology of RSV is characterized by massive replication leading to edema, excess mucus production, sloughing of dying infected epithelial cells and the infiltration of immune cells, mainly neutrophils. The combination of cell debris (epithelial and immune cells) with mucus and edema results in the formation of plugs that obstruct the smaller airways, the bronchioles, causing breathing difficulties during severe RSV disease. In humans, several observations suggest that

massive viral replication is responsible for severe RSV disease whereas infiltrating immune cells correlate with resolution of disease. First, analysis of lung tissues of fatal RSV cases with severe lower respiratory tract illness by Welliver and colleagues identified massive viral antigen, but near absence of $CD4^+$ and $CD8^+$ T cells and natural killer cells [28]. In the literature, some confusion about the role of T cells in human RSV-associated disease was risen by the observation of $CD3^+$ double negative T cells and $CD8^+$ T cells in biopsies from a child that had died with, but not due to (the cause of death was a car accident), a RSV infection [26]. Secondly, in previously healthy infants <2 years of age hospitalized for RSV infection, increased RSV viral load correlates with increased hospitalization duration [29]. Thirdly, neutrophil and T-cell responses in peripheral blood during severe primary RSV infection are delayed for about 2-3 days and 10 days, respectively, compared to the peak of disease severity/viral load [30]. Finally, experimental infection of adults with RSV clearly shows a positive correlation between viral load and disease, both at the onset and peak of disease [31]. Although somewhat delayed compared to the amount of RSV, neutrophil infiltration is a typical hallmark of severe RSV bronchiolitis, possibly contributing to RSV disease severity. It is important to note that these findings in humans, apart from chimpanzees the only natural host of RSV, contrast with observations in the mouse model of RSV. In mice, $CD4^+$ and $CD8^+$ T cells contribute to the clearance of RSV during a primary infection, but these cells also contribute to RSV disease, with a greater role for $CD8^+$ T cells than $CD4^+$ T cells [32].

1.3 RSV virion structure

RSV is a negative strand RNA virus that recently was reclassified by the International Committee on Taxonomy of Viruses and is thus no longer part of the *Paramyxoviridae* family. Currently the virus is classified within the order *Mononegavirales*, family *Pneumoviridae* and genus *Orthopneumovirus*. The genus *Orthopneumovirus* consists of the species *Bovine* -, *Human* - and *Murine orthopneumovirus* with the virus members bovine RSV (bRSV), human RSV (hRSV) and murine pneumonia virus (MPV), respectively. As we only worked with human RSV in this thesis we will use the abbreviation RSV in reference to human RSV. In addition to the genus *Orthopneumovirus* the *Pneumoviridae* family also consists of the genus *Metapneumovirus* with the species avian - and human metapneumovirus (hMPV). hMPV is the most closely related virus to RSV and an important cause of acute lower respiratory tract infections in infants besides RSV [33]. Both viruses cause very similar respiratory symptoms.

RSV virions are composed of ribonucleoprotein (RNP) structures surrounded by a lipid envelope (Fig. 2A). Their shape is pleomorphic. Electron cryotomography of cell culture grown RSV virions revealed a dynamic range from spherical virions of 100 to 1,000 nm in diameter to filamentous virions of 200 to 2,000 nm in length with intermediate virions composed of both spherical and filamentous regions [34, 35]. Depending on the virion morphology, on average 2-4 RNPs are traced in RSV virions [35]. A drop in infectivity due to freezing or heat coincides with a reduced fraction of filamentous virions, suggesting that filamentous RSV is more infectious and can convert to spherical RSV [34]. The RNP complex consists of a single, negative strand RNA genome and several viral proteins: the nucleoprotein (N) that completely covers the RNA strand, the phosphoprotein (P), the M2-1 protein and the large polymerase

subunit (L). The RNP complex is responsible for both mRNA transcription and synthesis of full length RNA genomes. The lipid envelope is derived from the host cell and contains three viral transmembrane proteins: the fusion protein (F), the attachment glycoprotein (G) and the small hydrophobic protein (SH), although the abundance of SH in virions is low. The two major surface glycoproteins, F and G, are the only targets for neutralizing antibodies [36]. The F protein is highly conserved among RSV strains. Therefore, the highly variable G protein is used for the classification of RSV strains. Just below the lipid envelope is a layer composed of the matrix protein (M). The RSV RNA genome is approximately 15,200 nucleotides long and encodes 10 genes in the order 3' leader-NS1-NS2-N-P-M-SH-G-F-M2-L-trailer 5', that are translated into 11 viral proteins (the M2 gene is translated in two proteins, M2-1 and M2-2) (Fig. 2B).

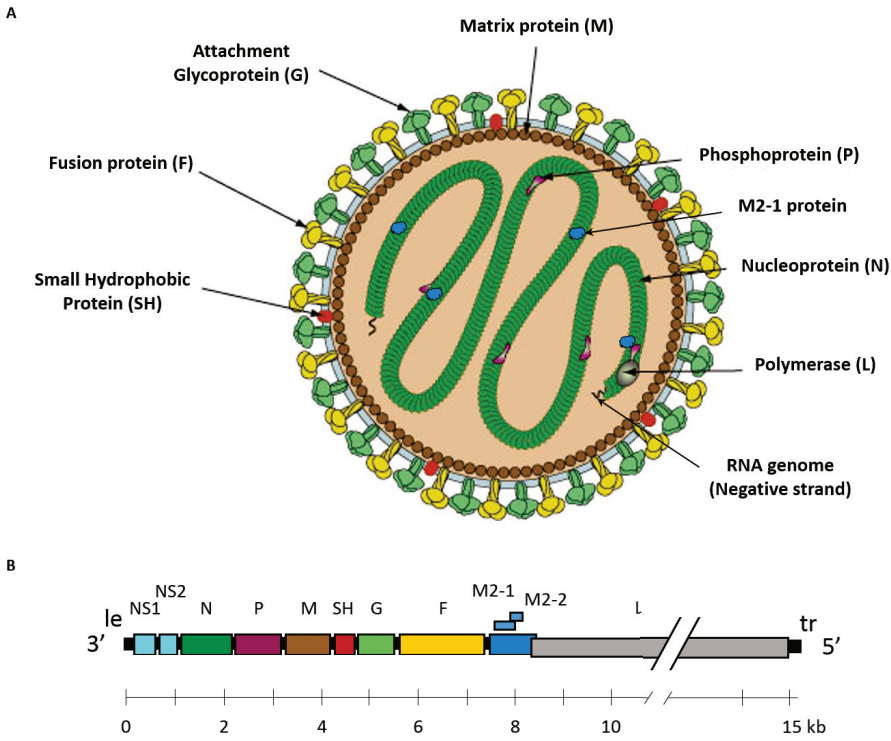

Figure 2: Structural organization of RSV. (A) Schematic representation of a RSV virion. Figure adapted from [37]. (B) RSV genome organization with scale bar (in kb). Le = leader, tr = trailer. Figure adapted from [38].

1.4 RSV infection cycle

A RSV infection starts with the attachment of the virion to the surface of a host cell. Initial experiments in immortalized stable cell lines suggested that attachment of RSV is mediated by the interaction of a heparin-binding domain of the attachment glycoprotein G with sulfated heparan-like glycosaminoglycans (GAG) on the cell surface [39, 40]. The prominent GAG heparan sulfate, however, is absent from the apical surface of well-differentiated human airway epithelial (HAE) cell cultures [41]. As these cultures closely resemble the natural tropism of RSV, heparan sulfate or related GAGs are unlikely to be the first receptors for RSV attachment *in vivo* [25, 27]. Recently, Johnson and colleagues indeed showed that soluble heparan sulfate neutralizes RSV in HeLa cells, but not in HAE cultures [42]. The G protein also contains a conserved CX3C motif that allows binding to the fractalkine receptor CX3CR1, thereby mimicking the chemokine fractalkine [43]. Preventing the interaction of the CX3C motif in G with CX3CR1 clearly reduces RSV infection in HAE cultures [42, 44, 45]. Interestingly, CX3CR1 is primarily expressed at the apical cilia of ciliated cells in HAE cultures and colocalizes with RSV particles upon attachment [45]. These results strongly argue that RSV attaches to the cell surface *in vivo* by interacting with CX3CR1 by the CX3C motif of G and they help explain the tropism of RSV for ciliated cells in the human respiratory tract. A mutant strain with complete deletion of G was strongly attenuated in HAE cultures [45]. This suggests that the fusion protein is the only RSV protein that is essential for entry and that F can also mediate attachment to HAE cultures, which is also evident in immortalized stable cell lines [46-48]. However, interaction of the G-CX3C motif with CX3CR1 strongly enhances attachment and infection of HAE cultures. Two other host proteins, annexin II and surfactant protein A, have also been identified as receptors for G in immortalized cell lines *in vitro*, yet their role in the more relevant HAE cultures or *in vivo* is currently unclear [49-51].

After attachment, fusion of the viral - and host membrane is mediated by the viral F protein. Several host proteins at the cell surface interact with the F protein and might act as a receptor for the F protein. These include Toll-like receptor (TLR)-4, intercellular adhesion molecule-1 (ICAM-1), nucleolin and epidermal growth factor receptor (EGFR) [52-55]. More recently, however, TLR-4 was shown not to be involved in the entry of RSV and thus unlikely to be a functional RSV receptor [56]. As with the candidate receptors for the G protein, substantial differences between cell lines and virus strains has generated confusion about the identity of the F protein receptor(s) *in vivo*. The EGFR, for example, appears important for fusion by the F protein of the RSV 2-20, but not for the F protein of the RSV-A2 lab strain [54]. Cell surface expressed nucleolin on the other hand binds a plethora of ligands such as carcinogenic - and anti-carcinogenic proteins, bacterial proteins and several other viruses ([57], reviewed in [58]). Possibly, interaction of F with cell surface nucleolin originates from the intrinsic broad binding characteristics of nucleolin rather than a specific interaction. So, despite the identification of several F interacting host proteins, a well-defined F receptor *in vivo* still needs to be determined.

The F protein is a trimeric type I membrane protein that initially is synthesized as a full length F_0 precursor protein in the endoplasmic reticulum (ER). Upon transport to the cell surface, F_0 is cleaved twice by a furin-like protease in the Golgi complex, which generates a fusion competent, disulfide

linked F_1 and F_2 fragment and a short fragment of 27 amino acids (p27) that is absent in the mature fusion competent F (Fig. 3A) [59, 60]. These cleavages are essential for transport to the cell surface and subsequent incorporation into virions [59, 61]. Krzyzaniak and colleagues, however, suggested that the second cleavage by a furin like protease only occurs during entry of a new host cell, implicating that RSV only becomes infectious during entry [62]. After full cleavage, the F_2-F_1 complex forms a metastable, prefusion form. The prefusion form undergoes dramatic conformational changes upon triggering and eventually forms a stable postfusion form. *In vitro* work revealed that low molarity could trigger this transition, however, the exact trigger during a natural RSV infection is currently unknown [63]. The transition from prefusion to postfusion is characterized by refolding of the heptad repeat (HR)-A region from each F_1 monomer into a long trimeric α-helix that inserts the adjacent hydrophobic fusion peptide at the N-terminus of each F_1 monomer into the host membrane (Fig. 3B). The F protein subsequently folds in the center, allowing the HR-B region of F_1 to bind to HR-A at the base of the extended α-helix and to form a stable 6-helix bundle [64, 65]. This way, the viral - and host membrane are brought together and the membranes eventually fuse. The exact route of RSV entry is still debated. Initial membrane fusion assays based on fluorophore dequenching, highlighted that RSV entry in HEp-2 cells occurs over a pH range of 5.5-8.5 and is resistant to treatment with ammonium chloride, a base that prevents endosomal acidification [66]. These results were interpreted as that RSV fusion occurs directly at the plasma membrane in a pH-independent manner, in analogy to other viruses of the closely related *Paramyxoviridae* family that enter the host cell in a pH-independent way. However, two alternative routes of RSV entry have been suggested. Kolokoltsov and colleagues used a targeted small interfering RNA (siRNA) library against host genes that are involved in membrane trafficking to demonstrate that RSV entry in HeLa cells involves clathrin-mediated endocytosis [67]. These results were subsequently confirmed by experiments with chlorpromazine, an inhibitor of clathrin-mediated endocytosis, and dominant negative mutants of Eps15 and Rab5, proteins that are involved in the assembly of clathrin-coated pits and formation of early endosomes, respectively. As RSV entry in HeLa cells was also pH-independent, a mechanism was proposed whereby RSV entry by clathrin-mediated endocytosis does not require early to late endosome transition and associated endosomal acidification. A role for clathrin-mediated endocytosis during RSV entry in HeLa cells was, however, not confirmed by Krzyzaniak and colleagues [62]. Inhibition of clathrin-mediated endocytosis by five different compounds (Chlorpromazine, pitstop-2, dynasore, dyngo-4a and dynol-34-2) did not inhibit RSV endocytosis or subsequent infection. RSV entry rather involved actin rearrangements and uptake of fluid, hallmarks of macropinocytosis. Maturation of macropinosomes during RSV entry was dependent on Rab5, but not Rab7, suggesting that RSV escapes macropinosomes before complete maturation. These results are in line with Kolokoltsov *et al.* who observed an important role for Rab5 during RSV entry [67]. Entry of RSV by macropinocytosis was confirmed in polarized epithelial 16HBE14o$^-$ cells [62]. Although these cells form polarized cell layers with functional tight junctions when grown under liquid covered culture conditions, no ciliated cells are formed [68]. Therefore, it would be interesting to confirm RSV entry by macropinocytosis in ciliated cells of well-differentiated HAE cultures in future experiments, as these air-liquid interphase cultures are the best models of RSV infections *in vivo*.

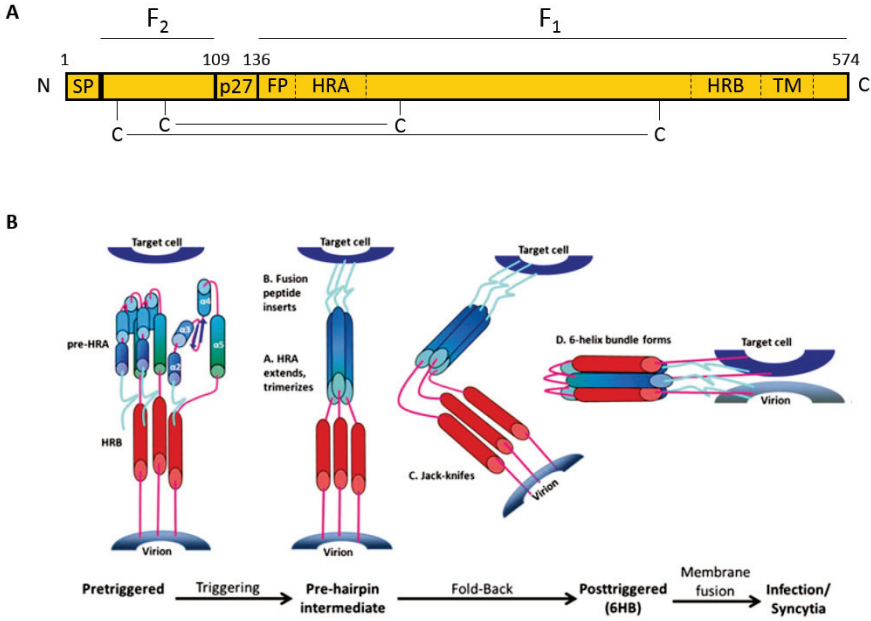

Figure 3: Fusion protein-mediated membrane fusion. (A) Structural organization of the F protein. The F protein consists of a N-terminal signal peptide (SP), a F_2 fragment, a 27-amino acids long peptide (p27) and a C-terminal F_1 fragment. Within the F_1 fragment, a N-terminal fusion peptide (FP), two heptad repeats (HR-A and HR-B) and the transmembrane region (TM) are localized. The F protein contains two furin-like cleavage sites (at position 109 and 136). Upon cleavage of both sites, mature F protein is formed by the F_2 and F_1 fragments connected by two disulfide bonds. (B) Schematic representation of the fusion process. Upon triggering of the trimeric F protein in the prefusion conformation, the three HR-A regions refold in a long trimeric α-helix with the insertion of the fusion peptides in the host membrane. Subsequent refolding at the center merges the HR-A helix with the HR-B regions to form a stable 6-helix bundle, thereby providing the force needed to merge the viral and host membrane. Figure adapted from [69].

Irrespective of the exact route of entry, fusion between the viral - and host membrane leads to the release of viral RNP complexes into the cytosol. RSV replication takes place in the cytosol and does not require the nuclear compartment of the cell. Upon release, the polymerase complex (N, P, L and M2-1) scans the single strand negative sense RNA genome starting from a single promoter in the 3' leader region and transcribes all 10 genes into separate mRNAs. The polymerase complex is hereby guided by conserved gene start and gene end sequences flanking each gene [70]. As the polymerase complex regularly detaches from the genome template, a gradient of viral mRNAs arises from the 3' genes (mostly transcribed) to the 5' genes (least transcribed) [71]. All mRNAs are 5' capped and 3' polyadenylated cotranscriptionally by intrinsic activities of the polymerase complex [72, 73]. A remarkable feature of the RSV genome organization is that the M2 and L gene partially overlap (Fig. 2B). As such the M2 gene end signal is located downstream of the L gene start signal. As transcription of the L gene is dependent on the M2 gene end signal, a model is proposed whereby the polymerase

complex scans back to the L gene start signal after it reaches the M2 gene end signal [74]. This however implies that the polymerase complex encounters the M2 gene end signal shortly after starting transcription at the L gene start signal. Collins and colleagues indeed found that the majority of L transcripts abort prematurely at the M2 gene end signal and that occasional read-through by the polymerase complex generates full length L transcripts [75]. Each mRNA is subsequently translated into one protein except for the M2 mRNA that encodes two, partially overlapping proteins, M2-1 and M2-2. Translation of the second open reading frame (ORF) (M2-2) occurs by ribosomes that terminate translation of the first ORF and reinitiate at the AUG start codon upstream [76]. Viral RNA synthesis is not randomly distributed over the cytoplasm, but occurs in virus-induced dense cytoplasmic structures, known as viral inclusion bodies (IB) (Fig. 4: IBs marked by an asterisk). These IBs are clearly present in infected cells at 6 hours post infection and expression of N and P is sufficient to form IBs [77-79]. In addition, M2-1, L, M and genomic RNA have also been shown to localize to the IBs [77-82]. F and G proteins are not detected within IBs, although F might interact with IBs during assembly [77, 83]. The relatively early induction of IBs and intense staining of viral RNP proteins suggest that IBs are the main sites of viral mRNA transcription, although some early genome amplification might be possible in IBs as well. Lindquist and colleagues identified a strong colocalization of genomic RNA and IBs late in infection (91% at 24 hours post infection) [78]. Another paper by Lifland *et al.*, however, identified genomic RNA in IBs at 6 hours post infection, but little to no genomic RNA in IBs at 12 or 24 hours post infection, despite high levels of N [79]. So it is currently not clear if IBs are the major sites of robust amplification of genomic RNA later in infection.

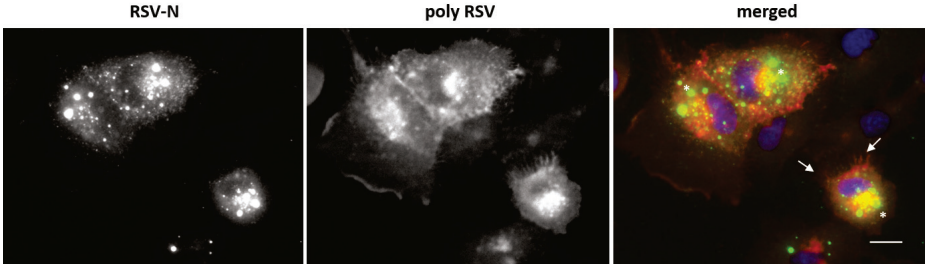

Figure 4: Inclusion bodies and viral filament formation in RSV infected cells. A549 cells were infected with RSV-A2 for 18 hours and stained with a nucleoprotein-specific antibody (left) and a polyclonal goat anti-RSV serum (middle). Both stainings were merged (right) with RSV-N (green), polyclonal RSV (red) and staining of nuclei with Hoechst (blue). Inclusion bodies were marked with an asterisk and viral filaments with an arrow. Scale bar = 10 μm. Pictures originate from our research group.

The N protein has two main functions. First, N protein monomers interact with each other to form decamer ring structures that are bound by both genomic and antigenomic viral RNA to form left handed helical nucleocapsid structures [84, 85]. These structures protect the viral RNA from degradation and serve as templates for both RNA transcription and replication. Secondly, N suppresses the induction of innate immune responses by different mechanisms. By completely covering the viral genome and antigenome, N prevents the recognition of viral RNA by cellular pattern recognition receptors. In addition, N directly interacts with protein kinase R, which prevents the phosphorylation of the α subunit of eukaryotic translation initiation factor 2 (eIF2α) and maintains protein translation during RSV infections [86]. N also sequesters the innate immunity mediators melanoma differentiation associated gene 5 (MDA5) and mitochondrial antiviral signaling protein (MAVS) to the IBs, which likely helps to suppress type I interferon (IFN) induction during RSV infections [79]. Two other signaling molecules, phosphorylated p38 mitogen activated protein kinase (MAPK) and O-linked N-acetylglucosamine transferase (OGT), are also sequestered to IBs, although it is not clear if this is mediated by N or any other RSV protein [87].

The P protein is highly phosphorylated and an essential cofactor for the viral polymerase complex during RNA transcription and replication [88]. The P protein interacts with all other members of the polymerase complex (N, L and M2-1) and is important for the elongation of the polymerase complex during transcription [81, 89-91]. It also binds to RNA-free N protein monomers where it functions as a chaperone molecule to maintain a pool of RNA-free N protein monomers that are readily available to bind and protect newly synthesized viral RNA [92]. Early after entry, uncoating of the RNP complex from the matrix layer is also dependent on the P protein [93].

The L protein is by far the largest protein encoded by RSV and comprises more than 40% of the total genome. It is the catalytic protein of the polymerase complex that synthesizes both mRNA and full length genomic RNA and has intrinsic capping and polyadenylation activity [72]. The L protein has been targeted for the development of small compound inhibitors with antiviral activity [94-96].

The M2 proteins have been identified as regulators of RSV transcription and replication. Although mRNA transcription occurs if N, P and L are expressed, M2-1 coexpression greatly enhances synthesis of full length mRNAs, highlighting that M2-1 is a transcription antitermination factor [97, 98]. M2-1 does not appear to have a role during RNA replication [98]. M2-1 binds both RNA and the P protein in a competitive manner through partially overlapping regions [81]. The crystal structure of M2-1 combined with targeted mutagenesis revealed that RNA binding and transcription elongation activity of M2-1 are strongly correlated [99]. In addition, M2-1 also interacts with the M protein, which connects the RNP complexes with the M protein and suggest that M2-1 is a structural protein [100]. High resolution imaging of RSV virions by cryo-electron tomography indeed confirmed that M2-1 connects the RNP structures with the matrix layer under the viral membrane in RSV virions [35]. M2-1 can also activate NF-κB, which involves the binding of M2-1 to relA [101].

As a RSV infection progresses with the accumulation of viral proteins, M2-2 proteins regulate RNA synthesis by reducing mRNA transcription and favoring replication of the RNA genome [102]. In

contrast to transcription, RNA replication requires that the polymerase complex ignores all gene start and - end signals. This leads to the synthesis of a full length, positive sense copy of the viral RNA genome, which is called the antigenome. The 3' end of the antigenome contains a promoter sequence that shares 88% sequence identity with the promoter of the genome and is used by the polymerase complex to synthesize full length, negative sense RNA genome copies.

The M protein is an important structural protein that forms a matrix layer below the viral envelope, which is mainly present in filamentous RSV in contrast to spherical RSV particles [34, 35]. Although M appears not to be essential for the initiation of virus filament formation, it is important for the elongation and maturation of virus filaments [103]. Recent crystallography suggests that M forms dimers and that the transition from dimers to higher order oligomers drives the viral filament formation [104]. In analogy to other negative strand RNA viruses, M reduces transcription activity of the RNP complex, which likely promotes RNP packaging in new virus filaments [82]. M possibly also enhances viral reproduction by reducing host gene transcription [105]. M is mainly found in the nucleus early after infection and translocates back to the cytoplasm late in infection. Nuclear import and - export of M are mediated by the importin β1 nuclear import receptor and the Crm1 nuclear export receptor, respectively [106, 107].

RSV encodes three transmembrane proteins, with the smallest one being SH. In infected cells, different isoforms of SH are expressed, *i.e.* unglycosylated, N-terminally truncated and glycosylated (Asn-3 or -52), but the exact role of these isoforms is currently not known [108]. In contrast to infected cells, SH is only present in virions at low abundance [109, 110]. SH appears to be dispensable for RSV growth, as SH deletion mutants equally replicate in cell culture and are only moderately attenuated *in vivo* [47, 111, 112]. Nevertheless, functional analysis of SH revealed that SH forms pentameric ion channels [113-115]. Fuentes and colleagues demonstrated that RSV SH inhibits tumor necrosis factor (TNF) signaling in analogy to the parainfluenza virus (PIV) type 5 SH protein and delays apoptosis [116]. This effect might be mediated by the interaction of SH with BCAP31, a protein involved in caspase-8-mediated apoptosis [117]. SH might also have an immunomodulatory role on IL-1β, a cytokine induced upon RSV infection, although current conflicting data urge for more validation of this surmised activity. Triantafilou and colleagues suggested that SH activates NLRP3 inflammasomes, leading to cleavage and secretion of IL-1β [118]. In contrast, SH has also been shown to suppress the secretion of IL1-β, both in human - and bovine RSV [119, 120]. Possibly, the use of primary lung epithelial cells versus stable cell lines account for these seemingly contradicting results.

The second transmembrane protein is G. It is a type II transmembrane protein with a short N-terminal cytoplasmic domain and a large C-terminal extracellular domain (Fig. 5). The extracellular domain is composed of two hypervariable mucin-like regions that enclose a conserved central domain. The two hypervariable regions contain several N-glycosylation sites (Asn-85, -103, -135, -237, -251 and -273) and numerous O-glycosylation sites, hence explaining the protein's name, glycosylated (G) protein. Glycosylation of these sites can increase the mass of the G protein up to three-fold in stable cell lines and possibly even up to six-fold in primary HAE cultures [121]. As these regions are highly variable

between RSV strains, G is mostly used to classify RSV strains in subgroups or hierarchical trees. The central domain contains a 13 amino acids long conserved region among RSV strains (164-176) that forms 2 disulfide bridges with the adjacent region (C173-C186 and C176-C182). These four cysteine residues together resemble a cysteine noose structural motif [122, 123]. The last 2 cysteine residues (C182 and C186) form a CX3C motif that mimicks the chemokine fractalkine. In addition to the full length G protein, a N-terminal truncated form of G is synthesized by translation initiation at a second start codon (position 48) in the transmembrane region followed by proteolytic removal of the remaining hydrophobic transmembrane region [124]. This truncated form of G is secreted from RSV infected cells. As described above, G is important for initial attachment, which is thought to occur by the interaction of the CX3C motif in the cysteine noose of G with CX3CR1 on ciliated epithelial cells in HAE cultures [42]. A deletion mutant of G was strongly attenuated, suggesting that G is important, but not completely indispensable for RSV infection in HAE cultures. These results have also been observed in some stable cell lines and in mice. Infection of HEp-2 cells and BALB/c mice with a RSV strain lacking G was strongly attenuated, whereas Vero cells were equally infected [47, 125]. Remarkably, a RSV strain that lacks full length G, but still expresses secreted G was not attenuated in HEp-2 cells, suggesting that secreted G is sufficient to overcome the *in vitro* attenuation of G deletion [125]. How exactly the secreted G could mediate cell attachment is, however, not clear. It would be interesting to test if this mutant RSV strain with preserved expression of secreted G is attenuated or not in HAE cultures.

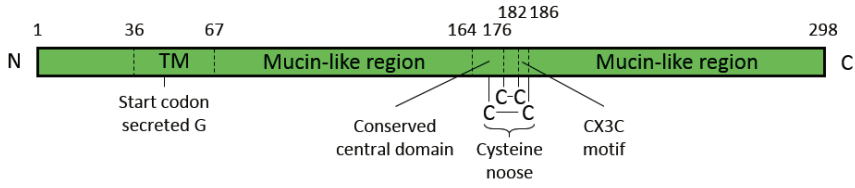

Figure 5: Structural organization of the G protein. The G protein consists of a short N-terminal cytoplasmic domain, a transmembrane domain (TM) and a large C-terminal extracellular domain. The extracellular domain contains two hypervariable mucin-like regions with multiple N- and O-glycosylation sites. In between the mucin-like regions a conserved central domain (164-176) forms two disulfide bonds (C173-C186 and C176-C182) with the adjacent CX3C motif (182-186). This CX3C motif functions as a fractalkine mimicry. The two disulfide bonds together resemble a cysteine noose structural motif. An alternative start codon in the TM domain is used to synthesize a secreted version of the G protein.

Several observations highlight an additional role for G during RSV infection apart from attachment, *i.e.* modulation of host immune responses. The high variability of the G protein sequence and strong glycosylation hamper the binding of (neutralizing) antibodies to G. This is strengthened by the secreted G that functions as a decoy receptor for G-specific antibodies [126]. Additionally, secreted G also impairs antiviral effects mediated by F- and G-specific antibodies involving pulmonary macrophages, FcgReceptors and complement activation, but not neutrophils [126, 127]. Secreted G might also impair innate immune responses such as induction of ICAM-1, IL-8 and CCL5 [128]. By interacting with DC-

SIGN and L-SIGN on dendritic cells, G directly reduces activation of dendritic cells, which likely lowers the induction of RSV-specific immune responses [129]. Furthermore, the CX3C motif in the cysteine noose of G mimics the chemokine fractalkine and suppresses both innate immune responses and adaptive immune responses [43, 130, 131]. For example, expression of the G-CX3C motif during a RSV infection reduces infiltration of $CX3CR1^{+}$ T cells among others in the lung [130]. Although G mimics fractalkine by binding to the fractalkine receptor CX3CR1, it is currently not clear how both proteins elicit an opposite response, *i.e.* fractalkine attracts T cells to the lung, whereas G reduces T cell infiltration in the lung. The cysteine noose of G also shares an interesting structural homology to the fourth subdomain of the TNF receptor [132]. So possibly, G modulates TNF-mediated immune responses, although to date no follow up data on this effect of G have been published.

In accordance with closely related paramyxoviruses the RSV-G protein might stabilize the F protein in its prefusion state to prevent premature transition to the postfusion state [133]. Although some prefusion F is present in recombinant RSV virions lacking G and SH, most F in these viruses is in the postfusion state [34]. In contrast, wild type RSV virions mainly consist of prefusion F, suggesting that G or SH, but most likely G, stabilizes F in its prefusion state.

Taken together, although G is not strictly necessary to initiate RSV infection, it strongly enhances attachment and plays an important role in the suppression of host immune responses against RSV *in vivo*.

The last transmembrane protein, F, is highly conserved among RSV strains and is the only indispensable transmembrane protein for RSV infection. As the F protein is so important for infection, F is an important target for neutralizing antibodies and the development of vaccines and antiviral compounds. As described above, F mediates fusion between the viral and host membrane during entry, but also mediates fusion between a RSV infected cell and non-infected neighbor cells, resulting in the formation of syncytia. The structures of pre - and postfusion F have been determined in 2013 and 2011, respectively, revealing a lollipop-like structure and a cone-like structure with extended stalk, respectively [134-136]. In addition to its role during fusion, F also induces innate immune responses (IL-6, IL-8 and TNF-α) by interacting with the TLR4-CD14 complex, a receptor complex known for the recognition of *e.g.* lipopolysaccharide [55]. Funchal and colleagues demonstrated that the interaction of F with TLR4 also induces the formation of neutrophil extracellular traps, which are composed of chromatin fibers bound by antimicrobial proteins that might possess antiviral activity [137]. It is not clear if the interaction of F with TLR4 yields any selective advantage for RSV replication.

RSV also encodes two, unique non-structural proteins (NS1 and NS2). Although not present in RSV virions, these proteins are strongly expressed in infected cells. NS1 and NS2 work independently and cooperatively in the suppression of host innate immune responses and their effector functions will be described more in detail in the next chapter.

As viral proteins are synthesized and genomic RNA is amplified, new virus particles are assembled and start to bud from infected cells. Newly produced RSV virions can be detected from 10-12 hours post infection, are maximally released around 24 hours post infection and continue to be released up to 48

hours post infection until the infected cell breaks down [138]. In accordance to the restricted entry of RSV by the apical surface of polarized epithelial cells, assembly and subsequent release of RSV virions is also restricted to the apical surface [25, 27, 139]. In *in vitro* cell cultures, up to 90% of newly produced virions remain cell associated, although this might be an artefact of immortalized cell lines and not be the case *in vivo* [140]. RSV assembly occurs at lipid raft domains in the plasma membrane that are enriched with the ganglioside GM1 and caveolin-1 [141-144]. Assembly typically involves the formation of filamentous projections of the plasma membrane, which can reach a length up to 10 µm (Fig. 4, virus filaments marked by arrows). These viral filaments are believed to generate the filamentous virions as F and G accumulate in the membrane and multiple RNP complexes are detected inside the viral filaments [145]. Viral filament formation appears to be driven by the viral proteins F, M, P and possibly N [146, 147]. The current model of RSV assembly and budding involves the formation of RNP complexes in the IBs that are often near the sites of virus filament formation in the plasma membrane [148]. Subsequently M interacts with the RNP complexes by M2-1 and guides the RNP complexes to the sites of filament formation, possibly by actin microfilaments [100, 103]. In parallel, viral glycoproteins (F, G and SH) are synthesized and transported by the secretory pathway (ER-Golgi-vesicle transport) to the plasma membrane, which is dependent on the apical recycling endosome [149]. At the lipid rafts in the plasma membrane, M forms a bridge between the RNP complexes and the cytoplasmic tails of the viral glycoproteins. Sorting of M to the lipid rafts is hereby dependent on the viral glycoproteins [150]. As the plasma membrane protrudes and elongates to a filamentous structure, a supporting matrix layer is formed just below the membrane. Oligomerization of the M protein appears not important for the initiation of virus filament formation, but is essential for the elongation [103, 104]. How exactly the final fission occurs is currently not known. As genome RNP complexes are more abundant in infected cells than antigenome RNP complexes, RSV virions contain mostly, but not exclusively, genome RNP complexes [138]. These results suggest that RNP incorporation in maturing filaments might be non-specific. Recently, an alternative way of RSV spreading was identified. Mehedi and colleagues demonstrated that RSV induces the formation of filopodia, thin cell protrusions containing actin filaments that are distinct from viral filaments [151]. These filopodia could spread RSV virions to neighboring cells.

1.5 Reference list

1. Blount, R.E., Jr., J.A. Morris, and R.E. Savage, *Recovery of cytopathogenic agent from chimpanzees with coryza.* Proc Soc Exp Biol Med, 1956. **92**(3): p. 544-9.
2. Chanock, R., B. Roizman, and R. Myers, *Recovery from infants with respiratory illness of a virus related to chimpanzee coryza agent (CCA). I. Isolation, properties and characterization.* Am J Hyg, 1957. **66**(3): p. 281-90.
3. Stensballe, L.G., J.K. Devasundaram, and E.A. Simoes, *Respiratory syncytial virus epidemics: the ups and downs of a seasonal virus.* Pediatr Infect Dis J, 2003. **22**(2 Suppl): p. S21-32.
4. Tang, J.W. and T.P. Loh, *Correlations between climate factors and incidence--a contributor to RSV seasonality.* Rev Med Virol, 2014. **24**(1): p. 15-34.
5. Glezen, W.P., et al., *Risk of primary infection and reinfection with respiratory syncytial virus.* Am J Dis Child, 1986. **140**(6): p. 543-6.
6. pediatrics, A.a.o. *Respiratory syncytial virus (RSV)*. 2015; Available from: https://www.healthychildren.org/English/health-issues/conditions/chest-lungs/Pages/Respiratory-Syncytial-Virus-RSV.aspx.
7. Nair, H., et al., *Global burden of acute lower respiratory infections due to respiratory syncytial virus in young children: a systematic review and meta-analysis.* Lancet, 2010. **375**(9725): p. 1545-55.
8. Lozano, R., et al., *Global and regional mortality from 235 causes of death for 20 age groups in 1990 and 2010: a systematic analysis for the Global Burden of Disease Study 2010.* Lancet, 2012. **380**(9859): p. 2095-128.
9. Stockman, L.J., et al., *Respiratory syncytial virus-associated hospitalizations among infants and young children in the United States, 1997-2006.* Pediatr Infect Dis J, 2012. **31**(1): p. 5-9.
10. Svensson, C., et al., *Incidence, risk factors and hospital burden in children under five years of age hospitalised with respiratory syncytial virus infections.* Acta Paediatr, 2015. **104**(9): p. 922-6.
11. Reeves, R.M., et al., *Estimating the burden of respiratory syncytial virus (RSV) on respiratory hospital admissions in children less than five years of age in England, 2007-2012.* Influenza Other Respir Viruses, 2017. **11**(2): p. 122-129.
12. Nokes, D.J., et al., *Respiratory syncytial virus infection and disease in infants and young children observed from birth in Kilifi District, Kenya.* Clin Infect Dis, 2008. **46**(1): p. 50-7.
13. Madhi, S.A., et al., *Five-year cohort study of hospitalization for respiratory syncytial virus associated lower respiratory tract infection in African children.* J Clin Virol, 2006. **36**(3): p. 215-21.
14. Boyce, T.G., et al., *Rates of hospitalization for respiratory syncytial virus infection among children in medicaid.* J Pediatr, 2000. **137**(6): p. 865-70.
15. Nielsen, H.E., et al., *Respiratory syncytial virus infection--risk factors for hospital admission: a case-control study.* Acta Paediatr, 2003. **92**(11): p. 1314-21.
16. Hall, C.B., *The burgeoning burden of respiratory syncytial virus among children.* Infect Disord Drug Targets, 2012. **12**(2): p. 92-7.
17. Sommer, C., B. Resch, and E.A. Simoes, *Risk factors for severe respiratory syncytial virus lower respiratory tract infection.* Open Microbiol J, 2011. **5**: p. 144-54.
18. Resch, B., P. Manzoni, and M. Lanari, *Severe respiratory syncytial virus (RSV) infection in infants with neuromuscular diseases and immune deficiency syndromes.* Paediatr Respir Rev, 2009. **10**(3): p. 148-53.
19. Lewinsohn, D.M., et al., *Phase I study of intravenous ribavirin treatment of respiratory syncytial virus pneumonia after marrow transplantation.* Antimicrob Agents Chemother, 1996. **40**(11): p. 2555-7.
20. Hall, C.B., C.E. Long, and K.C. Schnabel, *Respiratory syncytial virus infections in previously healthy working adults.* Clin Infect Dis, 2001. **33**(6): p. 792-6.

21. Falsey, A.R., *Respiratory syncytial virus infection in adults.* Semin Respir Crit Care Med, 2007. **28**(2): p. 171-81.
22. Widmer, K., et al., *Respiratory syncytial virus- and human metapneumovirus-associated emergency department and hospital burden in adults.* Influenza Other Respir Viruses, 2014. **8**(3): p. 347-52.
23. Pastula, S.T., et al., *Hospitalizations for Respiratory Syncytial Virus Among Adults in the United States, 1997-2012.* Open Forum Infect Dis, 2017. **4**(1): p. ofw270.
24. Widmer, K., et al., *Rates of hospitalizations for respiratory syncytial virus, human metapneumovirus, and influenza virus in older adults.* J Infect Dis, 2012. **206**(1): p. 56-62.
25. Zhang, L., et al., *Respiratory syncytial virus infection of human airway epithelial cells is polarized, specific to ciliated cells, and without obvious cytopathology.* J Virol, 2002. **76**(11): p. 5654-66.
26. Johnson, J.E., et al., *The histopathology of fatal untreated human respiratory syncytial virus infection.* Mod Pathol, 2007. **20**(1): p. 108-19.
27. Villenave, R., et al., *In vitro modeling of respiratory syncytial virus infection of pediatric bronchial epithelium, the primary target of infection in vivo.* Proc Natl Acad Sci U S A, 2012. **109**(13): p. 5040-5.
28. Welliver, T.P., et al., *Severe human lower respiratory tract illness caused by respiratory syncytial virus and influenza virus is characterized by the absence of pulmonary cytotoxic lymphocyte responses.* J Infect Dis, 2007. **195**(8): p. 1126-36.
29. El Saleeby, C.M., et al., *Respiratory syncytial virus load, viral dynamics, and disease severity in previously healthy naturally infected children.* J Infect Dis, 2011. **204**(7): p. 996-1002.
30. Lukens, M.V., et al., *A systemic neutrophil response precedes robust CD8(+) T-cell activation during natural respiratory syncytial virus infection in infants.* J Virol, 2010. **84**(5): p. 2374-83.
31. DeVincenzo, J.P., et al., *Viral load drives disease in humans experimentally infected with respiratory syncytial virus.* Am J Respir Crit Care Med, 2010. **182**(10): p. 1305-14.
32. Graham, B.S., et al., *Role of T lymphocyte subsets in the pathogenesis of primary infection and rechallenge with respiratory syncytial virus in mice.* J Clin Invest, 1991. **88**(3): p. 1026-33.
33. Ordas, J., et al., *Role of metapneumovirus in viral respiratory infections in young children.* J Clin Microbiol, 2006. **44**(8): p. 2739-42.
34. Liljeroos, L., et al., *Architecture of respiratory syncytial virus revealed by electron cryotomography.* Proc Natl Acad Sci U S A, 2013. **110**(27): p. 11133-8.
35. Kiss, G., et al., *Structural analysis of respiratory syncytial virus reveals the position of M2-1 between the matrix protein and the ribonucleoprotein complex.* J Virol, 2014. **88**(13): p. 7602-17.
36. Sastre, P., et al., *Comparison of affinity chromatography and adsorption to vaccinia virus recombinant infected cells for depletion of antibodies directed against respiratory syncytial virus glycoproteins present in a human immunoglobulin preparation.* J Med Virol, 2005. **76**(2): p. 248-55.
37. Swiss institute of Bioinformatics, V. *Pneumovirus*. Available from: http://viralzone.expasy.org/90?outline=all_by_species.
38. Collins, P.L. and B.S. Graham, *Viral and host factors in human respiratory syncytial virus pathogenesis.* J Virol, 2008. **82**(5): p. 2040-55.
39. Feldman, S.A., R.M. Hendry, and J.A. Beeler, *Identification of a linear heparin binding domain for human respiratory syncytial virus attachment glycoprotein G.* J Virol, 1999. **73**(8): p. 6610-7.
40. Hallak, L.K., et al., *Glycosaminoglycan sulfation requirements for respiratory syncytial virus infection.* J Virol, 2000. **74**(22): p. 10508-13.
41. Zhang, L., et al., *Infection of ciliated cells by human parainfluenza virus type 3 in an in vitro model of human airway epithelium.* J Virol, 2005. **79**(2): p. 1113-24.
42. Johnson, S.M., et al., *Respiratory Syncytial Virus Uses CX3CR1 as a Receptor on Primary Human Airway Epithelial Cultures.* PLoS Pathog, 2015. **11**(12): p. e1005318.

43. Tripp, R.A., et al., *CX3C chemokine mimicry by respiratory syncytial virus G glycoprotein.* Nat Immunol, 2001. **2**(8): p. 732-8.
44. Chirkova, T., et al., *CX3CR1 is an important surface molecule for respiratory syncytial virus infection in human airway epithelial cells.* J Gen Virol, 2015. **96**(9): p. 2543-56.
45. Jeong, K.I., et al., *CX3CR1 Is Expressed in Differentiated Human Ciliated Airway Cells and Co-Localizes with Respiratory Syncytial Virus on Cilia in a G Protein-Dependent Manner.* PLoS One, 2015. **10**(6): p. e0130517.
46. Karron, R.A., et al., *Respiratory syncytial virus (RSV) SH and G proteins are not essential for viral replication in vitro: clinical evaluation and molecular characterization of a cold-passaged, attenuated RSV subgroup B mutant.* Proc Natl Acad Sci U S A, 1997. **94**(25): p. 13961-6.
47. Techaarpornkul, S., N. Barretto, and M.E. Peeples, *Functional analysis of recombinant respiratory syncytial virus deletion mutants lacking the small hydrophobic and/or attachment glycoprotein gene.* J Virol, 2001. **75**(15): p. 6825-34.
48. Feldman, S.A., S. Audet, and J.A. Beeler, *The fusion glycoprotein of human respiratory syncytial virus facilitates virus attachment and infectivity via an interaction with cellular heparan sulfate.* J Virol, 2000. **74**(14): p. 6442-7.
49. Barr, F.E., et al., *Surfactant protein-A enhances uptake of respiratory syncytial virus by monocytes and U937 macrophages.* Am J Respir Cell Mol Biol, 2000. **23**(5): p. 586-92.
50. Hickling, T.P., et al., *Lung surfactant protein A provides a route of entry for respiratory syncytial virus into host cells.* Viral Immunol, 2000. **13**(1): p. 125-35.
51. Malhotra, R., et al., *Isolation and characterisation of potential respiratory syncytial virus receptor(s) on epithelial cells.* Microbes Infect, 2003. **5**(2): p. 123-33.
52. Behera, A.K., et al., *Blocking intercellular adhesion molecule-1 on human epithelial cells decreases respiratory syncytial virus infection.* Biochem Biophys Res Commun, 2001. **280**(1): p. 188-95.
53. Tayyari, F., et al., *Identification of nucleolin as a cellular receptor for human respiratory syncytial virus.* Nat Med, 2011. **17**(9): p. 1132-5.
54. Currier, M.G., et al., *EGFR Interacts with the Fusion Protein of Respiratory Syncytial Virus Strain 2-20 and Mediates Infection and Mucin Expression.* PLoS Pathog, 2016. **12**(5): p. e1005622.
55. Kurt-Jones, E.A., et al., *Pattern recognition receptors TLR4 and CD14 mediate response to respiratory syncytial virus.* Nat Immunol, 2000. **1**(5): p. 398-401.
56. Marr, N. and S.E. Turvey, *Role of human TLR4 in respiratory syncytial virus-induced NF-kappaB activation, viral entry and replication.* Innate Immun, 2012. **18**(6): p. 856-65.
57. Bose, S., M. Basu, and A.K. Banerjee, *Role of nucleolin in human parainfluenza virus type 3 infection of human lung epithelial cells.* J Virol, 2004. **78**(15): p. 8146-58.
58. Fujiki, H., T. Watanabe, and M. Suganuma, *Cell-surface nucleolin acts as a central mediator for carcinogenic, anti-carcinogenic, and disease-related ligands.* J Cancer Res Clin Oncol, 2014. **140**(5): p. 689-99.
59. Bolt, G., L.O. Pedersen, and H.H. Birkeslund, *Cleavage of the respiratory syncytial virus fusion protein is required for its surface expression: role of furin.* Virus Res, 2000. **68**(1): p. 25-33.
60. Gonzalez-Reyes, L., et al., *Cleavage of the human respiratory syncytial virus fusion protein at two distinct sites is required for activation of membrane fusion.* Proc Natl Acad Sci U S A, 2001. **98**(17): p. 9859-64.
61. Collins, P.L. and G. Mottet, *Post-translational processing and oligomerization of the fusion glycoprotein of human respiratory syncytial virus.* J Gen Virol, 1991. **72 (Pt 12)**: p. 3095-101.
62. Krzyzaniak, M.A., et al., *Host cell entry of respiratory syncytial virus involves macropinocytosis followed by proteolytic activation of the F protein.* PLoS Pathog, 2013. **9**(4): p. e1003309.
63. Chaiwatpongsakorn, S., et al., *Soluble respiratory syncytial virus fusion protein in the fully cleaved, pretriggered state is triggered by exposure to low-molarity buffer.* J Virol, 2011. **85**(8): p. 3968-77.

64. Zhao, X., et al., *Structural characterization of the human respiratory syncytial virus fusion protein core.* Proc Natl Acad Sci U S A, 2000. **97**(26): p. 14172-7.
65. McLellan, J.S., W.C. Ray, and M.E. Peeples, *Structure and function of respiratory syncytial virus surface glycoproteins.* Curr Top Microbiol Immunol, 2013. **372**: p. 83-104.
66. Srinivasakumar, N., P.L. Ogra, and T.D. Flanagan, *Characteristics of fusion of respiratory syncytial virus with HEp-2 cells as measured by R18 fluorescence dequenching assay.* J Virol, 1991. **65**(8): p. 4063-9.
67. Kolokoltsov, A.A., et al., *Small interfering RNA profiling reveals key role of clathrin-mediated endocytosis and early endosome formation for infection by respiratory syncytial virus.* J Virol, 2007. **81**(14): p. 7786-800.
68. Ehrhardt, C.F., B.; Kim, K.-J., *In vitro models of the Tracheo-Bronchial epithelium*, in *Drug absorption studies; in situ, in vitro and in silico models*, C. Ehrhardt, Editor. 2008.
69. Graham, B.S. and L.J. Anderson, *Challenges and opportunities for respiratory syncytial virus vaccines.* Curr Top Microbiol Immunol, 2013. **372**: p. 391-404.
70. Kuo, L., et al., *Effects of mutations in the gene-start and gene-end sequence motifs on transcription of monocistronic and dicistronic minigenomes of respiratory syncytial virus.* J Virol, 1996. **70**(10): p. 6892-901.
71. Barik, S., *Transcription of human respiratory syncytial virus genome RNA in vitro: requirement of cellular factor(s).* J Virol, 1992. **66**(11): p. 6813-8.
72. Barik, S., *The structure of the 5' terminal cap of the respiratory syncytial virus mRNA.* J Gen Virol, 1993. **74 (Pt 3)**: p. 485-90.
73. Liuzzi, M., et al., *Inhibitors of respiratory syncytial virus replication target cotranscriptional mRNA guanylylation by viral RNA-dependent RNA polymerase.* J Virol, 2005. **79**(20): p. 13105-15.
74. Fearns, R. and P.L. Collins, *Model for polymerase access to the overlapped L gene of respiratory syncytial virus.* J Virol, 1999. **73**(1): p. 388-97.
75. Collins, P.L., et al., *Gene overlap and site-specific attenuation of transcription of the viral polymerase L gene of human respiratory syncytial virus.* Proc Natl Acad Sci U S A, 1987. **84**(15): p. 5134-8.
76. Ahmadian, G., J.S. Randhawa, and A.J. Easton, *Expression of the ORF-2 protein of the human respiratory syncytial virus M2 gene is initiated by a ribosomal termination-dependent reinitiation mechanism.* EMBO J, 2000. **19**(11): p. 2681-9.
77. Garcia, J., et al., *Cytoplasmic inclusions of respiratory syncytial virus-infected cells: formation of inclusion bodies in transfected cells that coexpress the nucleoprotein, the phosphoprotein, and the 22K protein.* Virology, 1993. **195**(1): p. 243-7.
78. Lindquist, M.E., et al., *Respiratory syncytial virus induces host RNA stress granules to facilitate viral replication.* J Virol, 2010. **84**(23): p. 12274-84.
79. Lifland, A.W., et al., *Human respiratory syncytial virus nucleoprotein and inclusion bodies antagonize the innate immune response mediated by MDA5 and MAVS.* J Virol, 2012. **86**(15): p. 8245-58.
80. Carromeu, C., et al., *Intracellular localization of human respiratory syncytial virus L protein.* Arch Virol, 2007. **152**(12): p. 2259-63.
81. Blondot, M.L., et al., *Structure and functional analysis of the RNA- and viral phosphoprotein-binding domain of respiratory syncytial virus M2-1 protein.* PLoS Pathog, 2012. **8**(5): p. e1002734.
82. Ghildyal, R., et al., *Respiratory syncytial virus matrix protein associates with nucleocapsids in infected cells.* J Gen Virol, 2002. **83**(Pt 4): p. 753-7.
83. Baviskar, P.S., et al., *The respiratory syncytial virus fusion protein targets to the perimeter of inclusion bodies and facilitates filament formation by a cytoplasmic tail-dependent mechanism.* J Virol, 2013. **87**(19): p. 10730-41.
84. Tawar, R.G., et al., *Crystal structure of a nucleocapsid-like nucleoprotein-RNA complex of respiratory syncytial virus.* Science, 2009. **326**(5957): p. 1279-83.

85. Bakker, S.E., et al., *The respiratory syncytial virus nucleoprotein-RNA complex forms a left-handed helical nucleocapsid.* J Gen Virol, 2013. **94**(Pt 8): p. 1734-8.
86. Groskreutz, D.J., et al., *Respiratory syncytial virus limits alpha subunit of eukaryotic translation initiation factor 2 (eIF2alpha) phosphorylation to maintain translation and viral replication.* J Biol Chem, 2010. **285**(31): p. 24023-31.
87. Fricke, J., et al., *p38 and OGT sequestration into viral inclusion bodies in cells infected with human respiratory syncytial virus suppresses MK2 activities and stress granule assembly.* J Virol, 2013. **87**(3): p. 1333-47.
88. Grosfeld, H., M.G. Hill, and P.L. Collins, *RNA replication by respiratory syncytial virus (RSV) is directed by the N, P, and L proteins; transcription also occurs under these conditions but requires RSV superinfection for efficient synthesis of full-length mRNA.* J Virol, 1995. **69**(9): p. 5677-86.
89. Dupuy, L.C., et al., *Casein kinase 2-mediated phosphorylation of respiratory syncytial virus phosphoprotein P is essential for the transcription elongation activity of the viral polymerase; phosphorylation by casein kinase 1 occurs mainly at Ser(215) and is without effect.* J Virol, 1999. **73**(10): p. 8384-92.
90. Galloux, M., et al., *Characterization of a viral phosphoprotein binding site on the surface of the respiratory syncytial nucleoprotein.* J Virol, 2012. **86**(16): p. 8375-87.
91. Sourimant, J., et al., *Fine mapping and characterization of the L-polymerase-binding domain of the respiratory syncytial virus phosphoprotein.* J Virol, 2015. **89**(8): p. 4421-33.
92. Galloux, M., et al., *Identification and characterization of the binding site of the respiratory syncytial virus phosphoprotein to RNA-free nucleoprotein.* J Virol, 2015. **89**(7): p. 3484-96.
93. Asenjo, A., J.C. Gonzalez-Armas, and N. Villanueva, *Phosphorylation of human respiratory syncytial virus P protein at serine 54 regulates viral uncoating.* Virology, 2008. **380**(1): p. 26-33.
94. Tiong-Yip, C.L., et al., *Characterization of a respiratory syncytial virus L protein inhibitor.* Antimicrob Agents Chemother, 2014. **58**(7): p. 3867-73.
95. Wang, G., et al., *Discovery of 4'-chloromethyl-2'-deoxy-3',5'-di-O-isobutyryl-2'-fluorocytidine (ALS-8176), a first-in-class RSV polymerase inhibitor for treatment of human respiratory syncytial virus infection.* J Med Chem, 2015. **58**(4): p. 1862-78.
96. Hall, C.B., et al., *Ribavirin treatment of experimental respiratory syncytial viral infection. A controlled double-blind study in young adults.* JAMA, 1983. **249**(19): p. 2666-70.
97. Collins, P.L., et al., *Transcription elongation factor of respiratory syncytial virus, a nonsegmented negative-strand RNA virus.* Proc Natl Acad Sci U S A, 1996. **93**(1): p. 81-5.
98. Fearns, R. and P.L. Collins, *Role of the M2-1 transcription antitermination protein of respiratory syncytial virus in sequential transcription.* J Virol, 1999. **73**(7): p. 5852-64.
99. Tanner, S.J., et al., *Crystal structure of the essential transcription antiterminator M2-1 protein of human respiratory syncytial virus and implications of its phosphorylation.* Proc Natl Acad Sci U S A, 2014. **111**(4): p. 1580-5.
100. Li, D., et al., *Association of respiratory syncytial virus M protein with viral nucleocapsids is mediated by the M2-1 protein.* J Virol, 2008. **82**(17): p. 8863-70.
101. Reimers, K., K. Buchholz, and H. Werchau, *Respiratory syncytial virus M2-1 protein induces the activation of nuclear factor kappa B.* Virology, 2005. **331**(2): p. 260-8.
102. Bermingham, A. and P.L. Collins, *The M2-2 protein of human respiratory syncytial virus is a regulatory factor involved in the balance between RNA replication and transcription.* Proc Natl Acad Sci U S A, 1999. **96**(20): p. 11259-64.
103. Mitra, R., et al., *The human respiratory syncytial virus matrix protein is required for maturation of viral filaments.* J Virol, 2012. **86**(8): p. 4432-43.
104. Forster, A., et al., *Dimerization of matrix protein is required for budding of respiratory syncytial virus.* J Virol, 2015. **89**(8): p. 4624-35.
105. Ghildyal, R., et al., *The matrix protein of Human respiratory syncytial virus localises to the nucleus of infected cells and inhibits transcription.* Arch Virol, 2003. **148**(7): p. 1419-29.

106. Ghildyal, R., et al., *Nuclear import of the respiratory syncytial virus matrix protein is mediated by importin beta1 independent of importin alpha.* Biochemistry, 2005. **44**(38): p. 12887-95.
107. Ghildyal, R., et al., *The respiratory syncytial virus matrix protein possesses a Crm1-mediated nuclear export mechanism.* J Virol, 2009. **83**(11): p. 5353-62.
108. Olmsted, R.A. and P.L. Collins, *The 1A protein of respiratory syncytial virus is an integral membrane protein present as multiple, structurally distinct species.* J Virol, 1989. **63**(5): p. 2019-29.
109. Radhakrishnan, A., et al., *Protein analysis of purified respiratory syncytial virus particles reveals an important role for heat shock protein 90 in virus particle assembly.* Mol Cell Proteomics, 2010. **9**(9): p. 1829-48.
110. Rixon, H.W., et al., *The small hydrophobic (SH) protein accumulates within lipid-raft structures of the Golgi complex during respiratory syncytial virus infection.* J Gen Virol, 2004. **85**(Pt 5): p. 1153-65.
111. Bukreyev, A., et al., *Recombinant respiratory syncytial virus from which the entire SH gene has been deleted grows efficiently in cell culture and exhibits site-specific attenuation in the respiratory tract of the mouse.* J Virol, 1997. **71**(12): p. 8973-82.
112. Whitehead, S.S., et al., *Recombinant respiratory syncytial virus bearing a deletion of either the NS2 or SH gene is attenuated in chimpanzees.* J Virol, 1999. **73**(4): p. 3438-42.
113. Carter, S.D., et al., *Direct visualization of the small hydrophobic protein of human respiratory syncytial virus reveals the structural basis for membrane permeability.* FEBS Lett, 2010. **584**(13): p. 2786-90.
114. Gan, S.W., et al., *The small hydrophobic protein of the human respiratory syncytial virus forms pentameric ion channels.* J Biol Chem, 2012. **287**(29): p. 24671-89.
115. Li, Y., et al., *Inhibition of the human respiratory syncytial virus small hydrophobic protein and structural variations in a bicelle environment.* J Virol, 2014. **88**(20): p. 11899-914.
116. Fuentes, S., et al., *Function of the respiratory syncytial virus small hydrophobic protein.* J Virol, 2007. **81**(15): p. 8361-6.
117. Li, Y., et al., *Interaction between human BAP31 and respiratory syncytial virus small hydrophobic (SH) protein.* Virology, 2015. **482**: p. 105-10.
118. Triantafilou, K., et al., *Human respiratory syncytial virus viroporin SH: a viral recognition pathway used by the host to signal inflammasome activation.* Thorax, 2013. **68**(1): p. 66-75.
119. Taylor, G., et al., *Recombinant bovine respiratory syncytial virus with deletion of the SH gene induces increased apoptosis and pro-inflammatory cytokines in vitro, and is attenuated and induces protective immunity in calves.* J Gen Virol, 2014. **95**(Pt 6): p. 1244-54.
120. Russell, R.F., et al., *Partial Attenuation of Respiratory Syncytial Virus with a Deletion of a Small Hydrophobic Gene Is Associated with Elevated Interleukin-1beta Responses.* J Virol, 2015. **89**(17): p. 8974-81.
121. Kwilas, S., et al., *Respiratory syncytial virus grown in Vero cells contains a truncated attachment protein that alters its infectivity and dependence on glycosaminoglycans.* J Virol, 2009. **83**(20): p. 10710-8.
122. Langedijk, J.P., et al., *Proposed three-dimensional model for the attachment protein G of respiratory syncytial virus.* J Gen Virol, 1996. **77 (Pt 6)**: p. 1249-57.
123. Gorman, J.J., et al., *Determination of the disulfide bond arrangement of human respiratory syncytial virus attachment (G) protein by matrix-assisted laser desorption/ionization time-of-flight mass spectrometry.* Protein Sci, 1997. **6**(6): p. 1308-15.
124. Roberts, S.R., et al., *The membrane-associated and secreted forms of the respiratory syncytial virus attachment glycoprotein G are synthesized from alternative initiation codons.* J Virol, 1994. **68**(7): p. 4538-46.
125. Teng, M.N., S.S. Whitehead, and P.L. Collins, *Contribution of the respiratory syncytial virus G glycoprotein and its secreted and membrane-bound forms to virus replication in vitro and in vivo.* Virology, 2001. **289**(2): p. 283-96.

126. Bukreyev, A., et al., *The secreted form of respiratory syncytial virus G glycoprotein helps the virus evade antibody-mediated restriction of replication by acting as an antigen decoy and through effects on Fc receptor-bearing leukocytes.* J Virol, 2008. **82**(24): p. 12191-204.
127. Bukreyev, A., L. Yang, and P.L. Collins, *The secreted G protein of human respiratory syncytial virus antagonizes antibody-mediated restriction of replication involving macrophages and complement.* J Virol, 2012. **86**(19): p. 10880-4.
128. Arnold, R., et al., *Respiratory syncytial virus deficient in soluble G protein induced an increased proinflammatory response in human lung epithelial cells.* Virology, 2004. **330**(2): p. 384-97.
129. Johnson, T.R., J.S. McLellan, and B.S. Graham, *Respiratory syncytial virus glycoprotein G interacts with DC-SIGN and L-SIGN to activate ERK1 and ERK2.* J Virol, 2012. **86**(3): p. 1339-47.
130. Harcourt, J., et al., *Respiratory syncytial virus G protein and G protein CX3C motif adversely affect CX3CR1+ T cell responses.* J Immunol, 2006. **176**(3): p. 1600-8.
131. Polack, F.P., et al., *The cysteine-rich region of respiratory syncytial virus attachment protein inhibits innate immunity elicited by the virus and endotoxin.* Proc Natl Acad Sci U S A, 2005. **102**(25): p. 8996-9001.
132. Langedijk, J.P., et al., *Structural homology of the central conserved region of the attachment protein G of respiratory syncytial virus with the fourth subdomain of 55-kDa tumor necrosis factor receptor.* Virology, 1998. **243**(2): p. 293-302.
133. Porotto, M., et al., *Regulation of paramyxovirus fusion activation: the hemagglutinin-neuraminidase protein stabilizes the fusion protein in a pretriggered state.* J Virol, 2012. **86**(23): p. 12838-48.
134. McLellan, J.S., et al., *Structure of respiratory syncytial virus fusion glycoprotein in the postfusion conformation reveals preservation of neutralizing epitopes.* J Virol, 2011. **85**(15): p. 7788-96.
135. McLellan, J.S., et al., *Structure of RSV fusion glycoprotein trimer bound to a prefusion-specific neutralizing antibody.* Science, 2013. **340**(6136): p. 1113-7.
136. Swanson, K.A., et al., *Structural basis for immunization with postfusion respiratory syncytial virus fusion F glycoprotein (RSV F) to elicit high neutralizing antibody titers.* Proc Natl Acad Sci U S A, 2011. **108**(23): p. 9619-24.
137. Funchal, G.A., et al., *Respiratory syncytial virus fusion protein promotes TLR-4-dependent neutrophil extracellular trap formation by human neutrophils.* PLoS One, 2015. **10**(4): p. e0124082.
138. Collins, P.L., R. Fearns, and B.S. Graham, *Respiratory syncytial virus: virology, reverse genetics, and pathogenesis of disease.* Curr Top Microbiol Immunol, 2013. **372**: p. 3-38.
139. Roberts, S.R., R.W. Compans, and G.W. Wertz, *Respiratory syncytial virus matures at the apical surfaces of polarized epithelial cells.* J Virol, 1995. **69**(4): p. 2667-73.
140. Collins, P.L., *Human respiratory syncytial virus*, in *The biology of Paramyxoviruses*, S.S. K., Editor. 2011, Caister academic press.
141. Brown, G., H.W. Rixon, and R.J. Sugrue, *Respiratory syncytial virus assembly occurs in GM1-rich regions of the host-cell membrane and alters the cellular distribution of tyrosine phosphorylated caveolin-1.* J Gen Virol, 2002. **83**(Pt 8): p. 1841-50.
142. Brown, G., et al., *Caveolin-1 is incorporated into mature respiratory syncytial virus particles during virus assembly on the surface of virus-infected cells.* J Gen Virol, 2002. **83**(Pt 3): p. 611-21.
143. McCurdy, L.H. and B.S. Graham, *Role of plasma membrane lipid microdomains in respiratory syncytial virus filament formation.* J Virol, 2003. **77**(3): p. 1747-56.
144. McDonald, T.P., et al., *Evidence that the respiratory syncytial virus polymerase complex associates with lipid rafts in virus-infected cells: a proteomic analysis.* Virology, 2004. **330**(1): p. 147-57.
145. Santangelo, P.J. and G. Bao, *Dynamics of filamentous viral RNPs prior to egress.* Nucleic Acids Res, 2007. **35**(11): p. 3602-11.

146. Teng, M.N. and P.L. Collins, *Identification of the respiratory syncytial virus proteins required for formation and passage of helper-dependent infectious particles.* J Virol, 1998. **72**(7): p. 5707-16.
147. Meshram, C.D., et al., *The Respiratory Syncytial Virus Phosphoprotein, Matrix Protein, and Fusion Protein Carboxy-Terminal Domain Drive Efficient Filamentous Virus-Like Particle Formation.* J Virol, 2016. **90**(23): p. 10612-10628.
148. Jeffree, C.E., et al., *Ultrastructural analysis of the interaction between F-actin and respiratory syncytial virus during virus assembly.* Virology, 2007. **369**(2): p. 309-23.
149. Brock, S.C., J.R. Goldenring, and J.E. Crowe, Jr., *Apical recycling systems regulate directional budding of respiratory syncytial virus from polarized epithelial cells.* Proc Natl Acad Sci U S A, 2003. **100**(25): p. 15143-8.
150. Henderson, G., J. Murray, and R.P. Yeo, *Sorting of the respiratory syncytial virus matrix protein into detergent-resistant structures is dependent on cell-surface expression of the glycoproteins.* Virology, 2002. **300**(2): p. 244-54.
151. Mehedi, M., et al., *Actin-Related Protein 2 (ARP2) and Virus-Induced Filopodia Facilitate Human Respiratory Syncytial Virus Spread.* PLoS Pathog, 2016. **12**(12): p. e1006062.

Chapter II

Structure and functions of the RSV non-structural proteins 1 and 2

2.1 Induction and signaling of type I and type III interferon upon RSV infection

2.1.1 Innate recognition, signaling and response

Recognition of RNA viruses by PRRs

The innate immune system is an important early line of defense against pathogens that is induced by pattern recognition receptors (PRRs) that recognize pathogen associated molecular patterns (PAMPs). RNA viruses are recognized by several PRR families, such as toll-like receptors (TLRs), retinoic acid-inducible gene I-like receptors (RLRs), nucleotide binding oligomerization domain-like receptors (NLRs) and possibly by certain cytoplasmic DNA sensors. These receptors are able to recognize single stranded (ss)RNA - and double stranded (ds)RNA molecules that are intrinsically part of the viral life cycle. **TLR3** and **TLR7/8**, for example, are present in the endosome compartment where they recognize dsRNA and ssRNA, respectively. The **RLR** family consists of three cytoplasmic helicases, *i.e.* retinoic acid inducible gene I (RIG-I), MDA5 and laboratory of genetics and physiology 2 (LGP2). RIG-I is activated by 5' triphosphorylated ssRNA and - dsRNA and short dsRNA less than 1 kb, whereas MDA5 is activated by long dsRNA above 1 kb and mRNA lacking ribose 2'-O-methylation at the 5' cap structure [1-5]. LGP2 binds ssRNA and dsRNA, but cannot signal on its own. LGP2 is thought to function as a negative and positive regulator of RIG-I and MDA5-induced innate signaling. **NLRs** constitute a large, diverse family of cytoplasmic PRRs that can be activated by viral RNA or viral proteins, *e.g.* influenza A virus M2 protein. **Cytoplasmic DNA receptors**, such as Z-DNA binding protein 1 (ZBP1) and cyclic GMP-AMP synthase (cGAS), are well known to induce innate immune responses upon recognition of pathogen or host derived dsDNA in the cytoplasm. Yet, the Zα2 domain of ZBP1 also appears to recognize viral derived RNA [6-8]. Moreover, mice lacking cGAS are more susceptible for the positive strand RNA virus West-Nile virus [9]. These results suggest that cytoplasmic DNA receptors may also be involved in the induction of innate immune responses during infections with RNA viruses that lack any DNA intermediate, although further research is needed to understand the mechanism(s).

Innate signaling by PRRs

After PAMP recognition, PRRs induce a signaling cascade based on adaptor proteins and kinases that ultimately leads to the activation of transcription factors that induce expression of a diverse array of genes. TLR3 and -7 and RLR signaling, for example, converge at the activation of TNF receptor-associated factor 3 (TRAF3) (Fig. 1). TRAF3 activation by TLR3 and -7 occurs after interaction with the cytosolic adaptor proteins toll-like receptor adaptor molecule 1 (TICAM1) and myeloid differentiation primary response 88 (MyD88), respectively, whereas RLR-mediated activation of TRAF3 requires interaction with the mitochondrial associated adaptor MAVS. TRAF3 subsequently activates the kinases inhibitor of nuclear factor kappa B kinase subunit epsilon (IKBKE; also known as IKKε) and TANK binding kinase 1 (TBK1) [10, 11]. These kinases form a complex that phosphorylates and activates the transcription factors interferon regulatory factor (IRF) 3 and IRF7 [12, 13]. In contrast to constitutively expressed IRF3 that is present in the cytosol as an inactive form, IRF7 expression is generally low in normal cells but highly induced by type I IFN. Phosphorylated IRF3 and IRF7 can form homo- or

heterodimers that translocate to the nucleus where IRF3 interacts with the coactivators CBP (cyclic-AMP responsive element binding protein (CREB) binding protein) or p300. These transcription factors are important for the induction of type I and - III IFNs. In parallel, TLRs can also induce other transcription factors such as NF-κB, c-Jun, ATF2, … that are activated by upstream kinases such as the IKKα/β/γ complex, JNK and p38 MAPK (Fig. 1). These transcription factors are involved in the induction of cytokines, chemokines and IFNs.

Interferon induction and signaling

Type I IFNs consist of a family of IFN-α isoforms (13 genes that encode 12 different proteins) and IFN-β (one isoform) that can be expressed by all nucleated cells. Type III IFNs consist of three isoforms, IFN-λ1, -λ2 and -λ3 (also known as IL-29, IL-28A and IL-28B, respectively), but in contrast to type I IFNs expression is mostly limited to epithelial cells. Recently, Prokunina-Olsson and colleagues identified a fourth isoform, IFN-λ4, that is only expressed in some humans carrying a dinucleotide variation upstream of the IFN-λ3 gene [14]. Activation of the IFN-β promoter is regulated by four positive regulatory domains (PRDs) that are bound by IRF3 and -7 (PRD I and III), NF-κB (PRD II) and the heterodimer activator protein 1 (AP-1) (PRD IV). IFN-α promoters are less complex and only contain PRDI and -III like domains that are bound by IRF7.

Type I and type III IFNs are secreted after induction and bind to receptor complexes at the cell surface of other cells to induce an antiviral state. Type I IFNs bind to the IFN-α receptor (IFNAR), which clusters its two subunits, IFNAR1 and IFNAR2. Type III IFNs also bind to a heterodimeric receptor, composed of the subunits IL-10Rβ and IL-28Rα. Dimerization at both receptor complexes leads to the cross phosphorylation of two associated tyrosine kinases, janus kinase 1 (JAK1, associated to the cytoplasmic tail of IFNAR1 and IL-28Ra) and tyrosine kinase 2 (TYK2, associated to the cytoplasmic tail of IFNAR2 and IL-10Rβ). These activated kinases phosphorylate tyrosine residues on the receptor cytoplasmic tails, creating docking sites for the transcription factor family signal transducer and activator of transcription (STAT). JAK1 and TYK2 subsequently phosphorylate STAT members that can form homo- and heterodimers after release from the receptors. The STAT1-STAT2 heterodimer interacts with IRF9 to form the transcription factor complex ISGF3 that induces transcription of a plethora of interferon stimulated genes (ISGs), *e.g.* MxA, PKR, OAS, … with broad antiviral activities. In addition, key signaling proteins for IFN induction such as RIG-I and MDA5 are themselves ISGs, providing an activating feedback loop in the IFN induction pathway. JAK-STAT signaling induced by IFNs or other cytokines is regulated by several negative feedback loops, such as the suppressor of cytokine signaling (SOCS) family proteins that inactivate JAKs amongst other functions.

2.1.2 Innate response upon RSV infection

Recognition of RSV by PRRs

Upon RSV infection, airway epithelial cells, macrophages and dendritic cells are the main inducers of innate immune responses. Several TLRs have been identified that can act as PRRs for RSV (Fig. 1). Murine macrophages, for example, induce cytokines and chemokines *ex vivo* in a TLR2 and TLR6-dependent pathway upon RSV infection [15]. Mice lacking TLR2 and TLR6 have significantly higher RSV titers, suggesting that TLR2 and TLR6 play a role in suppressing RSV replication. Overexpression of TLR3 in RSV infected HEK293T cells increases the secretion of the chemokines CXCL8 and CCL5 [16]. In addition, TLR3 expression is upregulated by RSV in several cell lines, although it is unclear if this response is specifically induced by RSV to create a selective advantage, or just a host defense mechanism to detect viral infections more efficiently [16-18]. Liu and colleagues observed that TLR3 increases IFN-β secretion late in RSV infection, which clearly contrasted to the reduced IFN-β secretion by TLR3 early in infection [18]. A role for TLR4 as PRR for RSV is currently debated. Whereas some groups reported an impaired innate immune response in TLR4-deficient mice with prolonged viral presence in the lungs [19-21], others could not confirm TLR4-mediated immune responses upon RSV infection [22, 23]. Lukacs and colleagues observed that RSV infected TLR7-deficient mice experience increased lung pathology, suggesting that TLR7 might be important to temper immune responses [24]. Although TLRs might function as PRRs to induce certain cytokines and chemokines upon RSV infection, they are likely not the main PRRs for the induction of type I IFNs, at least not early after RSV infection and not in immune cells. Type I IFN production by macrophages and DCs from wild type and TLR1, -2, -4, -6 and-7 knockout mice is actually equal after RSV infection [15, 24].

RSV can also be detected by RLRs (Fig. 1). RLRs play an important role in the induction of type I and possibly type III IFNs upon recognition of RSV, as type I IFN expression is strongly hampered in the absence of MAVS, the adaptor protein for RIG-I and MDA5 [25, 26]. To estimate the importance of each receptor individually, several groups have selectively impeded expression of RIG-I or MDA5 by siRNA or gene knockout. These studies revealed that RIG-I is the most important RLR to detect RSV, although MDA5 might contribute to some extent to the induction of IFNs [27-29]. Liu and colleagues could coimmunoprecipitate viral mRNA with RIG-I, but not with MDA5, favoring the hypothesis that mainly RIG-I recognizes RSV RNA [18]. Later, however, both RIG-I and MDA5 were found colocalized with RSV genomic RNA and the N protein [30]. Interestingly, whereas RIG-I partially colocalized to RSV-induced IBs, MDA5 and MAVS were found nearly exclusively in the IBs, which was associated with a 27-fold reduction of IFN-β induction by Newcastle disease virus. These results suggest that MDA5 might be more important as PRR for RSV than initially thought and that the RSV-N protein evolved to sequester MDA5 to IBs in order to suppress IFN induction.

A third class of PRRs, the NLRs, have also been shown to be important for the recognition of RSV. NOD2 expression is induced by RSV in several cell lines and human peripheral blood mononuclear cells [31, 32]. Interestingly, NOD2 expression is enhanced early after infection (within 2 hours), whereas enhanced expression of RIG-I appears rather late in infection (8-16 hours) [18, 28, 31]. These results suggest that NOD2 might recognize RSV before RIG-I (Fig. 1). NOD2 activation by RSV depends

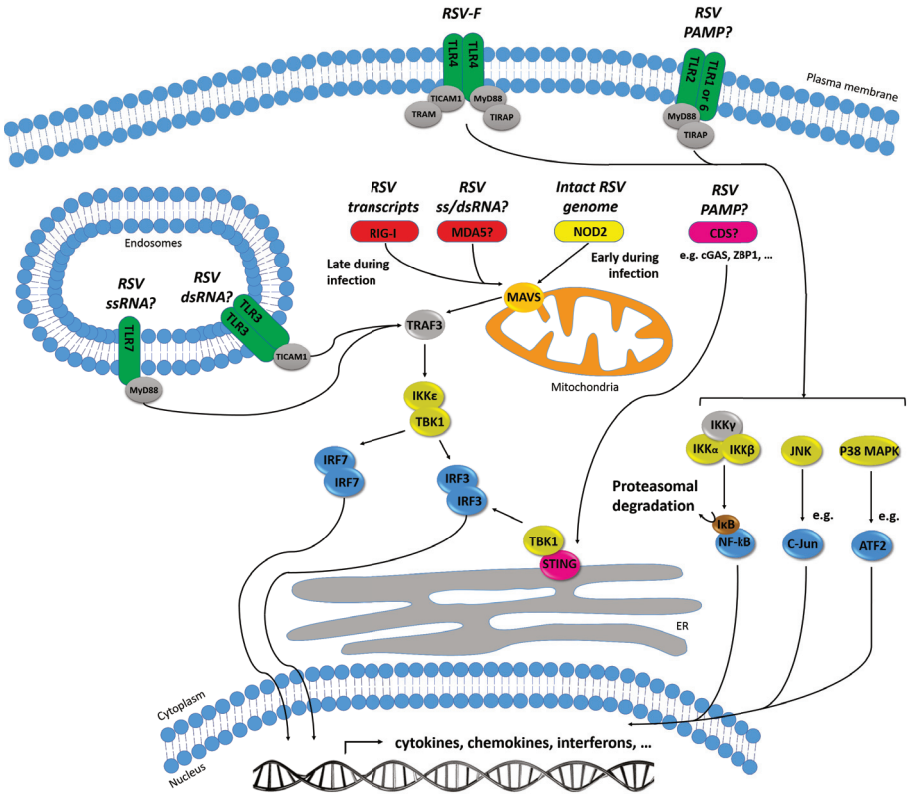

Figure 1: RSV-induced innate immune responses. Different families of pattern recognition receptors (PRRs) induce innate immune responses after activation by RSV-derived pathogen-associated molecular patterns (PAMP). Firstly, toll-like receptor (TLR)-2, -3, -4, -6 and -7 (marked in green) are involved in the production of cytokines and chemokines upon RSV infection, but are not necessary for the production of type I interferons. Secondly, RIG-I and possibly MDA5 (RIG-I-like receptors (RLRs), marked in red), are important in the induction of type I interferons. Thirdly, NOD2 (marked in yellow) also induces type I interferons upon RSV infection. Whereas NOD2 may be the most important PRR for type I interferon induction early during RSV infection, RIG-I may become the most important PRR only late(r) in infection. Currently, there is no evidence for a role of the cytoplasmic DNA sensors (CDS, marked in pink), which signal through the ER-associated STING protein, as PRRs during RSV infection. Activation of the RLRs or NOD2 induces their association with the mitochondrial associated MAVS protein, which activates TRAF3. TRAF3 subsequently activates the kinases IKKε and TBK1, which phosphorylate and activate the transcription factors IRF3 and IRF7. Activation of TLRs leads to the recruitment of adapter proteins, *e.g.* MyD88, TICAM1, TIRAP and TRAM. These adaptors can signal via TRAF3 or via the kinases IKKα/β/γ complex, JNK and p38 MAPK, leading to the activation of multiple transcription factors such as NF-κB, C-Jun and ATF2. The transcription factors activated by PRR signaling ultimately induce expression of cytokines, chemokines and interferons. Above each PRR we highlighted the confirmed or expected RSV-derived PAMP.

on the recognition of intact genomic ssRNA, which leads to the activation of IRF3 and possibly NF-κB and synthesis of IFN [31]. NOD2-induced activation of IRF3 is mediated by interaction of NOD2 with the adaptor protein MAVS by its nucleotide binding domain and leucine rich region, and not by its caspase recruitment domain (CARD) as is the case for the interaction of RIG-I with MAVS. NOD2 knockout mice induce about 6-fold lower IFN-β levels after RSV infection compared to wild type mice, which was associated with about 8-fold higher viral titers and increased lung pathology [31]. These results confirm a pivotal role of NOD2 as PRR for RSV.

Evidence for a role of cytoplasmic DNA receptors and the downstream protein STING in the induction of innate immune responses during RSV infection is currently lacking. Schoggins and colleagues found that cGAS overexpression tends to reduce RSV infection, however, this reduction was not significantly different [9]. Further research may elucidate if cytoplasmic DNA sensors and STING play a role during RSV infections.

RSV NS1 and NS2 proteins overcome innate responses upon RSV infection

Although several PRRs have been identified that can mount type I and III IFN responses after RSV infection (Fig. 1), analysis of nasal washes from infants hospitalized due to RSV identified low to undetectable levels of IFN-α and -β [33-35]. This in contrast to other respiratory viruses such as influenza A virus (IAV) and parainfluenza virus that mounted significant IFN-α and -β levels. In addition, type I IFNs are less frequently detected in non-hospitalized infants with RSV or hMPV infection compared to IAV [36]. An *in vitro* cell culture that closely resembles the *in vivo* tropism of RSV also could not detect type I IFNs after RSV infection [37]. These results highlight that RSV has intrinsic activities to suppress IFN induction *in vivo*. Two viral proteins, non-structural (NS) protein 1 and - 2, are not essential for RSV infection, but recombinant human or bovine RSV strains with deletions of NS1 and/or NS2 are strongly attenuated in immortalized stable cell cultures and in *in vivo* RSV infection models (cotton rats, chimpanzees and calves) [38-45]. Interestingly, a NS2 deletion mutant that is tested as live attenuated vaccine candidate is strongly attenuated in humans experimentally infected with RSV, confirming the importance of NS2 during RSV infection *in vivo* [46]. An attenuated RSV deletion mutant of NS2 displayed equal viral protein synthesis and genome replication as its parental, wild type strain, highlighting that NS2 favours RSV infection in some way independent of viral replication [38]. Schlender and colleagues were the first to demonstrate that NS1 and NS2 of bRSV suppress type I IFN-mediated antiviral responses [41]. Whereas wild type bRSV was only weakly inhibited by type I IFN, deletion of NS1 and NS2 separately or simultaneously rendered bRSV very sensitive to type I IFN. Recombinant rabies virus expressing NS1 and NS2 of bRSV was highly resistant to IFN-α in contrast to wild type rabies virus. These results suggested that bRSV NS1 and NS2 strongly counteract type I IFN antiviral responses independent of other RSV viral proteins. Valarcher and colleagues demonstrated that the NS proteins of bRSV suppress the induction of type I IFN after bRSV infection, with NS2 being stronger than NS1 [44]. Shortly later, NS proteins of human RSV were also identified as potent suppressors of both type I and type III IFN induction [43]. Opposite to bRSV, NS1 of human RSV appeared stronger than NS2.

2.2 Sequence and structure of the RSV non-structural protein 1 and 2

Since the NS1 and NS2 gene are located most proximal to the 3' leader region in the RSV genome, NS1 and NS2 are the most abundantly transcribed viral genes. Protein expression can be detected very early after infection (<5 hours) and is maximal between 8-18 hours post infection [47, 48]. In contrast to NS1, NS2 has a very limited half-life [49]. NS1 and NS2 are small proteins of 139 and 124 amino acids, respectively without sequence homology between each other except for the shared DLNP sequence at the C terminus (Fig. 2). No other homologous proteins have been found in the protein data bank, suggesting that NS1 and NS2 are unique proteins. The protein sequences of NS1 and NS2 are highly conserved between different human and bovine RSV strains (Fig. 2). Just recently, the crystal structure of NS1 was determined as a β-sandwich flanked by three α-helices [50]. Alignment of the crystal structures of NS1 and the N terminal domain of the M protein of RSV revealed a remarkable overlap, suggesting that NS1 might be a structural paralogue of M. Currently, no structural information on NS2 is available, possibly due to the unstable nature of NS2 [49]. The conformational state of NS1 and NS2 is still debated. NS1 has been identified as a monomer, dimer and possibly oligomer [49, 51, 52]. Although the NS1 crystal structure was made up of two molecules, a true dimer could however not be concluded based on the surface area of contact [50]. In line with this, size exclusion chromatography revealed that under physiological salt conditions NS1 predominantly is present as monomer. NS2 on the other hand possibly forms mono-, di- , tri-, tetra- and pentamers [49]. Co-immunoprecipitation revealed that in addition to NS1 and NS2 homomers, NS1 and NS2 also interact with each other to form heteromers [52, 53].

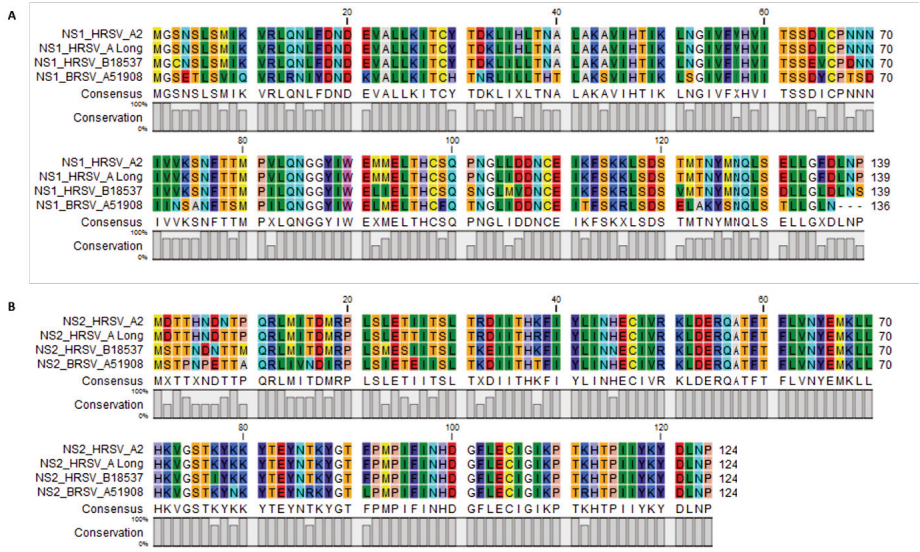

Figure 2: **Sequence alignment of the two non-structural (NS) proteins of RSV.** Alignment of the NS1 (A) and NS2 (B) amino acid sequence of three human RSV strains: *i.e.* RSV-A2, RSV-A long and RSV-B 18537 and the bovine RSV strain A51908. Sequence conservation of NS1: A2 vs A long = 138/139 AA (99%), A2 vs B 18537 = 121/139 AA (87%) and A2 vs bovine RSV = 94/136 AA (69%). Sequence conservation of NS2: A2 vs A long = 121/124 AA (98%), A2 vs B 18537 = 112/124 AA (90%) and A2 vs bovine RSV = 104/124 AA (84%).

2.3 The multiple NS protein effector functions

2.3.1 Suppression of interferon induction

NS1 and NS2 strongly reduce the induction of type I and type III interferon upon RSV infection [43, 50, 54-57]. Infection with recombinant viruses lacking NS1 or NS2 separately or simultaneously suggests that these proteins function individually and cooperatively to suppress IFN induction. They do so by targeting multiple proteins of the signaling cascade that starts with the recognition of PAMPs by PRRs and ends with the induction of IFN gene expression by several transcription factors.

NS1 and NS2 interfere with RIG-I

RIG-I is an important PRR for the recognition of RSV and a target protein for both NS1 and NS2 [27-29]. After ligand binding, RIG-I undergoes a conformational change that liberates the N-terminal two CARD domains and allows interaction with MAVS. Both NS1 and NS2 prevent the interaction of RIG-I with MAVS, albeit in a different manner. NS1 interacts with MAVS, whereas NS2, but not NS1, interacts with the N-terminal domain of RIG-I (Fig. 3) [58, 59]. In addition, RIG-I expression might be influenced by NS1, although current findings seem contradictory. Recombinant expressed RIG-I is strongly reduced by NS1, either expressed recombinantly or endogenously during a RSV infection [60]. Boyapalle and colleagues, however, observed that RSV-induced RIG-I expression is clearly lower in the absence of NS1, suggesting that NS1 promotes RIG-I expression during a RSV infection [59]. Since RIG-I is an ISG itself, this seems rather counterintuitive. In contrast to RIG-I, MAVS appears resistant to NS1 and/or NS2-mediated degradation [60]. These results highlight that the first signaling step in RIG-I-mediated IFN induction, the interaction of RIG-I with MAVS, is suppressed by both NS1 and NS2 and that RIG-I expression itself might be reduced by NS1. To our knowledge, no information has been published about the effect of NS1 and/or NS2 on the interaction of MDA5 or NOD2 with MAVS or on MDA5 expression levels.

NS1 and NS2 interfere with MAVS

Association of RLRs with MAVS leads to the activation of TRAF3 and the downstream serine/threonine kinases IKKε and TBK1. The effect of NS1 and NS2 on TRAF3, IKKε and TBK1 is currently inconclusive with some opposite results. NS1, either expressed recombinantly or endogenously during a RSV infection, has been found to clearly reduce recombinant expression of both TRAF3 and IKKε (Fig. 3) [53, 60]. Ren and colleagues, however, observed no difference in endogenous and recombinant TRAF3 and IKKε expression by NS1 [55]. Possibly, the different strains (RSV-A long versus RSV-A2) used or experimental timing might have caused these different observations, but this needs further confirmation. Recombinant expressed NS2 only modestly reduces TRAF3 expression and slightly enhances expression of IKKε (Fig. 3) [53, 60]. These effects of NS2 were, however, not reproduced with a recombinant RSV strain lacking NS1. Ling and colleagues also observed that recombinant expressed NS2 enhances recombinant expression of IKKε and TBK1 (Fig. 3) [58]. To our knowledge, no data have been published on the effect of NS1 on the expression of TBK1. Coexpression of NS1 and NS2 reduces recombinant IKKε expression, suggesting that the inhibitory effect of NS1 is dominant over the

enhancing effect of NS2 [53]. These results suggest that NS1 might suppress TRAF3 and IKKε expression, although more evidence is needed to confirm this hypothesis. Recombinant NS2 slightly suppresses TRAF3 expression and enhances IKKε and TBK1 expression, but these effects might relate to the artificial overexpression and not occur during a natural RSV infection.

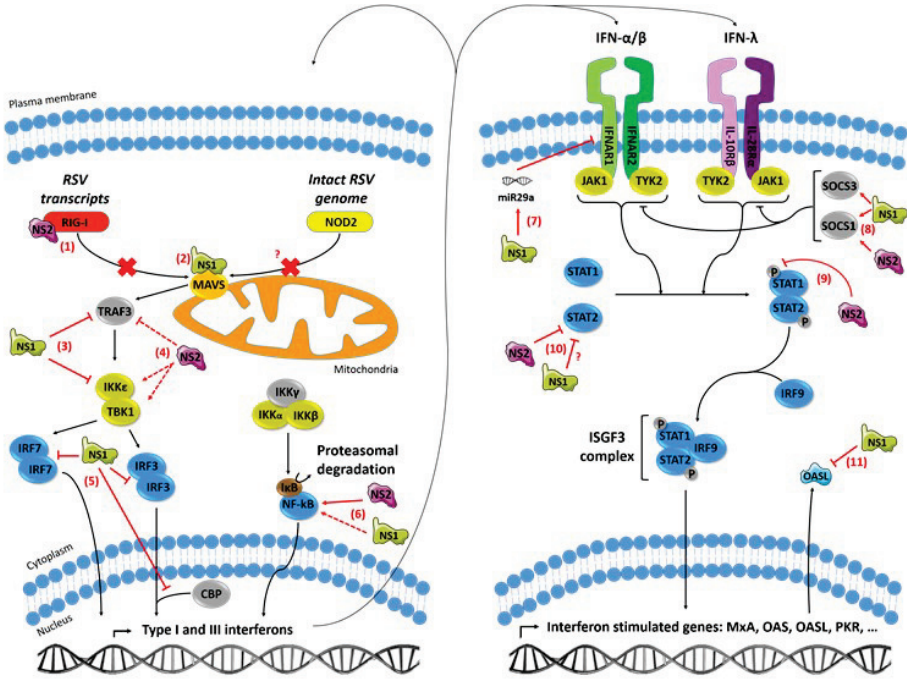

Figure 3: RSV NS1 and NS2 effector functions in suppressing interferon responses. Type I and III IFN responses are inhibited by NS1 and NS2 at multiple levels, both during the induction of type I and III IFNs (left panel) and during IFN-induced signaling (right panel). NS1 and NS2 prevent the interaction of RIG-I with MAVS by interacting with MAVS and RIG-I, respectively (1 and 2). Whether the interaction of NS1 with MAVS also prevents the interaction of NOD2 with MAVS is currently unclear. NS1 reduces protein expression of TRAF3 and IKKε (3), while NS2 modestly reduces TRAF3 and induces IKKε and TBK1 (4). NS1 subsequently inhibits IRF3 and IRF7 by different proposed mechanisms (5). NS1 reduces IRF3 and IRF7 protein expression and prevents the interaction between IRF3 and CBP, thereby lowering the binding of the IRF3-CBP complex to the IFN-β promoter. NS2, and to a lesser extent NS1, enhances the activation and nuclear translocation of NF-κB, although the exact mechanism is currently unclear (6). These NS1/NS2 effector functions (1-6) synergistically reduce the production of type I and III IFNs. Furthermore, NS1 and NS2 also suppress IFN-induced signaling/responses. NS1 induces miR29a expression, which targets the IFNAR1 mRNA, one of both subunits of the type I IFN receptor (7). NS1 and NS2 also induce expression of SOCS proteins (SOCS1 and -3), which negatively regulate the tyrosine kinases JAK1 and TYK2, that are important to transmit signaling from the type I and III IFN receptors (8). NS2 clearly inhibits JAK1/TYK2-mediated activation of STAT1/2 by reducing STAT1 phosphorylation (9) and reducing STAT2 protein expression (10). Some groups, however, reported that STAT2 expression can also be reduced by NS1 (see text). Recent evidence suggests that the NS proteins may also counteract antiviral effector functions of interferon stimulated genes, *e.g.* NS1 degrades the OASL protein. Full and dashed lines indicate robust or moderate inhibitory or stimulatory effector functions, respectively.

NS1 and NS2 interfere with the IRF and NF-κB transcription factors

Activated IKKε and TBK1 phosphorylate the transcription factors IRF3 and IRF7, which induces conformational changes that allow the formation of homo- and heterodimers that translocate to the nucleus. Phosphorylation of IκB, for example by the canonical IKKα/β/γ complex, initiates its degradation with subsequent release and nuclear translocation of NF-κB. The IRF and NF-κB transcription factors are essential for the induction of type I and III IFNs.

Several observations highlight that NS1 and NS2 impair the activation of IRF transcription factors and suppress their effector functions, *i.e.* inducing gene expression, although the exact mechanism is debated. Initial work highlights that NS1 and NS2 prevent nuclear translocation of IRF3. Whereas IRF3 nuclear translocation is similar early after infection with recombinant RSV wild type - and NS deletion strains, expression of NS1 and NS2 later in infection clearly prevents IRF3 nuclear translocation [56, 58, 61]. These results are supported by the observation that also cells infected with a bRSV strain lacking NS1 and NS2 have markedly higher levels of phosphorylated IRF3 in the nucleus than cells infected with wild type bRSV [54]. These publications, however, did not discriminate if the suppressed IRF3 nuclear translocation is a direct effector function of NS1 and/or NS2 or an indirect consequence of reduced IRF3 phosphorylation due to inhibition of proteins upstream in the signaling pathway. Transient expression of NS1 and/or NS2 in combination with IRF3 or IRF7 illustrated that NS1 can directly reduce expression of IRF3 and IRF7 (Fig. 3) [60]. In addition, NS1 overexpression in cells expressing a constitutive active form of IRF3 can still partially inhibit IRF3-dependent gene expression [50, 55]. This result confirms that NS1 is able to directly interfere with IRF3 effector functions. In contrast, Ren *et al.*, demonstrated that NS1 can interfere with IRF3-dependent gene expression without significantly affecting IRF3 expression, IRF3 phosphorylation and IRF3 nuclear translocation, but by preventing formation and binding of the IRF3/CBP complex to the IFN-β gene promoter (Fig. 3) [55].

NF-κB activation and nuclear translocation occurs early after RSV infection and is clearly enhanced by NS2 and to some extent by NS1 (Fig. 3) [48, 61]. NS protein-induced activation of NF-κB seems to counteract viral replication at first sight as NF-κB is an essential transcription factor for the induction of type I and type III IFN. NF-κB, however, is also an important transcription factor for the induction of antiapoptotic genes, which favours viral replication (see part 2.3.3).

Taken together, NS1 and NS2 suppress the induction of type I and type III IFN by targeting multiple proteins of the upstream signaling cascade, *i.e.* RIG-I, MAVS, TRAF3, αε, TBK1, IRF3 and IRF7. Although some of these effects have been confirmed in RSV infected cells, others could only be identified after recombinant expression. So future research is needed to elucidate the biological relevance of these recombinant responses.

2.3.2 Suppression of interferon signaling

Binding of type I and type III IFNs to their heterodimeric receptor complex induces a JAK-STAT signaling cascade that induces an antiviral state by gene expression of ISGs. In the presence of exogenously added IFN, recombinant RSV strains lacking NS proteins are attenuated in comparison to wild type RSV

strains [41, 60]. These results highlight that NS proteins also have effector functions downstream of the induction of IFN synthesis to suppress IFN-induced antiviral responses. In this part we will summarize at which steps of the IFN response the RSV NS proteins can interfere.

NS1 induces the expression of microRNA (miRNA) miR-29a, which targets the mRNA encoding IFNAR1, one of the two subunits of the type I IFN receptor (Fig. 3) [62]. This reduction in IFNAR1 expression lowers type I IFN signaling, thereby enhancing RSV replication.

Two tyrosine kinases, Jak1 and Tyk2, are responsible for the phosphorylation and activation of STAT proteins after activation of the type I and type III IFN receptor. Their kinase activity is strongly enhanced by cross phosphorylating each other upon receptor activation. Several groups reported that Tyk2 phosphorylation and total protein levels are not altered by the expression of NS1 and/or NS2, either recombinantly or during RSV infection [63-65]. To our knowledge, no such information has been published for Jak1. These results suggest that initial activation of Tyk2 and possibly Jak1 are not suppressed during a RSV infection.

Jak kinase activity is regulated by a negative feedback loop consisting of the SOCS family, with SOCS1 and -3 being the most performant inhibitors of Jak kinases. Several reports investigated the effect of NS1 and/or NS2 on SOCS1 and -3 expression, however, without a general consensus. Xu and colleagues observed that recombinant expression of NS1 induces SOCS1 but not SOCS3 expression, whereas RSV infection induces both SOCS1 and SOCS3 expression (Fig. 3) [66]. Zheng and colleagues, however, detected both SOCS1 and SOCS3 induction by recombinant expression of NS1, whereas NS2 only induces SOCS1 (Fig. 3) [67]. Infection with recombinant RSV lacking both NS proteins suggests that NS1 and/or NS2 rather suppresses SOCS1 expression, although this observation was much later (48 hours) compared to the previous reports (1-8 hours) [68]. Although additional confirmation is necessary, these results suggest that NS1 and/or NS2 might induce SOCS1 and -3 expression, thereby suppressing Jak activity and subsequent signaling.

STAT1/2 heterodimers are important for the induction of ISGs and are targets for NS1 and NS2. Infection with RSV slightly increases total STAT1 protein levels, likely because STAT proteins are themselves ISGs [63-65]. STAT1 phosphorylation induced by exogenous type I IFN, however, is clearly reduced by infection with RSV [63, 65, 69]. Infection with recombinant RSV strains lacking NS1 or NS2 revealed that NS2, but not NS1, reduces type I IFN-induced STAT1 phosphorylation (Fig. 3) [64]. Whether NS2 also reduces endogenous induced STAT1 phosphorylation during a RSV infection has not been published. Possibly, levels of phosphorylated STAT1 are (too) low to detect during a RSV infection, necessitating the addition of exogenous type I IFN to increase the levels of phosphorylated STAT1. Lo and colleagues indeed observed low quantities of phosphorylated STAT1 in RSV infected A549 cells that were not treated with type I IFN [65]. Interestingly, increasing the viral dose lowered the amount of phosphorylated STAT1, suggesting that a viral protein, likely NS2, might suppress STAT1 phosphorylation during a RSV infection. It can, however, not be excluded that the increased viral dose resulted in a stronger suppression of type I and type III IFN induction with subsequent lower induction of STAT1 phosphorylation. As Lo and colleagues only used wild type RSV, it would be interesting to test if recombinant RSV lacking NS2 induces higher STAT1 phosphorylation than wild type RSV in the absence of exogenous added type I IFN.

In contrast to STAT1, total STAT2 protein levels are clearly reduced by RSV infection [63, 65, 69]. STAT2 phosphorylation is also reduced, but the ratio between phosphorylated - and total STAT2 levels suggests that this is mainly the consequence of reduced total STAT2 levels and not due to a specific inhibition of STAT2 phosphorylation by RSV. Whether NS1, NS2 or both reduce STAT2 levels is currently debated. Several groups reported that recombinant expression of NS2, but not NS1, reduces STAT2 levels (Fig. 3) [53, 60, 64, 65]. Others, however, also observed reduced STAT2 levels after recombinant expression of NS1 (Fig. 3) [66, 69]. Lo and colleagues observed that, although recombinant expression of NS1 alone did not reduce STAT2 levels, coexpression of NS1 and NS2 reduces STAT2 levels stronger than NS2 alone [65]. Infections with recombinant RSV strains lacking NS1 or NS2 revealed that mainly NS2 reduces STAT2 levels [60, 64]. These results suggests that NS2 clearly reduces STAT2 levels, whereas NS1 might help reducing STAT2 levels, either on its own or only if coexpressed with NS2. In addition to reducing total STAT2 levels, RSV infection also seems to suppress nuclear translocation of the remaining STAT2 proteins, an effect that depends on NS1 and/or NS2 [65].

NS1 and possibly NS2 interfere with interferon stimulated genes

NS proteins also appear to suppress the antiviral activity of, at least some, ISGs. Cells expressing MxA or cells pretreated with type I IFN, only modestly limit RSV replication, whereas PIV3 replication is strongly reduced [70]. As these cells were only infected with wild type RSV, it cannot be excluded, however, that other viral proteins than the NS proteins also inhibit the antiviral functions of ISGs. A more direct proof of NS protein-mediated suppression of ISG antiviral activity was recently published. Dhar and colleagues observed that recombinant expressed NS1, but not NS2, degrades the 2'-5' oligoadenylate synthetase-like (OASL) protein (Fig. 3) [71]. OASL has some antiviral activity against RSV that depends on its two ubiquitin like domains, which are not present in the homologous ISG OAS. By degrading OASL, NS1 increases the viral yield. Whether NS1 expressed endogenously during a RSV infection also degrades endogenous OASL was, however, not investigated.

2.3.3 Other effector functions

In addition to counteracting IFN-induced antiviral responses by simultaneously targeting IFN induction and signaling, NS proteins also display other effector functions.

NS1 and NS2 interfere with the induction of apoptosis

NS1 and NS2 individually and cooperatively delay apoptosis in RSV infected cells, with NS2 being stronger than NS1 [48]. The early expression of NS1 and NS2 during infection activates the anti-apoptotic PDK-AKT-GSK pathway, although it is unclear how exactly this activation occurs. This leads to the inactivation of proapoptotic proteins and activation of anti-apoptotic proteins such as NF-κB, thereby preventing early apoptosis [48, 61]. Later in infection (>24 hours), activation of the PDK-AKT-GSK pathway drops, which increases the incidence of apoptosis [48]. Since NS1 and NS2 expression is

already maximal at 24 hours post infection and remains stable thereafter, induction of apoptosis late in infection is not due to a drop of NS protein expression. By delaying apoptosis, NS1 and NS2 allow prolonged RSV replication which strongly increases the viral yield (2-3 $\log_{10}$).

NS1 and NS2 interfere with the induction of miRNAs

In addition to miR-29a, NS proteins also regulate the expression of the miRNAs miR-24, let-7i and miR-30b [62, 72, 73]. Bakre and colleagues demonstrated that NS1 suppresses miR-24 expression [72]. Expression of four predicted target genes of miR-24, *i.e.* polo-like kinase (PLK) 3, casein kinase 1 gamma 1 (CSNK1G1), fibroblast growth factor receptor 3 and KLF6 was reduced in cells infected with a recombinant RSV strain lacking NS1, confirming that NS1 suppresses miR-24 expression. Whether inhibition of miR-24 enhances RSV replication or - yield was, however, not investigated. Further research might unravel the biological significance of miR-24 for RSV infection. Let-7i and miR-30b expression is upregulated during RSV infection by a type I IFN and NF-κB-dependent mechanism, respectively [73]. Infection with RSV strains lacking NS1 or NS2 further increases expression of let-7i and miR-30b, which can be expected for let-7i. For miR-30b, however, this seems counterintuitive as NS1 and especially NS2 are important for NF-κB activation during RSV infection [48, 61]. So possibly miR-30b expression is suppressed by NS1 and/or NS2 in a NF-κB independent mechanism.

NS1 and NS2 interfere with the adaptive immune response

The NS proteins also play a role in the development of adaptive immune responses during RSV infection. NS2 suppresses the development of cytotoxic T lymphocyte (CTL) responses in mice, whereas NS1 suppresses the maturation of human monocyte derived dendritic cells [57, 74]. Counteracting type I IFN responses by using STAT1-deficient mice and an IFNAR blocking antibody, however, largely abolished these suppressive effects, suggesting that these are an indirect consequence of NS protein-mediated suppression of type I IFN. In addition, NS1 can also modulate T cell responses in a type I IFN independent manner [75]. NS1 expression in dendritic cells suppresses the activation and proliferation of $CD103^+$ $CD8^+$ T cells and Th17 cells, while it promotes activation of IL-4 producing $CD4^+$ T cells. NS1 also promotes the proliferation of $CD4^+$ T cells, but this appears type I IFN-dependent. These results highlight that the NS proteins manipulate the development of adaptive immune responses following RSV infection, which relies largely, but not exclusively, on their capacity to suppress IFN responses.

NS2 induces shedding of infected epithelial cells

A typical hallmark of RSV infections *in vivo* is the obstruction of smaller airways by plugs consisting of infiltrating immune cells, mucus and shedded infected epithelial cells. Shedding of RSV infected epithelial cells involves two stages. First, the cells transform from a columnar to a rounded morphology but with conservation of the junctions with neighboring cells of the epithelial layer. Later, these

junctions are lost, thereby shedding the infected epithelial cells in the lumen. NS2 is necessary and sufficient to induce these morphological changes resulting in shedding of epithelial cells [76].

NS1 interferes with expression of Hox genes

NS1 might regulate expression of Hox genes by interacting with the histone H2BD, thereby inducing ubiquitination of H2BD [77]. Hox genes are a family of transcription factors involved in *e.g.* lung and gut development.

NS1 interferes with viral RNA synthesis

In an artificial minireplicon system, additional expression of NS1 strongly reduces synthesis of full length genomic and antigenomic RNA and subgenomic mRNA [47]. While RNA encapsidation is unaffected, NS1 expression appears to block subsequent use of the nucleocapsid complex by the polymerase. Infection with wild type RSV and RSV lacking both NS1 and NS2, however, revealed that nucleoprotein mRNA synthesis is not enhanced in the absence of NS1 and NS2 [56]. Genome and antigenome synthesis is strongly reduced in the absence of NS1 and NS2, which likely reflects the strong attenuation of this deletion strain. So NS1-mediated suppression of viral RNA synthesis might be an artefact of the minireplicon system and not occur during a natural RSV infection.

2.3.4 Mechanism(s) of effector functions

To understand the diversity of effectors functions, several groups investigated the subcellular localization of NS1 and NS2, either expressed recombinantly or endogenously during RSV infection. In the absence of NS2, NS1 localizes to the cytoplasm and nucleus [52, 53, 61, 77, 78], although one group reported that NS1 on its own localizes to the mitochondria by interacting with MAVS [59]. NS2 expression is mainly localized to the mitochondria and seems to induce mitochondrial localization of NS1 if NS1 and NS2 are coexpressed [52]. Interestingly, mitochondrial localization of NS1 and NS2 appears to be dependent on MAVS [60].

Taking into account the small size of NS1 and NS2, it is remarkable how many host genes are affected by NS1 and NS2. Goswami and colleagues hypothesized that NS1 and NS2 form a large, degradative complex of 300-750 kDa (called the NS degradasome (NSD)) whose enzymatic activity is enhanced by mitochondria via MAVS [60]. This complex appears to selectively degrade some innate immune signaling proteins, *e.g.* RIG-I, TRAF3, IKKε, IRF3, IRF7 and STAT2, while others are unaffected, *e.g.* MAVS, STAT1, TRIF and MyD88. In line with these results, RSV selectively induces human STAT2 degradation, but not mouse stat2 [65]. The NSD complex could also be purified from RSV infected cells and was shown to degrade RIG-I, however, it would be interesting to confirm that the other NS target proteins can also be degraded by NSD complexes purified from RSV infected cells [60]. Interestingly, in MAVS-deficient cells inoculated with IFN-α, wild type RSV is almost equally attenuated as RSV lacking NS1 and NS2, demonstrating the importance of MAVS in NS protein-mediated suppression of type I IFN signaling. The NS target proteins, but not the others, nicely relocate from the cytoplasm to the

mitochondria if NS1 and NS2 are expressed. These results support the hypothesis of the formation of a NSD complex that depends on MAVS to degrade innate immune proteins such as STAT2 amongst others.

The presence of the proteasome subunit α2 (PSMA2) from the 20S core proteasome in the NSD complex sparked the idea that the NSD complex might act in a similar way as the host 26S proteasome, or at least shares some common proteins [60]. Although currently being investigated, no detailed information is available on the exact protein composition of this NSD complex and how this complex relates to the host 26S proteasome. RSV-induced STAT2 and OASL degradation is blocked by the proteasome inhibitors MG132 and lactacystin [63, 64, 69, 71]. TRAF3 degradation, however, appears insensitive to MG132 [53], suggesting that NSD-mediated degradation of host proteins might be more complex and differ between proteins. Goswami and colleagues indeed found that MG132 only partially inhibited NSD proteolytic activity and hypothesized that non-proteasomal proteases might be responsible for some of the NSD activity [60]. Proteasome like activity of the NSD complex is further supported by the identification of NS1 and NS2 as possible inducers of ubiquitination of host proteins [69, 79]. NS1 is a putative Elongin B/C-CUL2/5-SOCS box (ECS)-type E3 ubiquitin ligase as it contains a near complete elongin C binding consensus sequence and binds to elongin C and cullin-2, two accessory proteins of ECS-type E3 ubiquitin ligase complexes [69]. NS1 possibly induces polyubiquitination of host proteins such as STAT2, although this could be mediated by NS2 as ubiquitination was only tested with coexpression of NS1 and NS2. Mutating three essential amino acids in the elongin C binding sequence abolishes NS1 protein expression and strongly attenuates RSV replication, confirming the importance of the elongin C binding site in NS1, at least for protein stability [78]. Although NS2 does not contain an elongin C binding consensus sequence like NS1, NS2 has been identified as an inducer of host protein ubiquitination, without evidence for NS1-mediated ubiquitination [79]. Ubiquitination activity of NS2 is strongly dependent on at least three residues, T36, L52 and P92, which also appear important for NS2-mediated STAT2 degradation. A recombinant RSV strain with these three amino acids mutated is nearly equally attenuated as a NS2 deletion strain, further confirming the importance of these residues for NS2-mediated effector functions. These results suggest that NS2 and possibly NS1 act as inducers of host protein ubiquitination, which may then be targeted by the NSD complex for degradation. In addition to STAT2, other innate immune proteins are selectively degraded by the NSD complex, whereas others are not. It is currently not known if NS1 and/or NS2 ubiquitinate these innate immune proteins in a selective manner and how this selectivity would be organized. The selective degradation of innate immune proteins by NS1, but not NS2, or vice versa indicates that these proteins indeed possess mechanisms to selectively degrade innate immune proteins.

Just recently, a crystal structure of NS1 revealed a remarkable structural homology with the N-terminal domain of the matrix protein of RSV, suggesting that these proteins are structural paralogues [50]. One clear difference between NS1 and M is the presence of an α-helix (called α3, residues 119-134) at the C terminus of NS1, which might, at least partially, be responsible for NS1 effector functions. A C-terminus truncated NS1 lacking helix α3 (NS1: 1-118) or mutation of three residues (Y125, L132/L133) that seem important for interaction of helix α3 with the rest of NS1, partially abrogates

NS1-mediated suppression of IFN-β induction. Furthermore, L132 and L133 seem important for NS1-mediated suppression of maturation of human monocyte derived dendritic cells and induction of cytokines and chemokines. Recombinant RSV strains with C-terminus truncated NS1 or carrying Y125 or L132/L133 mutations are strongly attenuated *in vitro.* These results confirm that helix α3 is important for, at least some, NS1-mediated effector functions.

2.4 Protein interactions of NS proteins

As NS1 and NS2 are small proteins, protein interactions with viral and host proteins are expected to contribute to the effector functions of NS1 and NS2. Recombinant expressed NS1 and NS2 can interact with each other, although it is unclear if this involves a direct interaction or takes place in a complex with host proteins [52, 53]. Whether NS1 and NS2 also interact during a RSV infection is currently not clear. Both NS1 and NS2 are detected in NSD complexes purified from RSV infected cells, suggesting that NS1 and NS2 at least can be part of the same complex. In addition, NS1 might also interact with the RSV proteins M and P, although further confirmation of these interactions is definitely necessary [49, 80]. As M is thought to form dimers and NS1 is a structural homolog of the N-terminal domain of M, an interaction between M and NS1 would be reasonable [50, 81]. Several host proteins have been identified that interact with NS1, *i.e.* cullin-2, elongin C, MAP1B, IRF3, CBP, MAVS and H2BD [52, 55, 59, 69, 77]. For NS2, MAP1B and RIG-I have been identified as interaction partners [52, 58].

A more comprehensive analysis of host proteins interacting with NS1 identified 221 host proteins that potentially interact directly or indirectly [82]. Wu and colleagues expressed NS1 and NS2 fused to the C-terminus of enhanced green fluorescent protein (EGFP) in HEK293T cells. EGFP constructs were immunoprecipitated and potential binding proteins were identified by mass spectrometry. Functional analysis of the 221 potential NS1 interacting proteins by ingenuity pathway analysis identified 20 functional groups with gene expression, cell signaling, cell cycle, post-translational modification and nucleic acid metabolism as most interesting categories at first sight for RSV replication. The cell cycle was further investigated and indicated that NS1 enriches A549 cells in the G1 phase of the cell cycle. These results confirm the observation that RSV induces a cell cycle arrest to enhance viral replication [83, 84].

2.5 General conclusion

In humans, RSV infections induce remarkably low levels of IFN. Two unique viral proteins, NS1 and NS2, strongly suppress the induction and signaling of IFN and likely also suppress antiviral activities of ISGs. NS1 and NS2 exert additional functions such as delaying cell apoptosis and suppressing adaptive immune responses to enhance viral replication.

2.6 Reference list

1. Yoneyama, M., et al., *The RNA helicase RIG-I has an essential function in double-stranded RNA-induced innate antiviral responses.* Nat Immunol, 2004. **5**(7): p. 730-7.
2. Pichlmair, A., et al., *RIG-I-mediated antiviral responses to single-stranded RNA bearing 5'-phosphates.* Science, 2006. **314**(5801): p. 997-1001.
3. Pichlmair, A., et al., *Activation of MDA5 requires higher-order RNA structures generated during virus infection.* J Virol, 2009. **83**(20): p. 10761-9.
4. Schlee, M., et al., *Recognition of 5' triphosphate by RIG-I helicase requires short blunt double-stranded RNA as contained in panhandle of negative-strand virus.* Immunity, 2009. **31**(1): p. 25-34.
5. Zust, R., et al., *Ribose 2'-O-methylation provides a molecular signature for the distinction of self and non-self mRNA dependent on the RNA sensor Mda5.* Nat Immunol, 2011. **12**(2): p. 137-43.
6. Thapa, R.J., et al., *DAI Senses Influenza A Virus Genomic RNA and Activates RIPK3-Dependent Cell Death.* Cell Host Microbe, 2016. **20**(5): p. 674-681.
7. Kesavardhana, S., et al., *ZBP1/DAI ubiquitination and sensing of influenza vRNPs activate programmed cell death.* J Exp Med, 2017. **214**(8): p. 2217-2229.
8. Maelfait, J., et al., *Sensing of viral and endogenous RNA by ZBP1/DAI induces necroptosis.* EMBO J, 2017. **36**(17): p. 2529-2543.
9. Schoggins, J.W., et al., *Pan-viral specificity of IFN-induced genes reveals new roles for cGAS in innate immunity.* Nature, 2014. **505**(7485): p. 691-5.
10. Hacker, H., et al., *Specificity in Toll-like receptor signalling through distinct effector functions of TRAF3 and TRAF6.* Nature, 2006. **439**(7073): p. 204-7.
11. Oganesyan, G., et al., *Critical role of TRAF3 in the Toll-like receptor-dependent and -independent antiviral response.* Nature, 2006. **439**(7073): p. 208-11.
12. Fitzgerald, K.A., et al., *IKKepsilon and TBK1 are essential components of the IRF3 signaling pathway.* Nat Immunol, 2003. **4**(5): p. 491-6.
13. Sharma, S., et al., *Triggering the interferon antiviral response through an IKK-related pathway.* Science, 2003. **300**(5622): p. 1148-51.
14. Prokunina-Olsson, L., et al., *A variant upstream of IFNL3 (IL28B) creating a new interferon gene IFNL4 is associated with impaired clearance of hepatitis C virus.* Nat Genet, 2013. **45**(2): p. 164-71.
15. Murawski, M.R., et al., *Respiratory syncytial virus activates innate immunity through Toll-like receptor 2.* J Virol, 2009. **83**(3): p. 1492-500.
16. Rudd, B.D., et al., *Differential role for TLR3 in respiratory syncytial virus-induced chemokine expression.* J Virol, 2005. **79**(6): p. 3350-7.
17. Groskreutz, D.J., et al., *Respiratory syncytial virus induces TLR3 protein and protein kinase R, leading to increased double-stranded RNA responsiveness in airway epithelial cells.* J Immunol, 2006. **176**(3): p. 1733-40.
18. Liu, P., et al., *Retinoic acid-inducible gene I mediates early antiviral response and Toll-like receptor 3 expression in respiratory syncytial virus-infected airway epithelial cells.* J Virol, 2007. **81**(3): p. 1401-11.
19. Kurt-Jones, E.A., et al., *Pattern recognition receptors TLR4 and CD14 mediate response to respiratory syncytial virus.* Nat Immunol, 2000. **1**(5): p. 398-401.
20. Haynes, L.M., et al., *Involvement of toll-like receptor 4 in innate immunity to respiratory syncytial virus.* J Virol, 2001. **75**(22): p. 10730-7.
21. Haeberle, H.A., et al., *Respiratory syncytial virus-induced activation of nuclear factor-kappaB in the lung involves alveolar macrophages and toll-like receptor 4-dependent pathways.* J Infect Dis, 2002. **186**(9): p. 1199-206.
22. Ehl, S., et al., *The role of Toll-like receptor 4 versus interleukin-12 in immunity to respiratory syncytial virus.* Eur J Immunol, 2004. **34**(4): p. 1146-53.

23. Marr, N. and S.E. Turvey, *Role of human TLR4 in respiratory syncytial virus-induced NF-kappaB activation, viral entry and replication.* Innate Immun, 2012. **18**(6): p. 856-65.
24. Lukacs, N.W., et al., *Respiratory virus-induced TLR7 activation controls IL-17-associated increased mucus via IL-23 regulation.* J Immunol, 2010. **185**(4): p. 2231-9.
25. Bhoj, V.G., et al., *MAVS and MyD88 are essential for innate immunity but not cytotoxic T lymphocyte response against respiratory syncytial virus.* Proc Natl Acad Sci U S A, 2008. **105**(37): p. 14046-51.
26. Demoor, T., et al., *IPS-1 signaling has a nonredundant role in mediating antiviral responses and the clearance of respiratory syncytial virus.* J Immunol, 2012. **189**(12): p. 5942-53.
27. Sasai, M., et al., *NAK-associated protein 1 participates in both the TLR3 and the cytoplasmic pathways in type I IFN induction.* J Immunol, 2006. **177**(12): p. 8676-83.
28. Loo, Y.M., et al., *Distinct RIG-I and MDA5 signaling by RNA viruses in innate immunity.* J Virol, 2008. **82**(1): p. 335-45.
29. Yoboua, F., et al., *Respiratory syncytial virus-mediated NF-kappa B p65 phosphorylation at serine 536 is dependent on RIG-I, TRAF6, and IKK beta.* J Virol, 2010. **84**(14): p. 7267-77.
30. Lifland, A.W., et al., *Human respiratory syncytial virus nucleoprotein and inclusion bodies antagonize the innate immune response mediated by MDA5 and MAVS.* J Virol, 2012. **86**(15): p. 8245-58.
31. Sabbah, A., et al., *Activation of innate immune antiviral responses by Nod2.* Nat Immunol, 2009. **10**(10): p. 1073-80.
32. Vissers, M., et al., *Respiratory syncytial virus infection augments NOD2 signaling in an IFN-beta-dependent manner in human primary cells.* Eur J Immunol, 2012. **42**(10): p. 2727-35.
33. Hall, C.B., et al., *Interferon production in children with respiratory syncytial, influenza, and parainfluenza virus infections.* J Pediatr, 1978. **93**(1): p. 28-32.
34. McIntosh, K., *Interferon in nasal secretions from infants with viral respiratory tract infections.* J Pediatr, 1978. **93**(1): p. 33-6.
35. Scagnolari, C., et al., *Gene expression of nucleic acid-sensing pattern recognition receptors in children hospitalized for respiratory syncytial virus-associated acute bronchiolitis.* Clin Vaccine Immunol, 2009. **16**(6): p. 816-23.
36. Melendi, G.A., et al., *Breastfeeding is associated with the production of type I interferon in infants infected with influenza virus.* Acta Paediatr, 2010. **99**(10): p. 1517-21.
37. Villenave, R., et al., *In vitro modeling of respiratory syncytial virus infection of pediatric bronchial epithelium, the primary target of infection in vivo.* Proc Natl Acad Sci U S A, 2012. **109**(13): p. 5040-5.
38. Teng, M.N. and P.L. Collins, *Altered growth characteristics of recombinant respiratory syncytial viruses which do not produce NS2 protein.* J Virol, 1999. **73**(1): p. 466-73.
39. Whitehead, S.S., et al., *Recombinant respiratory syncytial virus bearing a deletion of either the NS2 or SH gene is attenuated in chimpanzees.* J Virol, 1999. **73**(4): p. 3438-42.
40. Jin, H., et al., *Recombinant respiratory syncytial viruses with deletions in the NS1, NS2, SH, and M2-2 genes are attenuated in vitro and in vivo.* Virology, 2000. **273**(1): p. 210-8.
41. Schlender, J., et al., *Bovine respiratory syncytial virus nonstructural proteins NS1 and NS2 cooperatively antagonize alpha/beta interferon-induced antiviral response.* J Virol, 2000. **74**(18): p. 8234-42.
42. Teng, M.N., et al., *Recombinant respiratory syncytial virus that does not express the NS1 or M2-2 protein is highly attenuated and immunogenic in chimpanzees.* J Virol, 2000. **74**(19): p. 9317-21.
43. Spann, K.M., et al., *Suppression of the induction of alpha, beta, and lambda interferons by the NS1 and NS2 proteins of human respiratory syncytial virus in human epithelial cells and macrophages [corrected].* J Virol, 2004. **78**(8): p. 4363-9.
44. Valarcher, J.F., et al., *Role of alpha/beta interferons in the attenuation and immunogenicity of recombinant bovine respiratory syncytial viruses lacking NS proteins.* J Virol, 2003. **77**(15): p. 8426-39.

45. Buchholz, U.J., S. Finke, and K.K. Conzelmann, *Generation of bovine respiratory syncytial virus (BRSV) from cDNA: BRSV NS2 is not essential for virus replication in tissue culture, and the human RSV leader region acts as a functional BRSV genome promoter.* J Virol, 1999. **73**(1): p. 251-9.
46. Wright, P.F., et al., *The interferon antagonist NS2 protein of respiratory syncytial virus is an important virulence determinant for humans.* J Infect Dis, 2006. **193**(4): p. 573-81.
47. Atreya, P.L., M.E. Peeples, and P.L. Collins, *The NS1 protein of human respiratory syncytial virus is a potent inhibitor of minigenome transcription and RNA replication.* J Virol, 1998. **72**(2): p. 1452-61.
48. Bitko, V., et al., *Nonstructural proteins of respiratory syncytial virus suppress premature apoptosis by an NF-kappaB-dependent, interferon-independent mechanism and facilitate virus growth.* J Virol, 2007. **81**(4): p. 1786-95.
49. Evans, J.E., P.A. Cane, and C.R. Pringle, *Expression and characterisation of the NS1 and NS2 proteins of respiratory syncytial virus.* Virus Res, 1996. **43**(2): p. 155-61.
50. Chatterjee, S., et al., *Structural basis for human respiratory syncytial virus NS1-mediated modulation of host responses.* Nat Microbiol, 2017. **2**: p. 17101.
51. Pretel, E., G. Camporeale, and G. de Prat-Gay, *The non-structural NS1 protein unique to respiratory syncytial virus: a two-state folding monomer in quasi-equilibrium with a stable spherical oligomer.* PLoS One, 2013. **8**(9): p. e74338.
52. Swedan, S., et al., *Multiple functional domains and complexes of the two nonstructural proteins of human respiratory syncytial virus contribute to interferon suppression and cellular location.* J Virol, 2011. **85**(19): p. 10090-100.
53. Swedan, S., A. Musiyenko, and S. Barik, *Respiratory syncytial virus nonstructural proteins decrease levels of multiple members of the cellular interferon pathways.* J Virol, 2009. **83**(19): p. 9682-93.
54. Bossert, B., S. Marozin, and K.K. Conzelmann, *Nonstructural proteins NS1 and NS2 of bovine respiratory syncytial virus block activation of interferon regulatory factor 3.* J Virol, 2003. **77**(16): p. 8661-8.
55. Ren, J., et al., *A novel mechanism for the inhibition of interferon regulatory factor-3-dependent gene expression by human respiratory syncytial virus NS1 protein.* J Gen Virol, 2011. **92**(Pt 9): p. 2153-9.
56. Tran, K.C., B. He, and M.N. Teng, *Replacement of the respiratory syncytial virus nonstructural proteins NS1 and NS2 by the V protein of parainfluenza virus 5.* Virology, 2007. **368**(1): p. 73-82.
57. Munir, S., et al., *Nonstructural proteins 1 and 2 of respiratory syncytial virus suppress maturation of human dendritic cells.* J Virol, 2008. **82**(17): p. 8780-96.
58. Ling, Z., K.C. Tran, and M.N. Teng, *Human respiratory syncytial virus nonstructural protein NS2 antagonizes the activation of beta interferon transcription by interacting with RIG-I.* J Virol, 2009. **83**(8): p. 3734-42.
59. Boyapalle, S., et al., *Respiratory syncytial virus NS1 protein colocalizes with mitochondrial antiviral signaling protein MAVS following infection.* PLoS One, 2012. **7**(2): p. e29386.
60. Goswami, R., et al., *Viral degradasome hijacks mitochondria to suppress innate immunity.* Cell Res, 2013. **23**(8): p. 1025-42.
61. Spann, K.M., K.C. Tran, and P.L. Collins, *Effects of nonstructural proteins NS1 and NS2 of human respiratory syncytial virus on interferon regulatory factor 3, NF-kappaB, and proinflammatory cytokines.* J Virol, 2005. **79**(9): p. 5353-62.
62. Zhang, Y., et al., *Respiratory syncytial virus non-structural protein 1 facilitates virus replication through miR-29a-mediated inhibition of interferon-alpha receptor.* Biochem Biophys Res Commun, 2016. **478**(3): p. 1436-41.
63. Ramaswamy, M., et al., *Specific inhibition of type I interferon signal transduction by respiratory syncytial virus.* Am J Respir Cell Mol Biol, 2004. **30**(6): p. 893-900.

64. Ramaswamy, M., et al., *Respiratory syncytial virus nonstructural protein 2 specifically inhibits type I interferon signal transduction.* Virology, 2006. **344**(2): p. 328-39.
65. Lo, M.S., R.M. Brazas, and M.J. Holtzman, *Respiratory syncytial virus nonstructural proteins NS1 and NS2 mediate inhibition of Stat2 expression and alpha/beta interferon responsiveness.* J Virol, 2005. **79**(14): p. 9315-9.
66. Xu, X., et al., *Respiratory syncytial virus NS1 protein degrades STAT2 by inducing SOCS1 expression.* Intervirology, 2014. **57**(2): p. 65-73.
67. Zheng, J., et al., *Respiratory Syncytial Virus Nonstructural Proteins Upregulate SOCS1 and SOCS3 in the Different Manner from Endogenous IFN Signaling.* J Immunol Res, 2015. **2015**: p. 738547.
68. Moore, E.C., J. Barber, and R.A. Tripp, *Respiratory syncytial virus (RSV) attachment and nonstructural proteins modify the type I interferon response associated with suppressor of cytokine signaling (SOCS) proteins and IFN-stimulated gene-15 (ISG15).* Virol J, 2008. **5**: p. 116.
69. Elliott, J., et al., *Respiratory syncytial virus NS1 protein degrades STAT2 by using the Elongin-Cullin E3 ligase.* J Virol, 2007. **81**(7): p. 3428-36.
70. Atreya, P.L. and S. Kulkarni, *Respiratory syncytial virus strain A2 is resistant to the antiviral effects of type I interferons and human MxA.* Virology, 1999. **261**(2): p. 227-41.
71. Dhar, J., et al., *2'-5'-Oligoadenylate Synthetase-Like Protein Inhibits Respiratory Syncytial Virus Replication and Is Targeted by the Viral Nonstructural Protein 1.* J Virol, 2015. **89**(19): p. 10115-9.
72. Bakre, A., et al., *Human respiratory syncytial virus non-structural protein NS1 modifies miR-24 expression via transforming growth factor-beta.* J Gen Virol, 2015. **96**(11): p. 3179-91.
73. Thornburg, N.J., S.L. Hayward, and J.E. Crowe, Jr., *Respiratory syncytial virus regulates human microRNAs by using mechanisms involving beta interferon and NF-kappaB.* MBio, 2012. **3**(6).
74. Kotelkin, A., et al., *The NS2 protein of human respiratory syncytial virus suppresses the cytotoxic T-cell response as a consequence of suppressing the type I interferon response.* J Virol, 2006. **80**(12): p. 5958-67.
75. Munir, S., et al., *Respiratory syncytial virus interferon antagonist NS1 protein suppresses and skews the human T lymphocyte response.* PLoS Pathog, 2011. **7**(4): p. e1001336.
76. Liesman, R.M., et al., *RSV-encoded NS2 promotes epithelial cell shedding and distal airway obstruction.* J Clin Invest, 2014. **124**(5): p. 2219-33.
77. Tan, Y.R., et al., *Nonstructural protein-1 of respiratory syncytial virus regulates HOX gene expression through interacting with histone.* Mol Biol Rep, 2013. **40**(1): p. 675-9.
78. Straub, C.P., et al., *Mutation of the elongin C binding domain of human respiratory syncytial virus non-structural protein 1 (NS1) results in degradation of NS1 and attenuation of the virus.* Virol J, 2011. **8**: p. 252.
79. Whelan, J.N., et al., *Identification of Respiratory Syncytial Virus Nonstructural Protein 2 Residues Essential for Exploitation of the Host Ubiquitin System and Inhibition of Innate Immune Responses.* J Virol, 2016. **90**(14): p. 6453-63.
80. Hengst, U. and P. Kiefer, *Domains of human respiratory syncytial virus P protein essential for homodimerization and for binding to N and NS1 protein.* Virus Genes, 2000. **20**(3): p. 221-5.
81. Forster, A., et al., *Dimerization of matrix protein is required for budding of respiratory syncytial virus.* J Virol, 2015. **89**(8): p. 4624-35.
82. Wu, W., et al., *The interactome of the human respiratory syncytial virus NS1 protein highlights multiple effects on host cell biology.* J Virol, 2012. **86**(15): p. 7777-89.
83. Gibbs, J.D., et al., *Cell cycle arrest by transforming growth factor beta1 enhances replication of respiratory syncytial virus in lung epithelial cells.* J Virol, 2009. **83**(23): p. 12424-31.
84. Wu, W., et al., *Characterization of the interaction between human respiratory syncytial virus and the cell cycle in continuous cell culture and primary human airway epithelial cells.* J Virol, 2011. **85**(19): p. 10300-9.

Chapter III

High-throughput mapping of virus-host interactions by RNA interference

3.1 Discovery of RNA interference

In the 1980s, it became clear that expressing the antisense RNA strand of a gene could efficiently reduce the protein expression of that gene, a process called RNA interference (RNAi) later on. This phenomenon was identified in bacteria, plants, Drosophila, Xenopus and mammalian cells, suggesting that it involves an evolutionary conserved mechanism [1-5]. Initially it was thought that the antisense strand hybridizes with the mRNA resulting in the suppression of mRNA translation. More than a decade later, however, it was shown that injection of dsRNA in the nematode *Caenorhabditis elegans* is far more efficient in reducing gene expression than either single strand [6]. A few dsRNA molecules in a cell are already sufficient to mediate gene silencing, suggesting that RNAi involves a catalytic process rather than simply blocking mRNA translation. Further characterization of the RNAi mechanism revealed that short RNA fragments of 21-25 nucleotides generated from long dsRNA molecules mediate sequence-specific gene silencing by a so called RNA-induced silencing complex (RISC) [7-11]. The observation that transfection of chemical synthesized small RNA molecules in mammalian cell lines potently suppresses target gene expression opened a new scientific world and provided a powerful tool to study protein functions [12].

3.2 Mechanism of the canonical RNA interference pathway

The canonical RNAi pathway is used by two families of small, non-coding RNA, *i.e.* the small interfering RNAs (siRNAs) and microRNAs (miRNAs). The **siRNAs** are generated from long dsRNA molecules by Dicer, a cytosolic RNase III family enzyme, which cleaves long dsRNA into perfectly complementary siRNAs of 21-25 nucleotides with the help of two dsRNA binding proteins, TARBP2 and PRKRA (Fig. 1A) [13]. Long dsRNA can originate from the replication of RNA viruses, antisense transcription, self-annealing in transcripts or by experimental transfection. In the RISC loading complex (consisting of Dicer, TARBP2 and the RISC complex), the siRNAs generated by Dicer are transferred to the Argonaute2 protein in the RISC complex. This protein unwinds the siRNA and cleaves the passenger strand of the siRNA duplex, which is subsequently removed from the RISC complex. The other strand, the guide strand, remains attached to the Argonaute2 protein, which together form the functional RISC complex. The thermodynamic stability of the siRNA ends determines which strand will be the guide strand, which is typically the strand with the least stable 5' end [10, 11]. The guide strand subsequently guides the functional RISC complex to fully complementary mRNA targets that are cleaved by the Argonaute2 protein, the only Argonaute protein that cleaves the mRNA target [14]. The cleaved mRNA is released from the RISC complex, which can then target other mRNA molecules. Cleaved mRNA fragments with a 5' cap - or 3' poly A tail only are further degraded in the cytosol.

The second group, the **miRNAs**, are encoded endogenously by the genome and are synthesized as primary miRNAs upon transcription of their corresponding gene (Fig. 1B). These primary miRNAs typically contain hairpin structures that are excised in the nucleus by the Drosha/DGCR8 complex, yielding precursor miRNAs. The precursor miRNA molecules are exported from the nucleus to the cytoplasm by exportin5, although other proteins might complement the role of exportin5 [15, 16]. Precursor miRNAs are further processed by Dicer into mature miRNAs that are loaded in RISC

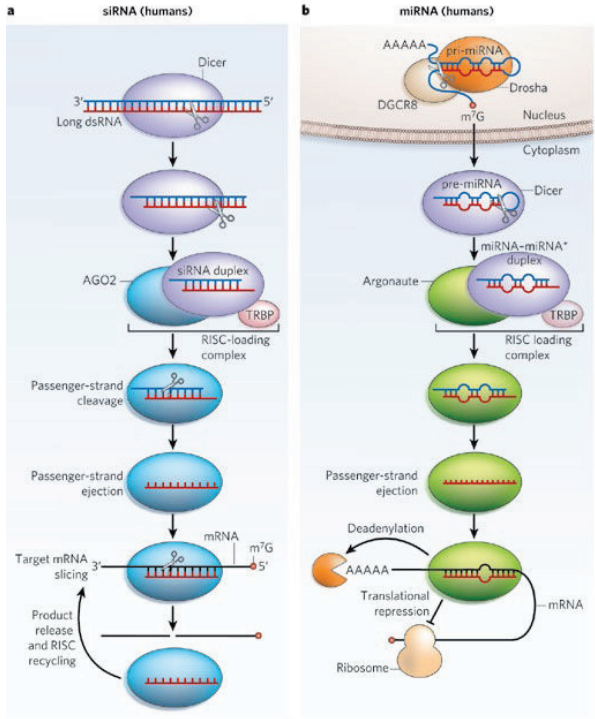

Figure 1: Canonical siRNA - and miRNA pathway. (A) siRNA pathway. SiRNAs (21-25 nucleotides) are generated from long dsRNA molecules by the endoribonuclease Dicer. SiRNAs are loaded into a RNA-induced silencing complex (RISC, here represented as AGO2 in blue) in a RISC loading complex consisting of the RISC complex, Dicer and the dsRNA binding protein TARBP2 (here represented as TRBP). The Argonaute protein will cleave the siRNA passenger strand, which is subsequently removed from the RISC complex. The mature RISC complex will cleave target mRNA molecules with complementarity to the siRNA guide strand through the Argonaute protein. The RISC complex is recycled for a next round and the cleaved mRNA fragments are further degraded. (B) miRNA pathway. Endogenously encoded miRNA genes are transcribed into primary-miRNAs that are cleaved by the Drosha/DGCR8 complex in the nucleus to form precursor-miRNAs. These precursor-miRNAs are translocated to the cytoplasm and further cleaved by Dicer. Mature miRNAs are loaded in the RISC complex. In contrast to siRNAs, miRNAs are typically only partially complementary to the 3' UTR of their target mRNAs and the Argonaute protein does not cleave the mRNA. Instead, mRNA translation is repressed or the mRNA is deadenylated followed by degradation. Figure adapted from [17].

complexes, although the exact mechanism in humans is not clear. In contrast to siRNAs, miRNAs typically are only partially complementary to the 3' untranslated region (UTR) of their target mRNA. As a result, mRNA targets are not cleaved, instead silencing is thought to occur by translation inhibition and degradation of the mRNA due to deadenylation. Interestingly, viral encoded miRNAs have been found in several deoxyribonucleic acid (DNA) viruses [18-20] and more particularly in the herpes virus family [21-25]. These miRNAs target both viral - and host mRNAs and play important roles in suppressing antiviral immune responses, regulating viral early gene expression and controlling the

balance between latent - and lytic states amongst others. To date no clear evidence exists of functional miRNAs encoded by RNA viruses, which might relate to the expectation that such a miRNA would destroy the viral RNA genome. In addition, most RNA viruses replicate in the cytoplasm, away from the Drosha/DGCR8 complex.

As a consequence of si/miRNA-mediated cleavage and degradation or translation inhibition of a target mRNA, synthesis of the corresponding protein drops, which leads to a reduction of the total protein level. This reduction in protein level is called a protein knockdown and the onset of knockdown is mainly determined by the stability (half-life) of the protein.

3.3 Pitfalls of the RNAi technology

Since its discovery, RNAi has proven its utility in exploring the functions of proteins in a cheap, fast and high-throughput compatible manner. Several pitfalls should, however, be considered carefully to avoid misinterpretation of knockdown phenotypes. These pitfalls can generally be subdivided in sequence-independent - and sequence-dependent off-target effects.

3.3.1 Sequence-independent off-target effects

As the name already indicates, sequence-independent off-target effects rely on general features of si/shRNA exposure irrespective of their sequence and can rather easily be controlled for by testing one or more non-targeting si/shRNA(s) in parallel. These non-targeting si/shRNAs are commercially available and are sequence optimized for a specific host to avoid unwanted RNA silencing as much as possible. Sequence-independent off-target effects might originate from *e.g.* cellular responses induced by cationic lipids used to transfect siRNAs into cells [26]. High levels of si/shRNAs might also saturate components of the RNAi machinery, which might hamper the functions of endogenous miRNAs in regulating gene expression. SiRNAs, for example, are excluded from the nucleus by exportin-5, which is also used by the endogenous miRNA pathway to export precursor-miRNAs [15, 27]. Generally, sequence-independent off-target effects can be reduced by lowering the concentration of si/shRNAs and transfection reagent as much as possible with preservation of efficient target knockdown. Fedorov and colleagues indeed observed a dose-dependent response of the transfection reagent lipofectamine2000 [26].

3.3.2 Sequence-dependent off-target effects

Sequence-dependent off-target effects rely on the specific sequence of si/shRNAs and should be monitored for each si/shRNA individually.

Sequence-dependent innate immune responses to siRNAs

Although siRNAs are generally poorly recognized as PAMPs by dsRNA sensing PRRs, some siRNAs are potent inducers of innate immune responses in a sequence-dependent manner [28-32]. This induction is dependent on the endosomal pathway and TLR7, a sensor for ssRNA [28-30]. Sequence alignment of siRNAs inducing innate immune responses versus non-inducers identified the motifs UGUGU and

GUCCUUCAA as potent inducers of IFN-α. Not all IFN-inducing siRNAs, however, contain these motifs, suggesting that other sequences likely also can activate TLR7. As TLR7 is mainly expressed in immune cells, siRNA experiments in stable cell lines that lack TLR7 expression should normally not be disturbed by siRNA-induced innate immune responses. *In vivo* or *in vitro* applications of siRNAs in the presence of TLR7 expressing cells should, however, carefully consider the possibility of siRNA-induced innate immune responses.

Immunostimulatory activity of siRNAs can be avoided by using siRNA delivery methods that do not use the endocytic pathway or by modifying residues in the siRNA duplex. Methylation of the ribose 2' hydroxyl group of guanosine and uridine residues is often used to abolish immunostimulatory activity of siRNAs with preservation of RNA silencing activity [33-36]. Incorporation of 2'deoxy uridine or - thymidine residues in siRNAs might even be better as this modification only counteracts immunostimulation without antagonizing TLR7 functions, in contrast to modification by methylation [35, 37].

Sequence-specific off-target effects and strategies to avoid these effects

Secondly, siRNAs might also act as miRNAs and unintentionally suppress the expression of genes with partial sequence complementarity in addition to cleavage of the fully complementary target mRNA [38, 39]. Complementarity between the siRNA seed region (nucleotide 2 to 8 starting from the 5' end of the guide strand) and 3' UTRs of mRNAs is the main driver of off-target silencing [40-42]. Not all mRNAs with seed complementarity in their 3' UTR, however, are silenced to the same extent, highlighting that other factors are also determining if a non-target mRNA is silenced or not. Thermostable seed matches with a high GC content and the presence of canonical Watson-Crick base pairing strongly enhance the chance of off-target silencing [43, 44]. In addition, the melting temperature of the adjacent non-seed region (nucleotide 8-15) and the GC content of the corresponding sequence in the mRNA 3' UTR are inversely correlated to the efficacy of off-target silencing [45]. Off-target silencing of genes can occur with a preservation or reduction of the mRNA template, suggesting that both translation inhibition and mRNA degradation can occur [38, 41]. Several reports highlight that siRNA-induced off-target silencing might strongly perturb results of RNAi screening [46-48]. Meier and colleagues, for example, used two different genome-wide siRNA libraries, one from Qiagen and one from Dharmacon, to investigate host genes involved in the replication of Uukuniemi virus [48]. Together, these siRNA screens identified 499 proviral genes and 63 antiviral genes. Strikingly, only 18 proviral genes (3,6%) and 2 antiviral genes (3,2%) were found in both siRNA screens. Moreover, they found that about 30% of primary hits following genome-wide siRNA screening consisted of genes that were not expressed in their cell model, suggesting that at least 30% of the primary hits represented off-target effects. Further characterization of the seed sequences revealed that about 8% and 0,08% of the siRNAs from the Qiagen and Dharmacon siRNA library, respectively, could inhibit Uukuniemi virus replication in a miRNA-like mechanism. Although this striking difference in predicted miRNA-like off-target effects of Qiagen versus Dharmacon siRNAs was not investigated further, differences in the algorithm to select siRNA sequences possibly contributed to this difference.

The fraction of possible off-target silencing siRNAs was, however, clearly higher in the list of primary hits, *i.e.* for 95 (~29%) of the 331 proviral genes identified with the Qiagen siRNA library and 6 (~3,2%) of the 186 proviral genes identified with the Dharmacon siRNA library, siRNAs with seed-induced off-target silencing were predicted. These results highlight the perturbation of primary siRNA screening results due to off-target silencing by siRNAs.

The chance of off-target silencing by siRNAs can be reduced by several means, such as proper design of the siRNA or by methylation of the ribose 2' hydroxyl group of the second nucleotide in the guide strand [49]. As off-target silencing by siRNAs appears concentration dependent, lowering the siRNA concentration might also help reducing off-target silencing [39]. A common strategy is pooling different siRNAs targeting the same gene, which allows lowering the concentration of each individual siRNA with maintenance of the total siRNA concentration and efficient target knockdown. Although most commercial sources for siRNAs pool up to 4 siRNAs per gene, Hannus and colleagues suggest that more complex pools of at least 30 different siRNAs per gene might be required to completely abolish siRNA-mediated off-target silencing [50]. Two strategies are widely used in the RNAi field to validate on-target RNAi knockdown phenotypes, *i.e.* redundancy and rescue. In redundancy, at least two different si/shRNAs with a different seed sequence targeting a gene are tested. If the knockdown phenotype is reproduced by these different si/shRNAs, then on-target silencing of the intended gene is likely causing the phenotype. In a rescue, si/shRNA-mediated knockdown of a gene of interest is restored by coexpressing a si/shRNA-resistant form of the gene of interest, which serves as the ultimate control of on-target RNAi knockdown phenotypes. Several approaches are used to express a si/shRNA-resistant gene. If available, an ortholog of the gene of interest with preserved functions and lacking the (complete) si/shRNA target sequence can be used. If a si/shRNA targets the 3'UTR of a gene of interest then the cDNA sequence lacking the 3'UTR can also be used. Lastly, the degeneracy of codons can be exploited by introducing wobble-base mutations in the si/shRNA target sequence which abolishes si/shRNA recognition without changing the amino acid sequence.

3.4 High-throughput virus-host screens

The discovery of the RNAi pathway and associated silencing of gene expression by the transfection of chemically synthesized siRNA molecules, has led to a huge explosion of research investigating protein functions in diverse cellular processes. One of the research fields that clearly benefits from the RNAi technology is virology. As obligate parasites, viruses hijack the host cellular machinery to replicate their genome and form new virus particles. With RNAi large numbers of host proteins can be shut down in parallel to investigate the role of these proteins during a virus infection. In the last decade, numerous large-scale RNAi screens have been performed to unravel the interaction between host cells and viruses (Table 1 gives an overview of RNAi screens with negative strand RNA viruses). The identification of critical host factors for viral replication is important to discover new potential targets for the development of antiviral drugs. De Clercq and Li recently provided a very nice overview of all approved antiviral drugs in the last 50 years (june 1963- april 2016) [51]. Ninety antiviral drugs have been approved to treat 9 viral diseases, of which 11 are currently discontinued. The vast majority of antiviral

drugs target viral proteins and are hence, especially for RNA viruses, vulnerable to the rise of drug-resistant mutant viruses. Targeting host proteins might lower the risk of developing drug resistance. Up till now, only few of the approved antiviral drugs target host molecules, *e.g.* Docosanol (approved use for herpes simplex virus (HSV)) is thought to modify the plasma membrane composition [52], Maraviroc (approved use for HIV) is a CCR5 antagonist and Podofilox (approved use for human papilloma virus related disease) destabilizes microtubuli. So the emerging knowledge on virus-host interactions might help in the discovery and development of antiviral drugs targeting host molecules in the future. In this section we will focus on high-throughput RNAi screens executed with viruses belonging to the order *Mononegavirales* and with influenza A virus.

In 2007, Kolokoltsov and colleagues published a siRNA screen for **RSV** covering a customized selection of 79 host genes from a membrane trafficking library [53]. Fourteen proviral genes and 15 antiviral genes were identified. Amongst the proviral genes, RSV infection was most strongly reduced upon knockdown of proteins involved in endocytosis, *e.g.* clathrin light chain B, the beta prime subunit of the clathrin adapter complex 1, dynamin-3 and Rab5A, highlighting a role for endocytosis in RSV infection, possibly through clathrin-mediated endocytosis. Other proviral genes included genes involved in actin dynamics such as the p21-activated kinase 1 (PAK1), Wiskott-Aldrich syndrome protein family member 2 and two members of the actin nucleation complex, *i.e.* actin-related protein 2/3 complex subunit 1b and -2. Yet, no large-scale RNAi screen has been published for RSV to date. RSV was recently reclassified in a new family, the *Pneumoviridae*, but it is evolutionary related to the *Paramyxoviridae* family with a number of shared orthologous genes.

To our knowledge high-throughput RNAi screening within the *Paramyxoviridae* family has only been published for the **henipaviruses**, which consist of the highly pathogenic hendra virus (HeV) and nipah virus (NiV). Deffrasnes and colleagues used a genome-wide SMARTpool® siRNA library in HeLa cells to investigate host proteins involved in HeV replication by using a recombinant luciferase expressing HeV strain [54]. On a total of 18,120 genes, 585 genes were found to enable HeV replication and 630 genes were found to inhibit HeV replication based on Z-scores ($Z \geq 2$ or $Z \leq -2$). Two hundred proviral genes were selected for further validated by siRNA pool deconvolution, *i.e.* the 4 siRNAs of each pool were tested separately on HeV replication. For 66 of those 200 genes at least 2/4 siRNAs reduced HeV replication, suggesting that on-target silencing caused the reduced HeV replication. About 2/3 of these genes were also important for the replication of wild type HeV and NiV. So in the end, about 0,24% of all genes included in the siRNA library were found to be important for henipavirus replication. Compared to the other genes, knockdown of fibrillarin had the largest negative impact on HeV and NiV replication. Interestingly, knockdown of fibrillarin also had a negative, but less extensive, impact on the replication of RSV and other Paramyxoviruses, such as measles virus and mumps virus, but not on replication of the Orthomyxovirus influenza A. Although HeV replication is cytoplasmic, the matrix protein translocates to the nucleus and nucleolus early after infection, where it interacts with fibrillarin [54]. In line with these results, the matrix protein of RSV also translocates to the nucleus early in infection despite cytoplasmic replication [55, 56]. An interactome analysis of the matrix protein of RSV

Table 1: Overview of RNAi screens for viruses of the order *Mononegavirales* and influenza A virus

Virus[a]	Targeted Genes	# of genes	company[b]	siRNA conc (nM)	virus strain	cell type	KD time	read out[c]	time of RO	# Hits[d]		Ref
										proviral	antiviral	
Pneumoviridae												
RSV	Custom library	79	Dha	50	rec RSV-GFP	HeLa	48h	GFP	20 hpi	14^{P}, 16^{V}	15^{P}	[53]
Paramyxoviridae												
HeV	Genome wide	18,120	Dha	40	rec HeV-Luc	HeLa	72h	Luc	24 hpi	585^{P}, 66^{V}	630^{P}	[54]
Rhabdoviridae												
VSV	Genome wide	22,909	Qia	15,4	rec VSV-eGFP	HeLa	52h	GFP	18 hpi	233^{V}	n/a	[58]
VSV	Genome wide	21,121	Dha	25	rec VSV-eGFP	HeLa	48h	GFP	7 hpi	$\geq 450^{P}$, 89^{V}	n/a	[59]
Filoviridae												
EBOV/MARV	Custom library	66	Dha	75	wild type	HEK293T	24h	IF	72 hpi	$8^{P}/3^{P}$	$0^{P}/4^{P}$	[61]
MARV	Genome wide	21,585	Amb	10	rec HIV-MARV GP-Luc	A549	48h	Luc	48 hpi	12^{V}	106^{V}	[62]
Bornaviridae												
BDV	Druggable genome	5,516	Amb	10	rec VSV-BDV G	Ol	36h	CPE	48 hpi	24^{V}	n/a	[63]
Orthomyxoviridae												
IAV	Genome wide	13,071	Amb	n/a[e]	rec A/WSN/33-VSV G-Luc	DL1	48h	Luc	24 hpi	110^{V}	n/a	[67]
IAV	Genome wide	17,877	Dha	50	A/PR/8/34	U2OS	72h	IF	12 hpi	312^{P},129^{V}	22^{P},4^{V}	[68]
IAV	custom library	1,745	Dha	25	A/PR/8/34	HBEC	72h	Vir titer	48 hpi	616 total[P f]		[69]
IAV	Genome wide	22,843	Qia	20	A/WSN/33	A549	48h	Vir titer/IF	24 hpi	287^{P},168^{V}	n/a	[70]
IAV	Genome wide	19,628	Qia, Inv, IDT	33,3	rec A/WSN/33-Luc and A/WSN/33	A549	48h	Luc/Vir titer	12, 24, 36 hpi	295^{V}, 219^{V}	n/a	[71]
IAV	Kinases	720	Dha	50	A/WSN/33	A549	48h	Vir titer	48 hpi	14^{V}	3^{V}	[72]
IAV	Genome wide	21,585	Amb	10	rec HIV-IAV HA/NA-Luc	A549	48h	Luc	48 hpi	4^{V}	42^{V}	[62]
IAV	Genome wide	16,368	TRC shRNA	-	A/WSN/33	A549	>2weeks	DS	4 weeks	110^{V}	-	[73]
IAV	Genome wide	21,415	TS	-	A/NY/55/2004	A549	48h	DS	72 hpi	138^{P}	-	[74]

[a] RSV = Respiratory syncytial virus, HeV = Hendra virus, VSV = Vesicular stomatitis virus, EBOV = Ebola virus, MARV = Marburg virus, BDV = Borna-disease virus and IAV = Influenza A virus

[b] Dha = Dharmacon, Qia = Qiagen, Amb = Ambion, Inv = Invitrogen and TS = Thermo Scientific

[c] Luc = Luciferase, IF = immunofluorescence, CPE = cytopathogenic effect, Vir titer = viral titer and DS = deep sequencing of surviving IAV infected cells

[d] primary hits (P) and validated hits (V) by siRNA redundancy

[e] library of dsRNA

[f] three different read-outs with each pro - and antiviral hits

KD = knockdown, RO = read-out, Ol = human oligodendroglial cell line, DL1 = Drosophila cells

on the other hand did not identify fibrillarin [57]. Fibrillarin catalyzes the modification of ribosomal RNA during ribosome maturation in the nucleolus and this activity appears important for HeV replication, but not for RSV replication [54]. These results highlight that fibrillarin is important for both HeV and RSV replication, but the precise role of fibrillarin might be different.

The **vesicular stomatitis virus** (VSV) is a prototype of the *Rhabdoviridae* family, which, next to the *Paramyxoviridae* and *Pneumoviridae* families, belongs to the order *Mononegavirales*. Two genome-wide siRNA screens have been performed with VSV. A first screen investigated the role of human genes in all stages of the VSV life cycle and identified 233 proviral genes [58]. About 42% of these genes were also identified as proviral genes after knockdown by siRNAs from another source. This illustrates that substantial differences, *e.g.* knockdown efficacy, exist between different siRNAs from different sources targeting the same gene. Several genes of these 233 proviral genes were identified as important host factors for VSV replication for the first time, e.g. SLC46A1, MAT2A and ADAL were found to be important during VSV entry/uncoating, gene expression and assembly/release, respectively. In addition, the coatomer complex I and its upstream regulators ARF1 and GBF1 were shown to be required for gene expression during VSV and two other negative stranded RNA viruses, the lymphocytic choriomeningitis virus and human parainfluenza virus type 3. In another screen, Lee and colleagues investigated the role of human genes in the early stages of VSV infection, *i.e.* entry/uncoating and viral gene expression [59]. In this screen at least 450 genes important for the early stages of VSV infection were identified. Only 89 of the 450 genes (~20%), however, were confirmed by at least 2 different siRNAs, suggesting that these genes are most reliably involved in VSV infection. A subset of 29 genes of the 450 genes were characterized further, which identified 3 genes, GPR149, PSCA and LSM5, as proviral genes involved in the entry phase of VSV and 20 genes involved in VSV gene expression. The response of the majority of these genes (13 of 23 genes), however, relied on knockdown by a single siRNA, urging the need to proof that on-target silencing caused the observed effects on VSV entry and gene expression.
The 2 RNAi screens for VSV infection described above identified 8 genes in common, *i.e.* the coatomer complex proteins COPB1, COPD, COPG and COPZ1, MAT2A, NHP2L1, SYVN1 and UTP6, highlighting the importance of these proteins during VSV infection. The coatomer complex indeed plays a role in VSV gene expression, whereas VSV entry is likely only indirectly blocked after long-term inhibition of the coatomer complex [60].

Ebola virus (EBOV) and **Marburg virus** (MARV) are two highly pathogenic viruses belonging to the *Filoviridae* family within the order *Mononegavirales*. Preliminary data on host genes involved in the infection cycle of these viruses is emerging. Spurgers and colleagues determined the protein composition of EBOV - and MARV virions and identified 66 host proteins [61]. To validate the biological significance of these proteins, EBOV and MARV infection efficacy was evaluated after silencing these 66 genes by using a custom siRNA library. Eight genes (HSPA5, RPL18, UBC, RPL3, RPL5, RPS6, DNAJB2 and Hist1H2BO) were found to enable EBOV infection, with the first 3 genes also being important for MARV infection. Remarkable, whereas RPS6 enhances EBOV infection, RPS6 suppresses MARV

infection. Three genes (HSPB1, DCD and ARF1) suppress MARV infection, without affecting EBOV infection. Cheng and colleagues performed a genome-wide siRNA screen followed by infection with a HIV virus like particle (VLP) carrying the MARV glycoprotein GP to mimick MARV entry [62]. They identified 12 and 106 genes that respectively enable and suppress MARV entry with at least 2 siRNAs per gene. Several of the identified host proteins were already known to be important during EBOV infection. Additional confirmation of the other host proteins in an infection with wild type MARV, however, is needed.

The **borna disease virus** (BDV) belongs to the *Bornaviridae* family within the order *Mononegavirales* and host genes involved in BDV entry were investigated in one siRNA screen. Clemente and colleagues investigated the role of a genome subset, 5512 druggable genes, in the entry of BDV [63]. Therefore, a recombinant VSV virus of which the G protein was replaced by the G protein of BDV was used. Initial hits were subsequently validated in infection with wild type BDV. Twenty-four genes were found to be required for the entry of BDV, of which 9 genes were also required for the entry of VSV. One of these 9 genes, DKFZP434F011, is a solute carrier currently renamed SLC22A23 and several other solute carriers have also been identified in a genome-wide siRNA screen for VSV [58]. The other 8 genes involved in VSV entry were, however, not identified in the two genome-wide siRNA screens for VSV [58, 59]. Among the 15 BDV-specific host factors there were 3 cellular proteases, furin, ADAM17 and cathepsin L [63]. Inhibitors against these proteases dose-dependently inhibit BDV infection, but not VSV or LCMV infection, confirming the biological significance of these proteases in the entry of BDV. Cathepsin L was recently also found in a screen for host proteins in the entry of MARV [62]. So cathepsin L might be a common host factor necessary for the entry of BDV and MARV by clathrin-dependent endocytosis and likely macropinocytosis, respectively [64-66].

Influenza A virus (IAV) belongs to the *Orthomyxoviridae* family and at least 9 different high-throughput RNAi screens have been performed to identify host genes involved in IAV replication. A first genome-wide screen was done in 2008 in drosophila cells and identified 110 host genes that enhance the replication of a recombinant influenza A/WSN/33 (H1N1) strain of which the haemagglutinin and neuraminidase gene were replaced by the VSV-G protein and *Renilla* luciferase [67]. These 110 host genes were identified by at least 2 different dsRNAs. Although the primary screen was rather artificial, this screen identified several host genes involved in cellular processes known to be important for influenza replication such as ATP6V0D1, COX6A1 and NXF1. About one year later, 4 large-scale siRNA screens were published nearly simultaneously, of which two involved the replication of the influenza A/Puerto Rico/8/34 (H1N1) strain [68, 69] and two the influenza A/WSN/33 (H1N1) strain [70, 71]. Brass and colleagues identified 129 proviral genes and 4 antiviral genes with at least 2 siRNAs per gene, which are involved in RNA splicing, proton transport and mRNA transport amongst other cellular processes [68]. One of the antiviral genes, interferon-induced transmembrane protein (IFITM) 3, led to the discovery of the important antiviral functions of the IFITM protein family (IFITM1, 2, 3). IFITM3 knockdown was tested by 11 distinct siRNAs of which 8 identified an antiviral role for IFITM3, with a clear correlation between knockdown efficiency and IAV replication. On-target silencing of IFITM3 was

further confirmed by restoring viral resistance upon rescuing IFITM3 expression. Shapira and colleagues first generated a list of host genes likely involved in IAV infection [69]. Therefore, they combined the results of a yeast-2-hybrid (Y2H) protein-protein interaction (PPI) screen of the 10 IAV proteins and IAV-induced gene expression data. As such, a selection of 1,745 genes was obtained and subsequently knocked down by siRNAs. In total, 616 host genes were found to be involved in the replication of IAV or the production of type I IFN (IFN-β) and highlighted possible novel roles for *e.g.* the WNT pathway. These results, however, were based on siRNA pools and were not validated by siRNA pool deconvolution. Karlas and colleagues identified 168 proviral genes, with at least 2 siRNAs per gene, for the replication of either influenza A/WSN/33 or influenza A/Hamburg/04/2009 (H1N1) with an overlap of 72 genes (~60%) [70]. A subset of these 72 genes (6 of 7 genes tested) were also important for the replication of a highly pathogenic avian influenza H5N1 strain (A/Vietnam/1203/2004), suggesting that, at least a part of, these genes play a crucial role in IAV infection independent of the subtype. The biological significance of two genes, CLK1 and CDKN1B, during IAV infection was further confirmed by using a CLK1 inhibitor and CDKN1B knockout mice. König and colleagues used a recombinant luciferase expressing influenza A/WSN/33 strain to perform a primary screen and validated subsequently with wild type influenza A/WSN/33 [71]. Of the 295 proviral genes identified by at least 2 siRNAs per gene in the primary screen, 219 were confirmed by at least 2 siRNAs per gene with the wild type strain. Functional clustering of the identified hits revealed 170 enriched categories that could be grouped into 11 broadly related functional groups, with kinase signaling, the ubiquitin pathway, phosphatase activity and ATPase/ion transport amongst the most enriched cellular processes.

In 2013, Bakre and colleagues published a focused, large-scale siRNA screen on the role of host kinases in the replication of influenza A/WSN/33 [72]. Three antiviral kinases and 14 proviral kinases were identified by a pool of 4 siRNAs in the primary screen and confirmed by an independent siRNA in a subsequent secondary experiment. Six of the 14 proviral kinases were also important in the replication of influenza A/New Caledonia/20/99. Several of these essential kinases are regulated by miRNAs induced upon influenza infection, supporting the biological significance of these kinases. Cheng and colleagues performed a genome-wide siRNA screen followed by infection with a HIV VLP carrying the HA and NA glycoproteins of an influenza H5N1 strain and influenza A/Puerto Rico/8/34, respectively [62]. Four genes enhanced and 42 genes suppressed cell entry by the H5N1 HA protein, which were identified by at least 2 siRNAs per gene.

In addition to the siRNA-mediated RNAi screens described above, two pooled lentiviral shRNA-mediated RNAi screens have been published for IAV [73, 74]. Su and colleagues identified 110 host genes, by at least 2 shRNA clones per gene, which likely promote influenza A/WSN/33 virus infection as their knockdown prevents influenza virus-induced cell death [73]. Thirty-eight of these genes are involved in the early stages of infection. The role of Itch, an E3 ubiquitin ligase, was further characterized and revealed that this ligase promotes the release of viral RNP complexes from the endosome into the cytosol during viral entry. Tran and colleagues used a similar approach to identify 138 host genes that likely enhance influenza A/New York/55/2004 (H3N2) virus infection [74]. A subset of these host genes, 127 of the 138 genes, were subsequently tested by siRNA-mediated knockdown,

of which about 2/3 provided protection against IAV infection. Silencing of 19 genes strongly (>85%) protected against influenza-induced cell death. Amongst these, the role of TNFSF13, TNFSF12-TNFSF13 and USP47 during IAV infection was investigated further and shown to be important during the late stage of IAV infection (TNFSF proteins) and during entry (USP47).

Although these 9 large-scale RNAi screens provide interesting host gene candidates that might be important in the IAV infection cycle, overlap between these screens is remarkably limited. Chou and colleagues reviewed the overlap between 7 of these 9 RNAi screens (all RNAi screens described above except for Cheng, H. *et al.* and Bakre, A. *et al.*) [75]. On a total of 1,362 host genes identified in these 7 RNAi screens as important for influenza virus infection, 1,229 genes (~90%) were uniquely identified in only one screen. Of the remaining overlapping genes, 113 genes were identified in 2 screens, 14 genes were identified in 3 screens and 6 genes were identified in 4 screens. Not a single gene, however, was identified in all 7 screens. The identification of these genes in multiple independent RNAi screens strengthens the reliability of their role during IAV infection. Among the genes with the highest overlap were members of the vacuolar H^+-ATPase, the COPI coatomer complex, members of nuclear import and - export complexes, ribosomal proteins and regulators of endocytosis and mRNA splicing, confirming cellular processes known to be intrinsically part of the IAV infection cycle. Pairwise comparisons between the 7 IAV RNAi screens revealed that experimental conditions, such as the used cell line, source of RNAi library, virus strain and read-out method, substantially contribute to the identification of host genes. RNAi screens using the same source of siRNA and viral strain for example share the highest number of host genes. A low number of overlapping host genes identified by multiple RNAi screens is likely not a unique characteristic of IAV, but seems applicable to viruses in general. Bushman and colleagues, for example, compared three siRNA screens for HIV infection [76]. These three screens together identified 842 host genes which seem important for HIV infection. Only 34 genes, however, were identified in at least 2 of these screens and only 3 genes, MED6, MED7 and RELA, were identified in all three screens.

3.5 Reference list

1. Coleman, J., P.J. Green, and M. Inouye, *The use of RNAs complementary to specific mRNAs to regulate the expression of individual bacterial genes.* Cell, 1984. **37**(2): p. 429-36.
2. Melton, D.A., *Injected anti-sense RNAs specifically block messenger RNA translation in vivo.* Proc Natl Acad Sci U S A, 1985. **82**(1): p. 144-8.
3. Rosenberg, U.B., et al., *Production of phenocopies by Kruppel antisense RNA injection into Drosophila embryos.* Nature, 1985. **313**(6004): p. 703-6.
4. Ecker, J.R. and R.W. Davis, *Inhibition of gene expression in plant cells by expression of antisense RNA.* Proc Natl Acad Sci U S A, 1986. **83**(15): p. 5372-6.
5. Izant, J.G. and H. Weintraub, *Constitutive and conditional suppression of exogenous and endogenous genes by anti-sense RNA.* Science, 1985. **229**(4711): p. 345-52.
6. Fire, A., et al., *Potent and specific genetic interference by double-stranded RNA in Caenorhabditis elegans.* Nature, 1998. **391**(6669): p. 806-11.
7. Hamilton, A.J. and D.C. Baulcombe, *A species of small antisense RNA in posttranscriptional gene silencing in plants.* Science, 1999. **286**(5441): p. 950-2.
8. Zamore, P.D., et al., *RNAi: double-stranded RNA directs the ATP-dependent cleavage of mRNA at 21 to 23 nucleotide intervals.* Cell, 2000. **101**(1): p. 25-33.
9. Elbashir, S.M., W. Lendeckel, and T. Tuschl, *RNA interference is mediated by 21- and 22-nucleotide RNAs.* Genes Dev, 2001. **15**(2): p. 188-200.
10. Hutvagner, G. and P.D. Zamore, *A microRNA in a multiple-turnover RNAi enzyme complex.* Science, 2002. **297**(5589): p. 2056-60.
11. Martinez, J., et al., *Single-stranded antisense siRNAs guide target RNA cleavage in RNAi.* Cell, 2002. **110**(5): p. 563-74.
12. Elbashir, S.M., et al., *Duplexes of 21-nucleotide RNAs mediate RNA interference in cultured mammalian cells.* Nature, 2001. **411**(6836): p. 494-8.
13. Kok, K.H., et al., *Human TRBP and PACT directly interact with each other and associate with dicer to facilitate the production of small interfering RNA.* J Biol Chem, 2007. **282**(24): p. 17649-57.
14. Liu, J., et al., *Argonaute2 is the catalytic engine of mammalian RNAi.* Science, 2004. **305**(5689): p. 1437-41.
15. Lund, E., et al., *Nuclear export of microRNA precursors.* Science, 2004. **303**(5654): p. 95-8.
16. Kim, Y.K., B. Kim, and V.N. Kim, *Re-evaluation of the roles of DROSHA, Export in 5, and DICER in microRNA biogenesis.* Proc Natl Acad Sci U S A, 2016. **113**(13): p. E1881-9.
17. Jinek, M. and J.A. Doudna, *A three-dimensional view of the molecular machinery of RNA interference.* Nature, 2009. **457**(7228): p. 405-12.
18. Sullivan, C.S., et al., *SV40-encoded microRNAs regulate viral gene expression and reduce susceptibility to cytotoxic T cells.* Nature, 2005. **435**(7042): p. 682-6.
19. Seo, G.J., et al., *Evolutionarily conserved function of a viral microRNA.* J Virol, 2008. **82**(20): p. 9823-8.
20. Xu, N., et al., *Adenovirus virus-associated RNAII-derived small RNAs are efficiently incorporated into the rna-induced silencing complex and associate with polyribosomes.* J Virol, 2007. **81**(19): p. 10540-9.
21. Pfeffer, S., et al., *Identification of virus-encoded microRNAs.* Science, 2004. **304**(5671): p. 734-6.
22. Cai, X., et al., *Kaposi's sarcoma-associated herpesvirus expresses an array of viral microRNAs in latently infected cells.* Proc Natl Acad Sci U S A, 2005. **102**(15): p. 5570-5.
23. Grey, F., et al., *Identification and characterization of human cytomegalovirus-encoded microRNAs.* J Virol, 2005. **79**(18): p. 12095-9.
24. Cai, X., et al., *Epstein-Barr virus microRNAs are evolutionarily conserved and differentially expressed.* PLoS Pathog, 2006. **2**(3): p. e23.

25. Umbach, J.L., et al., *MicroRNAs expressed by herpes simplex virus 1 during latent infection regulate viral mRNAs.* Nature, 2008. **454**(7205): p. 780-3.
26. Fedorov, Y., et al., *Different delivery methods-different expression profiles.* Nat Methods, 2005. **2**(4): p. 241.
27. Ohrt, T., et al., *In situ fluorescence analysis demonstrates active siRNA exclusion from the nucleus by Exportin 5.* Nucleic Acids Res, 2006. **34**(5): p. 1369-80.
28. Hornung, V., et al., *Sequence-specific potent induction of IFN-alpha by short interfering RNA in plasmacytoid dendritic cells through TLR7.* Nat Med, 2005. **11**(3): p. 263-70.
29. Judge, A.D., et al., *Sequence-dependent stimulation of the mammalian innate immune response by synthetic siRNA.* Nat Biotechnol, 2005. **23**(4): p. 457-62.
30. Sioud, M., *Induction of inflammatory cytokines and interferon responses by double-stranded and single-stranded siRNAs is sequence-dependent and requires endosomal localization.* J Mol Biol, 2005. **348**(5): p. 1079-90.
31. Bridge, A.J., et al., *Induction of an interferon response by RNAi vectors in mammalian cells.* Nat Genet, 2003. **34**(3): p. 263-4.
32. Sledz, C.A., et al., *Activation of the interferon system by short-interfering RNAs.* Nat Cell Biol, 2003. **5**(9): p. 834-9.
33. Morrissey, D.V., et al., *Potent and persistent in vivo anti-HBV activity of chemically modified siRNAs.* Nat Biotechnol, 2005. **23**(8): p. 1002-7.
34. Judge, A.D., et al., *Design of noninflammatory synthetic siRNA mediating potent gene silencing in vivo.* Mol Ther, 2006. **13**(3): p. 494-505.
35. Robbins, M., et al., *2'-O-methyl-modified RNAs act as TLR7 antagonists.* Mol Ther, 2007. **15**(9): p. 1663-9.
36. Robbins, M., et al., *Misinterpreting the therapeutic effects of small interfering RNA caused by immune stimulation.* Hum Gene Ther, 2008. **19**(10): p. 991-9.
37. Sioud, M., *Deciphering the code of innate immunity recognition of siRNAs.* Methods Mol Biol, 2009. **487**: p. 41-59.
38. Doench, J.G., C.P. Petersen, and P.A. Sharp, *siRNAs can function as miRNAs.* Genes Dev, 2003. **17**(4): p. 438-42.
39. Jackson, A.L., et al., *Expression profiling reveals off-target gene regulation by RNAi.* Nat Biotechnol, 2003. **21**(6): p. 635-7.
40. Birmingham, A., et al., *3' UTR seed matches, but not overall identity, are associated with RNAi off-targets.* Nat Methods, 2006. **3**(3): p. 199-204.
41. Jackson, A.L., et al., *Widespread siRNA "off-target" transcript silencing mediated by seed region sequence complementarity.* RNA, 2006. **12**(7): p. 1179-87.
42. Anderson, E.M., et al., *Experimental validation of the importance of seed complement frequency to siRNA specificity.* RNA, 2008. **14**(5): p. 853-61.
43. Gu, S., et al., *Weak base pairing in both seed and 3' regions reduces RNAi off-targets and enhances si/shRNA designs.* Nucleic Acids Res, 2014. **42**(19): p. 12169-76.
44. Ui-Tei, K., et al., *Thermodynamic stability and Watson-Crick base pairing in the seed duplex are major determinants of the efficiency of the siRNA-based off-target effect.* Nucleic Acids Res, 2008. **36**(22): p. 7100-9.
45. Kamola, P.J., et al., *The siRNA Non-seed Region and Its Target Sequences Are Auxiliary Determinants of Off-Target Effects.* PLoS Comput Biol, 2015. **11**(12): p. e1004656.
46. Lin, X., et al., *siRNA-mediated off-target gene silencing triggered by a 7 nt complementation.* Nucleic Acids Res, 2005. **33**(14): p. 4527-35.
47. Schultz, N., et al., *Off-target effects dominate a large-scale RNAi screen for modulators of the TGF-beta pathway and reveal microRNA regulation of TGFBR2.* Silence, 2011. **2**: p. 3.
48. Meier, R., et al., *Genome-wide small interfering RNA screens reveal VAMP3 as a novel host factor required for Uukuniemi virus late penetration.* J Virol, 2014. **88**(15): p. 8565-78.
49. Jackson, A.L., et al., *Position-specific chemical modification of siRNAs reduces "off-target" transcript silencing.* RNA, 2006. **12**(7): p. 1197-205.

50. Hannus, M., et al., *siPools: highly complex but accurately defined siRNA pools eliminate off-target effects.* Nucleic Acids Res, 2014. **42**(12): p. 8049-61.
51. De Clercq, E. and G. Li, *Approved Antiviral Drugs over the Past 50 Years.* Clin Microbiol Rev, 2016. **29**(3): p. 695-747.
52. Pope, L.E., et al., *The anti-herpes simplex virus activity of n-docosanol includes inhibition of the viral entry process.* Antiviral Res, 1998. **40**(1-2): p. 85-94.
53. Kolokoltsov, A.A., et al., *Small interfering RNA profiling reveals key role of clathrin-mediated endocytosis and early endosome formation for infection by respiratory syncytial virus.* J Virol, 2007. **81**(14): p. 7786-800.
54. Deffrasnes, C., et al., *Genome-wide siRNA Screening at Biosafety Level 4 Reveals a Crucial Role for Fibrillarin in Henipavirus Infection.* PLoS Pathog, 2016. **12**(3): p. e1005478.
55. Ghildyal, R., et al., *The matrix protein of Human respiratory syncytial virus localises to the nucleus of infected cells and inhibits transcription.* Arch Virol, 2003. **148**(7): p. 1419-29.
56. Ghildyal, R., et al., *Nuclear import of the respiratory syncytial virus matrix protein is mediated by importin beta1 independent of importin alpha.* Biochemistry, 2005. **44**(38): p. 12887-95.
57. Kipper, S., et al., *New host factors important for respiratory syncytial virus (RSV) replication revealed by a novel microfluidics screen for interactors of matrix (M) protein.* Mol Cell Proteomics, 2015. **14**(3): p. 532-43.
58. Panda, D., et al., *RNAi screening reveals requirement for host cell secretory pathway in infection by diverse families of negative-strand RNA viruses.* Proc Natl Acad Sci U S A, 2011. **108**(47): p. 19036-41.
59. Lee, A.S., R. Burdeinick-Kerr, and S.P. Whelan, *A genome-wide small interfering RNA screen identifies host factors required for vesicular stomatitis virus infection.* J Virol, 2014. **88**(15): p. 8355-60.
60. Cureton, D.K., R. Burdeinick-Kerr, and S.P. Whelan, *Genetic inactivation of COPI coatomer separately inhibits vesicular stomatitis virus entry and gene expression.* J Virol, 2012. **86**(2): p. 655-66.
61. Spurgers, K.B., et al., *Identification of essential filovirion-associated host factors by serial proteomic analysis and RNAi screen.* Mol Cell Proteomics, 2010. **9**(12): p. 2690-703.
62. Cheng, H., et al., *A parallel genome-wide RNAi screening strategy to identify host proteins important for entry of Marburg virus and H5N1 influenza virus.* Virol J, 2015. **12**: p. 194.
63. Clemente, R., et al., *Identification of host factors involved in borna disease virus cell entry through a small interfering RNA functional genetic screen.* J Virol, 2010. **84**(7): p. 3562-75.
64. Clemente, R. and J.C. de la Torre, *Cell entry of Borna disease virus follows a clathrin-mediated endocytosis pathway that requires Rab5 and microtubules.* J Virol, 2009. **83**(20): p. 10406-16.
65. Nanbo, A., et al., *Ebolavirus is internalized into host cells via macropinocytosis in a viral glycoprotein-dependent manner.* PLoS Pathog, 2010. **6**(9): p. e1001121.
66. Saeed, M.F., et al., *Cellular entry of ebola virus involves uptake by a macropinocytosis-like mechanism and subsequent trafficking through early and late endosomes.* PLoS Pathog, 2010. **6**(9): p. e1001110.
67. Hao, L., et al., *Drosophila RNAi screen identifies host genes important for influenza virus replication.* Nature, 2008. **454**(7206): p. 890-3.
68. Brass, A.L., et al., *The IFITM proteins mediate cellular resistance to influenza A H1N1 virus, West Nile virus, and dengue virus.* Cell, 2009. **139**(7): p. 1243-54.
69. Shapira, S.D., et al., *A physical and regulatory map of host-influenza interactions reveals pathways in H1N1 infection.* Cell, 2009. **139**(7): p. 1255-67.
70. Karlas, A., et al., *Genome-wide RNAi screen identifies human host factors crucial for influenza virus replication.* Nature, 2010. **463**(7282): p. 818-22.
71. Konig, R., et al., *Human host factors required for influenza virus replication.* Nature, 2010. **463**(7282): p. 813-7.
72. Bakre, A., et al., *Identification of Host Kinase Genes Required for Influenza Virus Replication and the Regulatory Role of MicroRNAs.* PLoS One, 2013. **8**(6): p. e66796.

73. Su, W.C., et al., *Pooled RNAi screen identifies ubiquitin ligase Itch as crucial for influenza A virus release from the endosome during virus entry.* Proc Natl Acad Sci U S A, 2013. **110**(43): p. 17516-21.
74. Tran, A.T., et al., *Knockdown of specific host factors protects against influenza virus-induced cell death.* Cell Death Dis, 2013. **4**: p. e769.
75. Chou, Y.C., et al., *Variations in genome-wide RNAi screens: lessons from influenza research.* J Clin Bioinforma, 2015. **5**: p. 2.
76. Bushman, F.D., et al., *Host cell factors in HIV replication: meta-analysis of genome-wide studies.* PLoS Pathog, 2009. **5**(5): p. e1000437.

Chapter IV

RSV-induced host responses

4.1 RSV regulated gene transcription in the host

One approach to understand the complex interplay between RSV and the host is the characterization of differentially expressed host genes upon RSV infection. Transcriptomics experiments using microarray technology have been performed on RSV infected human immortalized cells grown *in vitro*, on cells isolated from infected mice and on cells isolated from human clinical samples.

Zhang and colleagues investigated the induction of chemokines in RSV infected A549 cells and human small airway epithelial cells at 24 hours post infection and identified multiple chemokines that are upregulated in both cell lines upon infection [1]. One of these chemokines is the CX3C chemokine fractalkine, which is thought to function as a cellular receptor during RSV entry [2]. Tian and colleagues used HeLa cells to identify 1,359 RSV regulated genes at 12 hours post infection, of which 144 (~10%) appeared dependent on the induction of NF-κB by RSV [3]. These genes included chemokines, transcription factors involved in IFN responses, genes involved in metabolism and secreted proteins amongst others. Kong and colleagues identified 53 differentially expressed genes 30 min after RSV infection in A549 cells, highlighting that RSV modulated host gene expression already initiates early during the entry phase [4]. Further analysis demonstrated that STAT1 and STAT3 are activated upon RSV attachment. Later in infection, RSV NS2 might suppress the activation of STAT1 (see chapter 2: Structure and functions of the RSV non-structural proteins 1 and 2). Martinez and colleagues assessed different time points post infection to investigate the dynamics of differential gene expression [5]. Early after infection (< 6 hours), the urokinase-type plasminogen activator system and genes involved in cytoskeleton organization were amongst the strongest upregulated genes. Later (6-24 hours after infection), ISGs, genes related to oxidative stress and activation of NF-κB and immune response genes such as cytokines were clearly upregulated. Two groups used bronchial epithelial BEAS-2B cells and could identify several hundreds of differentially expressed genes [6, 7]. Zhou and colleagues used a microarray to unravel pathways involved in RSV-induced expression of IL-8 [8]. They observed RSV upregulated expression of the TLR adaptors MyD88, TRAM and TRIF.

Although mice are only semi-permissive to RSV, they are used as an animal model for RSV infections. Several groups have used mouse tissues or cells to investigate differential regulated genes upon RSV infection. In the lungs of RSV infected mice, strong innate immune responses are observed [9-11]. Janssen and colleagues demonstrated that the innate immune response is stronger at day 1 post infection compared to day 3, highlighting that the innate immune response mainly occurs before the peak of virus replication [9]. Ravi and colleagues infected pulmonary macrophages *ex vivo* and observed that 8,9% and 11,3% of all expressed genes were differentially regulated at 4 and 24 hours post infection, respectively [12]. Upregulated genes were mainly categorized in pathogen recognition -, IFN signaling - and antigen presentation pathways. Mosquera and colleagues used aged mice (>10 months of age) as a model for the increased risk of severe RSV disease observed in the elderly [13]. Chemokines, IFN response genes and inflammatory genes were upregulated by RSV infection, whereas some genes involved in antigen processing and presentation were downregulated, reflecting immunosenescence observed in the elderly. Young adult mice, however, were not investigated in parallel, making it difficult to correlate RSV-induced gene expression with high age.

Perhaps the most interesting samples include primary human cells. Ioannidis and colleagues cultured human tracheobronchial epithelial cells under air-liquid interphase and identified 336 differentially expressed genes upon RSV infection [14]. Several groups have used whole blood samples of infants hospitalized with acute RSV bronchiolitis and healthy matched controls to identify differentially regulated genes [15-17]. Interestingly, two of these groups identified IFI27 as the strongest induced gene upon RSV infection, which was also identified as the strongest upregulated gene in the tracheobronchial epithelial cell cultures of Ioannidis and colleagues [14-16]. IFI27 (also known as ISG12) is an ISG that promotes apoptosis by disturbing normal mitochondrial functions leading to increased release of cytochrome C, activation of Bax and loss of the mitochondrial membrane potential [18]. Other groups have used whole blood samples or nasopharyngeal aspirates from infants with variable clinical severity of RSV disease to correlate differential gene expression profiles to disease severity [19-21]. Van den Kieboom and colleagues identified a set of 5 genes, ubiquitin D, tetraspanin 8, mucin 13, β-microseminoprotein and chemokine ligand 7, whose expression in cells from nasopharyngeal aspirates correlated with disease severity [20]. Whereas Brand and colleagues identified olfactomedin-4, Jong and colleagues identified a set of 84 genes in the blood correlating with RSV disease severity [19, 21]. Although olfactomedin-4 was included in the set of 84 genes, none of the 5 markers identified by Van den Kieboom *et al.* were identified in this set. Possibly, this lack of accordance is caused by the different sample types.

In general, RSV upregulated genes were more abundant than downregulated genes. Recently, Dapat and Oshitani investigated the overlap of differentially regulated genes during a RSV infection identified by a set (7) of the above described microarray studies [22]. Pairwise comparisons between these 7 studies revealed that not more than 16% of the identified genes overlapped between two studies. This highlights that although a limited set of genes is common, most genes are uniquely identified within one study. Differences in experimental conditions, such as the source of cell material, virus strain, time of analysis and origin of the microarray plate likely causes this limited overlap.

4.2 RSV regulated protein expression in the host

Although transcriptomics data can provide valuable knowledge on the interaction of viruses with their host, differences in mRNA expression not necessarily coincide with differences in protein levels. Therefore, several groups have investigated changes in the host proteome during RSV infection. In the earlier days proteomics experiments were mostly carried out by using 2 dimensional difference gel electrophoresis (2D-DiGE). Although it is intrinsically biased for the detection of well-expressed proteins and its reproducibility has been a point of concern, 2D-DiGE provided the first knowledge on RSV-induced proteomics. Brasier and colleagues investigated the nuclear proteome in A549 cells and identified 24 differential proteins upon RSV infection [23]. Further analysis of these proteins revealed a nuclear heat shock response and disintegration of nuclear domain 10 (ND10) structures upon RSV infection. Jamaluddin and colleagues further optimized the analysis of the nuclear proteome and identified an additional 41 proteins that were differentially expressed or had a shift of the isoelectric point upon RSV infection [24]. Amongst these were several isoforms of the peroxiredoxin antioxidant

enzyme family. Peroxiredoxin-1 and -4 were shown to play an important role in the protection against RSV-induced oxidative damage of several nuclear proteins. Van Diepen and colleagues infected A549 cells with 4 different respiratory viruses, including RSV, and determined changes in the host proteome at 6, 12 or 24 hours post infection [25]. They identified 18 differentially expressed proteins upon RSV infection of which most are involved in the cytoskeleton and protein biosynthesis and modification. Hastie and colleagues used wild type RSV and a NS1 deletion strain to investigate candidate targets of the NS1 protein [26]. They identified 2 host proteins, actin-related protein (ARP)-3 and cytoplasmic thioredoxin reductase 1, with reduced expression upon wild type RSV infection. Fifteen proteins were upregulated upon infection with the NS1 deletion strain, of which 11 are known to be regulated by IFN, *e.g.* Mx1, IFN-induced protein with tetratricopeptide repeats (IFIT) 3 and ISG15. These results confirm that NS1 plays an important role in the suppression of IFN responses.

In the last two decades major progress has been achieved in the development of mass spectrometry and protein quantification techniques such as stable isotope labeling by amino acids in cell culture, isobaric tag for relative and absolute quantitation and recently label free quantification. These advancements combined with the capacity of mass spectrometry to detect thousands of proteins reproducibly, have made mass spectrometry the method of choice to investigate proteomics currently. Munday and colleagues were the first to use mass spectrometry without gel electrophoresis to investigate changes in the nuclear - and cytoplasmic proteome upon RSV-A2 and RSV-B infection [27, 28]. On a total of 1,081 quantified host proteins, only limited numbers of differentially expressed proteins upon RSV-A2 infection could be identified in the cytoplasm (14 upregulated - and 4 downregulated proteins), whereas massive changes in the nuclear proteome were observed (479 downregulated proteins) [27]. These proteins could be grouped into functional clusters such as cell growth, transcription regulation, molecular transport and protein and RNA trafficking for the nuclear proteome and cellular assembly and organization, cellular compromise and protein folding for the cytoplasmic proteome. Further analysis confirmed that several mitochondrial proteins, including respiratory chain pore complex proteins, were downregulated by RSV infection, highlighting RSV-induced changes of mitochondrial functions. Furthermore, multiple proteins of the nuclear pore complex were altered in expression, indicating that nucleocytoplasmic transport is affected by RSV infection. Several cell cycle regulatory proteins were reduced, confirming RSV-induced cell cycle arrest [29]. Although several members of ND10 structures were downregulated, its major component, promyelocytic leukemia protein, was upregulated in the nucleus upon RSV infection [27]. Immunofluorescence highlighted that ND10 structures were more abundant in RSV infected cells, which is opposite to the RSV-induced disintegration of ND10 structures seen by Brasier *et al.* [23]. In parallel to RSV-A2, Munday and colleagues also investigated the host proteome after infection with RSV-B [28]. They identified 112 differentially expressed proteins on a total of 904 quantified host proteins. In the nuclear proteome, both up- and downregulated proteins were identified, whereas in the cytoplasmic fraction only upregulated proteins were found. In comparison to RSV-A2, multiple identical and other mitochondrial proteins were downregulated upon RSV-B infection, suggesting that the modulation of mitochondrial functions by RSV is a broad response and not strain specific. A striking difference between RSV-A2 and RSV-B was the upregulation of proteins of the IFN response. Whereas

RSV-A2 only moderately upregulated expression of ISG15, STAT1, Mx1 and IFIT1 and even downregulated OAS3 (Fold change to mock: 3,9; 2,3; 1,8; 1,4 and 0,6; respectively), RSV-B strongly upregulated these proteins (Fold change to mock: n/a; 6,3; 11; 8,9 and 3,5; respectively). These results suggest that the suppression of IFN responses by RSV-A2 is stronger than RSV-B. Differences in the NS1 and/or NS2 sequence of RSV-A2 and RSV-B might account for this (NS1: 87% and NS2: 90% AA sequence conservation between RSV-A2 and RSV-B, see Fig. 2 of chapter 2). To explore the role of mitochondria during RSV infection further, Munday and colleagues have specifically focused on the mitochondrial proteome [30]. Upon RSV infection, several IFN-induced antiviral proteins, Mx1, ISG15 and OAS3, were shown to be translocated to the mitochondria. Moreover, the mitochondrial receptor TOM70 possessed antiviral activity, while its chaperone HSP90 acted proviral as demonstrated by siRNA-mediated knockdown of TOM70 and targeted inhibition of HSP90 by a small compound. Ternette and colleagues used a label free quantification approach to identify differentially expressed proteins upon RSV infection [31]. Sixty-nine differential proteins were identified involved in numerous cellular pathways. Further analysis confirmed induction of IFIT3 protein upon RSV infection, whereas different isoforms of 5'-3' exoribonuclease 2 were detected. Finally, Dave and colleagues did two RSV proteomics analysis in parallel, *i.e.* on total cell lysates and after lysate fractionation by in solution isoelectrofocusing, with multiple biological replicates [32]. As such, 5,010 and 3,247 host proteins could be quantified, respectively, making this the largest proteomics screen upon RSV infection. Of these proteins, 149 and 114 were differentially expressed, respectively, with most proteins possibly regulated by IFN, TNF-α and NF-κB2-mediated antiviral responses.

In analogy to the transcriptomics data, Dapat and Oshitani also determined the overlap of differentially expressed host proteins between most of the above described RSV proteomics screens [22]. Although some pairwise comparisons yielded relatively high numbers of overlapping proteins (up to 66%), others only yielded low numbers of overlapping proteins. A comparison was also made of all host factors identified by transcriptomics - (2,039 genes) and proteomics (814 proteins) screens, which identified 177 overlapping host factors. These results highlight that substantial differences between transcriptomics and proteomics data are possible. To identify biologically relevant host factors, a selection of factors that were identified in at least 2 screens was made, which resulted in a core set of 512 factors. Amongst these, IFN regulated genes were clearly enriched with Mx1, ISG15, IFIT1-3, IFI35, IFI44, STAT1, CCL2, ENO1, KLF4, PNPT1, RRBP1, SOD2 and WARS identified in at least 5 screens. This core set of 512 host factors and 10 RSV proteins (only M2-1 is in the network and shown as M2) was subsequently used to construct a RSV-host interaction network by implementing known interactions to these 512 factors. As a result, a network of 1,254 proteins with 1,989 interactions could be constructed (Fig. 1). Note that NS1 is by far the most interconnected viral protein (219 connections), suggesting a major interplay between the NS1 protein and host cell proteins.

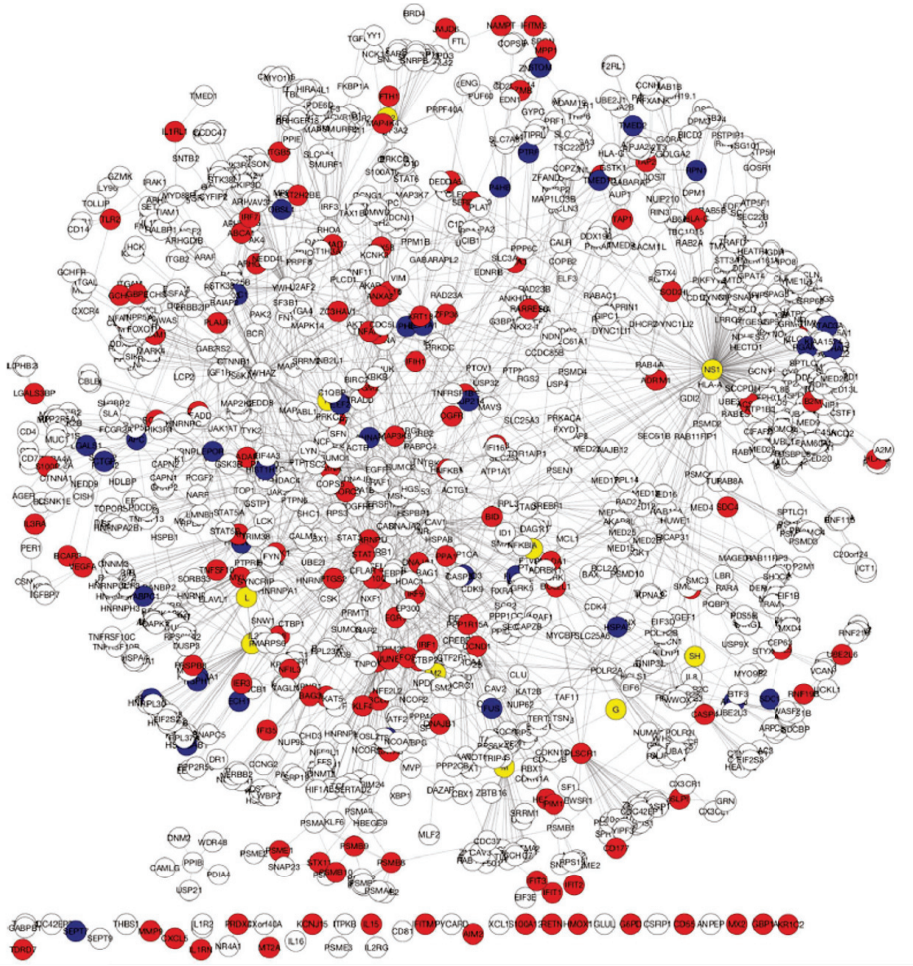

Figure 1: Interaction network between RSV and the human host. The network consists of 1,254 proteins (nodes) that are connected by 1,989 interactions (lines). RSV proteins are marked in yellow, upregulated host proteins upon RSV infection are marked in red and downregulated host proteins upon RSV infection are marked in blue. Figure taken from [22].

4.3 RSV regulated signaling pathways

In addition to changes in gene transcription and protein synthesis, signaling pathways can also be activated without affecting the total protein abundance. Dozens of post translational modifications of proteins are well known to regulate protein activity, functions and folding, *e.g.* phosphorylation, acetylation, glycosylation, amidation, hydroxylation, methylation and ubiquitination amongst many others. In the last two decades, several signaling pathways have been identified that are specifically activated during a RSV infection. In this section we will give an overview of the best characterized RSV-induced, phosphorylation-dependent signaling pathways. Although we will describe these pathways separately, these pathways are often strongly interconnected with each other.

EGFR

Several groups have reported that the EGFR is activated upon RSV infection. Most groups identified maximal EGFR activation around 24 hours post infection [33-35], whereas infection with a high multiplicity of infection (MOI) (~30) already activates the EGFR 15 min post infection during entry [36]. Currier and colleagues demonstrated that the F protein of RSV activates the EGFR with substantial differences between strains [35]. Compared to the F protein of the typical lab strain RSV-A2, F from the mucogenic clinical strain 2-20 more strongly activates the EGFR. Moreover, the EGFR might function as a receptor for F and enhance RSV entry, at least for RSV 2-20. RSV-induced activation of the EGFR leads to activation of MAPK3 (also known as ERK1), which contributes to an inflammatory response with the production of IL-8 and a cell survival response by shifting the balance towards anti-apoptotic Bcl2 proteins [33]. As such, EGFR activation plays a role in the production of matrix-metalloproteinase 10 and the chemokines CCL5 and CXCL10 upon RSV infection [37, 38].

MAPK

MAPKs are a well-known family of kinases involved in the signal transduction upon diverse stimuli such as growth factors, cytokines and cellular stress. These kinases typically signal in two consecutive steps with MAP3Ks activating MAP2Ks, which on their turn activate MAPKs. MAPKs can be subdivided into four groups, *i.e.* MAPK3/1 (also known as ERK1/2, respectively), MAPK14/11/12/13 (also known as p38 MAPKα/β/γ/δ, respectively), MAPK8/9/10 (also known as c-Jun N-terminal kinase (JNK) 1/2/3, respectively) and MAPK7 (also known as ERK5). RSV activates MAPKs.

MAPK1 and -3 are clearly activated biphasically during a RSV infection, *i.e.* early at attachment and late at replication [39, 40]. Their activation appears dependent on different protein kinase C (PRKC) isoforms (see below) and sphingosine-1-phosphate. Monick and colleagues observed an increased activation of Akt and MAPK3 late in infection due to enhanced synthesis of sphingosine-1-phosphate [41]. This contributed to the RSV-induced delay of apoptosis. Additionally, MAPK1 and -3 are activated in dendritic cells following interaction of the RSV-G protein with DC-SIGN and L-SIGN [42].

Similar to MAPK1 and -3, MAPK11-14 are also activated biphasically during a RSV infection, *i.e.* early and late [43-45]. One group, however, reported that MAPK14 is not activated late in infection,

but rather relocates from the cytoplasm to the viral-induced inclusion bodies [46]. Although MAPK11-14 activation is important in the induction of inflammatory cytokines such as TNF-α and IL-1β [47], MAPK11-14 activation also appears important for the infection of multiple respiratory viruses [43, 45, 48, 49]. Marchant and colleagues suggest that upon cell binding respiratory viruses can induce clustering of TLR4, which activates the MAPK11-14 pathway and promotes virus internalization [43].

RSV infection also activates MAPK8-10 by activation of the upstream MAP3K7 [50-52]. This results in the activation of the AP-1 transcription factor, which is, next to NF-κB, important in the induction of antiviral and proinflammatory genes. In addition, activation of MAPK8 and -9 also appears to play an important proviral role at the late stage of RSV infection by enhancing budding of newly produced virions [52].

Protein kinase C

The PRKC family consists of ten isotypes that can be subdivided in three groups, depending on their structural domains and cofactors necessary for their activation [53]. The classical PRKC isoforms (A, B (splice variant I and II) and G) are dependent on both diacylglycerol (DAG) and Ca^2 for their activation. The second group, the novel PRKC isoforms (D, E, H and Q), only require DAG binding for their activation and the last group, the atypical PRKC isoforms (Z and I), are activated without DAG or Ca^{2+}. PRKC isoforms are activated in two stages. First, PRKC in the cytosol is phosphorylated to correctly align catalytic residues and secondly, PRKC translocates from the cytosol to the plasma membrane where it is regulated by the second messenger molecules DAG and Ca^{2+}.

Several publications demonstrated that PRKC isoforms are involved in multiple phases of the RSV infection cycle [37, 39, 54-58]. In 2001, Monick and colleagues first described the activation of PRKC isoforms during a RSV infection in A549 cells [39]. Kinase activity assays demonstrated a biphasic activation of PRKC isoforms: PRKCZ and -D were activated early after infection (10 and 30 minutes post infection), whereas PRKCB1, -D, -E and -M (now renamed protein kinase D (PRKD) 1) were activated late in infection (24 and 48 hours post infection). The biphasic activation of PRKC isoforms nicely coincided with a biphasic activation of MAPK1. The importance of PRKC isoforms in a RSV infection is also evident in normal human bronchial epithelial cells. Inhibition of PRKCA by a pseudosubstrate peptide and a dominant negative mutant PRKCA reduces RSV replication [55]. Early after RSV infection PRKCA is activated, likely by the autophosphorylation of thr-638, and migrates from the cytoplasm to the plasma membrane where it colocalizes with the bound RSV virions. Although three dimensional images by confocal microscopy may be more conclusive than colocalization in two dimensional images. Fusion, but not RSV binding, is reduced by PRKCA inhibition [55]. These results suggest that after RSV binding activated PRKCA migrates to the plasma membrane where it colocalizes with the RSV virions and plays an important role during the fusion process. Activation and subsequent plasma membrane translocation of PRKCA was, however, not observed by Monick *et al*. [39]. Although membrane translocation was investigated at different times post infection (48h [39] versus 10 minutes [55]), a kinase activity assay at 10 or 30 minutes post infection did also not reveal PRKCA activation [39]. A role for PRKCD at the late stages of a RSV infection is also shown in polarized normal human nasal epithelial

cells [58]. Inhibition of PRKCD by rottlerin reduced G protein synthesis, viral filament formation and viral budding. Rottlerin is an ATP competitor with greater selectivity for PRKCD compared to other PRKC isoforms (IC_{50} PRKCD: 3-6 μM versus 30-100 μM for other PRKC isoforms) [59]. Although we should notify that Ca^{2+}/Calmodulin-dependent protein kinase III is equally inhibited by rottlerin as PRKCD (IC_{50} CaM kinase III: 5,3 μM). Taken together, these results suggest that different PRKC isoforms are activated during different stages of a RSV infection and that differences in cell lines or RSV strains used or small technical differences lead to a partial overlap in PRKC isoform identification.

Protein kinase D

PRKD was previously classified within the PRKC family as PRKCM and PRKCN, because these kinases share multiple features. PRKD contains membrane localization motifs, a cysteine rich repeat region, a pleckstrin-homology domain and a catalytic kinase domain and is bound by the phorbol ester family and DAG. The PRKD family consists of 3 isoforms, PRKD1, PRKD2 and PRKD3.

PRKD is phosphorylated during a RSV infection at two phases, early (2-3 hours) and late after infection (30-48 hours), with the former being stronger [60]. Infection with UV-inactivated RSV only induced phosphorylation of PRKD at 2-3 hours post infection, and not at 30-48 hours post infection. This suggests that early PRKD phosphorylation occurs during the entry phase, whereas late PRKD phosphorylation requires active RSV replication. RSV-induced phosphorylation of PRKD occurs at two serine residues in the activation loop at position 738 and 742 in human PRKD1 (position 744 and 748 in the mouse PRKD1 ortholog), two sites known to mediate activation of PRKD [61, 62]. However, as the amino acid sequence surrounding these two serine residues is nearly completely conserved in PRKD1 to -3, it is unclear which PRKD isoform(s) is (are) activated and if PRKD1 to -3 have a different role or not during a RSV infection. Different PRKC isoforms, PRKCD, -H and -Q, are known to directly or indirectly phosphorylate PRKD ser-738 and -742 depending on the stimulus and cell line [61, 63, 64]. So likely, PRKD is phosphorylated at ser-738 and -742 by PRKC during a RSV infection, although further research is necessary to confirm this and to determine which PRKC isoform is responsible for PRKD activation. As discussed in the previous section, different PRKC isoforms are activated during a RSV infection and are possible candidates to mediate PRKD phosphorylation. Activated PRKD at the late stage of a RSV infection disrupts apical junction complexes, composed of tight junctions and adherens junctions, and rearranges the apical actin cytoskeleton in 16HBE14O$^-$ bronchial epithelial cells [60]. This RSV-induced remodelling increased the permeability of the cell layer as measured by a reduction of the transepithelial electrical resistance and increased permeability to a fluorescently labeled dextran polymer. Masaki and colleagues, however, observed an increased tight junctional barrier after RSV infection in human nasal epithelial cells, marked by an increase of the transepithelial electrical resistance and expression of the tight junction markers claudin-4 and occludin [58]. A hallmark of severe RSV disease is the obstruction of the bronchioles by plugs consisting of shedded epithelial cells among other things, which is in line with the hypothesis that RSV disrupts the apical junctional complex. Future research might explore in more detail the biological relevance of this striking difference in RSV-induced changes of the epithelial barrier functions between cells derived from the

upper and lower respiratory tract. Interestingly, biphasic activated PRKD during a RSV infection coincides with a biphasic phosphorylation of cortactin at ser-405, which is prevented by the selective PRKD inhibitor CID755673 [60]. Cortactin is an actin binding protein known to regulate the organization of the actin cytoskeleton. Cellular functions of cortactin are regulated by phosphorylation of tyr-421, -470 and -486 by a diverse panel of tyrosine kinases (overview in [65]) and ser-405 and -418 by MAPK3/1 (previously named ERK1/2) and PAK1 [65-67]. As discussed in the previous section, MAPK1 is activated early and late during a RSV infection [39]. Although the exact mechanism of cell entry by RSV is still debated, several groups reported an important role of PAK1 during the entry process [36, 68, 69]. Possibly, MAPK1 and PAK1 directly phosphorylate cortactin ser-405 and/or -418 during a RSV infection. Whether cortactin tyr-421, -470 and -486 is (are) phosphorylated during a RSV infection is unknown at this moment.

RhoA

RhoA is a small GTPase protein of the Ras superfamily and involved in a plethora of biological functions, *e.g.* cytoskeletal organization, transcription, cell cycle progression, cell migration, cell-cell adhesion, cytokinesis, vesicle transport, cell transformation and formation of actin stress fibres (reviewed in [70]). Rho GTPases exist in two states: a GDP bound inactive form and a GTP bound active form. Transition between these two states is regulated by three protein groups: the guanine nucleotide exchange factors (GEFs) that promote GDP exchange for GTP, the GTPase activating proteins (GAPs) that promote GTP hydrolysis activity of the Rho GTPase and the guanine nucleotide dissociation inhibitors (GDI) that prevent dissociation of the guanine nucleotide and regulate the subcellular localization of the Rho GTPase. Activation of RhoA, and other Rho GTPases, involves two steps: first, GDP is exchanged for GTP and secondly, RhoA is translocated from the cytoplasm to the inner surface of the plasma membrane after isoprenylation of the carboxy-terminus of RhoA. Activated Rho GTPases exert their biological functions through conformation-specific interactions with effector proteins, such as serine/threonine kinases, tyrosine kinases, lipid kinases, lipases, oxidases and scaffolding proteins.

A role for RhoA during a RSV infection was first proposed in 1999 with the identification of RhoA as a possible RSV-F protein interacting host protein [71]. A follow-up study identified a RhoA derived peptide, $RhoA_{77\text{-}95}$, that inhibited RSV replication *in vitro* at an early stage, likely entry, prevented cell-to-cell fusion and reduced the RSV titer more than 100-fold in RSV infected BALB/c mice [72]. These results suggested that the $RhoA_{77\text{-}95}$ peptide could block RSV infection and syncytia formation by preventing the RhoA-F interaction. Further characterization of RhoA-derived peptides, however, revealed similarities with other polyanions, such as heparin and dextran sulphate that prevent viral attachment through direct interaction with the virus surface [73, 74]. So antiviral properties of RhoA-derived peptides are more likely the result of a more general inhibition of viral attachment and fusion, rather than specifically preventing a possible RhoA-RSV F interaction. Whether RhoA and RSV-F interact during a RSV infection is still debated. The RhoA-RSV F interaction was initially identified in an artificial yeast-two-hybrid screen and mammalian two-hybrid assay, but subsequently confirmed in RSV infected HEp-2 cells by co-immunoprecipitation [71]. In addition, $RhoA_{77\text{-}95}$ peptide

prevents the RhoA-RSV F interaction in ELISA in a dose-dependent manner, favoring the hypothesis that RhoA and RSV-F interact, whether or not during a RSV infection [72]. In contrast, mapping of the interaction domains revealed that $RhoA_{80-90}$, the region most critical for antiviral activity, and $RSV\text{-}F_{146-155}$, which completely resides in the buried hydrophobic fusion peptide, are not surface exposed [73, 75]. These findings disfavor the hypothesis of interaction between RhoA and RSV-F. Further studies are needed to elucidate if RhoA and RSV-F interact in the course of a RSV infection.

Irrespective of the question if RhoA and RSV-F interact, RhoA is activated during a RSV infection. Gower and colleagues observed that during RSV infection, RhoA is isoprenylated and translocates from the cytosol to the plasma membrane, which is a hallmark for Rho GTPase activation [76]. RhoA activation was confirmed by the observation that p130-Cas, a known substrate for Rho-dependent signaling [77], is phosphorylated biphasically during a RSV infection, *i.e.* 6-10h and 16-24h post infection. RSV infection of HEp-2 cells leads to the formation of actin stress fibers starting 10-12h post infection in a RhoA-dependent manner [76]. RhoA activation is also associated with RSV-induced syncytia formation, but is not essential for RSV replication, as viral titers and RSV-F expression are not reduced after treatment with two inhibitors of RhoA signaling, C3 exotoxin and Y-27632 [78]. Scanning electron microscopy revealed that RhoA signaling is important for the formation of RSV-induced viral filaments that are associated with the budding of filamentous RSV virions. Inhibition of RhoA by C3 exotoxin favours the formation of spherical virions at the cost of filamentous virions. Possibly, this is mediated by the RhoA-dependent selective recruitment of the RSV-F protein from non-lipid microdomains to the cholesterol-rich lipid microdomains in the plasma membrane, hence favoring viral filament formation [79]. As filamentous virions are thought to be more infectious than spherical virions, RhoA signaling seems to determine the infectivity of released RSV virions [80].

PI3K/AKT

The phosphatidylinositide 3-kinase (PI3K) family consists of lipid kinases that phosphorylate the 3' hydroxyl group of the inositol ring structure of different phosphatidylinositide lipids upon cell stimulation by *e.g.* growth factors or chemokines. PI3 kinases are subdivided in 3 different classes (I to III) depending on sequence similarity and function [81]. Class I PI3Ks are recruited to the cytoplasmic tail of receptor tyrosine kinases or to the $G_{\beta\gamma}$ subunit of G protein coupled receptors upon stimulation and generate phosphatidylinositide 3,4,5 trisphosphate (PIP_3). This second messenger recruits multiple effector proteins to the plasma membrane, such as AKT and others, that can bind to PIP_3 through at least two different domains: the FYVE - and pleckstrin homology domain [82]. AKT is subsequently activated by phosphorylation of thr-308 by 3-phosphoinositide-dependent protein kinase (PDPK) 1 and ser-473 by mechanistic Target of rapamycin (mTOR) in complex with sin1 and rictor [83, 84]. Class II and III PI3Ks are less well characterized and show a different phosphatidylinositide substrate specificity than class I PI3Ks. In addition, a related fourth class is sometimes formed and consists of the PI3K related protein kinases, such as ataxia-telangiectasia mutated (ATM), ataxia-telangiectasia and rad3 related (ATR), DNA-dependent protein kinase and mTOR.

PI3Ks exert a dual role during a RSV infection, *i.e.* PI3Ks delay cell death early in infection and play a role during virus assembly late in infection. Thomas and colleagues discovered that RSV-induced apoptotic cell death in A549 cells is substantially faster if PI3K activity is reduced by the inhibitor LY294002 (12h versus 24-48h in untreated cells) [85]. Although some caution is desired as LY294002 appears to inhibit other kinases as well at the used concentrations to inhibit PI3K [86]. As early as 30 minutes post infection, tyrosine phosphorylation of the p85 regulatory subunit of (class I) PI3K is found, suggesting that PI3K is activated early after infection. This was confirmed by the observation that immunoprecipitated PI3K from RSV infected A549 cells (30 min) phosphorylates phosphatidylinositol (PI) to form PI(3)P. Furthermore, the downstream effector of PI3K, AKT, is phosphorylated at ser-473 starting at 10 minutes post infection, reaches a maximum around 30 minutes post infection and is again completely absent around 24h post infection. Phosphorylation of GSK3, a downstream effector of AKT, nicely coincided with AKT activation during RSV infection. In addition, PI3K signaling is also important for regulating the transcriptional activity of RSV-induced NF-κB in the nucleus, but does not impact the nuclear translocation of NF-κB [85]. RSV-induced cell survival by a PI3K-dependent pathway was also confirmed in RSV inoculated neutrophils and eosinophils [87]. Interestingly, heat inactivated RSV equally delays apoptosis, suggesting that early binding of RSV is sufficient to trigger cell survival, at least in neutrophils. Stimulation of TLR7 and -8, which are present in endosomes and specifically recognize single stranded RNA, with ligands comparably delayed apoptosis in neutrophils. Inoculation of RSV to neutrophils with abrogated TLR7 and/or -8 function might elucidate the exact contribution of TLR7 and -8 in RSV-induced cell survival in future experiments. The two non-structural proteins encoded by RSV, NS1 and NS2, also play a role in RSV-induced cell survival. SiRNA-mediated knockdown of NS1 and NS2 clearly accelerates apoptosis of RSV infected A549 cells and is associated with a reduced activation of the PI3K-PDPK-AKT-GSK3 pathway, as measured from 5-48h post infection [34]. In combination with the results of Thomas *et al.*, this suggests that activation of the PI3K-PDPK-AKT-GSK3 pathway occurs in at least two phases. Cell binding of RSV virions, that lack NS1 and NS2 proteins, leads to an early activation around 30 minutes post infection that is followed by a second activation by newly expressed NS1 and NS2 that are detectable from at least 5 hours post infection. Bitko and colleagues nicely demonstrated that RSV growth and apoptosis are inversely correlated, suggesting that RSV-induced cell survival is a selective advantage for RSV growth [34].

In addition to its role in delaying cell apoptosis early after RSV infection, PI3K signaling is also involved in the late stage of a RSV infection during assembly. Jeffree and colleagues investigated the interaction between the host cytoskeleton and RSV during assembly [88]. Inhibition of PI3K activity by the inhibitor LY294002 reduces the formation of viral filaments, without affecting F protein expression or the formation of inclusion bodies. These results were confirmed by treatment with NSC23766, an inhibitor against Rac1-GTPase, suggesting that a PI3K-Rac1 signaling pathway plays a specific role during the formation of viral filaments. Recently, PI3K-δ activity was also shown to be important for RSV-induced upregulation of B7-H1 (CD274), an immune inhibitory ligand suppressing T-cell activation and cytokine production, in BEAS-2B cells [89].

4.4 Reference list

1. Zhang, Y., et al., *Expression of respiratory syncytial virus-induced chemokine gene networks in lower airway epithelial cells revealed by cDNA microarrays.* J Virol, 2001. **75**(19): p. 9044-58.
2. Johnson, S.M., et al., *Respiratory Syncytial Virus Uses CX3CR1 as a Receptor on Primary Human Airway Epithelial Cultures.* PLoS Pathog, 2015. **11**(12): p. e1005318.
3. Tian, B., et al., *Identification of NF-kappaB-dependent gene networks in respiratory syncytial virus-infected cells.* J Virol, 2002. **76**(13): p. 6800-14.
4. Kong, X., et al., *Respiratory syncytial virus infection activates STAT signaling in human epithelial cells.* Biochem Biophys Res Commun, 2003. **306**(2): p. 616-22.
5. Martinez, I., et al., *Distinct gene subsets are induced at different time points after human respiratory syncytial virus infection of A549 cells.* J Gen Virol, 2007. **88**(Pt 2): p. 570-81.
6. Mayer, A.K., et al., *Differential recognition of TLR-dependent microbial ligands in human bronchial epithelial cells.* J Immunol, 2007. **178**(5): p. 3134-42.
7. Huang, Y.C., et al., *Identification of gene biomarkers for respiratory syncytial virus infection in a bronchial epithelial cell line.* Genomic Med, 2008. **2**(3-4): p. 113-25.
8. Zhou, Y., et al., *Respiratory syncytial virus infection modulates interleukin8 production in respiratory epithelial cells through a transcription factoractivator protein1 signaling pathway.* Mol Med Rep, 2014. **10**(3): p. 1443-7.
9. Janssen, R., et al., *Host transcription profiles upon primary respiratory syncytial virus infection.* J Virol, 2007. **81**(11): p. 5958-67.
10. Schuurhof, A., et al., *Gene expression differences in lungs of mice during secondary immune responses to respiratory syncytial virus infection.* J Virol, 2010. **84**(18): p. 9584-94.
11. Pennings, J.L., et al., *Systemic signature of the lung response to respiratory syncytial virus infection.* PLoS One, 2011. **6**(6): p. e21461.
12. Ravi, L.I., et al., *A systems-based approach to analyse the host response in murine lung macrophages challenged with respiratory syncytial virus.* BMC Genomics, 2013. **14**: p. 190.
13. Mosquera, R.A., et al., *Functional and immune response to respiratory syncytial virus infection in aged BALB/c mice: a search for genes determining disease severity.* Exp Lung Res, 2014. **40**(1): p. 40-9.
14. Ioannidis, I., et al., *Plasticity and virus specificity of the airway epithelial cell immune response during respiratory virus infection.* J Virol, 2012. **86**(10): p. 5422-36.
15. Fjaerli, H.O., et al., *Whole blood gene expression in infants with respiratory syncytial virus bronchiolitis.* BMC Infect Dis, 2006. **6**: p. 175.
16. Bucasas, K.L., et al., *Global gene expression profiling in infants with acute respiratory syncytial virus broncholitis demonstrates systemic activation of interferon signaling networks.* Pediatr Infect Dis J, 2013. **32**(2): p. e68-76.
17. Mejias, A., et al., *Whole blood gene expression profiles to assess pathogenesis and disease severity in infants with respiratory syncytial virus infection.* PLoS Med, 2013. **10**(11): p. e1001549.
18. Rosebeck, S. and D.W. Leaman, *Mitochondrial localization and pro-apoptotic effects of the interferon-inducible protein ISG12a.* Apoptosis, 2008. **13**(4): p. 562-72.
19. Brand, H.K., et al., *Olfactomedin 4 Serves as a Marker for Disease Severity in Pediatric Respiratory Syncytial Virus (RSV) Infection.* PLoS One, 2015. **10**(7): p. e0131927.
20. van den Kieboom, C.H., et al., *Nasopharyngeal gene expression, a novel approach to study the course of respiratory syncytial virus infection.* Eur Respir J, 2015. **45**(3): p. 718-25.
21. Jong, V.L., et al., *Transcriptome assists prognosis of disease severity in respiratory syncytial virus infected infants.* Sci Rep, 2016. **6**: p. 36603.
22. Dapat, C. and H. Oshitani, *Novel insights into human respiratory syncytial virus-host factor interactions through integrated proteomics and transcriptomics analysis.* Expert Rev Anti Infect Ther, 2016. **14**(3): p. 285-97.

23. Brasier, A.R., et al., *Nuclear heat shock response and novel nuclear domain 10 reorganization in respiratory syncytial virus-infected a549 cells identified by high-resolution two-dimensional gel electrophoresis.* J Virol, 2004. **78**(21): p. 11461-76.
24. Jamaluddin, M., et al., *Role of peroxiredoxin 1 and peroxiredoxin 4 in protection of respiratory syncytial virus-induced cysteinyl oxidation of nuclear cytoskeletal proteins.* J Virol, 2010. **84**(18): p. 9533-45.
25. van Diepen, A., et al., *Quantitative proteome profiling of respiratory virus-infected lung epithelial cells.* J Proteomics, 2010. **73**(9): p. 1680-93.
26. Hastie, M.L., et al., *The human respiratory syncytial virus nonstructural protein 1 regulates type I and type II interferon pathways.* Mol Cell Proteomics, 2012. **11**(5): p. 108-27.
27. Munday, D.C., et al., *Quantitative proteomic analysis of A549 cells infected with human respiratory syncytial virus.* Mol Cell Proteomics, 2010. **9**(11): p. 2438-59.
28. Munday, D.C., J.A. Hiscox, and J.N. Barr, *Quantitative proteomic analysis of A549 cells infected with human respiratory syncytial virus subgroup B using SILAC coupled to LC-MS/MS.* Proteomics, 2010. **10**(23): p. 4320-34.
29. Gibbs, J.D., et al., *Cell cycle arrest by transforming growth factor beta1 enhances replication of respiratory syncytial virus in lung epithelial cells.* J Virol, 2009. **83**(23): p. 12424-31.
30. Munday, D.C., et al., *Proteomic analysis of mitochondria in respiratory epithelial cells infected with human respiratory syncytial virus and functional implications for virus and cell biology.* J Pharm Pharmacol, 2015. **67**(3): p. 300-18.
31. Ternette, N., et al., *Label-free quantitative proteomics reveals regulation of interferon-induced protein with tetratricopeptide repeats 3 (IFIT3) and 5'-3'-exoribonuclease 2 (XRN2) during respiratory syncytial virus infection.* Virol J, 2011. **8**(1): p. 442.
32. Dave, K.A., et al., *A comprehensive proteomic view of responses of A549 type II alveolar epithelial cells to human respiratory syncytial virus infection.* Mol Cell Proteomics, 2014. **13**(12): p. 3250-69.
33. Monick, M.M., et al., *Activation of the epidermal growth factor receptor by respiratory syncytial virus results in increased inflammation and delayed apoptosis.* J Biol Chem, 2005. **280**(3): p. 2147-58.
34. Bitko, V., et al., *Nonstructural proteins of respiratory syncytial virus suppress premature apoptosis by an NF-kappaB-dependent, interferon-independent mechanism and facilitate virus growth.* J Virol, 2007. **81**(4): p. 1786-95.
35. Currier, M.G., et al., *EGFR Interacts with the Fusion Protein of Respiratory Syncytial Virus Strain 2-20 and Mediates Infection and Mucin Expression.* PLoS Pathog, 2016. **12**(5): p. e1005622.
36. Krzyzaniak, M.A., et al., *Host cell entry of respiratory syncytial virus involves macropinocytosis followed by proteolytic activation of the F protein.* PLoS Pathog, 2013. **9**(4): p. e1003309.
37. Hirakawa, S., et al., *Marked induction of matrix metalloproteinase-10 by respiratory syncytial virus infection in human nasal epithelial cells.* J Med Virol, 2013. **85**(12): p. 2141-50.
38. Kalinowski, A., et al., *EGFR activation suppresses respiratory virus-induced IRF1-dependent CXCL10 production.* Am J Physiol Lung Cell Mol Physiol, 2014. **307**(2): p. L186-96.
39. Monick, M., et al., *Respiratory syncytial virus infection results in activation of multiple protein kinase C isoforms leading to activation of mitogen-activated protein kinase.* J Immunol, 2001. **166**(4): p. 2681-7.
40. Kong, X., et al., *ERK-1/2 activity is required for efficient RSV infection.* FEBS Lett, 2004. **559**(1-3): p. 33-8.
41. Monick, M.M., et al., *Sphingosine kinase mediates activation of extracellular signal-related kinase and Akt by respiratory syncytial virus.* Am J Respir Cell Mol Biol, 2004. **30**(6): p. 844-52.
42. Johnson, T.R., J.S. McLellan, and B.S. Graham, *Respiratory syncytial virus glycoprotein G interacts with DC-SIGN and L-SIGN to activate ERK1 and ERK2.* J Virol, 2012. **86**(3): p. 1339-47.

43. Marchant, D., et al., *Toll-like receptor 4-mediated activation of p38 mitogen-activated protein kinase is a determinant of respiratory virus entry and tropism.* J Virol, 2010. **84**(21): p. 11359-73.
44. Seki, E., et al., *Cytokine profiles, signalling pathways and effects of fluticasone propionate in respiratory syncytial virus-infected human foetal lung fibroblasts.* Cell Biol Int, 2013. **37**(4): p. 326-39.
45. Shin, H.B., et al., *Inhibition of respiratory syncytial virus replication and virus-induced p38 kinase activity by berberine.* Int Immunopharmacol, 2015. **27**(1): p. 65-8.
46. Fricke, J., et al., *p38 and OGT sequestration into viral inclusion bodies in cells infected with human respiratory syncytial virus suppresses MK2 activities and stress granule assembly.* J Virol, 2013. **87**(3): p. 1333-47.
47. Meusel, T.R. and F. Imani, *Viral induction of inflammatory cytokines in human epithelial cells follows a p38 mitogen-activated protein kinase-dependent but NF-kappa B-independent pathway.* J Immunol, 2003. **171**(7): p. 3768-74.
48. Choi, M.S., et al., *A novel p38 mitogen activated protein kinase (MAPK) specific inhibitor suppresses respiratory syncytial virus and influenza A virus replication by inhibiting virus-induced p38 MAPK activation.* Biochem Biophys Res Commun, 2016. **477**(3): p. 311-6.
49. McCaskill, J.L., et al., *Broad-Spectrum Inhibition of Respiratory Virus Infection by MicroRNA Mimics Targeting p38 MAPK Signaling.* Mol Ther Nucleic Acids, 2017. **7**: p. 256-266.
50. Stewart, M.J., et al., *c-Jun N-terminal kinase negatively regulates dsRNA and RSV induction of tumor necrosis factor- alpha transcription in human epithelial cells.* J Interferon Cytokine Res, 2006. **26**(8): p. 521-33.
51. Dey, N., et al., *TAK1 regulates NF-KappaB and AP-1 activation in airway epithelial cells following RSV infection.* Virology, 2011. **418**(2): p. 93-101.
52. Caly, L., et al., *c-Jun N-terminal kinase activity is required for efficient respiratory syncytial virus production.* Biochem Biophys Res Commun, 2017. **483**(1): p. 64-68.
53. Mayati, A., et al., *Protein Kinases C-Mediated Regulations of Drug Transporter Activity, Localization and Expression.* Int J Mol Sci, 2017. **18**(4).
54. Bitko, V. and S. Barik, *Persistent activation of RelA by respiratory syncytial virus involves protein kinase C, underphosphorylated IkappaBbeta, and sequestration of protein phosphatase 2A by the viral phosphoprotein.* J Virol, 1998. **72**(7): p. 5610-8.
55. San-Juan-Vergara, H., et al., *Protein kinase C-alpha activity is required for respiratory syncytial virus fusion to human bronchial epithelial cells.* J Virol, 2004. **78**(24): p. 13717-26.
56. Arnold, R. and W. Konig, *Respiratory syncytial virus infection of human lung endothelial cells enhances selectively intercellular adhesion molecule-1 expression.* J Immunol, 2005. **174**(11): p. 7359-67.
57. Ennaciri, J., R. Ahmad, and J. Menezes, *Interaction of monocytic cells with respiratory syncytial virus results in activation of NF-kappaB and PKC-alpha/beta leading to up-regulation of IL-15 gene expression.* J Leukoc Biol, 2007. **81**(3): p. 625-31.
58. Masaki, T., et al., *A nuclear factor-kappaB signaling pathway via protein kinase C delta regulates replication of respiratory syncytial virus in polarized normal human nasal epithelial cells.* Mol Biol Cell, 2011. **22**(13): p. 2144-56.
59. Gschwendt, M., et al., *Rottlerin, a novel protein kinase inhibitor.* Biochem Biophys Res Commun, 1994. **199**(1): p. 93-8.
60. Rezaee, F., et al., *Sustained protein kinase D activation mediates respiratory syncytial virus-induced airway barrier disruption.* J Virol, 2013. **87**(20): p. 11088-95.
61. Storz, P., H. Doppler, and A. Toker, *Protein kinase Cdelta selectively regulates protein kinase D-dependent activation of NF-kappaB in oxidative stress signaling.* Mol Cell Biol, 2004. **24**(7): p. 2614-26.
62. Olala, L.O., et al., *Protein kinase C and Src family kinases mediate angiotensin II-induced protein kinase D activation and acute aldosterone production.* Mol Cell Endocrinol, 2014. **392**(1-2): p. 173-81.

63. Brandlin, I., et al., *Protein kinase C (PKC)eta-mediated PKC mu activation modulates ERK and JNK signal pathways.* J Biol Chem, 2002. **277**(8): p. 6490-6.
64. Yuan, J., et al., *Protein kinase D is a downstream target of protein kinase Ctheta.* Biochem Biophys Res Commun, 2002. **291**(3): p. 444-52.
65. Kelley, L.C., et al., *Cortactin phosphorylated by ERK1/2 localizes to sites of dynamic actin regulation and is required for carcinoma lamellipodia persistence.* PLoS One, 2010. **5**(11): p. e13847.
66. Campbell, D.H., R.L. Sutherland, and R.J. Daly, *Signaling pathways and structural domains required for phosphorylation of EMS1/cortactin.* Cancer Res, 1999. **59**(20): p. 5376-85.
67. Grassart, A., et al., *Pak1 phosphorylation enhances cortactin-N-WASP interaction in clathrin-caveolin-independent endocytosis.* Traffic, 2010. **11**(8): p. 1079-91.
68. Kolokoltsov, A.A., et al., *Small interfering RNA profiling reveals key role of clathrin-mediated endocytosis and early endosome formation for infection by respiratory syncytial virus.* J Virol, 2007. **81**(14): p. 7786-800.
69. San-Juan-Vergara, H., et al., *Cholesterol-rich microdomains as docking platforms for respiratory syncytial virus in normal human bronchial epithelial cells.* J Virol, 2012. **86**(3): p. 1832-43.
70. Thumkeo, D., S. Watanabe, and S. Narumiya, *Physiological roles of Rho and Rho effectors in mammals.* Eur J Cell Biol, 2013. **92**(10-11): p. 303-15.
71. Pastey, M.K., J.E. Crowe, Jr., and B.S. Graham, *RhoA interacts with the fusion glycoprotein of respiratory syncytial virus and facilitates virus-induced syncytium formation.* J Virol, 1999. **73**(9): p. 7262-70.
72. Pastey, M.K., et al., *A RhoA-derived peptide inhibits syncytium formation induced by respiratory syncytial virus and parainfluenza virus type 3.* Nat Med, 2000. **6**(1): p. 35-40.
73. Budge, P.J., J. Lebowitz, and B.S. Graham, *Antiviral activity of RhoA-derived peptides against respiratory syncytial virus is dependent on formation of peptide dimers.* Antimicrob Agents Chemother, 2003. **47**(11): p. 3470-7.
74. Budge, P.J., et al., *RhoA-derived peptide dimers share mechanistic properties with other polyanionic inhibitors of respiratory syncytial virus (RSV), including disruption of viral attachment and dependence on RSV G.* J Virol, 2004. **78**(10): p. 5015-22.
75. McLellan, J.S., et al., *Structure-based design of a fusion glycoprotein vaccine for respiratory syncytial virus.* Science, 2013. **342**(6158): p. 592-8.
76. Gower, T.L., et al., *RhoA is activated during respiratory syncytial virus infection.* Virology, 2001. **283**(2): p. 188-96.
77. Tsuji, T., et al., *ROCK and mDia1 antagonize in Rho-dependent Rac activation in Swiss 3T3 fibroblasts.* J Cell Biol, 2002. **157**(5): p. 819-30.
78. Gower, T.L., et al., *RhoA signaling is required for respiratory syncytial virus-induced syncytium formation and filamentous virion morphology.* J Virol, 2005. **79**(9): p. 5326-36.
79. McCurdy, L.H. and B.S. Graham, *Role of plasma membrane lipid microdomains in respiratory syncytial virus filament formation.* J Virol, 2003. **77**(3): p. 1747-56.
80. Liljeroos, L., et al., *Architecture of respiratory syncytial virus revealed by electron cryotomography.* Proc Natl Acad Sci U S A, 2013. **110**(27): p. 11133-8.
81. Thorpe, L.M., H. Yuzugullu, and J.J. Zhao, *PI3K in cancer: divergent roles of isoforms, modes of activation and therapeutic targeting.* Nat Rev Cancer, 2015. **15**(1): p. 7-24.
82. Osaki, M., M. Oshimura, and H. Ito, *PI3K-Akt pathway: its functions and alterations in human cancer.* Apoptosis, 2004. **9**(6): p. 667-76.
83. Jacinto, E., et al., *SIN1/MIP1 maintains rictor-mTOR complex integrity and regulates Akt phosphorylation and substrate specificity.* Cell, 2006. **127**(1): p. 125-37.
84. Sarbassov, D.D., et al., *Phosphorylation and regulation of Akt/PKB by the rictor-mTOR complex.* Science, 2005. **307**(5712): p. 1098-101.

85. Thomas, K.W., et al., *Respiratory syncytial virus inhibits apoptosis and induces NF-kappa B activity through a phosphatidylinositol 3-kinase-dependent pathway.* J Biol Chem, 2002. **277**(1): p. 492-501.
86. Workman, P., et al., *Drugging the PI3 kinome: from chemical tools to drugs in the clinic.* Cancer Res, 2010. **70**(6): p. 2146-57.
87. Lindemans, C.A., et al., *Respiratory syncytial virus inhibits granulocyte apoptosis through a phosphatidylinositol 3-kinase and NF-kappaB-dependent mechanism.* J Immunol, 2006. **176**(9): p. 5529-37.
88. Jeffree, C.E., et al., *Ultrastructural analysis of the interaction between F-actin and respiratory syncytial virus during virus assembly.* Virology, 2007. **369**(2): p. 309-23.
89. Kan-o, K., et al., *PI3K-delta mediates double-stranded RNA-induced upregulation of B7-H1 in BEAS-2B airway epithelial cells.* Biochem Biophys Res Commun, 2013. **435**(2): p. 195-201.

Part II: Aims

RSV is a respiratory virus causing (severe) respiratory disease with a large impact on human health worldwide. Estimates on acute lower respiratory tract infections in children below 5 years of age demonstrate that RSV is the most important cause of lower respiratory tract disease in infants worldwide [1]. In the last years, RSV is also increasingly being recognized as an important respiratory pathogen for the elderly. Although RSV was discovered more than half a century ago, no effective vaccine has been approved to prevent RSV infections and associated disease. A vaccine trial with formalin-inactivated RSV in the early days turned out dramatically with enhanced disease in the vaccinated infants upon natural RSV infection and even two infants died [2]. To date, no effective therapeutic drug is available, limiting treatment options to mainly supportive care and oxygen supply. One humanized monoclonal antibody that targets the fusion protein of RSV, palivizumab (brand name Synagis®), is approved for prophylactic use in infants at increased risk of developing serious RSV disease. Palivizumab-induced protection, however, is only partial (55% reduction in hospitalization rate) and its high cost limits its use to infants at increased risk [3]. Therefore, there is a high need for the development of an effective vaccine and therapeutic drug(s), whose development have been hampered in part by the poor knowledge on the interaction of RSV with its host. For example, it is still debated how RSV enters the host cell and which cellular receptor(s) is (are) used during entry. A better understanding of the complex interplay between RSV and its host will help in the identification of novel candidate targets for antiviral drugs and the development of an effective RSV vaccine.

To gain more insight in the RSV infection cycle, we investigated the role of (a subset of) host genes during RSV infection. A first aim was to unravel phosphorylation-dependent signaling pathways activated and possibly exploited by a RSV infection. Therefore, we performed two high-throughput screens in parallel:

1) We evaluated the role of specific kinases in RSV infection by a gene by gene siRNA-based knockdown screen of the complete human kinome in a human lung epithelial cell line. We used a multiple-rounds-of-infection assay to cover all stages of the RSV infection cycle. We searched for kinases that either promote or counteract RSV infection. Primary hits were validated by testing different siRNAs per hit (redundancy). One kinase was further validated by confirming knockdown at mRNA and protein level and by evaluating phenotypic rescue. Finally, we generated a knockout cell line of this kinase through CRISPR/Cas9 technology.

2) We performed a mass spectrometry-based phosphoproteomics screen to identify RSV-induced (de)phosphorylation-events. To focus on the entry phase of RSV, we identified phosphorylation sites early after RSV infection (2 hours) and designed a strategy to discriminate attachment - from fusion-induced (de)phosphorylation-events. A selection of (de)phosphorylation-events were validated by using electrophoretic mobility shift assays.

A second aim was to identify protein-protein interactions of the two non-structural proteins of RSV, NS1 and NS2. Therefore, we used three different, complementary protein-protein interaction mapping techniques in parallel, *i.e.* proximity-based protein biotinylation (BioID), trapping of protein complexes

in virus-like particles (Virotrap) and antibody-mediated co-immunoprecipitation. A selection of candidate NS1 interactors identified by BioID were validated by co-immunoprecipitation. Finally, we compared our identified candidate NS1 and NS2 interactors with described NS1 and NS2 interactions from literature and determined the overlap between the three techniques.

Reference list

1. Nair, H., et al., *Global burden of acute lower respiratory infections due to respiratory syncytial virus in young children: a systematic review and meta-analysis.* Lancet, 2010. **375**(9725): p. 1545-55.
2. Kim, H.W., et al., *Respiratory syncytial virus disease in infants despite prior administration of antigenic inactivated vaccine.* Am J Epidemiol, 1969. **89**(4): p. 422-34.
3. *Palivizumab, a humanized respiratory syncytial virus monoclonal antibody, reduces hospitalization from respiratory syncytial virus infection in high-risk infants. The IMpact-RSV Study Group.* Pediatrics, 1998. **102**(3 Pt 1): p. 531-7.

Part III: Results

Chapter V

RNA interference screen to identify human kinases involved in RSV replication

Koen Sedeyn, Liesbet Martens, Marnik Vuylsteke, Bert Schepens and Xavier Saelens

Author contributions: K.S., B.S. and X.S. designed and discussed the experiments. K.S. performed the experiments. L.M. analysed the RNA sequencing data and M.V. did the statistical analysis.

5.1 Introduction

Protein kinases are a large family of enzymes that play crucial roles in the regulation of cellular signaling pathways. They do so by catalyzing the phosphorylation of protein substrates by transferring the gamma-phosphate group from ATP to certain amino acid side chains in the substrate. In higher eukaryotes protein phosphorylation almost exclusively occurs on serine, threonine and tyrosine residues, although some examples of histidine or aspartate phosphorylation are known in animals [1-3]. In 2002, Manning and colleagues described the human protein kinome consisting of 518 protein kinases, as the complete human genome sequence became available [4]. These 518 protein kinases can be subdivided phylogenetically into 7 groups: the tyrosine kinases (TK) and 6 groups of serine/threonine kinases: tyrosine kinase-like (TKL), sterile (STE), casein kinase (CK) 1, the PRKA, PRKG and PRKC subfamilies (AGC), the calcium/Calmodulin-dependent protein kinases (CAMK) and the CDK, MAPK, GSK3 and CLK subfamilies (CMGC) (Fig. 1). Most kinases contain an activation loop at the opening of the active site that regulates the activity of the kinase [5]. Often, the conformation of the activation loop is regulated itself by phosphorylation. Two types of activation loops have been identified [6]. First, the bifunctional gated activation loops, which regulate both substrate binding and phosphotransfer. Typically these loops block the active site in an unphosphorylated state and undergo a conformational change upon phosphorylation, which liberates the active site. Secondly, the non-gated activation loops only regulate the phosphotransfer, while substrate binding in the active site is irrespective of the phosphorylation status of the activation loop. Protein kinases are an important category of proteins for the development of inhibitory drugs, especially since most cancers are characterized by aberrant kinase activities. Currently, 37 kinase inhibitors have been approved by the United States food and drug administration, mainly for the treatment of different types of cancer [7]. The majority of these kinase inhibitors were approved in the last decade, highlighting the recent, fast progress in the development of kinase inhibitors (Fig. 2).

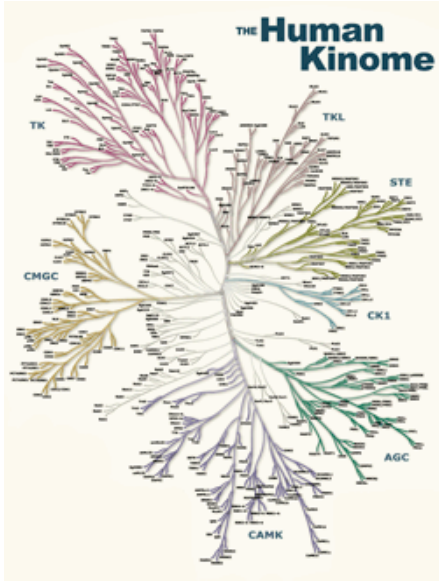

Figure 1: Phylogenetic tree of the human protein kinome. TK: tyrosine kinases, TKL: tyrosine kinase like, STE: sterile, CK1: casein kinase 1, AGC: containing PRKA, PRKG and PRKC, CAMK: Calcium and Calmodulin-dependent kinases, CMGC: containing CDK, MAPK, GSK3 and CLK. Figure taken from [16].

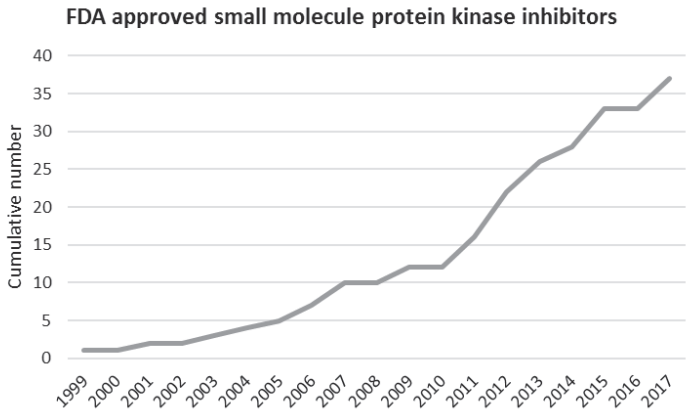

Figure 2: FDA approved small molecule protein kinase inhibitors. The Y-axis represents the cumulative number of inhibitors from 1999 to august 2017. List of inhibitors used from [7].

Although some kinase-dependent signaling pathways have been shown to be activated during RSV infection, *e.g.* EGFR, RhoA, PI3K, PRKC signaling (see chapter 4.3 for more details), a comprehensive analysis of the human kinome during RSV infection has not been published. To study kinases, small compound inhibitors are often used to inhibit specific kinases or families of kinases. Yet, these inhibitors have intrinsic disadvantages. Some of these inhibitors appear to be less specific than initially thought, which may lead to the wrong assignment of a biological response to a particular kinase. Additionally, conservation of the active site between isoforms of the same kinase family may lead to the failure of a kinase inhibitor to discriminate between different kinase isoforms. Small compound kinase inhibitors are also mostly limited to well-known kinases involved in major cellular signaling pathways. Some of these issues may be overcome by RNAi technology, which in principle allows to discriminate between closely related kinase isoforms. In addition, siRNA libraries are commercially available that can target the RNA of any known human kinase and thus there is no bias for well-studied kinases.

To explore the role of all known human kinases during RSV infection, we knocked down each human kinase one by one using RNAi technology followed by multiple rounds of RSV infection in a human lung epithelial cell line. Kinases with a pro- or antiviral role could subsequently be evaluated as candidate targets for the use of (approved) kinase inhibitors. Proviral kinases would be of particular interest as candidate targets for the development of a therapeutic small compound drug against RSV, whereas kinases that suppress RSV could be of interest in settings where enhanced virus replication is desired, *e.g.* production of a live-attenuated vaccine candidate.

5.2 Results

5.2.1 Experimental design

To explore host cell signaling pathways activated during the RSV infection cycle, a siRNA-mediated knockdown screen of the human kinome followed by a RSV infection was performed in a 96-well plate format. A high-throughput siRNA screen requires a stable cell line in which siRNA can be efficiently transfected. A549 cells, a human type II alveolar epithelial cell line, are easily transfected with siRNA and widely used in the RSV field. We first optimized a siRNA transfection/RSV infection protocol in A549 cells to maximize protein knockdown for prolonged experimental times. A549 cells were transfected with siRNA and then incubated for 48 hours, since knockdown at the protein level depends on the turnover time of a protein after siRNA-mediated degradation of the corresponding mRNA. At 48 hours post siRNA transfection, A549 cells were lysed to analyse protein levels by western blotting or infected with RSV. RSV replication was assessed with a semi-high-throughput read-out based on staining of plaques of RSV infected A549 cells in a 96-well format. As such, we covered all stages of the replication cycle from entry to budding. We used the lipid-based transfection reagent DharmaFECT-1 to deliver siRNAs in A549 cells as recommended by Dharmacon, the supplier of the human protein kinase siRNA library. The two human host genes nucleolin and PAK1 have been reported to play an important role during RSV infection. Nucleolin was identified as a possible receptor for RSV [8], whereas PAK1 regulates actin polymerization during cell entry [9-11]. SiRNA-mediated knockdown of nucleolin and PAK1 has been used to highlight their importance for RSV replication based on a single round of infection. We therefore included nucleolin and PAK1 siRNA knockdown as positive controls in our siRNA-mediated knockdown screen.

5.2.2 Optimization of siRNA-mediated knockdown in A549 cells

We optimized siRNA-mediated knockdown of nucleolin and PAK1 in A549 cells by using pools of 4 different siRNAs targeting each gene. In all experiments described below, where we included nucleolin and PAK1 knockdown, we used this pool of siRNAs. As negative controls, we treated A549 cells with culture medium only (untransfected), DharmaFECT-1 transfection reagent only (Dh 1) and a pool of 4 non-targeting (NT) siRNAs. These NT siRNAs were designed by Dharmacon to avoid, as much as possible, sequence homology with any human gene.

Optimization of cell numbers and concentration of siRNA transfection reagent

In order to maximize protein knockdown with the least possible cytotoxicity, we first optimized the number of A549 cells and the concentration of DharmaFECT-1. Increasing the concentration of DharmaFECT-1 generally increases knockdown efficiency, but at the cost of cell homeostasis which may lead to reduced cell growth. As we planned to infect siRNA transfected A549 cells with RSV, a confluent monolayer of A549 cells was desired at 48 hours post siRNA transfection. We seeded 3 amounts of A549 cells (7,500; 10,000 and 12,500 cells) in each well of a 96-well plate and transfected these with 3 dilutions of DharmaFECT-1 (1/500, 1/800 and 1/1200) in combination with 50 nM siRNA.

For both nucleolin and PAK1, we observed a clear correlation between knockdown efficiency on one hand and the number of A549 cells and DharmaFECT-1 concentration on the other hand. Increasing the number of A549 cells and increasing the dilution of DharmaFECT-1 reduced knockdown efficiency (Fig. 3A). For example, siRNA transfection of 7,500 A549 cells resulted in a complete knockdown of nucleolin and PAK1 irrespective of the DharmaFECT-1 dilution, whereas siRNA transfection of 12,500 cells resulted in a partial knockdown. Lysates from wild type, PAK1 - and PAK2 knockout mouse embryonic fibroblasts (MEFs) were used as a control to confirm the specificity of the PAK1-specific antibody used for detection of PAK1 by western blotting (Fig. 3A). As we obtained a confluent monolayer of A549 cells at 48 hours post siRNA transfection with 7,500 A549 cells, we selected this cell number and a DharmaFECT-1 dilution of 1/800 for subsequent experiments. This was slightly different from the Dharmacon recommendations for A549 cells (10.000 A549 cells, DharmaFECT-1 diluted 1/500).

Optimization of siRNA concentration

Since siRNA-mediated off-target silencing is concentration dependent [12, 13], we next investigated if lowering the siRNA concentration affected the knockdown efficiency of nucleolin in A549 cells. As shown in Fig. 3B, nucleolin expression was clearly reduced at a siRNA concentration of 25 and 50 nM, whereas nucleolin knockdown was not evident at a concentration of 5 nM. Note that the total amount of nucleolin in the NT siRNA transfected cells was lower in this experiment compared to the previous (Fig. 3A), which was caused by a reduced protein transfer during western blotting. As we initially planned to infect siRNA transfected A549 cells with RSV at 48 hours post siRNA transfection followed by 3 days of incubation to allow plaque formation, we investigated if nucleolin and PAK1 knockdown lasted until 5 days post siRNA transfection and if this was affected by the siRNA concentration. Knockdown of both nucleolin and PAK1 lasted at least until 5 days post siRNA transfection, independent of the used siRNA concentration (25 and 50 nM for nucleolin and 15 and 50 nM for PAK1)(Fig. 3C). As the number of A549 cells at 24 hours post siRNA transfection were only about half of the cell numbers in all later time points when the cells were confluent, we observed lower protein levels of nucleolin and PAK1 at 24 hours, which was also evident based on the lower actin protein levels. These results suggested that with our optimized siRNA transfection protocol, knockdown evaluated at the protein level would last during the complete RSV infection period from 2 until 5 days post siRNA transfection. To reduce the chance of off-target silencing while maintaining efficient knockdown, we selected a siRNA concentration of 15 nM to use in further experiments, unless otherwise stated.

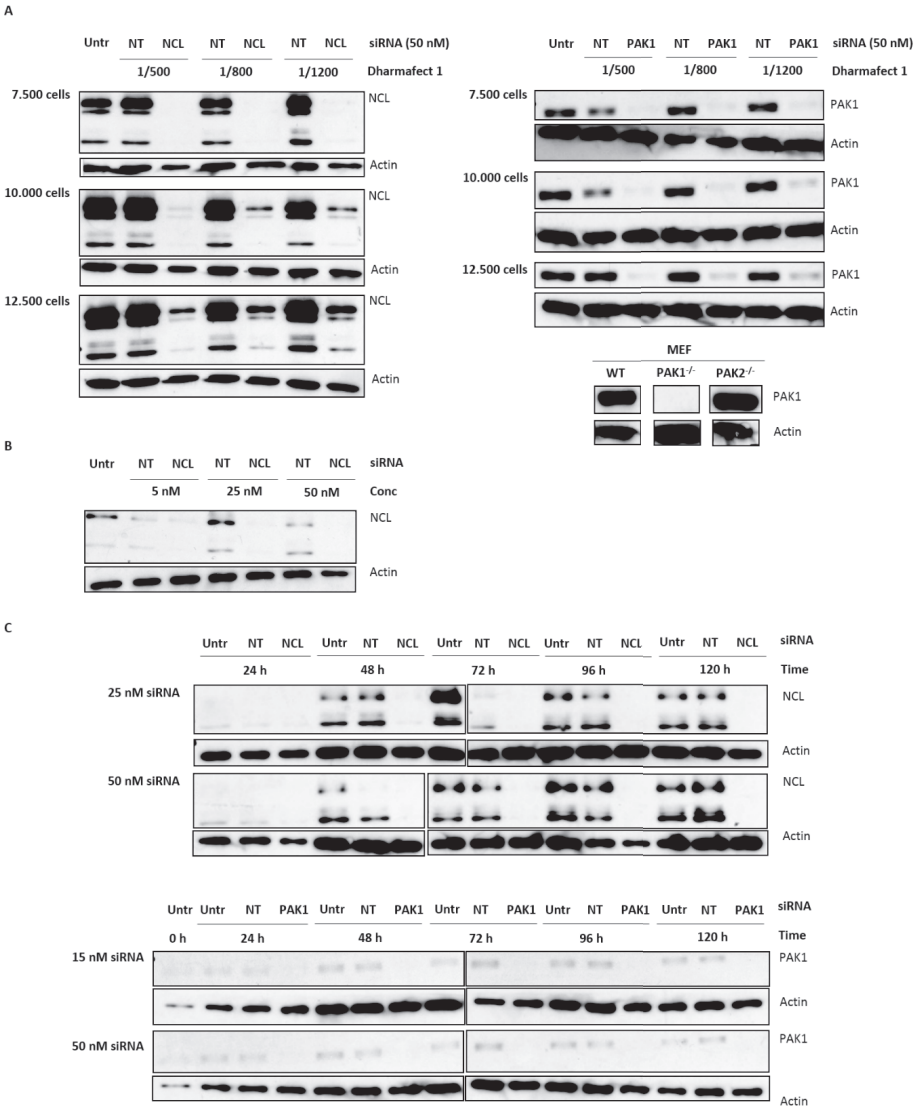

Figure 3: Optimization of siRNA transfection in A549 cells by evaluating nucleolin and PAK1 knockdown. A549 cells were seeded in 96-well plates and transfected with siRNAs the following day by using DharmaFECT-1 transfection reagent. SiRNA inocula were incubated on A549 cells for 48 hours after which lysates were prepared to detect nucleolin and PAK1 by western blotting. Actin detection was used as loading control. Untr = untransfected, NT = non-targeting siRNAs, NCL = nucleolin. (A) Optimization of the number of A549 cells at seeding (7,500; 10,000 or 12,500 cells) and dilution of DharmaFECT-1 (1/500, 1/800 or 1/1200). For PAK1, we tested lysates of wild type -, PAK1$^{-/-}$ - and PAK2$^{-/-}$ mouse embryonic fibroblasts (MEF) to confirm the specificity of the PAK1-specific antibody. (B) Optimization of the siRNA concentration with 7,500 cells at seeding and DharmaFECT-1 diluted 1/800. (C) Evaluation of the duration of knockdown from 1 to 5 days post siRNA transfection. Cell lysates were prepared at the indicated time post siRNA transfection.

Prolonged exposure to DharmaFECT-1 affects RSV plaque formation

To investigate the impact of our siRNA transfection protocol on RSV replication, we subsequently infected A549 cells at 48 hours post siRNA transfection with 50 plaque forming units (PFU) RSV-A2, a typical laboratory strain widely used in the RSV field. After 3 days, cells were fixed and RSV plaques were stained with a polyclonal goat anti-RSV serum directed against all RSV antigens. As the uptake of DharmaFECT-1/siRNA complexes is thought to be complete within 6 hours post siRNA transfection, we also investigated the impact of refreshing the culture medium at 6, 10, 24 and 48 hours post siRNA transfection on RSV plaque staining. RSV plaque morphology was affected by the duration of inoculating the DharmaFECT-1/siRNA complexes on A549 cells before replacing the culture medium (Fig. 4). If the siRNA inoculum was incubated for 24 or 48 hours, RSV plaque size was clearly enlarged compared to inoculation of 6 or 10 hours only. Likely, some cytotoxicity caused by prolonged exposure to DharmaFECT-1 affected RSV plaque formation, although we did not directly observe cytotoxicity by visual examination of A549 cell morphology during siRNA transfection. Replacing the siRNA inoculum 6 hours post transfection with fresh culture medium restored the normal RSV plaque phenotype (Fig. 4). We subsequently confirmed that nucleolin knockdown with replacement of the siRNA inoculum after 6 hours was as efficient as without replacement. Refreshing the siRNA inoculum after 6 hours resulted in a comparable nucleolin knockdown which lasted at least until 5 days post siRNA transfection (compare Fig. 5 with Fig. 3C). In summary, transfecting A549 cells for 6 hours with 15 nM siRNA and DharmaFECT-1 diluted 1/800 resulted in a strong knockdown of nucleolin which lasted at least until 5 days post siRNA transfection without clear cytotoxicity that affects RSV plaque formation.

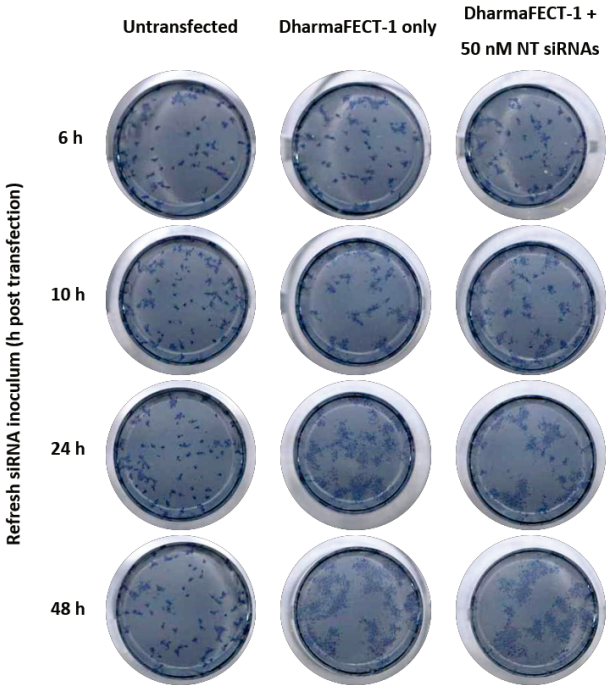

Figure 4: Prolonged exposure to DharmaFECT-1 affects RSV plaque formation. A549 cells (7,500) were seeded in 96-well plates and transfected with 50 nM siRNAs the following day by using DharmaFECT-1 transfection reagent (1/500). At different time points post siRNA transfection (6, 10, 24 or 48 hours), culture medium was refreshed. Forty-eight hours post siRNA transfection, cells were infected with 50 PFU RSV-A2 and fixed at 3 dpi. RSV plaques were stained with a polyclonal goat anti-RSV serum. NT = non-targeting.

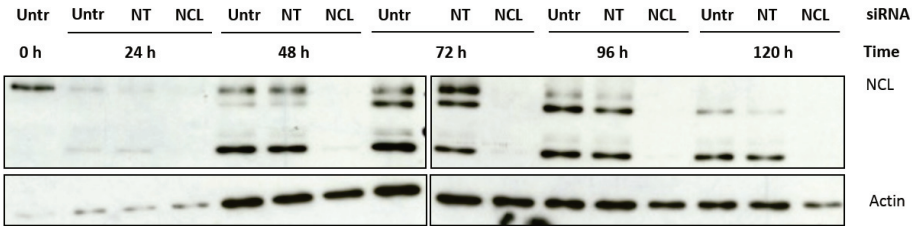

Figure 5: Knockdown of nucleolin is not affected by refreshing the culture medium at 6 hours post siRNA transfection. A549 cells (7,500) were seeded in 96-well plates and transfected with 15 nM siRNAs the following day by using DharmaFECT-1 transfection reagent (1/800). Six hours post siRNA transfection, culture medium was refreshed. Cell lysates were prepared at the indicated time post siRNA transfection. Nucleolin was detected by western blotting with actin staining as loading control. Untr = untransfected, NT = non-targeting, NCL = nucleolin.

Nucleolin and PAK1 knockdown does not reduce RSV plaque formation 3 days post infection (dpi)

We subsequently investigated if knockdown of nucleolin and PAK1 separately or combined reduced RSV plaque formation, *i.e.* a reduction in plaque numbers, - size and - intensity. We therefore infected A549 cells 48 hours post siRNA transfection with 80 PFU RSV-A2 for 3 days and immune-stained the fixed cells to visualize RSV plaques. As a positive control, we also transfected A549 cells with a RSV-nucleoprotein (RSV-N)-targeting siRNA. This RSV-N siRNA was designed to specifically target a conserved region in the nucleoprotein of RSV and was even evaluated in a phase IIb clinical trial in 2012 to evaluate its capacity to prevent bronchiolitis obliterans syndrome after RSV infection in lung transplant recipients [14, 15]. Note that in contrast to the pools of 4 siRNAs, the RSV-N siRNA was always used as a single siRNA at the same concentration of the total pools.

In comparison to negative control treated cells (untransfected, DharmaFECT-1 only and NT siRNAs), cells treated with siRNAs targeting nucleolin and PAK1 did not reduce the number, size or intensity of RSV plaques that were allowed to form until 3 dpi (Fig. 6A), despite a clear knockdown of nucleolin and PAK1 at 0 and 3 dpi (Fig. 6B). This result was in contrast to results from literature [8, 9], although we should remark that RSV replication was not measured in exactly the same way. We infected A549 cells with wild type RSV-A2 for about 3 rounds of infection before staining RSV plaques, whereas Tayyari *et al.* and Kolokoltsov *et al.* infected with a recombinant GFP expressing strain derived from RSV-A2 for one round of replication in 1HAEo- cells and HeLa cells, respectively, and counted the number of GFP positive cells. The RSV-N siRNA on the other hand clearly abolished the replication of RSV leading to a near complete absence of RSV plaques 3 dpi (Fig. 6A). To explore what caused the striking difference in reduction of RSV infection upon nucleolin and PAK1 knockdown, we tried to mimick the method of quantification of RSV infection used by Tayyari *et al.* and Kolokoltsov *et al.* as much as possible. Therefore, we infected siRNA transfected A549 cells with RSV-A2 for 24 hours (~ one round of replication) and stained RSV infected cells with a polyclonal goat anti-RSV serum for immunofluorescence-based imaging (Fig. 7). Additionally, we also investigated if flow cytometry could be used to quantify RSV infected cells after siRNA transfection (data not shown). Although we observed a reduction in the number of RSV infected cells after RSV-N siRNA transfection, this was not the case for nucleolin or PAK1 knockdown. These results suggested that the seemingly absent reduced RSV replication upon knockdown of nucleolin or PAK1 in our plaque assay of 3 days was not caused by the assay itself.

We decided to continue with our plaque assay as a read-out for RSV replication for several reasons. First, in our hands plaque assays were more compatible with semi-high-throughput screenings than immunofluorescence or flow cytometry. In particular, we did not make use of a high content automated imaging system but rather scored plaques or fluorescent foci manually. Flow cytometry on the other hand requires single cells, which makes stainings of large numbers of samples very labour-intensive. Secondly, RSV plaque formation requires multiple rounds of infection, meaning that all stages of the RSV infection cycle (entry, uncoating, replication, cytoskeleton-based transport, assembly, budding, cell-to-cell spreading) are covered. This is in contrast to immunofluorescence- or flow cytometry-based stainings of viral protein synthesis in a single round of infection, which only

partially covers the RSV infection cycle. Lastly, whereas RSV plaque formation was nearly completely abolished after RSV-N siRNA transfection, we could still detect RSV infected cells by immunofluorescence microscopy after RSV-N siRNA transfection, although the number of fluorescent foci was reduced by approximately 50% compared to the negative control set-ups (Fig. 6 and 7). This may indicate that inhibitory effects on RSV replication due to siRNA-mediated knockdown are amplified over multiple rounds of infection in a plaque assay in contrast to a single round of infection.

PAK1 and clathrin light chain B knockdown reduces RSV plaque size 5, 6 or 7 dpi

As knockdown of nucleolin and PAK1 did not reduce RSV plaque formation at 3 dpi, we looked for another host cell target that could serve as a positive control. We tested if RSV plaque formation was reduced after knockdown of a third host protein, clathrin light chain B (CLT B). CLT B was identified in the same screen as PAK1 and was proposed to be important for clathrin-mediated endocytosis during RSV entry as part of the clathrin triskelion [9]. Like PAK1, knockdown of CLT B significantly reportedly reduced RSV replication in a single round of infection. We also investigated if increasing the RSV infection period from 3 days to 5, 6 or 7 days would generate larger RSV plaques that may be more sensitive in detecting reduced RSV replication after host protein knockdown. We clearly observed that RSV plaque size increased with extending the RSV infection period, confirming that RSV plaque size is directly correlated to RSV replication (Fig. 8A). We observed a complete abolishment of RSV plaque formation after RSV-N siRNA transfection irrespective of the length of RSV infection (Fig. 8A). Knockdown of nucleolin, PAK1 and CLT B also reduced RSV plaque size in comparison to negative control treated cells at 5, 6 and 7 dpi (Fig. 8A). This was in contrast to the equal RSV plaque size at 3 dpi (Fig. 6A). We hypothesized that small reductions in RSV replication after knockdown of a host gene might require sufficient rounds of replication to observe a reduction in plaque size. Another explanation could be that not all cells are efficiently transfected with siRNA initially, which leads to clusters of non-transfected cells in the confluent monolayer by 48 hours post siRNA transfection. The reduced RSV plaque size after nucleolin knockdown was, however, only detected in this experiment and could not be reproduced in many subsequent experiments (see further). In parallel to staining RSV plaques, we also generated cell lysates to monitor knockdown of nucleolin, PAK1 and CLT B by western blotting. Knockdown of nucleolin, PAK1 and CLT B at least lasted until 7 dpi (~ 9 days post siRNA transfection) (Fig. 8B). In conclusion, knockdown of the host genes PAK1 or CLT B reduces the size of RSV plaques after 5 to 7 days of RSV infection. As the reduction in plaque size was most obvious at 6 dpi, we decided to infect siRNA transfected A549 cells for 6 days with RSV-A2 in our human kinase knockdown screen.

Conclusion

Transfection of A549 cells with 15 nM siRNA results in a clear protein knockdown at 48 hours post siRNA transfection, which lasts at least until 9 days post siRNA transfection. Cytotoxicity due to prolonged exposure to the siRNA inoculum can be avoided by refreshing the culture medium at 6 hours post siRNA transfection without affecting protein knockdown efficiency. Knockdown of host genes important for RSV replication most clearly reduce RSV plaque formation after multiple rounds of infection, e.g. 6 days post infection.

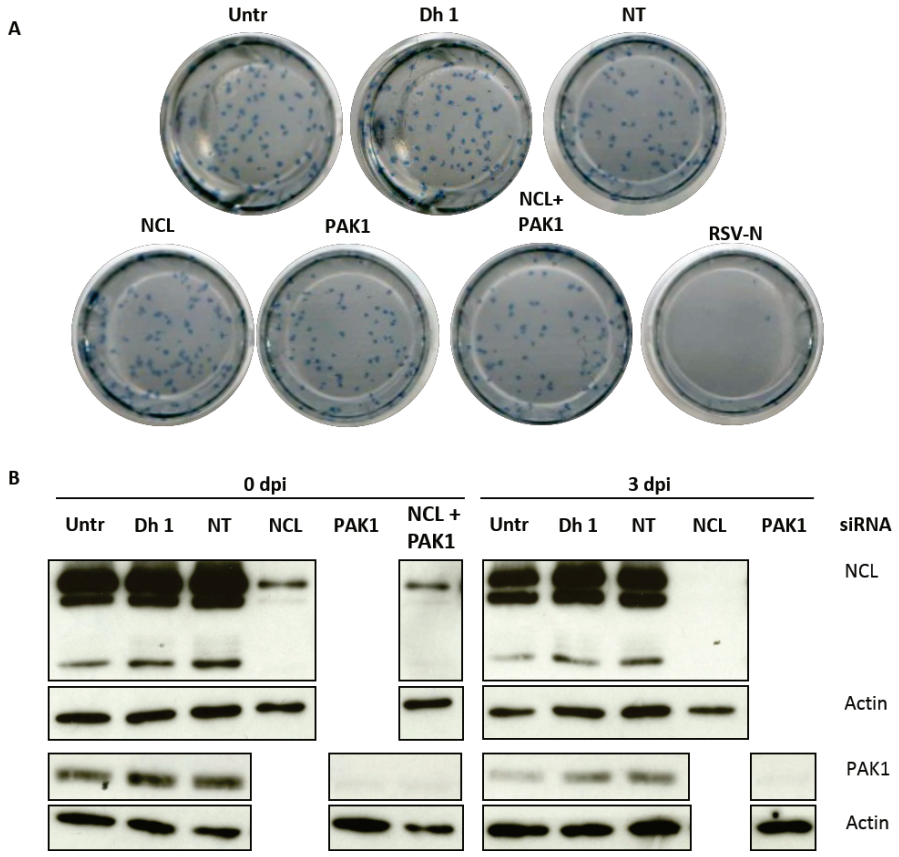

Figure 6: Nucleolin and PAK1 knockdown does not reduce RSV plaque formation 3 dpi. A549 cells (7,500) were seeded in 96-well plates and transfected with 15 nM siRNA by using DharmaFECT-1 (1/800). Six hours post siRNA transfection, culture medium was refreshed. At 48 hours post siRNA transfection, cells were infected with 80 PFU RSV-A2 for 3 days. (A) RSV plaque staining at 3 dpi. (B) Nucleolin and PAK1 detection by western blotting in lysates prepared 48 hours post siRNA transfection (0 dpi) and 5 days post siRNA transfection (3 dpi). Actin staining was used as loading control. Untr = untransfected, Dh 1 = DharmaFECT-1 only, NT = non-targeting, NCL = nucleolin.

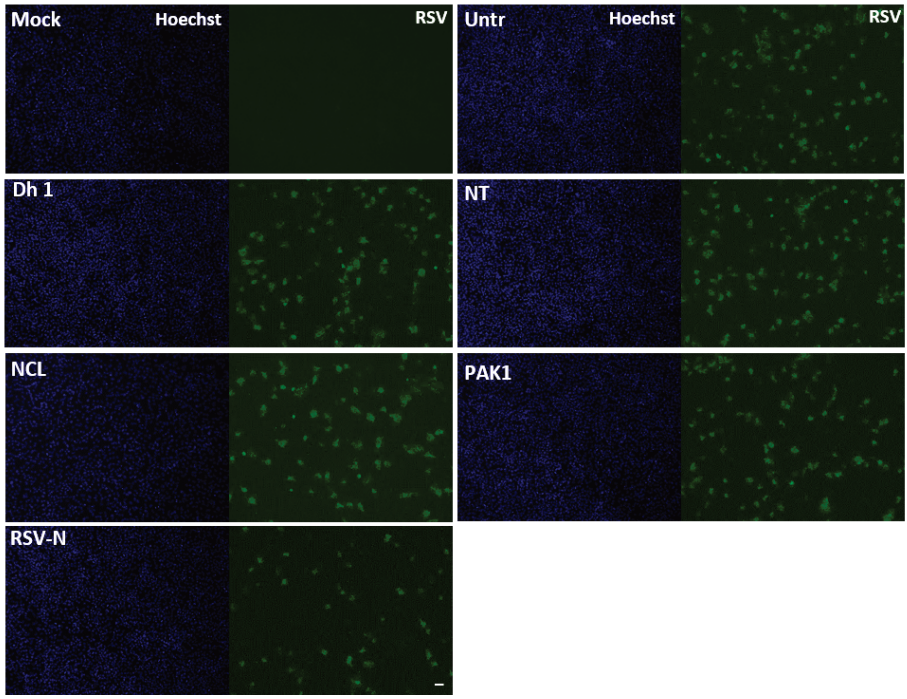

Figure 7: Nucleolin and PAK1 knockdown does not reduce the number of RSV infected cells as determined by immunofluorescence. A549 cells (7,500) were seeded in 96-well plates and transfected with 15 nM siRNA by using DharmaFECT-1 (1/800). Six hours post siRNA transfection, culture medium was refreshed. At 48 hours post siRNA transfection, cells were infected with RSV-A2 (MOI ~ 0,05) for 24 hours. As a control, untransfected A549 cells were mock infected in parallel (Mock, upper left). RSV infected cells were stained with a polyclonal goat anti-RSV serum. Cell nuclei were stained with Hoechst. Scale Bar = 50 µm.

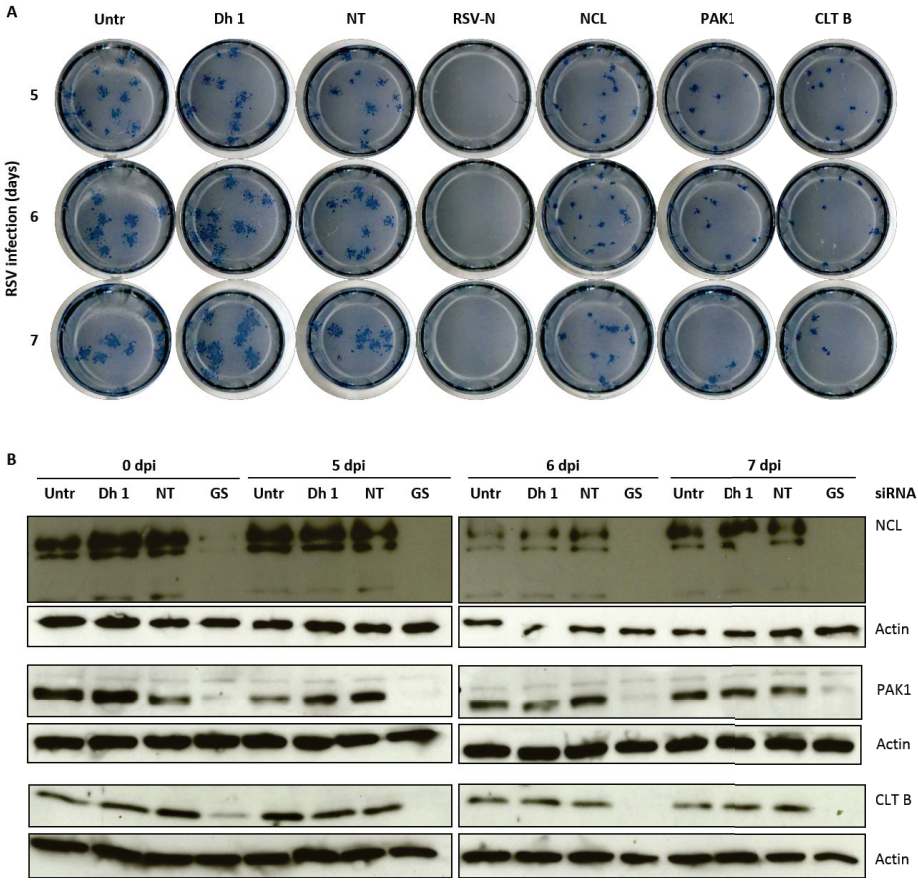

Figure 8: PAK1 and clathrin light chain B knockdown reduces RSV plaque size 5, 6 or 7 dpi. A549 cells (7,500) were seeded in 96-well plates and transfected with 15 nM siRNA by using DharmaFECT-1 (1/500). Six hours post siRNA transfection, culture medium was refreshed. At 48 hours post siRNA transfection, cells were infected with 50, 30 or 15 PFU RSV-A2 for 5, 6 or 7 days, respectively. (A) RSV plaque staining. (B) Nucleolin, PAK1 and clathrin light chain B detection by western blotting in lysates prepared 48 hours post siRNA transfection (0 dpi) and 5, 6 or 7 dpi. Actin staining was used as loading control. The reduced RSV plaque size after nucleolin knockdown was, however, only detected in this experiment and could not be reproduced in many subsequent experiments. Untr = untransfected, Dh 1 = DharmaFECT-1 only, NT = non-targeting, GS = gene specific, NCL = nucleolin, CLT B = clathrin light chain B.

5.2.3 SiRNA-mediated knockdown screen of human kinases during RSV infection

We purchased the *siGENOME®SMARTpool® siRNA library-Human protein Kinase* from Dharmacon. This library consists of pools of 4 different siRNAs per kinase, targeting 714 different human kinases that are divided over nine 96-well plates (80 kinases/plate, one kinase/well). Each siRNA consists of 2 complementary RNA strands that form a 19 base pair (bp) duplex with 2 overhanging dT nucleotides at the 3' end of each RNA strand. Dharmacon guarantees a knockdown of each kinase at mRNA level of at least 75% by 3 out of the 4 siRNAs used at 100 nM. The advantage of pooling siRNAs against a gene of interest is that the concentration of each individual siRNA can be reduced without affecting knockdown efficiency. Since off-target silencing depends on the siRNA concentration, it is believed that pooling siRNAs reduces the risk of off-target silencing. In 2002, Manning and colleagues published the human kinome, consisting of 518 protein kinases and 106 protein kinase pseudogenes [4]. An update of this initial kinome in 2007 lowered the number of pseudogenes to 102 [16]. The vast majority of the human kinome described by Manning *et al.* is targeted in the *siGENOME®SMARTpool® siRNA library-Human protein Kinase* from Dharmacon (502 of 518 protein kinases, Fig. 9). In addition, 212 human kinase genes that phosphorylate non-protein molecules are also targeted in the Dharmacon siRNA library. So in contrast to what the name of the library suggests, not only protein kinases, but also kinases that phosphorylate other substrates than proteins are targeted with this library. A complete list of protein kinases described by Manning *et al.* and kinases targeted by the *siGENOME® SMARTpool® siRNA library-Human protein kinase* from Dharmacon can be found on figshare (www.figshare.com, login: koen.sedeyn@vib-ugent.be, password: PhDKoenSedeynNov2017).

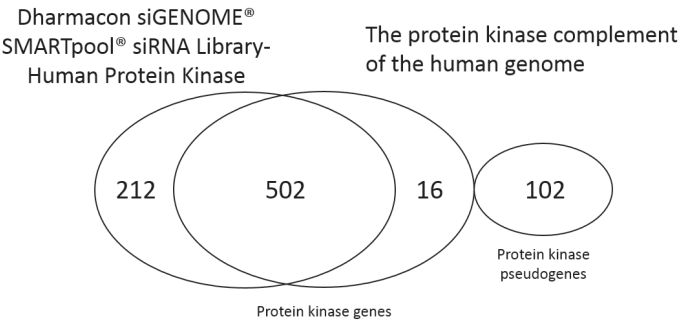

Figure 9: Unique and overlapping kinase genes in the Dharmacon siGENOME®SMARTpool® siRNA library-Human Protein kinase and the human protein kinase complement. The Human Protein kinase siRNA library consists of 714 kinases, whereas the human protein kinase complement consists of 518 kinases [4].

SiRNA-mediated knockdown screen based on RSV plaque quantification at 6 days post infection

As described in the previous section, a reduced RSV plaque size after knockdown of the human host genes PAK1 and CLT B was most obvious if RSV plaques were stained 6 dpi. Therefore, we performed a first siRNA-mediated knockdown screen of the human kinome with read-out by immune-staining of RSV plaques at 6 dpi (Fig. 10). We transfected the kinase siRNA library (15 nM siRNAs per well) in A549 cells in triplicate with on every 96-well plate the following controls in duplicate or triplicate: untransfected, DharmaFECT-1 only, NT -, nucleolin -, PAK1 -, CLT B siRNAs and RSV-N siRNA. To monitor for plate effects, we randomly distributed these controls over 2 non-adjacent rows. In addition, we did not use the outermost rows and columns of each 96-well plate to avoid any edge effects. The screen involved fifty-four 96-well plates in total, that were analysed in 9 separate experiments involving one plate from the kinase siRNA library at a time. Forty-eight hours post siRNA transfection, we infected these cells with 25 PFU RSV-A2. At 24 and 48 hours post siRNA transfection we visually monitored cell morphology for cytotoxicity. As depletion of the PLK1 protein in cancer cells strongly reduces cell proliferation and induces apoptosis, PLK1-targeting siRNAs are often used as controls in RNAi experiments to monitor siRNA transfection efficacy. As expected, we observed clear cytotoxicity in our siRNA-mediated knockdown screen after PLK1 siRNA transfection. Six days after RSV infection, the cells were fixed and RSV plaques were stained with a polyclonal goat anti-RSV serum. RSV plaque size was then visually compared to several replicates of negative control treated cells (untransfected, DharmaFECT-1 only, non-targeting siRNA) and scored as follows: if the plaque size was clearly reduced or increased in all three replicates, a green score was assigned. If the plaque size was clearly reduced or increased in two replicates or moderately reduced or increased in all three replicates, an orange score was assigned. Finally, if the plaque size was clearly reduced or increased in only one replicate or moderately reduced or increased in one or two replicates, a red score was assigned. The plaque size was scored by two researchers in a blind manner, *i.e.* without prior knowledge on the scores assigned by the other researcher, after which the scores were merged. Based on this scoring system we identified 191 kinases for which the siRNA-based knockdown was associated with a reduced RSV plaque size (green: 40, orange: 71 and red: 80), suggesting that these kinases or associated signaling pathways may be important during a RSV infection (Fig. 11, upper left oval; Suppl. table 1, which can also be found on figshare: www.figshare.com, login: koen.sedeyn@vib-ugent.be, password: PhDKoenSedeynNov2017). We also identified 55 kinases for which the siRNA-based knockdown was associated with an increased RSV plaque size (green: 25, orange: 25 and red: 5)(Fig. 11, lower left oval; Suppl. table 1), suggesting a possible antiviral role for these kinases or associated signaling pathways.

SiRNA-mediated knockdown screen based on RSV plaque quantification at 3 or 4 days post infection

Since the RSV plaque size after 6 days of infection was relatively large, observing an enhancement of plaque size was not always obvious. We therefore performed a second siRNA-mediated knockdown screen of the human kinome with staining of RSV plaques at 3 or 4 dpi (Fig. 10). Basically, this second screen was performed as the first screen, except that we infected with 60 PFU RSV-A2 and stained RSV plaques at 3 or 4 dpi (for 4 and 5 out of the nine 96-well plates from the kinase siRNA library, plaques

were stained at 3 and 4 dpi, respectively). We initially stained RSV plaques at 3 dpi, however, we observed smaller plaques than expected after analysing the first 4 kinase siRNA library plates. Therefore, we prolonged the RSV infection to 4 days for the remaining 5 kinase siRNA library plates. The same scoring system as described above was used to identify kinases that either increased or reduced RSV plaque size after knockdown. In this screen, which also involved fifty-four 96-well plates in total, we identified 31 kinases for which the siRNA-based knockdown was associated with a reduced RSV plaque size (green: 10, orange: 18, red: 3) (Fig. 11, upper right oval; Suppl. table 1). We also identified 76 kinases for which the siRNA-based knockdown was associated with an increased RSV plaque size (green: 45, orange: 26 and red: 5) (Fig. 11, lower right oval; Suppl. table 1). Note that some kinases with either reduced or increased RSV plaque size after knockdown were identified in both screens (Fig. 11, intersections). We also identified 14 kinases with opposite effects in both screens upon knockdown, *i.e.* reduced RSV plaque size in the screen of 6 dpi and increased RSV plaque size in the screen of 3/4 dpi (Suppl. table 1). Taken together, these results highlight a bias for the identification of kinases that reduced plaque size in the first knockdown screen (read-out of plaques 6 dpi) and kinases that increased plaque size in the second knockdown screen (read-out of plaques 3 or 4 dpi).

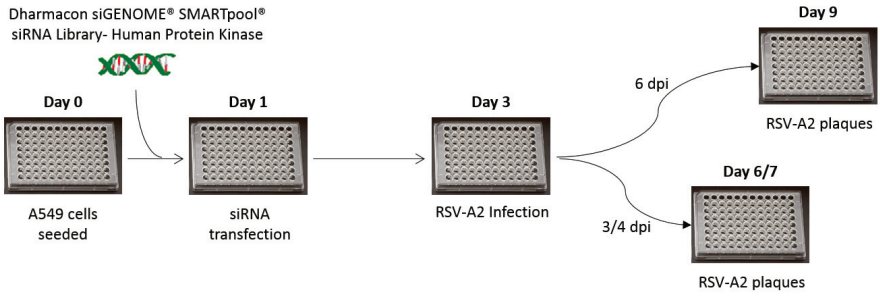

Figure 10: Experimental layout of the siRNA-mediated human kinome knockdown screen. A549 cells (6,000) were seeded in 96-well plates and transfected with the Dharmacon siGENOME®SMARTpool® siRNA library-Human Protein kinase (15 nM) in triplicate by using DharmaFECT-1 (1/800). Six hours post siRNA transfection, culture medium was refreshed. At 48 hours post siRNA transfection, cells were infected with RSV-A2 and RSV plaques were stained. The screen was performed twice: first we infected with 40 PFU for 6 days and secondly we infected with 120 PFU for 3 or 4 days.

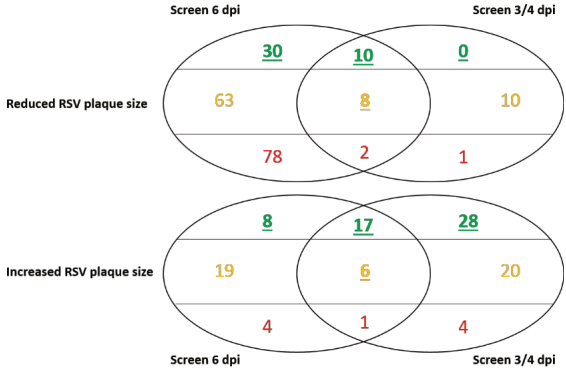

Figure 11: Number of primary hits in both siRNA-mediated human kinome knockdown screens. Kinases with a reduced or increased RSV plaque size upon knockdown were assigned a color score: Green: clear phenotype in all three replicates, Yellow: clear phenotype in two replicates or moderate phenotype in all three replicates and Red: clear phenotype in one replicate or moderate effect in one or two replicates. Kinase hits with a different color score in both screens were classified according to their best score.

SiRNA-mediated knockdown screen based on altered RSV replication kinetics as a read-out

To narrow down the number of kinases, we only retained kinases for which we found no evidence that their knockdown in A549 cells resulted in cytotoxicity and that either were assigned a green score in at least one of both screens or that received an orange score in both screens. As such, we retained 104 kinases to study further (Suppl. table 1: genes in bold). Since we hypothesized that RSV plaque size is a good proxy for the extent of RSV replication, we investigated RSV replication more quantitatively. Therefore, we transfected A549 cells in individual 96-wells in triplicate with 15 nM siRNAs targeting the 104 retained kinases. As before, positive control siRNAs targeting PAK1, CLT B and RSV-N were included. Forty-eight hours post siRNA transfection, we infected these cells with RSV-A2 (MOI ~ 0,003) and harvested cell culture supernatants daily from 2 until 5 or 6 days post infection. Subsequently we titrated the infectious RSV virions present in the harvested cell culture supernatants and plotted the titer in function of time (Suppl. Fig. 1: in order to not overload the graphs we only show the negative control treated cells, cells transfected with RSV-N, PAK1 and CLT B siRNAs and cells transfected with siRNAs targeting 10 selected kinases (see further)). As expected, knocking down RSV-N strongly reduced the RSV titer with on average 3-4 $\log_{10}$ units (Suppl. Fig. 1). CLT B and PAK1 knockdown on the other hand only modestly reduced the RSV titer about 1,5-3,0-fold (Suppl. Fig. 1a). We performed two statistical analyses on the kinetics of RSV replication after kinase knockdown. We compared the average titer over all time points and the slope of the RSV growth curve between negative control treated cells (untransfected, DharmaFECT-1 only and NT siRNA) and kinase siRNA treated cells. The first statistical analysis identified 40 kinases with an average RSV titer that was significantly ($p < 0,01$) different from the average titer of negative control treated cells (Suppl. table 2, which can also be found on figshare: www.figshare.com, login: koen.sedeyn@vib-ugent.be, password: PhDKoenSedeynNov2017). With the second statistical analysis, we identified 41 kinases with a

significantly ($p < 0,01$) different growth slope compared to negative control treated cells (Suppl. table 2). Of these kinases, 33 were significantly different in both statistical tests. Some kinases that were significantly different in one or both statistical tests had an opposite biological response for RSV plaque size and RSV kinetics. For example, knockdown of ERK8 significantly reduced the RSV titer as found in both statistical tests that were applied to the kinetics data, although we had observed an enlargement of the RSV plaque size when ERK8 was knocked down. Possibly, knockdown of these kinases had resulted in a degree of cytotoxicity, even though visual inspection of the cell monolayer by light microscopy over the course of the kinetics experiment did not suggest this, which could have resulted in an aberrant, large plaque staining. The kinases of which the knockdown resulted in such an intuitively contradictory outcome were excluded from further analysis.

We eventually selected 10 kinases, of which the knockdown was associated with both reduced RSV plaque size and new virus production over time or, alternatively, increased RSV plaque size and - titer, for further analysis (Table 1, Suppl. Fig. 1). Two of these kinases, CSNK1G1 and ephrin receptor B2 (EPHB2) were retained, despite the absence of statistical significance in the RSV kinetics. We did retain these kinases as literature-based evidence suggested that they might play a role during RSV infection. RSV-NS1 for example suppresses the expression of miR-24, which targets CSNK1G1 mRNA for degradation [17], whereas Ephrin receptors and - ligands have been shown to function as cellular receptors for different viruses such as the Henipah viruses and Kaposi's sarcoma-associated herpesvirus [18-20]. Knockdown of 3 kinases, anti-Mullerian hormone receptor type 2 (AMHR2), CSNK1G1 and tau tubulin kinase 1 (TTBK1), increased RSV plaque size and titer, suggesting that these kinases and/or associated signaling pathways have an antiviral role during a RSV infection. Knockdown of 7 kinases, EPHB2, interleukin-1 receptor-associated kinase 3 (IRAK3), myosin light chain kinase 4 (MYLK4), platelet derived growth factor receptor β (PDGFRB), phosphoinositide-3-kinase regulatory subunit 5 (PIK3R5), polynucleotide kinase 3'-phosphatase (PNKP) and protein kinase cAMP-activated catalytic subunit γ (PRKACG), reduced RSV plaque size and titer, suggesting that these kinases and/or associated signaling pathways promote a RSV infection.

Table 1: Selection of 10 kinase hits involved in RSV infection.

Gene Name	Gene ID	Plaque size	Kinetics		
		response	response	Statistical Analysis	
				1	2
AMHR2	269	+	+	n.s.	v
CSNK1G1	53944	+	+	n.s.	n.s.
TTBK1	84630	+	+	v	v
EPHB2	2048	-	-	n.s.	n.s.
IRAK3	11213	-	-	v	v
MYLK4	340156	-	-	v	v
PDGFRB	5159	-	-	v	v
PIK3R5	23533	-	-	v	v
PNKP	11284	-	-	v	v
PRKACG	5568	-	-	v	v

+ = increased, - = reduced

n.s. = not significant, v = significant ($p < 0,01$)

5.2.4 Validation of 10 selected human kinases by siRNA deconvolution

Since siRNAs can suppress mRNAs with partial sequence complementarity in a miRNA-like manner, off-target silencing should be carefully considered when analyzing siRNA knockdown results. A way of evaluating off-target silencing is to investigate siRNA knockdown phenotypes by different siRNAs targeting the same gene of interest. If knockdown of a gene of interest by at least two different siRNAs results in the same phenotype, then the phenotype is likely caused by the specific knockdown of the gene of interest. To investigate the on-target specificity of the 10 kinase siRNA pools described in table 1, we deconvoluted the siRNA pools and transfected A549 cells with 15 nM of the 4 different siRNAs separately per kinase for 48 hours. We also deconvoluted the non-targeting siRNA pool and tested non-targeting siRNA #2, #3 and #4. We excluded non-targeting siRNA #1 as it was reported by Dharmacon that it could reduce EGFR mRNA expression by 50% in a cell - and assay-dependent manner. It has been shown that RSV-F binds to the EGFR which induces EGFR phosphorylation in a strain-dependent manner [21]. To limit the workload in this experiment, we only included the RSV-N siRNA and not nucleolin, PAK1 or CLT B siRNAs. RSV plaques were stained either at 3 days post infection for kinases whose knockdown increased plaque size (AMHR2, CSNK1G1 and TTBK1) or at 6 days post infection for kinases whose knockdown reduced plaque size (EPHB2, IRAK3, MYLK4, PIK3R5, PDGFRB, PNKP and PRKACG). As shown in Fig. 12A, transfection of A549 cells with AMHR2 siRNA #1 and #2 moderately increased RSV plaque size compared to negative control treated cells. However, we should note that non-targeting siRNA #2 also increased RSV plaque size 3 days post infection in this experiment. For CSNK1G1, RSV plaque size was only increased by siRNA #4, which clearly caused cytotoxicity leading to enlarged plaque stainings. A549 cells transfected with TTBK1 siRNAs only showed a moderate increased RSV plaque size with siRNA #1. Taken together, the increased RSV plaque size observed after knockdown of CSNK1G1 and TTBK1 with the pool of 4 siRNAs could not be reproduced by at least 2 separate siRNAs from these pools, suggesting that off-target silencing by the single siRNA causing an increased plaque size may be responsible for this phenotype. Although knockdown of AMHR2 by 2 different siRNAs increased RSV plaque size, these effects were not very pronounced, so we decided to not further investigate the role of AMHR2 during RSV infection.

Knockdown of EPHB2 and PRKACG by none of the 4 siRNAs reduced RSV plaque size as we observed in the screens with the siRNA pools (Fig. 12B). For PDGFRB, PIK3R5 and PNKP we could only confirm a slight reduction of the RSV plaque size by one of the 4 siRNAs (siRNA #1 for PDGFRB and PNKP and siRNA #4 for PIK3R5). So likely, the reduced RSV plaque size after knockdown of PDGFRB, PIK3R5 and PNKP by the pool of 4 siRNAs in the screens was caused by this single siRNA. Hence, we could not exclude the possibility that those single siRNAs caused a reduced RSV plaque size by off-target silencing. The most convincing results were obtained for the interleukin-1 receptor-associated kinase 3 (IRAK3) and myosin light chain kinase 4 (MYLK4). In line with the Dharmacon guarantee that at least 3 out of the 4 siRNAs mediate knockdown of at least 75%, we could identify 3 siRNAs targeting IRAK3 and MYLK4 with a reduced RSV plaque size after knockdown. IRAK3 knockdown by siRNA #1 and #4 clearly reduced RSV plaque size, while knockdown by siRNA #2 moderately reduced RSV plaque size (Fig. 12B). For MYLK4, we observed a clear reduction of RSV plaque size after knockdown by siRNA #2,

#3 and #4. In this experiment, MYLK4 siRNA #1 did not reduce RSV plaque size. Taken together, knockdown of IRAK3 and MYLK4 by three different siRNAs reduced subsequent RSV plaque size, suggesting that on-target silencing of IRAK3 and MYLK4 causes a reduced RSV plaque size.

IRAK3 is one of the 4 members of the IRAK kinase family which are important in the Toll/IL-R signaling pathways. Upon activation of TLRs or the IL-1R by ligand binding, a multiprotein complex composed of the adaptor protein MyD88, IRAK2 and IRAK4 is recruited to the cytoplasmic tail of the TLR or IL-1R. This complex activates the downstream kinase IRAK1 by IRAK4-mediated phosphorylation of IRAK1. IRAK1 subsequently associates with TRAF6, which leads to the activation of NF-κB by activation of the IKK complex. IRAK1/TRAF6 can also activate JNK and p38 MAPK signaling. IRAK3 is a negative regulator of this pathway by suppressing the activation of IRAK4 and IRAK1 and is normally mainly expressed in monocytes and macrophages.

MYLK4 is one of the four members of the MYLK kinase family, a family of serine/threonine protein kinases. MYLK1, MYLK2 and MYLK3 are well-known kinases that phosphorylate the regulatory light chains of myosin, thereby facilitating the contractile activity in smooth -, skeletal - and cardiac muscle cells, respectively. Additionally, MYLK1 also regulates myosin activities in non-muscle cells. In contrast, information on specific functions of MYLK4 is currently lacking. Although it was assigned as a MYLK kinase based on sequence homology, it is not yet clear if MYLK4 phosphorylates the regulatory light chains of myosin as MYLK1-3 do. Looking back at our original screening data, we also found no evidence that knockdown of MYLK1 and MYLK3 affected RSV plaque size, whereas MYLK2 knockdown only reduced RSV plaque size in the screen at 3 dpi (where it was assigned an orange score). MYLK2, however, was not investigated in the RSV replication kinetics.

We decided to investigate the role of IRAK3 and MYLK4 during a RSV infection further.

A

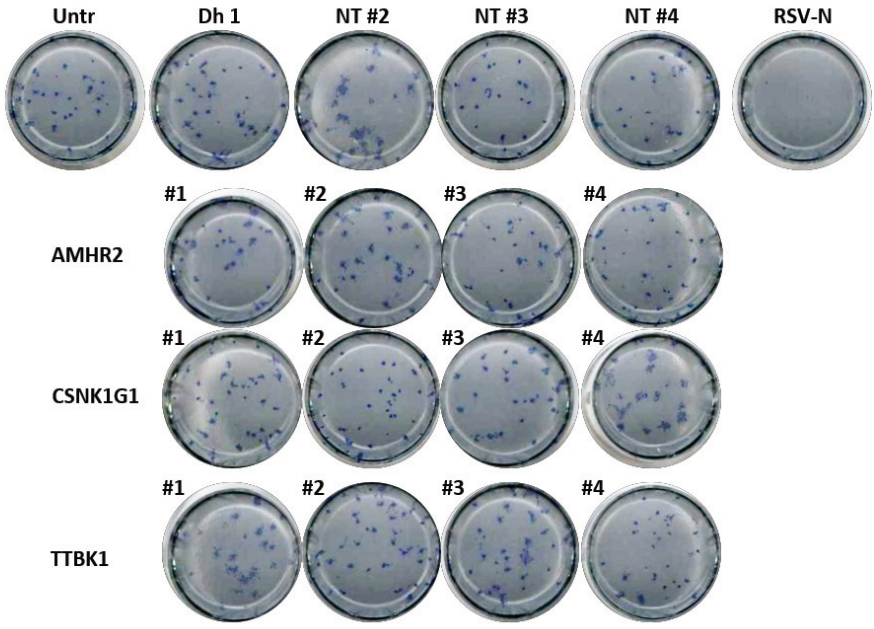

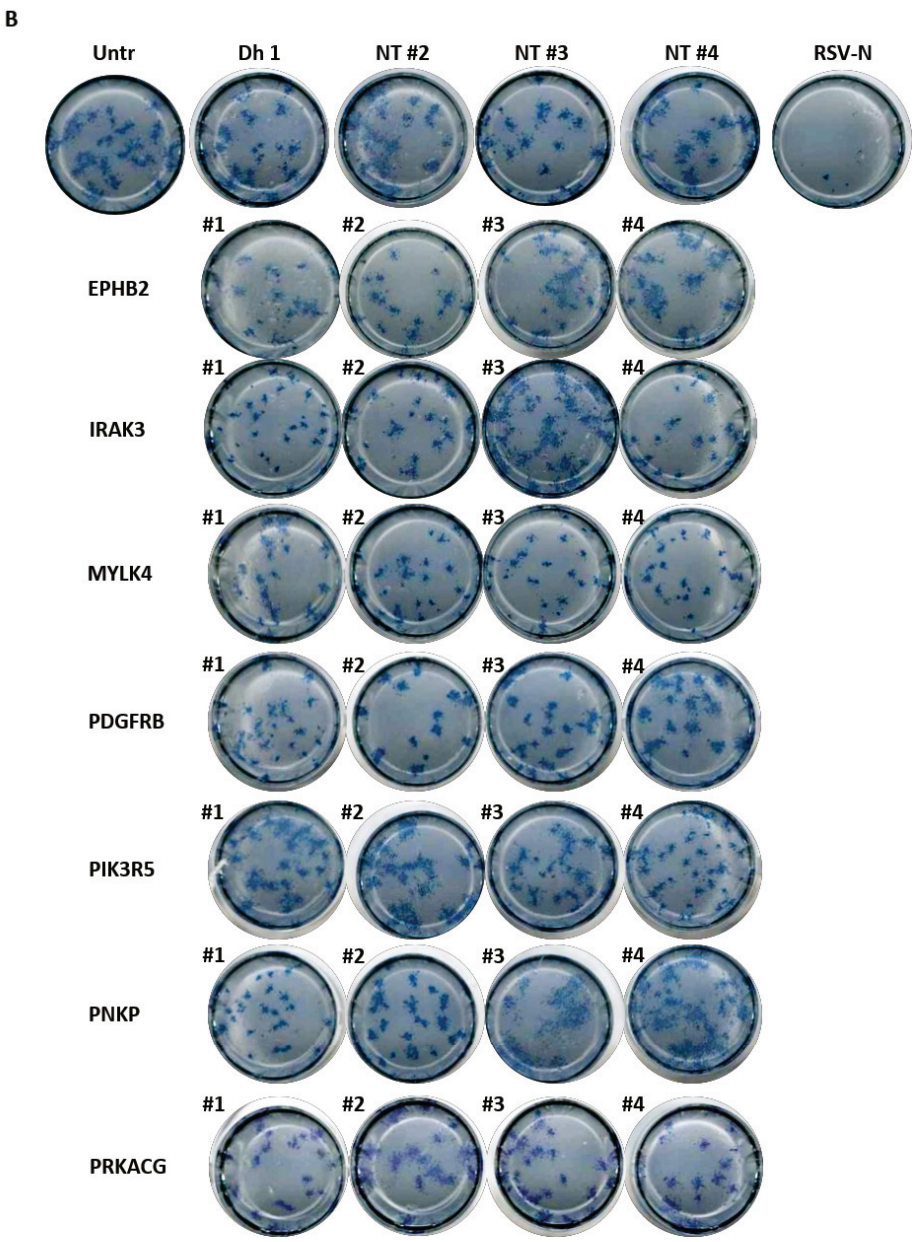

Figure 12: Validation of 10 selected kinases by siRNA pool deconvolution. A549 cells were seeded in 96-well plates and transfected with 15 nM individual siRNA by using DharmaFECT-1 (1/800). Six hours post siRNA transfection, culture medium was refreshed. At 48 hours post siRNA transfection, cells were infected with 35 PFU RSV-A2 for 3 days (A) or 6 days (B).

5.2.5 Validation of the potential proviral function of the kinases IRAK3 and MYLK4

Knockdown of IRAK3 and MYLK4 does not reduce RSV plaque size in two other immortalized, stable cell lines

We investigated if IRAK3 and MYLK4 knockdown also reduced RSV plaque size in other immortalized, stable cell lines than A549 cells. We first tested if several human cell lines, *i.e.* HeLa, HEp-2 and Calu-1 cells, were efficiently transfectable with siRNA by DharmaFECT-1 by investigating nucleolin knockdown. We should remark that HEp-2 cells originate from a HeLa cell contamination and not from a carcinoma of the larynx as initially thought (information from ATCC). Nevertheless, we tested both HeLa and HEp-2 cells as they evolved separately in the last decades. Calu-1 cells originate from a human metastasis of the pleura of the lung. SiRNA transfection in HeLa and Calu-1 cells appeared to be as efficient as in A549 cells since we observed a strong reduction of nucleolin expression in these cells after siRNA-mediated knockdown of this target (Fig. 13A). HEp-2 cells on the other hand only showed a moderate nucleolin knockdown, suggesting that siRNA transfection was less efficient in these cells compared to A549 cells. In contrast to our previous experience in RSV permissive HEp-2 cells and HeLa cells, we had no experience with RSV infections of Calu-1 cells. Based on literature, we found that Calu-3 cells are RSV permissive [22], but we could not find any publication describing RSV infections in Calu-1 cells. Therefore, we tested if Calu-1 cells were RSV permissive. Whereas HeLa cells and HEp-2 cells were easily infected by RSV, we could barely infect Calu-1 cells (data not shown). We therefore only tested IRAK3 and MYLK4 knockdown followed by a RSV infection in HeLa cells and HEp-2 cells. In contrast to A549 cells, we only observed a slight reduction in RSV plaque size in HeLa cells after IRAK3 siRNA #4 transfection (Fig. 13B). Neither of the MYLK4 siRNAs could reduce RSV plaque size in HeLa cells. In HEp-2 cells we only observed a slight reduction in RSV plaque size after IRAK3 siRNA #3, which was the only IRAK3-specific siRNA that did not reduce RSV plaque size in A549 cells (Fig. 12B). Transfection of the RSV-N siRNA on the other hand clearly abolished RSV replication in both HeLa and HEp-2 cells (Fig. 13B). One possible explanation for the lack of a clear effect of IRAK3 or MYLK4 knockdown on the RSV plaque size could be the presence of single nucleotide polymorphisms in the siRNA target regions that differ between A549 cells on one hand and HeLa and HEp-2 cells on the other hand. However, this seems unlikely as multiple siRNAs targeting IRAK3 and MYLK4 failed to reduce RSV plaque size in HeLa and HEp-2 cells. As HeLa cells originate from cervical tissue, which is not part of the natural tropism of RSV, cell or tissue-specific differences with lung-derived A549 cells may be responsible for the difference in RSV plaque size reduction after IRAK3 and MYLK4 knockdown. In conclusion, we were not able to confirm reduced RSV plaque size in HeLa and HEp-2 cells after IRAK3 and MYLK4 knockdown as previously seen in A549 cells.

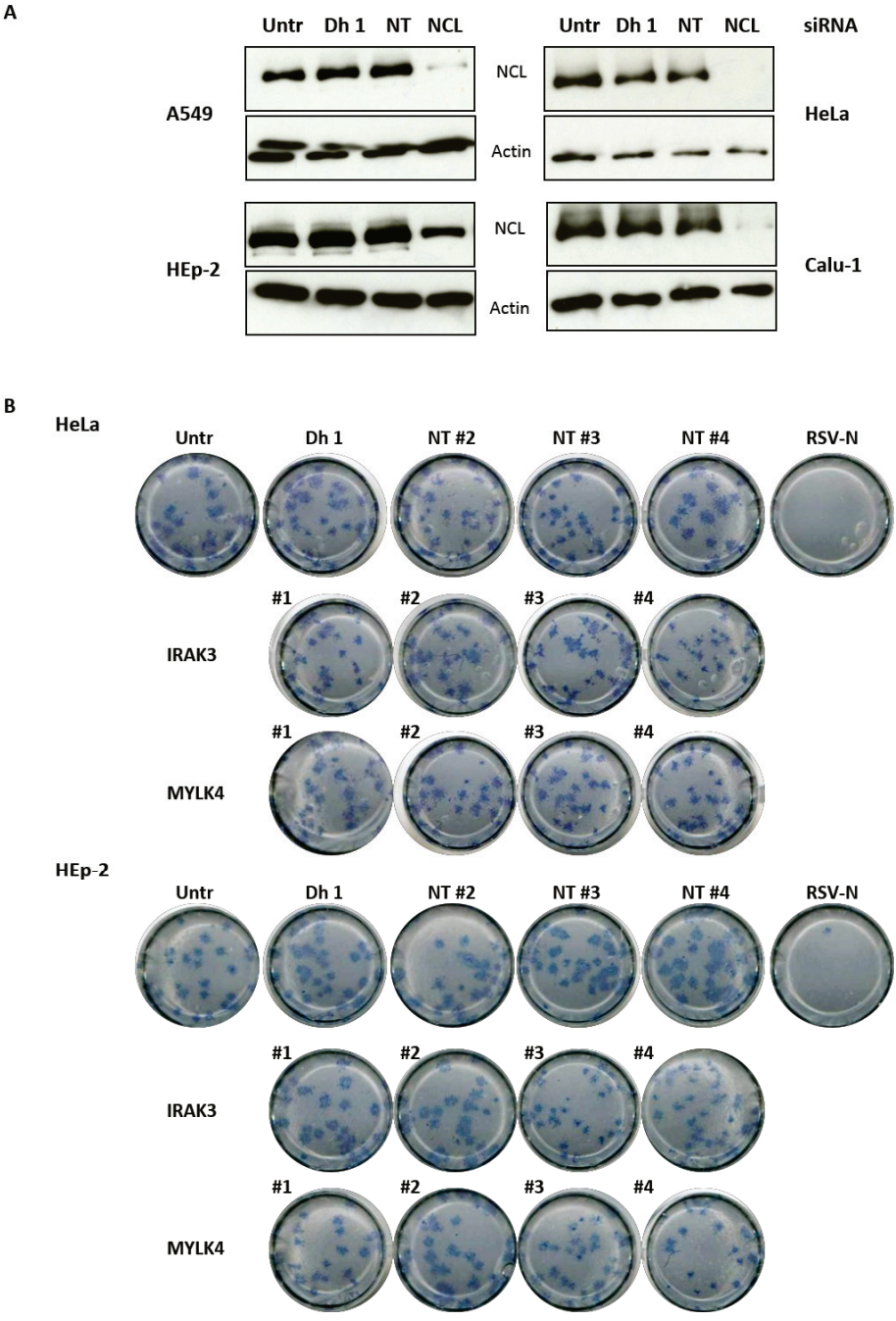
A
Untr
Dh 1
NT
NCL
Untr
Dh 1
NT
NCL
siRNA
A549
NCL
Actin
HeLa
HEp-2
NCL
Actin
Calu-1
B
HeLa
Untr
Dh 1
NT #2
NT #3
NT #4
RSV-N
IRAK3
#1
#2
#3
#4
MYLK4
#1
#2
#3
#4
HEp-2
Untr
Dh 1
NT #2
NT #3
NT #4
RSV-N
IRAK3
#1
#2
#3
#4
MYLK4
#1
#2
#3
#4

Figure 13: Knockdown of IRAK3 and MYLK4 does not reduce RSV plaque size in HeLa or Hep-2 cells. (A) Confirmation of siRNA transfection in HeLa, HEp-2 and Calu-1 cells by evaluating nucleolin knockdown. HeLa and Calu-1 cells were transfected with DharmaFECT-1 diluted 1/800 and HEp-2 cells were transfected with DharmaFECT-1 diluted 1/500 with 15 nM siRNA. A549 cells were used as a control. (B) RSV plaque assay in HeLa and HEp-2 cells 6 dpi. Untr = untransfected, Dh 1 = DharmaFECT-1 only, NT = non-targeting and NCL = nucleolin.

IRAK3 and MYLK4 are possibly important during the late stages of RSV infection

As RSV plaques originate from multiple rounds of infection, all phases of the RSV infection cycle (entry, uncoating, replication, cytoskeleton-based transport, assembly, budding and cell to cell spreading) are covered in this assay. Knockdown of IRAK3 and MYLK4 could impact one of these phases and hence reduce RSV plaque size. To estimate in which phase of the RSV infection cycle IRAK3 and MYLK4 play an important role, we infected A549 cells 48 hours post siRNA transfection with RSV-A2 (MOI~0,1) for a single round of infection (16h) covering the early phases, but not the late assembly, budding and cell spreading. RSV infected cells were stained with a polyclonal goat anti-RSV serum and quantified by immunofluorescence. In parallel we infected siRNA transfected A549 cells with RSV-A2 for 6 days and stained RSV plaques. Compared to negative control treated cells, knockdown of PAK1 and CLT B clearly reduced RSV plaque size, but did not reduce the number of RSV infected cells as measured by immunofluorescence (Fig. 14). These results confirm that PAK1 and CLT B promote a RSV infection, but possibly not during the initial RSV entry phase as suggested by Kolokoltsov and colleagues [9]. A slight, but significant (P = 0,0174), reduction of the number of RSV infected cells was observed after nucleolin knockdown, although RSV plaque size was unaffected. Whereas RSV plaques were hardly detectable upon transfection of RSV-N siRNA, only a 3-fold reduction of RSV infected cells was observed, which is in line with previous observations (Fig. 6 and 7). Unexpectedly, a reduction of RSV infected cells was observed after transfection of non-targeting siRNA #2. As the variation was relatively high compared to other siRNA treatments and plaque size was unaffected, we considered this reduction as random variation, without real biological meaning. RSV plaque size was clearly reduced after IRAK3 knockdown by siRNA #1, #2 and a pool of #1 to #4, but could not be reproduced for siRNA #4 (Fig. 14A). Knockdown of MYLK4 by siRNA #3, #4 and a pool of #1 to #4 clearly reduced RSV plaque size, while siRNA #1 moderately reduced RSV plaque size (Fig. 14A). Despite the reduced RSV plaque size after knockdown of IRAK3 and MYLK4 by several siRNAs, none of these reduced the number of RSV infected cells as measured by immunofluorescence (Fig. 14B). These results suggest that IRAK3 and MYLK4 likely don't play an important role during the initial entry, uncoating and replication phase of a RSV infection, but possibly during the late stages of the RSV infection cycle.

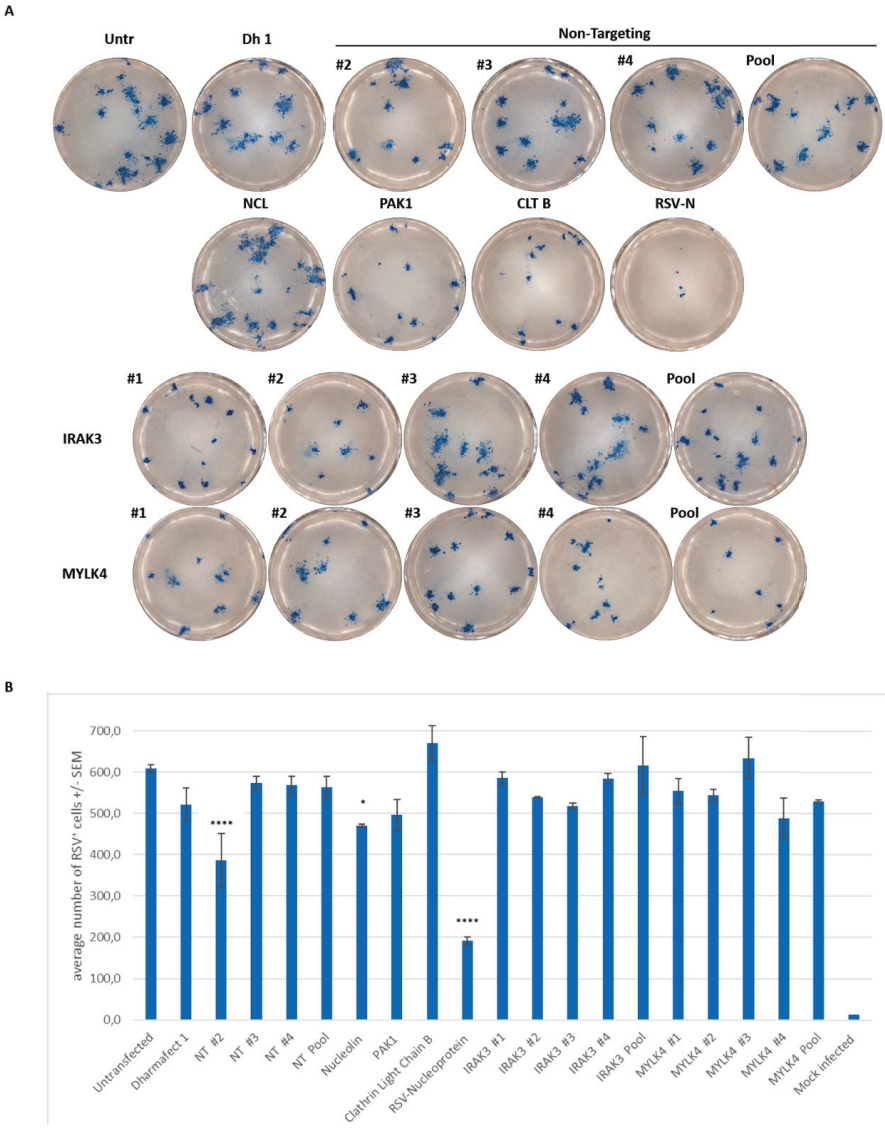

Figure 14: IRAK3 and MYLK4 are possibly important during the late stages of RSV infection. A549 cells were seeded in 96-well plates and transfected with 15 nM siRNA by using DharmaFECT-1 (1/800). Six hours post siRNA transfection, culture medium was refreshed. At 48 hours post siRNA transfection, cells were infected with 35 PFU RSV-A2 with plaque staining 6 dpi (A) or with RSV-A2 (MOI ~ 0,075) for 16 hours followed by immunofluorescence-based quantification of RSV infected cells (B). Bars represent the average number of RSV-positive cells +/- standard error of the means (SEM) of 2 biological replicates. Statistics: one-way ANOVA with Dunnett's multiple comparison testing correction: * $p < 0,05$, **** $p = 0,0001$. Untr = untransfected, Dh 1 = DharmaFECT-1 only, NT = non-targeting, NCL = nucleolin, CLT B = clathrin light chain B.

Knockdown of IRAK3 and MYLK4 does not reduce the metabolic activity of cells

We hypothesized that IRAK3 and/or MYLK4 knockdown could potentially reduce the metabolic activity of cells, creating an unfavorable environment for RSV replication rather than a specific role of IRAK3 and MYLK4 during a RSV infection. To test this hypothesis we transfected A549 cells with IRAK3 and MYLK4 siRNAs and measured the cellular metabolic activity 2 days post siRNA transfection with a colorimetric assay based on the activity of dehydrogenase enzymes found in metabolically active cells. In parallel we also infected siRNA transfected A549 cells with RSV for 3 or 6 days at 48 hours post siRNA transfection and measured cell metabolism. As such, we investigated if a RSV infection influences the cell metabolism of IRAK3 or MYLK4 siRNA transfected cells. We used gossypol, a plant derived polyphenol compound, as a positive control, since our lab observed a reduction of cell metabolism in A549 cells after gossypol administration (Kenny Roose, Unpublished observation). As expected, we observed a clear reduction of cell metabolism upon administration of 250 µg/ml gossypol, whereas a lower concentration of 10 or 50 µg/ml gossypol did not reduce cell metabolism (Fig. 15). None of the IRAK3 or MYLK4-targeting siRNAs reduced the cellular metabolism, both in mock and RSV-A2 infected A549 cells 6 days post infection (Fig. 15). Similar results were obtained for siRNA transfected A549 cells at 0 and 3 days post infection (data not shown). These results suggest that the reduced RSV plaque size after IRAK3 and MYLK4 knockdown is not caused by a general reduction of cellular metabolism.

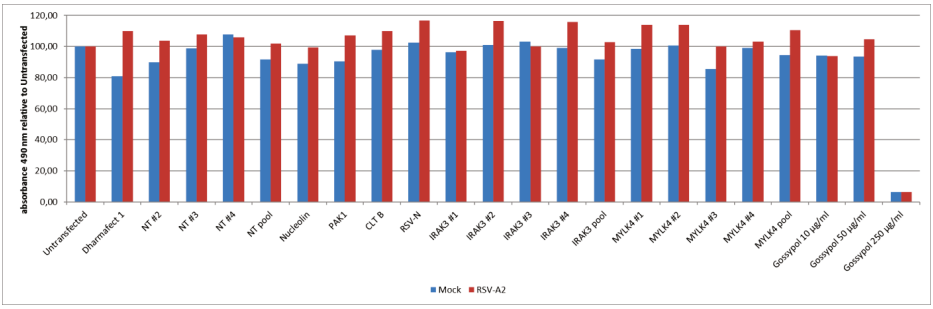

Figure 15: Knockdown of IRAK3 and MYLK4 does not reduce the cell metabolism. We used a MTS-based cellular metabolism assay to quantify the cellular metabolism. A549 cells were seeded in 96-well plates and transfected with 15 nM siRNA by using DharmaFECT-1 (1/800). Six hours post siRNA transfection, culture medium was refreshed. As a control, cells were treated with Gossypol. At 48 hours post siRNA transfection, cells were either mock infected or infected with 35 PFU RSV-A2 for 6 days. At 6 dpi, MTS conversion by dehydrogenase enzymes was measured. Absorbance values at 490 nm were set relative to the untransfected control.

IRAK3 and MYLK4-targeting siRNAs do not induce type I interferons

It has been published that siRNAs can induce the production of type I interferon in a sequence-dependent manner [23-27]. Type I IFN induction upon siRNA recognition, however, mainly occurs *in vivo* by plasmacytoid dendritic cells and normally does not occur in stable epithelial cell lines *in vitro*. Nevertheless, we wanted to be sure that the reduced RSV plaque size after transfection of IRAK3 and

MYLK4-targeting siRNAs was not caused by type I IFN induction. Therefore we investigated if the IRAK3 and/or MYLK4-specific siRNAs induced type I IFN production upon transfection in A549 cells. Although RSV NS1 and NS2 strongly counteract the production and signaling of type I IFNs, siRNA transfected A549 cells were only infected with RSV 2 days post siRNA transfection. If one of the siRNAs would induce the production of type I IFNs, an antiviral state may have been elicited in the A549 cells before RSV infection and hence reduce RSV replication. To measure the induction of type I IFNs we used a luciferase-based reporter assay consisting of the firefly luciferase under control of the IFIT1 promoter in HEK293T cells. We transfected A549 cells with IRAK3 siRNA #1 and #2, MYLK4 siRNA #1 and #4 and with a panel of 16 randomly chosen siRNAs targeting the 8 other primary kinase hits listed in table 1. As a positive control we also transfected poly I:C as an inducer of type I IFN production. Twenty-four and 48 hours post transfection we collected an aliquot of the cell culture supernatants. The supernatants were then inoculated on the reporter HEK293T cells for 24 hours and firefly luciferase was measured after lysis. Transfection of poly I:C in A549 cells induced a modest 3 to 4-fold increase of firefly luciferase expression in the reporter HEK293T cells compared to untransfected cells (Fig. 16). Low expression levels of RLRs in A549 cells likely limited a robust induction of type I IFN production upon poly I:C transfection. In contrast, the IRAK3 and MYLK4-targeting siRNAs and our random panel of 16 siRNAs did not show any induction of firefly luciferase expression compared to the negative control siRNAs. These results suggest that the reduced RSV plaque size after IRAK3 and MYLK4 knockdown is not caused by a siRNA sequence-specific induction of type I IFNs.

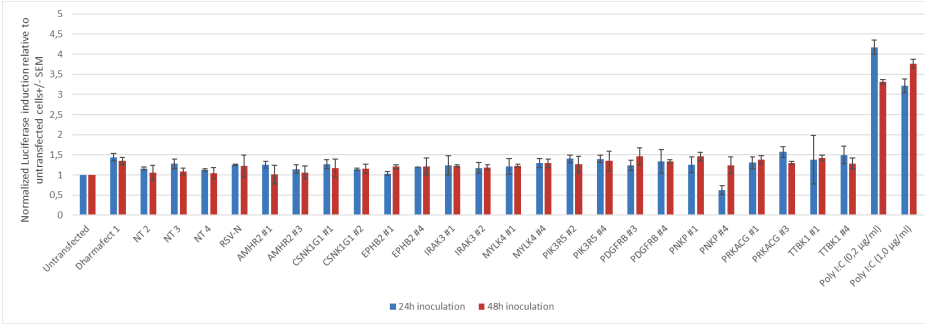

Figure 16: IRAK3 and MYLK4-targeting siRNAs do not induce type I IFNs SiRNAs (15 nM) were transfected in A549 cells for 24 or 48 hours, after which culture medium was harvested. As a control for interferon induction, 2 concentrations of poly I:C (0,2 and 1,0 µg/ml) were transfected in parallel. Meanwhile, HEK293T cells were transfected with a luciferase reporter plasmid expressing firefly luciferase under the control of the interferon inducible promoter of the human IFIT1 gene and a plasmid expressing *Renilla* luciferase constitutively to normalize for transfection efficacy. The harvested culture medium was incubated on the reporter HEK293T cells for 24 hours, followed by measuring luciferase protein levels. Firefly luciferase values were normalized for *Renilla* luciferase values and calculated relative to the untransfected control. Bars represent the average of two biological replicates +/- SEM.

MYLK4, but not IRAK3, is expressed in A549 cells at the mRNA level

To confirm that IRAK3 and MYLK4 function as proviral kinases during a RSV infection, we investigated if IRAK3 and MYLK4 are expressed in A549 cells. If on-target silencing of IRAK3 and MYLK4 is causing the reduced RSV plaque size, mRNA expression of IRAK3 and MYLK4 should be detectable in wild type A549 cells, unless RSV specifically induces IRAK3 and/or MYLK4 expression. At first, we inspected literature and the human protein atlas, a database for expression of human genes. According to the human protein atlas (Version 17), IRAK3 is mainly expressed in monocytes and macrophages, but not in A549 cells, whereas MYLK4 mRNA expression is low, but detectable in A549 cells. We performed a RT-PCR on RNA isolated from untransfected A549 cells that were either mock or RSV-A2 infected at a MOI of 1 and 5 for 4, 9 or 24 hours. After purifying total cellular RNA, we generated cDNA by using a oligodT primer. As such we investigated if IRAK3 and/or MYLK4 are expressed in A549 cells and if their expression is influenced by a RSV infection. To monitor if cDNA synthesis was successful, we PCR-amplified DDX39B cDNA in parallel, a gene that is expressed ubiquitously. As controls for IRAK3 and MYLK4 PCR efficacy, we also performed our IRAK3 and MYLK4-specific PCR on two expression vectors encoding IRAK3 and MYLK4 cDNA (pEXPR-IRAK3 and pEXPR-MYLK4, respectively).

As expected, we observed a strong single band with the IRAK3 and MYLK4-specific PCR on the IRAK3 and MYLK4 expression vectors (Fig. 17, lane 1 and 2). In accordance with literature and the human protein atlas, we could not identify IRAK3 expression in A549 cells, both in mock and RSV-A2 infected cells (Fig. 17, lane 2 for each cDNA sample). In contrast, MYLK4 mRNA was detected in all samples except for the mock sample at 24h post infection (Fig. 17, lane 4 for each cDNA sample). The absence of DDX39B cDNA in this sample, however, suggests that cDNA synthesis for this sample had failed. Although the intensity of the amplified MYLK4 cDNA band differed between mock and RSV-A2 samples, it strongly correlated to the intensity of the DDX39B band. This suggests that the difference in MYLK4 cDNA amplification was more likely the result of a difference in the efficiency of the RT-PCR than a real difference in MYLK4 expression. In conclusion, we could not detect IRAK3 mRNA expression in A549 cells, whereas MYLK4 mRNA expression was present in A549 cells, likely independent of a RSV infection.

We also tried to detect endogenous IRAK3 and MYLK4 at the protein level in both mock and RSV-A2 infected A549 cells by western blotting and immunofluorescence. In line with the RT-PCR result, endogenous IRAK3 could not be detected by western blotting (data not shown). Although we could detect MYLK4 mRNA in A549 cells, we were not able to detect endogenous MYLK4 protein in A549 cells both by western blotting and immunofluorescence (data not shown). Upon transient overexpression of MYLK4 in HEK293T cells we could clearly detect MYLK4 expression, which mainly resided in the cytoplasm (Fig. 18, Suppl. Fig. 2). These results suggest that endogenous MYLK4 protein levels were likely too low to detect by western blotting or immunofluorescence.

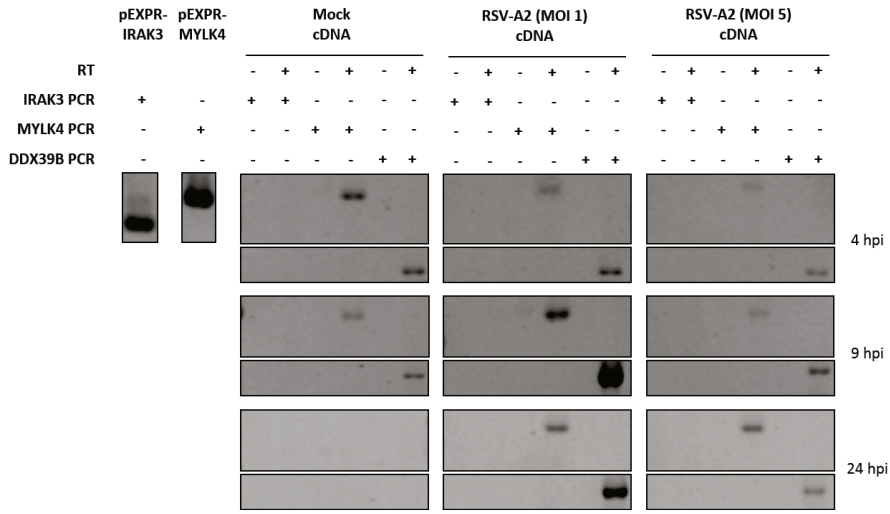

Figure 17: RT-PCR on endogenous IRAK3 and MYLK4 mRNA in A549 cells. A549 cells were mock infected or infected with RSV-A2 (MOI ~ 1 or ~ 5) for 4, 9 or 24 hours and total cellular RNA was isolated. mRNA was reverse transcribed into cDNA by using an oligodT primer. For each sample, a negative control without reverse transcriptase (RT) was run in parallel. The cDNA was subsequently used in a PCR specific for IRAK3, MYLK4 or DDX39B, with the latter being used as a positive control for known expression in A549 cells. As a positive control for the IRAK3 - and MYLK4-specific PCR, we used expression vectors containing IRAK3 or MYLK4 cDNA (pEXPR-IRAK3 and pEXPR-MYLK4, respectively).

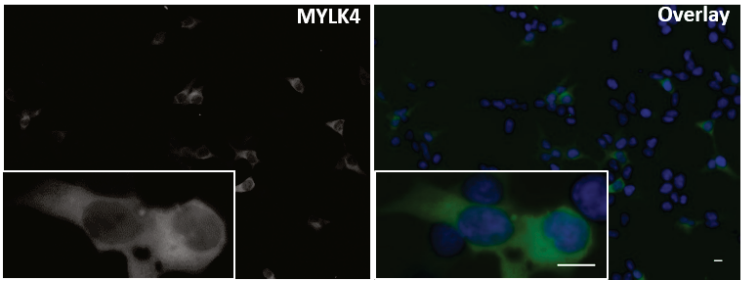

Figure 18: Immunofluorescence-based detection of MYLK4 after transient overexpression in HEK293T cells. HEK293T cells were transfected with an expression vector for MYLK4 under the control of the constitutive cytomegalovirus immediate-early (CMV-IE) promoter. Twenty-four hours post transfection, MYLK4 was stained with a MYLK4-specific antibody (left) and nuclei were stained with Hoechst (right, overlay). Inset = higher magnification. Scale bar = 10 µm.

Knockdown of IRAK3 and MYLK4 by additional siRNAs does not reduce RSV plaque size

As we were not able to detect IRAK3 mRNA expression in A549 cells by RT-PCR, off-target silencing by IRAK3 siRNA #1 and/or #2 could have been the cause of the reduced RSV plaque size. To investigate this further we purchased 4 extra siRNAs targeting IRAK3 and MYLK4 from another source (Qiagen), which we labeled as siRNA #5 to #8. We tested if knockdown of IRAK3 and MYLK4 by these siRNAs also reduced RSV plaque size. A549 cells were transfected with siRNA #5 to #8 from Qiagen and IRAK3 siRNA #1 and #2 and MYLK4 siRNA #1 and #4 from Dharmacon. At 48 hours post siRNA transfection, A549 cells were infected with 35 PFU RSV-A2 for 6 days. In accordance to previous experiments RSV plaque size was strongly reduced upon RSV-N siRNA transfection and clearly reduced upon PAK1 and CLT B knockdown in comparison to negative control treated cells (Fig. 19). Knockdown of nucleolin did not affect RSV plaque size. Transfection of A549 cells with IRAK3-targeting siRNA #5 to #8 did not reduce RSV plaque size, although we could also not reproduce the reduced RSV plaque size after transfection of IRAK3-targeting siRNA #1 and #2 (Fig. 19). Knockdown of MYLK4 by siRNA #1 and #4 and particularly the pool of #1 and #4, clearly reduced RSV plaque size as previously observed. However, MYLK4 siRNA #5 to #8 did not reduce RSV plaque size. Simultaneous knockdown of IRAK3 (by siRNA #1 and #2) and MYLK4 (by siRNA #1 and #4) also reduced RSV plaque size, which likely was caused by the knockdown of MYLK4 and not of IRAK3. We hypothesized that MYLK4 siRNA #1 and #4 from Dharmacon were possibly more potent in knocking down MYLK4 compared to the MYLK4 siRNAs #5 to #8 from Qiagen. As we could not reproduce the reduced RSV plaque size after IRAK3 knockdown and were not able to detect IRAK3 mRNA expression in mock and RSV-A2 infected A549 cells, we decided to not further investigate the observed effect on RSV replication upon knockdown with siRNAs that were designed to target IRAK3 mRNA.

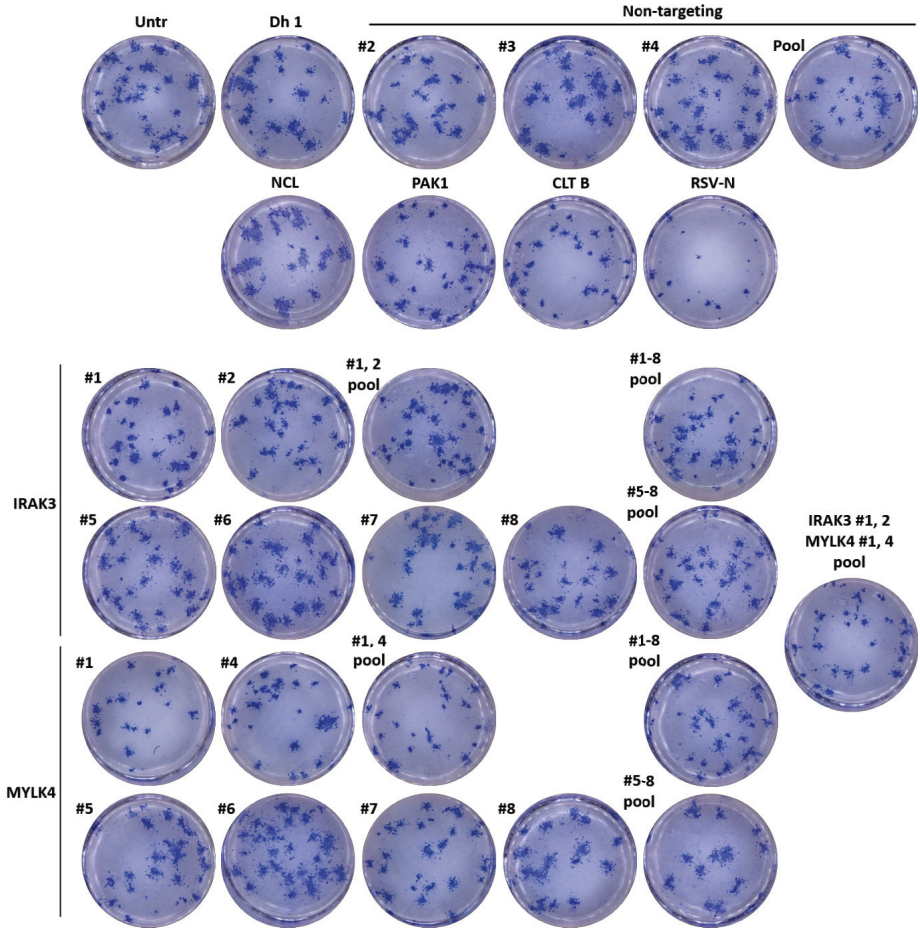

Figure 19: Knockdown of IRAK3 and MYLK4 by siRNAs from Qiagen. A549 cells were seeded in 96-well plates and transfected with 15 nM siRNA by using DharmaFECT-1 (1/800). Six hours post siRNA transfection, culture medium was refreshed. At 48 hours post siRNA transfection, cells were infected with 35 PFU RSV-A2 for 6 days. SiRNAs #1 to #4 are from Dharmacon, siRNAs #5 to #8 are from Qiagen. Untr = untransfected, Dh 1 = DharmaFECT-1 only, NCL = nucleolin and CLT B = clathrin light chain B.

5.2.6 Further validation of the potential proviral kinase MYLK4

Knockdown of endogenous MYLK4 mRNA

Of the 8 MYLK4-targeting siRNAs that we tested (#1 to #4 from Dharmacon and #5 to #8 from Qiagen), siRNA #1 and #4 most potently reduced RSV plaque size, whereas siRNAs #5 to #8 did not reduce the RSV plaque size. To evaluate the knockdown efficacy of endogenous MYLK4 mRNA by these 8 different siRNAs we performed a RT-qPCR. Therefore, we transfected A549 cells with siRNAs for 48 hours and lysed the cells to purify total cellular RNA. We synthesized cDNA by using a mix of oligodT primer and a MYLK4-specific primer and subsequently used the cDNA in a quantitative PCR for MYLK4 and 3 human reference genes, β-actin, ubiquitin C and peptidylprolyl isomerase A, that were selected in advance for stable expression during MYLK4 knockdown. Although we tested an untransfected control in this experiment, it was excluded from the analysis, because we obtained an equal PCR amplification value in our negative control cDNA sample (without reverse transcriptase), suggesting that genomic DNA was present in the RNA sample extracted from this untransfected control. Therefore we set our normalized MYLK4 expression levels relative to the DharmaFECT-1 only control (Fig. 20). Although we observed some variation in MYLK4 expression levels in the negative control samples, we observed a clear knockdown of endogenous MYLK4 mRNA with all 4 siRNAs from Dharmacon (#1-#4). In contrast, siRNA #5 and #7 from Qiagen barely reduced MYLK4 expression, while siRNA #6 and #8 reduced MYLK4 expression, but less efficient compared to siRNA #1 to #4. Although this experiment has been performed only once, these results suggest that the MYLK4-targeting siRNAs from Dharmacon are more efficient than the siRNAs from Qiagen.

Knockdown of overexpressed MYLK4 protein

We wanted to confirm that knockdown of MYLK4 not only occurs at mRNA level, but also at protein level. In addition, we also tested if there was a difference in knockdown efficiency at protein level between MYLK4 siRNA #1 to #4 from Dharmacon and siRNA #5 to #8 from Qiagen as seen on endogenous MYLK4 mRNA. Since we were not able to detect endogenous MYLK4 protein by western blotting or immunofluorescence, we investigated if overexpressed MYLK4 could be reduced by MYLK4 siRNA #1 to #8. We cotransfected A549 cells with siRNA and the MYLK4 expression vector pEXPR-MYLK4 or an empty vector (pEmpty) as control by using DharmaFECT-1. Twenty-four hours post transfection, cell lysates were prepared and MYLK4 expression was investigated by western blotting. MYLK4 was clearly detected after transfection of A549 cells with 20 or 100 ng of pEXPR-MYLK4, whereas no MYLK4 was detected in the empty vector control (Fig. 21A, lane 3-6). This confirmed that although the MYLK4-specific antibody was capable of detecting MYLK4 by western blotting, endogenous MYLK4 levels were likely too low to be detected. In addition to the upper band running at the expected molecular weight (44,5 kDa), we also detected two smaller bands. Cotransfection of MYLK4 siRNA #1 to #4 comparably reduced MYLK4 protein levels in comparison to the non-targeting siRNAs (Fig. 21A, lane 7-14 and 19-20), which is mostly in line with the knockdown of endogenous MYLK4 mRNA. MYLK4 siRNA #5 to #8 more variably reduced MYLK4 protein levels. Whereas siRNA #5

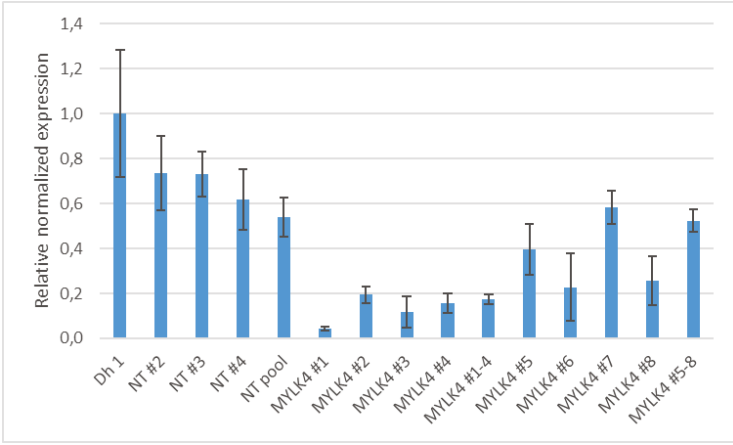

Figure 20: RT-qPCR to confirm knockdown of endogenous MYLK4 mRNA. A549 cells were seeded in 96-well plates and transfected with 15 nM siRNA by using DharmaFECT-1 (1/800). Six hours post siRNA transfection, culture medium was refreshed. Forty-eight hours post siRNA transfection total cellular RNA was isolated and mRNA was reverse transcribed into cDNA by using a mix of oligodT primer and a MYLK4-specific primer. As a control, for each sample cDNA synthesis was performed without reverse transcriptase in parallel. MYLK4 and three reference genes, ACTB, UBC and PPIA, were amplified in a quantitative PCR by using SYBRgreen. MYLK4 expression was normalized for the three reference genes and set relative to the DharmaFECT-1 only control (Dh 1). Bars represent average values of three technical replicates +/- SEM. NT = non-targeting siRNA.

reduced MYLK4 equally as siRNA #1 to #4, siRNA #7 only weakly reduced MYLK4 protein levels (Fig. 21A, lane 15 and 17). SiRNA #6 and #8 most strongly reduced MYLK4 protein levels (Fig. 21A, lane 16 and 18). These results are not entirely consistent with the analysis by RT-qPCR of the knockdown of endogenous MYLK4 mRNA, with siRNA #5 to #8 being inferior to siRNA #1 to #4. As the intensities of the two smaller bands also reduced after MYLK4 knockdown, they likely represent MYLK4 degradation products.

Since MYLK4 siRNA #5, #6 and #8 appeared non-inferior to siRNA #1 to #4 in reducing MYLK4 protein at 24 hours after MYLK4 overexpression, we investigated if there was a difference in duration of knockdown. SiRNAs from Dharmacon could reduce nucleolin, PAK1 and CLT B protein levels at least up to 9 days post siRNA transfection and possibly duration of knockdown of host genes by Qiagen siRNAs was shorter. We therefore investigated knockdown of overexpressed MYLK4 at 3 and 6 days post transfection. In contrast to the previous experiment where we lysed cells at 24 hours post transfection, we observed cytotoxicity and low transfection efficacy due to plasmid DNA transfection in A549 cells with transfection periods exceeding 24 hours. Therefore we had to reduce the amount of transfected plasmids in this experiment. Transfection of 1 and 5 ng of the pEXPR-MYLK4 vector was insufficient to detect overexpressed MYLK4 at 3 days post transfection, whereas 25 ng of pEXPR-MYLK4 resulted in a clear MYLK4 protein band (Fig. 21B, lane 3-8). Transfection of 100 ng plasmid DNA was toxic for the

A549 cells at 3 days post transfection, leading to a reduced MYLK4 overexpression (Fig. 21B, lane 10). Cotransfection of MYLK4 siRNA #1 to #8, with the exception of #7, completely reduced MYLK4 overexpression (Fig. 21B, lane 11-23). SiRNA #7 only partially reduced MYLK4 overexpression in accordance to the earlier time point of 24 hours (Fig. 21A). We should also remark that MYLK4 siRNA #3 was not tested in this experiment as our stock was temporarily finished completely. We also observed that MYLK4 overexpression was reduced in non-targeting siRNA #2 transfected cells compared to the other non-targeting siRNAs (Fig. 21B, lane 11). However, this was not seen at 24 hours post transfection (Fig. 21A), so possibly transfection of the pEXPR-MYLK4 vector was lower in this sample compared to all other samples. In conclusion, we confirmed that MYLK4 siRNA #1 to #8 reduced MYLK4 protein levels upon overexpression, albeit with different efficacy. We could not conclude that, at least in the context of MYLK4 overexpression, MYLK4 siRNA #1 to #4 from Dharmacon were superior to MYLK4 siRNA #5 to #8 from Qiagen, both in terms of efficacy and in duration of MYLK4 knockdown.

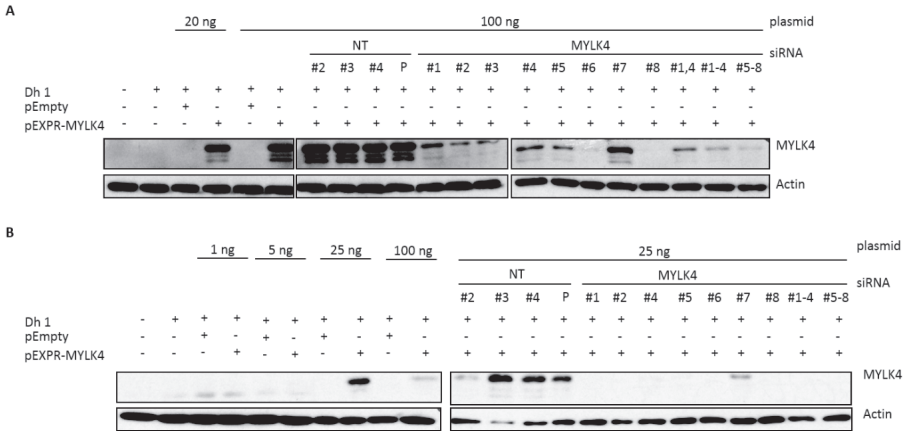

Figure 21: Knockdown of MYLK4 at the protein level after transient overexpression. A549 cells were seeded in 96-well plates and cotransfected with 15 nM siRNA and a MYLK4 expression vector (pEXPR-MYLK4, varying amounts in ng) by using DharmaFECT-1 (1/500). As a control, cells were transfected with the MYLK4 expression vector only or an equal amount of an empty vector (pEmpty). Six hours post transfection, culture medium was refreshed. Twenty-four hours (A) and 3 days (B) post transfection cell lysates were prepared and MYLK4 was detected by western blotting. Actin detection was used as a loading control. NT = non-targeting.

MYLK4-targeting siRNAs from Dharmacon reduce RSV plaque size of both laboratory and clinical RSV isolates

In aforementioned experiments we only tested the effect of MYLK4 knockdown on the replication of RSV-A2, a typical laboratory RSV strain widely used in the RSV field. To investigate the role of MYLK4 further, we tested if the plaque size of other RSV strains would also be affected after MYLK4 siRNA transfection. As previously, siRNA transfected A549 cells were infected with RSV at 48 hours post siRNA transfection. We infected the cells with the laboratory strains RSV-A long and RSV-B1 (Fig. 22A and B, respectively), three clinical RSV-A isolates: RSV-A2001, RSV-A MAD/GM2_13/12 and RSV-A MON/9/92 (Fig. 22C and D and Suppl. Fig. 3A, respectively) and two clinical RSV-B isolates: RSV-B MAD/GM3_7/13 and RSV-B MAD/GM3_5/13 (Fig. 22E and Suppl. Fig. 3B, respectively). For all strains tested, we observed a clear reduction in RSV plaque size after knockdown of PAK1 and CLT B, whereas nucleolin knockdown did not reduce plaque size. With the exception of the clinical RSV-B MAD/GM3_7/13 isolate, we observed a near complete abolishment of RSV plaque formation after RSV-N transfection for all strains. This effect was observed in two independent experiments, suggesting that the clinical isolate RSV-B MAD/GM3_7/13 is resistant to the antiviral effects of the RSV-N siRNA, possibly due to one or more mutations in the siRNA target site. For the MYLK4-targeting siRNAs we observed some differences between different strains, although a clear trend was present. For most strains, we observed that several individual siRNAs from Dharmacon (#1 to #4) reduced RSV plaque size and especially the pool of siRNA #1 to #4, for example with RSV-A long, RSV-A2001 and RSV-A MAD/GM2_13/12 (Fig. 22A, C and D, respectively). In contrast, siRNAs from Qiagen mostly did not reduce RSV plaque size, although some reduction was observed for RSV-A MAD/GM2_13/12 (Fig. 22D). Taken together, these results confirm our previous observations with RSV-A2, suggesting that MYLK4 is important for the *in vitro* replication of both laboratory and clinical RSV isolates.

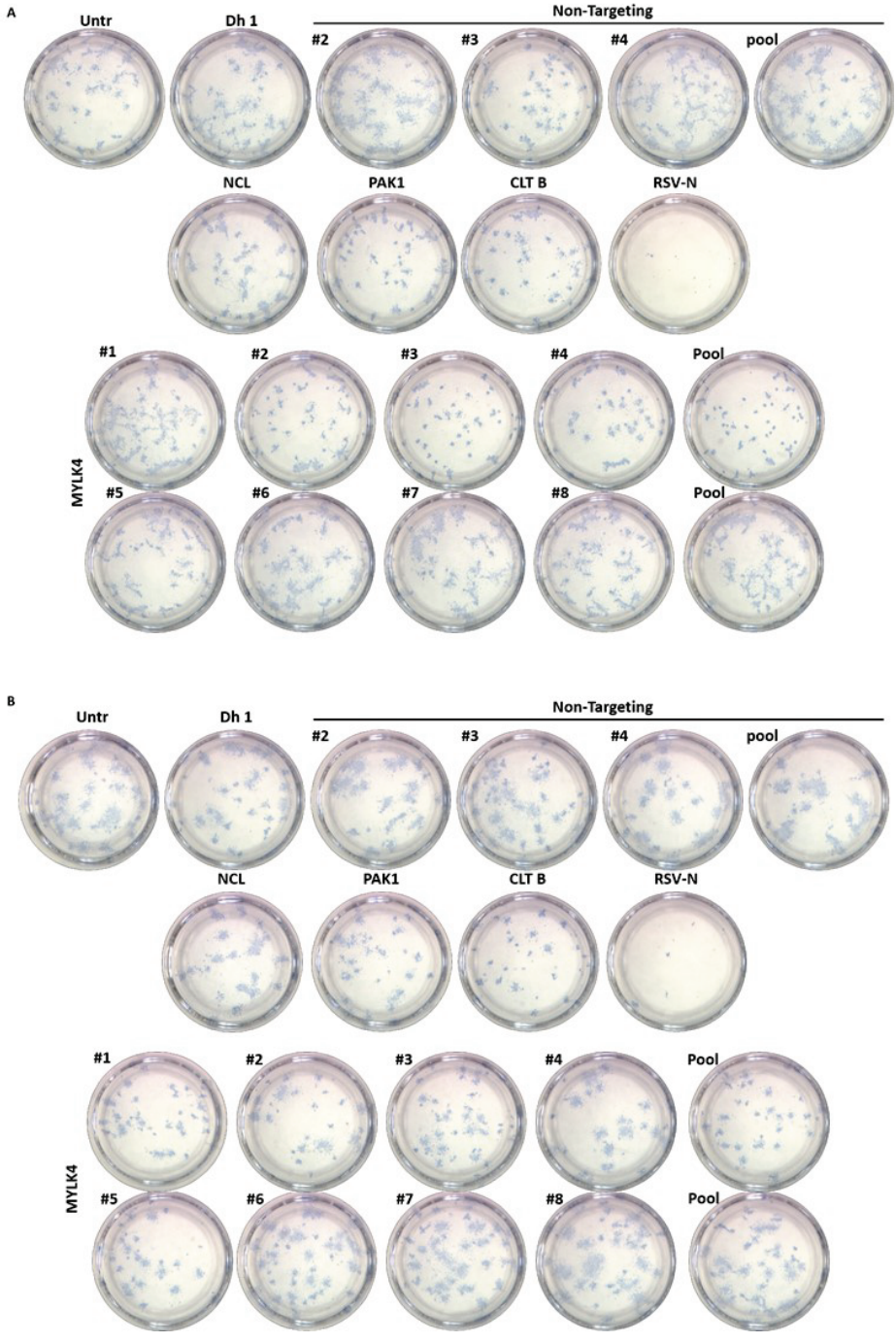
A
Untr
Dh 1
Non-Targeting
#2
#3
#4
pool
NCL
PAK1
CLT B
RSV-N
MYLK4
#1
#2
#3
#4
Pool
#5
#6
#7
#8
Pool
B
Untr
Dh 1
Non-Targeting
#2
#3
#4
pool
NCL
PAK1
CLT B
RSV-N
MYLK4
#1
#2
#3
#4
Pool
#5
#6
#7
#8
Pool

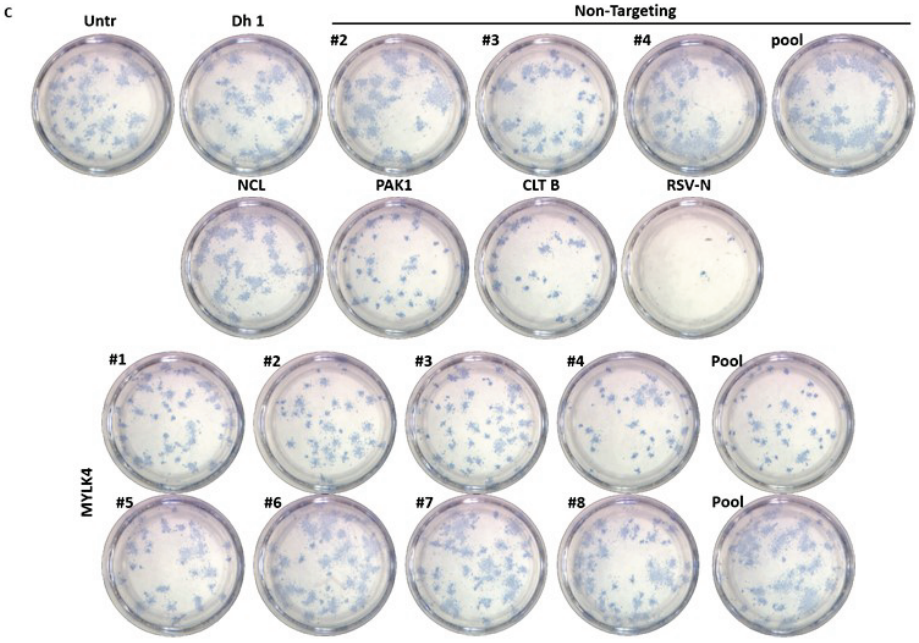
C
Untr
Dh 1
Non-Targeting
#2
#3
#4
pool
NCL
PAK1
CLT B
RSV-N
MYLK4
#1
#2
#3
#4
Pool
#5
#6
#7
#8
Pool

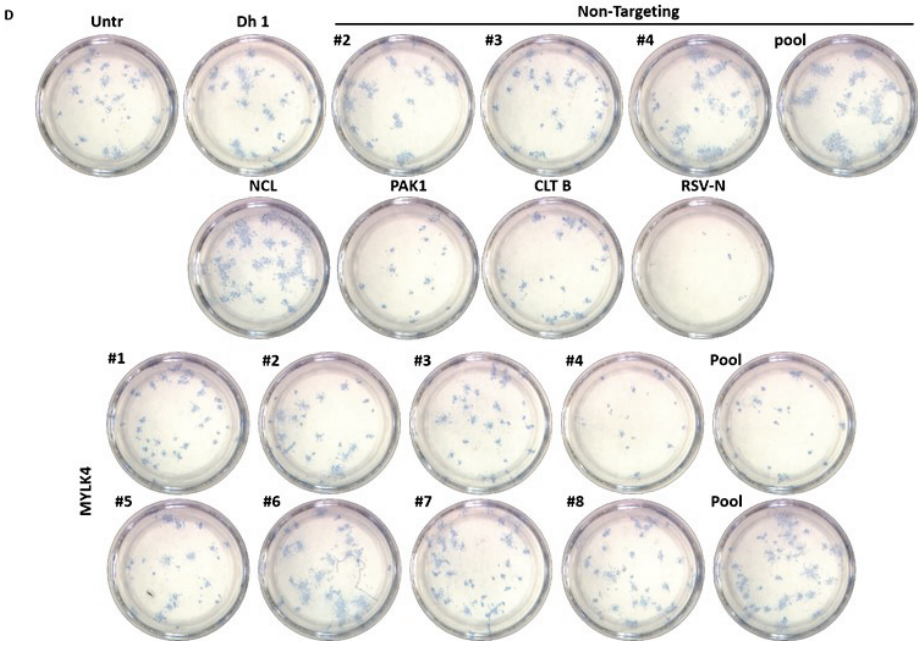
D
Untr
Dh 1
Non-Targeting
#2
#3
#4
pool
NCL
PAK1
CLT B
RSV-N
MYLK4
#1
#2
#3
#4
Pool
#5
#6
#7
#8
Pool

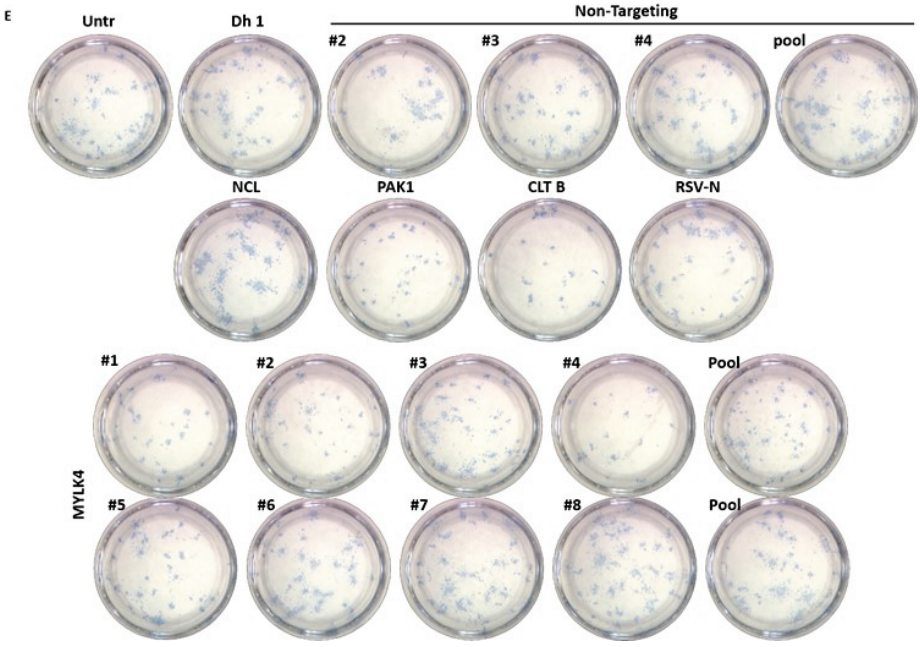

Figure 22: MYLK4-targeting siRNAs from Dharmacon reduce RSV plaque size of both laboratory and clinical RSV isolates. A549 cells were seeded in 96-well plates and transfected with 15 nM siRNA by using DharmaFECT-1 (1/500). Six hours post siRNA transfection, culture medium was refreshed. Forty-eight hours post siRNA transfection cells were infected with (A) RSV-A long for 4 days, (B) RSV-B1 for 5 days, (C) RSV-A2001 for 5 days, (D) RSV-A MAD/GM2_13/12 for 6 days and (E) RSV-B MAD/GM3_7/13 for 6 days. Untr = untransfected, Dh 1 = DharmaFECT-1 only, NCL = nucleolin, CLT B = clathrin light chain B.

RSV plaque size is not restored upon rescue of MYLK4 expression

Upon transfection of different MYLK4-targeting siRNAs, *e.g.* siRNA #1 and #4, we observed a clear reduction of RSV plaque size, suggesting that on-target silencing of MYLK4 caused the reduced RSV plaque size. Although MYLK4 siRNA #6 and #8 were somewhat less efficient in knocking down endogenous MYLK4 mRNA levels compared to siRNA #1 to #4, they were more efficient in knocking down overexpressed MYLK4 protein. Yet, these siRNAs did not result in a reduced RSV plaque size, which is still intriguing to us. An established method to validate on-target specificity of RNAi is to rescue expression of the targeted gene, for example by making use of the degeneracy of codons. An expression vector for the gene of interest with introduced silent wobble base mutations in the siRNA target region should not be affected by that siRNA. As such, siRNA target recognition can be completely abolished while maintaining the wild type amino acid sequence of the gene of interest. By cotransfecting the mutated expression vector with siRNAs against the gene of interest, endogenous expression of the gene of interest is restored by expression from the mutated vector. If a phenotype after knocking down a gene of interest is restored to the normal phenotype, then the gene of interest is highly likely responsible for the phenotype. To investigate if on-target silencing of MYLK4 caused the reduced RSV plaque size, we introduced 5 silent wobble base mutations in the target sites of siRNA #1 and #4 in the MYLK4 expression vector. We called this new mutated vector pEXPR-MYLK4_siRes (siRNA Resistant) and for clarity renamed the wild type pEXPR-MYLK4 vector pEXPR-MYLK4_siSen (siRNA Sensitive). We first investigated if siRNA recognition was indeed abolished by the introduction of the silent mutations. We cotransfected A549 cells with MYLK4 siRNA and plasmid DNA (empty vector, pEXPR-MYLK4_siSen and pEXPR-MYLK4_siRes) for 24 hours, lysed the cells and determined MYLK4 protein levels by western blotting. Since we experienced cytotoxicity after plasmid DNA transfection in A549 cells with DharmaFECT-1 as explained before, we now cotransfected with K2 transfection reagent. Transfection of 100 ng pEXPR-MYLK4_siSen and pEXPR-MYLK4_siRes clearly induced MYLK4 expression in comparison to the empty vector control (Fig. 23, upper panel, lane 6-8). Expression levels of the siRNA resistant MYLK4 were slightly lower than the siRNA sensitive MYLK4. Cotransfection of MYLK4 siRNAs clearly reduced expression of the siRNA sensitive MYLK4 in comparison to non-targeting siRNAs with efficacies comparable to previous experiments (Fig. 23, middle panel; compare with Fig. 21A). In contrast, knockdown of the siRNA resistant MYLK4 was completely absent with siRNA #1 and #4, while unaffected by the other MYLK4-targeting siRNAs (Fig. 23, lower panel). To estimate MYLK4 protein knockdown efficacy, protein band intensities were normalized to the actin loading control and calculated relative to the average intensity of the non-targeting siRNA treated samples (Fig. 23, values below the blots). These results confirmed that by introducing silent mutations in the MYLK4 siRNA #1 and #4 target sequence of a MYLK4 expression vector, overexpression of MYLK4 becomes resistant to these siRNAs.

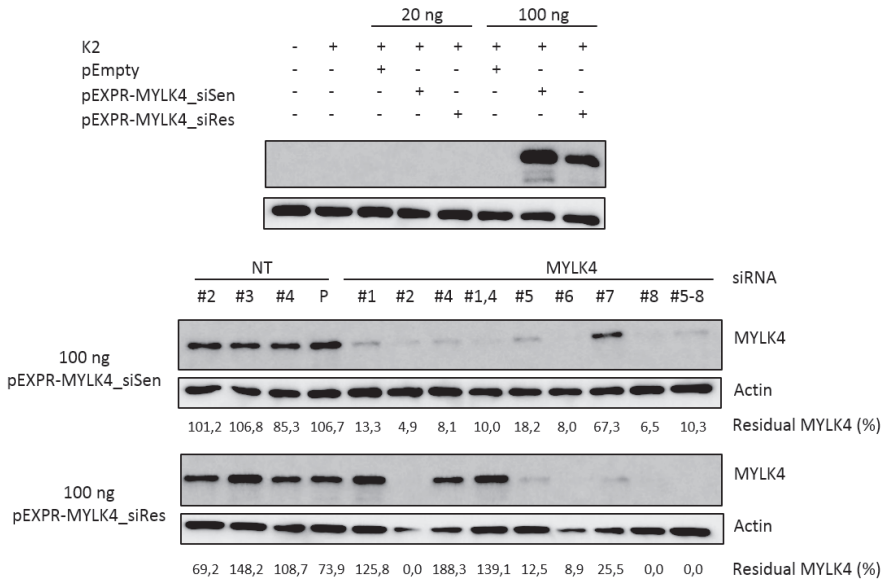

Figure 23: Knockdown of MYLK4 at the protein level after transient overexpression of wild type MYLK4 and siRNA #1 and #4-resistant MYLK4. A549 cells were seeded in 96-well plates and cotransfected with 15 nM siRNA and an expression vector for wild type MYLK4 (pEXPR-MYLK4_siSen) or siRNA #1 and #4-resistant MYLK4 (pEXPR-MYLK4_siRes) by using K2 transfection reagent. As a control, cells were transfected with the MYLK4 expression vectors only or an equal amount of an empty vector (pEmpty). Six hours post transfection, culture medium was refreshed. Twenty-four hours post transfection cell lysates were prepared and MYLK4 was detected by western blotting. Actin detection was used as a loading control. MYLK4 siRNA #3 was not included in this experiment as our stock temporarily ran out. MYLK4 protein band intensities were quantified and normalized for the intensity of the actin band. Residual MYLK4 (%) was calculated by dividing the normalized MYLK4 intensity for each sample by the average normalized MYLK4 intensity of the four NT siRNA treated samples. NT = non-targeting.

As the silent mutations prevented MYLK4 siRNA #1 and #4 recognition, the pEXPR-MYLK4_siRes vector could be used to investigate RSV replication during MYLK4 rescue. Unfortunately, transfection of plasmid DNA in A549 cells with the K2 transfection reagent (and many others that we tested) also caused cytotoxicity. This allowed the generation of cell lysates relatively early after transfection, *e.g.* 24 hours, but was incompatible with the generation of RSV plaques after an infection of 6 days. To overcome this issue, we changed our strategy and used lentiviral transduction to generate stably transduced A549 cells encoding doxycycline inducible siRNA #1 and #4 resistant MYLK4. These transduced A549 cells were transfected with siRNA and stimulated with 1 µg/ml doxycycline (+ dox) or medium only (- dox) as a negative control at 6 hours post siRNA transfection to induce MYLK4 expression. At 48 hours post siRNA transfection, cells were either lysed or infected with RSV-A2 for 6 days in the presence or absence of 1 µg/ml doxycycline to maintain MYLK4 expression during the RSV

infection. We also prepared cell lysates at 6 days post infection. In the presence of doxycycline, we observed a clear induction of MYLK4 expression that was resistant to MYLK4 siRNA #1 and #4 (Fig. 24A). MYLK4 expression levels were slightly lower at 6 days post infection relative to 0 days post infection. As doxycycline is stable in culture medium for about 48 hours, the concentration of doxycycline possibly lowered during the infection time of 6 days, hence lowering MYLK4 overexpression. In the absence of doxycycline, cells transfected with non-targeting siRNAs or without siRNA (untransfected and DharmaFECT-1 only) clearly showed normal RSV plaque sizes as seen previously at 6 days post infection (Fig. 24B, - Dox). As expected RSV-N siRNA transfected cells strongly abolished RSV plaque formation, whereas MYLK4 siRNA #1 and #4 clearly reduced RSV plaque size. However, RSV plaques were not rescued to the normal RSV plaque size in MYLK4 siRNA #1, #4 and #1,4 pool transfected cells in the presence of doxycycline (Fig. 24B, + Dox). At first glance these results suggest that the reduced RSV plaque size after transfection of MYLK4 siRNA #1 and #4 is not caused by the specific knockdown of MYLK4, but could originate from off-target silencing of one or more human genes. However, we cannot say for sure that the overexpressed MYLK4 protein behaves identically as the endogenous MYLK4. It has been described for example that binding profiles of kinase inhibitors can substantially differ between the endogenous and recombinant form of a kinase [28].

In theory, if MYLK4 is important and limiting during a RSV infection, it could be expected that overexpressing MYLK4 before the RSV infection would enhance RSV plaque size. In this experiment the negative control treated cells that overexpress MYLK4 in the presence of doxycycline resemble such a situation. However, we did not observe an increased RSV plaque size in the negative control treated cells upon doxycycline-induced MYLK4 overexpression (Fig. 24B, + Dox).

MYLK4-targeting siRNAs reduce RSV plaque size in A549 cells originating from the ATCC collection

We also tested if RSV plaque size was comparably reduced in A549 cells from ATCC as in the A549 cells used during the kinome knockdown screen. We transfected A549 cells from ATCC with siRNA for 48 hours and infected these with RSV-A2 for 6 days. Transfection of RSV-N siRNA almost completely abolished RSV plaque formation, whereas MYLK4 siRNA #4 and #1,4 pool clearly reduced RSV plaque size compared to the negative control treated cells (Fig. 25). MYLK4 siRNA #1 on the other hand slightly reduced RSV plaque size. In conclusion, we observed a comparable reduction of RSV plaque size after MYLK4 knockdown in A549 cells from ATCC as in the A549 cells used for the kinome knockdown screen.

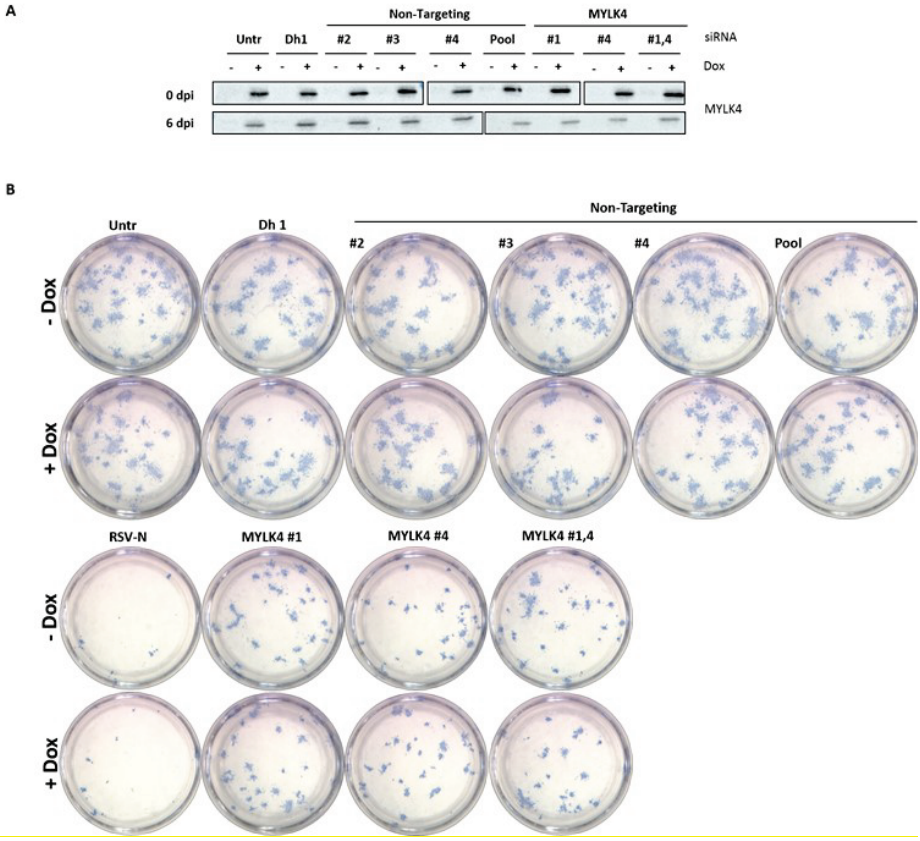

Figure 24: RSV plaque size is not restored upon rescue of MYLK4 expression. Stable transduced A549 cells encoding siRNA #1 and #4-resistant MYLK4 under the control of a doxycycline inducible minimal CMV-IE promoter were seeded in 96-well plates and transfected with 15 nM siRNA with DharmaFECT-1 (1/500). Six hours post siRNA transfection, culture medium was replaced by medium with or without 1 µg/ml doxycycline (+ and - Dox, respectively). Forty-eight hours post siRNA transfection cell lysates were prepared to detect MYLK4 expression by western blotting (A) or cells were infected with 35 PFU RSV-A2 for 6 days (B). In addition, we also prepared cell lysates at 6 dpi to detect MYLK4 expression (A). Untr = untransfected and Dh 1 = DharmaFECT-1 only.

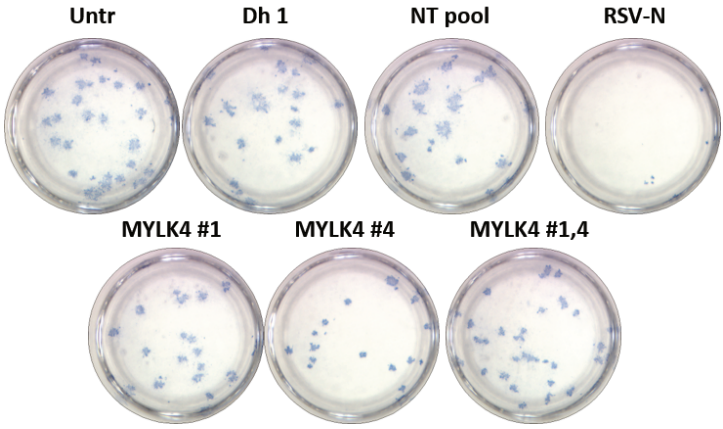

Figure 25: MYLK4-targeting siRNAs reduce RSV plaque size in A549 cells from the ATCC collection. A549 cells originating from the ATCC culture collection were seeded in 96-well plates and transfected with 15 nM siRNA by using DharmaFECT-1 (1/650). Six hours post siRNA transfection, culture medium was refreshed. Forty-eight hours post siRNA transfection cells were infected with RSV-A2 for 6 days. Untr = untransfected, Dh 1 = DharmaFECT-1 only and NT = non-targeting.

RSV plaque size is not reduced in MYLK4 knockout A549 cells

Since siRNA-mediated knockdown generally not completely abolishes protein expression and not all cells are transfected with siRNA to the same extent, knockdown phenotypes may be disturbed by residual protein expression of the targeted gene of interest. Completely abolishing the expression of a gene of interest can be achieved by generating a full knockout. With the recent advances in the CRISPR/Cas9-mediated genome engineering technology, creating a knockout cell line became possible in basically every lab. We therefore generated MYLK4 knockout A549 cells by using the CRISPR/Cas9 technology. We did this in parallel in the A549 cells that were used in the knockdown screen and all subsequent validation experiments and in the A549 cells originating from ATCC. For clarity, we will subsequently refer to these cells as A549 and A549 ATCC cells, respectively. First, we designed three guide RNAs (gRNAs) against MYLK4 by analyzing the MYLK4 exon sequences in two online gRNA design tools (MIT CRISPR Design tool [29] and CRISPOR [30]). Three gRNAs, targeting MYLK4 exon 2, 3 and 6, respectively, with a high specificity and out-of-frame score were retained. We cloned these gRNAs under control of the human U6 promoter in the pX458-w/t Cas9-2A-EGFP vector encoding the *Streptococcus pyogenes* derived Cas9 nuclease and EGFP. These vectors were subsequently transfected in A549 and A549 ATCC cells and EGFP positive cells were sorted as single cells in a 96-well plate by fluorescence activated cell sorting (FACS) 48 hours post transfection. As a control we also sorted one plate with A549 ATCC cells from the EGFP negative population, which were used as monoclonal, wild type A549 ATCC cells. In addition to the sorted single cells, we also collected the remaining EGFP positive cell population as a polyclonal pool of cells. The polyclonal pool of transfected cells was used to investigate for each of the three gRNAs if the gRNA was active in directing Cas9-

mediated cleavage of the genomic MYLK4 DNA. Genomic DNA was extracted from the pool of cells and used to amplify the regions surrounding the expected Cas9 cleavage sites by PCR. PCR fragments of 1090 bp, 1379 bp and 1296 bp were expected for gRNA1, - 2 and - 3, respectively. These PCR fragments were then heated to 95°C and cooled down gradually to 25°C to allow reannealing of the DNA. As the pool of cells is expected to contain a mix of wild type and Cas9-mediated small insertion/deletion mutant cells, reannealing is expected to form homo- and heteroduplex DNA. We then cleaved the DNA with Surveyor® nuclease, an endonuclease that specifically cleaves at mismatches in DNA duplexes, and analysed the DNA on agarose gel. So if a gRNA was active and induced Cas9-mediated cleavage, then the mix of homo- and heteroduplex DNA is expected to yield a full length PCR fragment (homoduplex) and two smaller PCR fragments (cleaved heteroduplex) upon surveyor® nuclease cleavage. For gRNA1 we observed a single band of 1090 bp for wild type, untransfected A549 cells containing only homoduplex DNA, whereas two extra bands of 692 bp and 399 bp as expected were detected for gRNA1 transfected A549 cells (Fig. 26, lane 2 and 3, two extra bands highlighted with an asterisk). For gRNA2, we also observed the expected single band of 1379 bp for wild type, untransfected A549 cells and two extra bands of 876 and 504 bp as expected for gRNA2 transfected cells (Fig. 26, lane 4 and 5, two extra bands highlighted with an arrowhead). We also observed an unexpected fourth band around 700 bp, for which we had not clear-cut explanation. For gRNA3, the expected PCR fragment of 1296 bp was very faint, even in the wild type, untransfected cells, making it hard to draw firm conclusions on the activity of gRNA3 (Fig. 26, lane 6 and 7). In conclusion, we confirmed that gRNA1 and - 2 were active in directing Cas9-mediated genomic DNA cleavage in at least part of the A549 cells from the pool, whereas for gRNA3 we found no evidence for Cas9-mediated cleavage, but we could not exclude that gRNA3 was active.

As we found evidence of Cas9-mediated cleavage of MYLK4 genomic DNA with gRNA1 and - 2 in the pool of transfected cells, we continued with the corresponding single cell clones. As outlined in table 2, depending on the cell line and gRNA, about 16% to 27% of the single cell clones survived and started dividing. Of the expanded monoclonal cells we PCR-amplified the genomic DNA region surrounding the expected Cas9 cleavage site. PCR fragments present as single bands of the expected size were sequenced and aligned to the wild type MYLK4 sequence. We found that 5 out of 15 and 8 out of 24 successfully sequenced PCR fragments were mutated in gRNA1 and -2 transfected A549 cells, respectively. Mutations rates were even higher in the A549 ATCC cells. We found 3 out of 7 and 8 out of 12 successfully sequenced PCR fragments mutated in gRNA1 and – 2 transfected cells, respectively. As the MYLK4 gene is located on chromosome 6, which is present as 2 copies in the hypotriploid genome of A549 cells [31, 32], we investigated if both MYLK4 alleles were mutated. We used the online tool TIDE (Tracking of INDELS by Decomposition), which decomposes overlapping Sanger sequencing chromatograms to estimate the frequency and positions of insertions or deletions [33]. We found 2 A549 clones with frameshifts in both MYLK4 alleles for both gRNA1 (clone #7 and #9) and gRNA2 (clone #3 and #22)(Suppl. Fig. 4 and 5, respectively). We also found 2 and 3 A549 ATCC clones with frameshifts in both MYLK4 alleles for gRNA1 (clone #15 and #16) and gRNA2 (clone #1, #4 and #5), respectively (Suppl. Fig. 6 and 7, respectively). Based on the TIDE prediction of the length of insertions and/or

deletions, we estimated that for all these mutant clones truncated MYLK4 proteins of maximally 93 amino acids would be generated (with wild type MYLK4 being 388 amino acids long). These results suggest that all selected mutant clones are deficient in MYLK4. As the endogenous MYLK4 protein levels in A549 cells were too low to detect by western blotting or immunofluorescence, we could not check for the absence of MYLK4 protein in these mutant clones unfortunately.

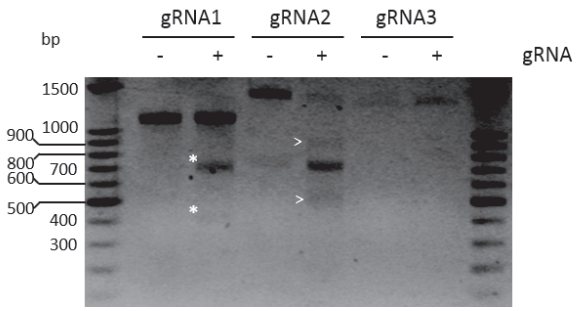

Figure 26: MYLK4 Guide RNA selection by Surveyor® Nuclease-mediated heteroduplex cleavage. Three Cas9 guide RNAs (gRNA1, 2 and 3) were designed to target MYLK4 exon 2, 3 and 6, respectively. A549 cells were transfected with a pX458-w/t Cas9-2A-EGFP vector encoding the Cas9-EGFP fusion protein and one of the three gRNAs (+ gRNA). As a control, we used non-transfected A549 cells (- gRNA). Forty eight hours post transfection, EGFP positive cells were sorted by FACS as a polyclonal pool of cells. Genomic DNA regions surrounding the expected Cas9 cleavage sites were amplified by PCR yielding the following expected fragments: gRNA1: 1,090 bp; gRNA2: 1,379 bp and gRNA3: 1,296 bp. The PCR fragments were subsequently denatured and gradually cooled down to allow the formation of homo - and heteroduplex PCR fragments due to Cas9-mediated small insertions/deletions. The PCR fragments were digested by the mismatch-specific endonuclease Surveyor® nuclease. * and > indicate expected Surveyor® nuclease generated fragments of 692 bp and 399 bp for gRNA1 and 876 bp and 504 bp for gRNA2.

Table 2: Number of clones at the various steps in selecting MYLK4$^{-/-}$ A549 clones

	A549		A549 ATCC	
	gRNA1	gRNA2	gRNA1	gRNA2
# surviving single cells[a]	19	26	16	19
gDNA extraction successful	17	26	13	16
PCR: single band, expected size	16	25	8	12
Sequencing PCR fragment				
Unsuccessful	1	1	1	0
Wild type	10	16	4	4
Mutated	5	8	3	8
TIDE: frameshift in both MYLK4 alleles	2	2	2	3

[a] From 96 single cells

All expected MYLK4$^{-/-}$ clones and wild type MYLK4$^{+/+}$ A549 and A549 ATCC cells were subsequently infected with 60 or 30 PFU RSV-A2 for 3 and 6 days, respectively, to investigate the effect of the absence of MYLK4 on RSV plaque size. Upon RSV infection, most cells of one MYLK4$^{-/-}$ A549 clone (clone #22 of gRNA2) died, whereas no clear cytotoxicity was observed in these cells before infection (data not shown). Of the three remaining MYLK4$^{-/-}$ A549 clones, none showed a reduced RSV plaque size compared to the polyclonal MYLK4$^{+/+}$ A549 cells, both at 3 and 6 days post infection (Fig. 27A). For the wild type, MYLK4$^{+/+}$ A549 ATCC cells, we observed slightly enlarged RSV plaques at 3 dpi, but not at 6 dpi, in one of the two tested monoclonal cells (clone A) compared to the polyclonal cells (Fig. 27B, upper panel). This may highlight that some biological variation exists between different wild type monoclonal A549 ATCC cells. Of all MYLK4$^{-/-}$ A549 ATCC clones, only clone 04 of gRNA2 showed a slight reduction in RSV plaque size compared to the MYLK4$^{+/+}$ A549 ATCC cells at 3 dpi, but not at 6 dpi. In conclusion, with this experiment we could not prove that knocking out MYLK4 in A549 and A549 ATCC cells is associated with reduced RSV plaque size as we observed before with knocking down MYLK4 by siRNAs. Yet, we can also not prove that our presumed MYLK4 knockout clones are really defective in the synthesis of MYLK4 protein.

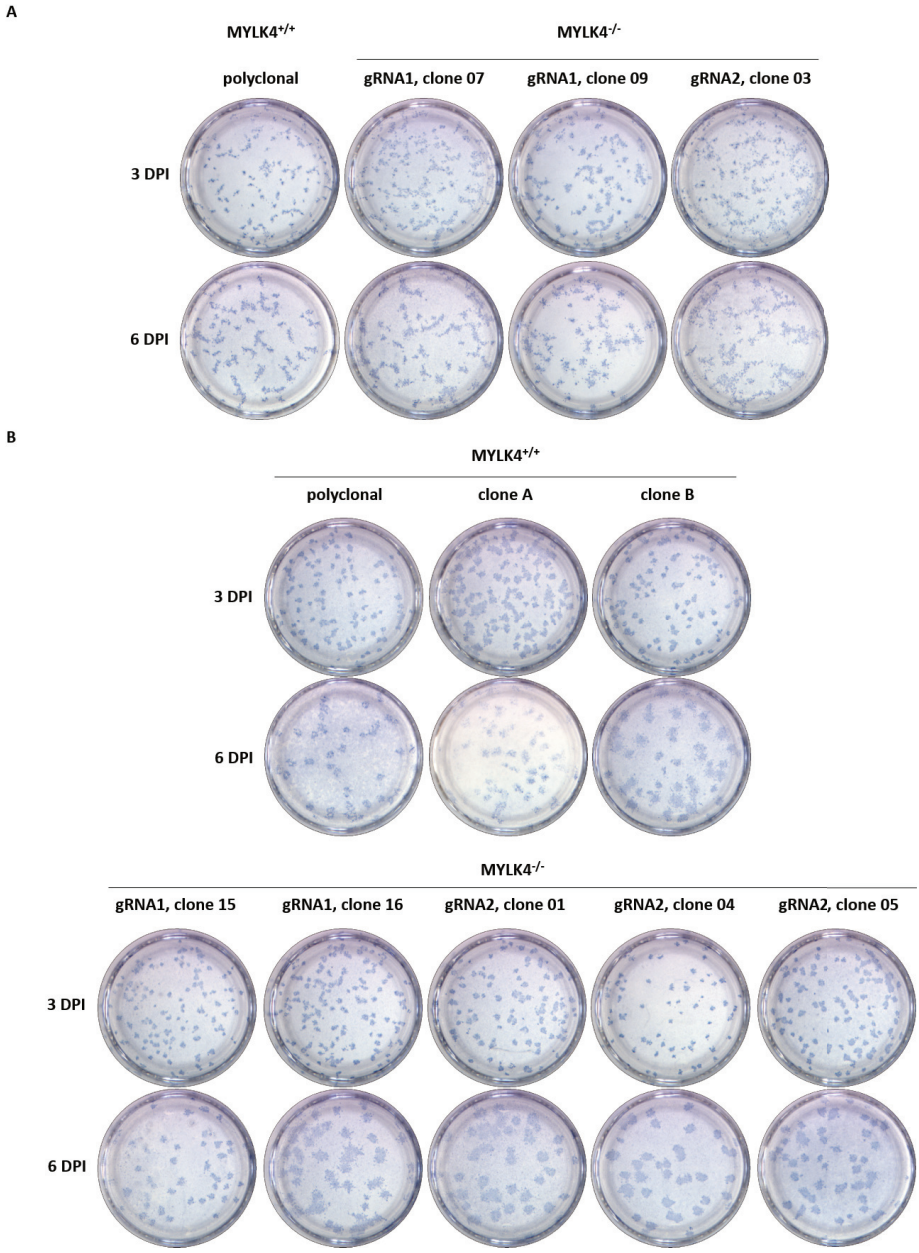

Figure 27: RSV plaque formation in wild type - and MYLK4 knockout A549 cells. (A) Wild type, polyclonal A549 cells and three different MYLK4$^{-/-}$, single cell A549 clones were infected with RSV-A2 for 3 or 6 days. Clone #22 of gRNA2 was excluded as cells died upon RSV infection. (B) Wild type, polyclonal A549 ATCC cells, two wild type, single cell A549 ATCC clones and five different MYLK4$^{-/-}$, single cell A549 ATCC clones were infected with RSV-A2 for 3 or 6 days.

5.3 Discussion

To unravel phosphorylation-dependent signaling pathways that are activated and possibly exploited by a RSV infection, we investigated the role of 714 human kinases during RSV infection by siRNA-mediated knockdown of each kinase one by one in A549 cells, a model lung epithelial cell line. To our knowledge this is the first high-throughput screen to investigate the role of (a subset of) host genes during RSV infection. To unambiguously cover all stages of the RSV infection cycle we measured RSV reproduction in a semi-quantitative manner by staining RSV plaques formed by multiple rounds of infection. This in contrast to immunofluorescence- or flow cytometry-based quantification of newly produced RSV proteins in a single round of infection. Additionally, in our hands RSV plaques were more compatible with semi-high-throughput screening and appeared more sensitive in detecting aberrated RSV replication compared to immunofluorescence- or flow cytometry-based read-outs. We used siRNAs targeting three host genes, *i.e.* nucleolin, PAK1 and CLT B, and one viral gene, the nucleoprotein, as positive controls. In line with literature, we observed a clear reduction in RSV plaque size at 6 dpi after knockdown of PAK1 and CLT B, highlighting that these proteins are important during RSV infection [9]. Furthermore, we observed a near complete abolishment of RSV plaque formation after transfection of the RSV-N siRNA [15], although one clinical RSV isolate, RSV-B MAD/GM3_7/13, was resistant against this RSV-N siRNA. Despite a clear knockdown of nucleolin at protein level, we did not observe a reduced RSV plaque size after transfection of siRNAs targeting nucleolin in A549 cells, in contrast to literature [8]. Even if we quantified RSV replication by a single round of infection as Tayyari and colleagues did, we could not observe a reduction in RSV replication after nucleolin knockdown. Although we cannot exclude that this striking difference is caused by differences in the used cell lines (A549 vs 1HAEo- cells) and/or RSV strains (RSV-A2 vs a recombinant GFP expressing RSV strain derived from RSV-A2), we found no evidence that nucleolin is used as a cellular receptor by RSV or that nucleolin plays an important role during RSV infection. This is in agreement with the observation that recombinant RSV-F protein fails to interact with recombinant nucleolin, even at high concentrations (personal communications with Dr. J. Mclellan).

The siRNA-mediated knockdown screen of the human kinome followed by RSV infection was performed twice, with staining of RSV plaques at 6 dpi and at 3 or 4 dpi. We identified 104 kinases for which the siRNA-based knockdown was associated with a reduced or increased RSV plaque size in all three replicates in one or both screens or in two of the three replicates in both screens. These 104 kinases were further validated by assessing RSV replication in a quantitative manner by determining the infectious RSV titer in the cell culture supernatans after knockdown. We subsequently combined the results of the RSV replication kinetics with the results from the initial screens based on RSV plaques to select 10 kinases for further validation. For 3 kinases, AMHR2, CSNK1G1 and TTBK1, we observed an increase in RSV plaque size and - titer upon knockdown, suggesting that these kinases possess an antiviral role during RSV infection. For 7 kinases, EPHB2, IRAK3, MYLK4, PIK3R5, PDGFRB, PNKP and PRKACG, we observed a reduced RSV plaque size and - titer upon knockdown, suggesting that these kinases possess a proviral role during RSV infection. The on-target specificity of the siRNA pools targeting these 10 kinases was further validated by deconvoluting the siRNA pools into 4 separate siRNAs. For the majority of these kinases, however, we only observed a reduced or increased RSV

plaque size with maximum 1 of the 4 siRNAs, raising the possibility that the aberrated plaque size was caused by off-target silencing by a single siRNA in the siRNA pools. These results highlight that a substantial fraction of primary hits in large-scale RNAi experiments may be caused by off-target silencing induced by siRNAs, as seen previously [34, 35]. SiRNA-mediated off-target silencing should be a major point of caution in the interpretation of large-scale RNAi results. Initially, we observed a reduced RSV plaque size by at least 2 different siRNAs targeting IRAK3, suggesting that on-target silencing of IRAK3 reduced RSV plaque size. IRAK3 is a member of the family of IRAK kinases, which are important in the initiation of signaling upon activation of TLRs and the IL-1 receptor. Whereas IRAK1, 2 and 4 promote TLRs/IL-1 receptor signaling, IRAK3 is a negative regulator of this signaling. We hypothesized that by knocking down IRAK3, increased signaling of TLRs or the IL-1 receptor would increase innate immune responses that could have caused the reduced RSV plaque size and - titer. However, in line with literature and a database for expression of human genes, we were not able to detect IRAK3 mRNA expression in A549 cells by RT-PCR. The seemingly absent expression of IRAK3 in A549 cells combined with difficulties in reproducing the reduced RSV plaque size after transfection of the IRAK3-targeting siRNAs, convinced us that the reduced RSV plaque size was likely not caused by on-target silencing of IRAK3 mRNA.

We demonstrated that targeting MYLK4 by a pool of 4 siRNAs from Dharmacon reduced RSV plaque size and the titer of infectious virions released in the cell culture supernatants in A549 cells. Upon deconvolution of this MYLK4 siRNA pool in the 4 separate siRNAs, we observed a reduced RSV plaque size by at least 2 different siRNAs in two sources of A549 cells, but not in HeLa or Hep-2 cells. Moreover, this reduction in RSV plaque size was not only observed for the RSV-A2 strain, but also for the laboratory strains RSV-A long and RSV-B1 and for 5 clinical RSV isolates (3 RSV-A strains and 2 RSV-B strains). We found no evidence that the reduction in RSV plaque size upon transfection of MYLK4-targeting siRNAs was caused by a general reduction in cell metabolism or by siRNA-induced production of IFNs. We also tested 4 siRNAs targeting MYLK4 from Qiagen, however, none of these siRNAs reduced the size of RSV plaques in A549 cells. We were able to detect endogenous MYLK4 mRNA expression in A549 cells by RT-PCR and confirmed knockdown at the mRNA level by all 4 siRNAs from Dharmacon and by 2 siRNAs from Qiagen. At first glance, siRNAs from Dharmacon appeared superior over siRNAs from Qiagen in knocking down MYLK4 mRNA, highlighting a possible cause of the difference in plaque size reduction observed for siRNAs originating from Dharmacon and Qiagen. Yet, we have not been able to detect endogenous MYLK4 at the protein level, which may be caused by low to absent expression levels or by a too low affinity of the MYLK4-specific antibody that we used to detect endogenous MYLK4 protein. Upon overexpression of MYLK4, we demonstrated knockdown of MYLK4 at the protein level by all 4 siRNAs from Dharmacon and by 3 siRNAs from Qiagen, with the siRNAs from Qiagen being superior over the siRNAs from Dharmacon. To confirm that on-target silencing of MYLK4 by the Dharmacon siRNAs #1 and #4 caused the reduced RSV plaque size, we performed a rescue experiment. Although we could clearly detect MYLK4 expression by western blotting upon rescue, we did not observe a rescue of the RSV plaque phenotype. As substrates of MYLK4 are not known currently, we could, however, not investigate if this overexpressed MYLK4 fully recapitulates cellular functions of endogenous MYLK4. In addition, we used the CRISPR/Cas9 technology to generate

several A549 single cell clones of which we believe that they are a full knockout of MYLK4, based on sequencing of a part of the genomic MYLK4 locus surrounding the expected Cas9 cleavage site. RSV infection of these single cell clones and wild type cells resulted in plaques with equal size. Since we have not been able to detect endogenous MYLK4 at the protein level, however, we were unable to confirm the absence of MYLK4 protein in these MYLK4 knockout clones.

The myosin light chain kinase (MYLK) family consists of four calcium and calmodulin-dependent serine/threonine protein kinases, MYLK1-4, although the calcium/calmodulin dependency of MYLK3 is debated [36, 37]. MYLK1-3 regulate the activity of the actin motor protein myosin by phosphorylating the regulatory light chain of myosin [36, 38-40]. As such MYLK1, -2 and -3 regulate the contractile activity of smooth -, skeletal - and cardiac muscle cells, respectively. In addition, MYLK1 also plays a role in cellular processes such as cytokinesis, phagocytosis and cell motility in non-muscle cells. In contrast to MYLK1-3, any functional information on MYLK4 is currently lacking. MYLK4 has been identified as a monoallelic expressed gene in colorectal cancer cell lines and was found to be downregulated at both the mRNA level and protein level in cardiac tissue from patients suffering from heart failure compared to healthy controls [41, 42]. The biological relevance of these findings to our results, however, is unclear. Aligning the MYLK4 and MYLK1 amino acid sequence highlights that the vast majority of the MYLK4 protein overlaps with the catalytic kinase domain of MYLK1 with about 55% sequence conservation between the kinase domains of MYLK4 and MYLK1. In comparison, sequence conservation with the kinase domain of MYLK2 and MYLK3 was 64% and 74%, respectively. Although experimental confirmation is necessary, these results suggest that MYLK4 may act as a kinase that phosphorylates the regulatory light chain of myosin as MYLK1-3 do. At first sight MYLK4 appears to lack the actin and calmodulin binding domains present in MYLK1, although these domains are also not present in MYLK2 and MYLK3, with the exception of one calmodulin binding domain in MYLK2. MYLK1 and the motor protein myosin have been shown to play a role during viral infections [43-50]. Although we did not observe a reduction in RSV plaque size after MYLK1 knockdown and experimental evidence is yet lacking, MYLK4 may function in a similar/identical manner during viral infection as MYLK1. Infection of monocytes with feline infectious peritonitis virus leads to the synthesis of viral proteins in the plasma membrane, which are internalized upon antibody binding in a MYLK1 and myosin-I and VI-dependent manner [45]. As such, the monocyte evades antibody-mediated cell lysis. Interestingly, antibody-mediated internalization of the F and G protein expressed in the plasma membrane upon RSV infection was recently shown [50], although it is not directly clear to us how these results could be implemented on our results as we did not add any viral protein-specific antibody to the A549 cells. The non-muscle myosin heavy chains (NMMHC)-IIa and IIb are used as cellular receptors for the entry of several viruses from diverse families, including several members of the herpesvirus family and the bunyavirus severe fever with thrombocytopenia syndrome virus (SFTSV) [43, 44, 46, 47, 49]. Upon infection with HSV-1 and SFTSV, the NMMHC-IIa and IIb were shown to relocate from the cytoplasm to the cell surface, which was dependent on MYLK1-mediated phosphorylation of the myosin regulatory light chain [43, 46, 47]. Inhibition of MYLK1 by the inhibitor ML-7 thereby reduced infection with HSV-1 and SFTSV, confirming the importance of the NMMHC-IIa and IIb in the entry of these viruses. In contrast to the proviral role of the NMMHC-IIa and IIb, the non-muscle myosin II has also

been reported to suppress membrane fusion and subsequent infection of the paramyxovirus Sendai virus [48]. Although these results highlight a role for myosin during the entry phase of several viruses, we did not observe a reduction in the number of cells expressing newly synthesized RSV proteins in a single round of infection experiment upon transfection of MYLK4-targeting siRNAs. These results suggest that a possible role for MYLK4 during RSV infection rather involves late stages of the RSV infection cycle. During RSV infection, viral RNPs synthesized in cytoplasmic IBs and viral transmembrane proteins synthesized in the ER/Golgi are thought to be transported to the site of virion assembly at the plasma membrane by myosin-driven transport along actin filaments [51, 52]. As such, MYLK4 knockdown may reduce this myosin-driven transport, leading to reduced virion assembly and release, thereby causing a smaller RSV plaque size. Recently, Mehedi and colleagues found that RSV infected A549 cells, but not calu-3 or Vero cells, induce the formation of filopodia which can reach more than 50 µm in length and which contain actin filaments [53]. These filopodia were used to transport RSV to neighboring uninfected cells. Currently, we are testing if we can also detect RSV-induced filopodia formation and if the length of these filopodia is reduced upon transfection of MYLK4-targeting siRNAs, which could explain the reduced RSV plaque size.

Although we observed a reduced RSV plaque size upon transfection of several, unrelated MYLK4-targeting siRNAs, a number of observations indicate that the reduced RSV plaque size may not be caused by on-target silencing of MYLK4, but rather might depend on off-target effects. First, the knockdown efficiency of MYLK4 by the different siRNAs did not always correlate to the RSV plaque phenotype. For example, MYLK4 siRNA #6 and #8 most strongly reduced overexpressed MYLK4 protein, yet these siRNAs did not reduce RSV plaque size. Secondly, we did not observe a restored RSV plaque formation upon rescue of MYLK4 expression. Lastly, RSV plaque formation was not hampered in single cell A549 clones expected to lack MYLK4 protein expression. As described in more detail in chapter 3 section 3, off-target effects of RNAi technology are divided in sequence-independent and sequence-dependent effects. As we did not observe reductions in RSV plaque size upon transfection of several non-targeting siRNAs, sequence-independent effects of the MYLK4-targeting siRNAs are unlikely to have caused the reduced RSV plaque size. Furthermore, we found no evidence of IFN induction by MYLK4 siRNA #1 and #4, although we did not yet test IFN induction by the other MYLK4-targeting siRNAs. These results suggest that sequence-dependent off-target silencing of mRNAs by miRNA-like mechanisms are the most plausible cause of possible off-target effects caused by the MYLK4-targeting siRNAs. To investigate this, we are currently analyzing transcriptome data obtained by RNA sequencing from A549 cells transfected with 15 nM non-targeting siRNA #2, RSV-N siRNA, MYLK4 siRNA #1 and MYLK4 siRNA #4. The RNA sequencing was performed twice to evaluate the reproducibility of possible off-target effects. One of our goals is to identify one or more gene(s) with a reduced expression at the mRNA level in both cells transfected with MYLK4 siRNA #1 and #4 compared to the cells transfected with non-targeting siRNA #2 or the RSV-N siRNA, which we consider as a non-targeting siRNA for the human genome as it was optimized to contain at least 3 mismatches with every human gene [15]. Although further analysis is needed, RNA sequencing results unexpectedly indicate that the expression of several hundreds of genes is deregulated (> 2-fold), with the vast majority downregulated, in cells transfected with MYLK4-targeting siRNA #1 or #4 compared to the non-

targeting siRNA #2 or the RSV-N siRNA. Even if we compare the non-targeting siRNA #2 with the RSV-N siRNA, which both have been optimized to reduce off-target silencing of human genes, a few hundred genes are differentially regulated. These numbers are 10 to 30-fold higher compared to previous microarray-based estimates of off-target silenced genes upon transfection of siRNAs at a ~ 7-fold higher concentration (100 nM) [54, 55]. Taken together, these results highlight that siRNAs used at concentrations typically applied in RNAi experiments may easily deregulate hundreds of genes and that microarray-based estimates of off-target silencing may underestimate this significant problem.

A number of kinases and/or associated signaling pathways have been shown to be activated during RSV infection with some kinases being essential for RSV infection. We expected that these kinases, or at least a part of, would be identified in our siRNA-mediated knockdown screen of the human kinome. Although some of these kinases were indeed identified in our primary screens, most kinases only moderately affected RSV plaque size and were omitted during subsequent validation experiments. For example, the **EGFR** is activated during RSV infection [10, 56, 57], yet we did not find an altered RSV plaque size upon knockdown of the EGFR. In line with our observations, Currier and colleagues only observed a reduced replication of the RSV 2-20 strain and not of the RSV-A2 strain upon EGFR knockdown [21]. **CSNK2a** is necessary for RSV replication, likely by phosphorylating thr-205 of the RSV-M protein, which is essential for M oligomerization [58, 59]. Of the two tested CSNK2a isoforms in our screen, we only observed a moderate reduced plaque size at 6 dpi for CSNK2a1 in one of the three biological replicates, so this was not investigated further. In the siRNA-mediated knockdown screen performed by Kolokoltsov and colleagues, two kinases important for RSV replication were identified, *i.e.* **PAK1** and **MAP4K2** [9]. None of these two kinases, however, affected the RSV plaque size in our screen. This is particularly striking for PAK1, as we observed a reduced RSV plaque size after PAK1 knockdown by the same pool of 4 siRNAs that were purchased independently of the siRNA library. Possibly, some technical failure at the well containing the PAK1-targeting siRNAs during our screen has led to the absence of plaque size reduction. Several members of the **MAPK** family are essential for RSV infection [60-62]. Yet, we only observed a moderate reduction of RSV plaque size upon knockdown of MAPK8 and 11 in our initial screen, which we did not select for further analysis. The **PRKC** family is also essential for RSV infection [63-65]. In our screen, knockdown of PRKCE and -Q reduced RSV plaques only in one of the three biological replicates. Knockdown of two other isoforms, PRKCD and PRKCZ, gave opposite results on RSV plaque size in both primary knockdown screens (staining of RSV plaques at 6 and 3/4 dpi). Yet two other isoforms, PRKCA and PRKCG, enhanced RSV plaque size upon knockdown. PRKCG was subsequently tested in the RSV replication kinetics, but we could not observe an increase in the RSV titer upon PRKCG knockdown. **PRKD** is persistently activated during the course of a RSV infection [66]. We observed an increased plaque size in all three biological replicates at 6 dpi upon knockdown of PRKD3, however, in the subsequent RSV replication kinetics we observed a reduction in titer. Lastly, RSV activates a **PI3K/Akt**-dependent pathway to suppress premature apoptosis of the infected cell [67]. Of the nine PI3K isoforms that were tested in the primary knockdown screens, only isoform C2B and R3 (named as PIK3C2B and PIK3R3 in the library) moderately increased RSV plaque size at 6 dpi in all three biological replicates. These isoforms were, however, not selected to test in the RSV replication kinetics. Knockdown of AKT1 enhanced RSV plaque size at 6 dpi

and had a trend of increasing the RSV titer, however, this increase was not significant. Therefore, AKT1 was not investigated further. Knockdown of AKT3 on the other hand only reduced RSV plaque size in one biological replicate.

Overall, we were surprised that so few kinase-targeting siRNAs affected RSV plaque formation in a consistent manner and that it was hard to confirm the importance of a number of published kinases during RSV infection. Yet, we believe that important roles for certain kinases during RSV infections cannot be excluded with our results. We hypothesize that some characteristics of siRNA-mediated knockdown may have contributed to false negative results in our primary knockdown screens. As siRNA-mediated knockdown not completely abolishes protein expression, small residual expression levels of kinases may have been sufficient to allow normal RSV replication, especially since kinases are catalytic enzymes. Possibly, a portion of cells in our assay were not transfected with siRNA. We transfected subconfluent A549 cells with siRNA for 48 hours, meaning that cells could divide 1 or 2 times to reach confluency at 48 hours post siRNA transfection. If a cell was not transfected, we expect that this cell would result in a small cluster of cells without siRNA. If a RSV virion initiates infection within such a cluster, than normal RSV replication is expected to occur, at least until a siRNA transfected cells is reached. As we infected with a limited number of plaque forming units, a fair number of such "siRNA-free" clusters could have contributed to false negative results. Although we did not test this, fluorescently labeled siRNAs could have been used to determine the percentage of transfected cells. Most published kinases important for RSV replication have been identified by using kinase inhibitors. Although often claimed to be kinase-specific, these inhibitors often tend to inhibit different families of kinases with comparable IC_{50} values. These inhibitors generally also do not allow to discriminate between different kinase isoforms. With our siRNA-mediated knockdown screen we aimed to discriminate between closely related kinase isoforms. Yet, the intrinsic capacity of siRNAs to knock down one isoform at a time may have been a bottleneck to identify kinases important for RSV replication, as other kinase isoforms might compensate for the loss of a single isoform. In addition to compensation between kinase isoforms, alternative signaling pathways may also have been activated during the rather long assay of 6 days of RSV infection. As siRNA transfected A549 cells had reached confluency by the time of RSV infection, such compensatory circuits might be much more tolerated compared to dividing cells.

5.4 Conclusion

Knockdown of MYLK4 by multiple siRNAs reduced the plaque size of both laboratory and clinical RSV isolates of both the A and B subtype, which initially suggested that MYLK4 plays an important role during RSV infection. Restoring MYLK4 expression during siRNA-mediated knockdown of endogenous MYLK4, however, did not rescue the RSV plaque phenotype. Furthermore, RSV plaque formation was not reduced in MYLK4 knockout cells. These results suggest that off-target silencing by multiple MYLK4-targeting siRNAs caused the reduced RSV plaque size. Preliminary RNA sequencing results indeed suggest that siRNAs may target several hundreds of transcripts. Our study highlights the importance of profound validation of RNAi results by other techniques and shows that siRNAs used at concentrations widely applied in the RNAi field may be less specific than generally assumed.

5.5 Material and methods

Cells

A549 cells (a kind gift from Dr M.L. Hammarskjold, University of Virginia-School of Medicine, USA or ATCC, CCL-185 (a kind gift from Prof. Dr. Sven Eyckerman, Ghent University, Belgium)) and Hep-2 cells (ATCC, CCL-23) were grown in Dulbecco's modified eagle medium (DMEM) supplemented with 10% heat-inactivated fetal calve serum (FCS) and 2 mM L-glutamine (BE17-605F, Lonza) at 37°C and 5% CO_2. HEK293T cells (a kind gift from Dr M. Hall, University of Birmingham, Birmingham, UK) and HeLa cells (ATCC, CCL-2) were grown as A549 cells, but medium was supplemented with 0,4 mM sodium-pyruvate (S8636, Sigma-Aldrich) and 0,1 mM non-essential amino acids (BE13-114E, Lonza). Calu-1 cells (ATCC, HTB-54) were grown in RPMI1640 medium supplemented with 10% FCS and 2 mM L-glutamine at 37°C and 5% CO_2.

SiRNA sequences

We used the siGENOME® SMARTpool® siRNA Library- Human Protein Kinase (G-003505, lot #09174, GE Healthcare Dharmacon, Inc., Lafayette, CO), which consists of pools of 4 siRNAs targeting 714 different human kinases. A list of the siRNAs targeting nucleolin, PAK1, clathrin light chain B, RSV-nucleoprotein (target sequence: GGCUCUUAGCAAAGUCAAG), AMHR2, CSNK1G1, EPHB2, IRAK3, MYLK4, NEK5, PIK3R5, PDGFRB, PNKP, PRKACG and TTBK1 can be found in supplementary table 3. Non-targeting siRNAs used as negative control are also included in supplementary table 3. All siRNAs, except IRAK3 siRNA #5-8 and MYLK4 siRNA #5-8, were purchased from Dharmacon (GE Healthcare Dharmacon, Inc., Lafayette, CO) and consist of two complementary RNA strands of 19 nucleotides with the addition of 2 dT overhangs at each 3' end. IRAK3 siRNA #5-8 and MYLK4 siRNA #5-8 were purchased from Qiagen and consist of two complementary RNA strands of 19 nucleotides with the addition of a 2 dT overhang at the 3' end of the sense strand and 2 nucleotides complementary to the target sequence at the 3' end of the antisense strand.

SiRNA transfection

In 96-well plates, 5.000 A549 cells per well (unless otherwise specified) were seeded in 85 µl complete DMEM medium and grown overnight at 37°C and 5% CO_2. SiRNA and DharmaFECT-1 transfection reagent (T-2001, GE Healthcare Dharmacon, Inc., Lafayette, CO) were diluted in Opti-MEM™ reduced serum medium to a final concentration of 150 nM and dilution of 1/80, respectively (each in 10 µl per well), unless otherwise specified. SiRNA and DharmaFECT-1 were mixed and incubated at room temperature (RT) for 20 min, to allow lipid-siRNA complex formation. Complete DMEM medium was added to a final volume of 100 µl per well, resulting in a final siRNA concentration of 15 nM and DharmaFECT-1 diluted 1/800. SiRNA inoculum was added to A549 cells for 6h and subsequently replaced by complete DMEM medium, unless otherwise stated. Forty-eight hours post siRNA transfection, A549 cells were either lysed or infected with RSV. We monitored for cytotoxicity at 24h and 48h post siRNA transfection by visual inspection of the cell monolayer with light microscopy.

RSV cultivation and plaque assay

We used laboratory RSV strains (RSV-A2 (ATCC-VR1540); RSV-A long (ATCC-VR26), a kind gift from Dr Rik De Swart, Erasmus MC, Rotterdam, The Netherlands and RSV-B1 (ATCC-VR1580)) and clinical RSV strains (RSV-A2001 (BEI resource), RSV-A MAD/GM2_13/12, RSV-A MON/9/92, RSV-B MAD/GM3_7/13 and RSV-B MAD/GM3_5/13, the latter 4 being a kind gift from Prof. Dr. José Melero, Instituto de Salud Carlos III, Madrid, Spain). RSV stocks were prepared by inoculating HEp-2 cells with RSV in DMEM medium supplemented with 2% FCS and 2 mM L-glutamine until cytopathogenic effects were visible. Supernatants and HEp-2 cells were collected with a cell scraper and centrifuged at 1,000 x g for 8 min. Cleared supernatants was mixed with polyethylene glycol-6000 to a final concentration of 10% and incubated at 4°C for 4 hours with constant shaking. Polyethylene glycol was centrifuged at 3,000 x g for 30 min and supernatants was removed. The virus containing pellet was gently washed and resuspended in Hank's balanced salt solution supplemented with 20% sucrose. The resuspended virus was aliquoted in cryovials, snap frozen in liquid nitrogen and stored at -80°C.

Confluent monolayers of A549 cells (at 48h post siRNA transfection or after overnight incubation upon cell seeding) were washed with Opti-MEM™ reduced serum medium to remove serum containing DMEM medium. About 35 plaque forming units (PFU) were added per 96-well in Opti-MEM™ reduced serum medium and allowed to enter A549 cells for 4h at 37°C. After 4h, the RSV inoculum was replaced by DMEM medium supplemented with 2% FCS, 2 mM L-glutamine and 0,6% (w:v) avicel RC-851 (FMC biopolymers). RSV infection was allowed to continue for 3 to 7 days at 37°C depending on the experiment, after which the culture medium was removed and cells were fixed with 4% paraformaldehyde in phosphate buffered saline (PBS) for 20 min at RT. Cells were then washed 2x with PBS and permeabilized with 0,2% Triton-X100 for 10 min at RT. Cells were blocked with 1% bovine serum albumin (BSA, A4503 Sigma-Aldrich) in PBS for at least 1h. RSV plaques were stained with a polyclonal goat anti-RSV serum (AB1128, EMD Millipore) diluted 1:1000 in 0,5% BSA in PBS for 2h at RT and a horseradish peroxidase conjugated anti-goat IgG (Sc-2020, Santa Cruz biotechnology, Inc.) diluted 1:3000 in 0,5% BSA in PBS for 1h at RT. After each antibody inoculation, cells were washed 4x with PBS. Plaques were visualized by TrueBlue™ Peroxidase substrate (5510, Sera Care) and washed with water when plaque intensity was satisfactory.

SDS-PAGE and western blotting

Total cell lysates were prepared with a low salt lysis buffer (50 mM Tris pH 8.0, 150 mM NaCl, 5 mM EDTA, 1% NP40, 0.1% SDS and complete protease inhibitor cocktail (04693132001, Sigma-Aldrich)). Lysis of cells was allowed for 20 min on ice. Cell lysates were boiled for 10 min at 99°C in 1x Laemmli buffer supplemented with 4,2% (v:v) β-mercaptoethanol. Proteins were separated by SDS-PAGE and semi-dry blotted on nitrocellulose membranes. Membranes were blocked with a 4% (w:v) low fat milk solution in PBS with 0,1% Tween20. Proteins were detected by the following primary antibodies: nucleolin (C23 (MS-3): sc-8031, Santa Cruz biotechnology, Inc.), PAK1 (2602, Cell signaling technology), Clathrin light chain B (Clathrin LCB (H-60): sc-28277, Santa Cruz biotechnology, Inc.) and MYLK4 (24309-1-AP, Proteintech). As a control for equal loading, we detected actin (MAB1501, Chemicon

international). We used secondary Amersham ECL Mouse or Rabbit IgG, HRP-linked whole Ab (NA931 and NA934, respectively, GE healthcare) and Pierce™ ECL Western blotting substrate (32106, ThermoFisher Scientific). Protein bands were visualized with radiographic films or a chemiluminescence imager (Amersham Imager 600, GE Healthcare). Band intensities were quantified by Melanie™ software and normalized to the intensity of the reference gene Actin.

RNA isolation

A549 cells were detached by a 0,05% trypsin/1 mM EDTA solution and centrifuged at 400 x g for 5 min. The cell pellet was resuspended in 200 µl PBS and RNA was extracted by using the High Pure RNA isolation kit (11 828 665 001, Roche) according to the manufacturer's protocol with small adaptations. Briefly, cells were lysed for 10 min at RT and the lysate was transferred to filter tubes containing two layers of glass fiber fleece. After centrifugation, DNA was degraded on the filter by incubating DNase I for 15 min at RT. After consecutive washing steps, RNA was eluted from the filter with water and quantified spectrophotometrically at 260 nm. RNA was either used directly to reverse transcribe into complementary DNA (cDNA) or stored at -80°C for later use.

RT-PCR

RNA was reverse transcribed into cDNA by using the transcriptor first strand cDNA synthesis kit (04 897 030 001, Roche) according to the manufacturer's protocol. Briefly, five µg RNA was mixed with anchored oligo dT primer at a final concentration of 2,5 µM and heated to 65°C for 10 min to denature secondary RNA structures. After denaturation, we added the following components: transcriptor reverse transcriptase reaction buffer, protector RNase inhibitor, deoxynucleotide mix and transcriptor reverse transcriptase. As a negative control we also prepared a parallel sample without the reverse transcriptase. cDNA synthesis was performed for 1 hour at 50°C, followed by heat inactivating the reverse transcriptase for 5 min at 85°C.

IRAK3, MYLK4 and DDX39B cDNA was amplified by PCR with the following gene-specific primers: IRAK3 (forward: AACAGCCAATGTCACCGTGGAT, reverse: GCAGCCAACTCTAGTATGTTTGGG), MYLK4 (forward: AGCTGTACGATGCCTTCGAGTCTA, reverse: GGAAAGGCGACAAACCGCTAAGTA) and DDX39B (forward: GTTATGGCAGAGAACGATGTGGA, reverse: GTCTTCTACCGTGTCTGTTCAATGTAGGA). Five µl cDNA was PCR amplified with phusion HF DNA polymerase (F530L, Thermo Fisher scientific). PCR products were separated by 1,5% agarose and stained with ethidium bromide.

RT-qPCR

RNA was reverse transcribed into cDNA as described above except that we used a mix of oligo dT primer and a MYLK4-specific primer (GGAAAGGCGACAAACCGCTAAGTA), both at a final concentration of 2,5 µM. We amplified cDNA quantitatively by using the Sensifast™ SYBR® No-ROX kit (BIO-98020, Bioline) in a Roche lightcycler® 480 instrument. We used the following gene-specific primers: MYLK4 (forward: AGCTGTACGATGCCTTCGAGTCTA, reverse: CAGGATGGTATCAAGCTCCGTCAA), ACTB

(forward: CTCTTCCAGCCTTCCTTCCT, reverse: AGCACTGTGTTGGCGTACAG), UBC (forward: ATTTGGGTCGCGGTTCTTG, reverse: TGCCTTGACATTCTCGATGGT), PPIA (forward: GCATACGGGTCCTGGCATCTTGTCC, reverse: ATGGTGATCTTCTTGCTGGTCTTGC). Cp values were analysed by qBase+ and MYLK4 expression values were normalised to the reference genes ACTB, UBC and PPIA. Normalized MYLK4 expression values were calculated relative to DharmaFECT-1 treatment.

Immunofluorescence

A549 cells or HEK293T cells were fixed with 4% paraformaldehyde for 20 min, permeabilised with 0,2% Triton-X100 in PBS for 10 min and subsequently blocked with 1% BSA in PBS for 2 hours at RT. RSV infected cells were stained with a polyclonal goat anti-RSV serum (AB1128, EMD Millipore) diluted 1:3000 in 0,5% BSA in PBS for 1h at RT and an Alexa fluor 488 conjugated donkey anti-goat IgG (Invitrogen) diluted 1:500 in 0,5% BSA in PBS for 1h at RT. MYLK4 was stained with a polyclonal rabbit antiserum (24309-1-AP, Proteintech) and an Alexa fluor 488 conjugated donkey anti-rabbit IgG (Invitrogen) diluted 1:500 in 0,5% BSA in PBS for 1h at RT. After each antibody inoculation, cells were washed 4x with 0,1% Tween20 in PBS. Cell nuclei were stained with Hoechst (Invitrogen) for 15 min at RT. For the quantification of RSV infected cells, immunofluorescent pictures were taken with a Nikon AZ100M macroscope and analysed in Volocity (Perkin Elmer). Infected cells were detected by the tool "find spots" which searches for fluorescent signals above background after setting a treshold automatically. Counted spots were finally normalized for the surface area of analysis.

Cell viability assay

We measured cell viability by using the CellTiter 96® Aqueous Non-Radioactive Cell Proliferation assay (G5421, Promega) according to the manufacturer's protocol with small adaptations. This colorimetric assay determines the conversion of a novel tetrazolium compound (3-(4,5-dimethylthiazol-2-yl)-5-(3-carboxymethoxyphenyl)-2-(4-sulfophenyl)-2H-tetrazolium; MTS) to its soluble formazan product by dehydrogenase enzymes found in metabolically active cells in the presence of an electron coupling reagent (PMS). Briefly, we dissolved 46 mg MTS in 23 ml of PBS and adjusted the pH to 6,0-6,5. We added 100 µl PMS (10x) solution to 2,0 ml MTS solution, mixed well and filtered the solution through a 0,2 µm filter. We added 10 µl of MTS/PMS solution per 96-well and incubated the cells further at 37°C and 5% CO_2. We measured the absorbance at 490 nm at 20 min, 1h , 2h and 4h post inoculation. As the colorimetric reaction occurred fast, we selected the earliest measurement of 20 min to avoid saturation. Absorbance values were calculated relative to untransfected A549 cells.

IFN induction assay

To investigate the potential induction of IFN by MYLK4 siRNA #1 and #4, we used an IFN reporter plasmid (pISRE-Fluc, stratagene) with firefly luciferase under control of the IFN inducible IFIT1 promoter. We transfected 3 million HEK293T cells by polyethyleneimine (PEI, 23966-1, polysciences Inc.) with 5 µg pISRE-Fluc plasmid and 1 µg of a plasmid with *Renilla* luciferase under control of the constitutive CMV-IE promoter. Briefly, DNA and PEI were diluted in Opti-MEM™ reduced serum

medium and mixed for 10 minutes at RT in a 1:5 ratio (5 µl PEI (1 mg/ml) per µg of DNA). DNA:PEI complexes were added to the HEK293T cells dropwise and culture medium was refreshed after 6h. In parallel, A549 cells were transfected with siRNA (15 nM) or Poly I:C (0,2 or 1,0 µg/ml) by DharmaFECT-1 (diluted 1/500) as described above. Poly I:C was used as a positive control for IFN induction. Twenty-four hours post transfection, HEK293T cells were detached, 30.000 cells seeded in 96-well plates and grown overnight. HEK293T cells were subsequently inoculated for 24 hours with A549 culture supernatans harvested at 24 or 48 hours post transfection. Firefly – and *Renilla* luciferase were detected by using the dual-luciferase reporter assay system (E1910, Promega) according to the manufacturer's protocol and a luminometer (Glomax, Promega). Firefly luciferase values were divided by *Renilla* luciferase values to normalize for transfection efficacy.

Cloning of IRAK3 and MYLK4 expression vectors

By using Gateway® cloning technology we transferred the IRAK3 and MYLK4 cDNA sequence from the corresponding entry vectors from the human ORFeome library v8.1 (CCSB human ORFeome collection) into a destination vector for mammalian constitutive expression by the CMV-IE promoter. This destination vector contains a Flag tag and myc tag just outside of the LR recombination sites, thereby fusing a Flag tag and myc tag in frame at the N - and C terminus, respectively, of IRAK3 or MYLK4. The resulting expression plasmids were named pEXPR-IRAK3 and pEXPR-MYLK4, respectively. In order to perform MYLK4 rescue experiments, we generated a pENTRY-MYLK4 vector carrying 5 silent wobble base mutations in the target sequence of MYLK4 siRNA #1 (WT: TGACGGAGCTTGATACCAT; mutant: TGAC**T**GA**A**CT**C**GA**C**AC**A**AT) and #4 (WT: CCAGAGGCATGAAGGACAA; mutant: C**A**AG**G**GG**A**ATGAA**A**GA**T**AA). We chose wobble base mutations that generate codons with a codon usage as similar as possible to the wild type codon. This pENTRY-MYLK4_siRes vector was subsequently recombined with the same destination vector as mentioned above to generate an expression plasmid, called pEXPR-MYLK4_siRes vector, which allows constitutive expression of MYLK4 siRNA #1 and #4 resistant MYLK4 in mammalian cells.

By using Gateway® cloning technology we transferred the MYLK4 encoding sequence from the pENTRY-MYLK4_siRes vector to a lentiviral destination vector, pDG2-Flag-rtTA3. This destination vector encodes a reverse tetracycline transactivator and puromycin resistance marker under control of the constitutive SV40 early promoter. The resulting expression vector was called pDG2-MYLK4_siRes-Flag-rtTA3 and encodes MYLK4 siRNA #1 and #4 resistant MYLK4 with a C-terminal Flag tag under control of a doxycycline inducible promoter (minimal CMV promoter with 6 tetracycline operator sequences). This vector also encodes the necessary lentiviral packaging signals.

Lentiviral transduction of A549 cells

We generated lentiviral transduced A549 cells with doxycycline inducible expression of MYLK4 siRNA #1 and #4 resistant MYLK4 and GFP. HEK293T cells (T75 falcon) were cotransfected by PEI (1:5) with 4 µg pDG2-MYLK4_siRes-Flag-rtTA3 or pDG2-GFP-rtTA3 plasmid, two helper plasmids (1,2 µg pMD2-VSV-G and 2,6 µg pCMV-ΔR8.91) and 1 µg of a plasmid constitutively expressing GFP to monitor

transfection efficacy. As a negative control, we also cotransfected HEK293T cells with all plasmids except for the pDG2-MYLK4_siRes-Flag-rtTA3 or pDG2-GFP-rtTA3 plasmid. Forty-eight hours post transfection, cell culture supernatant was collected and filtered through a 0,45 µm low protein binding filter to remove cell debris from the lentiviral particles. To increase the infection efficacy of the lentiviral particles, we added 8 µg/ml hexadimethrine bromide (polybrene) (107689, Sigma-Aldrich) to the lentiviral inoculum before addition to A549 cells. Seventy-two hours post inoculation, we selected stable transduced A549 cells by adding 2 µg/ml puromycin dihydrochloride (P8833, Sigma-Aldrich) to the culture medium. Puromycin selection was maintained for 48 hours, which was sufficient to kill all cells in the parallel negative control setting. Surviving A549 cells were expanded in normal culture medium without puromycin dihydrochloride, stored in liquid nitrogen and used to investigate RSV replication in the absence or presence of 1 µg/ml doxycycline hyclate (D9891, Sigma-Aldrich).

CRISPR/Cas9-mediated MYLK4 knockout

We used two gRNA design tools (the MIT Crispr design tool [29] and CRISPOR [30]) to select three gRNAs targeting MYLK4 with a high specificity and out of frame score and a low off target score in both tools. These three gRNAs, gRNA1 (GGGGACCAGGATTCAAGATC), gRNA2 (CAAACGCCGACCTGACGGAA) and gRNA3 (AATGTCGTTCTTAGACTCGA) target exon 2, 3 and 6 of MYLK4, respectively, that are present in all predicted MYLK4 transcripts. Each gRNA was cloned in the pSpCas9(BB)-2A-EGFP vector, which encodes a fusion protein between *Streptococcus pyogenes* derived Cas9 and 2A-EGFP at the C terminus. BpiI-mediated cleavage of this vector allows incorporation of gRNA duplexes under control of the human U6 RNA polymerase III promoter. For each gRNA a forward primer was synthesized by adding a CACCG sequence to the 5' end of the gRNA, whereas a reversed primer was synthesized by adding a AAAC sequence to the 5' end of the reverse complement sequence of the gRNA. Per gRNA 100 pmol of both forward and reverse primer was diluted in a total volume of 10 µl buffer (3 mM Hepes pH 7.5, 10 mM potassium acetate). This mix was heated to 100°C and gently cooled to RT to allow primer hybridization. The hybridized primers were subsequently diluted 200 times in ultrapure water. Two µl of each gRNA duplex was mixed with 100 ng pSpCas9(BB)-2A-EGFP plasmid, T4 ligation buffer, 2.5 units T4 DNA ligase (EL011, Thermo Fisher scientific) and 1 µl FastDigest BpiI (FD1014, Thermo Fisher scientific) in a total volume of 20 µl. This mix was incubated for 6 cycles of 5 min at 37°C and 5 min at 21°C to allow incorporation of each gRNA duplex in the empty Cas9 expression vector and transformed in *Escherichia coli* MC1061. Plasmids with insertion of each gRNA duplex were selected by colony PCR and verified by Sanger sequencing.

Three hundred thousand A549 cells from both sources (gift of M.L. Hammarskjold or ATCC) were separately transfected by lipofectamine 3000 (L3000-001, Thermo Fisher scientific) with 1 µg of pSpCas9(BB)-2A-EGFP plasmids containing each MYLK4 gRNA duplex. Forty-eight hours post transfection, A549 cells were detached to single cells, washed and resuspended in presort buffer (PBS with 1% BSA, 5 mM EDTA, 100 U/ml penicillin and 100 µg/ml streptomycin (15140122, Thermo fisher scientific)). Ninety-six single GFP positive A549 cells were sorted by FACS (BD FACS ARIA II) and seeded in a 96-well plate in conditioned A549 cell medium (0,22 µm filtered culture medium from near

confluent A549 cells grown for 3 days mixed with fresh culture medium in a 1:2 balance). In addition, we seeded the remaining GFP positive A549 cells as a polyclonal pool of cells. These polyclonal pools were used to test which gRNAs could cleave the genomic MYLK4 gene. Therefore, genomic DNA from 30.000 A549 cells was extracted by resuspending the cells in 30 µl QuickExtract™ DNA extraction solution (QE0905T, Illumina) and incubation at 65°C for 6 min and 98°C for 2 min. This genomic DNA was then used to PCR amplify the region surrounding the expected gRNA guided Cas9 cleavage site by using Kapa HiFi HotStart Ready mix (KK2601, Roche). We used the following primers: gRNA1 (forward: AAAGGACTCATTCGGGAGCG, reverse: CCGCGTGAGGAACTCAAGAT), gRNA2 (forward: ACAGAGGTCAAGGGTGATGC, reverse: GCTGTGGATACGCAATGCTG), gRNA3 (forward: TGGCAAAGCCCAGCTCATAA, reverse: ACCACTTTCCTCCAGGTTGC). The PCR products were purified by magnetic HighPrep™ PCR beads (AC-60050, Magbio): briefly, we added 18 µl resuspended beads per 10 µl PCR sample and incubated 10 min at RT. Supernatans was removed and the beads were washed twice with 200 µl 70% ethanol. When all the ethanol was evaporated, beads were resuspended in distilled water to elute DNA, which was then cleared from the beads. After purification, PCR products were treated with the mismatch-specific Surveyor® nuclease (706020, IDT). Therefore, we diluted 400 ng PCR product in Surveyor buffer (10 mM Tris-HCl pH 8.8, 1.5 mM $MgCl_2$, 50 mM KCl) and denatured/rehybridized the DNA in a thermal cycler according to the manufacturer's protocol. We then added 0,15M $MgCl_2$, 1 µl Surveyor® enhancer S and 1 µl Surveyor® nuclease S and incubated for 1 hour at 42°C. We then added Surveyor® Stop solution to terminate the nuclease reaction. Finally, we analysed the Surveyor® nuclease cleavage products by DNA agarose gel electrophoresis.

Single cell clones were analysed by extracting genomic DNA, PCR-based amplification of the region surrounding the expected gRNA guided Cas9 cleavage and purification of the PCR product as described above. The PCR products were sequenced by Sanger sequencing with the following primers: gRNA1 (CCTTTCTTTGCAGTCAAGAG) and gRNA2 (GGTGACGGGTGATTTTGCT). Sanger sequencing chromatograms were analysed by the tracking of indels by decomposition (TIDE) software tool to investigate how many alleles have insertion/deletion mutations and if these mutations result in a frame shift leading to a premature stop codon. Single cell clones with an expected premature stopcodon in both MYLK4 alleles were considered as MYLK4 knockout clones and used to investigate RSV replication by plaque assay.

Statistics

Repeated measurements data analysis: RSV replication kinetics data were analyzed as repeated measurements using the residual maximum likelihood (REML) approach as implemented in Genstat v18 [68]. Briefly, a linear mixed model with treatment (108 levels: 106 knockdown, 1 positive control, 1 composite negative control (Untransfected, DharmaFECT-1 and Non-targeting siRNAs)), time and treatment x time interaction as fixed terms, experiment as random term, and subject.time used as residual term, was fitted to the data. Times of measurement were set at equal intervals and an autoregressive correlation structure of order 1 with equal variances (i.e. homogeneity across time) was selected as best model fit, based on the Aikake Information Coefficient. Significances of the fixed terms

and significances of changes in differences between the 106 knockdown and negative control over time were assessed by an F-test; significances of overall differences between the 106 knockdown and negative control irrespective time, were assessed by a Wald test.

5.6 Acknowledgements

We thank Dr. Céline Van den Broeke (Ghent, Belgium) for providing the MEF cell lysates, Prof. Dr. José Melero (Madrid, Spain) for providing the clinical RSV isolates, Prof. Dr. Rik De Swart (Rotterdam, The Netherlands) for providing the RSV A long strain, Dr. Philippe De Groote for providing the pDG2-Flag-rtTA3 vector and Prof. Dr. Sven Eyckerman (Ghent, Belgium) for providing the A549 cells from the ATCC cell culture collection. We thank Amanda Gonçalves for guiding with the microscopy analysis. We also thank Dr. Francis Santens and Gert Van Isterdael for helping us with the design of the protocol and the FACS-based cell sorting, respectively, to generate knockout A549 cells clones.

5.7 Reference list

1. Besant, P.G. and P.V. Attwood, *Detection of a mammalian histone H4 kinase that has yeast histidine kinase-like enzymic activity.* Int J Biochem Cell Biol, 2000. **32**(2): p. 243-53.
2. Muimo, R., et al., *Histidine phosphorylation of annexin I in airway epithelia.* J Biol Chem, 2000. **275**(47): p. 36632-6.
3. Wagner, P.D. and N.D. Vu, *Histidine to aspartate phosphotransferase activity of nm23 proteins: phosphorylation of aldolase C on Asp-319.* Biochem J, 2000. **346 Pt 3**: p. 623-30.
4. Manning, G., et al., *The protein kinase complement of the human genome.* Science, 2002. **298**(5600): p. 1912-34.
5. Wang, Q., J.A. Zorn, and J. Kuriyan, *A structural atlas of kinases inhibited by clinically approved drugs.* Methods Enzymol, 2014. **548**: p. 23-67.
6. Adams, J.A., *Activation loop phosphorylation and catalysis in protein kinases: is there functional evidence for the autoinhibitor model?* Biochemistry, 2003. **42**(3): p. 601-7.
7. Roskoski, R.J. *FDA-approved protein kinase inhibitors*. 2017; Available from: http://www.brimr.org/PKI/PKIs.htm.
8. Tayyari, F., et al., *Identification of nucleolin as a cellular receptor for human respiratory syncytial virus.* Nat Med, 2011. **17**(9): p. 1132-5.
9. Kolokoltsov, A.A., et al., *Small interfering RNA profiling reveals key role of clathrin-mediated endocytosis and early endosome formation for infection by respiratory syncytial virus.* J Virol, 2007. **81**(14): p. 7786-800.
10. Krzyzaniak, M.A., et al., *Host cell entry of respiratory syncytial virus involves macropinocytosis followed by proteolytic activation of the F protein.* PLoS Pathog, 2013. **9**(4): p. e1003309.
11. San-Juan-Vergara, H., et al., *Cholesterol-rich microdomains as docking platforms for respiratory syncytial virus in normal human bronchial epithelial cells.* J Virol, 2012. **86**(3): p. 1832-43.
12. Jackson, A.L., et al., *Expression profiling reveals off-target gene regulation by RNAi.* Nat Biotechnol, 2003. **21**(6): p. 635-7.
13. Semizarov, D., et al., *Specificity of short interfering RNA determined through gene expression signatures.* Proc Natl Acad Sci U S A, 2003. **100**(11): p. 6347-52.
14. Gottlieb, J., et al., *ALN-RSV01 for prevention of bronchiolitis obliterans syndrome after respiratory syncytial virus infection in lung transplant recipients.* J Heart Lung Transplant, 2016. **35**(2): p. 213-21.
15. Alvarez, R., et al., *RNA interference-mediated silencing of the respiratory syncytial virus nucleocapsid defines a potent antiviral strategy.* Antimicrob Agents Chemother, 2009. **53**(9): p. 3952-62.
16. institute, S. *Genomics, evolution and function of protein kinases*. 2014; Available from: http://kinase.com/human/kinome/.
17. Bakre, A., et al., *Human respiratory syncytial virus non-structural protein NS1 modifies miR-24 expression via transforming growth factor-beta.* J Gen Virol, 2015. **96**(11): p. 3179-91.
18. Hahn, A.S., et al., *The ephrin receptor tyrosine kinase A2 is a cellular receptor for Kaposi's sarcoma-associated herpesvirus.* Nat Med, 2012. **18**(6): p. 961-6.
19. Bonaparte, M.I., et al., *Ephrin-B2 ligand is a functional receptor for Hendra virus and Nipah virus.* Proc Natl Acad Sci U S A, 2005. **102**(30): p. 10652-7.
20. Chakraborty, S., et al., *Kaposi's sarcoma-associated herpesvirus interacts with EphrinA2 receptor to amplify signaling essential for productive infection.* Proc Natl Acad Sci U S A, 2012. **109**(19): p. E1163-72.
21. Currier, M.G., et al., *EGFR Interacts with the Fusion Protein of Respiratory Syncytial Virus Strain 2-20 and Mediates Infection and Mucin Expression.* PLoS Pathog, 2016. **12**(5): p. e1005622.
22. Harcourt, J.L., et al., *Evaluation of the Calu-3 cell line as a model of in vitro respiratory syncytial virus infection.* J Virol Methods, 2011. **174**(1-2): p. 144-9.
23. Bridge, A.J., et al., *Induction of an interferon response by RNAi vectors in mammalian cells.* Nat Genet, 2003. **34**(3): p. 263-4.

24. Sledz, C.A., et al., *Activation of the interferon system by short-interfering RNAs.* Nat Cell Biol, 2003. **5**(9): p. 834-9.
25. Hornung, V., et al., *Sequence-specific potent induction of IFN-alpha by short interfering RNA in plasmacytoid dendritic cells through TLR7.* Nat Med, 2005. **11**(3): p. 263-70.
26. Judge, A.D., et al., *Sequence-dependent stimulation of the mammalian innate immune response by synthetic siRNA.* Nat Biotechnol, 2005. **23**(4): p. 457-62.
27. Sioud, M., *Induction of inflammatory cytokines and interferon responses by double-stranded and single-stranded siRNAs is sequence-dependent and requires endosomal localization.* J Mol Biol, 2005. **348**(5): p. 1079-90.
28. Patricelli, M.P., et al., *In situ kinase profiling reveals functionally relevant properties of native kinases.* Chem Biol, 2011. **18**(6): p. 699-710.
29. Zhang Lab, M. *Crispr design*. 2015; Available from: http://crispr.mit.edu:8079/.
30. Haeussler, M., et al., *Evaluation of off-target and on-target scoring algorithms and integration into the guide RNA selection tool CRISPOR.* Genome Biol, 2016. **17**(1): p. 148.
31. Peng, K.J., et al., *Characterization of two human lung adenocarcinoma cell lines by reciprocal chromosome painting.* Dongwuxue Yanjiu, 2010. **31**(2): p. 113-21.
32. Isaka, T., et al., *Chromosomal variations within aneuploid cancer lines.* J Histochem Cytochem, 2003. **51**(10): p. 1343-53.
33. Brinkman, E.K., et al., *Easy quantitative assessment of genome editing by sequence trace decomposition.* Nucleic Acids Res, 2014. **42**(22): p. e168.
34. Schultz, N., et al., *Off-target effects dominate a large-scale RNAi screen for modulators of the TGF-beta pathway and reveal microRNA regulation of TGFBR2.* Silence, 2011. **2**: p. 3.
35. Meier, R., et al., *Genome-wide small interfering RNA screens reveal VAMP3 as a novel host factor required for Uukuniemi virus late penetration.* J Virol, 2014. **88**(15): p. 8565-78.
36. Chan, J.Y., et al., *Identification of cardiac-specific myosin light chain kinase.* Circ Res, 2008. **102**(5): p. 571-80.
37. Taniguchi, M., et al., *New Isoform of Cardiac Myosin Light Chain Kinase and the Role of Cardiac Myosin Phosphorylation in alpha1-Adrenoceptor Mediated Inotropic Response.* PLoS One, 2015. **10**(10): p. e0141130.
38. Sellers, J.R., *Regulation of cytoplasmic and smooth muscle myosin.* Curr Opin Cell Biol, 1991. **3**(1): p. 98-104.
39. Zhi, G., et al., *Myosin light chain kinase and myosin phosphorylation effect frequency-dependent potentiation of skeletal muscle contraction.* Proc Natl Acad Sci U S A, 2005. **102**(48): p. 17519-24.
40. Ikebe, M., et al., *Structural requirement of the regulatory light chain of smooth muscle myosin as a substrate for myosin light chain kinase.* J Biol Chem, 1994. **269**(45): p. 28165-72.
41. Lee, R.D., M.Y. Song, and J.K. Lee, *Large-scale profiling and identification of potential regulatory mechanisms for allelic gene expression in colorectal cancer cells.* Gene, 2013. **512**(1): p. 16-22.
42. Herrer, I., et al., *RNA-sequencing analysis reveals new alterations in cardiomyocyte cytoskeletal genes in patients with heart failure.* Lab Invest, 2014. **94**(6): p. 645-53.
43. Arii, J., et al., *Non-muscle myosin IIA is a functional entry receptor for herpes simplex virus-1.* Nature, 2010. **467**(7317): p. 859-62.
44. Valiya Veettil, M., et al., *Interaction of c-Cbl with myosin IIA regulates Bleb associated macropinocytosis of Kaposi's sarcoma-associated herpesvirus.* PLoS Pathog, 2010. **6**(12): p. e1001238.
45. Dewerchin, H.L., et al., *Myosins 1 and 6, myosin light chain kinase, actin and microtubules cooperate during antibody-mediated internalisation and trafficking of membrane-expressed viral antigens in feline infectious peritonitis virus infected monocytes.* Vet Res, 2014. **45**: p. 17.
46. Sun, Y., et al., *Nonmuscle myosin heavy chain IIA is a critical factor contributing to the efficiency of early infection of severe fever with thrombocytopenia syndrome virus.* J Virol, 2014. **88**(1): p. 237-48.

47. Arii, J., et al., *Nonmuscle myosin heavy chain IIb mediates herpes simplex virus 1 entry.* J Virol, 2015. **89**(3): p. 1879-88.
48. Das, P., et al., *Phosphorylation of Nonmuscle myosin II-A regulatory light chain resists Sendai virus fusion with host cells.* Sci Rep, 2015. **5**: p. 10395.
49. Xiong, D., et al., *Nonmuscle myosin heavy chain IIA mediates Epstein-Barr virus infection of nasopharyngeal epithelial cells.* Proc Natl Acad Sci U S A, 2015. **112**(35): p. 11036-41.
50. Leemans, A., et al., *Antibody-Induced Internalization of the Human Respiratory Syncytial Virus Fusion Protein.* J Virol, 2017. **91**(14).
51. Brock, S.C., J.R. Goldenring, and J.E. Crowe, Jr., *Apical recycling systems regulate directional budding of respiratory syncytial virus from polarized epithelial cells.* Proc Natl Acad Sci U S A, 2003. **100**(25): p. 15143-8.
52. Santangelo, P.J. and G. Bao, *Dynamics of filamentous viral RNPs prior to egress.* Nucleic Acids Res, 2007. **35**(11): p. 3602-11.
53. Mehedi, M., et al., *Actin-Related Protein 2 (ARP2) and Virus-Induced Filopodia Facilitate Human Respiratory Syncytial Virus Spread.* PLoS Pathog, 2016. **12**(12): p. e1006062.
54. Birmingham, A., et al., *3' UTR seed matches, but not overall identity, are associated with RNAi off-targets.* Nat Methods, 2006. **3**(3): p. 199-204.
55. Jackson, A.L., et al., *Widespread siRNA "off-target" transcript silencing mediated by seed region sequence complementarity.* RNA, 2006. **12**(7): p. 1179-87.
56. Monick, M.M., et al., *Activation of the epidermal growth factor receptor by respiratory syncytial virus results in increased inflammation and delayed apoptosis.* J Biol Chem, 2005. **280**(3): p. 2147-58.
57. Bitko, V., et al., *Nonstructural proteins of respiratory syncytial virus suppress premature apoptosis by an NF-kappaB-dependent, interferon-independent mechanism and facilitate virus growth.* J Virol, 2007. **81**(4): p. 1786-95.
58. Bajorek, M., et al., *The Thr205 phosphorylation site within respiratory syncytial virus matrix (M) protein modulates M oligomerization and virus production.* J Virol, 2014. **88**(11): p. 6380-93.
59. Caly, L., H.M. Li, and D. Jans, *Host Factors Modulating RSV Infection: Use of Small Interfering RNAs to Probe Functional Importance.* Methods Mol Biol, 2016. **1442**: p. 93-117.
60. Kong, X., et al., *ERK-1/2 activity is required for efficient RSV infection.* FEBS Lett, 2004. **559**(1-3): p. 33-8.
61. Marchant, D., et al., *Toll-like receptor 4-mediated activation of p38 mitogen-activated protein kinase is a determinant of respiratory virus entry and tropism.* J Virol, 2010. **84**(21): p. 11359-73.
62. Caly, L., et al., *c-Jun N-terminal kinase activity is required for efficient respiratory syncytial virus production.* Biochem Biophys Res Commun, 2017. **483**(1): p. 64-68.
63. Monick, M., et al., *Respiratory syncytial virus infection results in activation of multiple protein kinase C isoforms leading to activation of mitogen-activated protein kinase.* J Immunol, 2001. **166**(4): p. 2681-7.
64. San-Juan-Vergara, H., et al., *Protein kinase C-alpha activity is required for respiratory syncytial virus fusion to human bronchial epithelial cells.* J Virol, 2004. **78**(24): p. 13717-26.
65. Masaki, T., et al., *A nuclear factor-kappaB signaling pathway via protein kinase C delta regulates replication of respiratory syncytial virus in polarized normal human nasal epithelial cells.* Mol Biol Cell, 2011. **22**(13): p. 2144-56.
66. Rezaee, F., et al., *Sustained protein kinase D activation mediates respiratory syncytial virus-induced airway barrier disruption.* J Virol, 2013. **87**(20): p. 11088-95.
67. Thomas, K.W., et al., *Respiratory syncytial virus inhibits apoptosis and induces NF-kappa B activity through a phosphatidylinositol 3-kinase-dependent pathway.* J Biol Chem, 2002. **277**(1): p. 492-501.
68. Payne R., M.D., Harding S., *An Introduction to the Genstat Command Language (18th Edition), Part 3 Procedures*, V. International, Editor. 2015.

5.8 Supplementary figures

A

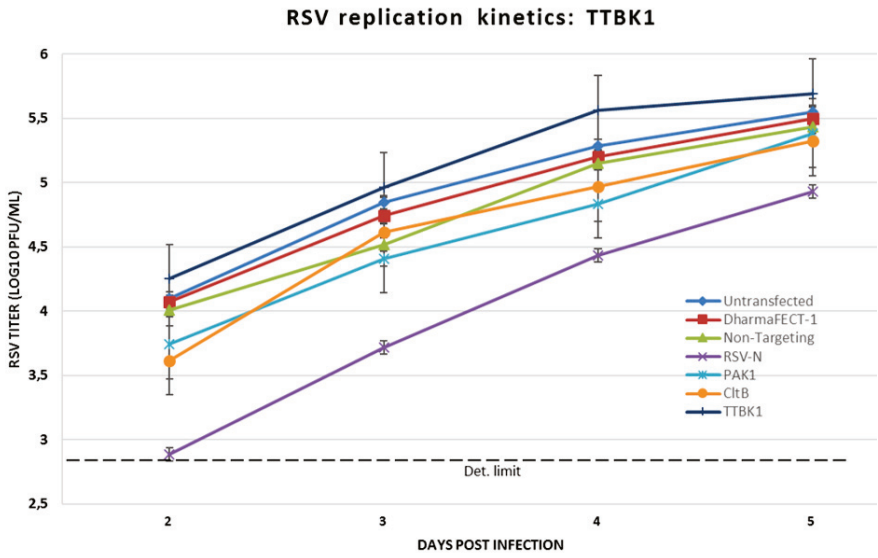

B

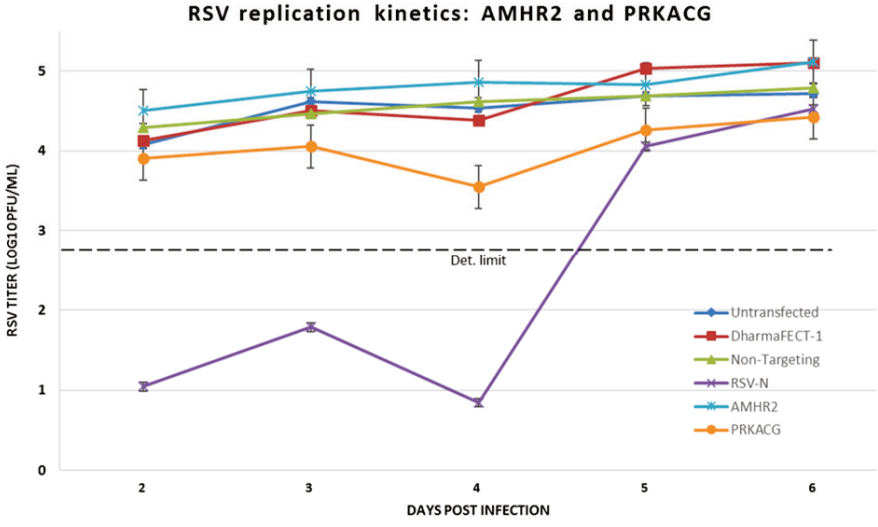

C

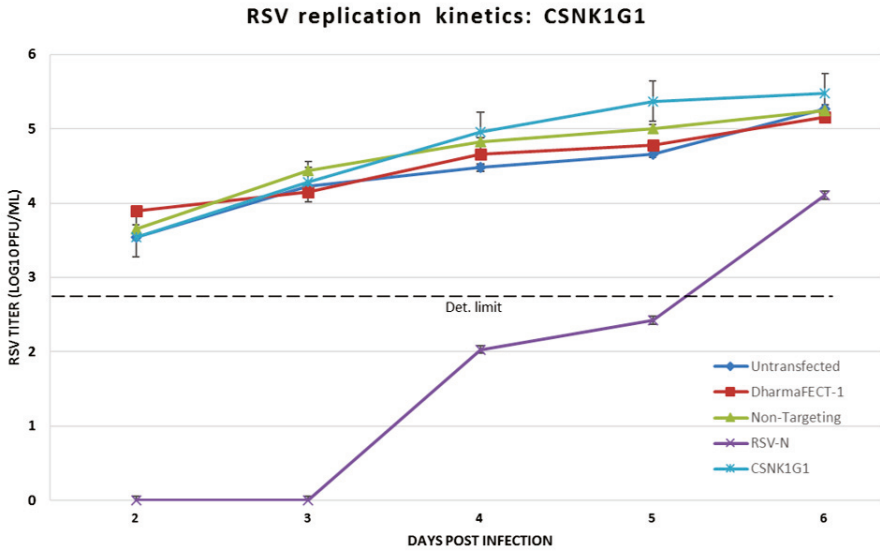
RSV replication kinetics: CSNK1G1
RSV TITER (LOG10PFU/ML)
DAYS POST INFECTION
Det. limit
Untransfected
DharmaFECT-1
Non-Targeting
RSV-N
CSNK1G1

D

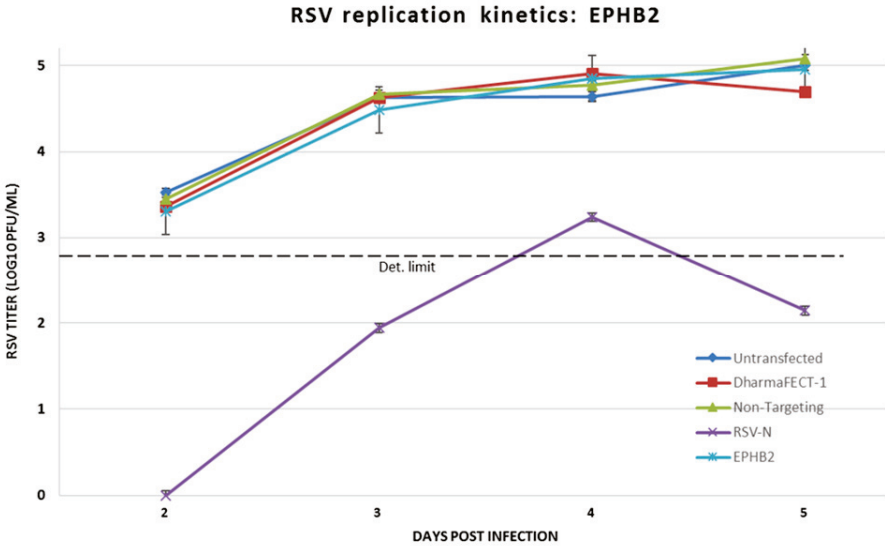
RSV replication kinetics: EPHB2
RSV TITER (LOG10PFU/ML)
DAYS POST INFECTION
Det. limit
Untransfected
DharmaFECT-1
Non-Targeting
RSV-N
EPHB2

E

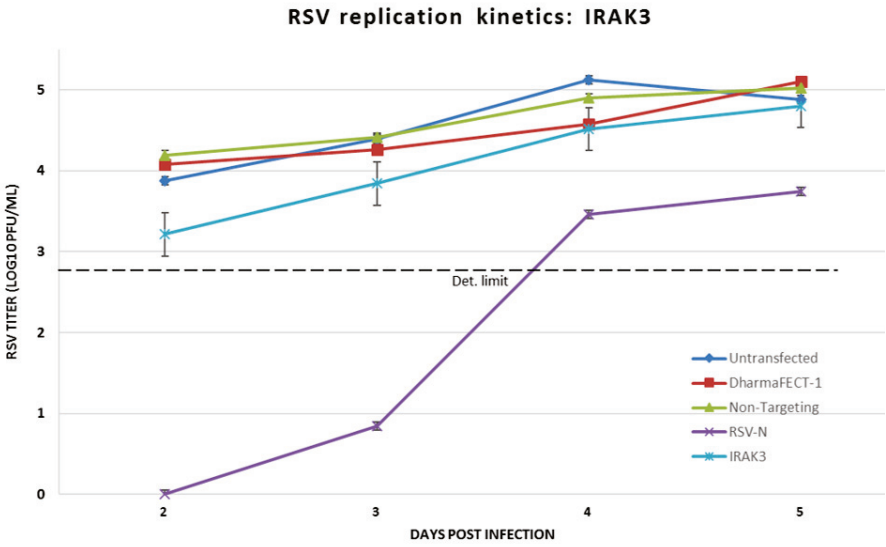
RSV replication kinetics: IRAK3
RSV TITER (LOG10 PFU/ML)
DAYS POST INFECTION
Det. limit
Untransfected
DharmaFECT-1
Non-Targeting
RSV-N
IRAK3

F

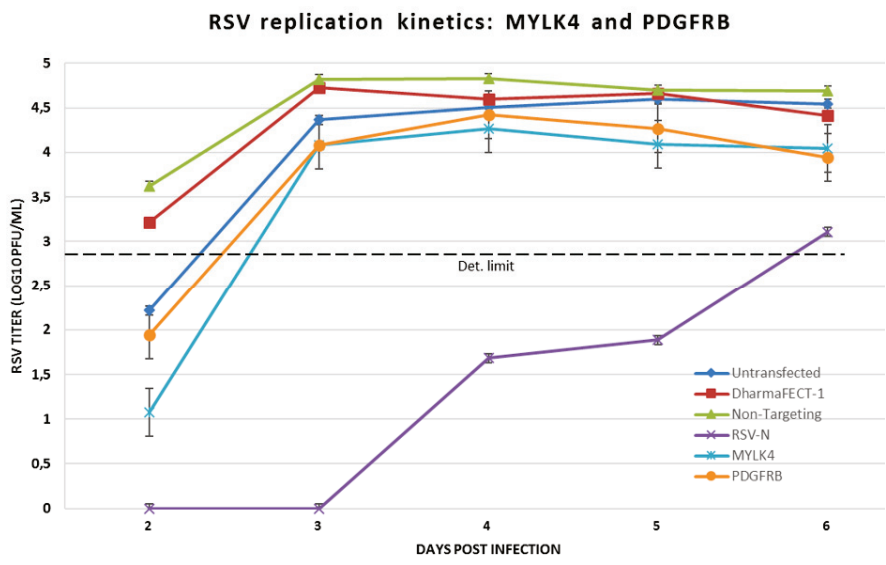
RSV replication kinetics: MYLK4 and PDGFRB
RSV TITER (LOG10 PFU/ML)
DAYS POST INFECTION
Det. limit
Untransfected
DharmaFECT-1
Non-Targeting
RSV-N
MYLK4
PDGFRB

G

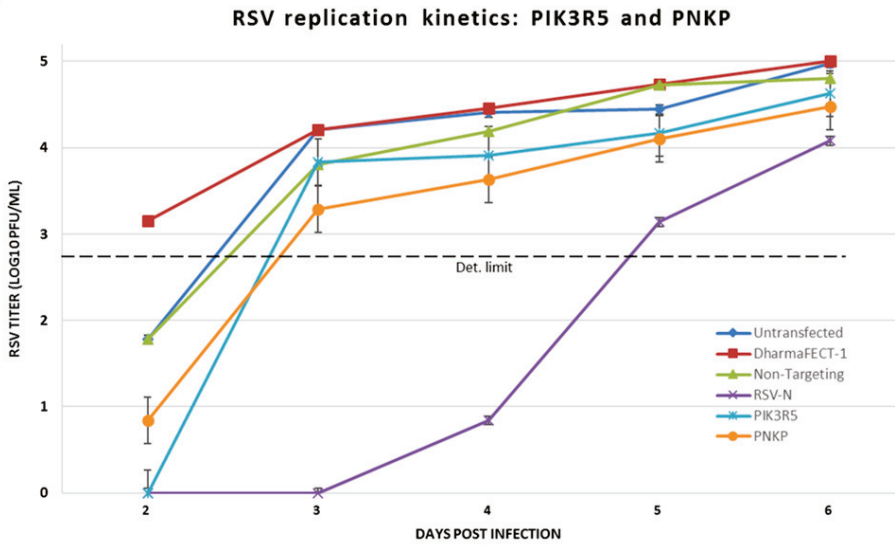

Supplementary figure 1: RSV replication kinetics. A549 cells were seeded in 96-well plates and transfected with 15 nM siRNA by using DharmaFECT-1 (1/800). Six hours post siRNA transfection, culture medium was refreshed. Forty-eight hours post siRNA transfection, cells were infected with RSV-A2 (MOI ~ 0,003) and cell culture supernatants was harvested daily from 2 until 5 or 6 days post infection. Viral titers were plotted over time as the average titer +/- SEM of 3 biological replicates. To not overload the graphs we only show the curves for the control treated cells (untransfected, DharmaFECT-1, Non-targeting siRNAs and RSV-N siRNA) and 10 kinases that were selected for further validation, *i.e.*TTBK1 (A), AMHR2 and PRKACG (B), CSNK1G1 (C), EPHB2 (D), IRAK3 (E), MYLK4 and PDGFRB (F) and PIK3R5 and PNKP (G). As a control we also tested PAK1 and CLT B siRNAs (A). In each graph we marked the detection (Det.) limit (Log_{10} PFU/ml ~ 2,82). Note that for some titers we could measure an average titer below the detection limit as the titer of one or two of the three biological replicates were above the detection limit.

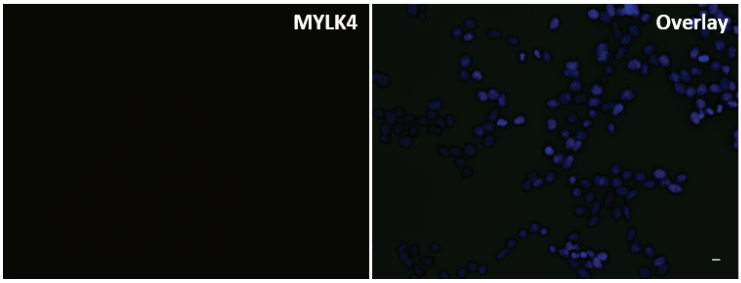

Supplementary figure 2: Secondary antibody only control for immunofluorescence-based detection of MYLK4 after transient overexpression in HEK293T cells. HEK293T cells were transfected with an expression vector for MYLK4 under the control of the constitutive CMV-IE promoter. Twenty-four hours post transfection, HEK293T cells were stained with the anti-rabbit secondary antibody only (left) and nuclei were stained with Hoechst (right, overlay). Scale bar = 10 µm.

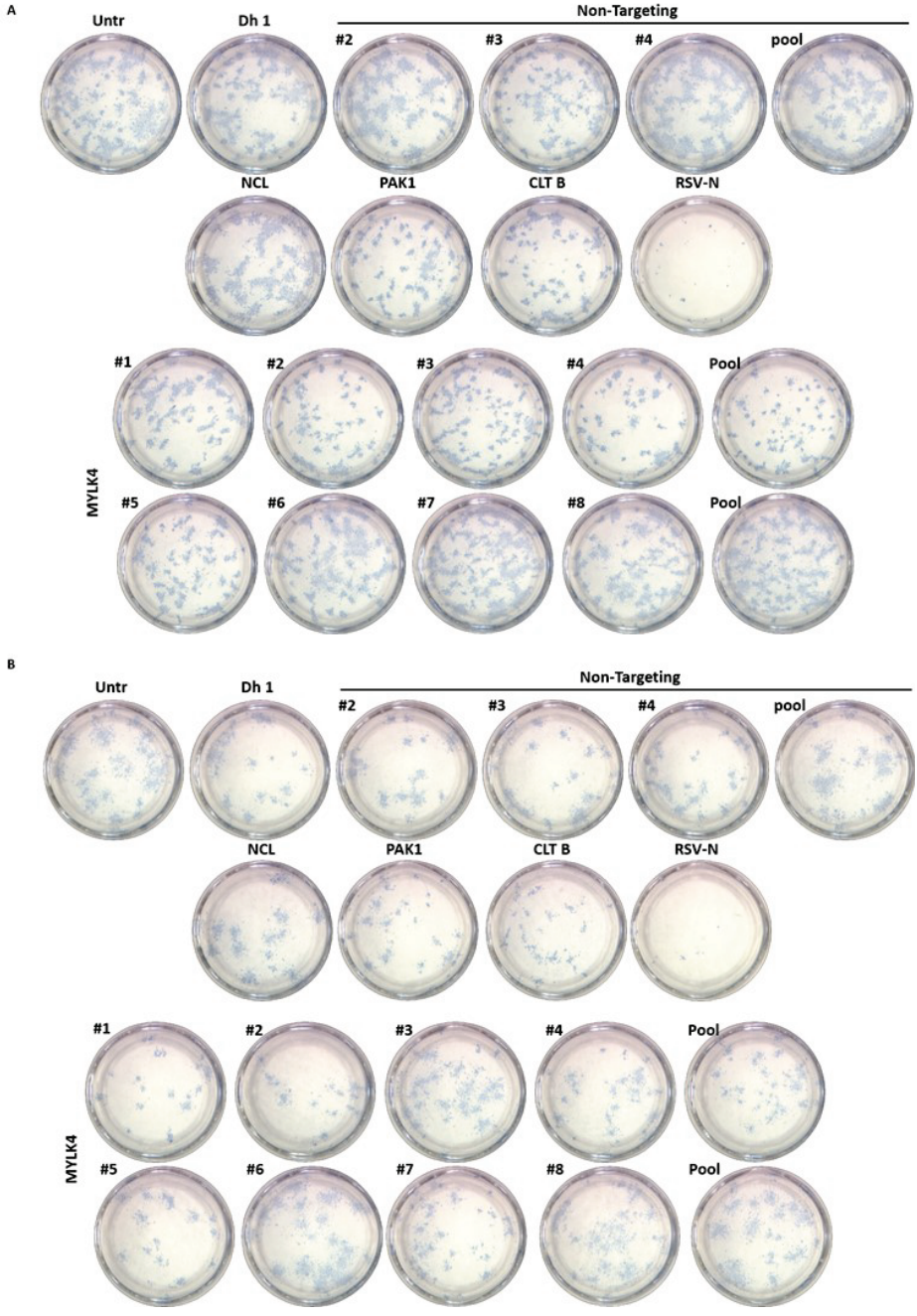

Supplementary figure 3: MYLK4-targeting siRNAs from Dharmacon reduce RSV plaque size of both laboratory and clinical RSV isolates. A549 cells were seeded in 96-well plates and transfected with 15 nM siRNA by using DharmaFECT-1 (1/500). Six hours post siRNA transfection, culture medium was

refreshed. Forty-eight hours post siRNA transfection cells were infected with (A) RSV-A MON/9/92 for 6 days and (B) RSV-B MAD/GM3_5/13 for 6 days. Untr = untransfected, Dh 1 = DharmaFECT-1 only, NCL = nucleolin, CLT B = clathrin light chain B.

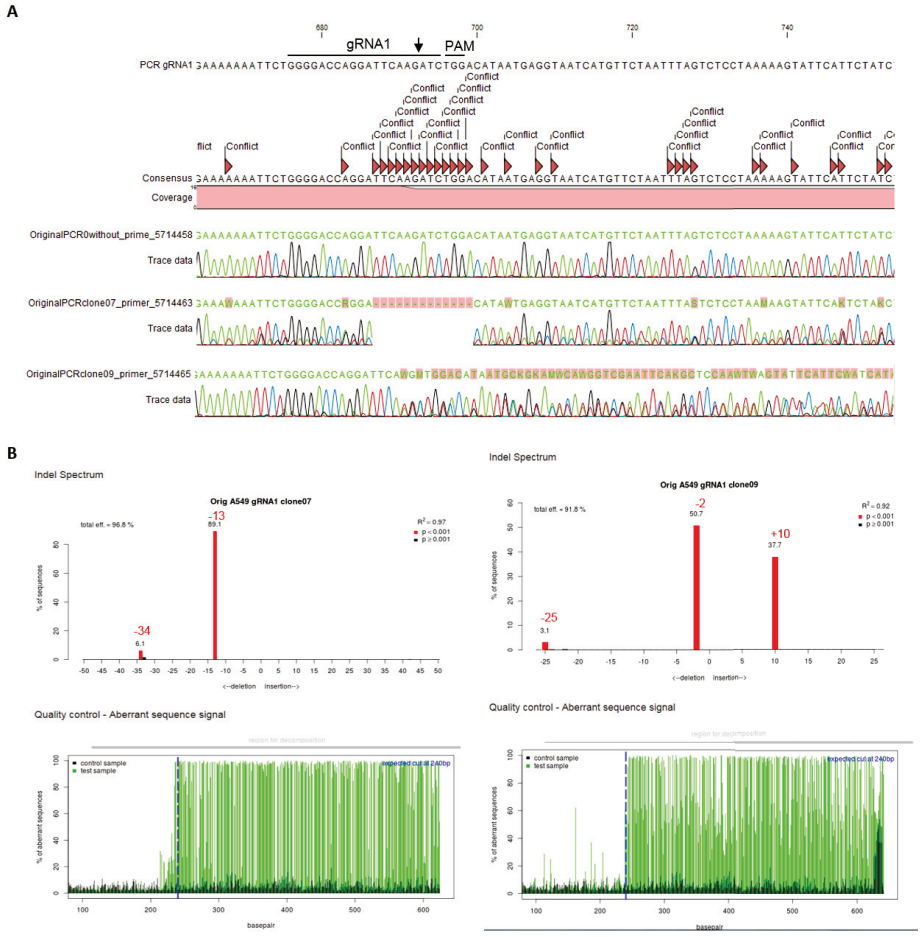

Supplementary figure 4: Genomic MYLK4 sequence analysis in A549 cells expressing guideRNA1. (A) Sanger sequencing of the PCR-amplified genomic MYLK4 region surrounding the expected Cas9 cleavage site from wild type A549 cells (= "*without*" chromatogram) and single cell clones #7 and #9 that were transfected with the pX458-w/t Cas9-2A-EGFP vector expressing Cas9-EGFP and gRNA1. On top of the consensus sequence we marked the gRNA1 sequence, the PAM sequence and the expected Cas9 cleavage site (arrow). (B) TIDE analysis of the Sanger sequencing chromatogram of clone #7 and #9.

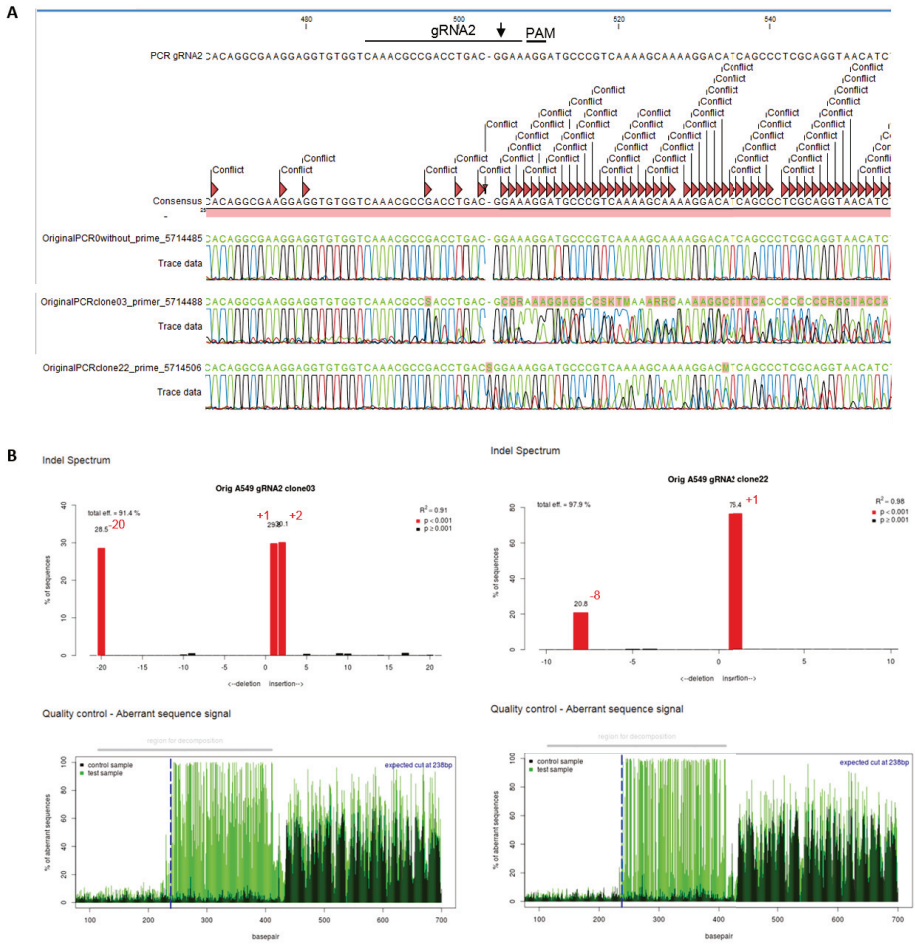

Supplementary figure 5: Genomic MYLK4 sequence analysis in A549 cells expressing guideRNA2. (A) Sanger sequencing of the PCR-amplified genomic MYLK4 region surrounding the expected Cas9 cleavage site from wild type A549 cells (= "*without*" chromatogram) and single cell clone #3 and #22 that were transfected with the pX458-w/t Cas9-2A-EGFP vector expressing Cas9-EGFP and gRNA2. On top of the consensus sequence we marked the gRNA2 sequence, the PAM sequence and the expected Cas9 cleavage site (arrow). (B) TIDE analysis of the Sanger sequencing chromatogram of clone #3 and #22.

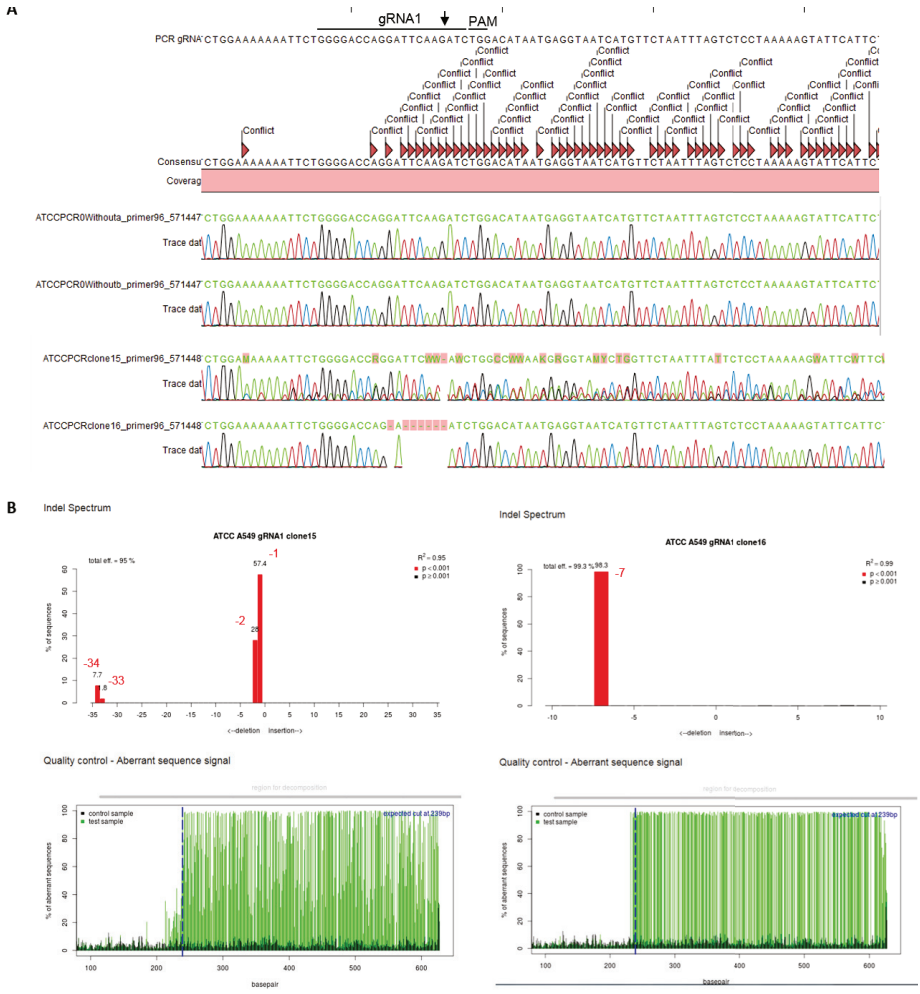

Supplementary figure 6: Genomic MYLK4 sequence analysis in A549 ATCC cells expressing guideRNA1. (A) Sanger sequencing of the PCR-amplified genomic MYLK4 region surrounding the expected Cas9 cleavage site from two wild type, single cell A549 ATCC clones (= "*without a"* and *"without b"* chromatogram) and single cell clone #15 and #16 that were transfected with the pX458-w/t Cas9-2A-EGFP vector expressing Cas9-EGFP and gRNA1. On top of the consensus sequence we marked the gRNA1 sequence, the PAM sequence and the expected Cas9 cleavage site (arrow). (B) TIDE analysis of the Sanger sequencing chromatogram of clone #15 and #16.

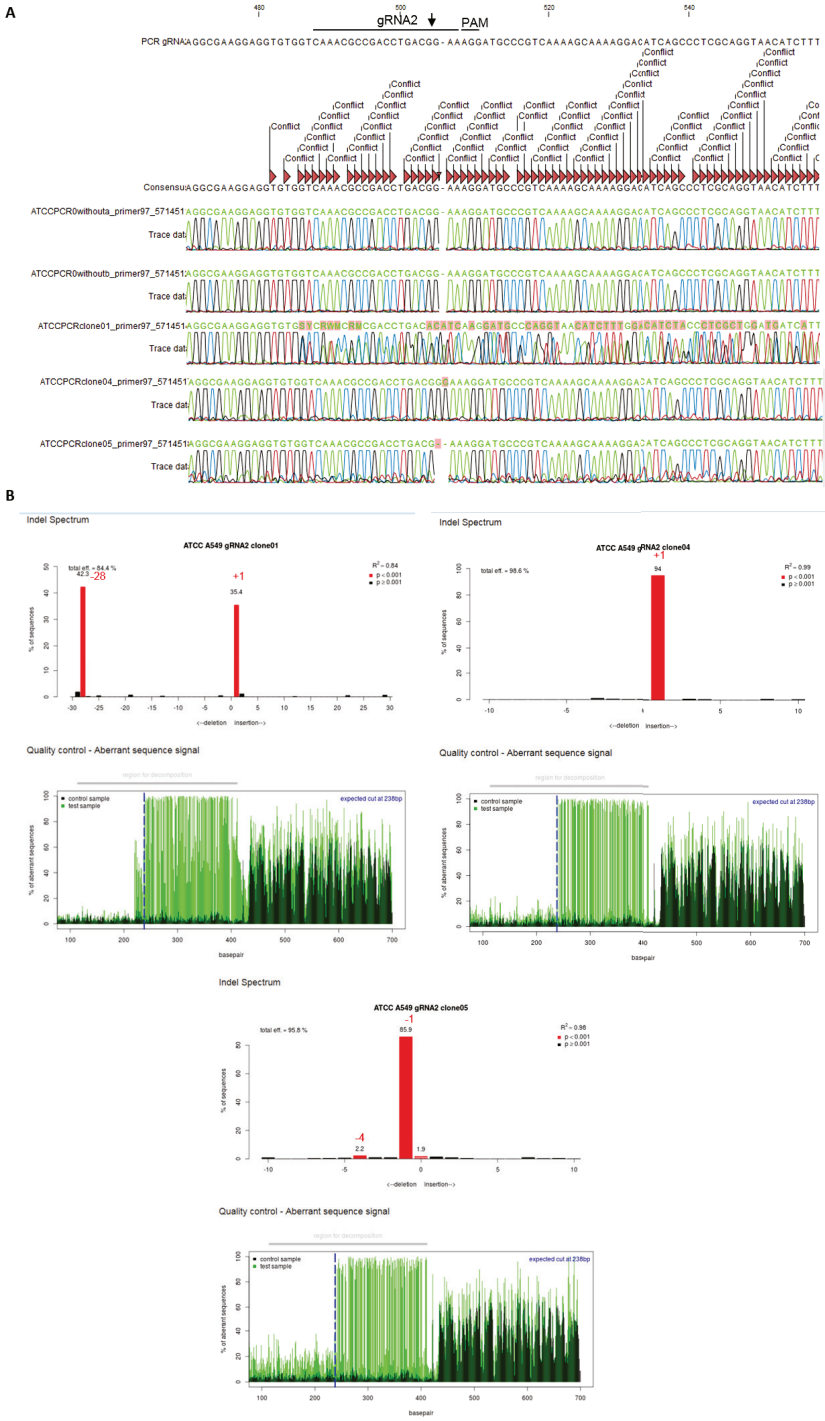
A
gRNA2
PAM
PCR gRNA
Consensus
ATCCPCR0withouta_primer97_571451
ATCCPCR0withoutb_primer97_571451
ATCCPCRclone01_primer97_571451
ATCCPCRclone04_primer97_571451
ATCCPCRclone05_primer97_571451
Trace data
B
Indel Spectrum
ATCC A549 gRNA2 clone01
ATCC A549 gRNA2 clone04
ATCC A549 gRNA2 clone05
Quality control - Aberrant sequence signal
control sample
test sample
expected cut at 238bp
basepair
% of sequences
% of aberrant sequences
<--deletion insertion-->
region for decomposition

Supplementary figure 7: Genomic MYLK4 sequence analysis in A549 ATCC cells expressing guideRNA2. (A) Sanger sequencing of the PCR-amplified genomic MYLK4 region surrounding the expected Cas9 cleavage site from two wild type, single cell A549 ATCC clones (= "*without a"* and *"without b"* chromatogram) and single cell clone #1, #4 and #5 that were transfected with the pX458-w/t Cas9-2A-EGFP vector expressing Cas9-EGFP and gRNA2. On top of the consensus sequence we marked the gRNA2 sequence, the PAM sequence and the expected Cas9 cleavage site (arrow). (B) TIDE analysis of the Sanger sequencing chromatogram of clone #1, #4 and #5.

5.9 Supplementary tables

Supplementary table 1: Primary hits from the human kinome knockdown screens (6 or 3/4 dpi)

Gene Name	Gene ID	Upon siRNA-mediated knockdown			
		Reduced RSV plaque size		Increased RSV plaque size	
		Screen		Screen	
		6 DPI	3/4 DPI	6 DPI	3/4 DPI
DKFZP761P0423	**157285**				
AATK	**9625**				
ADCK2	**90956**				
AK3	**205**				
EPHB6	**2051**				
PSKH1	**5681**				
LTK	**4058**				
MAP3K1	**4214**				
STK22D	**83942**				
MYLK4	**340156**				
GK	**2710**				
IRAK3	**11213**				
KIAA1811	**84446**				
MERTK	**10461**				
PRKACG	**5568**				
STK16	**8576**				
NEK5	**341676**				
RIOK3	8780				
ACVR1B	**91**				
ALK	**238**				
BCR	613				
CDK3	1018				
CDKL1	**8814**				
CDKN2C	**1031**				
DYRK3	**8444**				
DYRK4	**8798**				
EPHB2	**2048**				
FN3KRP	79672				
HUNK	**30811**				
MAGI-3	**260425**				
MAP4K5	**11183**				
MARK4	**57787**				
MET	**4233**				
MGC4796	**83931**				
MPP2	**4355**				
PIK3R5	**23533**				
PASK	23178				
PDGFRB	**5159**				
PFKL	**5211**				

Supplementary table 1 continued…

Gene Name	Gene ID	Upon siRNA-mediated knockdown			
		Reduced RSV plaque size		Increased RSV plaque size	
		Screen		Screen	
		6 DPI	3/4 DPI	6 DPI	3/4 DPI
PIK3C2A	**5286**				
PNKP	**11284**				
SSTK	**83983**				
STK11	6794				
STK23	**26576**				
UCK1	**83549**				
VRK2	**7444**				
VRK3	**51231**				
WNK4	**65266**				
ADCK4	79934				
ARAF1	369				
ATM	472				
ATR	545				
BMPR2	659				
BMX	660				
BRAF	673				
CAMK2B	816				
CASK	8573				
CHUK	1147				
COL4A3BP	10087				
CRKL	1399				
CSNK1A1	1452				
DLG2	1740				
ERBB3	**2065**				
ETNK1	55500				
FGFR2	2263				
GRK5	2869				
HAK	115701				
HK3	3101				
HRI	27102				
JAK3	3718				
LCK	3932				
LMTK2	22853				
MAP3K10	4294				
MAP3K12	7786				
MAP3K14	9020				
MAP3K15	389840				
MAP3K9	4293				
MAP4K1	11184				
MARK1	4139				

Supplementary table 1 continued…

Gene Name	Gene ID	Upon siRNA-mediated knockdown			
		Reduced RSV plaque size		Increased RSV plaque size	
		Screen		Screen	
		6 DPI	3/4 DPI	6 DPI	3/4 DPI
MAST2	23139				
MPP3	4356				
NEK1	4750				
NEK7	140609				
NME3	4832				
NME6	10201				
NRBP	29959				
NYD-SP25	89882				
PACSIN1	29993				
PAK4	10298				
PAK6	56924				
PANK1	53354				
PCK1	5105				
PHKG1	5260				
PIP5K1A	**8394**				
PKIB	5570				
PKM2	5315				
PLK3	1263				
PRKAB1	5564				
PTK6	5753				
RAF1	5894				
RPS6KA6	27330				
RPS6KB2	6199				
SGK	6446				
SPHK2	56848				
STK22B	**23617**				
STK24	8428				
STK38L	23012				
SYK	6850				
TP53RK	112858				
TRIO	7204				
ZAK	51776				
ARK5	9891				
ERN1	2081				
LYN	4067				
MAPK11	**5600**				
MYLK2	85366				
NEK3	4752				
PCTK1	**5127**				
ROCK1	6093				
RP6-213H19.1	51765				
SPHK1	8877				

Supplementary table 1 continued…

Gene Name	Gene ID	Upon siRNA-mediated knockdown			
		Reduced RSV plaque size		Increased RSV plaque size	
		Screen		Screen	
		6 DPI	3/4 DPI	6 DPI	3/4 DPI
PRKACB	5567				
RBKS	64080				
AK2	204				
AKT3	10000				
C14ORF20	283629				
CAMK1	8536				
CAMK1D	57118				
CAMKK2	10645				
CDC7	8317				
CDK10	8558				
CDKL4	344387				
CDKN2D	1032				
CKM	1158				
CRIM1	51232				
CSNK1A1L	122011				
CSNK1D	1453				
CSNK2A1	1457				
CSNK2B	1460				
DDR1	780				
DDR2	4921				
DGKB	1607				
EPHA2	1969				
EPHA3	2042				
EPHA4	2043				
EPHA5	2044				
FGFRL1	53834				
FRDA	2395				
FYN	2534				
GAK	2580				
GRK1	6011				
GRK4	2868				
GRK7	131890				
GSG2	83903				
GSK3B	2932				
GUCY2F	2986				
GUK1	2987				
HUS1	3364				
ILK-2	55522				
KALRN	8997				
KCNH2	3757				
KDR	3791				
KIAA1639	57729				
KIAA1765	85443				
LIMK2	3985				
LOC390226	390226				
LRRK2	120892				
MAP2K2	5605				

Supplementary table 1 continued…

Gene Name	Gene ID	Upon siRNA-mediated knockdown			
		Reduced RSV plaque size		Increased RSV plaque size	
		Screen		Screen	
		6 DPI	3/4 DPI	6 DPI	3/4 DPI
MAP3K11	4296				
MAP4K3	8491				
MAPK8	5599				
NME5	8382				
OSR1	9943				
PANK2	80025				
PAPSS2	9060				
PCK2	5106				
PCTK2	5128				
PDK1	5163				
PFKFB3	5209				
PFKFB4	5210				
PHKA2	5256				
PI4KII	55361				
PIP5KL1	138429				
PRKAA1	5562				
PRKCE	5581				
PRKCQ	5588				
PRKDC	5591				
PTK9	5756				
RIPK3	11035				
RPS6KC1	26750				
SCAP1	8631				
SGK2	10110				
SSTK	83983				
STK17A	9263				
STK25	10494				
STK31	56164				
TAF1	6872				
TEK	7010				
ULK1	8408				
URKL1	54963				
XYLB	9942				
PTK2	5747				
BUB1B	**701**				
FRAP1	**2475**				
HK2	**3099**				
HSMDPKIN	**55561**				
PRPF4B	**8899**				
TTBK1	**84630**				
CHEK1	**1111**				
CKMT2	**1160**				

Supplementary table 1 continued…

Gene Name	Gene ID	Upon siRNA-mediated knockdown			
		Reduced RSV plaque size		Increased RSV plaque size	
		Screen		Screen	
		6 DPI	3/4 DPI	6 DPI	3/4 DPI
DGKD	**8527**				
ILK	**3611**				
NAGK	**55577**				
PIK4CA	**5297**				
CALM3	**808**				
ITPKC	**80271**				
LMTK3	114783				
MAPK7	**5598**				
MOS	**4342**				
CIB2	**10518**				
GUCY2D	3000				
STK17B	**9262**				
IKBKB	3551				
MAP3K13	9175				
AURKC	**6795**				
ACVR1C	**130399**				
ANKRD3	54101				
AURKA	6790				
BRD4	**23476**				
CCRK	**23552**				
CDC42BPB	**9578**				
CSNK1G1	**53944**				
DGKG	**1608**				
DGKQ	**1609**				
DYRK1A	**1859**				
EFNA3	**1944**				
ERK8	**225689**				
EXOSC10	**5394**				
FES	**2242**				
FLJ10761	**55224**				
FLJ13052	**65220**				
GALK1	**2584**				
GCK	**2645**				
GSK3A	**2931**				
IKBKG	**8517**				
MAP3K8	**1326**				
MST1R	**4486**				
NLK	**51701**				
PDPK1	**5170**				
PIP5K2C	79837				
PRKCA	5578				
PYCS	**5832**				
STK10	6793				
AKT1	**207**				
FLJ23074	**80122**				
HIPK2	28996				
MVK	**4598**				
NPR2	**4882**				
PFKM	**5213**				

Supplementary table 1 continued…

Gene Name	Gene ID	Upon siRNA-mediated knockdown			
		Reduced RSV plaque size		Increased RSV plaque size	
		Screen		Screen	
		6 DPI	3/4 DPI	6 DPI	3/4 DPI
PRKAR1B	5575				
PRKD3	**23683**				
ACVR2B	93				
AK1	203				
CAMK1G	57172				
CAMKIINALPHA	55450				
CSF1R	1436				
DUSTYPK	25778				
FGFR1	2260				
HIPK3	10114				
ITK	3702				
JAK2	3717				
PDXK	8566				
PFKFB1	5207				
PIP5K3	200576				
PRKWNK1	65125				
PTK2B	2185				
RELA	5970				
SNRK	54861				
TNK2	10188				
TTK	7272				
UHMK1	127933				
BRD3	8019				
CDK4	1019				
CDK9	1025				
CDKN2B	1030				
CLK4	57396				
FGFR4	2264				
IKBKAP	8518				
IPMK	253430				
MAPKAPK3	7867				
PDK2	5164				
PIK3C2B	5287				
PIK3R3	8503				
PRKCG	**5582**				
PRKWNK3	65267				
PSKH2	85481				
STK3	6788				
STK35	140901				
TOPK	55872				
TPK1	27010				
TESK1	7016				
ACVR2	92				

Supplementary table 1 continued…

Gene Name	Gene ID	Upon siRNA-mediated knockdown			
		Reduced RSV plaque size		Increased RSV plaque size	
		Screen		Screen	
		6 DPI	3/4 DPI	6 DPI	3/4 DPI
ACVR2	92				
ADCK5	203054				
PANK4	55229				
STK19	8859				
CHEK2	11200				
DKFZP434C131	25989				
PACE-1	57147				
PHKB	5257				
CDKL5	**6792**				
MAP2K7	**5609**				
EPHA1	**2041**				
IGF2R	3482				
NTRK1	**4914**				
PKLR	**5313**				
PRKCZ	**5590**				
AMHR2	**269**				
ITPK1	3705				
MAP2K3	5606				
PFKP	5214				
PRKCD	**5580**				
ROR2	4920				
FUK	197258				

Genes in bold: were tested in a subsequent RSV growth kinetic experiment

Strong phenotypic response in all three biological replicates

Strong phenotypic response in two biological replicates or moderate phenotypic response in all three biological replicates

strong phenotypic response in one biological replicate or moderate phenotypic response in one or two biological replicates

Supplementary table 2: RSV replication kinetics of 104 human kinases: statistical analysis

Gene name	Gene ID	Statistical analysis 1 (average titer)		Statistical analysis 2 (slope of curve)		RSV kinetics	RSV plaque size
		Wald statistic	Probability	F statistic	Probability		
AATK	9625	1.27	0.260	0.63	0.640	red	red
ACVR1B	91	1.19	0.276	0.45	0.770	red	red
ACVR1C	130399	0.71	0.398	0.22	0.926	inc	inc
ADCK2	90956	0.78	0.378	0.58	0.677	inc	red
AK3	205	0.79	0.373	0.92	0.451	red	red
AKT1	207	0.06	0.814	0.05	0.996	inc	inc
ALK	238	2.66	0.103	3.78	**0.004**	red	red
AMHR2	269	4.42	0.036	4.88	**<0.001**	inc	inc
AURKC	6795	10.61	**0.001**	3.11	0.014	red	inc
BRD4	23476	3.13	0.077	1.46	0.213	red	inc
BUB1B	701	1.61	0.205	1.57	0.178	red	inc
CALM3	808	7.75	**0.005**	4.01	**0.003**	red	inc
CCRK	23552	1.63	0.202	0.74	0.565	inc	inc
CDC42BPB	9578	7.21	**0.007**	4.86	**<0.001**	inc	inc
CDKL1	8814	1.94	0.163	1.90	0.108	red	red
CDKL5	6792	3.82	0.051	4.00	**0.003**	red	both
CDKN2C	1031	10.62	**0.001**	3.41	**0.009**	red	red
CHEK1	1111	0.62	0.432	0.89	0.469	inc	inc
CIB2	10518	3.26	0.071	1.15	0.331	red	inc
CKMT2	1160	5.83	0.016	1.94	0.100	red	inc
CLT B	1212	1.46	0.227	4.35	**0.002**	red	red
CSNK1G1	53944	0.03	0.852	1.64	0.161	inc	inc
DGKD	8527	0.61	0.436	1.55	0.184	inc	inc
DGKG	1608	15.04	**<0.001**	5.88	**<0.001**	red	inc
DGKQ	1609	0.37	0.541	0.18	0.949	inc	inc
DKFZP761P0423	157285	6.71	0.010	2.17	0.069	red	red
DYRK1A	1859	0.96	0.327	1.55	0.184	inc	inc
DYRK3	8444	0.23	0.628	2.30	0.056	inc	red
DYRK4	8798	1.11	0.292	1.47	0.210	inc	red
EFNA3	1944	8.30	**0.004**	4.13	**0.002**	red	inc
EPHA1	2041	3.03	0.082	2.02	0.089	red	both
EphB2	2048	0.47	0.492	0.98	0.419	red	red
EPHB6	2051	2.95	0.086	1.08	0.365	red	red
ERBB3	2065	0.59	0.441	2.68	0.030	red	red
ERK8	225689	11.33	**<0.001**	4.13	**0.002**	red	inc
EXOSC10	5394	0.49	0.483	2.78	0.025	inc	inc
FES	2242	0.10	0.750	4.42	**0.001**	inc	inc
FLJ10761	55224	27.37	**<0.001**	10.65	**<0.001**	red	inc
FLJ13052	65220	0.17	0.681	0.97	0.422	red	inc
FLJ23074	80122	7.23	**0.007**	6.97	**<0.001**	inc	inc
FRAP1	2475	68.51	**<0.001**	18.33	**<0.001**	red	inc
GALK1	2584	2.09	0.149	3.08	0.015	inc	inc
GCK	2645	6.04	0.014	1.84	0.117	red	inc
GK	2710	10.36	**0.001**	7.60	**<0.001**	red	red
GSK3A	2931	1.92	0.166	0.57	0.685	inc	inc
HK2	3099	9.49	**0.002**	3.72	**0.005**	red	inc
HSMDPKIN	55561	9.31	**0.002**	2.36	0.051	red	inc
HUNK	30811	24.93	**<0.001**	9.13	**<0.001**	red	red
IKBKG	8517	0.21	0.650	0.20	0.941	inc	inc
ILK	3611	1.89	0.170	3.63	**0.006**	inc	inc
IRAK3	11213	14.19	**<0.001**	5.51	**<0.001**	red	red
ITPKC	80271	10.90	**<0.001**	4.27	**0.002**	red	inc
KIAA1811	84446	7.56	**0.006**	2.74	0.027	red	red
LTK	4058	0.02	0.879	0.56	0.692	inc	red
MAGI3	260425	0.26	0.609	0.79	0.529	inc	red

Supplementary table 2 continued…

Gene name	Gene ID	Statistical analysis 1 (average titer)		Statistical analysis 2 (slope of curve)		RSV kinetics	RSV plaque size
		Wald statistic	Probability	F statistic	Probability		
MAP2K7	5609	0.00	0.977	2.78	0.025	inc	both
MAP3K1	4214	1.30	0.254	0.65	0.628	red	red
MAP3K8	1326	16.08	**<0.001**	10.45	**<0.001**	inc	inc
MAP4K5	11183	9.14	**0.003**	6.08	**<0.001**	red	red
MAPK11	5600	5.04	0.025	1.61	0.168	red	red
MAPK7	5598	7.01	**0.008**	4.29	**0.002**	red	inc
MARK4	57787	12.87	**<0.001**	5.06	**<0.001**	red	red
MERTK	10461	2.43	0.119	1.23	0.294	red	red
MET	4233	6.81	**0.009**	4.10	**0.003**	red	red
MGC4796	83931	12.20	**<0.001**	3.86	**0.004**	red	red
MOS	4342	0.52	0.471	0.18	0.951	red	inc
MPP2	4355	7.09	**0.008**	3.52	**0.007**	inc	red
MST1R	4486	0.07	0.785	6.38	**<0.001**	inc	inc
MVK	4598	4.29	0.038	1.36	0.244	red	inc
MYLK4	340156	37.67	**<0.001**	18.90	**<0.001**	red	red
NAGK	55577	7.17	**0.007**	1.89	0.109	red	inc
NEK5	341676	1.34	0.247	1.24	0.290	red	red
NLK	51701	15.16	**<0.001**	4.06	**0.003**	red	inc
NPR2	4882	3.72	0.054	3.25	0.011	red	inc
NTRK1	4914	1.06	0.303	2.98	0.018	red	both
PIK3R5	23533	37.82	**<0.001**	18.22	**<0.001**	red	red
PAK1	5058	0.65	0.421	3.05	0.016	red	red
PCTK1	5127	0.92	0.339	1.13	0.342	red	red
PDGFRB	5159	20.04	**<0.001**	9.14	**<0.001**	red	red
PDPK1	5170	5.03	0.025	3.02	0.017	red	inc
PFKL	5211	3.17	0.075	0.87	0.480	inc	red
PFKM	5213	0.94	0.333	4.81	**<0.001**	red	inc
PIK3C2A	5286	0.11	0.737	0.92	0.449	inc	red
PIK4CA	5297	9.25	**0.002**	5.94	**<0.001**	red	inc
PIP5K1A	8394	8.66	**0.003**	9.40	**<0.001**	red	red
PKLR	5313	2.36	0.124	0.71	0.585	red	both
PNKP	11284	37.80	**<0.001**	13.03	**<0.001**	red	red
PRKACG	5568	28.70	**<0.001**	16.26	**<0.001**	red	red
PRKCD	5580	0.33	0.565	0.34	0.852	red	both
PRKCG	5582	0.35	0.553	0.68	0.608	inc	inc
PRKCN	23683	13.25	**<0.001**	8.91	**<0.001**	red	inc
PRKCZ	5590	0.56	0.453	1.05	0.379	red	both
PRPF4B	8899	4.56	0.033	1.81	0.123	red	inc
PSKH1	5681	9.85	**0.002**	3.22	0.012	red	red
PYCS	5832	20.72	**<0.001**	5.69	**<0.001**	red	inc
SSTK	83983	8.54	**0.003**	3.21	0.012	red	red
STK16	8576	2.41	0.121	2.72	0.028	red	red
STK17B	9262	7.30	**0.007**	3.34	0.010	red	inc
STK22B	23617	17.06	**<0.001**	13.45	**<0.001**	red	red
STK22D	83942	1.23	0.268	0.68	0.606	red	red
STK23	26576	1.58	0.209	1.22	0.300	red	red
TTBK1	84630	38.42	**<0.001**	11.87	**<0.001**	inc	inc
UCK1	83549	2.60	0.107	0.84	0.499	inc	red
VRK2	7444	6.25	0.012	2.43	0.045	red	red
VRK3	51231	0.13	0.715	0.22	0.929	inc	red
WNK4	65266	1.45	0.228	1.40	0.231	red	red

Genes in bold: statistically significant in at least one of both tests ($p < 0,01$).

Red = reduced, inc = increased

Supplementary table 3: siRNA sequences

Gene		catalogue number
Non-Targeting	siRNA #2	D-001210-02
	siRNA #3	D-001210-03
	siRNA #4	D-001210-04
Nucleolin	siRNA #1	D-003854-01
	siRNA #2	D-003854-02
	siRNA #3	D-003854-03
	siRNA #4	D-003854-04
PAK1	siRNA #1	D-003521-03
	siRNA #2	D-003521-05
	siRNA #3	D-003521-07
	siRNA #4	D-003521-21
Clathrin light chain B	siRNA #1	D-004003-01
	siRNA #2	D-004003-02
	siRNA #3	D-004003-03
	siRNA #4	D-004003-04
RSV-nucleoprotein	siRNA	[15]
AMHR2	siRNA #1	D-005307-01
	siRNA #2	D-005307-03
	siRNA #3	D-005307-04
	siRNA #4	D-005307-05
CSNK1G1	siRNA #1	D-004666-05
	siRNA #2	D-004666-06
	siRNA #3	D-004666-07
	siRNA #4	D-004666-08
EPHB2	siRNA #1	D-003122-07
	siRNA #2	D-003122-08
	siRNA #3	D-003122-25
	siRNA #4	D-003122-26
IRAK3	siRNA #1	D-004762-01
	siRNA #2	D-004762-02
	siRNA #3	D-004762-03
	siRNA #4	D-004762-04
	siRNA #5	SI02224278
	siRNA #6	SI02224285
	siRNA #7	SI00095431
	siRNA #8	SI04438868
MYLK4	siRNA #1	D-027171-01
	siRNA #2	D-027171-02
	siRNA #3	D-027171-03
	siRNA #4	D-027171-04
	siRNA #5	SI00500969
	siRNA #6	SI03068653
	siRNA #7	SI03102071
	siRNA #8	SI03120236

PIK3R5	siRNA #1	D-020619-01
	siRNA #2	D-020619-02
	siRNA #3	D-020619-03
	siRNA #4	D-020619-04
PDGFRB	siRNA #1	D-003163-05
	siRNA #2	D-003163-06
	siRNA #3	D-003163-07
	siRNA #4	D-003163-09
PNKP	siRNA #1	D-006783-03
	siRNA #2	D-006783-04
	siRNA #3	D-006783-05
	siRNA #4	D-006783-06
PRKACG	siRNA #1	D-004651-01
	siRNA #2	D-004651-02
	siRNA #3	D-004651-04
	siRNA #4	D-004651-06
TTBK1	siRNA #1	D-004680-01
	siRNA #2	D-004680-03
	siRNA #3	D-004680-05
	siRNA #4	D-004680-18

Chapter VI

A phosphoproteomics study of RSV infection

Koen Sedeyn, Delphi Van Haver, Francis Impens, Marnik Vuylsteke, Bert Schepens and Xavier Saelens

Author contributions: K.S., F.I., B.S. and X.S. designed and discussed the experiments. K.S. performed the experiments except for the mass spectrometry-based identification of proteins and phosphosites, which was done by D.V.H. and F.I.. The statistical analysis was done by M.V. and K.S. analysed the protein and phosphosite data.

6.1 Introduction

Viruses are obligate parasites that require a host cell for their replication and assembly of progeny virions. Most viral genomes only encode for a limited number of viral genes, necessitating viruses to hijack the host cell machinery. To do so, viruses typically modulate host cell signaling pathways to create a cellular environment favorable for viral replication [1-4]. As protein phosphorylation is one of the main drivers of signaling pathways, large-scale phosphoproteomics screens have been performed for a wide range of viruses, e.g. influenza virus [5, 6], rift valley fever virus [7], sendai virus [8], VSV [9], hepatitis C virus [10], Japanese encephalitis virus [11], porcine reproductive and respiratory syndrome virus [12], West-Nile virus [13], HIV [14-17], rotavirus [18] and several herpesviruses [19-23]. These screens have identified a rather wide range of differentially regulated phosphosites, *i.e.* from a few dozens to more than 1,000. Differences in the time of analysis post infection, method of phosphopeptide enrichment and method of detection (*e.g.* protein microarrays versus mass-spectrometry) affect the number of identified differentially regulated phosphosites. Most screens identified phosphosites rather late during infection, thereby identifying several hundreds of phosphosites that often mapped to innate immune responses. A phosphoproteomics screen for HIV-1 could identify 239 differentially regulated phosphosites already after 1 minute of HIV-1 exposure, highlighting that phosphorylation events can occur very rapidly [14]. To date, no large-scale phosphoproteomics screen has been published for RSV.

To characterize signaling pathways that are modulated by RSV, we performed a large-scale phosphoproteomics screen. To avoid a bias towards innate immune responses, we opted to focus our screen at an early time point post infection, *i.e.* during RSV entry. By quantifying RSV-induced changes in host protein phosphorylation we aimed to identify significant numbers of (de)phosphorylation-events that could be mapped to particular cellular pathways by using software tools such as ingenuity pathway analysis or kinase enrichment analysis. Such an analysis was set in part to try to complement the results obtained from the human kinome knockdown experiments (see chapter V). Pathways perturbed in response to RSV infection could subsequently be evaluated as candidate targets for the development of therapeutic drugs against RSV by using specific kinase inhibitors. Since the route of entry of RSV in host cells is currently still a matter of debate, we decided to focus our screen on the entry phase of a RSV infection. RSV entry consists of two stages, *i.e.* attachment and virion-host cell membrane fusion. Although *in vitro* data in immortalized stable cell lines allocate an important role for the interaction of the attachment protein G with heparan sulphate, recent evidence in primary cell cultures suggests that not heparan sulphate, but the interaction of G with the fractalkine receptor CX3CR1 is important during RSV entry *in vivo* [24]. After attachment, fusion between the viral - and host membrane is mediated by the F protein. Several plasma membrane proteins have been identified that interact with the F protein and proposed as RSV receptor, however, follow-up publications confirming these findings are currently lacking [25-27]. Ideally, one should perform a phosphoproteomics screen in primary HAE cultures, of which the infection by RSV is thought to share multiple characteristics with RSV infections in humans. Phosphopeptides generated by proteolytic digests, however, are often present in small amounts, necessitating the selective enrichment of

phosphopeptides by *e.g.* immobilized metal affinity chromatography or titanium dioxide for their identification by mass spectrometry. This requires the use of large cell numbers, which is incompatible with primary cell cultures. Therefore we decided to use A549 cells for our phosphoproteomics screen during RSV infection. In addition, we designed a strategy to discriminate attachment from fusion-induced signaling.

6.2 Results

6.2.1 Experimental design

As we aimed to map RSV modulated signaling pathways during the entry phase of RSV, we first rationalized our time point of analysis for quantifying (de)phosphorylation-events of host proteins. Krzyzaniak and colleagues investigated the entry route of RSV and amongst others demonstrated that RSV virions can efficiently bind to the cell surface at 4°C [28]. RSV inoculation at 4°C is often used to synchronize attachment of RSV to the cell surface as membrane fusion and subsequent infection does not occur at this temperature. Thirty minutes after transfer of cells to 37°C, RSV particles were found to be endocytosed and fusion between the viral and host membrane became detectable. On average fusion occurred 50 min after endocytosis. So in theory, inoculation of RSV for 1 hour at 4°C, followed by a transfer to 37°C for about 80 minutes should result in an enrichment of cells where RSV entry has taken place or is in progress. However, incubation of cells at lower temperature will induce phosphorylation events associated with cold responses [29]. To avoid cold-induced signaling events and enrich for RSV entry-induced host protein (de)phosphorylation, we directly inoculated A549 cells with RSV for 2 hours at 37°C without a cold step.

In addition, we aimed to discriminate RSV attachment from RSV fusion-induced host protein (de)phosphorylation. Palivizumab, a humanized mouse monoclonal antibody that neutralizes RSV and is used prophylactically to prevent severe RSV disease in at risk children, blocks the fusion process by preventing conformational changes of the fusion protein, without affecting RSV attachment [30]. We therefore hypothesized that incubation of RSV with palivizumab prior to the inoculation of A549 cells would prevent fusion-induced signaling, without affecting attachment-induced signaling. As a control, we treated RSV with an isotype matching, irrelevant antibody.

6.2.2 Identification of RSV-associated (de)phosphorylation-events

Experimental set-up

A549 cells were mock infected or infected with RSV-A2 (MOI 2) that had been pretreated with 100 nM palivizumab, 100 nM of an irrelevant isotype control antibody or without antibody for 2 hours at 37°C (Fig. 1A). Each experiment was performed in quadruplicate. Two hours post infection, we prepared cell lysates and digested proteins by trypsin. Peptides were subsequently identified and quantified by liquid chromatography-tandem mass spectrometry (LC-MS/MS) using label-free quantification (LFQ) in two parallel runs. First, total peptides were quantified to normalize for differences in protein expression (shotgun proteomics) and secondly, phosphopeptides were quantified after enrichment by TiO_2 (Fig. 1A). As a control, in parallel, A549 cells were also incubated further for 24 hours and stained for RSV infected cells. As expected, palivizumab prevented RSV-A2 fusion and subsequent infection, whereas the isotype control antibody did not affect RSV-A2 infection as compared to non-treated RSV-A2 (Fig. 1B). The punctuate RSV staining in palivizumab treated RSV-A2 infected A549 cells that is absent in mock inoculated A549 cells, most likely represent attached RSV virions that failed to fuse their viral membrane with the host membrane. As we did not investigate this further by *e.g.* confocal microscopy, it is unclear if these RSV virions are still at the cell surface or “trapped” inside the cell in endosomes.

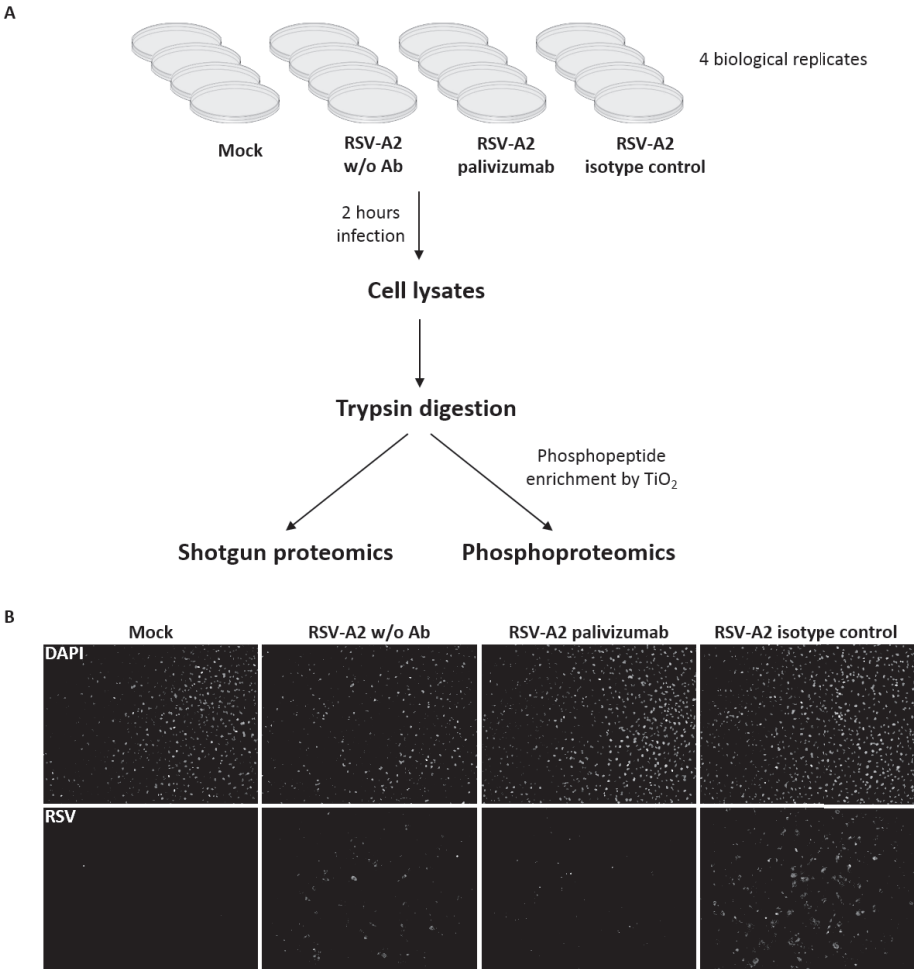

Figure 1: Set-up of the phosphoproteomics screen at an early time point after RSV infection. (A) Experimental layout of the phosphoproteomics screen. A549 cells were seeded in 14-cm petri-dishes in 4 biological replicates. The following day cells were mock infected or infected with RSV-A2 (MOI ~ 2) preincubated without antibody, with 100 nM palivizumab or with 100 nM isotype control antibody for 30 min at 37°C. Two hours post infection, cell lysates were prepared and proteins were digested by trypsin. Peptides were identified by LC-MS/MS with LFQ, whereas phosphopeptides were identified by LC-MS/MS with LFQ after enrichment by TiO_2 beads. (B) Validation of the antibody treatments during the phosphoproteomics screen. Cells were treated as for the screen, but infection was allowed for 24 hours. RSV infected cells were stained with a polyclonal goat anti-RSV serum. Cell nuclei were stained with Hoechst.

We were able to identify and quantify 3,220 different human proteins in the shotgun proteomics, that were detected in at least 3 of the 4 biological replicates of at least one treatment group (A complete list of the shotgun proteomics can be found on figshare (www.figshare.com, login: koen.sedeyn@vib-ugent.be, password: PhDKoenSedeynNov2017)). In addition, we detected 3 RSV proteins, the matrix - , nucleo - and phosphoprotein in all three RSV-A2 infected groups, but not in the mock infected A549 cells. As expected, we also identified the constant domains of the IgG1 heavy chain and Ig κ light chain in the samples treated with palivizumab or isotype control antibody, but not in the mock or RSV-A2 without antibody samples. The variable domains of the heavy - and light chain of palivizumab were only detected in the palivizumab treated RSV-A2 infected A549 cell samples. Altogether, these results confirm that RSV infection and antibody treatments were executed correctly.

Identification of phosphopeptides

Upon enrichment of phosphopeptides, we were able to identify and quantify 4,996 different phosphosites derived from 1,933 different human proteins, that were detected in at least 3 of the 4 biological replicates of at least one treatment group (A complete list of the phosphoproteomics can be found on figshare (www.figshare.com, login: koen.sedeyn@vib-ugent.be, password: PhDKoenSedeynNov2017)). The vast majority of these phosphosites were serine residues (4,514; 90,4%), followed by threonine residues (457; 9,1%) and only a few tyrosine residues (25; 0,5%). Of these 4,996 phosphosites, 3,574 (71,5%) were identified on mono-phosphorylated peptides, 1,287 (25,8%) on di-phosphorylated peptides and 135 (2,7%) on tri-phosphorylated peptides. In addition, we also identified one viral phosphosite, *i.e.* ser-232 of the RSV phosphoprotein, which is known as one of the major phosphosites of the phosphoprotein and important for the transcription elongation activity of the polymerase complex [31-34]. Only phosphosites for which the corresponding protein expression levels were quantified in the shotgun proteomics were retained for further statistical analysis.

To identify RSV-induced changes in the abundance of phosphosites, we did a statistical analysis on the combination of phosphopeptide - and protein abundance levels. Such normalization for protein expression is important, as differences in phosphopeptide abundance might reflect differences in total protein levels without a difference in phosphorylation. For each phosphopeptide we calculated the average protein - and phosphopeptide abundance values of the 4 biological replicates for each of the 4 treatments. Subsequently, we retained phosphopeptides with a significant ($P<0,05$) interaction effect between the 4 treatments, suggesting that at least one treatment results in a change in phosphopeptide abundance that is not caused by an equivalent change in protein abundance. As such, we retained 88 phosphopeptides. Of these 88 phosphopeptides we selected the ones with a significant ($P<0,05$) change in abundance between mock and non-treated RSV-A2 infected A549 cells, narrowing down the number of phosphopeptides to 21. Eight of these phosphopeptides were significantly more abundant in RSV-A2 infected cells compared to mock infected cells, suggesting that these phosphopeptides are phosphorylated by RSV (Table 1, upper part). Thirteen of these phosphopeptides were significantly less abundant in RSV-A2 infected cells compared to mock infected cells, suggesting that these phosphopeptides are dephosphorylated by RSV (Table 1, lower part).

Identification of phosphosites

Assigning the exact phosphosite in these phosphopeptides is not always straightforward. For mono-phosphorylated peptides, the identified phosphosite can be readily assigned. For di- or tri-phosphorylated peptides, however, changes in the phosphopeptide abundance might reflect changes in phosphorylation of one of the phosphosites or multiple phosphosites simultaneously in the peptide. Therefore we added the column multiplicity in table 1, which displays if a phosphosite was identified in a mono - (1), di - (2) or tri- (3) phosphorylated peptide. For di- and tri-phosphorylated peptides we provided other phosphosites that were also detected in the peptide in our screen that could account for the change in phosphopeptide abundance (see legend of table 1 remark c). For simplicity, we will keep on referring to phosphopeptides instead of phosphosites, as for di- and tri-phosphorylated peptides we cannot assign with 100% certainty which phosphosite caused a change in phosphopeptide abundance.

Table 1: RSV-modulated (de)phosphorylation-events

RSV-induced phosphorylation

Protein name	Uniprot code	Phosphosite	Localization prob score[a]	Multiplicity[b]	p-value interaction	p-value mock vs RSV-A2 w/o Ab
MLPH	Q9BV36	S266	0,8535	1	0,00165	0,02719
PUM2	Q8TB72	S178[C]	0,9889	2	0,01669	0,04537
RANBP2	P49792	T779[C]	0,9066	2	0,00325	0,01574
ANKHD1	Q8IWZ3	S93[C]	0,7983	2	0,00100	0,00569
ANKHD1	Q8IWZ3	S95[C]	0,9249	2	0,00176	0,00827
CTTN	Q14247	T399[C]	0,7825	2	0,00061	0,00825
FOXK1	P85037	S441	0,9998	1	0,02030	0,04062
EIF3B	P55884	S152[C]	1,0000	2	0,00641	0,04365

RSV-induced dephosphorylation

Protein name	Uniprot code	Phosphosite	Localization prob score[a]	Multiplicity[b]	p-value interaction	p-value mock vs RSV-A2 w/o Ab
TOR1AIP1	Q5JTV8	S215	0,9972	1	0,00753	0,04379
DYNC1LI1	Q9Y6G9	S510	0,8908	1	0,03705	0,04294
MAP7D1	Q3KQU3	T97[C]	1,0000	2	0,02727	0,04777
PRPF4B	Q13523	S387[C]	0,7984	2	0,01770	0,03355
RPS6	P62753	S247[C]	0,9181	3	0,00889	0,02778
TBC1D5	Q92609	S554	0,9928	1	0,02417	0,03415
AHNAK	Q09666	S5790[C]	0,8449	2	0,00070	0,00830
RRP1	P56182	S291	0,9999	1	0,03932	0,02128
PTPN12	Q05209	T587	0,8872	1	0,03939	0,04229
RRBP1	Q9P2E9	S1277	0,7918	1	0,03539	0,01880
ACIN1	Q9UKV3	S365	0,9763	1	0,01080	0,01821
NAA10	P41227	S182	1,0000	1	0,00082	0,00682
PAK2	Q13177	T169	0,9989	1	0,04855	0,02165

a: Localization probability score: the closer to 1, the more reliable the phosphosite allocation was.

b: Multiplicity: value of 1, 2 or 3, indicating if a phosphosite was identified in a mono-, di- or tri-phosphorylated peptide, respectively.

c: Other identified phosphosites within the same phosphopeptide: PUM2_S182, RANBP2_S781/S788, ANKHD1_S93/S95, CTTN_T401/S405, eIF3B_S154/S164, MAP7D1_S93/S113/S116/S125, PRPF4B_S381, RPS6_S235/S236/S240, AHNAK_S5780, S5782/S5793/T5794

RSV Infection-associated phosphorylation events

The shotgun proteomics revealed that the vast majority of host proteins was not differentially expressed between mock - and RSV-A2 infected cells, which can be expected as we investigated a relatively early time point (2 hpi). This is also highlighted in figure 2 and 3, with very similar protein levels for all 4 treatments for the vast majority of phosphopeptides. Whereas protein phosphorylation and dephosphorylation can occur within minutes after a stimulus, differential protein expression typically takes more time. Of the 8 RSV upregulated phosphopeptides, phosphorylation of three peptides from melanophilin (MLPH), pumilio-2 (PUM2) and RAN binding protein 2 (RANBP2) seems to be mediated by the attachment of RSV, as palivizumab did not prevent these phosphorylations (Fig. 2 A-C). For the other 5 phosphopeptides, our antibody treatments were not always biologically consistent. Whereas the phosphopeptides from the ankyrin repeat and KH domain-containing protein 1 (ANKHD1), cortactin (CTTN) and forkhead box protein K1 (FOXK1) were significantly upregulated in non-treated RSV-A2 infected A549 cells compared to mock treated cells, both palivizumab and the isotype control antibody prevented this upregulation (Fig. 2 D-G). Why the isotype control antibody, that does not prevent RSV attachment and fusion, prevented these phosphorylations is unclear. For the phosphopeptide from the eukaryotic translation initiation factor 3B (eIF3B) we observed that only the isotype control antibody, but not palivizumab, prevented RSV-A2 induced phosphorylation (Fig. 2 H). Again, it is currently unclear to us how this could be explained biologically.

We also observed 13 phosphopeptides that were significantly downregulated in non-treated RSV-A2 infected A549 cells compared to mock infected A549 cells. Six phosphopeptides from Torsin-1A-interacting protein 1 (TOR1AIP1), cytoplasmic dynein 1 light intermediate chain 1 (DYNC1Li1), MAP7 domain-containing protein 1 (MAP7D1), serine/threonine-protein kinase PRP4 homolog (PRPF4B), 40S ribosomal protein S6 (RPS6) and TBC1 domain family member 5 (TBC1D5) were not downregulated in palivizumab treated RSV-A2 infected cells, suggesting that these RSV-induced dephosphorylations might be induced during the RSV fusion process (Fig. 3 A-F). Although isotype control antibody treated RSV-A2 tended to induce dephosphorylation of these phosphopeptides as did non-treated RSV-A2, this was not significantly different compared to mock infected cells or palivizumab treated RSV-A2 infected cells. Only for TOR1AIP1, we identified a significant difference between the isotype control antibody and palivizumab. Four phosphopeptides from neuroblast differentiation-associated protein AHNAK (AHNAK), ribosomal RNA processing protein 1 homolog A (RRP1), tyrosine-protein phosphatase non-receptor type 12 (PTPN12) and ribosome-binding protein 1 (RRBP1) had a trend of being downregulated in RSV-A2 infected cells irrespective of the antibody treatment, suggesting that these dephosphorylations might be induced by RSV attachment (Fig. 3 G-J). Phosphopeptides from apoptotic chromatin condensation inducer in the nucleus (ACIN1), N-alpha-acetyltransferase 10 (NAA10) and p-21 activated kinase 2 (PAK2) were not fully biologically consistent. Whereas these phosphopeptides were significantly downregulated in non-treated RSV-A2 infected cells compared to mock infected cells, we did not observe a reduction in isotype control antibody treated RSV-A2 infected cells (Fig. 3 K-M).

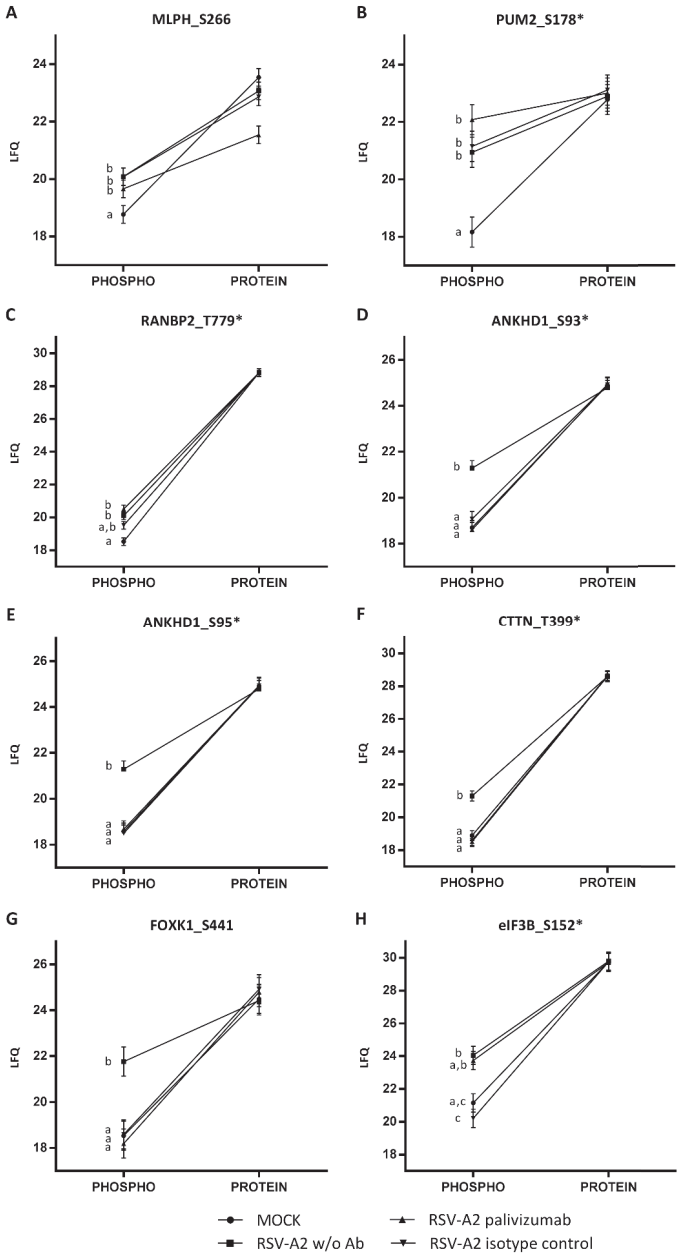

Figure 2: RSV-induced phosphorylations. LFQ values for the phosphopeptides and corresponding proteins are shown (Y-axis). (A) MLPH ser-266, (B) PUM2 ser-178, (C) RANBP2 thr-779, (D) ANKHD1 ser-93, (E) ANKHD1 ser-95, (F) CTTN thr-399, (G) FOXK1 ser-441 and (H) eIF3B ser-152. Phosphosites that were identified in di- or tri-phosphorylated peptides are marked with *. Treatment groups with an equal letter (a, b or c) were statistically not significantly different.

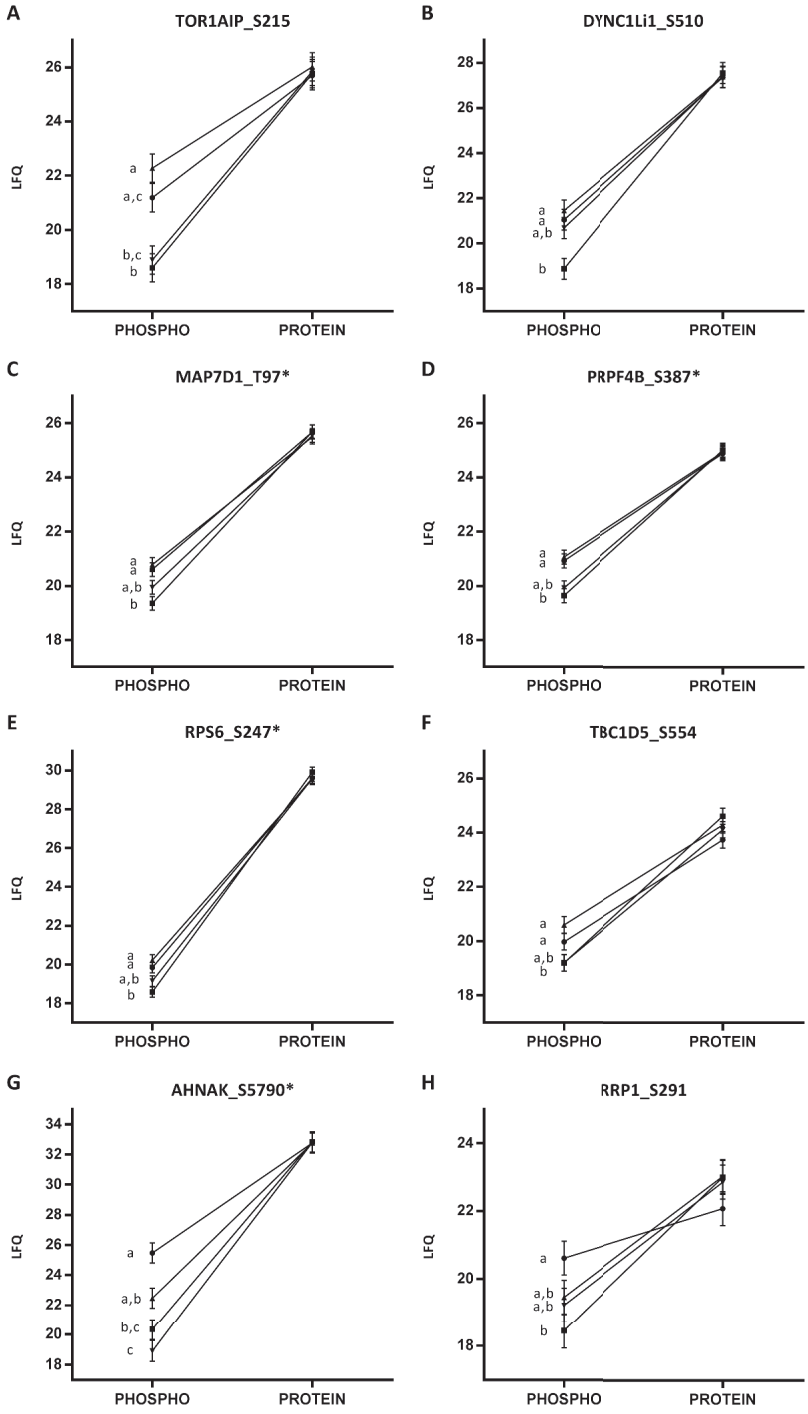
A
TOR1AIP_S215
LFQ
PHOSPHO
PROTEIN
B
DYNC1Li1_S510
C
MAP7D1_T97*
D
PRPF4B_S387*
E
RPS6_S247*
F
TBC1D5_S554
G
AHNAK_S5790*
H
RRP1_S291

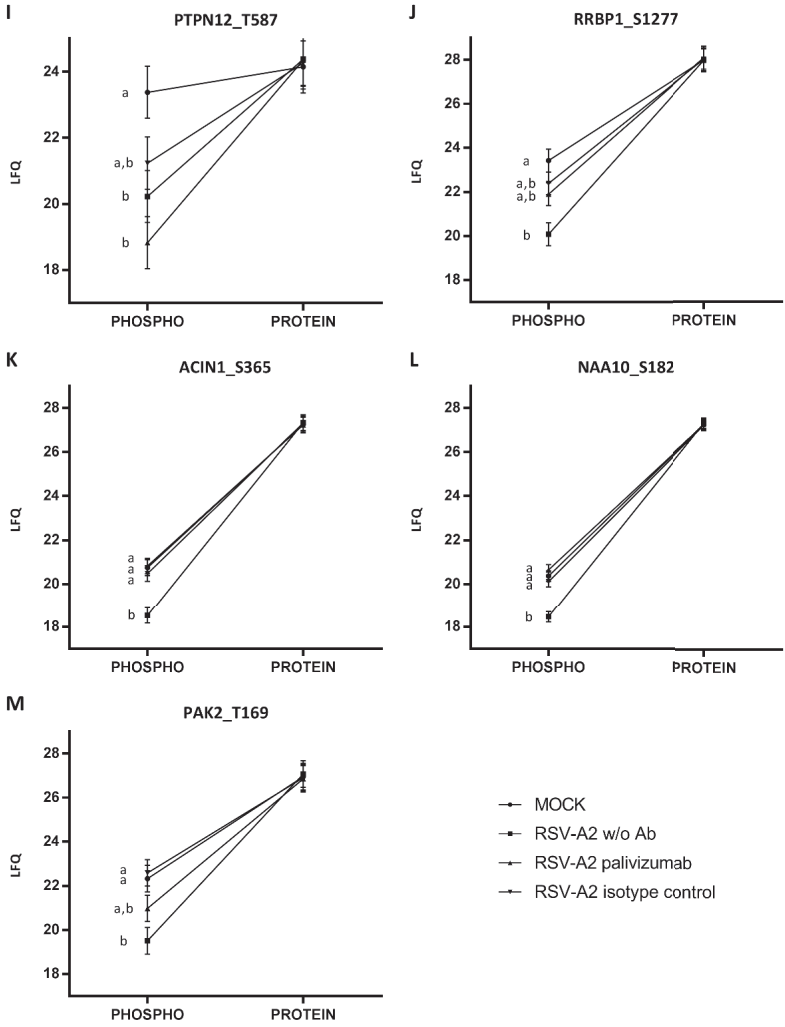

Figure 3: RSV-induced dephosphorylations. LFQ values for the phosphopeptides and corresponding proteins are shown (Y-axis). (A) TOR1AIP ser-215, (B) DYNC1Li1 ser-510, (C) MAP7D1 thr-97, (D) PRPF4B ser-387, (E) RPS6 ser-247, (F) TBC1D5 ser-554, (G) AHNAK ser-5790, (H) RRP1 ser-291, (I) PTPN12 thr-587, (J) RRBP1 ser-1277, (K) ACIN1 ser-365, (L) NAA10 ser-182 and (M) PAK2 thr-169. Phosphosites that were identified in di- or tri-phosphorylated peptides are marked with *. Treatment groups with an equal letter (a, b or c) were statistically not significantly different.

RSV Infection-associated kinase and phosphatase activity

We subsequently investigated if the predicted phosphosites differentially regulated after RSV infection had already been identified in other phosphoproteomics screens by using two databases, *i.e.* the general protein database Uniprot and the post translational modification database PhosphoSitePlus. As shown in table 2, the vast majority of the predicted phosphosites are known in one or both databases, except for thr-587 in PTPN12, which might represent a novel identified phosphosite. We also used three different online tools, phosida [35], networkin [36] and kinase enrichment analysis (KEA) 2, to predict upstream kinases of the phosphosites that might be activated or inactivated by RSV. Whereas phosida and networkin predict upstream kinases based on motifs in the primary amino acid sequence, KEA2 uses manually curated kinase-substrate interactions from literature. For 10 out of the 21 phosphosites at least one tool predicted a kinase (Table 2). Phosphorylation of ser-387 in PRPF4B by CDK2 was predicted by both phosida and KEA2, whereas RPS6 ser-247 phosphorylation by CK1, ATM and PRKCα was predicted by 2 of the 3 kinase tools. In addition, we also searched for phosphatases that could be regulated by RSV and hence explain the RSV modulated phosphosites. In contrast to kinase prediction tools, however, phosphatase prediction tools are limited, so we only used the DEPOD database [37]. Of all 21 proteins with a RSV modulated phosphosite, only cortactin and PAK2 were found in the database. Cortactin is regulated by the tyrosine phosphatase PTP1B on tyr-446, whereas PAK2 is regulated by the PP2Cα phosphatase, however, the target site(s) of this phosphatase in PAK2 is (are) unknown. Although RPS6 was not found back in the DEPOD database as a substrate for phosphatases, it has been shown that phosphorylated ser-247 of RPS6 is a substrate for the ser/thr protein phosphatase type 1 (PP1) [38, 39].

Identification of RSV infection-associated pathway activation

We further looked up the known cellular functions of the 21 RSV modulated phosphoproteins and could group more than half of the proteins in 4 different functional categories that are biologically relevant to RSV infection (summarized in Table 3).

- *Actin dynamics, cytoskeleton rearrangements and - transport, cell shape*

A first category involves proteins with a role in actin dynamics, cytoskeleton rearrangements and - transport and cell shape, processes that are important during the entry phase of RSV [28]. Six proteins, CTTN, DYNC1Li1, PTPN12, PAK2, TBC1D5 and NAA10 could be grouped in this category. CTTN plays a role in endocytosis and in the organization of the actin cytoskeleton [40, 41]. Interestingly, it has already been published that RSV induces CTTN phosphorylation on ser-405 biphasically in a PRKD-dependent manner [42]. Since we identified CTTN thr-399 phosphorylation on a di-phosphorylated peptide and both thr-401 - and ser-405 phosphorylation in our screen, it is likely that the increased abundance of this di-phosphorylated peptide after RSV infection is caused by ser-405 phosphorylation. We cannot, however, exclude that RSV induces thr-399 phosphorylation, alone or together with ser-405 phosphorylation. DYNC1Li1 is the non-catalytic component of the cytoplasmic dynein 1 complex and thought to connect dynein with cargo to be transported along the microtubuli. PTPN12 is a protein tyrosine phosphatase that dephosphorylates protein tyrosine kinase 2 beta (PTK2B) amongst others

[43], with PTK2B playing a role in organizing the actin cytoskeleton [44]. PAK2 is a serine/threonine kinase with a large number of substrates, *e.g.* the ribosomal protein S6, and is involved in organizing the cytoskeleton. TBC1D5 may function as a GTPase activating protein for Rab effector proteins and as such regulate cytoskeleton-based transport [45, 46]. NAA10 is the catalytic subunit of an acetyltransferase complex that inactivates MYLK by acetylation [47]. MYLK phosphorylates PTK2B and myosin light chains, thereby regulating the organization of and transport along the actin cytoskeleton.

Table 2: RSV-modulated (de)phosphorylation-events: novelty and predicted upstream kinases

RSV-induced phosphorylation

Protein name	Phospho-site	Phosphosite described		Predicted kinase		
		Uniprot	PSPlus[a]	Phosida[b]	Networkin[c]	KEA2[d]
MLPH	S266	No	Yes			
PUM2	S178	Yes	Yes			
RANBP2	T779	Yes	Yes		TTK	
ANKHD1	S93	No	Yes			
ANKHD1	S95	No	Yes			
CTTN	T399	Yes	Yes	CAMK2, DDR kinase	PAK1, PAK2	
FOXK1	S441	Yes	Yes	GSK3		
EIF3B	S152	Yes	Yes	PLK1	CK2α	

RSV-induced dephosphorylation

Protein name	Phospho-site	Phosphosite described		Predicted kinase		
		Uniprot	PSPlus[a]	Phosida[b]	Networkin[c]	KEA2[d]
TOR1AIP1	S215	Yes	Yes			
DYNC1LI1	S510	Yes	Yes			
MAP7D1	T97	Yes	Yes			
PRPF4B	S387	Yes	Yes	CK1, CDK1/2, CAMK2		CDK2, PRKDC, MAPK14
RPS6	S247	Yes	Yes	CK1, DDR kinase	CK1, ATM, PRKCα,β	ATM, PRKCα, PRKDC
TBC1D5	S554	Yes	Yes	GSK3	PRKCβ	
AHNAK	S5790	Yes	Yes		AKT1	
RRP1	S291	No	Yes			
PTPN12	T587	No	No			
RRBP1	S1277	Yes	Yes			
ACIN1	S365	Yes	Yes	CK2		
NAA10	S182	Yes	Yes	GSK3		
PAK2	T169	Yes	Yes			

a: PhosphoSitePlus

b: Phosida: kinase prediction tool based on motifs in the primary amino acid sequence [35].

c: Networkin: kinase prediction tool based on motifs in the primary amino acid sequence [36].

d: Kinase enrichment analysis 2: kinase prediction tool based on curated kinase-substrate interactions from literature.

DDR = DNA Damage response kinase: ATM/ATR

- *Protein translation*

A second category comprises four proteins, eIF3B, RPS6, RRBP1 and RRP1, which are known to play a role in protein translation. EIF3B is the RNA binding component of the EIF3 translation initiation complex that recruits other translation initiation factors and helps in identifying the AUG start codon [48]. RPS6 is one of the structural proteins of the small 40S ribosomal subunit and the major target for different cellular kinases, such as the S6 kinase, the 90 kDa ribosomal S6 kinase family, PKA and casein kinase 1 (recently reviewed in [49]). These kinases phosphorylate 5 conserved serine residues at the C-terminus of RPS6 at positions 235, 236, 240, 244 and 247. RRBP1 is a transmembrane protein in the endoplasmic reticulum membrane that functions as a receptor for ribosomes. Finally, RRP1 is thought to be essential for the generation of the 28S ribosomal RNA [50].

- *Cell death*

The third category involves two proteins with a role in regulating cell death, *i.e.* ANKHD1 and ACIN1. A truncated splice variant of ANKHD1 has been identified as a prosurvival protein by inhibiting caspase activity [51]. ACIN1 is a substrate of caspase-3 and induces chromatin condensation without DNA fragmentation [52].

- *RNA binding*

The last category consists of the RNA binding protein PUM2, which functions as a post transcriptional inhibitor by binding to the 3' UTR of target mRNAs. The pumilio proteins have also been identified as possible positive regulators of RIG-I signaling by enhancing the recognition of viral RNA by LGP2 [53]. Interestingly, the PUM2 binding consensus RNA sequence (5'-UGUANAUA-3') is present in the RSV antigenome sequence and in the mRNAs encoding the RSV fusion and - large polymerase protein. We hypothesized that PUM2 might bind these RSV sequences and hence be a target for RSV-induced phosphorylation.

Table 3: Cellular functions of RSV-modulated phosphoproteins.

Actin dynamics, cytoskeleton rearrangements and - transport and cell shape	
Protein name	**Functions**
CTTN	Role in receptor-mediated endocytosis by clathrin-coated pits
	Role in intracellular protein transport and endocytosis
	Contributes to the organization of the actin cytoskeleton and cell shape
	Role in the formation of lamellipodia and in cell migration
	In complex with ABL1 and MYLK regulates cortical actin-based cytoskeletal rearrangements
DYNC1LI1	Non-catalytic accessory component of the cytoplasmic dynein 1 complex
	Dynein 1 complex involved in cargo transport along microtubules
PTPN12	Dephosphorylates cellular tyrosine kinases, such as PTK2B
	PTK2B is a tyrosine kinase that *e.g.* regulates reorganization of the actin cytoskeleton
PAK2	S/T kinase involved in *e.g.* cytoskeleton regulation, cell motility
	Phosphorylates many substrates, *e.g.* ribosomal protein S6
TBC1D5	May act as a GTPase-activating protein (GAP) for Rab family protein(s)
NAA10	Catalytic subunit of the N-terminal acetyltransferase A complex
	Represses MYLK kinase activity by acetylation

Protein translation	
Protein name	**Functions**
EIF3B	RNA binding component of the eukaryotic translation initiation factor 3 complex
	eIF3 complex facilitates recruitment of other translation initiation factors
	eIF3 complex facilitates scanning of the mRNA for AUG recognition
RPS6	40S ribosomal protein S6
RRBP1	Ribosome receptor that regulates interaction between ribosomes and the ER membrane
RRP1	Possible critical role in the generation of 28S rRNA

Cell death	
Protein name	**Functions**
ANKHD1	May possess an antiapoptotic effect through its regulation of caspases
ACIN1	Induces apoptotic chromatin condensation after activation by caspase-3

RNA binding	
Protein name	**Functions**
PUM2	Sequence-specific RNA-binding protein
	Post-transcriptional repressor by binding the 3'-UTR of mRNA targets
	Binds to an RNA consensus sequence (5'-UGUANAUA-3') which is present in RSV genome
	Plays a role in cytoplasmic sensing of viral infection

6.2.3 Validation of RSV-associated (de)phosphorylation-events

One well-established way to validate stimulus-induced changes in protein phosphorylation is by using a phosphosite-specific antibody. Although such antibodies are often commercially available for well-studied proteins and phosphosites, this is clearly less the case for proteins and phosphosites that are less well studied. In the absence of phosphosite-specific antibodies, an alternative technique can be used to study protein phosphorylation, *i.e.* phosphorylation-dependent mobility shifts of proteins in SDS-PAGE. This technique relies on the observation that most proteins run slower (*i.e.* display a higher apparent molecular weight) in SDS-PAGE if phosphorylated compared to their unphosphorylated form. This is thought to be the result of reduced SDS binding at the phosphorylation site due to the negative charge [54]. Since not all proteins are characterized by such a phosphorylation-dependent mobility shift, however, this technique is not feasible for every protein and should be tested for each protein empirically. Furthermore, target protein-specific antibodies must be available that work in western blotting.

To validate a subset of the identified RSV modulated phosphopeptides we searched for commercially available phosphosite-specific antibodies. We selected 5 phosphopeptides that were identified as mono-phosphorylated peptides of which the exact phosphosite should be reliable. These included the phosphopeptides containing the phosphosites PAK2 thr-169, NAA10 ser-182, DYNC1Li1 ser-510, PTPN12 thr-587 and TBC1D5 ser-554. Unfortunately, we could not find commercially available antibodies specific for these phosphosites. Instead we ordered total protein-specific antibodies for these proteins to test for phosphorylation-induced mobility shifts. Additionally, we also selected 3 phosphopeptides that were identified as di-or tri-phosphorylated peptides: *i.e.* the peptides containing the phosphosites CTTN thr-399, RPS6 ser-247 and PUM2 ser-178. For PUM2 we could not find commercially available antibodies specific for phosphorylated ser-178 or ser-182, whereas for CTTN and RPS6, antibodies specific for phosphorylated ser-405 and ser-235, -236, -240, -244 and -247, respectively, are commercially available. As we had total protein antibodies in house for CTTN, RPS6 and PUM2, however, we first tested these for phosphorylation-associated mobility shifts.

To investigate RSV-induced (de)phosphorylation of CTTN, RPS6 and PUM2 we infected A549 cells with 2 or 16 MOI of RSV-A2 or with a mock inoculum as control for 2 hours. This was done in duplicate with a pretreatment of the inocula for 30 min either in the absence or presence of 30 µg/ml dextran sulphate. Dextran sulphate is a polyanion that binds to RSV virions, thereby preventing attachment to cells. This allowed us to discriminate the specificity of RSV-induced (de)phosphorylation. Two hours post infection, we prepared cell lysates and treated these with or without lambda phosphatase. As shown in figure 4A, we were able to detect total protein levels of CTTN and RPS6, but not of PUM2 (data not shown). We observed two protein bands of CTTN in lysates not treated with lambda phosphatase, whereas only the lower band was present in lysates treated with lambda phosphatase, suggesting that CTTN is present in cells both as a non-phosphorylated form (lower band) and a phosphorylated form (upper band). RSV infection dose-dependently increased the intensity of the upper, phosphorylated CTTN band (compare lane 1, 3 and 5 in Fig. 4A). Interestingly, preventing RSV attachment by dextran sulphate abolished the RSV-induced increase in intensity of the upper,

phosphorylated CTTN band (compare lane 7, 9 and 11 in Fig. 4A). These results confirm that CTTN is phosphorylated during RSV entry. For RPS6, we mainly observed a single band that migrated faster after lambda phosphatase treatment, suggesting that (almost) all RPS6 proteins in normal, untreated cells are present as a phosphorylated form. Infection with RSV, however, did not cause a shift of the single RPS6 band to the height that corresponds to the unphosphorylated form (compare lane 1, 3 and 5 in Fig. 4A). So with this mobility shift assay we could not confirm that RSV induces a dephosphorylation of RPS6.

In a second experiment we investigated the RSV-induced (de)phosphorylation of PAK2, NAA10, DYNC1Li1, PUM2, PTPN12 and TBC1D5. We used a similar experimental set-up as for CTTN and RPS6, with some adaptations (for details see the material and methods section). Basically, adaptations include the use of a different MOI (5 instead of 2 or 16) of RSV-A2 infection, a lysis buffer without phosphatase inhibitors and a higher number of lambda phosphatase units. In addition we tested a different PUM2 antibody. As shown in figure 4B, we were able to detect total protein levels of PAK2, NAA10 and DYNC1Li1. In contrast, we could not detect total protein levels of PUM2, PTPN12 and TBC1D5 (data not shown). As we did not investigate this further yet, we cannot say if this is caused by a (too) low expression level of these proteins, or due to a poor affinity of the used primary antibodies. We detected two bands for PAK2, running at the same height in both lysates treated with and without lambda phosphate. So these two bands likely represent different PAK2 isoforms, but not different phosphorylation forms of PAK2. Although at first sight PAK2 bands were more intense in RSV infected cells compared to mock treated cells, we also observed a stronger total protein staining by ponceau, suggesting unequal protein loading rather than a difference in protein expression (compare lane 1 and 3 in Fig. 4B). For NAA10, we also observed two bands, which both seemed to reduce in abundance with lambda phosphatase treatment (compare lane 1 with 2 and lane 3 with 4 in Fig. 4B). Possibly dephosphorylation of NAA10 reduces the protein stability, hence explaining the lower protein abundance. Although it is difficult to make firm conclusions, we found no evidence of RSV-induced NAA10 dephosphorylation in this single assay. We only observed one band for DYNC1Li1, suggesting that a phosphorylation-dependent mobility shift assay is not feasible with DYNC1Li1 (Fig. 4B).

Taken together, we could only confirm that RSV induces phosphorylation of CTTN, although phosphorylation-dependent mobility shift assays do not provide information on the exact phosphosite location. For all other investigated proteins further optimization of the blotting/protein staining methods might enhance protein detection and validate if a phosphorylation-dependent electrophoretic mobility shift occurs. If this is the case, we could investigate if RSV affects the phosphorylation state of the protein.

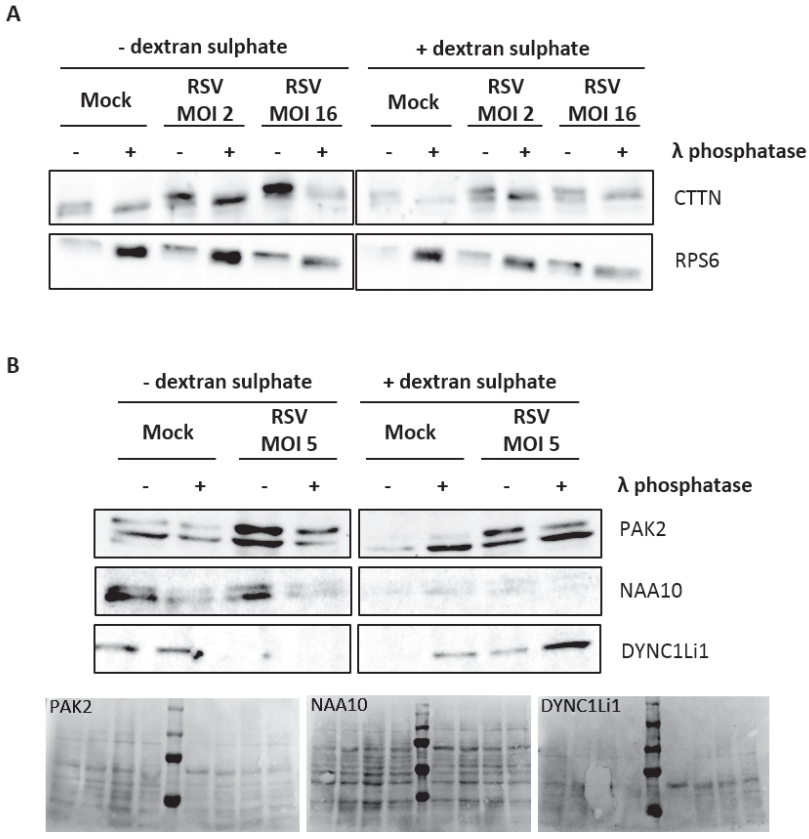

Figure 4: Validation of RSV-induced phosphorylation/dephosphorylation by electrophoretic mobility shift assays. A549 cells were mock infected or infected with RSV-A2, preincubated with or without 30 µg/ml dextran sulphate for 30 min at 37°C. Two hours after infection, cell lysates were prepared and treated with or without lambda phosphatase. (A) Electrophoretic mobility shift assays for CTTN and RPS6. (B) Electrophoretic mobility shift assays for PAK2, NAA10 and DYNC1Li1. Pictures below show ponceau staining of the blotted proteins to document comparable protein loading.

6.3 Discussion

Although RSV was discovered more than half a century ago, the complex interplay between the host and RSV remains far from elucidated. To characterize phosphorylation-dependent signaling pathways that are activated during a RSV infection we performed a mass spectrometry-based phosphoproteomics experiment. To our knowledge, this is the first unbiased screen for the identification of host protein phosphorylation events upon RSV infection. As several groups identified different routes of entry during RSV infection, we focused our screen on the very initial phases of RSV infection, *i.e.* attachment and fusion, and quantified protein phosphorylations changes 2 hours post RSV infection. Fusion may take place directly at the plasma membrane as originally thought or, as shown more recently, occur in endosomes following clathrin-mediated endocytosis or macropinocytosis [28, 55, 56]. Resolving the crystal structure of the prefusion F conformation gained structural insights in the fusion process [57], yet what signal exactly triggers the F protein to shift from the prefusion - to the postfusion conformation is currently not clear. In contrast to *e.g.* influenza virus haemagglutinin, endosomal acidification is unnecessary for RSV entry, suggesting that if entry occurs by endocytosis, fusion takes place before the formation of late endosomes. With our phosphoproteomics screen we aimed to identify phosphorylation events and associated signaling pathways that could provide hints to the RSV receptor(s) and the mechanism(s) used during RSV entry *in vitro*.

We could identify and quantify 3,220 different human proteins and 3 viral proteins. After selective enrichment of phosphopeptides, we identified and quantified 4,996 different phosphosites from 1,933 different human proteins and one viral phosphosite, Ser-232 on the phosphoprotein [31-34]. To identify phosphorylation events that are specifically modulated by RSV infection, we compared the abundance of phosphopeptides from mock and RSV-A2 infected cells with normalization for the abundance of the corresponding proteins. This provided a selected list of 8 and 13 phosphopeptides that are significantly up- and downregulated upon RSV infection, respectively. To understand the biological relevance of these RSV modulated phosphorylation events we explored the reported biological functions of the corresponding proteins and identified 4 functional categories that are relevant for RSV.

Actin, either as a monomer or as filaments, plays an important role at various stages of RSV infection such as transcription, assembly and budding. RSV transcription is enhanced by actin, which binds to the viral RNP complex through its divalent-cation-binding domain, and is further enhanced in the presence of profilin, an actin-regulatory protein [58-60]. The interaction of actin with the RNP complex probably explains the presence of actin inside purified RSV virions [61]. Moreover, actin filaments are important for the transport of viral RNP complexes from the site of synthesis (inclusion bodies) to the site of budding at the plasma membrane, which is mediated by the RSV-M protein [62-64]. The final budding of RSV virions also requires actin filaments as the destabilizing inhibitor cytochalasin D inhibits virus release [58]. Recently, a novel way of RSV spreading by the induction of filopodia was shown to be dependent on the ARP2 protein, a subunit of the actin filament nucleation complex ARP2/3 [65]. In

addition, cytochalasin D also inhibits RSV entry, highlighting that actin filaments are important during RSV entry [28, 66]. Moreover, several cytoskeleton proteins have been shown to be differentially expressed upon RSV infection [67]. In line with these observations we identified several proteins involved in regulating the actin cytoskeleton, *i.e.* **CTTN**, **PTPN12**, **PAK2** and **NAA10**, with RSV modulated phosphorylation events. Krzyzaniak and colleagues observed drastic changes in the cell shape and actin distribution 30 minutes after RSV infection, characterized by transient actin filament depolymerisation and the formation of actin filled blebs at the cell surface [28]. This was associated with signaling cascades involving the EGFR, Cdc42, PAK1 and neural Wiskott-Aldrich syndrome protein (N-WASP). Our screen identified RSV-induced upregulation of a di-phosphorylated peptide from **CTTN** containing phosphorylated thr-399. As we also identified CTTN thr-401 and ser-405 phosphorylation, one of these sites may have caused the RSV-induced upregulation of the di-phosphorylated peptide. This RSV-induced CTTN phosphorylation was subsequently confirmed by an electrophoretic mobility shift assay. These results appear to confirm previous observations that CTTN is phosphorylated at ser-405 within 3 hours after RSV infection [42]. Ser-405 phosphorylation increases the interaction of CTTN with N-WASP, an activator of the nucleation activity of the ARP2/3 complex [68]. Although a proteomics analysis upon RSV infection suggested complete absence of CTTN at 24 hours post infection, others demonstrated that total CTTN protein levels are unaffected during RSV infection [42, 69].

We identified a RSV-induced dephosphorylation of thr-587 in the tyrosine phosphatase **PTPN12**. This site likely represents a novel phosphosite as it could not be found in large databases of phosphosites. PTPN12 associates with and dephosphorylates a variety of proteins that directly or indirectly regulate the actin cytoskeleton, *e.g.* proline-serine-threonine phosphatase interacting protein 1 (PSTPIP1), PTK2B and paxillin [43, 70, 71]. PSTPIP1 hereby serves as a scaffold protein between PTPN12 and N-WASP, allowing PTPN12-mediated dephosphorylation of N-WASP [71]. PTK2B is a tyrosine kinase that interacts with many proteins, *e.g.* the Rho-related GTP-binding protein RhoU [72]. Ectopic expression of RhoU in NIH3T3 cells induces the formation of filopodia, a loss of actin stress fibres and membrane blebbing [73]. Interestingly, Krzyzaniak and colleagues observed a reduction of the number of actin stress fibres and membrane blebbing during RSV entry [28]. So possibly, these responses during RSV entry depend on a PTPN12-PTK2B-RhoU pathway. Paxillin is a protein linking the actin filaments to the plasma membrane at focal adhesion complexes. The molecular consequence of PTPN12 thr-587 phosphorylation on its functions or phosphatase activity, for example for its association with PSTPIP1, PTK2B and paxillin, is currently unclear.

We also observed a RSV-induced dephosphorylation of thr-169 of **PAK2**, although our isotype control antibody, that at first glance did not affect RSV infection, prevented this RSV-induced dephosphorylation. Yet, several reports highlight a role for PAK1 during RSV entry [28, 55, 74]. By extension, PAK2 may also regulate RSV entry, *e.g.* by activating the filamentous actin regulator MAPK5 through phosphorylation of the upstream MAPK6 [75]. Specific information on the biological function of PAK2 thr-169 phosphorylation is currently limited. A phosphoproteomics screen in HEK293T cells expressing the angiotensin II type 1 receptor revealed an increased PAK2 thr-169 phosphorylation

upon stimulation with a modified angiotensin (SII: angiotensin with substitutions at position 1, 4 and 8 with Sarcosine, Ile and Ile, respectively) that is biased towards β-arrestin-mediated signaling [76].

A final protein involved in regulating the actin cytoskeleton was **NAA10**. We observed a RSV-induced dephosphorylation of ser-182 of NAA10, the catalytic subunit of the N-terminal acetyltransferase A complex. As was the case with PAK2, the isotype control antibody unexpectedly also prevented this RSV-induced NAA10 dephosphorylation. NAA10 interacts with MYLK, which leads to the acetylation and inactivation of MYLK [47]. MYLK regulates the activity of the actin filament motor protein myosin by phosphorylating the regulatory light chains. In addition, MYLK also phosphorylates the tyrosine kinase PTK2B [77]. Interestingly, activation of the angiotensin II type 1 receptor in HEK293T cells induces blebbing of the cell membrane which is dependent on β-arrestin-2 and is mediated by a RhoA/Rock/MYLK-dependent pathway [78]. Although expression levels of angiotensin II type 1 receptor are low in A549 cells according to the human protein atlas and our A549 transcriptome analysis, expression is absent in a wide range of other stable cell lines (human protein atlas).

Taken together, these RSV modulated phosphorylation events likely contribute to the drastic remodelling of the actin cytoskeleton during RSV entry and point towards a possible role for the angiotensin II type 1 receptor during membrane blebbing seen at RSV entry.

Upon cellular stress, *e.g.* during a viral infection, cells may induce the formation of stress granules (SGs), which are dense cytoplasmic structures accumulating RNA and RNA binding proteins in a state of translational arrest. As such, SGs function as safe havens to protect cellular mRNAs during cellular stress. RSV infection induces the formation of SGs, which is dependent on the activation of PKR and which are distinct from the viral inclusion bodies [79-81]. Induction of SGs, however, only occurs in a subset of RSV infected cells, suggesting that RSV has evolved mechanisms to suppress the formation of SGs. Several reports indeed highlight that RSV modulates the induction of SGs and associated translation arrest. Groskreutz and colleagues found that although PKR was activated during RSV infection, subsequent phosphorylation of the eIF2α was basically absent, leading to an unaffected cellular protein translation [82]. This appeared due to binding of the N protein to PKR, thereby sequestering the PKR protein away from eIF2α and by the association of the phosphatase PP2a to eIF2α. Secondly, the 5' trailer region of the RSV genome suppresses the formation of SGs [79]. Lastly, the O-linked N-acetylglucosamine transferase enzyme is sequestered from the SGs to the viral IBs during RSV infection, thereby lowering the essential O-linked N-acetylglucosamine modifications of several proteins required to accumulate untranslated mRNAs in SGs [83, 84].

In our phosphoproteomics screen, we identified 4 RSV-modulated (de)phosphorylation-events that potentially affect protein translation. We identified a RSV-induced upregulation of a di-phosphorylated peptide from the translation initiation factor **eIF3B** containing phosphorylated ser-152, although phosphorylated ser-154 and - ser-164 were also identified in the screen and may have caused the RSV-induced upregulation. Unexpectedly, the irrelevant, isotype control antibody prevented this RSV-induced upregulation. These results confirm a previous characterization of the

protein composition and posttranslational modifications of the eIF3 complex, that identified mono-, di- and tri-phosphorylated peptides containing phosphorylated ser-152, ser-154 and ser-164 of eIF3B [85]. Any functional data on the role of these phosphorylation sites, however, is currently lacking. EIF3B Ser-154 is predicted as a substrate site for casein kinase 2 according to phosida, providing a possible link to the role of casein kinase 2 in the phosphorylation of the RSV-M and -P protein [33, 86].

We also identified a RSV-induced downregulation of a tri-phosphorylated peptide containing phosphorylated ser-247 of **RPS6**, which at first glance appears dependent on the fusion process. Other identified phosphosites within this phosphopeptide included ser-235, ser-236 and ser-240 and may have contributed to this RSV-induced downregulation. Although we observed a shift in the electrophoretic mobility of RPS6 in SDS-PAGE depending on its phosphorylation, we could not confirm RSV-induced dephosphorylation of RPS6 in this assay. RPS6 Ser-247 phosphorylation is regulated by the kinases CK1, ATM and the phosphatase PP1 [38, 39]. Yet, the biological role of ser-247 phosphorylation in RPS6 is currently unclear. RPS6 ser-235/236 phosphorylation is regulated by several kinases such as the S6 kinases, CK1, PKA and the p90 ribosomal S6 kinase (RSK) family [49]. The L protein of Theiler's encephalomyelitis virus, a murine cardiovirus of the *Picornaviridae* family, interacts with the RSK family kinases by a DDDVF motif (oral presentation by Michael Peeters at the fourth annual meeting of the Belgian society for virology, December 8th 2016, Brussels). A DDDVF motif is not present in any RSV protein, however a DVF and DDD motif are present in the RSV-N and -M protein, respectively. Although we did not yet investigate this, RSV-N and/or -M may interact with the RSK family kinases, thereby regulating RPS6 phosphorylation of ser-235/236.

Ser-1277 and ser-291 of **RRBP1** and **RRP1**, respectively, were downregulated by RSV infection, possibly due to attachment of RSV. RRBP1 is a transmembrane protein of the ER membrane which binds to ribosomes, whereas RRP1 plays a role in the late stage of nucleologenesis and may be essential for the generation of 28S rRNA [50]. Interestingly, RRBP1 expression at both the mRNA level and protein level is upregulated upon RSV infection, as identified by several RSV transcriptomics and proteomics screens [87-91]. Although these phosphosites have been identified in large-scale phosphoproteomics screens, a specific biological function is currently not known.

6.4 Conclusion

We could identify 8 and 13 phosphopeptides that were more and less abundant in RSV infected cells compared to mock infected cells, respectively, suggesting that these peptides harbor RSV-induced phosphorylation and dephosphorylation events, respectively. RSV-induced phosphorylation of cortactin, likely at serine-405, could be confirmed by an electrophoretic mobility shift assay and confirms published results. For the other identified phosphosites, no phosphosite-specific antibodies are commercially available, necessitating the need to generate such antibodies first to validate our findings.

6.5 Material and methods

Materials

Acetonitrile (ACN), Trifluoroacetic acid (TFA), Formic acid (FA) were purchased from Biosolve, HEPES, Dithiothreitol (DTT) and Iodoacetamide from Sigma Aldrich, NH_4OH from Merck and Urea from Biorad.

Cells

A549 cells (a kind gift from M.L. Hammarskjold - University of Virginia-School of Medicine) and Hep-2 cells (ATCC, CCL-23) were grown in Dulbecco's modified eagle medium (DMEM) supplemented with 10% heat-inactivated FCS, 2 mM L-glutamine (BE17-605F, Lonza), 100 U/ml penicillin and 100 µg/ml streptomycin (15140122, ThermoFisher scientific) (~complete DMEM medium) at 37°C and 5% CO_2.

RSV stock preparation

We prepared a high concentrated, pure stock of the laboratory RSV strain A2 (ATCC-VR1540). Subconfluent HEp-2 cells were washed with DMEM buffer (DMEM medium supplemented with 1 mM HEPES, 100 U/ml penicillin and 100 µg/ml streptomycin) and subsequently inoculated with RSV-A2 (MOI 0,1) in DMEM buffer. After 4 hours, DMEM buffer was replaced by complete DMEM medium and cells were incubated further for 3 days when cytopathogenic effects were clearly visible. To harvest RSV virions as pure as possible, supernatans was collected without scraping the HEp-2 cells. Cell debris was removed by centrifuging (1,000 x g, 10 min at 4°C) the supernatans twice. Virions in the supernatans were pelleted through a 30% (w/v) sucrose cushion in Hank's balanced salt solution supplemented with 25 mM HEPES pH 7.2 by ultracentrifugation at ~ 50,000 x g for 90 min at 4°C. Pellets were gently washed and resuspended in Hank's balanced salt solution supplemented with 20% sucrose and penicillin/streptomycin. The resuspended virus was aliquoted in cryovials, snap frozen in liquid nitrogen and stored at -80°C. To generate a virus-free mock inoculum as comparable as possible to the RSV-A2 inoculum, in parallel, HEp-2 cells were inoculated with DMEM buffer without virus and treated in exactly the same way.

Sample preparation

Six million A549 cells were seeded in 14 cm petri dishes in 25 ml complete DMEM medium and incubated overnight. Mock inoculum or RSV-A2 virus were diluted in Opti-MEM™ reduced serum medium, mixed without or with antibody (palivizumab (a humanized mouse monoclonal IgG1,$_\kappa$ antibody from MedImmune) or human IgG1,$_\kappa$ isotype control antibody (0151K-14, Southern Biotech)) and incubated for 30 min at 37°C. Meanwhile, A549 cells were washed with Opti-MEM™ reduced serum medium. After 30 minutes, A549 cells were inoculated with mock - or RSV-A2 inoculum and incubated for 2 hours at 37°C and 5% CO_2. Cell lysates were prepared by washing the A549 cells with ice cold PBS and inoculation with 10 ml freshly prepared urea lysis buffer (8M urea, 50 mM NH_4HCO_3, 1 mM sodium orthovanadate, 1 tablet PhosSTOP™ phosphatase inhibitors (04906845001, Sigma-Aldrich)) for 20 min at room temperature to avoid urea precipitation. Cell lysates were collected by

scraping the petri-dishes and were sonicated (5 intervals of 5 sec sonication/5 sec rest). Cell debris was removed by centrifugation at 4,332 x g for 15 min at 4°C. Cleared supernatans was snap frozen in liquid nitrogen and stored at -80°C until further processing. In parallel to the lysates, we also allowed RSV-A2 infection to proceed for 24 hours to control if palivizumab prevented RSV-A2 fusion. These A549 cells were fixed for 20 min with 4% paraformaldehyde, permeabilised with 0,2% Triton-X100 for 10 min and subsequently blocked with 1% BSA in PBS for 2 hours at RT. RSV infected cells were stained with a polyclonal goat anti-RSV serum (AB1128, EMD Millipore) diluted 1:3000 in 0,5% BSA in PBS for 1h at RT and an Alexa fluor 488 conjugated donkey anti-goat IgG (Invitrogen) diluted 1:500 in 0,5% BSA in PBS for 1h at RT. After each antibody inoculation, cells were washed 4x with 0,1% Tween20 in PBS. Cell nuclei were stained with Hoechst (Invitrogen) for 15 min at RT.

The protein concentration in the cell lysates of each replicate was measured using a BCA assay and equal protein amounts, each containing 2 mg of total protein, were used for further analysis. Proteins in each sample were reduced by adding 5 mM DTT and incubation for 30 minutes at 55˚C. Alkylation of the proteins was done by addition of 10 mM iodoacetamide and incubation for 15 minutes at room temperature in the dark. The samples were diluted with 20 mM HEPES pH 8.0 to a urea concentration of 4 M and the proteins were digested with 8 µg lysyl endopeptidase (Wako) (1/250, w/w) for 4 hours at room temperature. All samples were further diluted with 20 mM HEPES pH 8.0 to a final urea concentration of 2 M and proteins were digested with 20 µg trypsin (Promega) (1/100, w/w) overnight at 37˚C. Peptides were then purified on a SampliQ SPE C18 cartridge (Agilent) and 100 µg of vacuum dried peptides of each sample was used for shotgun analysis, while the remainder was used for phosphopeptide enrichment.

Phosphopeptide enrichment

MagReSyn Ti-IMAC beads (2 mg, ReSyn Biosciences) were equilibrated and phosphopeptides were enriched according to the instructions of the manufacturer [92], using a different loading buffer containing 80% ACN and 6% TFA.

LC-MS/MS (phosphoenriched samples and shotgun samples marked in italics)

The phospho-enriched peptide samples were completely dried and re-dissolved in 20 µl loading solvent (0.1% TFA in water/ACN (98:2, v/v)). 10 µL (*6 µl*) of the peptide mixtures were analyzed by LC–MS/MS system on an Ultimate 3000 RSLC nano LC (Thermo) in-line connected to a Q Exactive HF mass spectrometer (Thermo). The peptides were first loaded on a trapping column (made in-house, 100 µm internal diameter (I.D.) × 20 mm, 5 µm beads C18 Reprosil-HD, Dr. Maisch, Ammerbuch-Entringen, Germany) and after flushing from the trapping column, peptides were loaded on an analytical column (made in-house, 75 µm I.D. × 400 mm, 1.9 µm beads C18 Reprosil-HD, Dr. Maisch) using a non-linear 150 min gradient from 2 to 56% solvent B (0.1% FA in water/ACN, 20/80 (v/v)), all at a flow rate of 250 nL/min. Peptide separation was followed by a 10 min wash reaching 99% solvent B and re-equilibration

with solvent A (0.1% FA in water). The column temperature was kept constant at 50°C in a column oven (CoControl 3.3.05, Sonation).

The Q Exactive HF mass spectrometer was operated in data-dependent, positive ionization mode, automatically switching between MS and MS/MS acquisition for the 16 most abundant peaks in a given MS spectrum. The source voltage was set to 3 kV and the capillary temperature was set at 250°C. One MS1 scan (m/z 375-1500, AGC target 3E6 ions, maximum ion injection time of 60 ms) acquired at a resolution of 60,000 (at 200 m/z) was followed by up to 16 tandem MS scans (resolution of 15,000 at 200 m/z) of the most intense ions fulfilling predefined selection criteria (AGC target 1E5 ions, maximum ion injection time of 80 ms (*45 ms*), isolation window of 1.5 m/z, fixed first mass of 145 m/z, spectrum data type: centroid, under fill ratio 1%, intensity threshold 1.3E4 (*2.2E4*), exclusion of unassigned, singly charged precursors, peptide match preferred, exclude isotopes on, dynamic exclusion time of 12 s). The HCD collision energy was set to 32% Normalized Collision Energy and the polydimethylcyclosiloxane background ion at 445.12003 Da was used for internal calibration (lock mass).

Data Analysis (phosphoenriched samples and shotgun samples marked in italics)

Data analysis was performed with MaxQuant (version 1.5.3.30)[93] using the Andromeda search engine [94] with default search settings including a false discovery rate set at 1% on both the peptide and protein level. Spectra were searched against human proteins in the UniProt/Swiss-Prot database (database release version of November 2016 containing 20,117 human protein sequences,[95]) supplemented with the RSV Synagis antibody sequence. The mass tolerance for precursor and fragment ions was set to 20 and 4.5 ppm, respectively, during the main search. Enzyme specificity was set as C-terminal to arginine and lysine (trypsin), also allowing cleavage at arginine/lysine-proline bonds with a maximum of three missed cleavages. Carbamidomethylation of cysteine residues was set as a fixed modification and variable modifications were set to oxidation of methionine residues (to sulfoxides), acetylation of protein N-termini and phosphorylation of serine, threonine and tyrosine residues.

Proteins in the shotgun analysis were quantified by the MaxLFQ algorithm [96] integrated in the MaxQuant software. Only proteins with at least one unique or razor peptide were retained leading to the identification of 4,524 proteins. A minimum ratio count of two unique or razor peptides was required for quantification of 3,227 proteins. Further data analysis was performed with the Perseus software (version 1.5.3.0, [97]) after loading the shotgun samples protein groups file from MaxQuant. Proteins only identified by site and reverse database hits were removed and replicate samples were grouped. Proteins with less than three valid values in at least one group were removed and missing values were imputed from a normal distribution around the detection limit.

For the data analysis of the phospho-enriched samples, the phospho(STY)sites file from MaxQuant was loaded in the Perseus software. Phosphosites with a localization probability lower than 0.75 were

removed and the site table was expanded. The replicate samples were grouped according to the sample type (Mock, RSV-A2 w/o Ab, RSV-A2 palivizumab or RSV-A2 isotype control Ab). Phosphosites with less than three valid values in at least one sample type were removed and missing values were imputed from a normal distribution around the detection limit.

Phospho-mobility shift assay of CTTN, RPS6 and PUM2

In 6-well plates, 400.000 A549 cells were seeded in complete DMEM medium and incubated overnight at 37°C and 5%CO_2. The following day, A549 cells were incubated for 2 hours at 37°C with mock - or RSV-A2 inocula that were pretreated for 30 min at 37°C with or without 30 µg/ml dextran sulfate sodium salt (02160110, MP biomedicals) in Opti-MEM™ reduced serum medium. After 2 hours, A549 cell lysates were prepared as described above (sample preparation) with 1 ml lysis buffer. Proteins were enriched and purified from the lysate on an Amicon ultra centrifugal filter with a molecular weight cut-off of 3 kDa (UFC500324, Merck Millipore) and resuspended in PBS.

Purified proteins were subsequently treated with 200 units lambda protein phosphatase (P0753, New England Biolabs) or buffer only as a control for 1 hour at 30°C according to the manufacturer's protocol. After 1 hour, lambda protein phosphatase was inactivated by the addition of Na_2EDTA at a final concentration of 50 mM and inoculation at 65°C for 1 hour.

The proteins were then finally boiled for 10 min at 99°C in 1x Laemmli buffer supplemented with 4,2% (v:v) β-mercaptoethanol, separated by SDS-PAGE and semi-dry blotted on nitrocellulose membranes. Membranes were blocked with a 4% (w:v) low fat milk solution in PBS with 0,1% Tween20. Total cortactin -, RPS6 - and PUM2 protein levels were detected by cortactin antibody H-191 (sc-11408, Santa Cruz Biotechnology, Inc.), S6 ribosomal protein antibody 5G10 (2217, Cell signaling technology) and pumilio-2 antibody (A300-202A, Bethyl laboratories) by overnight incubation at 4°C in tris buffered saline-0,1% Tween20. We used secondary Amersham ECL Rabbit IgG, HRP-linked whole Ab (NA934, GE healthcare) and Pierce™ ECL Western blotting substrate (32106, ThermoFisher Scientific). Protein bands were visualized with a chemiluminescence imager (Amersham Imager 600, GE Healthcare).

Phospho-mobility shift assay of PAK2, NAA10, DYNC1Li1, PUM2, PTPN12 and TBC1D5

In 9 cm petri dishes, 3.4 million A549 cells were seeded in complete DMEM medium and incubated overnight at 37°C and 5% CO_2. Cells were mock - or RSV-A2 infected for 2 hours as described above for CTTN and RPS6, but cell lysates were prepared differently. After 2 hours, cells were washed and detached by trypsin/EDTA and pelleted by centrifugation at 400 x g for 5 min. Cells were lysed by resuspending the cell pellet in low salt lysis buffer (50 mM Tris pH 8.0, 150 mM NaCl, 5 mM EDTA, 1% NP40, 0.1% SDS and complete protease inhibitor cocktail (04693132001, Sigma-Aldrich)) on cells for 20 min on ice. Cell lysates were treated with lambda protein phosphatase as described above for CTTN and RPS6, except that we used 1,000 units instead of 200. Total PAK2 -, NAA10 -, DYNC1Li1 -, PUM2 -, PTPN12 - and TBC1D5 protein levels were detected by PAK2 antibody (2608, Cell signaling technology), ARD1A (NAA10) antibody (9046, Cell signaling technology), DYNC1Li1 antibody (ABIN2790248, Antibodies-online), PUM2 antibody (12323, Cell signaling technology), PTP-PEST (PTPN12)(AG10)

antibody (4864 Cell signaling technology) and TBC1D5 (E-9) antibody (sc-376296, Santa Cruz biotechnology, Inc.), respectively, by overnight incubation at 4°C in tris buffered saline-0,1% Tween20 with 5% (w/v) BSA. We used secondary Amersham ECL Mouse and Rabbit IgG, HRP-linked whole Ab (NA931 and NA934, respectively, GE healthcare) and Pierce™ ECL Western blotting substrate (32106, ThermoFisher Scientific). Protein bands were visualized with a chemiluminescence imager (Amersham Imager 600, GE Healthcare). As a control for equal loading, blots were stained with ponceau S before blocking.

Statistics

To examine to what extent significant changes observed in phosphorylation abundances in response to the mock/RSV inocula were (partially) resulting from changes in peptide quantities, the experiment was laid out in a completely randomized design with three replicates, and phosphopeptide and peptide quantities were analyzed jointly by fitting a linear mixed model of the following form to each of the 4,996 phosphorylated peptides separately: $y_{ijk} = \mu + \alpha_i + \beta_j + \alpha\beta_{ij} + \gamma_k + \varepsilon_{ijk}$, where y_{ijk} = log-transformed LFQ intensity reflecting the phosphopeptide and peptide abundances (i = 1…2) measured in the k-th replicate (k = 1…3) of the j-th mock/RSV inocula (j = 1…4; Mock, RSV-A2 isotype control Ab, RSV-A2 w/o Ab, RSV-A2 palivizumab).

The fixed part of the model consists of:

μ = the overall mean (intercept)

α_i = the term modeling the phosphorylation effect,

β_j = the term modeling the inocula effect, and

$\alpha\beta_{ij}$ = the interaction term modeling the inocula-specific phosphorylation

The random model terms, assumed to follow a normal distribution with zero mean and variance σ^2, are:

γ_k = main effect of the k-th replicate, and

ε_{ijk} = the random error (i.e. residual) for sample ijk.

The linear mixed model was fitted by the residual maximum likelihood (REML) approach as implemented in Genstat v18 [98]. Significances of the fixed main terms and their interaction were assessed by an F-test. Significances of pairwise comparisons between predicted means of inocula-specific phosphorylation were assessed by an t-test.

6.6 Acknowledgements

We thank Prof. Dr. Frans Van Roy (Ghent, Belgium) for providing the cortactin and PUM2 antibodies and Prof. Dr. Bart Lambrecht (Ghent, Belgium) for providing the RPS6 antibody. We also thank Jarne Pauwels and Prof. Dr. Kris Gevaert (Ghent, Belgium) for giving advice and performing a try-out mass spectrometry-based identification of proteins from A549 cells.

6.7 Reference list

1. Schweneker, M., et al., *HIV-induced changes in T cell signaling pathways.* J Immunol, 2008. **180**(10): p. 6490-500.
2. Gaur, P., A. Munjhal, and S.K. Lal, *Influenza virus and cell signaling pathways.* Med Sci Monit, 2011. **17**(6): p. RA148-54.
3. Ruggieri, A., et al., *Interplay between Hepatitis C Virus and Redox Cell Signaling.* Int J Mol Sci, 2013. **14**(3): p. 4705-21.
4. Guo, H., W.J. Kaiser, and E.S. Mocarski, *Manipulation of apoptosis and necroptosis signaling by herpesviruses.* Med Microbiol Immunol, 2015. **204**(3): p. 439-48.
5. Dapat, C., et al., *Quantitative phosphoproteomic analysis of host responses in human lung epithelial (A549) cells during influenza virus infection.* Virus Res, 2014. **179**: p. 53-63.
6. Soderholm, S., et al., *Phosphoproteomics to Characterize Host Response During Influenza A Virus Infection of Human Macrophages.* Mol Cell Proteomics, 2016. **15**(10): p. 3203-3219.
7. Popova, T.G., et al., *Reverse-phase phosphoproteome analysis of signaling pathways induced by Rift valley fever virus in human small airway epithelial cells.* PLoS One, 2010. **5**(11): p. e13805.
8. Ohman, T., et al., *Phosphoproteome characterization reveals that Sendai virus infection activates mTOR signaling in human epithelial cells.* Proteomics, 2015. **15**(12): p. 2087-97.
9. Kandasamy, R.K., et al., *A time-resolved molecular map of the macrophage response to VSV infection.* NPJ Syst Biol Appl, 2016. **2**: p. 16027.
10. Lu, N.T., et al., *Phospho-Network Analysis Identifies and Quantifies Hepatitis C Virus (HCV)-induced Hepatocellular Carcinoma (HCC) Proteins Regulating Viral-mediated Tumor Growth.* Cancer Genomics Proteomics, 2016. **13**(5): p. 339-57.
11. Ye, J., et al., *Quantitative phosphoproteomic analysis identifies the critical role of JNK1 in neuroinflammation induced by Japanese encephalitis virus.* Sci Signal, 2016. **9**(448): p. ra98.
12. Luo, R., et al., *Label-free quantitative phosphoproteomic analysis reveals differentially regulated proteins and pathway in PRRSV-infected pulmonary alveolar macrophages.* J Proteome Res, 2014. **13**(3): p. 1270-80.
13. Zhang, H., et al., *Quantitative Label-Free Phosphoproteomics Reveals Differentially Regulated Protein Phosphorylation Involved in West Nile Virus-Induced Host Inflammatory Response.* J Proteome Res, 2015. **14**(12): p. 5157-68.
14. Wojcechowskyj, J.A., et al., *Quantitative phosphoproteomics reveals extensive cellular reprogramming during HIV-1 entry.* Cell Host Microbe, 2013. **13**(5): p. 613-23.
15. Greenwood, E.J., et al., *Temporal proteomic analysis of HIV infection reveals remodelling of the host phosphoproteome by lentiviral Vif variants.* Elife, 2016. **5**.
16. Len, A.C., et al., *HIV-1 Activates T Cell Signaling Independently of Antigen to Drive Viral Spread.* Cell Rep, 2017. **18**(4): p. 1062-1074.
17. Lucera, M.B., et al., *HIV signaling through CD4 and CCR5 activates Rho family GTPases that are required for optimal infection of primary CD4+ T cells.* Retrovirology, 2017. **14**(1): p. 4.
18. Chattopadhyay, S., et al., *Tyrosine phosphorylation modulates mitochondrial chaperonin Hsp60 and delays rotavirus NSP4-mediated apoptotic signaling in host cells.* Cell Microbiol, 2017. **19**(3).
19. Stahl, J.A., et al., *Phosphoproteomic analyses reveal signaling pathways that facilitate lytic gammaherpesvirus replication.* PLoS Pathog, 2013. **9**(9): p. e1003583.
20. Kato, A., et al., *Herpes simplex virus 1 protein kinase Us3 phosphorylates viral dUTPase and regulates its catalytic activity in infected cells.* J Virol, 2014. **88**(1): p. 655-66.
21. Li, R., et al., *Phosphoproteomic Profiling Reveals Epstein-Barr Virus Protein Kinase Integration of DNA Damage Response and Mitotic Signaling.* PLoS Pathog, 2015. **11**(12): p. e1005346.
22. Oberstein, A., et al., *Human cytomegalovirus pUL97 kinase induces global changes in the infected cell phosphoproteome.* Proteomics, 2015. **15**(12): p. 2006-22.

23. Avey, D., et al., *Phosphoproteomic Analysis of KSHV-Infected Cells Reveals Roles of ORF45-Activated RSK during Lytic Replication.* PLoS Pathog, 2015. **11**(7): p. e1004993.
24. Johnson, S.M., et al., *Respiratory Syncytial Virus Uses CX3CR1 as a Receptor on Primary Human Airway Epithelial Cultures.* PLoS Pathog, 2015. **11**(12): p. e1005318.
25. Behera, A.K., et al., *Blocking intercellular adhesion molecule-1 on human epithelial cells decreases respiratory syncytial virus infection.* Biochem Biophys Res Commun, 2001. **280**(1): p. 188-95.
26. Tayyari, F., et al., *Identification of nucleolin as a cellular receptor for human respiratory syncytial virus.* Nat Med, 2011. **17**(9): p. 1132-5.
27. Currier, M.G., et al., *EGFR Interacts with the Fusion Protein of Respiratory Syncytial Virus Strain 2-20 and Mediates Infection and Mucin Expression.* PLoS Pathog, 2016. **12**(5): p. e1005622.
28. Krzyzaniak, M.A., et al., *Host cell entry of respiratory syncytial virus involves macropinocytosis followed by proteolytic activation of the F protein.* PLoS Pathog, 2013. **9**(4): p. e1003309.
29. Kaufmann, H., et al., *Influence of low temperature on productivity, proteome and protein phosphorylation of CHO cells.* Biotechnol Bioeng, 1999. **63**(5): p. 573-82.
30. Huang, K., et al., *Respiratory syncytial virus-neutralizing monoclonal antibodies motavizumab and palivizumab inhibit fusion.* J Virol, 2010. **84**(16): p. 8132-40.
31. Barik, S., T. McLean, and L.C. Dupuy, *Phosphorylation of Ser232 directly regulates the transcriptional activity of the P protein of human respiratory syncytial virus: phosphorylation of Ser237 may play an accessory role.* Virology, 1995. **213**(2): p. 405-12.
32. Sanchez-Seco, M.P., et al., *C-terminal phosphorylation of human respiratory syncytial virus P protein occurs mainly at serine residue 232.* J Gen Virol, 1995. **76 (Pt 2)**: p. 425-30.
33. Dupuy, L.C., et al., *Casein kinase 2-mediated phosphorylation of respiratory syncytial virus phosphoprotein P is essential for the transcription elongation activity of the viral polymerase; phosphorylation by casein kinase 1 occurs mainly at Ser(215) and is without effect.* J Virol, 1999. **73**(10): p. 8384-92.
34. Lu, B., et al., *The major phosphorylation sites of the respiratory syncytial virus phosphoprotein are dispensable for virus replication in vitro.* J Virol, 2002. **76**(21): p. 10776-84.
35. Gnad, F., J. Gunawardena, and M. Mann, *PHOSIDA 2011: the posttranslational modification database.* Nucleic Acids Res, 2011. **39**(Database issue): p. D253-60.
36. Horn, H., et al., *KinomeXplorer: an integrated platform for kinome biology studies.* Nat Methods, 2014. **11**(6): p. 603-4.
37. Duan, G., X. Li, and M. Kohn, *The human DEPhOsphorylation database DEPOD: a 2015 update.* Nucleic Acids Res, 2015. **43**(Database issue): p. D531-5.
38. Li, Y., et al., *Relationship between ATM and ribosomal protein S6 revealed by the chemical inhibition of Ser/Thr protein phosphatase type 1.* Biosci Biotechnol Biochem, 2012. **76**(3): p. 486-94.
39. Hutchinson, J.A., et al., *Regulation of ribosomal protein S6 phosphorylation by casein kinase 1 and protein phosphatase 1.* J Biol Chem, 2011. **286**(10): p. 8688-96.
40. Eiseler, T., et al., *Protein kinase D controls actin polymerization and cell motility through phosphorylation of cortactin.* J Biol Chem, 2010. **285**(24): p. 18672-83.
41. Kelley, L.C., et al., *Cortactin phosphorylated by ERK1/2 localizes to sites of dynamic actin regulation and is required for carcinoma lamellipodia persistence.* PLoS One, 2010. **5**(11): p. e13847.
42. Rezaee, F., et al., *Sustained protein kinase D activation mediates respiratory syncytial virus-induced airway barrier disruption.* J Virol, 2013. **87**(20): p. 11088-95.
43. Lyons, P.D., et al., *Inhibition of the catalytic activity of cell adhesion kinase beta by protein-tyrosine phosphatase-PEST-mediated dephosphorylation.* J Biol Chem, 2001. **276**(26): p. 24422-31.
44. Du, Q.S., et al., *Inhibition of PYK2-induced actin cytoskeleton reorganization, PYK2 autophosphorylation and focal adhesion targeting by FAK.* J Cell Sci, 2001. **114**(Pt 16): p. 2977-87.

45. Pan, X., et al., *TBC-domain GAPs for Rab GTPases accelerate GTP hydrolysis by a dual-finger mechanism.* Nature, 2006. **442**(7100): p. 303-6.
46. Seaman, M.N., et al., *Membrane recruitment of the cargo-selective retromer subcomplex is catalysed by the small GTPase Rab7 and inhibited by the Rab-GAP TBC1D5.* J Cell Sci, 2009. **122**(Pt 14): p. 2371-82.
47. Shin, D.H., et al., *Arrest defective-1 controls tumor cell behavior by acetylating myosin light chain kinase.* PLoS One, 2009. **4**(10): p. e7451.
48. Masutani, M., et al., *Reconstitution reveals the functional core of mammalian eIF3.* EMBO J, 2007. **26**(14): p. 3373-83.
49. Meyuhas, O., *Ribosomal Protein S6 Phosphorylation: Four Decades of Research.* Int Rev Cell Mol Biol, 2015. **320**: p. 41-73.
50. Savino, T.M., et al., *The nucleolar antigen Nop52, the human homologue of the yeast ribosomal RNA processing RRP1, is recruited at late stages of nucleologenesis.* J Cell Sci, 1999. **112 (Pt 12)**: p. 1889-900.
51. Miles, M.C., et al., *Molecular and functional characterization of a novel splice variant of ANKHD1 that lacks the KH domain and its role in cell survival and apoptosis.* FEBS J, 2005. **272**(16): p. 4091-102.
52. Sahara, S., et al., *Acinus is a caspase-3-activated protein required for apoptotic chromatin condensation.* Nature, 1999. **401**(6749): p. 168-73.
53. Narita, R., et al., *A novel function of human Pumilio proteins in cytoplasmic sensing of viral infection.* PLoS Pathog, 2014. **10**(10): p. e1004417.
54. Lee, C.R., et al., *Phosphorylation-Dependent Mobility Shift of Proteins on SDS-PAGE is Due to Decreased Binding of SDS.* Bull. Korean Chem. Soc., 2013. **34**(7): p. 2063-2066.
55. Kolokoltsov, A.A., et al., *Small interfering RNA profiling reveals key role of clathrin-mediated endocytosis and early endosome formation for infection by respiratory syncytial virus.* J Virol, 2007. **81**(14): p. 7786-800.
56. Srinivasakumar, N., P.L. Ogra, and T.D. Flanagan, *Characteristics of fusion of respiratory syncytial virus with HEp-2 cells as measured by R18 fluorescence dequenching assay.* J Virol, 1991. **65**(8): p. 4063-9.
57. McLellan, J.S., et al., *Structure of RSV fusion glycoprotein trimer bound to a prefusion-specific neutralizing antibody.* Science, 2013. **340**(6136): p. 1113-7.
58. Burke, E., et al., *Role of cellular actin in the gene expression and morphogenesis of human respiratory syncytial virus.* Virology, 1998. **252**(1): p. 137-48.
59. Burke, E., et al., *Profilin is required for optimal actin-dependent transcription of respiratory syncytial virus genome RNA.* J Virol, 2000. **74**(2): p. 669-75.
60. Harpen, M., et al., *Mutational analysis reveals a noncontractile but interactive role of actin and profilin in viral RNA-dependent RNA synthesis.* J Virol, 2009. **83**(21): p. 10869-76.
61. Radhakrishnan, A., et al., *Protein analysis of purified respiratory syncytial virus particles reveals an important role for heat shock protein 90 in virus particle assembly.* Mol Cell Proteomics, 2010. **9**(9): p. 1829-48.
62. Santangelo, P.J. and G. Bao, *Dynamics of filamentous viral RNPs prior to egress.* Nucleic Acids Res, 2007. **35**(11): p. 3602-11.
63. Mitra, R., et al., *The human respiratory syncytial virus matrix protein is required for maturation of viral filaments.* J Virol, 2012. **86**(8): p. 4432-43.
64. Oliveira, A.P., et al., *Human respiratory syncytial virus N, P and M protein interactions in HEK-293T cells.* Virus Res, 2013. **177**(1): p. 108-12.
65. Mehedi, M., et al., *Actin-Related Protein 2 (ARP2) and Virus-Induced Filopodia Facilitate Human Respiratory Syncytial Virus Spread.* PLoS Pathog, 2016. **12**(12): p. e1006062.
66. Kallewaard, N.L., A.L. Bowen, and J.E. Crowe, Jr., *Cooperativity of actin and microtubule elements during replication of respiratory syncytial virus.* Virology, 2005. **331**(1): p. 73-81.
67. van Diepen, A., et al., *Quantitative proteome profiling of respiratory virus-infected lung epithelial cells.* J Proteomics, 2010. **73**(9): p. 1680-93.

68. Grassart, A., et al., *Pak1 phosphorylation enhances cortactin-N-WASP interaction in clathrin-caveolin-independent endocytosis.* Traffic, 2010. **11**(8): p. 1079-91.
69. Ternette, N., et al., *Label-free quantitative proteomics reveals regulation of interferon-induced protein with tetratricopeptide repeats 3 (IFIT3) and 5'-3'-exoribonuclease 2 (XRN2) during respiratory syncytial virus infection.* Virol J, 2011. **8**(1): p. 442.
70. Chen, L.M., D. Bailey, and C. Fernandez-Valle, *Association of beta 1 integrin with focal adhesion kinase and paxillin in differentiating Schwann cells.* J Neurosci, 2000. **20**(10): p. 3776-84.
71. Cote, J.F., et al., *PSTPIP is a substrate of PTP-PEST and serves as a scaffold guiding PTP-PEST toward a specific dephosphorylation of WASP.* J Biol Chem, 2002. **277**(4): p. 2973-86.
72. Ruusala, A. and P. Aspenstrom, *The atypical Rho GTPase Wrch1 collaborates with the nonreceptor tyrosine kinases Pyk2 and Src in regulating cytoskeletal dynamics.* Mol Cell Biol, 2008. **28**(5): p. 1802-14.
73. Saras, J., P. Wollberg, and P. Aspenstrom, *Wrch1 is a GTPase-deficient Cdc42-like protein with unusual binding characteristics and cellular effects.* Exp Cell Res, 2004. **299**(2): p. 356-69.
74. San-Juan-Vergara, H., et al., *Cholesterol-rich microdomains as docking platforms for respiratory syncytial virus in normal human bronchial epithelial cells.* J Virol, 2012. **86**(3): p. 1832-43.
75. De la Mota-Peynado, A., J. Chernoff, and A. Beeser, *Identification of the atypical MAPK Erk3 as a novel substrate for p21-activated kinase (Pak) activity.* J Biol Chem, 2011. **286**(15): p. 13603-11.
76. Xiao, K., et al., *Global phosphorylation analysis of beta-arrestin-mediated signaling downstream of a seven transmembrane receptor (7TMR).* Proc Natl Acad Sci U S A, 2010. **107**(34): p. 15299-304.
77. Xu, J., et al., *Nonmuscle myosin light-chain kinase mediates neutrophil transmigration in sepsis-induced lung inflammation by activating beta2 integrins.* Nat Immunol, 2008. **9**(8): p. 880-6.
78. Godin, C.M. and S.S. Ferguson, *The angiotensin II type 1 receptor induces membrane blebbing by coupling to Rho A, Rho kinase, and myosin light chain kinase.* Mol Pharmacol, 2010. **77**(6): p. 903-11.
79. Hanley, L.L., et al., *Roles of the respiratory syncytial virus trailer region: effects of mutations on genome production and stress granule formation.* Virology, 2010. **406**(2): p. 241-52.
80. Lindquist, M.E., et al., *Respiratory syncytial virus induces host RNA stress granules to facilitate viral replication.* J Virol, 2010. **84**(23): p. 12274-84.
81. Lindquist, M.E., et al., *Activation of protein kinase R is required for induction of stress granules by respiratory syncytial virus but dispensable for viral replication.* Virology, 2011. **413**(1): p. 103-10.
82. Groskreutz, D.J., et al., *Respiratory syncytial virus limits alpha subunit of eukaryotic translation initiation factor 2 (eIF2alpha) phosphorylation to maintain translation and viral replication.* J Biol Chem, 2010. **285**(31): p. 24023-31.
83. Fricke, J., et al., *p38 and OGT sequestration into viral inclusion bodies in cells infected with human respiratory syncytial virus suppresses MK2 activities and stress granule assembly.* J Virol, 2013. **87**(3): p. 1333-47.
84. Ohn, T., et al., *A functional RNAi screen links O-GlcNAc modification of ribosomal proteins to stress granule and processing body assembly.* Nat Cell Biol, 2008. **10**(10): p. 1224-31.
85. Damoc, E., et al., *Structural characterization of the human eukaryotic initiation factor 3 protein complex by mass spectrometry.* Mol Cell Proteomics, 2007. **6**(7): p. 1135-46.
86. Bajorek, M., et al., *The Thr205 phosphorylation site within respiratory syncytial virus matrix (M) protein modulates M oligomerization and virus production.* J Virol, 2014. **88**(11): p. 6380-93.
87. Martinez, I., et al., *Distinct gene subsets are induced at different time points after human respiratory syncytial virus infection of A549 cells.* J Gen Virol, 2007. **88**(Pt 2): p. 570-81.
88. Mayer, A.K., et al., *Differential recognition of TLR-dependent microbial ligands in human bronchial epithelial cells.* J Immunol, 2007. **178**(5): p. 3134-42.

89. Munday, D.C., et al., *Quantitative proteomic analysis of A549 cells infected with human respiratory syncytial virus.* Mol Cell Proteomics, 2010. **9**(11): p. 2438-59.
90. Munday, D.C., J.A. Hiscox, and J.N. Barr, *Quantitative proteomic analysis of A549 cells infected with human respiratory syncytial virus subgroup B using SILAC coupled to LC-MS/MS.* Proteomics, 2010. **10**(23): p. 4320-34.
91. Dave, K.A., et al., *A comprehensive proteomic view of responses of A549 type II alveolar epithelial cells to human respiratory syncytial virus infection.* Mol Cell Proteomics, 2014. **13**(12): p. 3250-69.
92. Biosciences, R. *MagReSyn® Ti-IMAC*. 2017; Available from: http://www.resynbio.com/index_htm_files/IFU_IMAC.pdf.
93. Cox, J. and M. Mann, *MaxQuant enables high peptide identification rates, individualized p.p.b.-range mass accuracies and proteome-wide protein quantification.* Nat Biotechnol, 2008. **26**(12): p. 1367-72.
94. Cox, J., et al., *Andromeda: a peptide search engine integrated into the MaxQuant environment.* J Proteome Res, 2011. **10**(4): p. 1794-805.
95. Uniprot. 2016; Available from: www.uniprot.org.
96. Cox, J., et al., *Accurate proteome-wide label-free quantification by delayed normalization and maximal peptide ratio extraction, termed MaxLFQ.* Mol Cell Proteomics, 2014. **13**(9): p. 2513-26.
97. Tyanova, S., et al., *The Perseus computational platform for comprehensive analysis of (prote)omics data.* Nat Methods, 2016. **13**(9): p. 731-40.
98. Payne R., M.D., Harding S., *An Introduction to the Genstat Command Language (18th Edition), Part 3 Procedures*, V. International, Editor. 2015.

Chapter VII

Interactome analysis of the RSV non-structural proteins 1 and 2

Koen Sedeyn, Delphi Van Haver, Francis Impens, Delphine De Sutter, Sven Eyckerman, Bert Schepens and Xavier Saelens

Author contributions: K.S., F.I., S.E., B.S. and X.S. designed and discussed the experiments. For BioID and affinity purification, K.S. performed the experiments except for the mass spectrometry-based identification of proteins, which was done by D.V.H. and F.I.. For Virotrap, K.S. cloned and validated the expression vectors, while D.D.S and S.E. performed the actual Virotrap experiment and mass spectrometry-based identification of proteins. K.S. analysed the proxeome/interactome data by pathway tools.

7.1 Introduction

Protein-protein interactions (PPIs) play crucial roles in the cellular functions of proteins. As a consequence, characterization of the PPIs of proteins can greatly enhance the understanding of the molecular actions of proteins. Over the years, many techniques have been developed to study PPIs, which all have intrinsic advantages and limitations. Commonly used PPI mapping techniques are yeast-two-hybrid and antibody-mediated affinity purification. Although these techniques have been and still are being used successfully to study PPIs, considerable challenges must be taken into account. The yeast-two-hybrid method requires that the bait and prey protein interact in the nucleus of the yeast cells. For mammalian proteins that do not normally reside in the nucleus this prerequisite of Y2H is a limitation because protein folding and modifications such as phosphorylations and methylations that occur in the natural environment of the candidate bait and prey proteins may be compromised in the yeast cell nucleus. Antibody-mediated affinity purification is usually performed in a homologous cell background but is executed after cell lysis. The lysis step creates the possibility for proteins that not necessarily colocalize in an intact cell to interact with each other. In addition, transient and weak interactions are easily lost during cell lysis and subsequent purification steps. Therefore, several techniques have been developed to study PPIs in the endogenous cellular context, such as BioID and Virotrap.

BioID makes use of the *E. coli* derived DNA-binding biotin protein ligase BirA [1]. As BirA is highly selective in biotinylating its substrate peptide, a more promiscuous point mutant (R118G) of BirA has been generated. The BirA-R118G mutant has also lost its DNA binding capacity. In the presence of ATP, this point mutant of BirA converts biotin into the highly reactive biotinoyl-5'-AMP, and covalently links biotin to primary amines (*e.g.* N-terminus of proteins and Lysine side chains) that are in its vicinity (Fig. 1). By fusing BirA-R118G to a protein of interest, proteins in the proximity (estimated to be around 10 nm) of the bait can become selectively biotinylated. Natural biotinylation is a rare protein modification that is thought to be limited to 4 carboxylase proteins in animals [2]. Therefore, in BioID, enrichment of biotinylated proteins after cell lysis basically corresponds to these "proxeome" proteins. Proxeome proteins can, but not necessarily, represent interactors of the bait protein. One of the strengths of BioID is that interacting proteins are labeled in their natural context and that weak or transient interactions might be sufficient for biotinylation. Additionally, biotinylated proteins can be enriched with high affinity by streptavidin, which permits the use of rigorous washing steps.

Virotrap is a PPI mapping technique that was developed at the Center for Medical Biotechnology. This technique exploits the characteristic of the p55 GAG protein of HIV-1 to form VLPs that are released from the cell upon expression [3]. Fusion of a bait protein to GAG may allow the formation of VLPs that are secreted in the culture medium with bait interacting proteins "trapped" inside these VLPs (Fig. 2). After selective enrichment of VLPs from the culture medium, proteins inside the VLPs can be identified. Analogous to BioID, Virotrap allows the identification of PPIs in their natural context. As shown in figure 3, Virotrap allows the identification of core PPIs that can be identified by several commonly used PPI techniques, but, more interestingly, also of PPIs that are missed by these other PPI techniques. These results highlight that Virotrap is a complementary approach to study PPIs.

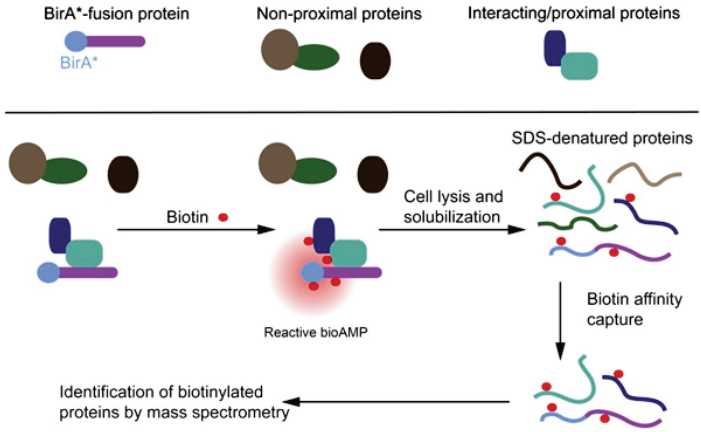

Figure 1: Schematic outline of proximity-based protein biotinylation (BioID). In BioID, a promiscuous point mutant (R118G) of the *E. coli* derived biotin ligase BirA (marked as BirA*) is genetically fused to a bait protein of interest (highlighted in purple). Upon expression of the bait-BirA* fusion protein an excess of free biotin is added. The BirA* protein will convert biotin and ATP into the highly reactive bioAMP. As such, candidate interacting proteins or proteins in the proximity of the bait may get biotinylated by the BirA* protein. After cell lysis biotinylated proteins can be enriched efficiently by *e.g.* streptavidin, followed by their identification by mass spectrometry. Figure taken from [1].

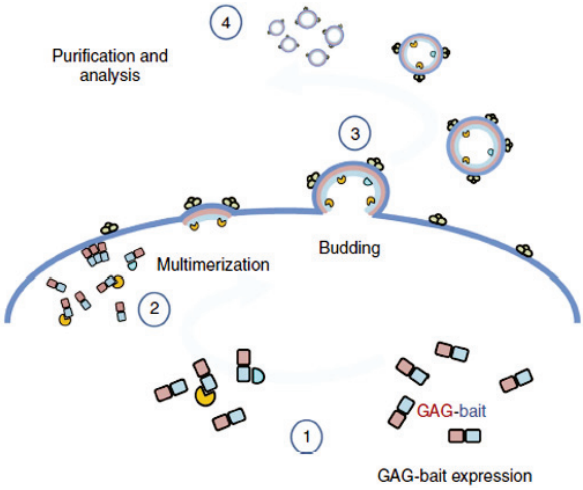

Figure 2: Schematic outline of Virotrap. In Virotrap, a bait protein of interest is genetically fused to the p55 GAG protein of HIV-1 and expressed in the cytoplasm to allow protein-protein interactions to occur with the bait (1). The p55 GAG moiety subsequently recruits the fusion protein, with associated candidate interactors, to the plasma membrane and induces the formation of VLPs (2). These VLPs bud from the plasma membrane, thereby trapping candidate interactors of the bait protein inside the VLPs (3). Upon coexpression, flag-tagged VSV-G (highlighted as green trimers) will be incorporated in the membrane of the VLPs and allows efficient affinity purification of the VLPs (4). Trapped proteins can be identified by mass spectrometry. Figure taken from [3].

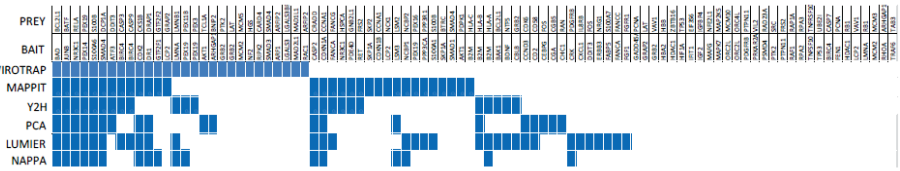

Figure 3: Comparison of different protein-protein interaction mapping techniques for the identification of a set of known protein-protein interactions. A positive reference set of 92 known PPIs were tested with different PPI mapping techniques, *i.e.* Virotrap, mammalian protein-protein interaction trap (MAPPIT), Y2H, protein fragment complementation assay (PCA), Lumier and nucleic acid programmable protein arrays (NAPPA). Confirmed bait-prey interactions were marked in blue. As a negative control, a random reference set of 92 bait-prey pairs was tested (not shown). For Virotrap, 5% false-positive interactions were detected. Figure taken from [3].

A typical hallmark of RSV infections is the low to undetectable levels of type I and III IFN that is induced by the host. This is attributed to the concerted actions of the two non-structural proteins, NS1 and NS2 [4-8]. Multiple key proteins that are involved in the induction and signaling of type I - and type III IFN are reduced in abundance in the presence of NS1 and/or NS2. NS1 (19,4 kDa) and NS2 (18,6 kDa) lack enzymatic activity and thus their PPIs with host proteins help explain their capacity to interfere with the host IFN response. It has been proposed that NS1 and NS2 form so called "NS degradasome" complexes that might function as proteasome like structures [9]. Within these complexes, purified by size exclusion chromatography, the α2 subunit of the 20S core proteasome was identified, suggesting a close interconnection between the NS degradasome and the 26S proteasome complex. A more comprehensive analysis of NS1 interactions with host proteins based on affinity purification identified 221 candidate interactors [10]. Functional analysis of a subset of these candidate interactors revealed a possible role for NS1 in inducing a cell cycle arrest at the G_0/G_1 phase. Although these results provided a first insight in candidate NS1 interactors, weak or transient interactions might have been missed during the affinity purification approach.

To expand the knowledge on candidate NS1 and NS2 interactors we used three different PPI techniques, *i.e.* BioID and Virotrap, discussed above, and conventional affinity purification followed by label free quantification (LFQ)-mass spectrometry. For BioID, we generated three stable cell lines that allowed conditional (doxycycline inducible) expression of NS1 or NS2 fused to the promiscuous BirA biotin ligase. For Virotrap, we fused NS1 and NS2 to the HIV-1 p55 GAG protein and determined VLP trapped proteins. Finally, we performed a conventional affinity purification after expression of epitope-tagged NS1 and NS2.

7.2 Results

7.2.1 The RSV NS1 and NS2 proxeome studied with BioID

To study PPIs of the RSV-NS1 and -NS2 proteins, we first used the proximity-based biotinylation technique BioID. Therefore we generated stable transduced cell lines that allowed doxycycline inducible expression of the biotin ligase BirA-R118G (which we will name BirA* hereafter) fused with RSV-NS1, -NS2 or the human host protein MYLK4, which served as a non-virus-derived control.

Generation of stable Flp-In™ T-REx™ 293 cells expressing doxycycline inducible RSV-NS1, -NS2 or MYLK4 fused to the biotin ligase BirA*.

To generate the stable cell lines we used Flp-In™ T-REx™ 293 cells. These cells are HEK293-derived cells with two stable integrated plasmids and can be used to express a gene of interest by the administration of doxycycline to the culture medium. The first integrated plasmid encodes β-galactosidase (*lacZ* gene) and a zeocin selection marker preceded by a FRT recombination site and an AUG startcodon (Fig. 4A). The second plasmid codes for the tetracycline repressor (TetR) and a blasticidin resistance marker. The Gateway® cloning compatible destination vector pDest_pcDNA5-BirA*-Flag (Suppl. Fig. 1A) is applicable with these cells as it encodes the mammalian resistance marker hygromycin B without start codon preceded by a FRT recombination site and the BirA*-Flag protein under control of the CMV-IE promoter with a Tet operator. Through Gateway® cloning, bait proteins can be inserted in frame at the N-terminus of the BirA*-Flag protein in the pDest-pcDNA5-BirA*-Flag vector. Cotransfection of a pcDNA5-bait-BirA*-Flag plasmid and a Flp recombinase expression vector (*e.g.* pOG44) in Flp-In™ T-REx™ 293 cells, will lead to Flp recombinase-mediated insertion of the pcDNA5 vector at the FRT site preceding the *lacZ* gene and the zeocin resistance marker (Fig. 4B). Only cells that correctly inserted the pcDNA5 plasmid at the FRT site will express a functional hygromycin B resistance protein and can be selected. Additionally, stable integration will lead to a loss of expression of β-galactosidase - and the zeocin resistance marker. The constitutively expressed TetR will repress bait-BirA*-Flag expression in the absence of doxycycline.

In a first step we cloned the codon optimized RSV-NS1 and -NS2 and MYLK4 sequence in frame at the N-terminus of the Flag-tagged BirA* in the destination plasmid pDest_pcDNA5-BirA*-Flag. We named these plasmids pcDNA5-NS1-BirA*-Flag, pcDNA5-NS2-BirA*-Flag and pcDNA5-MYLK4-BirA*-Flag, respectively (Suppl. Fig. 1B-D). These plasmids were first transiently transfected in HEK293T cells for 24 hours to confirm expression of the BirA* fusion proteins by western blotting and immunofluorescence. In contrast to Flp-In™ T-REx™ 293 cells, HEK293T cells do not express the tetracycline repressor, so expression of the BirA* fusion proteins was expected. As controls, we also transfected the pDest_pcDNA5-BirA*-Flag vector and two expression plasmids encoding Flag-tagged codon optimized RSV-NS1 and -NS2 without the BirA* moiety, to investigate the effect of BirA* fusion on the subcellular localization of NS1 and NS2.

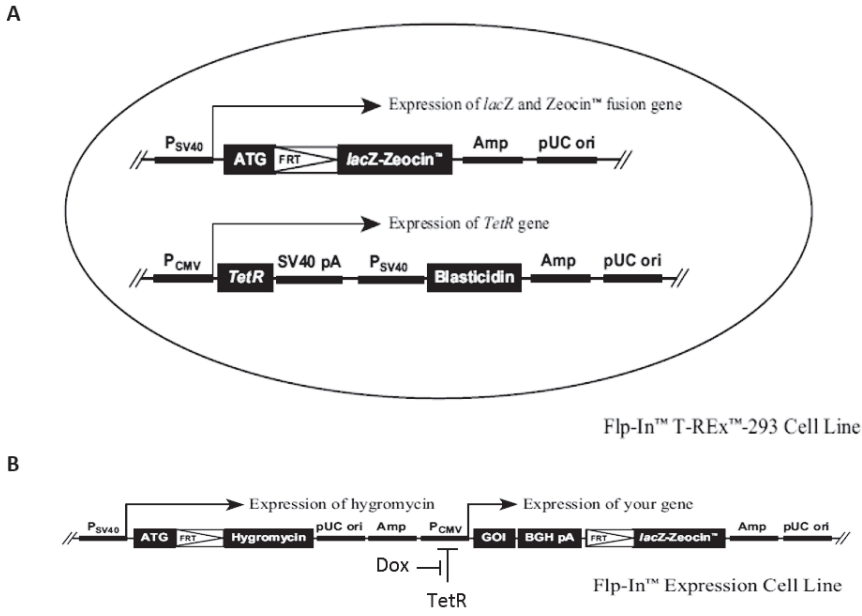

Figure 4: Flp-In™ T-REx™ 293 cells. (A) schematic representation of the two stably, independently integrated plasmids in Flp-In™ T-REx™ 293 cells. The upper plasmid encodes a lacZ and zeocin resistance gene preceded by a FRT recombination site and AUG start codon under the control of the constitutive SV40 early promoter. The FRT site can be used to stably integrate a plasmid containing a FRT site by Flp recombinase-mediated recombination. The lower plasmid encodes a tetracycline repressor under the control of the constitutive CMV immediate/early promoter. (B): schematic representation of a stably integrated plasmid encoding a gene of interest (GOI) under control of a doxycycline inducible CMV immediate-early/Tet operator promoter after Flp recombinase-mediated recombination at the FRT site in Flp-In™ T-REx™ 293 cells. Figures adapted from ThermoFisher Scientific.

As shown in figure 5A we observed a main protein band around 50 kDa after transfection of the pcDNA5-NS1-BirA*-Flag - and pcDNA5-NS2-BirA*-Flag plasmids that likely corresponds to the full length NS1-BirA*-Flag (theoretical mass of 53,8 kDa) and NS2-BirA*-Flag (theoretical mass of 53,0 kDa).Several other bands were also present, however, these bands were only observed after transient transfection and not in the stable cell lines (see further). We therefore did not investigate these bands further. MYLK4-BirA*-Flag and BirA*-Flag alone were detected as single bands corresponding to their theoretical mass of 82,9 kDa and 36,9 kDa, respectively (Fig. 5A, BirA*-Flag alone was marked as: -). As expected, we only detected MYLK4-BirA*-Flag with a MYLK4-specific antibody. Unexpectedly, we could not observe expression of NS1-Flag (theoretical mass of 19,4 kDa) by western blotting, whereas NS2-Flag was expressed as two bands (theoretical mass of 18,6 kDa). Immunofluorescence-based detection of expression largely corresponded to the western blotting results. For all NS constructs, MYLK4-BirA*-Flag and BirA*-Flag alone (pDestination), Flag staining was observed, whereas untransfected cells and secondary antibody only controls did not stain (Fig. 5B, Suppl. Fig. 2). Although staining of the NS1

proteins was somewhat weaker compared to the NS2 - and MYLK4 proteins, we could detect NS1 expression. Recombinant expression of NS1 alone has been published to localize to the cytoplasm and nucleus, whereas NS2 expression mainly localizes to the mitochondria [8, 11, 12]. In accordance, we observed that NS1-Flag and NS1-BirA*-Flag are expressed in both the cytoplasm and nucleus, suggesting that BirA* fusion does not affect NS1 localization. For NS2-Flag and NS2-BirA*-Flag, expression was mainly detected in the cytoplasm, with a substantial number of cells having a bright, spotted pattern of expression, which likely corresponds with a mitochondrial localization (see Fig. 5B inset in NS2-Flag). MYLK4-BirA*-Flag expression was mainly cytoplasmic, whereas BirA*-Flag alone localized to both cytoplasm and nucleus. Taken together, these results confirm that our pcDNA5 vectors are functional in expressing NS1-BirA*-Flag, NS2-BirA*-Flag and MYLK4-BirA*-Flag and that the fusion of BirA* to NS1 and NS2 has no major impact on their subcellular localization.

As we were surprised that we could not detect NS1-Flag expression by western blotting despite expression in immunofluorescence (Fig. 5), we performed a repeat experiment with transfection of different amounts of the pEXPR-NS1-Flag - and pEXPR-NS2-Flag plasmids in HEK293T cells. In contrast to the first experiment, we could now clearly detect expression of both NS1-Flag and NS2-Flag by western blotting, with NS1-Flag expression being stronger than NS2-Flag (Fig. 6). These results likely reflect the unstable nature of the NS2 protein. In accordance to literature, NS1 ran slightly faster than NS2, despite the slightly higher theoretical mass of NS1 [11, 13]. The Flag-tagged NS1 and NS2 proteins appeared as two bands in the western blots with the upper band corresponding to the expected molecular weight and the lower band running slightly faster. The lower bands possibly represent truncated forms of NS1 and NS2. These results confirm that our NS1-Flag and NS2-Flag expression vectors are functional.

To investigate if the biotin ligation activity of BirA* after fusion to NS1, NS2 or MYLK4 is still intact, we transiently transfected the corresponding pcDNA5 vectors in HEK293T cells for 48 hours and incubated the cells with 50 µM biotin after 24 hours. Fourty-eight hours post transfection we prepared cell lysates and detected biotinylated proteins with HRP-coupled streptavidin in western blotting. Upon expression of NS1-BirA*-Flag and NS2-BirA*-Flag we detected multiple streptavidin-reactive protein bands, which likely also included the NS1-BirA*-Flag and NS2-BirA*-Flag proteins themselves (Fig. 7). For MYLK4-BirA*-Flag we observed only one band that likely corresponded to MYLK4-BirA*-Flag itself, considering the molecular weight. Transfection of the pDest_pcDNA5-BirA*-Flag vector did not result in the detection of streptavidin-reactive proteins, despite the apparent expression of BirA*-Flag alone (Fig. 5 and 7). These results suggest that the diversity of proteins in the proxeomes of NS1, NS2 and MYLK4 might be different with the highest diversity for NS1 and the lowest for MYLK4. As we did not monitor the expression levels of the three BirA* fusion proteins in this experiment, it is possible that differences in expression of the biotin ligase have caused the difference in protein diversity. The strong intensity of the single band of MYLK4-BirA*-Flag suggests that the biotin ligation activity of BirA* is not hampered by MYLK4 fusion, at least not on self-biotinylation. These results confirm that the BirA* moieties in NS1-BirA*-Flag, NS2-BirA*-Flag and MYLK4-BirA*-Flag are functionally active in biotinylating proteins.

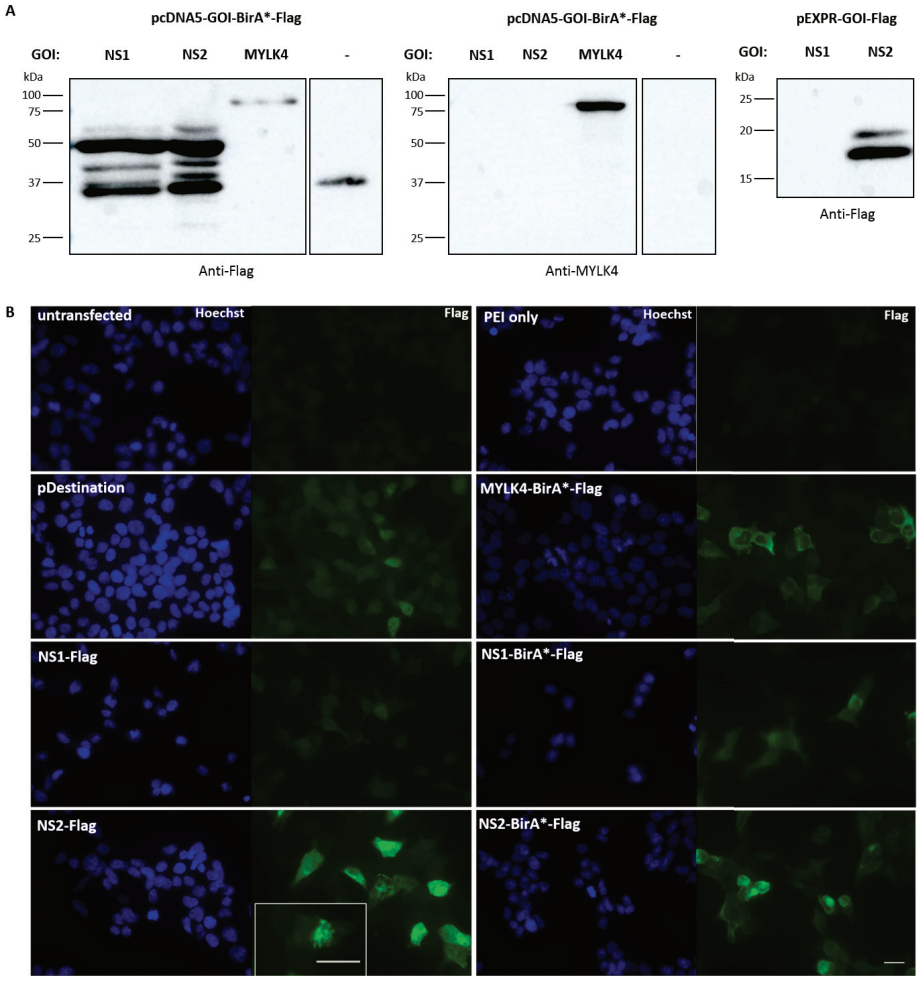

Figure 5: Expression of NS1-BirA*-Flag, NS2-BirA*Flag, MYLK4-BirA*-Flag, NS1-Flag and NS2-Flag after transient transfection in HEK293T cells. HEK293T cells in 24-well plates were transiently transfected with 300 ng pcDNA5-GOI-BirA*-Flag plasmid, pDest_pcDNA5-BirA*-Flag plasmid (marked as: -) or pEXPR-GOI-Flag plasmid for 24 hours. GOI = gene of interest. (A) Western blot-based detection by using a Flag-tag or MYLK4-specific antibody. (B) immunofluorescence-based detection by using a Flag-tag-specific antibody and staining of the nuclei by Hoechst. Inset in NS2-Flag: higher magnification. Scale bar = 10 µm.

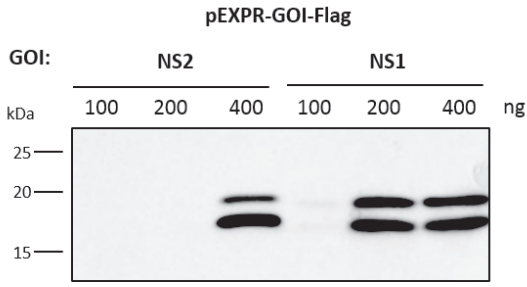

Figure 6: Expression of NS1-Flag and NS2-Flag after transient transfection in HEK293T cells. HEK293T cells in 48-well plates were transiently transfected with 100, 200 or 400 ng of pEXPR-GOI-Flag plasmid for 24 hours. GOI = gene of interest. NS1-Flag and NS2-Flag were detected by a Flag-tag-specific antibody.

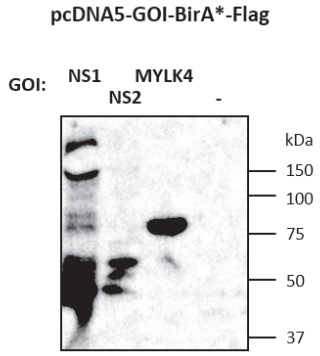

Figure 7: Protein biotinylation assay by NS1-BirA*-Flag, NS2-BirA*Flag and MYLK4-BirA*-Flag after transient transfection in HEK293T cells. HEK293T cells in 96-well plates were transiently transfected with 100 ng of pcDNA5-GOI-BirA*-Flag plasmid or pDest_pcDNA5-BirA*-Flag plasmid for 48 hours. After 24 hours, we added 50 µM biotin to the culture medium. GOI = gene of interest. Biotinylated proteins were detected by HRP-coupled streptavidin.

As we could validate the functionality of the NS1-, NS2- and MYLK4-BirA* fusion proteins, we used the respective pcDNA5 expression vectors to generate stably transduced cell lines. The pcDNA5 vectors were cotransfected in Flp In^{TM} T-REx^{TM} 293 cells with the Flp recombinase expression vector pOG44. As a negative control, we also transfected Flp In^{TM} T-REx^{TM} 293 cells with the pcDNA5 vectors only in parallel. Stably transduced cells were selected by the inoculation of hygromycin B in the culture medium for at least 3 days. We named these cell lines HEK-NS1-BirA*-Flag, HEK-NS2-BirA*-Flag and HEK-MYLK4-BirA*-Flag.

Validation of stable Flp In™ T-REx™ 293 cells expressing doxycycline inducible RSV-NS1, -NS2 or MYLK4 fused to the biotin ligase BirA*.

After the selection of stable HEK293 derived cells expressing NS1-BirA*-Flag, NS2-BirA*-Flag or MYLK4-BirA*-Flag, we validated these cell lines. As the stable integration of the pcDNA5 vectors at the FRT recombination site in the Flp In™ T-REx™ 293 cells should obliterate zeocin resistance, we first investigated zeocin sensitivity of the stable cell lines. All three selected stable cell lines did not survive in 100 µg/ml zeocin (data not shown). Untransfected Flp In™ T-REx™ 293 cells on the other hand survived both in the absence and presence of 100 µg/ml zeocin. These results suggest that the pcDNA5 vectors are correctly integrated at the FRT recombination site in the HEK-NS1-BirA*-Flag, HEK-NS2-BirA*-Flag and HEK-MYLK4-BirA*-Flag stable cell lines.

We subsequently determined if NS1-, NS2- or MYLK4-BirA*-Flag expression is inducible by doxycycline and if these fusion proteins have biotin ligase activity. The three stable cell lines and untransfected Flp In™ T-REx™ 293 cells were treated with different concentrations of doxycycline for 3 days. All three BirA* fusion proteins were clearly expressed after inoculation of 1,000 or 20 ng/ml doxycycline, but not in the absence of doxycycline or when a low concentration (0,3 ng/ml) of doxycycline was used (Fig. 8A). As expected, no Flag-specific signal was detected in the parental Flp In™ T-REx™ 293 cells treated with doxycycline. To investigate the biotinylation activity of doxycycline-induced NS1-, NS2- and MYLK4-BirA*-Flag proteins, we detected biotinylated proteins after treating the three stable cell lines and untransfected Flp In™ T-REx™ 293 cells with doxycycline for 48 hours and the addition of 50 or 0 µM biotin after 24 hours. Although signals were rather weak, we observed protein biotinylation after doxycycline-induced expression of NS1- and NS2-BirA*-Flag only when exogenous biotin was added (Fig. 8B). After doxycycline-induced expression of MYLK4-BirA*-Flag we observed a clear streptavidin-reactive band that likely corresponds to biotinylated MYLK4-BirA*-Flag itself, and a second band of lower molecular size. These bands were also weakly detected in the absence of exogenously added biotin. Presumably, the fetal calve serum that was added in the culture medium might be a (limited) source of biotin. Streptavidin-reactive bands were not observed in untransfected Flp In™ T-REx™ 293 cells. Taken together, these results highlight that the stable cell lines HEK-NS1-BirA*-Flag, HEK-NS2-BirA*-Flag and HEK-MYLK4-BirA*-Flag, express NS1-, NS2- and MYLK4-BirA*-Flag protein, respectively, in the presence of doxycycline and that these BirA* fusion proteins have intrinsic protein biotinylation activity.

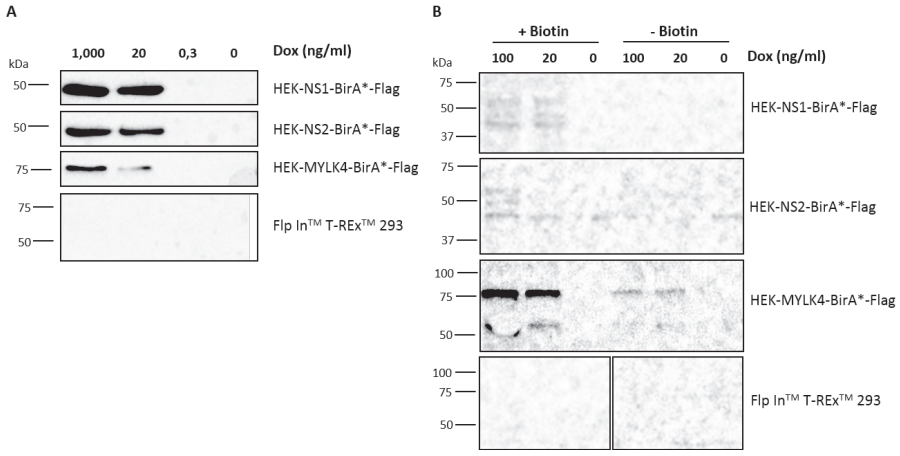

Figure 8: Validation of stable HEK-NS1-BirA*Flag, HEK-NS2-BirA*-Flag and HEK-MYLK4-BirA*-Flag cells. (A) Induction of NS1-BirA*-Flag, NS2-BirA*-Flag and MYLK4-BirA*-Flag expression upon doxycycline administration for 3 days as detected with a Flag-tag-specific antibody. As a negative control, untransfected Flp In™ T-REx™ 293 cells were used. (B) Protein biotinylation assay by NS1-BirA*-Flag, NS2-BirA*Flag and MYLK4-BirA*-Flag after doxycycline-induced expression for 48 hours with or without the addition of 50 µM biotin after 24 hours. Biotinylated proteins were detected by HRP-coupled streptavidin. As a negative control, untransfected Flp In™ T-REx™ 293 cells were used.

NS1-, NS2- and MYLK4 proxeome screen

We subsequently used our stable HEK-NS1-BirA*-Flag, HEK-NS2-BirA*-Flag and HEK-MYLK4-BirA*-Flag cell lines in a large-scale experiment to determine the proxeomes of NS1, NS2 and MYLK4. As outlined in figure 9, 4 biological replicates for each stable cell line were used. These were induced with 20 ng/ml doxycycline for 48 hours or not induced. Twenty-four hours after induction, 50 µM biotin was added to the culture medium of all samples for the remaining 24 hours. After cell lysates were prepared, we enriched for biotinylated proteins with streptavidin coated beads. To monitor for doxycycline-induced expression of the BirA* fusion proteins and protein biotinylation, aliquots were taken and analysed by western blotting. In agreement with previous results, we observed a clear induction of NS1-BirA*-Flag, NS2-BirA*-Flag and MYLK4-BirA*-Flag expression after doxycycline administration, but not in the absence of doxycycline, for all 4 biological replicates (Suppl. Fig. 3). In addition, western blot detection of biotinylated proteins revealed the highest diversity of proteins for NS1-BirA*-Flag, a lower diversity for NS2-BirA*-Flag and the lowest diversity for MYLK4-BirA*-Flag (Suppl. Fig. 4). Although substantial amounts of biotinylated proteins were still present in the supernatans after streptavidin-based enrichment, we clearly enriched for biotinylated proteins on the streptavidin beads and decided to continue with these. The streptavidin purified proteins were subsequently digested by trypsin on the beads and identified and quantified by a LC-MS/MS approach with LFQ.

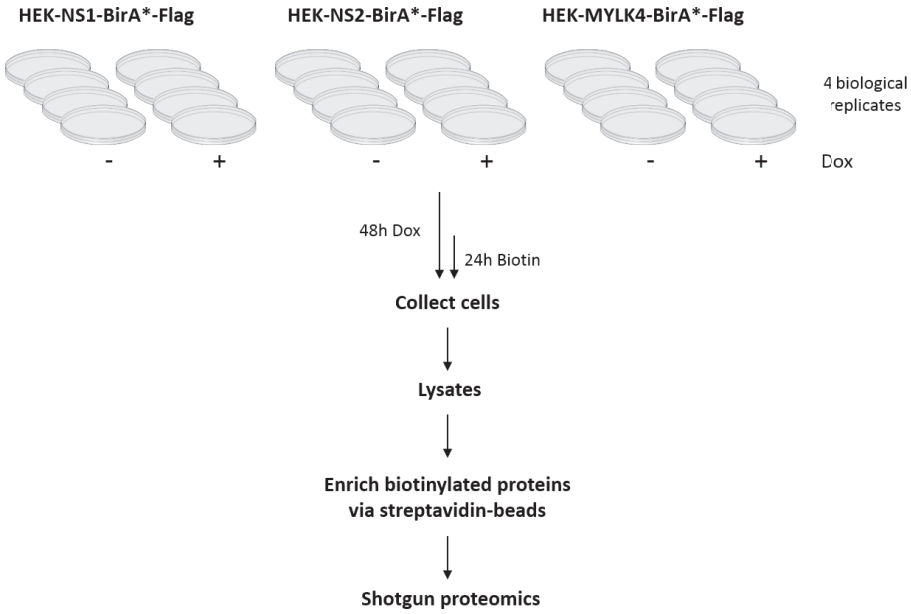

Figure 9: Experimental layout of the BioID screen to determine the NS1, NS2 and MYLK4 proxeomes. Of each stable cell line (HEK-NS1-BirA*Flag, HEK-NS2-BirA*-Flag and HEK-MYLK4-BirA*-Flag) sixteen 14-cm petri-dishes were seeded with 5 million cells. Half of the plates were induced with doxycycline (20 ng/ml) for 48 hours, whereas the other half was non-induced. After 24 hours, all cells were inoculated with 50 µM biotin. Forty-eight hours after induction, cells were collected and pooled per two petri-dishes, resulting in 4 biological replicates with or without induction of NS1-BirA*-Flag, NS2-BirA*-Flag or MYLK4-BirA*-Flag expression. After cell lysis, biotinylated proteins were enriched by streptavidin beads and identified by LC-MS/MS with LFQ.

We could identify and quantify 2,875; 2,338 and 2,009 human proteins that were present in at least 3 of the 4 biological replicates either in the presence or absence of doxycycline treatment or in both for HEK-NS1-BirA*-Flag, HEK-NS2-BirA*-Flag and HEK-MYLK4-BirA*-Flag derived samples, respectively. For each quantified protein we compared the protein intensities between the doxycycline-induced samples and non-induced samples with a T-test on the average LFQ values and calculated the - logP value (FDR = 0,01 and S_0 = 2). In addition the Log_2 fold change (FC) was calculated of the average LFQ intensity values of the doxycycline-induced samples over non-induced samples (Log_2 (LFQ + dox/LFQ - dox)). These two values, -logP and Log_2 FC, were plotted in a volcano plot for every quantified protein (Fig. 10). As such, we were able to identify 836, 345 and 47 host proteins that were significantly enriched after doxycycline-induced expression of NS1-BirA*-Flag, NS2-BirA*-Flag and MYLK4-BirA*-Flag, respectively, relative to their respective non-induced controls. These protein numbers nicely correspond to the difference in diversity of biotinylated proteins that we previously detected by western blotting (Fig. 7). We subsequently determined which identified proteins overlapped between the three BirA* fusion proteins. As shown in figure 11, 22 proteins were identified in the proxeomes

of all three BirA* fusion proteins, 18 overlapped between NS1-BirA*-Flag and MYLK4-BirA*-Flag and 1 overlapped between NS2-BirA*-Flag and MYLK4-BirA*-Flag. We assumed that proteins present in the proxeomes of one or both NS protein(s) and the control MYLK4 protein are more likely candidate interactors of the shared BirA* protein than real common interactors. Therefore we excluded these proteins from the NS1- and NS2 proxeomes. We identified 214 proteins that overlapped between NS1-BirA*-Flag and NS2-BirA*-Flag. Since NS1 and NS2 work individually and cooperatively in suppressing type I - and type III IFN responses, common interacting proteins can be expected. We also identified 582, 108 and 6 proteins that are unique for NS1-BirA*-Flag, NS2-BirA*-Flag and MYLK4-BirA*-Flag, respectively. Based on these selection criteria we defined a NS1 proxeome of 796 proteins (Suppl. Table 1) and a NS2 proxeome of 322 proteins (Suppl. Table 2). For the MYLK4 proxeome we retained all 47 proteins, although the vast majority of these proteins possibly represent BirA* interactors (Suppl. Table 3). These proxeome lists can also be found on figshare (www.figshare.com, login: koen.sedeyn@vib-ugent.be, password: PhDKoenSedeynNov2017). We also identified 61, 119 and 1 host protein(s) that were (was) significantly downregulated after doxycycline-induced expression of NS1-BirA*-Flag, NS2-BirA*-Flag and MYLK4-BirA*-Flag, respectively (a list with these proteins can be found on figshare (www.figshare.com, login: koen.sedeyn@vib-ugent.be, password: PhDKoenSedeynNov2017)). For NS1 and NS2 these included the 4 known carboxylase proteins that are naturally biotinylated, *i.e.* acetyl CoA -, puryvate -, methylcrotonyl CoA - and propionyl CoA carboxylase. Although these 4 carboxylases were also downregulated after induction of MYLK4-BirA*-Flag, the reduction level was not statistically significant. So, it appears that overexpression of a BirA* fusion protein reduces the natural endogenous biotinylation of these 4 carboxylases.

We also directly compared the protein intensities of the doxycycline-induced NS1-BirA*-Flag or NS2-BirA*-Flag samples with the doxycycline-induced MYLK4-BirA*-Flag samples and could identify a NS1' proxeome of 701 proteins and a NS2' proxeome of 252 proteins, respectively (data not shown). These NS1' and NS2' proxeomes showed an overlap of about 54% and 49%, respectively, with the NS1 and NS2 proxeomes. Yet, whereas some previously identified NS1 interaction partners were identified in the NS1 proxeome (see below), only one of these interaction partners (CBP) could be identified in the NS1' proxeome. Therefore we decided to continue with the NS1 and NS2 proxeome in favor of the NS1' and NS2' proxeomes.

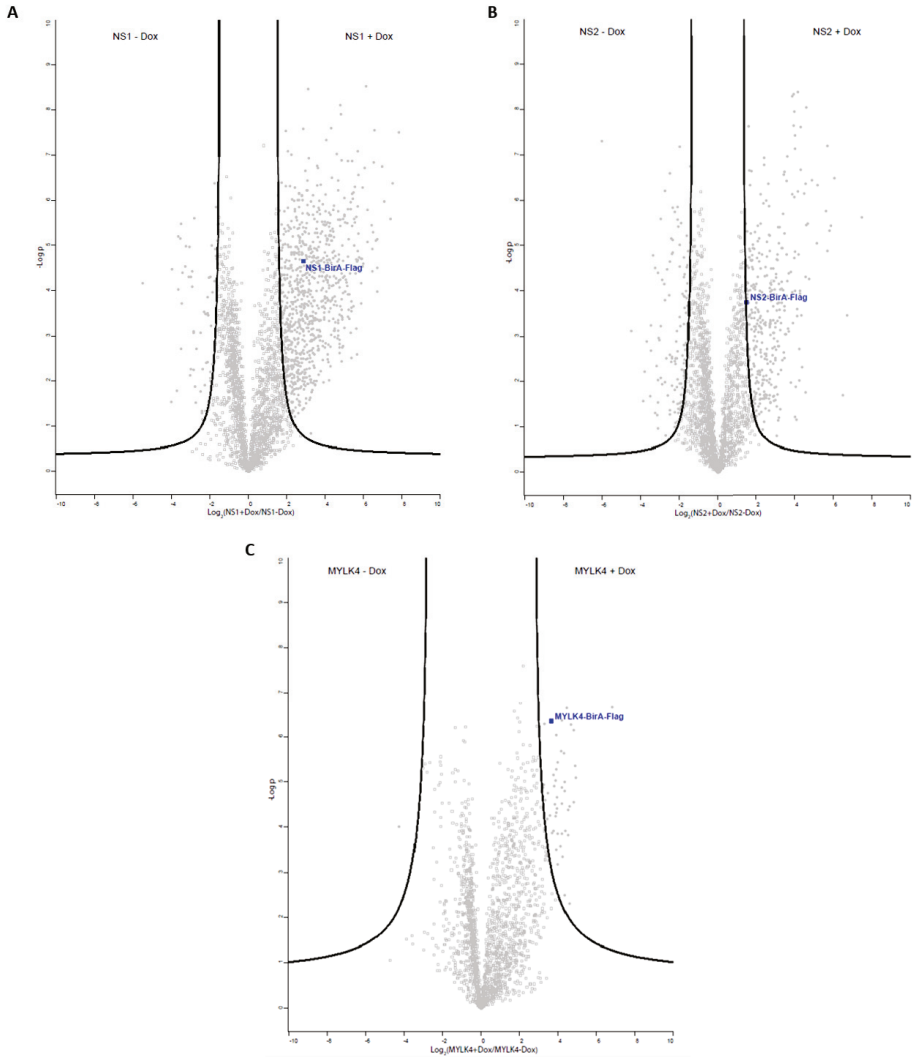

Figure 10: Volcano plots of identified proteins in the NS1, NS2 and MYLK4 BioID screen. All identified proteins were plotted according to the Log_2 fold change of their LFQ value in the doxycycline-induced samples (+ Dox) relative to the non-induced samples (- Dox) (X-axis) and the statistical significance (Y-axis, -Log (p-value) of a t-test). The two black curves represent the selection cut-off for selection of significantly enriched proteins, with proteins on the right side of the right curve representing the proxeome. (A) NS1 proxeome, (B) NS2 proxeome and (C) MYLK4 proxeome. The BirA*-Flag fusion proteins are highlighted in bold.

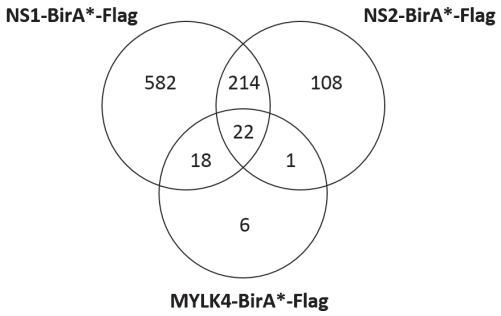

Figure 11: The number of unique and overlapping candidate interactors in the NS1, NS2 and MYLK4 proxeomes.

Validation of the NS1 and NS2 proxeomes by the presence of known interaction partners

To validate our BioID approach to identify novel interaction partners of NS1 and NS2, we first investigated if published interaction partners of NS1 (MAVS, IRF3, CBP, cullin-2, elongin C and MAP1B) and NS2 (RIG-I and MAP1B) were found in their respective proxeome [12-16]. In addition, we also searched for other key proteins (possibly) involved in the induction and signaling of type I - and type III IFN upon RSV infection, *i.e.* MDA-5, LGP2, TLR3, NOD2, TRIF, MyD88, TRAF3, TBK1, IKKε, IRF7, JAK1, TYK2, STAT1, STAT2 and IRF9. We could identify the previously described NS1 interaction partners MAVS and elongin C in the NS1 proxeome (Table 1). MAP1B was enriched about 2-fold after NS1-BirA*-Flag expression compared to non-induced cells, however, this was not significant enough to be included in the NS1 proxeome. Although cullin-2 was not enriched, we identified cullin-3 in the NS1 proxeome. In addition to elongin C, we also identified elongin B in the NS1 proxeome. The IRF3 and CBP proteins could not be detected in the screen. For the NS2 interaction partners, MAP1B was not enriched after NS2-BirA*-Flag expression compared to non-induced cells, whereas RIG-I could not be detected. Of all other key proteins known to be involved in type I and type III IFN induction and signaling, only TBK1 and STAT1 were detected in our screen. Although both proteins were enriched after NS1-BirA*-Flag and NS2-BirA*-Flag expression, this was not significant enough to be included in the NS1- and NS2 proxeomes. The absence of detection of most proteins involved in type I and type III IFN induction and signaling is likely caused by the fact that expression of most of these proteins is low to absent and only induced in the presence of IFN. In addition, we also compared our NS1 proxeome with the list of 221 NS1 interaction partners identified in HEK293T cells with affinity purification by Wu and colleagues and found 23 overlapping proteins [10]. Taken together, these results highlight that our BioID approach is able to identify known and novel interaction partners of NS1 and NS2.

Table 1: Proteins involved in IFN induction and signaling in the NS1 and NS2 proxeomes

IFN induction							
		NS1			NS2		
Protein IDs	Gene name	Log2 (NS1+Dox/ NS1-Dox)	-LOG (P-value)	Significant	Log2 (NS2+Dox/ NS2-Dox)	-LOG (P-value)	Significant
Q7Z434	MAVS	3,99	4,30	+	1,24	1,06	-
Q9UHD2	TBK1	0,99	2,02	-	1,50	2,94	-

IFN signaling							
		NS1			NS2		
Protein IDs	Gene name	Log2 (NS1+Dox/ NS1-Dox)	-LOG (P-value)	Significant	Log2 (NS2+Dox/ NS2-Dox)	-LOG (P-value)	Significant
P42224	STAT1	0,41	1,29	-	0,15	0,30	-

Others							
		NS1			NS2		
Protein IDs	Gene name	Log2 (NS1+Dox/ NS1-Dox)	-LOG (P-value)	Significant	Log2 (NS2+Dox/ NS2-Dox)	-LOG (P-value)	Significant
Q15370	ELOB	2,24	2,07	+	1,97	1,72	+
Q15369	ELOC	3,56	3,36	+	1,09	0,91	-
Q13617	CUL2	-0,07	0,24	-	-0,79	0,52	-
Q13618	CUL3	4,14	2,82	+	n.d.	n.d.	n.d.
P46821	MAP1B	1,15	3,82	-	-0,56	2,17	-

n.d.: not detected

Validation of the NS1 and NS2 proxeomes by the number of interferon regulated genes

We subsequently estimated the number of interferon regulated gene products in the NS1, NS2 and MYLK4 proxeome with the interferome database v2.01 [17]. Interestingly, 128 of the 796 (~16%) proteins of the NS1 proxeome and 92 of the 322 (~29%) proteins of the NS2 proxeome were identified as interferon regulated genes (Suppl. Table 1 and 2). At first glance, these results suggest that, in addition to suppressing key molecules involved in the induction and signaling of type I and type III IFN, NS1 and NS2 might also impair the IFN response by modulating effector functions of large numbers of interferon regulated gene products. For the MYLK4 proxeome we identified 18 of the 47 (~ 38%) proteins as interferon regulated gene products (Suppl. Table 3). This number appeared rather high at first sight, however, the vast majority of proteins identified in the MYLK4 proxeome were also identified in the NS1 and/or NS2 proxeome. Of the 6 proteins uniquely identified in the MYLK4 proxeome, 2 were identified as interferon regulated gene products.

Validation of the NS1 and NS2 proxeomes by pathway analysis

To explore the biological relevance of the NS1- and NS2 proxeome further and identify novel, interesting NS1 and/or NS2 protein interaction partners, we analysed the proxeomes with two software tools, *i.e.* STRING and ingenuity pathway analysis (IPA). STRING is based on a database with known and predicted protein-protein interactions, which can be both physical and functional [18]. IPA on the other hand is a software program developed by Qiagen that uses curated information extracted from literature to identify cellular pathways in high-throughput lists of genes or proteins. Functional analysis of the NS1 proxeome in STRING revealed a highly interconnected network, with mRNA processing and splicing as the most significant pathway (Fig. 12A). These results were confirmed by IPA, which identified the cleavage and polyadenylation of precursor mRNA pathway, protein ubiquitination and RhoA signaling amongst the most enriched pathways (Fig. 12B). Interestingly, 10 of the 12 protein members of the cleavage and polyadenylation of precursor mRNA pathway were identified in the NS1 proxeome, highlighting that this pathway might be affected by NS1.

Analysis of the NS2 proxeome on the other hand revealed three main clusters of proteins in STRING. The first cluster consisted of proteins involved in the organization and functions of centrosomes and biogenesis of cilia, *e.g.* several components of the HAUS augmin-like complex, centrosomal proteins (CEPs), pericentriolar material 1 (PCM1), ALMS1, centriolar coiled-coil protein 110 (CCP110) and oral-facial-digital syndrome 1 (OFD1) protein (Fig. 13A box 1). A second cluster involved multiple structural proteins of the 26S proteasome complex (PSM isoforms) and proteins with E3 ubiquitin ligase activity (ANAPC1, -4, CDC23, KEAP1, FBXW9, HECTD1) (Fig. 13A box 2). A final cluster was strongly enriched for chaperones and related proteins, *e.g.* several CCT isoforms, PFDN isoforms and PDCL (Fig. 13A box 3). These results were partially confirmed by IPA, most clearly for the protein ubiquitin pathway as the most significant enriched pathway (Fig. 13B).

A

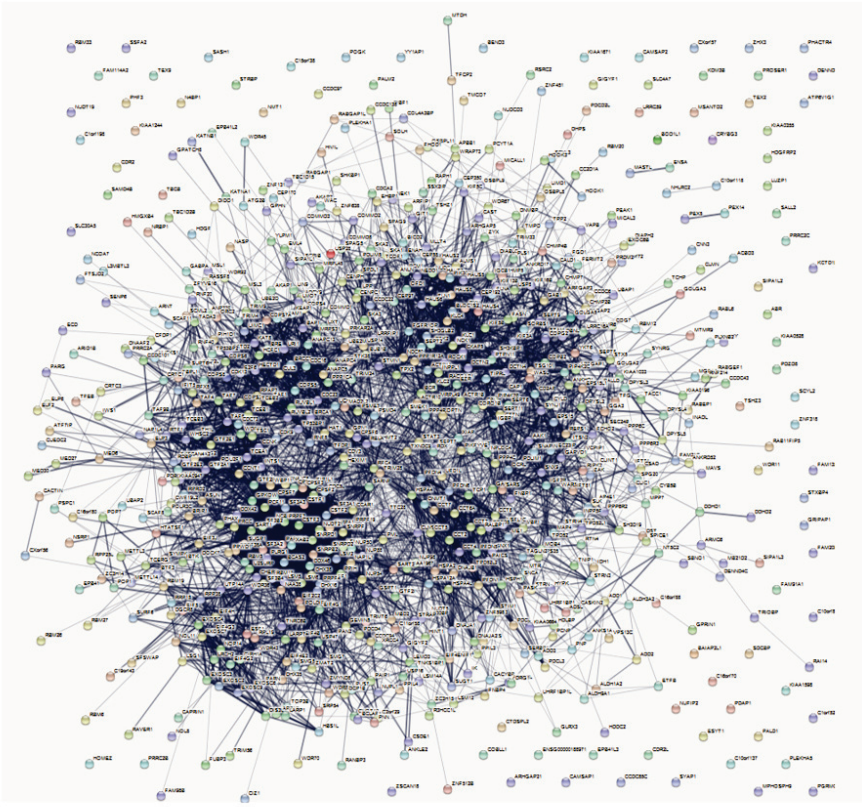

B

Top Canonical Pathways

Name	p-value	Overlap
Cleavage and Polyadenylation of Pre-mRNA	2,67E-13	83,3 % 10/12
Protein Ubiquitination Pathway	6,00E-07	10,6 % 28/265
Systemic Lupus Erythematosus Signaling	1,03E-05	10,2 % 23/225
RhoA Signaling	1,30E-05	12,9 % 16/124
Assembly of RNA Polymerase II Complex	7,67E-05	18,0 % 9/50

1 2 3 4 5 6 7 8 9 ›

Figure 12: Functional network analysis of the NS1 proxeome. (A) Functional and physical protein-protein interaction network determined by STRING. (B) Enriched cellular pathways determined by ingenuity pathway analysis. This list represents the 5 most significantly enriched pathways with their p-value. For each pathway, the number of identified proteins in the input list and the total number of proteins known for that pathway is shown (overlap).

A

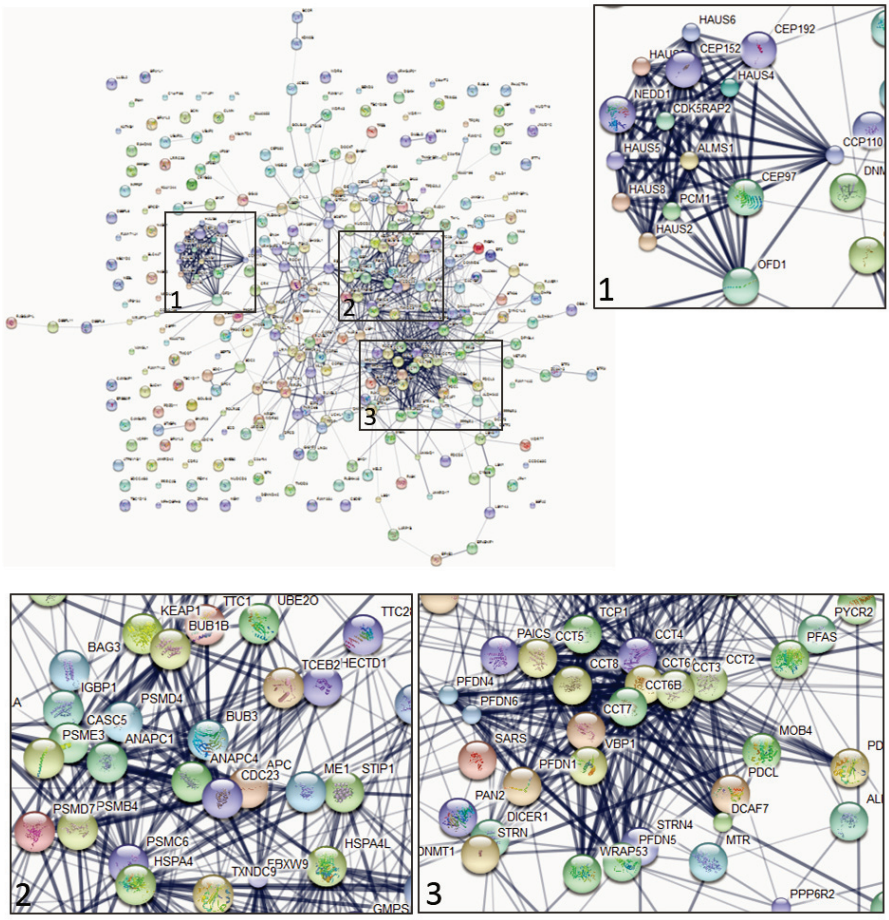

B

Top Canonical Pathways

Name	p-value	Overlap
Protein Ubiquitination Pathway	2,96E-09	7,5 % 20/265
NRF2-mediated Oxidative Stress Response	3,19E-05	6,2 % 12/193
Integrin Signaling	4,37E-04	5,0 % 11/219
Fcγ Receptor-mediated Phagocytosis in Macrophages and Monocytes	4,60E-04	7,5 % 7/93
Purine Nucleotides De Novo Biosynthesis II	4,83E-04	27,3 % 3/11

Figure 13: Functional network analysis of the NS2 proxeome. (A) Functional and physical protein-protein interaction network determined by STRING. Box 1-3 focus on particular subnetworks, *i.e.* centrosomes and biogenesis of cilia, proteasome complex and E3 ubiquitin ligases, and chaperones, respectively. (B) Enriched cellular pathways determined by ingenuity pathway analysis. This list represents the 5 most significantly enriched pathways with their p-value. For each pathway, the number of identified proteins in the input list and the total number of proteins known for that pathway is shown (overlap).

Validation of the cleavage and polyadenylation of precursor mRNA pathway

As we were intrigued by the identification of nearly all protein members of the cleavage and polyadenylation of precursor mRNA pathway in the NS1 proxeome we studied these proteins further. We hypothesized that by interacting with proteins involved in the processing of host mRNAs, NS1 could possibly affect host transcription, thereby creating a favourable environment for viral replication. Although IPA allocates 12 proteins to the cleavage and polyadenylation of precursor mRNA pathway, we identified a 13th protein belonging to this pathway, *i.e.* cleavage and polyadenylation specificity factor subunit (CPSF) 7. Eleven of these 13 proteins, CPSF1 to -3, CPSF5 to -7, cleavage stimulation factor subunit (CSTF) 1 to -3, WD repeat domain 33 (WDR33) and poly (A) polymerase alpha (PAPOLA), were significantly enriched after NS1-BirA*-Flag expression, whereas CPSF4 and polyadenylate-binding nuclear protein 1 (PABPN1) were detected but not enriched (Suppl. Fig. 5A). With the exception of CSTF2, most of these proteins were identified, but not significantly enriched after expression of either NS2-BirA*-Flag or MYLK4-BirA*-Flag (Suppl. Fig. 5B and C). To validate these proteins as candidate NS1 interactors, we performed co-immunoprecipitation experiments. To mimick the BioID screen as much as possible we transfected Flp-In^{TM} T-REx^{TM}-293 cells with plasmids constitutively expressing NS1-Flag, NS2-Flag or an empty vector control. We included NS2-Flag as a negative control to test the specificity of the candidate NS1 interactors, although CSTF2 might interact with both NS1 and NS2. Twenty-four hours later we determined if protein members of the cleavage and polyadenylation of precursor mRNA pathway could be coimmunoprecipitated with NS1-Flag or NS2-Flag. Except for CPSF5, we tested all candidate NS1 interactors, CPSF4 as a control for the absence of NS1 interaction and MAVS as a positive control for NS1 interaction [14]. Although we could clearly detect NS1-Flag expression, we did not observe NS2-Flag expression in this experiment, possibly caused by the unstable nature of NS2 (Fig. 14, INPUT-upper blot). We could unambiguously identify endogenous expression of MAVS and all tested candidate NS1 interactors, except for CPSF4 and CPSF7 (Fig. 14, INPUT-blot 2-11). Although we were able to immunoprecipitate NS1-Flag with a Flag-tag-specific antibody (Fig. 14, CoIP-upper blot), none of the tested candidate NS1 interactors coimmunoprecipitated with NS1 under the conditions that we used (Fig. 14, CoIP-blot 3-11). The published NS1 interactor MAVS, however, was also not coimmunoprecipitated with NS1 (the band that is visible in the CoIP blot of MAVS represents the heavy chain fragment of the Flag-tag-specific antibody used for immunoprecipitation) (Fig. 14, CoIP-blot 2). So, with these experiments we could not confirm the interaction of NS1 with any protein of the cleavage and polyadenylation of precursor mRNA pathway. However, as we could not coimmunoprecipitate MAVS, further optimization of the experimental conditions (time of expression, lysis and wash conditions) during co-immunoprecipitation may allow us to provide evidence using another PPI method that these proteins possibly interact with NS1. We note that these co-immunoprecipitation experiments relied on interactions with endogenous levels of the candidate interactors.

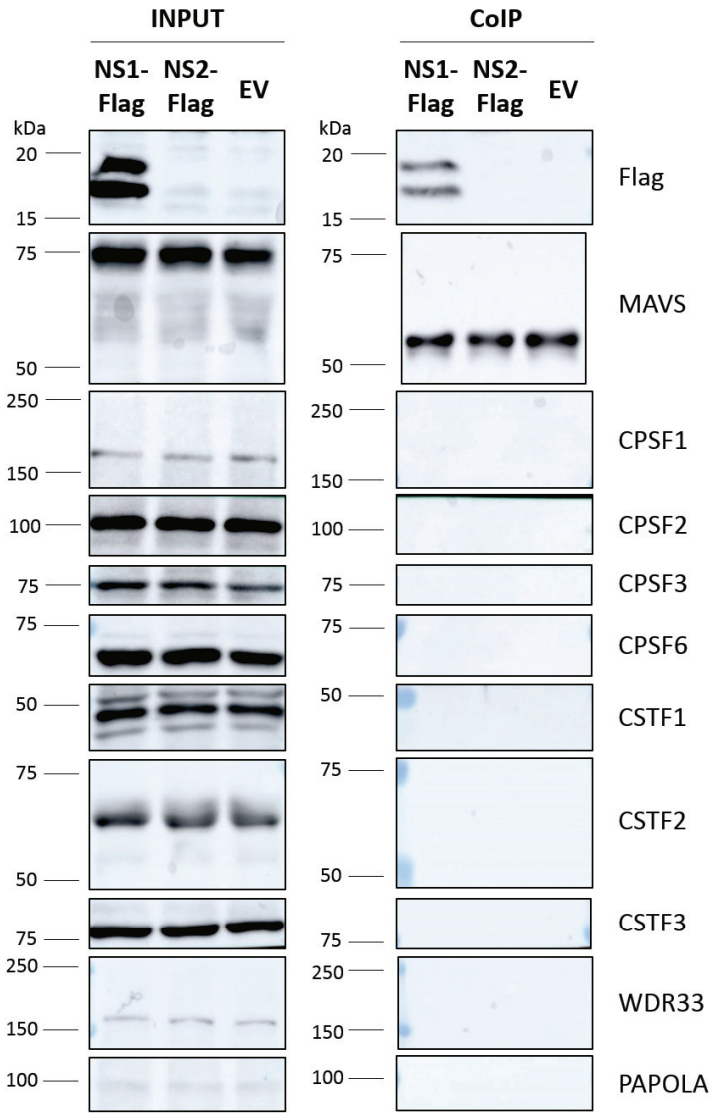

Figure 14: Validation of protein-protein interactions between NS1 and members of the cleavage and polyadenylation of precursor mRNA pathway by co-immunoprecipitation. NS1-Flag and NS2-Flag were immunoprecipitated with a Flag-tag-specific antibody after transient overexpression in HEK293T cells. As a control HEK293T cells were transfected with an empty vector (EV). Input samples (INPUT) and samples after co-immunoprecipitation (CoIP) were analysed for the presence of NS1-Flag, NS2-Flag, MAVS and 11 members of the cleavage and polyadenylation of precursor mRNA pathway: *i.e.* CPSF1-4, CPSF6-7, CSTF1-3, WDR33 and PAPOLA. As we could not unambiguously detect CPSF4 and CPSF7, we did not include the blots for these proteins.

7.2.2 Study of the NS1 and NS2 interactome using Virotrap

Generation of GAG-NS1 and GAG-NS2 expression vectors

In a second approach to study the interactome of RSV NS1 and - NS2, we used the PPI mapping technique Virotrap. Therefore, we cloned the codon optimized sequences of RSV-NS1 and -NS2 in frame at the C-terminus of the HIV-1 p55-GAG protein in the pMET7-GAG vector, which allows strong expression of the GAG fusion protein by the SR alpha promoter, which is composed of the simian virus 40 early promoter and the R segment and part of the U5 sequence (R-U5') of the long terminal repeat of human T-cell leukemia virus type 1 (Suppl. Fig. 6). To verify if GAG-NS1 and GAG-NS2 are expressed, we transfected the corresponding pMET7 vectors in HEK293T cells, lysed the cells 24 hours later and stained western blots with a p24-GAG-specific antibody. In addition, we also transfected a pMET7 vector expressing GAG-Ras as a positive control, an irrelevant plasmid or no plasmid as negative controls. We observed a clear band at the expected molecular weight for full length p55-GAG-Ras (79,4 kDa) and p55-GAG-NS1 (74,7 kDa), whereas two bands were observed for p55-GAG-NS2 (73,9 kDa) (Fig. 15). In accordance with the higher protein stability of NS1 compared to NS2, we observed a stronger expression of GAG-NS1 compared to GAG-NS2. In addition to the full length p55-GAG, we also observed weak bands at lower molecular weight that might correspond to GAG fusion proteins that lost the N-terminal p17 fragment of GAG, possibly due to host proteases. These results confirm that GAG-NS1 and GAG-NS2 are expressed upon transfection of the pMET7-GAG-NS1 and pMET7-GAG-NS2 plasmid, respectively.

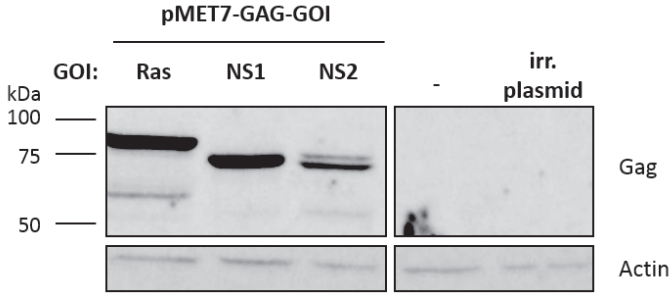

Figure 15: Expression of GAG-Ras, GAG-NS1 and GAG-NS2 after transient transfection in HEK293T cells. HEK293T cells in 12-well plates were transiently transfected with 1 µg of pMET7-GAG-GOI plasmid, an irrelevant (irr.) plasmid or without (-) plasmid for 24 hours by using FuGENE transfection reagent. GOI = gene of interest. The GAG-fusion proteins were detected by a p24-GAG-specific antibody.

NS1 and NS2 interactome screen

To study the NS1 and NS2 interactome by Virotrap we transfected HEK293T cells in 75-cm² falcons with expression vectors for GAG-NS1, GAG-NS2 or GAG-eDHFR as irrelevant control, which expresses the *Escherichia coli* derived dihydrofolate reductase (eDHFR) (Fig. 16). With a molecular weight of ~ 18 kDa, eDHFR is very similar in size compared to NS1 (~ 19,4 kDa) and NS2 (~ 18,6 kDa). Transfections were done in triplicate with the cotransfection of expression vectors for Flag-tagged VSV-G and VSV-G and an empty vector. VSV-G/VSV-G-Flag trimers will end-up in the membranes of the VLPs and allow a fast, straightforward purification of VLPs from the culture supernatans. Forty-eight hours post transfection, culture medium was harvested and VLPs were purified by using a biotinylated Flag-tag-specific antibody coupled to streptavidin beads. The VLPs were lysed with a mild detergent, amphipol (APol) A8-35, which also allows subsequent acid-induced precipitation of protein/APol complexes. These protein complexes were finally boiled and identified by LC-MS/MS with LFQ.

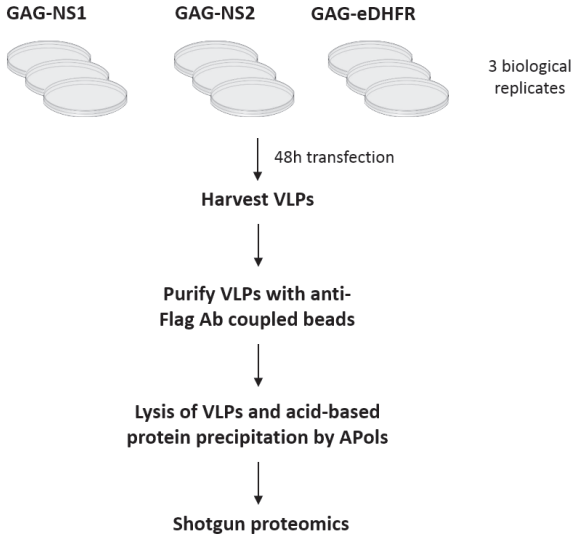

Figure 16: Experimental layout of the NS1 and NS2 Virotrap screen. HEK293T cells in 75-cm² falcons were transfected with pMET7-GAG-NS1, pMET7-GAG-NS2 or pMET7-GAG-eDHFR in combination with expression vectors for Flag-tagged VSV-G and VSV-G and an empty vector in 3 biological replicates. Forty-eight hours after transfection VLPs were harvested and purified by using streptavidin beads bound by a Flag tag-specific antibody. Purified VLPs were lysed by APol A8-35 and released protein/APol complexes were precipitated by acidification. Proteins were identified by LC-MS/MS with LFQ.

We could identify and quantify 276 host proteins that were present in all three biological replicates for at least one of the GAG fusion proteins. These quantified proteins were analysed in two pairwise comparisons, *i.e.* GAG-NS1 vs GAG-eDHFR and GAG-NS2 vs GAG-eDHFR. As such, we could identify 40 and 54 proteins that were significantly enriched with GAG-NS1 - and GAG-NS2 VLPs, respectively, compared to GAG-eDHFR VLPs (Fig. 17 and Table 2, which can also be found on figshare

(www.figshare.com, login: koen.sedeyn@vib-ugent.be, password: PhDKoenSedeynNov2017)). Of these proteins, 28 were enriched by both GAG-NS1 and GAG-NS2 VLPs. We could also identify 4 and 6 proteins (with an overlap of 3 proteins) that were significantly enriched with GAG-eDHFR VLPs compared to GAG-NS1 and GAG-NS2 VLPs, respectively (Table 3). We investigated the degree of overlap between our 40 candidate NS1 interactors and the 221 candidate NS1 interactors identified in HEK293T cells by Wu and colleagues [10]. Three proteins, prostate tumor overexpressed 1 (PTOV1), valosin containing protein (VCP) and RAD23 homolog B (RAD23B), were common between both screens.

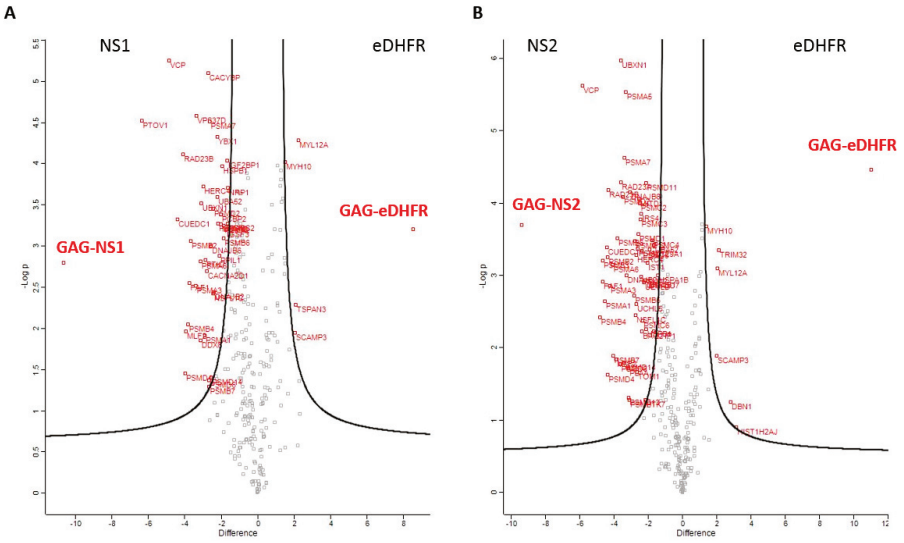

Figure 17: Volcano plots of identified proteins upon Virotrap with NS1, NS2 and the irrelevant eDHFR control. All identified proteins were plotted according to the Log_2 fold change of their LFQ value in the NS1 (A) or NS2 (B) Virotrap relative to the irrelevant eDHFR Virotrap (X-axis) and the statistical significance (Y-axis, -Log (p-value) of a t-test). The two black curves represent the selection cut-off for selection of significantly enriched proteins. The GAG-bait proteins are highlighted in bold.

Table 2: NS1 and NS2 interactome identified by Virotrap

Protein IDs	Gene names	NS1		NS2	
		Log2 FC (NS1/eDHFR)	-LOG (P-value)	Log2 FC (NS2/eDHFR)	-LOG (P-value)
Q86YD1	PTOV1	6,37	4,52	*n.s.*	*n.s.*
P55072	VCP	4,86	5,25	5,86	5,62
P49720	PSMB3	*n.s.*	*n.s.*	4,67	3,20
Q9NWM3	CUEDC1	4,42	3,33	4,40	3,39
P54727	RAD23B	4,10	4,12	4,33	4,19
P55036	PSMD4	3,97	1,46	4,38	1,63
Q15773	MLF2	3,95	1,96	3,88	1,84
P28070	PSMB4	3,82	2,05	4,82	2,42
Q9UNN5	FAF1	3,73	2,55	4,66	2,91
P49721	PSMB2	3,66	3,06	4,38	3,25

P54725	RAD23A	*n.s.*	*n.s.*	3,62	4,29
P25788	PSMA3	3,41	2,52	4,26	2,86
Q86XT2	VPS37D	3,36	4,58	*n.s.*	*n.s.*
Q9Y263	PLAA	*n.s.*	*n.s.*	3,15	1,71
P60900	PSMA6	3,14	2,82	4,08	3,15
Q9UNM6	PSMD13	*n.s.*	*n.s.*	3,14	1,31
P20618	PSMB1	*n.s.*	*n.s.*	3,13	1,28
P26196	DDX6	3,12	1,86	*n.s.*	*n.s.*
Q04323	UBXN1	3,10	3,52	3,61	5,97
Q5GLZ8	HERC4	2,98	3,73	2,71	3,28
P25786	PSMA1	2,91	1,92	4,53	2,64
Q13308	PTK7	2,85	2,83	2,15	1,27
P28074	PSMB5	*n.s.*	*n.s.*	2,83	2,72
P54289	CACNA2D1	2,80	2,69	*n.s.*	*n.s.*
O00232	PSMD12	*n.s.*	*n.s.*	2,80	3,47
Q9Y5K5	UCHL5	*n.s.*	*n.s.*	2,71	2,60
Q9HB71	CACYBP	2,70	5,10	*n.s.*	*n.s.*
Q15008	PSMD6	2,68	1,37	3,64	1,78
Q99436	PSMB7	2,68	1,30	4,06	1,88
O60784	TOM1	*n.s.*	*n.s.*	2,66	1,66
O14818;Q8TAA3	PSMA7;PSMA8	2,62	4,51	3,39	4,63
P62191	PSMC1	*n.s.*	*n.s.*	2,62	3,37
Q99460	PSMD1	*n.s.*	*n.s.*	2,59	3,57
O75190	DNAJB6	2,57	3,00	3,09	4,15
Q8WV92	MITD1	*n.s.*	*n.s.*	2,53	4,05
O00487	PSMD14	2,54	1,40	3,39	1,80
P17980	PSMC3	*n.s.*	*n.s.*	2,46	3,77
Q9UNZ2	NSFL1C	2,45	2,42	2,74	2,45
Q13200	PSMD2	2,42	3,45	3,47	4,09
O14654	IRS4	*n.s.*	*n.s.*	2,41	3,85
P62195	PSMC5	*n.s.*	*n.s.*	2,39	3,34
P25686	DNAJB2	2,39	2,44	3,25	3,00
O95816	BAG2	*n.s.*	*n.s.*	2,36	2,23
P62333	PSMC6	*n.s.*	*n.s.*	2,32	2,37
Q8IX04	UEVLD	*n.s.*	*n.s.*	2,24	2,90
P67809	YBX1	2,21	4,33	*n.s.*	*n.s.*
P62987;P62979;P0CG47;P0CG48	UBA52;RPS27A;UBB;UBC	2,20	3,59	1,67	3,42
P28066	PSMA5	2,17	3,28	3,31	5,53
P25685	DNAJB1	*n.s.*	*n.s.*	2,17	2,93
O00231	PSMD11	*n.s.*	*n.s.*	2,13	4,28
Q9Y3C6	PPIL1	2,11	2,88	*n.s.*	*n.s.*
P53990	IST1	*n.s.*	*n.s.*	2,06	3,18
Q9HCE1	MOV10	2,01	3,27	*n.s.*	*n.s.*
Q99615	DNAJC7	*n.s.*	*n.s.*	2,01	2,93
Q15366	PCBP2	2,01	3,39	*n.s.*	*n.s.*
P04792	HSPB1	1,94	3,97	2,14	2,25
Q99808	SLC29A1	*n.s.*	*n.s.*	1,93	3,36
P25787	PSMA2	1,87	3,25	2,43	2,98
P28072	PSMB6	1,86	3,09	3,79	3,51
P43686	PSMC4	*n.s.*	*n.s.*	1,78	3,48
O75054	IGSF3	1,74	3,20	*n.s.*	*n.s.*
P31948	STIP1	*n.s.*	*n.s.*	1,69	2,23
Q9NZI8	IGF2BP1	1,66	4,03	*n.s.*	*n.s.*
O14786	NRP1	1,64	3,70	*n.s.*	*n.s.*
P35998	PSMC2	1,62	3,27	2,51	3,99
P0DMV9;P0DMV8	HSPA1B;HSPA1A	*n.s.*	*n.s.*	1,42	3,00

FC = fold change

n.s. = not significantly different from the irrelevant eDHFR control

Table 3: eDHFR interactome identified by Virotrap relative to NS1 or NS2

Protein IDs	Gene names	NS1		NS2	
		Log2 FC (NS1/eDHFR)	-LOG (P-value)	Log2 FC (NS2/eDHFR)	-LOG (P-value)
Q99878;…	HIST1H2A isotypes	*n.s.*	*n.s.*	-3,15	0,90
Q16643	DBN1	*n.s.*	*n.s.*	-2,79	1,25
P19105;O14950;P24844	MYL12A;MYL12B;MYL9	-2,26	4,28	-2,06	3,10
Q13049	TRIM32	*n.s.*	*n.s.*	-2,13	3,35
O60637	TSPAN3	-2,08	2,29	*n.s.*	*n.s.*
O14828	SCAMP3	-2,04	1,95	-2,00	1,88
P35580	MYH10	-1,50	4,02	-1,37	3,68

FC = fold change

n.s. = not significantly different from the irrelevant eDHFR control

Validation of the candidate NS1 and NS2 interactors by pathway analysis

To explore the possible biological relevance of the 40 and 54 candidate interactors of NS1 and NS2, respectively, identified by Virotrap, we analysed these proteins in STRING and IPA. For NS1, both STRING and IPA identified the proteasome-mediated degradation of ubiquitinated proteins as the most significantly enriched pathway (Fig. 18). This is of particular interest, as the protein ubiquitination pathway was also highly enriched in the NS1 proxeome identified by BioID (Fig. 12). In the STRING network, multiple proteins of the 26S proteasome complex were clustered together (Fig. 18A box 1). We also identified several proteins that interact with the HIV-1 GAG protein (personal communication with Prof. Dr. Sven Eyckerman), *i.e.* MOV10, insulin-like growth factor 2 mRNA binding protein 1, DEAD-box helicase 6 (DDX6) and Y-box binding protein 1 (Fig. 18A box 2). At first glance, these GAG protein interactors serve as an internal control. However, why these proteins were significantly more enriched in GAG-NS1 VLPs compared to GAG-eDHFR VLPs, which also contain the GAG protein, is currently unclear to us. Possibly, fusion of the NS1 and eDHFR bait proteins to GAG differentially affects the interaction of certain human proteins to GAG.

STRING and IPA also identified the proteasome-mediated degradation of ubiquitinated proteins as the most significantly enriched pathway for the candidate NS2 interactors (Fig. 19). Again, this is in agreement with the NS2 proxeome identified by BioID (Fig. 13). Compared to NS1, even more proteins of the 26S proteasome complex were identified for NS2 (Fix. 17A box 1). Taken together, these Virotrap results strongly argue that both NS1 and NS2 interact with (part of) the 26S proteasome components.

A

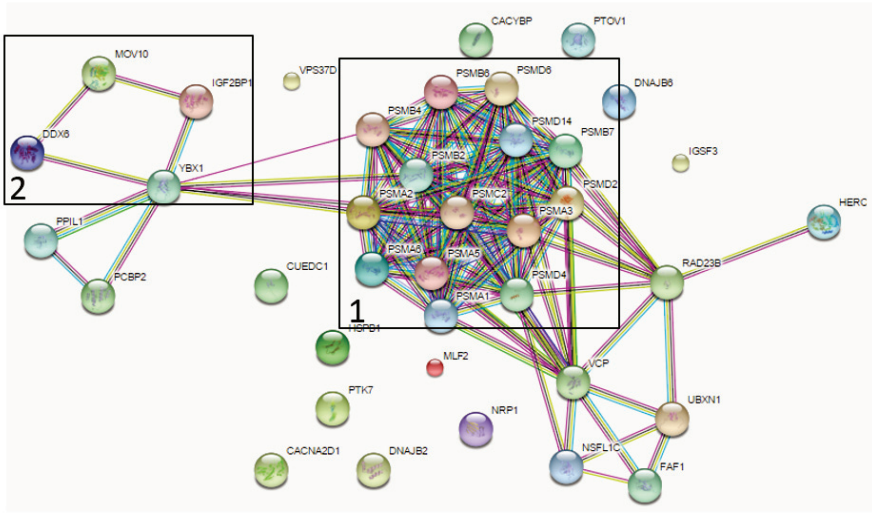

B

Top Canonical Pathways

Name	p-value	Overlap
Protein Ubiquitination Pathway	5,48E-23	6,4 % 17/265
Aldosterone Signaling in Epithelial Cells	3,31E-03	1,8 % 3/168
NRF2-mediated Oxidative Stress Response	4,88E-03	1,6 % 3/193
Oxidized GTP and dGTP Detoxification	5,34E-03	33,3 % 1/3
IL-15 Production	4,87E-02	3,6 % 1/28

Figure 18: Functional network analysis of the candidate interactors of NS1 identified by Virotrap. (A) Functional and physical protein-protein interaction network determined by STRING. Box 1 highlights a subnetwork of components of the 26S proteasome complex, whereas box 2 highlights proteins known to interact with GAG. (B) Enriched cellular pathways determined by ingenuity pathway analysis. This list represents the 5 most significantly enriched pathways with their p-value. For each pathway, the number of identified proteins in the input list and the total number of proteins known for that pathway is shown (overlap).

A

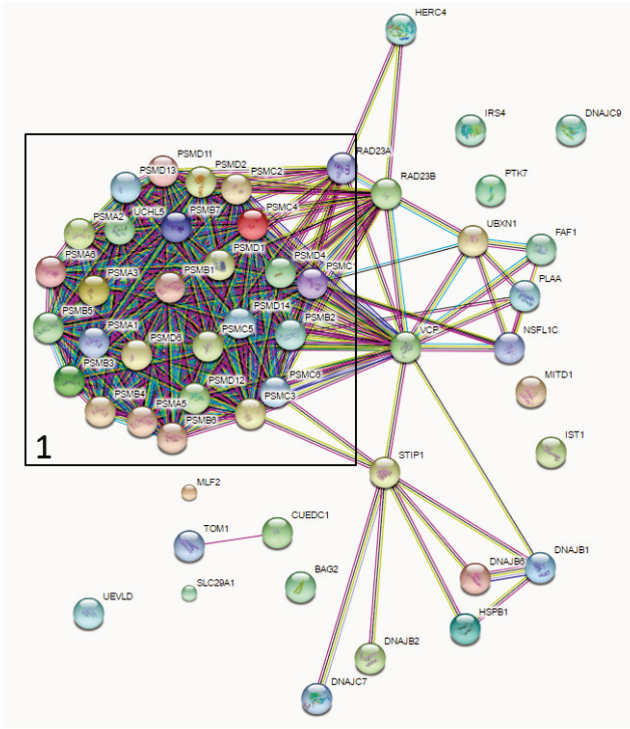

B

Top Canonical Pathways

Name	p-value	Overlap
Protein Ubiquitination Pathway	1,07E-43	10,9 % 29/265
NRF2-mediated Oxidative Stress Response	7,20E-05	2,6 % 5/193
Aldosterone Signaling in Epithelial Cells	5,52E-04	2,4 % 4/168
Antigen Presentation Pathway	3,31E-03	5,3 % 2/38
IL-15 Production	6,12E-02	3,6 % 1/28

Figure 19: Functional network analysis of the candidate interactors of NS2 identified by Virotrap (A) Functional and physical protein-protein interaction network determined by STRING. Box 1 highlights a subnetwork of components of the 26S proteasome complex. (B) Enriched cellular pathways determined by ingenuity pathway analysis. This list represents the 5 most significantly enriched pathways with their p-value. For each pathway, the number of identified proteins in the input list and the total number of proteins known for that pathway is shown (overlap).

7.2.3 Study of the NS1 and NS2 interactome using affinity purification

NS1 and NS2 interactome screen

In a final approach to study protein-protein interactions of the RSV NS1 and - NS2 proteins, we used a conventional affinity purification protocol. To mimic the BioID proxeome screen as much as possible we used the same cell line, *i.e.* Flp-In™ T-REx™ 293 cells. We transiently transfected plasmids encoding C-terminally Flag-tagged NS1 and - NS2 or an empty vector control in these cells for 24 hours in 4 biological replicates (Fig. 20A). Additionally we also transfected a plasmid encoding MYLK4 with a N-terminal Flag tag and C-terminal Myc tag to validate candidate interactors of MYLK4. After 24 hours, we prepared cell lysates and immunoprecipitated Flag-tagged proteins and associated interactors with a Flag-tag-specific antibody and protein G sepharose beads. Co-immunoprecipitated proteins were subsequently identified and quantified by a LC-MS/MS approach with LFQ.

To monitor for expression of the Flag tagged proteins during the affinity purification screen, we stained an aliquot of the cell lysates with a Flag antibody. Although we observed some background staining in the empty vector control, we could clearly detect expression of NS1-Flag and Flag-MYLK4-Myc (Fig. 20B). NS2-Flag expression, however, was not distinguishable from background staining, suggesting that NS2-Flag expression was low to undetectable. These results confirm previous observations with NS2 expression being less stable than NS1 expression. Nevertheless, we continued with the mass spectrometry-based identification of candidate interactors of NS1, NS2 and MYLK4.

After mass spectrometry-based identification and quantification of proteins we compared the LFQ values of proteins of the NS1-Flag, NS2-Flag and Flag-MYLK4-Myc samples relative to the empty vector control. We could quantify 903, 1059 and 881 proteins that were present in at least 3 of the 4 biological replicates of the empty vector control and/or NS1-Flag, NS2-Flag and Flag-MYLK4-Myc, respectively. Of these quantified proteins, 2, 114 and 10 were significantly enriched with NS1-Flag, NS2-Flag and Flag-MYLK4-Myc, respectively, relative to the empty vector control (Fig. 21 and Suppl. Table 4-6, which can also be found on figshare (www.figshare.com, login: koen.sedeyn@vib-ugent.be, password: PhDKoenSedeynNov2017)). These proteins represent candidate interactors of NS1, NS2 and MYLK4. In line with the western blotting results, we could clearly detect NS1-Flag and Flag-MYLK4-Myc by mass spectrometry, but not NS2-Flag (Fig. 21). Since the NS2-Flag bait was not detected, we realize that it is difficult to interpret the possible biological meaning of the 114 candidate NS2 interactors. Nevertheless, we used these candidate NS2 interactors in subsequent preliminary analysis. Although only 2 proteins were identified as candidate NS1 interactors by affinity purification, oxysterol binding protein-like 8 (OSBPL8) was also identified in HEK293T cells by Wu and colleagues [10].

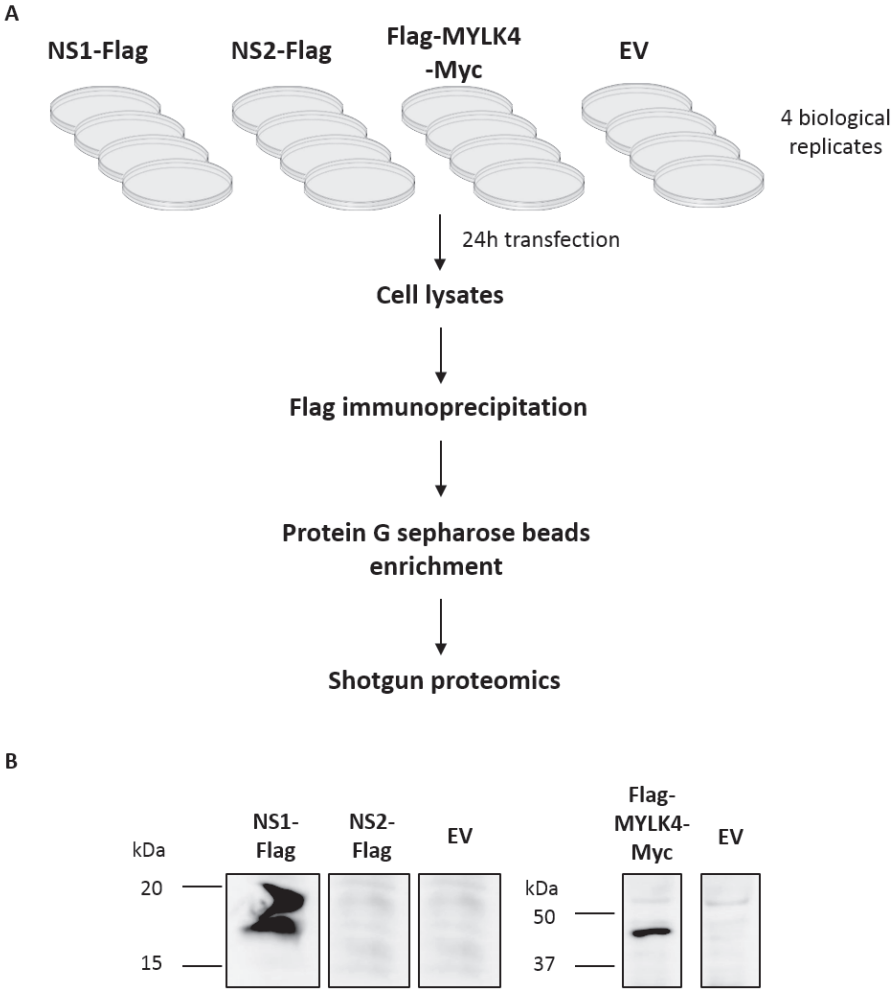

Figure 20: NS1, NS2 and MYLK4 affinity purification screen. (A) Experimental layout of the affinity purification screen. In 9-cm petri-dishes, Flp IN™ T-REx™ 293 cells were transiently transfected with pEXPR-NS1-Flag, pEXPR-NS2-Flag, pEXPR-Flag-MYLK4-Myc or with an empty vector (EV) control for 24 hours in 4 biological replicates. After cell lysis, Flag-tagged NS1, NS2 and MYLK4 were immunoprecipitated with a Flag-tag-specific antibody and protein G sepharose beads. Copurified proteins were detected by LC-MS/MS with LFQ. (B) Validation of NS1-Flag, NS2-Flag and Flag-MYLK4-Myc expression in the affinity purification screen by using a Flag-tag-specific antibody.

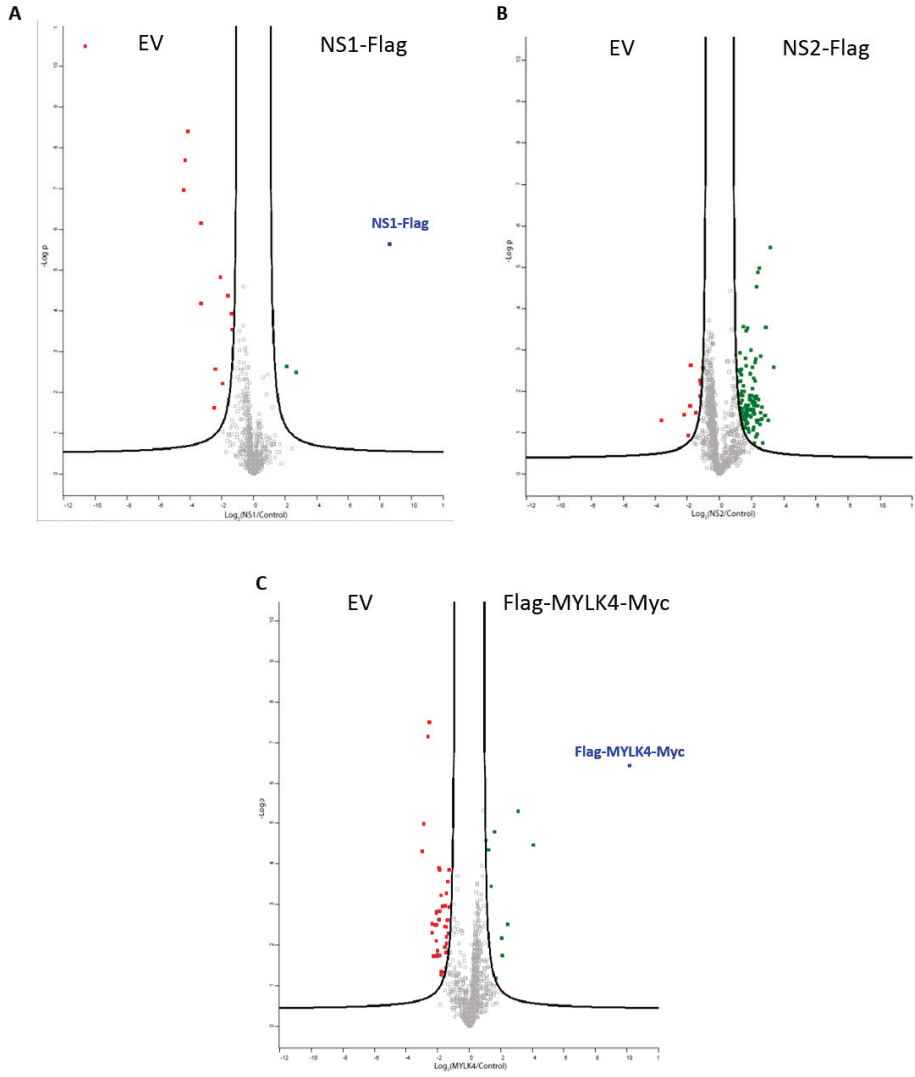

Figure 21: Volcano plots of NS1, NS2 and MYLK4 affinity purified proteins. All identified proteins were plotted according to the Log_2 fold change of their LFQ value in the NS1 (A), NS2 (B) or MYLK4 (C) affinity purification relative to the empty vector (EV) control (X-axis) and the statistical significance (Y-axis, -Log (p-value) of a t-test). The two black curves represent the selection cut-off for selection of significantly enriched proteins. The NS1-Flag and Flag-MYLK4-Myc bait proteins are highlighted in bold.

Validation of the candidate NS1 and NS2 interactors by pathway analysis

As with the BioID - and Virotrap screens, we also analysed the candidate interactors identified by affinity purification with STRING and IPA. Since we only identified a high number of candidate interactors for NS2, we only did these analysis for NS2. Both STRING and IPA identified actin cytoskeleton organization and signaling as one of the most enriched pathways (Fig. 22). Additionally, IPA also identified signaling by Rho GTPases and epithelial adherens junctions as strongly enriched pathways.

A

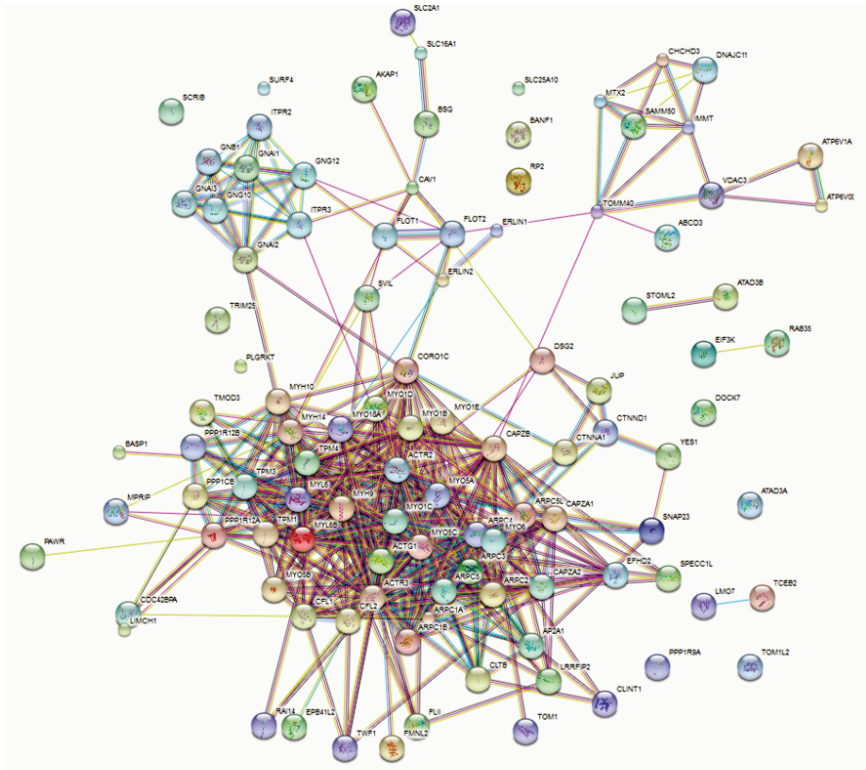

B

Top Canonical Pathways

Name	p-value	Overlap
Epithelial Adherens Junction Signaling	3,87E-25	14,4 % 21/146
RhoGDI Signaling	4,38E-25	12,7 % 22/173
Actin Cytoskeleton Signaling	1,98E-22	9,7 % 22/227
RhoA Signaling	1,02E-21	14,5 % 18/124
Signaling by Rho Family GTPases	1,40E-21	8,9 % 22/248

1 2 3 4 5 6 7 8 9 ›

Figure 22: Functional network analysis of the candidate interactors of NS2 identified by affinity purification. (A) Functional and physical protein-protein interaction network determined by STRING. (B) Enriched cellular pathways determined by ingenuity pathway analysis. This list represents the 5 most significantly enriched pathways with their p-value. For each pathway, the number of identified proteins in the input list and the total number of proteins known for that pathway is shown (overlap).

7.2.4 NS1 and NS2 interactome: overlap between BioID, Virotrap and affinity purification

To further validate the candidate NS1, NS2 and MYLK4 interactors, we searched for overlapping proteins between the BioID proxeome, Virotrap and affinity purification results. MYLK4 was not included in the Virotrap analysis, and so for MYLK4 we determined the overlap of BioID and affinity purification only. As shown in figure 23, very few proteins were found by more than one of the three PPI identification techniques. For NS1 and NS2, no proteins were identified in all three PPI methods. For NS1, 3 proteins were found in both BioID and Virotrap, whereas 1 protein was found in both BioID and affinity purification (Table 4). For NS2, 5 proteins were found in both BioID and Virotrap, 9 proteins were found in both BioID and affinity purification and 1 protein was found in both Virotrap and affinity purification (Table 4). For MYLK4 we used the complete proxeome set of 47 proteins, which consists of 6 proteins unique to MYLK4 and 41 proteins that overlapped with NS1 and/or NS2 (Suppl. Table 3). Therefore, this protein set might include aspecific binding proteins or interactors of the BirA* biotin ligase. When we used this complete set, 2 proteins were found in both BioID and affinity purification (Table 4). If we were more stringent and only tested the MYLK4 unique proxeome of 6 proteins, than 1 overlapping protein was found between BioID and affinity purification.

We considered proteins identified in at least two PPI mapping techniques as more reliable and performed a literature search to better understand their known biological function(s) (overview in Table 4).

Of the 4 candidate NS1 interactors that were identified by two methods, PSMD4 and calcyclin-binding protein (CACYBP) are involved in proteasomal degradation of ubiquitinated proteins. PSMD4 is a subunit of the 26S proteasome where it functions as a receptor for the polyubiquitin chains on proteins, whereas CACYBP might function as a molecular bridge in E3 ubiquitin ligase complexes [19]. NSFL1 cofactor p47 (NSFL1C) is a negative regulator of the ATPase activity of VCP, an ER ATPase involved in the maintenance of the ER network during cell division [20]. OSBPL8 is a lipid transporter that shuttles between the ER and plasma membrane, thereby delivering phosphatidylserine to the plasma membrane and removing phosphatidylinositol-4-phosphate [21].

Also for NS2, three subunits of the 26S proteasome were identified, *i.e.* PSMB4, PSMC6 and PSMD4. Although elongin C has been identified as an interactor of NS1, but not NS2 [15], we identified elongin B as an interactor of NS2. The elongin BC complex appears to function as an adaptor in E3 ubiquitin ligase complexes such as the VHL complex and SOCS family proteins. Two co-chaperones, DnaJ heat shock protein family member C7 and stress-induced phosphoprotein 1, were identified as candidate NS2 interactors. Another functional group consists of the ARP2/3 proteins and tropomodulin-3 (TMOD3) that regulate the (de)polymerization and branching of actin filaments. Interestingly, ARP2 was recently identified as an important host factor for the release of progeny RSV virions [22]. More specifically, the RSV fusion protein appears to induce the formation of filopodia in an ARP2-dependent fashion, which facilitate the spread of RSV virions to neighboring cells. Possibly, NS2 also plays a role in this process by interacting with ARP2 and -3. Several proteins involved in vesicle transport and membrane fusion were also identified by us as candidate NS2 interactors, *i.e.* myosin-Vb (MYO5B), synaptosome-associated Protein 23 (SNAP23), target of myb1 membrane trafficking

protein (TOM1) and protein phosphatase 1 regulatory subunit 12A (PPP1R12A), the regulatory subunit of the myosin phosphatase. Other candidate NS2 interactors include desmoglein-2 (DSG2), a component of intercellular desmosome junctions, and dedicator of cytokinesis 7 (DOCK7), a guanine nucleotide exchange factor for the Rho GTPases Rac1 and Rac3.

For MYLK4, based on the overlap between BioID and affinity purification, we identified 2 interactors, SKP1 and STUB1, with SKP1 being unique for the MYLK4 proxeome, whereas STUB1 was also identified in the proxeomes of NS1, NS2 and MYLK4. These results suggest that STUB1 might be an aspecific binding protein or an interactor of the BirA* biotin ligase. SKP1 functions as an adaptor protein between the cullin-1 and F box protein in SCF ubiquitin ligase complexes. STUB1 is an E3 ubiquitin ligase of misfolded chaperone substrates and inhibits the ATPase activity of several chaperones such as HSP90, HSP70 and HSC70.

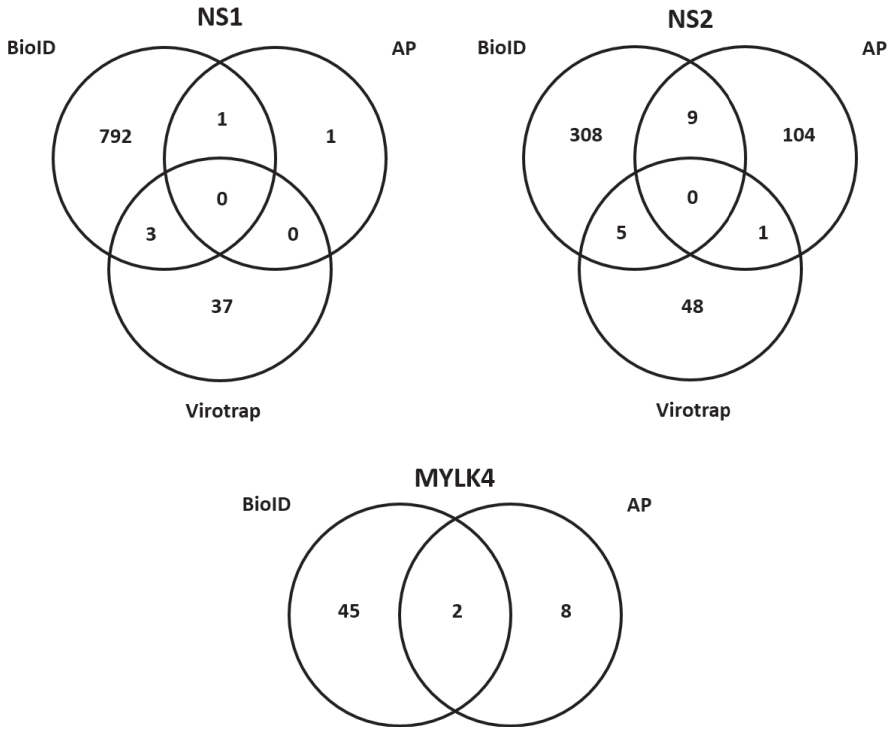

Figure 23: The number of unique and overlapping candidate interactors identified by BioID, Virotrap and affinity purification (AP) for NS1, NS2 and MYLK4. Note that for MYLK4 we used the complete MYLK4 proxeome, which showed a high overlap with NS1 and NS2, suggesting that some of these proteins may interact with the BirA* moiety instead of MYLK4.

Table 4: Candidate interactors of NS1, NS2 or MYLK4 identified in at least 2 of the 3 PPI mapping techniques

NS1

Protein ID	Gene name	PPI screens	Functions
P55036	PSMD4	BioID, VT	Component of the 26S proteasome. Acts as an ubiquitin receptor subunit with a preference for longer polyubiquitin chains
Q9HB71	CACYBP	BioID, VT	May be involved in ubiquitination and proteasomal degradation of target proteins by acting as a molecular bridge in ubiquitin E3 complexes
Q9UNZ2	NSFL1C	BioID, VT	Reduces the ATPase activity of VCP, an ER ATPase necessary for the maintenance of the ER network at mitosis. Inhibits the activity of cathepsin L *in vitro*
Q9BZF1	OSBPL8	BioID, AP	Lipid transporter involved in lipid countertransport between the ER and the plasma membrane

NS2

Protein ID	Gene name	PPI screens	Functions
P28070	PSMB4	BioID, VT	Component of the 20S core proteasome complex
P55036	PSMC6	BioID, VT	Component of the 26S proteasome. Belongs to the heterohexameric ring of AAA proteins that unfolds ubiquitinated target proteins
P62333	PSMD4	BioID, VT	Component of the 26S proteasome. Acts as an ubiquitin receptor subunit with a preference for longer polyubiquitin chains
Q15370	ELOB	BioID, AP	Regulatory subunit B of the transcription elongation factor elongin Together with regulatory subunit C (elongin BC complex) involved as adapter protein in the proteasomal degradation of target proteins by different E3 ubiquitin ligase complexes
Q99615	DNAJC7	BioID, VT	Co-chaperone regulating the molecular chaperones HSP70 and HSP90 in folding of steroid receptors
P31948	STIP1	BioID, VT	Co-chaperone for HSP90AA1
P61160	ACTR2	BioID, AP	ATP-binding component of the Arp2/3 complex, which is involved in regulating polymerization and branching of actin filaments
P61158	ACTR3	BioID, AP	ATP-binding component of the Arp2/3 complex which is involved in regulating polymerization and branching of actin filaments. Role in ciliogenesis
Q9NYL9	TMOD3	BioID, AP	Blocks the elongation and depolymerization of actin filaments at the pointed end
Q9ULV0	MYO5B	BioID, AP	May be involved in vesicular trafficking by its association with the CART complex Together with RAB11A and RAB8A participates in epithelial cell polarization
O00161	SNAP23	BioID, AP	Essential component of the high affinity receptor for the general membrane fusion machinery Important regulator of transport vesicle docking and fusion
O60784	TOM1	VT, AP	May be involved in intracellular trafficking
O14974	PPP1R12A	BioID, AP	Regulatory subunit of myosin phosphatase
Q14126	DSG2	BioID, AP	Component of intercellular desmosome junctions
Q96N67	DOCK7	BioID, AP	Guanine nucleotide exchange factor, which activates Rac1 and Rac3 Rho small GTPases.

MYLK4

Protein ID	Gene name	PPI screens	Functions
P63208	SKP1	BioID, AP	Essential component of the SCF (SKP1-CUL1-F-box protein) ubiquitin ligase complex In the SCF complex, serves as an adapter that links the F-box protein to CUL1
Q9UNE7	STUB1	BioID, AP	E3 ubiquitin-protein ligase which targets misfolded chaperone substrates

7.3 Discussion

Upon viral infection of a host cell, PRRs can recognize viral RNA molecules, *e.g.* double stranded RNA, that are part of the viral infection cycle. Activated PRRs typically induce innate immune responses by inducing the production of type I and III IFNs. RSV infections can be recognized by several PRRs such as RIG-I and NOD2 [23, 24]. A remarkable feature of RSV infections, however, is the low to absent induction of type I IFNs [25-27]. Two viral proteins, the NS1 and NS2 protein, have been identified as important suppressors of the induction of type I and type III IFN responses upon RSV infection. By acting individually and synergistically, these proteins reduce both the production and signaling of type I and type III IFNs (a detailed description on NS1 and NS2 functions is provided in chapter 2 of this thesis). NS1 and NS2, for example, prevent the interaction of RIG-I with the adaptor protein MAVS [13, 14]. Although debated, some groups have reported that NS1 reduces the expression of TRAF3 and IKKε, two proteins downstream of MAVS [9, 11]. NS1 and NS2 also reduce IRF3 and IRF7-induced gene expression, with different mechanisms being proposed, *i.e.* by reducing the expression of IRF3 and IRF7 [9], by suppressing the nuclear translocation of IRF3 and IRF7 [8, 13, 28] or by preventing the formation of the IRF3/CBP transcription activation complex [16]. In addition to suppressing the production of type I and type III IFNs, NS1 and NS2 also suppress IFN-induced signaling. NS2 prevents IFN-induced STAT1 phosphorylation and lowers the total STAT2 protein levels, whereas NS1 possibly also contributes in reducing total STAT2 protein levels [9, 15, 29, 30]. Moreover, NS1 promotes the degradation of the ISG OASL in a proteasome-dependent manner, supporting the hypothesis that the NS proteins may also directly suppress IFN-induced antiviral proteins [31]. Taken together, these results highlight that the NS proteins counteract IFN-induced antiviral responses at different levels.

NS1 and NS2 are unique viral proteins without significant homology to any other known protein. Just recently, the crystal structure of the NS1 protein has been published, demonstrating that the NS1 protein is a structural paralog of the N-terminal domain of the RSV matrix protein [32]. As NS1 and NS2 are small proteins, it is believed that NS1 and NS2 interact with host proteins to carry out their diverse cellular functions. Wu and colleagues were the first to investigate host proteins interacting with the NS1 and NS2 protein [10]. They used an affinity purification approach followed by mass spectrometry and could identify 221 candidate NS1 interactors. Further validation of these candidate interactors revealed that NS1 promotes a cell cycle arrest in the G1 phase. Although this work provides a first overview on candidate NS1 interactors, identification of PPIs by affinity purification relies on the generation of crude cell lysates, which possess the risk of identifying false positive and - negative interactions. We therefore used three complementary PPI mapping techniques to study candidate interactors of NS1 and NS2, *i.e.* BioID [1], Virotrap [3] and affinity purification. In contrast to affinity purification, BioID and Virotrap do not rely on the identification of PPIs after cell lysis, allowing the identification of PPIs in their natural cellular context. BioID measures the proxeome of a bait protein, which is thought to be around 10 nm, and is believed to be able to also detect transient and weak PPIs, which may be lost during cell lysis or subsequent washing steps in affinity purification.

To study the proxeomes of NS1 and NS2 by BioID, we generated stable transduced HEK293T-derived cell lines that allowed doxycycline inducible expressing of the promiscuous biotin ligase BirA* fused to the RSV-NS1, -NS2 or human MYLK4 protein, with the latter being used as a non-virus-derived control. Staining of the NS1- and NS2-BirA* fusion proteins or NS1 and NS2 alone by immunofluorescence revealed that the subcellular localization of NS1 and NS2 was not affected by fusing the BirA* protein to NS1 and NS2. In line with previous reports on the subcellular localization of recombinantly expressed NS1 or NS2, we observed that NS1 resided both in the cytoplasm and the nucleus, whereas in most cells NS2 could be detected as bright spots in the cytoplasm, likely representing mitochondrial localization [8, 11, 12]. Confocal microscopy with co-staining of a mitochondrial marker may confirm mitochondrial localization of NS2 and the NS2-BirA* fusion protein. We defined a NS1 and NS2 proxeome of 796 and 322 proteins, respectively, with an overlap of 214 proteins, that were significantly enriched by streptavidin-beads upon expression of the NS1- or NS2-BirA* fusion proteins, but not upon expression of the MYLK4-BirA* fusion protein. In addition, we identified 6 proteins in the MYLK4 proxeome that were not identified in the NS1 and/or NS2 proxeome. These numbers are more or less in the same range as other published BioID screens. BioID screens of the human proteins PLK4 [33], nuclear lamins [34], A-kinase anchoring protein 8 [35], EphA2 [36], heterogeneous nuclear ribonucleoprotein M and myelin expression factor 2 [37], identified 48, 50-250, 428, 215, 133 and 110 proteins, respectively. Two BioID screens of viral proteins, HIV-1 GAG [38] and human CMV pUL103 [39], have identified 47 and 1,126 host proteins, respectively. This relatively large difference in proxeome size may rely on intrinsic differences of these two viral proteins, and/or on different experimental settings, such as the cut-off to define proxeome proteins or the method of enrichment of biotinylated proteins (immunoprecipitation versus streptavidin binding). With our BioID screen we could confirm the previously published NS1 interactors MAVS and elongin C, whereas MAP1B was enriched, but not significantly [12, 14, 15]. Moreover, we also identified elongin B, in the NS1 proxeome, confirming that NS1 may assemble into an ECS-type E3 ubiquitin ligase complex [15]. Although we did not identify the ECS-type E3 ubiquitin ligase component cullin-2 in the NS1 proxeome, we did find cullin-3, a component of the BTB-CUL3-RBX1 (BCR)-type E3 ubiquitin ligase complexes. This raises the hypothesis that in addition to ECS-type E3 ubiquitin ligase complexes, NS1 possibly also assembles into BCR-type E3 ubiquitin ligase complexes. Pathway analysis of the NS1 interactome revealed that nearly all components of the cleavage and polyadenylation of precursor mRNA pathway, *i.e.* CPSF1-3, CPSF5-7, CSTF1-3, WDR33 and PAPOLA, were present in the NS1 interactome. Although not validated further, CPSF5 expression at the protein level was downregulated upon RSV infection in a proteomics experiment [40]. We hypothesized that NS1 may interact with one or more proteins of this pathway, thereby bringing the multiprotein complex in proximity of the BirA* protein, leading to the biotinylation of these proteins. By interacting with one or more proteins of this pathway, NS1 may affect the processing of host precursor mRNA molecules, either selectively or generally, thereby favoring viral replication. In line with this hypothesis, NS1 and NS1-BirA* expression was observed in both the cytoplasm and in the nucleus, with the latter being the subcellular localization of the proteins of the cleavage and polyadenylation of precursor mRNA pathway. Interestingly, several viral proteins of a wide range of viruses have been shown to interact with proteins of the cleavage and

polyadenylation of precursor mRNA pathway. For example, the non-structural protein of the M segment of rift valley fever virus interacts with CPSF2 [41]. CPSF3 plays a role during HIV-1 infection. Calzado and colleagues demonstrated that the HIV-1 Tat protein enhances the expression of CPSF3 and that CPSF3 promotes viral gene expression [42]. In contrast, de la Vega and colleagues observed that CPSF3 reduces basal gene expression from the HIV-1 long terminal repeat promoter by directly interacting with this promoter [43]. Moreover, they found that the HIV-1 Tat protein interacts with CPSF3 to prevent this repressive activity of CPSF3. CPSF4 has also been identified as a target for viral proteins. The NS1 protein of influenza virus interacts with CPSF4, thereby preventing the 3' end cleavage and polyadenylation of host mRNAs [44]. As such, influenza prevents the initial IRF3-dependent gene expression of antiviral genes and the production of IFN-β later on, which increases the virulence [45]. Two residues of the RNA binding motif of influenza A NS1, Phe-103 and Met-106, have been shown to be important for the binding of NS1 to CPSF4 [46, 47]. The human papilloma virus E2 protein also interacts with CPSF4, thereby enhancing the expression of the late viral genes [48]. The non-natural presence of CPSF6 in the cytoplasm due to C-terminal truncation of CPSF6 restricts HIV-1 infection due to CPSF6-mediated stabilization of the HIV-1 capsid core, which prevents subsequent nuclear entry [49, 50]. A viral evolution study, however, demonstrated that CPSF6 also has a proviral role during HIV-1 infection [51], possibly by guiding the integration of the HIV-1 genome into transcriptionally active euchromatin [52]. Taken together, these results highlight a close interplay between viral proteins and the cleavage and polyadenylation of precursor mRNA pathway. To confirm that RSV-NS1 interacts with one or more proteins of the cleavage and polyadenylation of precursor mRNA pathway, we performed a co-immunoprecipitation. Although we could unambiguously identify endogenous expression of CPSF1-3, CPSF6, CSTF1-3, WDR33 and PAPOLA, none of these proteins were coimmunoprecipitated with NS1. We should mention, however, that this co-immunoprecipitation was based on a single experiment performed just recently. Yet, affinity purification detects PPIs outside the natural cellular context. Other PPI mapping techniques that detect PPIs in the natural cellular context, *e.g.* fluorescence life-time imaging microscopy, may be better techniques to validate the PPIs identified by BioID.

In addition, pathway analysis of the NS1 proxeome by IPA identified protein ubiquitination and RhoA signaling as enriched pathways. RhoA signaling is activated upon RSV infection and has been implicated in the RSV-induced formation of actin stress fibres, syncytia and viral filaments [53-56]. Although initial *in vitro* results suggested that the RSV-F protein interacts with RhoA [57, 58], further characterization of the domains of RhoA and RSV-F responsible for interaction revealed that these domains are not surface exposed [59, 60]. Our results suggest a possible role for NS1 in the RSV-induced activation of RhoA signaling.

Pathway analysis of the NS2 proxeome by STRING identified a cluster of proteins involved in the organization of centrosomes and the biogenesis of cilia, *i.e.* PCM1, ALMS1, CEP97 and CCP110 amongst others. Whereas PCM1 is thought to be involved in ciliogenesis, depletion of ALMS1 leads to abnormal, stunted cilia without affecting ciliogenesis [61, 62]. In contrast, CEP97 and CCP110 are negative regulators of ciliogenesis [63]. Post-mortem lung autopsies and well-differentiated HAE cell cultures

highlight that RSV primarily infects ciliated epithelial cells lining the respiratory tract [26, 64, 65]. Moreover, NS2 has been shown to cause a transition from a columnar cell morphology to a rounded cell morphology, including the loss of cilia, which eventually leads to the shedding of the infected epithelial cell into the airway lumen [66]. Although further confirmation is necessary, our results highlight that the NS2-induced loss of cilia may involve PCM1, ALMS1, CEP97 and CCP110. Furthermore, pathway analysis of the NS2 proxeome also identified an enrichment of subunits of the 26S proteasome and the protein ubiquitination pathway.

In parallel to the BioID screen, we studied the NS1 and NS2 interactome by two other PPI mapping techniques, *i.e.* Virotrap and affinity purification. With Virotrap, we could identify 40 and 54 candidate interactors of NS1 and NS2, respectively, with an overlap of 28 proteins. Pathway analysis of these NS1 and NS2 candidate interactors identified a strong enrichment of the protein ubiquitination pathway and many subunits of the 26S proteasome for both NS1 and NS2. These results suggest that both NS1 and NS2 closely interact with the 26S proteasome. In contrast to BioID, we could not identify MAVS for example as a candidate NS1 interactor by Virotrap, which likely relates to intrinsic differences between these techniques. We expect that the mitochondrial association of MAVS does not hamper biotinylation in BioID, but hampers incorporation in VLPs in Virotrap. More specifically, the VLPs are formed at the plasma membrane and their size (~ 145 nm diameter) is too small to incorporate whole mitochondria (~ 0,5-1 µm diameter). By using affinity purification, we identified 2, 114 and 10 candidate interactors of NS1, NS2 and MYLK4, respectively, although the interpretation of the candidate interactors of NS2 is complicated by the lack of detection of the NS2-Flag bait protein in the affinity purification screen. A preliminary pathway analysis of the candidate NS2 interactors highlighted the enrichment of signaling by Rho GTPases, actin cytoskeleton signaling and epithelial adherens junction signaling. Possibly, candidate NS2 interactors of the latter pathway may be involved in the NS2-induced cell rounding and - shedding of RSV infected epithelial cells [66].

Pathway analysis of the candidate interactors of NS1 and NS2 identified by BioID and Virotrap revealed an interesting overlap of the protein ubiquitination pathway and subunits of the 26S proteasome. Looking back in the NS1 proxeome, we found two 26S proteasome subunits, PSMD4 and PSME3. We hypothesized that proteasome-mediated degradation of the NS1-BirA* and/or NS2-BirA* fusion protein(s) in the BioID screens could have caused the biotinylation of subunits of the proteasome, rather than an interaction between NS1 and/or NS2 with the proteasome. The identification of a large number of subunits of the proteasome in the Virotrap screens, however, disfavours this hypothesis and suggests that NS1 and NS2 indeed specifically interact with one or more subunits of the proteasome complex. This is further confirmed by the absence of proteasome subunits in the proxeomes of MYLK4 and other published human and viral bait proteins [33-39]. We observed more proteasome subunits as candidate interactors of NS2 compared to NS1, both in BioID and Virotrap, suggesting that NS2 may interact more strongly with one or more subunits than NS1. Our results seem to confirm the existence of a so called “NS degradasome” (NSD) [9]. Goswami and colleagues could isolate multiprotein complexes assembled by the NS proteins of 300-750 kDa in size upon overexpression of NS1 and NS2 or upon RSV infection. They identified the presence of the PSMA2

protein in this NSD, suggesting a link between the proteasome and the NSD. Our results suggest that both NS1 and NS2 indeed may assemble into a NSD by interacting with one or more subunits of the proteasome complex. We identified PSMA2 as a candidate NS1 and NS2 interactor in the Virotrap screens, but not in the BioID screens. The size of the 20S core proteasome is about 750 kDa [67], suggesting that the NSD is not formed by the interaction of NS1 and NS2 with a complete 20S core proteasome, but is rather formed as a unique multiprotein complex of NS proteins and a part of the proteasome subunits. In line with this hypothesis, the NSD complex was only partially inhibited by the proteasome inhibitor MG132 [9]. Moreover, we also identified the protein ubiquitination pathway as highly enriched in the NS1 and NS2 interactomes, confirming previous observations that NS2 and possibly NS1 induce host protein ubiquitination [15, 68]. In analogy to the 26S proteasome, NS1 and/or NS2-mediated host protein ubiquitination might be necessary for subsequent degradation by the NSD complex. As such, the formation of a NSD complex and NS-induced host protein ubiquitination may explain the broad, but selective, protein degradative capacity of NS1 and NS2. In agreement with the NSD concept, we hypothesize that the NS1 - and NS2 proxeomes identified by BioID may contain substrates of such a NSD complex and hence explain the fairly large number of proteins compared to the number of candidate interactors identified by Virotrap. Upon the turn-over of substrates in the NSD complex, the BirA* moiety that was coupled to NS1 or NS2 may have biotinylated these substrates, leading to their subsequent enrichment and detection. This hypothesis assumes that peptides generated by the NSD complex are not further degraded into amino acids and that such biotinylated peptides were subsequently enriched by the streptavidin-beads.

We determined the overlap of candidate interactors of NS1, NS2 and MYLK4 identified by BioID, Virotrap and affinity purification, as proteins identified by different PPI mapping techniques are more likely real interactors. Although we could not identify a single candidate interactor of NS1 or NS2 by all three PPI mapping techniques, we identified 4 candidate interactors of NS1 and 15 candidate interactors of NS2 by 2 of the 3 PPI mapping techniques. These included several subunits of the 26S proteasome, *i.e.* **PSMB4** and **PSMC6** for NS2 and **PSMD4** for both NS1 and NS2. Two proteins of E3 ubiquitin ligase complexes were found, *i.e.* **CACYBP** for NS1, which recruits the E3 ubiquitin ligase siah1, which is involved in the degradation of β-catenin upon p53-activation [19] and **elongin B** for NS2, which forms an adaptor complex with elongin C for the ECS-type E3 ubiquitin ligases. For NS1 we also found **NSFL1C**, a cofactor of the ER ATPase VCP, which is involved in the maintenance of the ER network upon cell division [20]. *In vitro* data have shown that a subdomain of NSFL1C inhibits cathepsin L [69]. Interestingly, cathepsin L-mediated cleavage of the RSV-G protein in Vero cells reduces the infectivity of progeny RSV virions about 5-fold in HAE cultures [70]. So possibly, by interacting with NSFL1C, NS1 may regulate the infectivity of progeny RSV virions by affecting NSFL1C-mediated inhibition of cathepsin L. A fourth candidate interactor of NS1 was **OSBPL8**, a lipid transporter between the ER and the plasma membrane, which was shown to bind cholesterol and to inhibit cholesterol biosynthesis [71]. Several reports have highlighted the importance of cholesterol-rich lipid microdomains in the assembly and release of RSV virions [72-74], although Bajimaya and colleagues recently demonstrated that cholesterol-depletion did not affect virion production, but rather affected the stability and infectivity of the released virions [75]. Additional NS2 candidate interactors included

the actin filament regulators **ARP2** and **-3** (gene names ACTR2 and -3), which form the ARP2/3 complex responsible for the branching of daughter filaments on other actin filaments and **TMOD3**. Actin and -filaments are known to be important at various stages in the RSV infection cycle, *i.e.* during entry, transcription, assembly and budding [76-79]. Moreover, ARP2 was recently identified as an important host factor for RSV spreading by RSV-induced formation of filopodia in A549 cells [22]. NS2 may regulate the organisation of the actin cytoskeleton by interacting with ARP2/3 and/or TMOD3. Four other NS2 candidate interactors, **MYO5B**, **SNAP23**, **TOM1** and **PPP1R12A**, are involved in vesicle transport and/or membrane fusion. *In vivo*, RSV entry and budding in respiratory epithelial cells is restricted to the apical surface, necessitating a directed transport of viral proteins to the apical site of the cell for virion assembly. Brock and colleagues demonstrated that MYO5B-dependent transport of apical recycling endosomes on actin filaments are important for RSV virion production [80]. PPP1R12A is the regulatory subunit of the myosin phosphatase, which is phosphorylated and inactivated by Rho-associated kinase upon RhoA activation. The myosin phosphatase dephosphorylates the regulatory light chain of myosin, thereby regulating the binding of the motor protein myosin on actin in non-muscle cells. So our results suggest that NS2 may regulate (apical-directed) vesicle transport and membrane fusion by interacting with MYO5B, SNAP23, TOM1 and/or PPP1R12A. We also identified the desmosome junction component **DSG2** as a candidate NS2 interactor. Possibly, NS2 may affect desmosome junctions as a part of the NS2-induced cell shedding of RSV-infected epithelial cells [66]. The last candidate interactor of NS2 was **DOCK7**, a GEF of the Rho GTPases Rac1 and Rac3, but not of cdc42. Rac1 is an activator of PAK1, which is known to be important during RSV infection [78, 81, 82].

We compared the NS1 proxeome/interactome identified by BioID, Virotrap and affinity purification with the NS1 interactome identified by affinity purification by Wu and colleagues [10]. Of the 221 proteins identified by Wu and colleagues, 23 (~ 10%) were found in the NS1 proxeome of 796 proteins identified by BioID. Moreover, we identified an overlap of 3 proteins (~ 7,5%) with the 40 candidate NS1 interactors identified by Virotrap. Although we only identified 2 candidate NS1 interactors by affinity purification, one overlapping protein was identified. In contrast to Wu and colleagues, who could not identify any previously known NS1 interactor, we could confirm the interaction of NS1 with MAVS and elongin C by BioID. Nevertheless, we expected to see a higher degree of overlap between our NS1 interactome analysis and the one of Wu and colleagues. Whereas both studies were performed in HEK293T cells, some difference in timing was present. In the BioID and Virotrap screen, we transfected cells for 48 hours, whereas for the affinity purification screen we transfected cells for 24 hours as Wu and colleagues did. Yet, we do not expect that this would have a significant impact on the detection of candidate NS1 interactors. The low degree of overlap is more likely caused by intrinsic differences of the used PPI mapping techniques. Whereas affinity purification relies on the identification of PPIs after cell lysis, BioID and Virotrap allow the identification of PPIs in their natural environment. This is highlighted in figure 3, where a comparison was made of different PPI mapping techniques to identify a set of known PPIs. Whereas some PPIs were detected by (nearly) all PPI mapping techniques, others were uniquely identified by one specific technique. Therefore, we are convinced that candidate interactors identified by a single PPI mapping technique in this study should also be considered as possible interactors of NS1 and/or NS2.

7.4 Conclusion

To better understand the interplay between the host and the RSV non-structural proteins, we investigated the NS1 and NS2 interactome by 3 different protein-protein interaction mapping techniques. Although the overlap of candidate interactors between the techniques was low, we identified several subunits of the proteasome complex in 2 of the 3 techniques. Our results highlight a possible interaction of NS1 and NS2 with (subunits of) the host proteasome and may help in the characterization of the proposed “NS degradasome”. This multiprotein complex may explain the NS protein induced degradation of multiple key signaling proteins of the innate immune system. Confirmation of the candidate interactions with endogenously expressed NS1 and NS2 in a natural RSV infection will strengthen our results.

7.5 Material and methods

Cells and reagents

HEK293T cells (a gift from Dr M. Hall, University of Birmingham, Birmingham, UK) were grown in Dulbecco's modified eagle medium (DMEM) supplemented with 10% heat-inactivated FCS, 2 mM L-glutamine (BE17-605F, Lonza) and 0,4 mM sodium-pyruvate (S8636, Sigma-Aldrich) at 37°C and 5% CO_2. Flp-In™ T-REx™-293 cells (a kind gift from Prof. Dr. Sven Eyckerman, originally from ThermoFisher Scientific, R78007) were grown as HEK293T cells, except for the addition of 100 µg/ml zeocin (R25001, ThermoFisher scientific) and 15 µg/ml blasticidin S (15205, Sigma-Aldrich) in the culture medium. Doxycycline hyclate was purchased from Sigma-Aldrich (D9891).

Transient transfection

In 12-, 24-, 48- or 96-well plates, $2{,}5x10^5$, $1x10^5$, $6x10^4$ or $1{,}5x10^4$ HEK293T cells were seeded per well, respectively, and grown overnight. The following day, cells were transfected with varying amounts of plasmid DNA (for details see results section) by PEI (23966-1, polysciences Inc.) in a 1:5 ratio (5 µl PEI (1 mg/ml) per µg of DNA) or by FuGENE® HD transfection reagent (E2311, Promega) in a 1:3 ratio (1 µl FuGENE per µg DNA). Briefly, DNA and PEI or FuGENE were diluted in Opti-MEM™ reduced serum medium and mixed for 10 minutes at RT. DNA complexes were added to the HEK293T cells dropwise and culture medium was refreshed after 6h. Twenty-four hours post transfection, cells were either lysed with low salt lysis buffer (50 mM Tris pH 8.0, 150 mM NaCl, 5 mM EDTA, 1% NP40, 0.1% SDS and complete protease inhibitor cocktail (04693132001, Sigma-Aldrich)) for 20 min on ice, fixed with 4% paraformaldehyde in PBS for 20 min at RT for immunofluorescent staining or incubated with 50 µM D-Biotin (B4501, Sigma-Aldrich) for 24 hours for the biotinylation experiment.

Western blotting

Total cell lysates were boiled for 10 min at 99°C in 1x Laemmli buffer supplemented with 4,2% (v:v) β-mercaptoethanol. Proteins were separated by SDS-PAGE and semi-dry blotted on nitrocellulose membranes. Membranes were blocked with a 4% (w:v) low fat milk solution in PBS with 0,1% Tween20. Proteins were detected by the following primary antibodies: Flag tag (F7425, Sigma-Aldrich), MYLK4 (24309-1-AP, Proteintech), p24-GAG (9071, Abcam). As a control for equal loading, we detected actin (MAB1501, Chemicon international). We used secondary Amersham ECL Mouse or Rabbit IgG, HRP-linked whole Ab (NA931 and NA934, respectively, GE healthcare) or streptavidin-HRP (RPN1231, Amersham life science). Protein bands were visualized by Pierce™ ECL Western blotting substrate (32106, ThermoFisher Scientific) and a chemiluminescence imager (Amersham Imager 600, GE Healthcare).

Immunofluorescence

Fixed HEK293T cells were permeabilised with 0,2% Triton-X100 in PBS for 7 min and blocked with 1% BSA in PBS overnight at 4°C. The following day, cells were incubated with a primary anti-Flag antibody (F7425, Sigma-Aldrich) and a Dylight fluor 488 conjugated donkey anti-rabbit secondary antibody (Pierce), both for 1 hour at RT. Cell nuclei were stained with Hoechst (invitrogen).

Generation of stable cell lines for BioID

Six-hundred thousand Flp-In™ T-REx™ 293 cells were seeded per well in 6-well plates in their culture medium, however, without the addition of zeocin and grown overnight at 37°C and 5% CO_2. The following day, cells were cotransfected with 900 ng of a Flp recombinase expressing plasmid (pOG44) and 100 ng of pcDNA5-NS1-BirA*-Flag, pcDNA5-NS2-BirA*-Flag or pcDNA5-MYLK4-BirA*-Flag with PEI (as described above). As a negative control, we transfected cells with the pcDNA5 plasmids without the Flp recombinase expressing plasmid in parallel. Culture medium was refreshed after 24 hours and cells were detached at 48 hours post transfection. Cells were subsequently seeded in 12-well plates at 100.000 cells per well in culture medium without zeocin, but supplemented with a dilution series of hygromycin B (0, 10, 50, 100, 200 or 400 µg/ml) to select stable transduced cells. Cells were monitored for cell death and we selected the lowest concentration of hygromycin B that was sufficient to kill all negative control transfected cells. Cotransfected cells that survived in this hygromycin B concentration were then selected as stable transduced cells and kept in culture.

BioID proxeome screen

For each stable cell line (HEK-NS1-BirA*-Flag, HEK-NS2-BirA*-Flag and HEK-MYLK4-BirA*-Flag) sixteen 14-cm petri-dishes were seeded with 5 million cells in 20 ml DMEM medium supplemented with L-glutamine, 10% fetal calve serum and sodium pyruvate and grown overnight at 37°C and 5% CO_2. The following day, half (8) of the plates were inoculated with 20 ng/ml doxycycline for 48 hours, whereas the other half were not inoculated with doxycycline. After 24 hours we added D-biotin at a final concentration of 50 µM to all 16 petri-dishes. The following day, we replaced the biotin containing culture medium with biotin- and serum-free DMEM medium supplemented with L-glutamine and sodium pyruvate three hours before collecting the cells. After three hours, cells were gently washed with ice-cold PBS and collected in 750 µl PBS by scraping the cells of the petri-dish. Cells from 2 petri-dishes were combined as one biological sample. Cells were centrifuged at 500 x g for 5 min and washed with 2 ml PBS. After another centrifugation at 500 x g for 5 min, supernatans was removed and cell pellets were stored at -20°C. Cell pellets were resuspended in 1 ml lysis buffer (50 mM Tris-HCl pH 7.5, 150 mM NaCl, 1% NP40, 1 mM EDTA, 1 mM EGTA, 0,5% sodium deoxycholate, 0,1% SDS and complete protease inhibitor cocktail (04693132001, Sigma-Aldrich)). We added 210 units benzonase® nuclease (E1014, Sigma-Aldrich) and incubated at 4°C for 1h with agitation. Cell lysates were subsequently sonicated at 30% amplitude (3 intervals of 9 sec sonication/5 sec rest) and centrifuged at 4,332 x g for 15 min at 4°C to remove the insoluble fraction. The supernatant fraction was collected and from each sample an aliquot was taken to monitor bait-BirA*-Flag expression. Meanwhile, streptavidin-

sepharose High performance beads (17-5113-01, GE healthcare life sciences) were washed 3 times with 20x bedvolume lysis buffer without sodium deoxycholate and protease inhibitors. Washed beads, corresponding to 20 µl slurry, were added to each sample and incubated for 3 hours at 4°C with constant rotation. After 3 hours, beads were pelleted by centrifugation at 400 x g for 1 min. The supernatant was removed and beads were washed 3x in 1 ml lysis buffer without sodium deoxycholate and protease inhibitors. An aliquot of both the supernatans and beads was taken to monitor protein biotinylation and streptavidin-based enrichment of biotinylated proteins. Beads were subsequently washed another 3 times with trypsin digestion buffer (20 mM Tris-HCl pH 8.0 and 2 mM $CaCl_2$) and finally resuspended in 150 µl trypsin digestion buffer.

The beads were subsequently incubated for 4 hours with 1 µg trypsin (V5111, Promega) at 37˚C. Beads were removed, another 1 µg of trypsin was added and proteins were further digested overnight at 37˚C. Peptides were purified on Omix C18 tips (A57003100, Agilent), dried and re-dissolved in 20 µl loading solvent (0.1% TFA in water/acetonitrile (98:2, v/v)) of which 2 µl was injected for LC-MS/MS analysis.

LC–MS/MS Analysis

The peptide mixtures were analyzed by LC–MS/MS on an Ultimate 3000 RSLC nano LC (Thermo) in-line connected to a Q Exactive mass spectrometer (Thermo). The peptides were first loaded on a trapping column (made in-house, 100 µm internal diameter (I.D.) × 20 mm, 5 µm beads C18 Reprosil-HD, Dr. Maisch, Ammerbuch-Entringen, Germany) and after flushing from the trapping column, peptides were loaded on an analytical column (made in-house, 75 µm I.D. × 150 mm, 3 µm beads C18 Reprosil-HD, Dr. Maisch) packed in the needle. Peptides were loaded with loading solvent and separated with a linear gradient from 98% solvent A (0.1% formic acid in water) to 55% solvent B (0.1% formic acid in water/acetonitrile, 20/80 (v/v)) in 120 min at a constant flow rate of 300 nL/min, followed by a 5 min wash reaching 99% solvent B.

The mass spectrometer was operated in data-dependent, positive ionization mode, automatically switching between MS and MS/MS acquisition for the 10 most abundant peaks in a given MS spectrum. The source voltage was 4.1 kV, and the capillary temperature was 275°C. One MS1 scan (m/z 400–2,000, AGC target 3×10^6 ions, maximum ion injection time 80 ms), acquired at a resolution of 70,000 (at 200 m/z), was followed by up to 10 tandem MS scans (resolution 17,500 at 200 m/z) of the most intense ions fulfilling predefined selection criteria (AGC target 5×10^4 ions, maximum ion injection time 60 ms, isolation window 2 Da, fixed first mass 140 m/z, spectrum data type: centroid, underfill ratio 2%, intensity threshold $1.7xE^4$, exclusion of unassigned, 1, 5-8, >8 positively charged precursors, peptide match preferred, exclude isotopes on, dynamic exclusion time 50 s). The HCD collision energy was set to 25% Normalized Collision Energy and the polydimethylcyclosiloxane background ion at 445.120025 Da was used for internal calibration (lock mass).

Data analysis

Data analysis was performed with MaxQuant (version 1.5.6.5, [83]) using the Andromeda search engine [84] with default search settings including a false discovery rate set at 1% on both the peptide and protein level. Spectra were searched against human proteins in the UniProt/Swiss-Prot database (database release version of November 2016 containing 20,141 human protein sequences, [85]) supplemented with the NS1-BirA*-Flag/NS2-BirA*-Flag/MYLK4-BirA*-Flag sequence (BioID) or the NS1-Flag/NS2-Flag/Flag-MYLK4-Myc sequence (affinity purification). The mass tolerance for precursor and fragment ions was set to 20 and 4.5 ppm, respectively, during the main search. Enzyme specificity was set to C-terminal to arginine and lysine, also allowing cleavage at arginine/lysine-proline bonds with a maximum of two missed cleavages. Variable modifications were set to oxidation of methionine residues (to sulfoxides), acetylation of protein N-termini and phosphorylation of serine, threonine and tyrosine residues. A minimum of one unique or razor peptide was required for identification. Matching between runs was enabled with an alignment time window of 20 minutes and a match time window of 1 minute. Proteins were quantified by the MaxLFQ algorithm integrated in the MaxQuant software. A minimum ratio count of two unique or razor peptides was required for quantification.

Further data analysis was performed with the Perseus software (version 1.5.5.3, [86]) after loading the protein groups file from MaxQuant. First, proteins only identified by site, reverse database hits and potential contaminants were removed. LFQ intensities were log2 transformed. Replicate samples were grouped and proteins with less than 3 valid values in at least one group were removed. Missing values were imputed with values from the lower part of the normal distribution representing the detection limit, and a two-sample t-test was performed with a permutation-based FDR of 0.01 and a S0 value of 2, with a total of 1,000 randomizations.

Co-immunoprecipitation

Three million Flp-In™ T-REx™ 293 cells were seeded in 9 cm petri-dishes in 10 ml DMEM medium supplemented with 10% heat-inactivated FCS, 2 mM L-glutamine (BE17-605F, Lonza) and 0,4 mM sodium-pyruvate (S8636, Sigma-Aldrich) and grown at 37°C and 5% CO_2. The following day, cells were transfected with 10 µg pEXPR-NS1-Flag, pEXPR-NS2-Flag or with an empty vector by using PEI in a 1:4 ratio as described above. Twenty-four hours post transfection, cells were gently washed with 1 ml ice-cold PBS and lysed in 600 µl low salt, low detergent lysis buffer (50 mM Tris-HCl pH 8.0, 150 mM NaCl, 5 mM EDTA, 0.1% NP40 and complete protease inhibitor cocktail (04693132001, Sigma-Aldrich)) for 20 min on ice. We used a low detergent concentration to preserve protein-protein interactions as much as possible. Cell lysates were centrifuged at 16,000 x g for 3 min to remove the insoluble fraction. Supernatans was harvested and an aliquot was taken as the CoIP input sample. We subsequently incubated the supernatans with 10 µg/ml mouse IgG1 antiFlag-M2 antibody (F3165, Sigma-Aldrich) for 3 hours at 4°C with constant rotation. Meanwhile, protein G sepharose beads (17-0618-01, GE healthcare) were washed 3 times with low salt, low detergent lysis buffer without protease inhibitors. After 3 hours, Flag complexes were immunoprecipitated by the addition of protein G sepharose beads

for 1 hour at 4°C with constant rotation. Beads were centrifuged at 1,000 x g for 5 min, washed 4 times with 0,5 ml - and finally resuspended in 50 µl low salt, low detergent lysis buffer without protease inhibitors. Beads were boiled for 10 min at 99°C in 2x Laemmli buffer supplemented with 4,2% (v:v) β-mercaptoethanol. Supernatans was collected, loaded on SDS-PAGE and blotted as described above, except that we used Pierce protein free T20 blocking buffer (37573, ThermoFischer scientific). Proteins were detected by the following primary antibodies: rabbit anti-Flag (F7425, Sigma-Aldrich), mouse anti-MAVS (E-3)(sc-166583, Santa Cruz biotechnology Inc.), rabbit anti-CPSF1-4, - CPSF6-7, - CSTF1-3, - WDR33 and - PAPOLA (A301-580A, A301-581A, A301-091A, A301-585A, A301-356A, A301-359A, A301-151A, A301-250A, A301-092A, A301-096A and A301-010A, Bethyl laboratories).

Virotrap screen

A detailed protocol can be found in [87]. Ten-million HEK293T cells were seeded in 75-cm² flasks and grown overnight at 37°C and 8% CO_2. The following day cells were transfected with 3,75 µg of pMET7-GAG-NS1, pMET7-GAG-NS2 or pMET7-GAG-eDHFR in combination with 3,75 µg of a Virotrap plasmid mix (an empty vector (pSVsport), pcDNA3-Flag-VSV-G and pMD2.G in a 15:4:2 (wt/wt/wt) ratio) by using PEI (1:5). Plasmid DNA and PEI were mixed for 10 min at RT. Meanwhile, culture medium was refreshed with DMEM medium supplemented with 2% FCS. After 10 min, DNA:PEI complexes were added to the cells. Six hours post transfection, culture medium was refreshed with DMEM medium supplemented with 10% FCS. Forty-eight hours post transfection secreted VLPs were harvested as follows. Culture medium was harvested and centrifuged at 1,500 x g for 3 min to remove any cells and filtered through a 0.45 µm filter. Paramagnetic MyOne Streptavidin T1 beads (20 µl per falcon) were washed with Tris wash buffer (TWB; 20 mM Tris-HCl, pH 7.5, 150 mM NaCl in Milli-Q water) and subsequently incubated with 2 µl of anti-Flag BioM2 antibody (F9291, Sigma-Aldrich) for 10 min at room temperature while rotating. After 10 min beads were washed with TWB. The beads were subsequently incubated with the filtered supernatants for 2h at RT to capture VLPs and washed twice with TWB. VLPs were eluted from the beads by adding 4 µg Flag peptide (F3290, Sigma-Aldrich) with 30 min incubation at 37°C while shaking. The supernatans containing the VLPs was harvested. VLPs were lysed by adding Amphipol A8-35 (A835, Anatrace) to a final concentration of 100 ng/µl with 10 min incubation at RT. Protein aggregates were precipitated by acidifying the samples to pH 3 with formic acid and centrifugation at 8,600 x g for 5 min. Precipitates were redissolved in 50 mM triethylammonium bicarbonate buffer. Samples were heated at 95°C for 5 min and cooled down on ice. Samples were subsequently treated with 0,25 µg trypsin (V5111, Promega) and incubated overnight at 37°C. Samples were acidified to pH 3.0 by adding 1,5-2µl of 5% TFA and centrifuged at 8,600 x g for 5 min. Peptides were subsequently analysed by LC-MS/MS in a very similar way as for the BioID screen (see above). Data analysis was done using Mascot software (for details see [87]). Proteins were searched in the Uniprot/Swiss-prot database of all human proteins, bovine proteins, HIV-1 GAG protein, the VSV-G protein, the Flag-VSV-G fusion protein and the EGFP protein. Only proteins that were identified in all three replicates of at least one group were retained.

Affinity purification screen

Four million Flp-In™ T-REx™ 293 cells were seeded in 9 cm petri-dishes in 10 ml DMEM medium supplemented with 10% heat-inactivated FCS, 2 mM L-glutamine (BE17-605F, Lonza), 0.4 mM sodium-pyruvate (S8636, Sigma-Aldrich) and 100 U/ml penicillin and 100 µg/ml streptomycin (15140122, Thermo fisher scientific)) and grown at 37°C and 5% CO_2. The following day, cells were transfected with 10 µg pEXPR-NS1-Flag, pEXPR-NS2-Flag, pEXPR-Flag-MYLK4-Myc or with an empty vector by using PEI in a 1:4 ratio as described above. Twenty-four hours post transfection, cells were gently washed with 1 ml ice-cold PBS and lysed in 1 ml low salt, low detergent lysis buffer (50 mM Tris-HCl pH 8.0, 150 mM NaCl, 5 mM EDTA, 0.1% NP40 and complete protease inhibitor cocktail (04693132001, Sigma-Aldrich)) for 20 min on ice. We used a low detergent concentration to preserve protein-protein interactions as much as possible. Cell lysates were centrifuged at 16,000 x g for 3 min to remove the insoluble fraction. We subsequently incubated the supernatans with 4 µg/ml rabbit antiFlag antibody (F7425, Sigma-Aldrich) for 3 hours at 4°C with constant rotation. Meanwhile, protein G sepharose beads (17-0618-01, GE healthcare) were washed 3 times with low salt, low detergent lysis buffer without protease inhibitors. After 3 hours, Flag complexes were immunoprecipitated by the addition of protein G sepharose beads for 1 hour at 4°C with constant rotation. Beads were centrifuged at 1,000 x g for 5 min and washed once with 0,5 ml of low salt, low detergent lysis buffer without protease inhibitors. Beads were subsequently washed 3 times with 1 ml trypsin digestion buffer and finally resuspended in 150 µl trypsin digestion buffer. Beads were subsequently digested with trypsin for mass spectrometry-based identification of affinity purified proteins (similar as for the BioID screen: see above).

7.6 Acknowledgements

We thank Prof. Dr. Anne-Claude Gingras (Lunenfeld-Tanenbaum research institute at Mount Sinai Hospital, Toronto, Canada) for providing the pDest_pcDNA5-BirA*-Flag vector, Prof. Dr. Sven Eyckerman (Ghent, Belgium) for providing the pOG44-Flp recombinase - and pMET7-GAG vector, and Prof. Dr. Rudi Beyaert (Ghent, Belgium) for providing the MAVS antibody. We also thank Noortje Samyn for helping with the Virotrap experiment.

7.7 reference list

1. Roux, K.J., et al., *A promiscuous biotin ligase fusion protein identifies proximal and interacting proteins in mammalian cells.* J Cell Biol, 2012. **196**(6): p. 801-10.
2. Bramwell, M.E., *Characterization of biotinylated proteins in mammalian cells using 125I-streptavidin.* J Biochem Biophys Methods, 1987. **15**(3-4): p. 125-32.
3. Eyckerman, S., et al., *Trapping mammalian protein complexes in viral particles.* Nat Commun, 2016. **7**: p. 11416.
4. Teng, M.N. and P.L. Collins, *Altered growth characteristics of recombinant respiratory syncytial viruses which do not produce NS2 protein.* J Virol, 1999. **73**(1): p. 466-73.
5. Whitehead, S.S., et al., *Recombinant respiratory syncytial virus bearing a deletion of either the NS2 or SH gene is attenuated in chimpanzees.* J Virol, 1999. **73**(4): p. 3438-42.
6. Jin, H., et al., *Recombinant respiratory syncytial viruses with deletions in the NS1, NS2, SH, and M2-2 genes are attenuated in vitro and in vivo.* Virology, 2000. **273**(1): p. 210-8.
7. Teng, M.N., et al., *Recombinant respiratory syncytial virus that does not express the NS1 or M2-2 protein is highly attenuated and immunogenic in chimpanzees.* J Virol, 2000. **74**(19): p. 9317-21.
8. Spann, K.M., K.C. Tran, and P.L. Collins, *Effects of nonstructural proteins NS1 and NS2 of human respiratory syncytial virus on interferon regulatory factor 3, NF-kappaB, and proinflammatory cytokines.* J Virol, 2005. **79**(9): p. 5353-62.
9. Goswami, R., et al., *Viral degradasome hijacks mitochondria to suppress innate immunity.* Cell Res, 2013. **23**(8): p. 1025-42.
10. Wu, W., et al., *The interactome of the human respiratory syncytial virus NS1 protein highlights multiple effects on host cell biology.* J Virol, 2012. **86**(15): p. 7777-89.
11. Swedan, S., A. Musiyenko, and S. Barik, *Respiratory syncytial virus nonstructural proteins decrease levels of multiple members of the cellular interferon pathways.* J Virol, 2009. **83**(19): p. 9682-93.
12. Swedan, S., et al., *Multiple functional domains and complexes of the two nonstructural proteins of human respiratory syncytial virus contribute to interferon suppression and cellular location.* J Virol, 2011. **85**(19): p. 10090-100.
13. Ling, Z., K.C. Tran, and M.N. Teng, *Human respiratory syncytial virus nonstructural protein NS2 antagonizes the activation of beta interferon transcription by interacting with RIG-I.* J Virol, 2009. **83**(8): p. 3734-42.
14. Boyapalle, S., et al., *Respiratory syncytial virus NS1 protein colocalizes with mitochondrial antiviral signaling protein MAVS following infection.* PLoS One, 2012. **7**(2): p. e29386.
15. Elliott, J., et al., *Respiratory syncytial virus NS1 protein degrades STAT2 by using the Elongin-Cullin E3 ligase.* J Virol, 2007. **81**(7): p. 3428-36.
16. Ren, J., et al., *A novel mechanism for the inhibition of interferon regulatory factor-3-dependent gene expression by human respiratory syncytial virus NS1 protein.* J Gen Virol, 2011. **92**(Pt 9): p. 2153-9.
17. Rusinova, I., et al., *Interferome v2.0: an updated database of annotated interferon-regulated genes.* Nucleic Acids Res, 2013. **41**(Database issue): p. D1040-6.
18. Szklarczyk, D., et al., *The STRING database in 2017: quality-controlled protein-protein association networks, made broadly accessible.* Nucleic Acids Res, 2017. **45**(D1): p. D362-D368.
19. Santelli, E., et al., *Structural analysis of Siah1-Siah-interacting protein interactions and insights into the assembly of an E3 ligase multiprotein complex.* J Biol Chem, 2005. **280**(40): p. 34278-87.
20. Kano, F., et al., *The maintenance of the endoplasmic reticulum network is regulated by p47, a cofactor of p97, through phosphorylation by cdc2 kinase.* Genes Cells, 2005. **10**(4): p. 333-44.
21. Chung, J., et al., *INTRACELLULAR TRANSPORT. PI4P/phosphatidylserine countertransport at ORP5- and ORP8-mediated ER-plasma membrane contacts.* Science, 2015. **349**(6246): p. 428-32.

22. Mehedi, M., et al., *Actin-Related Protein 2 (ARP2) and Virus-Induced Filopodia Facilitate Human Respiratory Syncytial Virus Spread.* PLoS Pathog, 2016. **12**(12): p. e1006062.
23. Loo, Y.M., et al., *Distinct RIG-I and MDA5 signaling by RNA viruses in innate immunity.* J Virol, 2008. **82**(1): p. 335-45.
24. Sabbah, A., et al., *Activation of innate immune antiviral responses by Nod2.* Nat Immunol, 2009. **10**(10): p. 1073-80.
25. Hall, C.B., et al., *Interferon production in children with respiratory syncytial, influenza, and parainfluenza virus infections.* J Pediatr, 1978. **93**(1): p. 28-32.
26. Villenave, R., et al., *In vitro modeling of respiratory syncytial virus infection of pediatric bronchial epithelium, the primary target of infection in vivo.* Proc Natl Acad Sci U S A, 2012. **109**(13): p. 5040-5.
27. McIntosh, K., *Interferon in nasal secretions from infants with viral respiratory tract infections.* J Pediatr, 1978. **93**(1): p. 33-6.
28. Tran, K.C., B. He, and M.N. Teng, *Replacement of the respiratory syncytial virus nonstructural proteins NS1 and NS2 by the V protein of parainfluenza virus 5.* Virology, 2007. **368**(1): p. 73-82.
29. Lo, M.S., R.M. Brazas, and M.J. Holtzman, *Respiratory syncytial virus nonstructural proteins NS1 and NS2 mediate inhibition of Stat2 expression and alpha/beta interferon responsiveness.* J Virol, 2005. **79**(14): p. 9315-9.
30. Ramaswamy, M., et al., *Respiratory syncytial virus nonstructural protein 2 specifically inhibits type I interferon signal transduction.* Virology, 2006. **344**(2): p. 328-39.
31. Dhar, J., et al., *2'-5'-Oligoadenylate Synthetase-Like Protein Inhibits Respiratory Syncytial Virus Replication and Is Targeted by the Viral Nonstructural Protein 1.* J Virol, 2015. **89**(19): p. 10115-9.
32. Chatterjee, S., et al., *Structural basis for human respiratory syncytial virus NS1-mediated modulation of host responses.* Nat Microbiol, 2017. **2**: p. 17101.
33. Kazazian, K., et al., *Plk4 Promotes Cancer Invasion and Metastasis through Arp2/3 Complex Regulation of the Actin Cytoskeleton.* Cancer Res, 2017. **77**(2): p. 434-447.
34. Mehus, A.A., R.H. Anderson, and K.J. Roux, *BioID Identification of Lamin-Associated Proteins.* Methods Enzymol, 2016. **569**: p. 3-22.
35. Lopez-Soop, G., et al., *AKAP95 interacts with nucleoporin TPR in mitosis and is important for the spindle assembly checkpoint.* Cell Cycle, 2017. **16**(10): p. 947-956.
36. Perez White, B.E., et al., *EphA2 proteomics in human keratinocytes reveals a novel association with afadin and epidermal tight junctions.* J Cell Sci, 2017. **130**(1): p. 111-118.
37. Johnston, W.L., et al., *C. elegans SUP-46, an HNRNPM family RNA-binding protein that prevents paternally-mediated epigenetic sterility.* BMC Biol, 2017. **15**(1): p. 61.
38. Le Sage, V., et al., *Proteomic analysis of HIV-1 Gag interacting partners using proximity-dependent biotinylation.* Virol J, 2015. **12**: p. 138.
39. Ortiz, D.A., J.E. Glassbrook, and P.E. Pellett, *Protein-Protein Interactions Suggest Novel Activities of Human Cytomegalovirus Tegument Protein pUL103.* J Virol, 2016. **90**(17): p. 7798-810.
40. Jamaluddin, M., et al., *Role of peroxiredoxin 1 and peroxiredoxin 4 in protection of respiratory syncytial virus-induced cysteinyl oxidation of nuclear cytoskeletal proteins.* J Virol, 2010. **84**(18): p. 9533-45.
41. Engdahl, C., et al., *The Rift Valley Fever virus protein NSm and putative cellular protein interactions.* Virol J, 2012. **9**: p. 139.
42. Calzado, M.A., R. Sancho, and E. Munoz, *Human immunodeficiency virus type 1 Tat increases the expression of cleavage and polyadenylation specificity factor 73-kilodalton subunit modulating cellular and viral expression.* J Virol, 2004. **78**(13): p. 6846-54.
43. de la Vega, L., et al., *The 73 kDa subunit of the CPSF complex binds to the HIV-1 LTR promoter and functions as a negative regulatory factor that is inhibited by the HIV-1 Tat protein.* J Mol Biol, 2007. **372**(2): p. 317-30.

44. Nemeroff, M.E., et al., *Influenza virus NS1 protein interacts with the cellular 30 kDa subunit of CPSF and inhibits 3'end formation of cellular pre-mRNAs.* Mol Cell, 1998. **1**(7): p. 991-1000.
45. Noah, D.L., K.Y. Twu, and R.M. Krug, *Cellular antiviral responses against influenza A virus are countered at the posttranscriptional level by the viral NS1A protein via its binding to a cellular protein required for the 3' end processing of cellular pre-mRNAS.* Virology, 2003. **307**(2): p. 386-95.
46. Kochs, G., A. Garcia-Sastre, and L. Martinez-Sobrido, *Multiple anti-interferon actions of the influenza A virus NS1 protein.* J Virol, 2007. **81**(13): p. 7011-21.
47. Steidle, S., et al., *Glycine 184 in nonstructural protein NS1 determines the virulence of influenza A virus strain PR8 without affecting the host interferon response.* J Virol, 2010. **84**(24): p. 12761-70.
48. Johansson, C., et al., *HPV-16 E2 contributes to induction of HPV-16 late gene expression by inhibiting early polyadenylation.* EMBO J, 2012. **31**(14): p. 3212-27.
49. Lee, K., et al., *Flexible use of nuclear import pathways by HIV-1.* Cell Host Microbe, 2010. **7**(3): p. 221-33.
50. De Iaco, A., et al., *TNPO3 protects HIV-1 replication from CPSF6-mediated capsid stabilization in the host cell cytoplasm.* Retrovirology, 2013. **10**: p. 20.
51. Henning, M.S., et al., *In vivo functions of CPSF6 for HIV-1 as revealed by HIV-1 capsid evolution in HLA-B27-positive subjects.* PLoS Pathog, 2014. **10**(1): p. e1003868.
52. Sowd, G.A., et al., *A critical role for alternative polyadenylation factor CPSF6 in targeting HIV-1 integration to transcriptionally active chromatin.* Proc Natl Acad Sci U S A, 2016. **113**(8): p. E1054-63.
53. Gower, T.L., et al., *RhoA is activated during respiratory syncytial virus infection.* Virology, 2001. **283**(2): p. 188-96.
54. Tsuji, T., et al., *ROCK and mDia1 antagonize in Rho-dependent Rac activation in Swiss 3T3 fibroblasts.* J Cell Biol, 2002. **157**(5): p. 819-30.
55. McCurdy, L.H. and B.S. Graham, *Role of plasma membrane lipid microdomains in respiratory syncytial virus filament formation.* J Virol, 2003. **77**(3): p. 1747-56.
56. Gower, T.L., et al., *RhoA signaling is required for respiratory syncytial virus-induced syncytium formation and filamentous virion morphology.* J Virol, 2005. **79**(9): p. 5326-36.
57. Pastey, M.K., J.E. Crowe, Jr., and B.S. Graham, *RhoA interacts with the fusion glycoprotein of respiratory syncytial virus and facilitates virus-induced syncytium formation.* J Virol, 1999. **73**(9): p. 7262-70.
58. Pastey, M.K., et al., *A RhoA-derived peptide inhibits syncytium formation induced by respiratory syncytial virus and parainfluenza virus type 3.* Nat Med, 2000. **6**(1): p. 35-40.
59. Budge, P.J., J. Lebowitz, and B.S. Graham, *Antiviral activity of RhoA-derived peptides against respiratory syncytial virus is dependent on formation of peptide dimers.* Antimicrob Agents Chemother, 2003. **47**(11): p. 3470-7.
60. McLellan, J.S., et al., *Structure-based design of a fusion glycoprotein vaccine for respiratory syncytial virus.* Science, 2013. **342**(6158): p. 592-8.
61. Villumsen, B.H., et al., *A new cellular stress response that triggers centriolar satellite reorganization and ciliogenesis.* EMBO J, 2013. **32**(23): p. 3029-40.
62. Graser, S., et al., *Cep164, a novel centriole appendage protein required for primary cilium formation.* J Cell Biol, 2007. **179**(2): p. 321-30.
63. Spektor, A., et al., *Cep97 and CP110 suppress a cilia assembly program.* Cell, 2007. **130**(4): p. 678-90.
64. Zhang, L., et al., *Respiratory syncytial virus infection of human airway epithelial cells is polarized, specific to ciliated cells, and without obvious cytopathology.* J Virol, 2002. **76**(11): p. 5654-66.
65. Johnson, J.E., et al., *The histopathology of fatal untreated human respiratory syncytial virus infection.* Mod Pathol, 2007. **20**(1): p. 108-19.

66. Liesman, R.M., et al., *RSV-encoded NS2 promotes epithelial cell shedding and distal airway obstruction.* J Clin Invest, 2014. **124**(5): p. 2219-33.
67. Tanahashi, N., et al., *Molecular structure of 20S and 26S proteasomes.* Enzyme Protein, 1993. **47**(4-6): p. 241-51.
68. Whelan, J.N., et al., *Identification of Respiratory Syncytial Virus Nonstructural Protein 2 Residues Essential for Exploitation of the Host Ubiquitin System and Inhibition of Innate Immune Responses.* J Virol, 2016. **90**(14): p. 6453-63.
69. Soukenik, M., et al., *The SEP domain of p47 acts as a reversible competitive inhibitor of cathepsin L.* FEBS Lett, 2004. **576**(3): p. 358-62.
70. Corry, J., et al., *Preventing Cleavage of the Respiratory Syncytial Virus Attachment Protein in Vero Cells Rescues the Infectivity of Progeny Virus for Primary Human Airway Cultures.* J Virol, 2015. **90**(3): p. 1311-20.
71. Zhou, T., et al., *OSBP-related protein 8 (ORP8) regulates plasma and liver tissue lipid levels and interacts with the nucleoporin Nup62.* PLoS One, 2011. **6**(6): p. e21078.
72. Yeo, D.S., et al., *Evidence that selective changes in the lipid composition of raft-membranes occur during respiratory syncytial virus infection.* Virology, 2009. **386**(1): p. 168-82.
73. Chang, T.H., et al., *Cholesterol-rich lipid rafts are required for release of infectious human respiratory syncytial virus particles.* Virology, 2012. **422**(2): p. 205-13.
74. Ludwig, A., et al., *Caveolae provide a specialized membrane environment for respiratory syncytial virus assembly.* J Cell Sci, 2017. **130**(6): p. 1037-1050.
75. Bajimaya, S., et al., *Cholesterol is required for stability and infectivity of influenza A and respiratory syncytial viruses.* Virology, 2017. **510**: p. 234-241.
76. Burke, E., et al., *Role of cellular actin in the gene expression and morphogenesis of human respiratory syncytial virus.* Virology, 1998. **252**(1): p. 137-48.
77. Kallewaard, N.L., A.L. Bowen, and J.E. Crowe, Jr., *Cooperativity of actin and microtubule elements during replication of respiratory syncytial virus.* Virology, 2005. **331**(1): p. 73-81.
78. Krzyzaniak, M.A., et al., *Host cell entry of respiratory syncytial virus involves macropinocytosis followed by proteolytic activation of the F protein.* PLoS Pathog, 2013. **9**(4): p. e1003309.
79. Santangelo, P.J. and G. Bao, *Dynamics of filamentous viral RNPs prior to egress.* Nucleic Acids Res, 2007. **35**(11): p. 3602-11.
80. Brock, S.C., J.R. Goldenring, and J.E. Crowe, Jr., *Apical recycling systems regulate directional budding of respiratory syncytial virus from polarized epithelial cells.* Proc Natl Acad Sci U S A, 2003. **100**(25): p. 15143-8.
81. Kolokoltsov, A.A., et al., *Small interfering RNA profiling reveals key role of clathrin-mediated endocytosis and early endosome formation for infection by respiratory syncytial virus.* J Virol, 2007. **81**(14): p. 7786-800.
82. San-Juan-Vergara, H., et al., *Cholesterol-rich microdomains as docking platforms for respiratory syncytial virus in normal human bronchial epithelial cells.* J Virol, 2012. **86**(3): p. 1832-43.
83. Cox, J. and M. Mann, *MaxQuant enables high peptide identification rates, individualized p.p.b.-range mass accuracies and proteome-wide protein quantification.* Nat Biotechnol, 2008. **26**(12): p. 1367-72.
84. Cox, J., et al., *Andromeda: a peptide search engine integrated into the MaxQuant environment.* J Proteome Res, 2011. **10**(4): p. 1794-805.
85. Uniprot. 2016; Available from: www.uniprot.org.
86. Tyanova, S., et al., *The Perseus computational platform for comprehensive analysis of (prote)omics data.* Nat Methods, 2016. **13**(9): p. 731-40.
87. Titeca, K., et al., *Analyzing trapped protein complexes by Virotrap and SFINX.* Nat Protoc, 2017. **12**(5): p. 881-898.

7.8 Supplementary figures

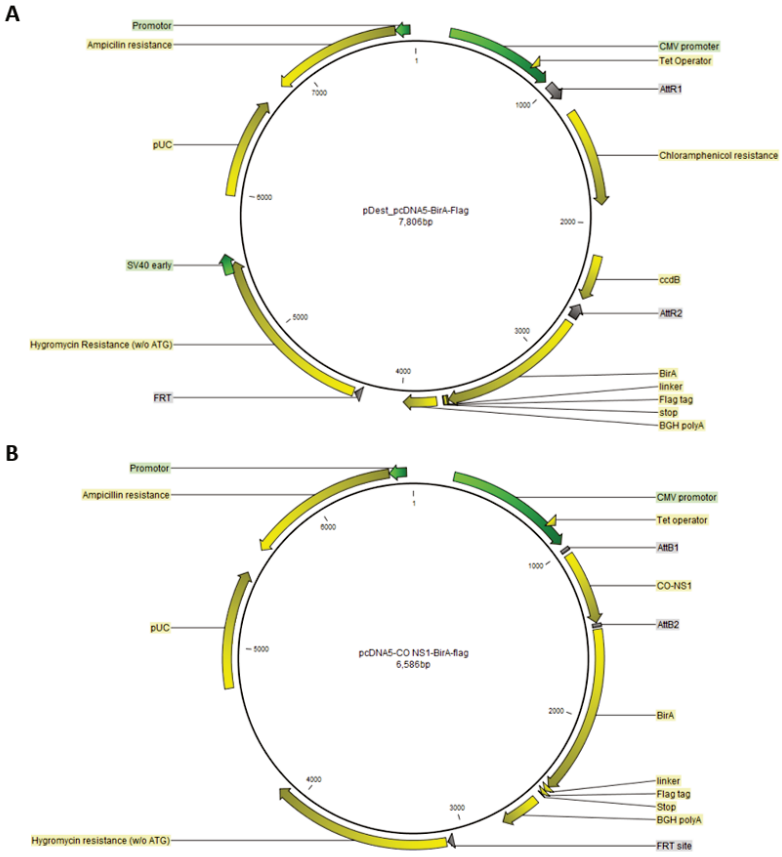

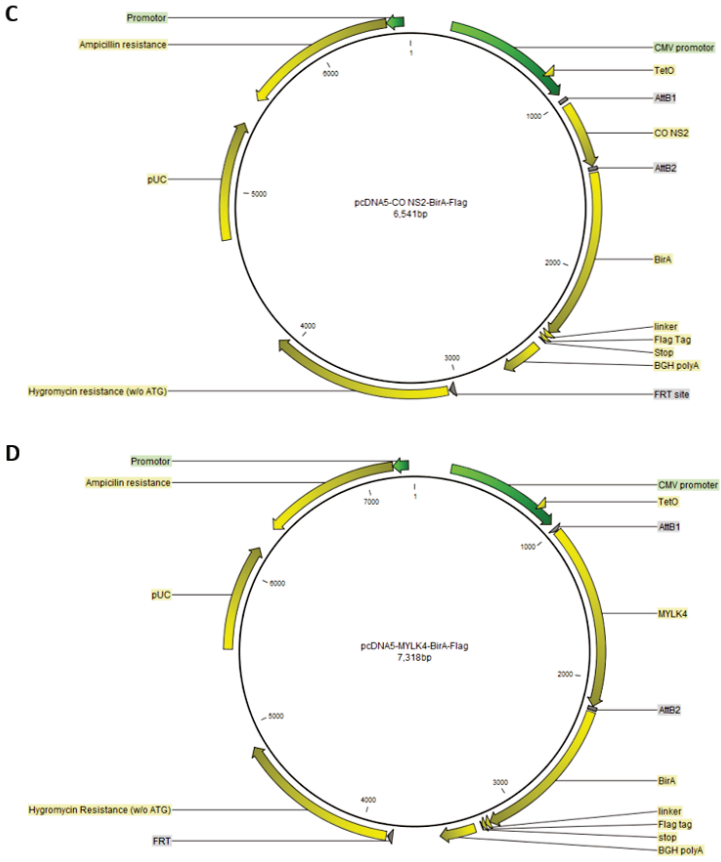

Supplementary figure 1: Plasmid maps of BioID vectors. (A) pDest_pcDNA5-BirA*-Flag. (B) pcDNA5-NS1-BirA*-Flag. (C) pcDNA5-NS2-BirA*-Flag. (D) pcDNA5-MYLK4-BirA*-Flag. CO = codon optimized.

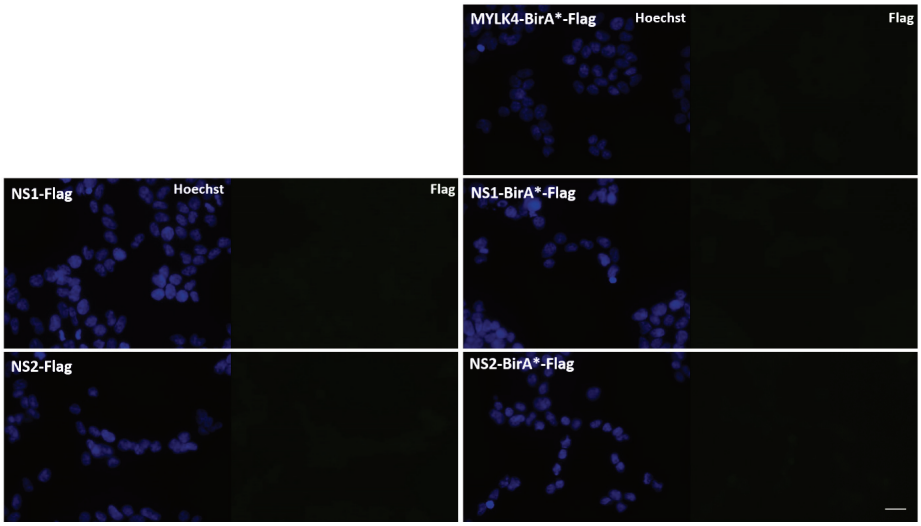

Supplementary figure 2: Secondary antibody only controls for the expression of NS1-BirA*-Flag, NS2-BirA*Flag, MYLK4-BirA*-Flag, NS1-Flag and NS2-Flag after transient transfection in HEK293T cells. HEK293T cells in 24-well plates were transiently transfected with 300 ng pcDNA5-GOI-BirA*-Flag plasmid or pEXPR-GOI-Flag plasmid for 24 hours. GOI = gene of interest. Nuclei were stained by Hoechst. Scale bar = 10 µm.

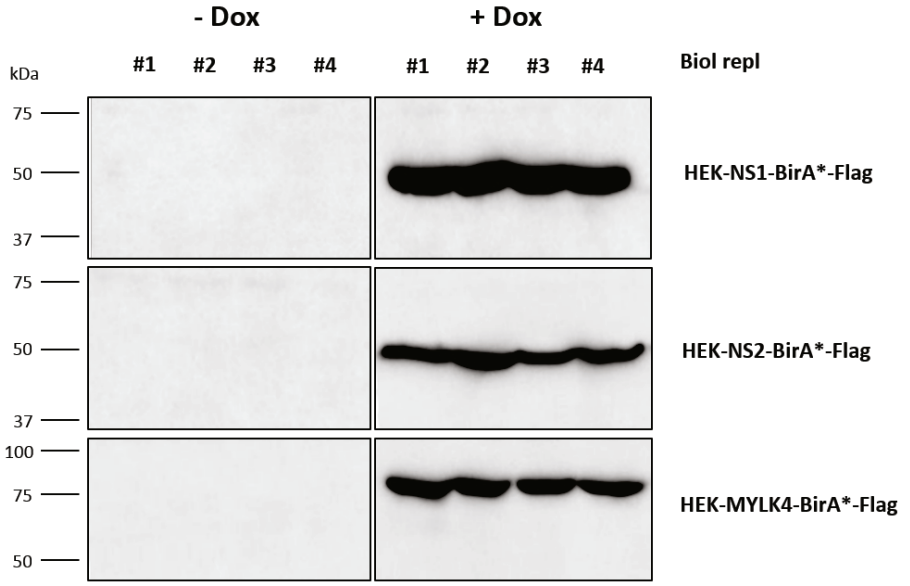

Supplementary figure 3: Validation of doxycycline-induced expression of NS1-BirA*-Flag, NS2-BirA*-Flag and MYLK4-BirA*-Flag in the BioID screen. Detection with a Flag-tag-specific antibody.

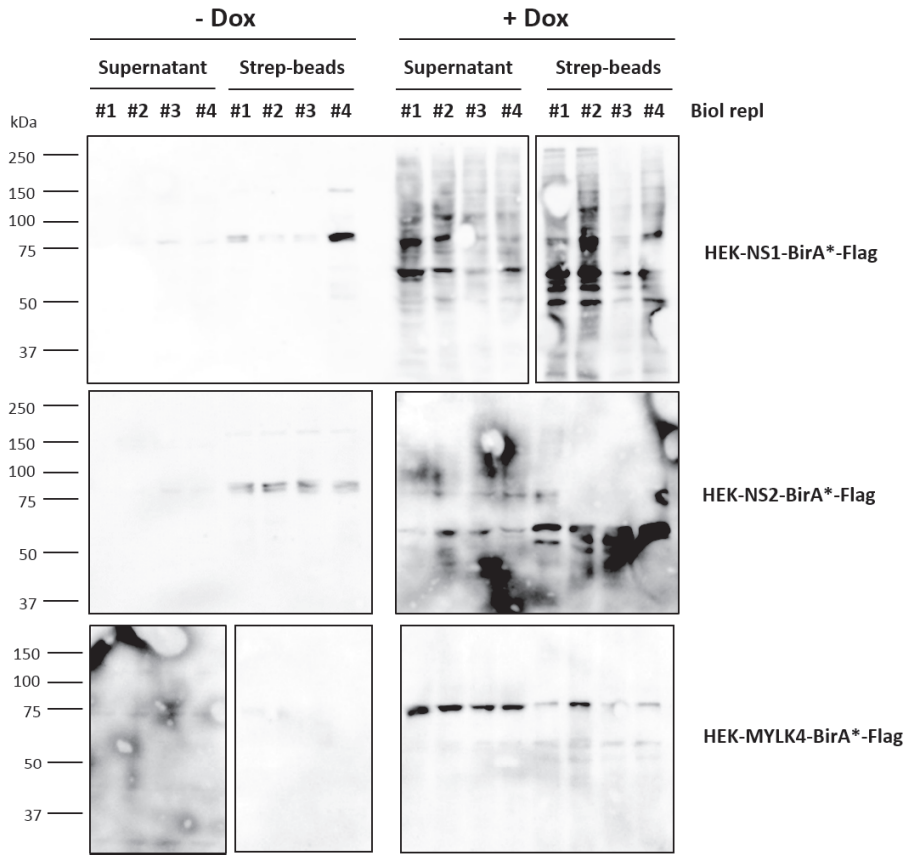

Supplementary figure 4: Validation of the enrichment of biotinylated proteins in the BioID screen. After enrichment of biotinylated proteins by streptavidin beads, an aliquot of the supernatans and the streptavidin beads was taken for western blot analysis. Biotinylated proteins were detected with HRP coupled streptavidin.

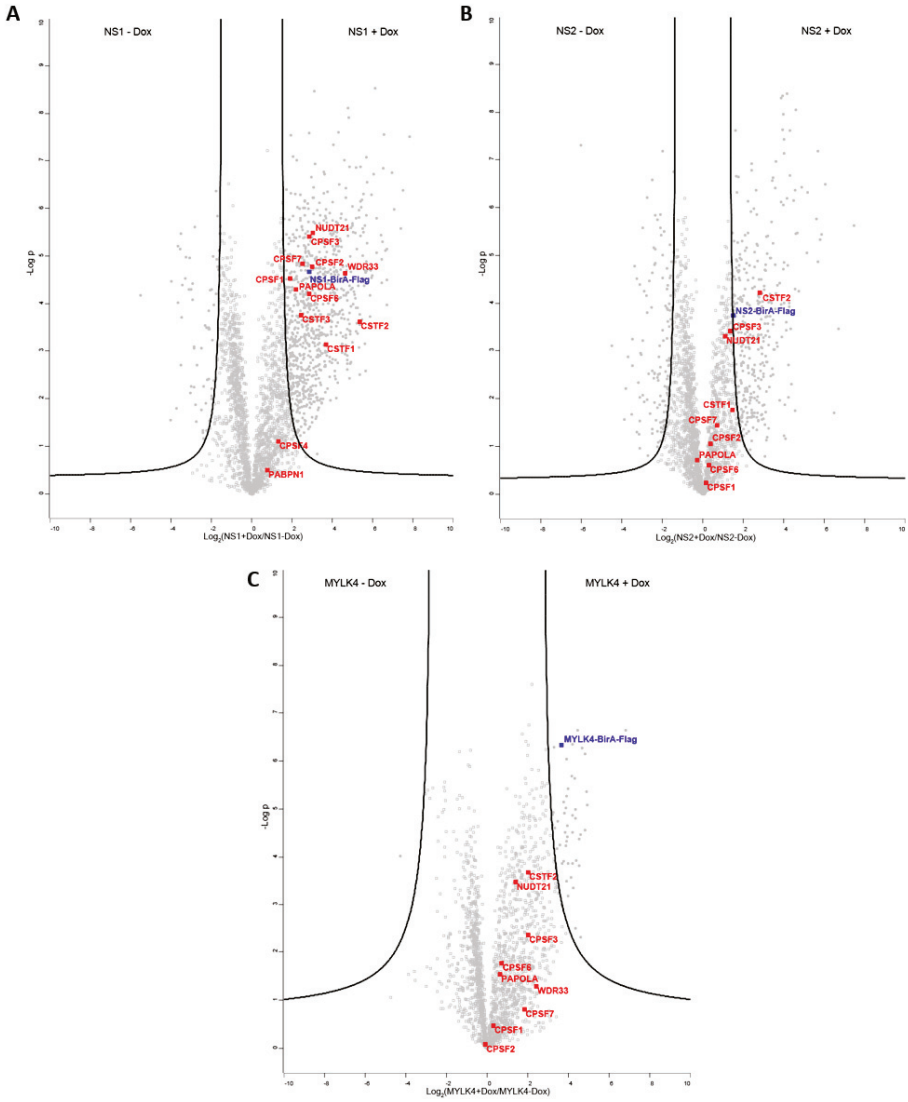

Supplementary figure 5: Volcano plots of the identified proteins in the BioID screen with NS1, NS2 and MYLK4. All identified proteins were plotted according to the Log_2 fold change of their LFQ value in the doxycycline-induced samples relative to the non-induced samples for NS1-BirA*-Flag (A), NS2-BirA*-Flag (B) or MYLK4-BirA*-Flag (C) (X-axis) and the statistical significance (Y-axis, -Log (p-value) of a t-test). The two black curves represent the selection cut-off for selection of significantly enriched proteins. NS1-BirA*-Flag, NS2-BirA*-Flag and MYLK4-BirA*-Flag are highlighted in blue, whereas members of the cleavage and polyadenylation of precursor mRNA pathway are highlighted in red.

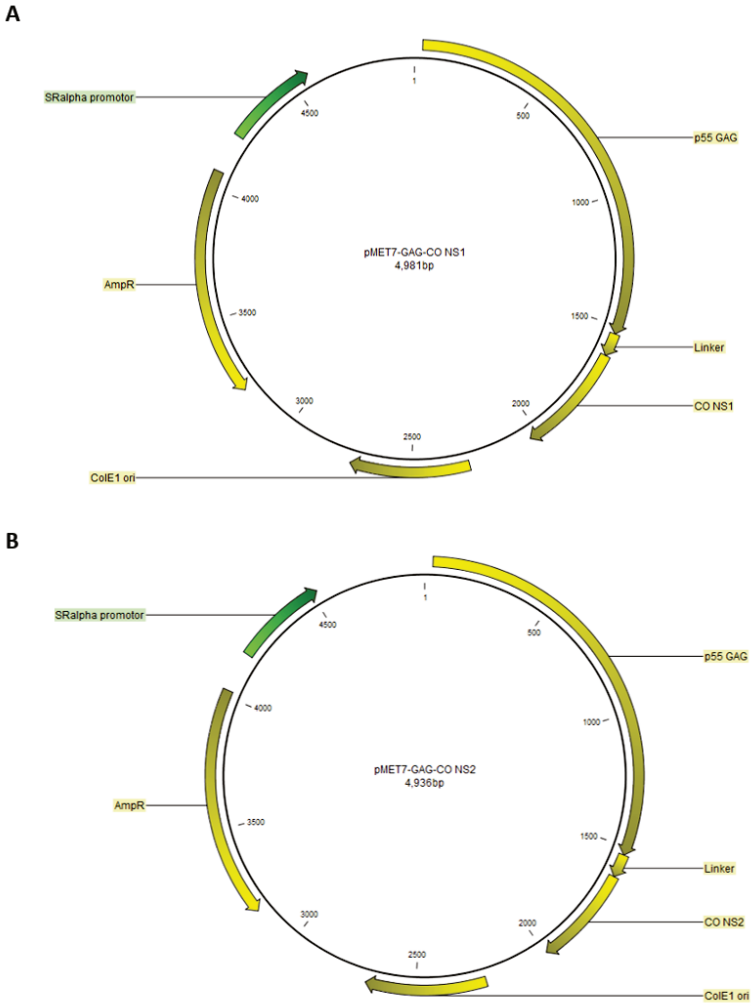

Supplementary figure 6: Plasmid maps of Virotrap vectors. (A) pMET7-GAG-NS1. (B) pMET7-GAG-NS2. CO = codon optimized

7.9 Supplementary tables

Supplementary table 1: NS1 proxeome identified by BioID

protein IDs	Gene names	Log2FC (NS1+Dox/ NS1-Dox)	-Log(P)	IRG gene	protein IDs	Gene names	Log2FC (NS1+Dox/N S1-Dox)	-Log(P)	IRG gene
Q9UPQ9	TNR6B	7,82	7,51	No	P33240	CSTF2	5,34	3,62	No
Q96JH7	VCIP1	7,50	6,39	No	P37802	TAGL2	5,33	2,51	No
O60271	JIP4	6,94	6,75	No	Q86TX2	ACOT1	5,32	3,08	Yes
Q9NSK0	KLC4	6,68	3,98	No	Q8IX90	SKA3	5,31	5,97	No
O43290	SNUT1	6,63	5,11	No	P55010	IF5	5,30	5,82	No
Q5VT52	RPRD2	6,53	6,85	Yes	Q9H6T3	RPAP3	5,27	4,38	No
Q8NDI1	EHBP1	6,46	5,30	No	Q92625	ANS1A	5,24	3,37	No
Q96BY7	ATG2B	6,45	4,93	No	Q15427	SF3B4	5,24	3,92	No
Q13625	ASPP2	6,43	4,44	No	Q9Y2Z0	SGT1	5,20	3,59	No
O94830	DDHD2	6,20	5,80	Yes	Q96A49	SYAP1	5,17	6,87	No
Q96RT1	ERBIN	6,18	5,08	No	Q96BD8	SKA1	5,16	5,80	No
Q8NB46	ANR52	6,12	8,53	No	O43815	STRN	5,13	5,50	Yes
Q8IY67	RAVR1	6,05	6,73	No	Q13426	XRCC4	5,13	4,11	Yes
Q9P2N5	RBM27	5,95	4,60	No	Q96EA4	SPDLY	5,09	4,19	No
Q5VZ89	DEN4C	5,93	6,29	No	Q08379	GOGA2	5,07	4,25	No
P42566	EPS15	5,90	4,71	No	O60925	PFD1	5,01	3,99	No
Q9Y4E1	FA21C	5,87	3,73	No	O75150	BRE1B	5,00	5,69	No
Q5H9R7	PP6R3	5,86	4,17	No	P18615	NELFE	4,99	6,05	No
Q9BPU6	DPYL5	5,85	4,71	No	Q05682	CALD1	4,99	3,18	No
A0MZ66	SHOT1	5,73	4,74	No	P50542	PEX5	4,97	4,33	No
Q6IN85	P4R3A	5,71	6,56	No	O75170	PP6R2	4,97	5,65	No
O75153	CLUH	5,69	5,27	Yes	O75381	PEX14	4,92	4,30	No
Q14145	KEAP1	5,69	4,68	No	Q9BTA9	WAC	4,92	2,78	No
Q9NRA8	4ET	5,68	7,09	No	Q5T8P6	RBM26	4,90	3,95	No
Q9C0C9	UBE2O	5,67	5,86	No	P51648	AL3A2	4,90	4,67	No
O60826	CCD22	5,64	4,66	No	O94788	AL1A2	4,89	5,60	No
Q8NI08	NCOA7	5,62	2,59	Yes	Q5T5Y3	CAMP1	4,89	2,75	No
Q92574	TSC1	5,61	5,64	No	Q13561	DCTN2	4,86	3,36	No
Q8IWZ8	SUGP1	5,60	3,16	Yes	Q8WUQ7	CATIN	4,86	5,00	No
Q07866	KLC1	5,59	4,51	No	Q9NW82	WDR70	4,85	6,88	No
Q5SW79	CE170	5,59	4,70	No	Q9H910	HN1L	4,85	3,58	Yes
Q5VTR2	BRE1A	5,55	4,39	No	Q13123	RED	4,85	4,39	No
O60566	BUB1B	5,54	5,51	Yes	P48634	PRC2A	4,83	3,82	No
Q9H0B6	KLC2	5,52	6,30	Yes	Q9NX08	COMD8	4,83	3,44	No
Q8NHV4	NEDD1	5,49	5,01	No	Q9H089	LSG1	4,81	7,92	No
Q9UKX7	NUP50	5,48	4,54	No	Q68DK7	MSL1	4,78	3,66	No
Q9BT92	TCHP	5,46	6,18	No	O75410	TACC1	4,76	4,25	Yes
Q96D71	REPS1	5,42	6,04	No	O15212	PFD6	4,76	5,57	No
Q9Y5K5	UCHL5	5,39	6,88	No	O94763	RMP	4,76	8,11	No
Q8TEP8	CE192	5,35	3,77	No	O60573	IF4E2	4,75	5,43	No
P61011	SRP54	5,34	3,56	No	P13984	T2FB	4,74	2,82	No

Supplementary table 1 continued …

protein IDs	Gene names	Log2FC (NS1+Dox/ NS1-Dox)	-log(P)	IRG gene	protein IDs	Gene names	Log2FC (NS1+Dox/NS1-Dox)	-Log(P)	IRG gene
Q9ULV3	CIZ1	4,74	3,47	No	Q9BRZ2	TRI56	4,38	3,85	No
P21675	TAF1	4,74	5,57	No	Q96MX6	WDR92	4,35	5,37	No
Q9P013	CWC15	4,73	2,74	No	Q96MW1	CCD43	4,34	4,11	No
Q96K76	UBP47	4,73	4,07	No	Q9BVL2	NUP58	4,34	6,51	No
Q7Z3T8	ZFY16	4,73	2,92	No	Q9UPU7	TBD2B	4,33	3,80	No
Q8N6T3	ARFG1	4,72	2,63	No	Q13435	SF3B2	4,32	5,11	No
Q86XP3	DDX42	4,69	4,70	No	Q99471	PFD5	4,31	7,60	No
Q05D32	CTSL2	4,69	4,23	No	Q06265	EXOS9	4,29	4,61	No
O60292	SI1L3	4,67	6,23	No	Q15020	SART3	4,28	5,11	Yes
Q9BT25	HAUS8	4,67	5,58	No	Q9UJX5	APC4	4,28	5,22	No
Q92783	STAM1	4,66	4,18	No	Q8NEN9	PDZD8	4,26	2,34	Yes
Q8N8S7	ENAH	4,66	3,35	No	Q9NRY5	F1142	4,26	3,61	No
Q9Y6Y8	S23IP	4,66	3,13	No	Q9ULW0	TPX2	4,26	2,76	Yes
Q96PY6	NEK1	4,65	3,01	No	P62310	LSM3	4,25	5,68	Yes
Q6XZF7	DNMBP	4,65	5,76	Yes	Q8WUA2	PPIL4	4,24	3,77	No
Q9C0J8	WDR33	4,61	4,65	Yes	P60510	PP4C	4,24	5,22	No
P23381	SYWC	4,60	2,94	No	Q86VS8	HOOK3	4,23	5,24	No
Q14241	ELOA1	4,59	3,68	No	Q9Y5K6	CD2AP	4,23	4,31	Yes
P55196	AFAD	4,57	7,03	No	Q9BRX9	WDR83	4,22	4,67	No
Q9NQC7	CYLD	4,56	4,55	Yes	Q86U44	MTA70	4,21	5,50	No
Q9HAU0	PKHA5	4,55	4,29	No	O75113	N4BP1	4,20	5,72	Yes
Q16555	DPYL2	4,53	4,17	No	O14929	HAT1	4,19	4,06	No
O43426	SYNJ1	4,51	4,47	No	O75934	SPF27	4,19	2,02	No
O75179	ANR17	4,50	4,78	No	P37840	SYUA	4,19	5,03	No
Q5T6F2	UBAP2	4,50	3,31	No	Q9NQX3	GEPH	4,19	5,42	No
Q9H4I2	ZHX3	4,49	3,78	Yes	Q8IWZ3	ANKH1	4,18	4,70	No
P49366	DHYS	4,49	3,12	No	Q9BXB4	OSB11	4,17	3,34	No
Q9UKK9	NUDT5	4,48	2,97	Yes	P30566	PUR8	4,17	5,22	No
Q9H2H8	PPIL3	4,47	3,88	Yes	Q659A1	ICE2	4,16	4,12	No
Q15208	STK38	4,47	3,16	No	P52655	TF2AA	4,15	2,42	No
P49023	PAXI	4,45	4,47	No	Q9NWS0	PIHD1	4,15	3,80	No
Q9NQP4	PFD4	4,45	5,89	No	Q13618	CUL3	4,14	2,82	Yes
Q9P2D0	IBTK	4,45	3,70	No	Q9H3P2	NELFA	4,12	4,19	No
O75665	OFD1	4,44	4,32	No	Q6Y7W6	PERQ2	4,12	5,15	No
O95905	ECD	4,43	4,88	No	Q9H501	ESF1	4,11	2,48	No
Q7Z4H7	HAUS6	4,43	5,20	No	O43719	HTSF1	4,11	3,78	No
O94913	PCF11	4,43	3,12	No	O75534	CSDE1	4,11	5,52	Yes
P49750	YLPM1	4,41	3,39	Yes	P49585	PCY1A	4,11	4,22	No
Q8TBC5	ZSC18	4,41	5,32	No	Q99961; Q99962	SH3GL1; SH3GL2	4,11	2,60	No
Q92541	RTF1	4,40	5,80	No	P78318	IGBP1	4,10	4,61	No
O14531	DPYL4	4,39	4,13	No	Q92734	TFG	4,09	4,34	No
O43395	PRPF3	4,38	4,72	Yes	Q9H7Z6	KAT8	4,09	5,12	Yes

Supplementary table 1 continued …

protein IDs	Gene names	Log2FC (NS1+Dox/ NS1-Dox)	-Log(P)	IRG gene	protein IDs	Gene names	Log2FC (NS1+Dox/ NS1-Dox)	-Log(P)	IRG gene
P61289	PSME3	4,08	3,84	No	Q8IVD9	NUDC3	3,78	3,78	No
Q9ULE6	PALD	4,08	4,67	No	Q9UBC2	EP15R	3,77	4,01	No
Q9P2D6	F135A	4,08	4,55	No	Q7Z4V5	HDGR2	3,75	2,22	No
Q92917	GPKOW	4,08	4,77	No	Q9H5V9	CX056	3,75	4,66	No
O95453	PARN	4,06	5,15	No	P46108	CRK	3,74	3,34	No
Q69YH5	CDCA2	4,04	5,04	No	P29144	TPP2	3,74	6,35	No
Q9NPD3	EXOS4	4,04	7,34	No	Q86X02	CDR2L	3,74	5,27	No
P55327	TPD52	4,03	4,25	Yes	Q9P2F8	SI1L2	3,74	2,99	No
Q6PJT7	ZC3HE	4,03	4,33	No	Q0PNE2	ELP6	3,73	4,43	No
Q9Y2D5	AKAP2	4,02	3,98	Yes	Q13868	EXOS2	3,71	5,09	No
Q9Y2H2	SAC2	4,02	3,74	No	Q9UKY7	CDV3	3,70	5,71	No
O00743	PPP6	4,02	6,14	No	Q53EZ4	CEP55	3,70	2,91	Yes
Q4V328	GRAP1	4,01	5,76	No	Q9Y333	LSM2	3,70	3,11	No
Q9NQT5	EXOS3	4,00	5,22	No	Q92599	SEPT8	3,69	4,33	Yes
Q7Z434	MAVS	3,99	4,30	Yes	Q9ULT8	HECD1	3,68	3,35	No
Q7Z5L2	R3HCL	3,99	4,30	No	Q05048	CSTF1	3,68	3,14	Yes
Q12800	TFCP2	3,98	2,84	No	P54578	UBP14	3,68	5,99	No
Q9H3P7	GCP60	3,98	3,83	No	Q9NR46	SHLB2	3,66	5,80	No
Q96I25	SPF45	3,98	4,86	No	Q9NZ52	GGA3	3,66	3,33	No
Q15024	EXOS7	3,97	5,45	No	Q96EV2	RBM33	3,65	2,68	No
Q15276	RABE1	3,96	2,75	No	Q5PRF9	SMAG2	3,64	2,14	No
Q96SU4	OSBL9	3,96	3,62	No	Q96GX5	GWL	3,64	4,60	No
O75461	E2F6	3,95	3,87	No	Q96B97	SH3K1	3,64	4,67	No
Q14195	DPYL3	3,95	5,53	No	Q9UJX4	APC5	3,64	2,98	No
Q15942	ZYX	3,94	3,52	Yes	P61163	ACTZ	3,63	2,72	No
Q68CZ6	HAUS3	3,94	3,42	Yes	P27540	ARNT	3,63	3,01	No
P49189	AL9A1	3,93	3,36	No	Q9UPM8	AP4E1	3,63	4,98	Yes
Q9NTZ6	RBM12	3,91	4,63	Yes	Q92890	UFD1	3,63	5,84	No
Q8N5Y2	MS3L1	3,89	4,22	No	Q9Y2W2	WBP11	3,62	3,61	No
Q9UK61	TASOR	3,89	4,72	No	Q13480	GAB1	3,61	6,72	Yes
O00193	SMAP	3,88	4,41	No	P50990	TCPQ	3,60	5,19	No
Q9H0G5	NSRP1	3,88	5,48	No	P28290	SSFA2	3,60	2,69	Yes
Q96RG2	PASK	3,87	3,78	Yes	P55036	PSMD4	3,60	4,18	No
A6NKD9	CC85C	3,87	4,06	No	A8MXV4	NUD19	3,60	2,78	No
Q13442	HAP28	3,86	2,47	No	P61758	PFD3	3,59	4,75	No
Q6P1N0	C2D1A	3,85	2,78	No	Q9Y450	HBS1L	3,57	4,62	Yes
P49773	HINT1	3,85	5,91	Yes	Q9NY27	PP4R2	3,57	5,53	No
Q9UPN9	TRI33	3,84	2,88	No	P38398	BRCA1	3,56	5,75	No
Q99575	POP1	3,83	4,32	No	O75808	CAN15	3,56	3,14	No
Q9H2J4	PDCL3	3,83	3,64	No	Q8IWX8	CHERP	3,56	6,77	No
Q9NR28	DBLOH	3,82	5,53	No	Q15369	ELOC	3,56	3,36	No
Q7Z3E2	CC186	3,79	4,68	No	Q6P1J9	CDC73	3,56	5,29	No
O95684	FR1OP	3,78	4,49	No	Q8IZ21	PHAR4	3,55	4,90	No

Supplementary table 1 continued …

protein IDs	Gene names	Log2FC (NS1+Dox/ NS1-Dox)	-Log(P)	IRG gene	protein IDs	Gene names	Log2FC (NS1+Dox/ NS1-Dox)	-Log(P)	IRG gene
Q12874	SF3A3	3,55	6,33	Yes	Q15637	SF01	3,33	3,45	No
Q15723	ELF2	3,55	4,62	No	Q8N0X7	SPG20	3,33	4,86	Yes
Q99426	TBCB	3,55	3,68	No	Q6ZWJ1	STXB4	3,32	3,33	No
Q96DF8	DGC14	3,54	4,00	No	O75874	IDHC	3,32	4,54	No
P25685	DNJB1	3,53	4,73	No	Q8IW35	CEP97	3,31	3,05	No
Q7RTP6	MICA3	3,53	4,63	No	Q8TD16	BICD2	3,31	3,86	No
Q13325	IFIT5	3,53	4,48	Yes	Q7Z417	NUFP2	3,31	4,31	No
Q96LT7	CI072	3,52	4,92	No	Q5JSZ5	PRC2B	3,30	2,44	No
Q92905	CSN5	3,51	2,01	No	Q9Y2U8	MAN1	3,30	3,66	No
Q5VT06	CE350	3,51	5,37	No	Q8WWI1	LMO7	3,30	1,81	No
Q9NVA2	SEPT11	3,48	3,50	Yes	Q13371	PHLP	3,29	4,56	No
Q01968	OCRL	3,47	2,96	No	O94927	HAUS5	3,29	3,27	Yes
P54105	ICLN	3,47	2,95	No	Q15025	TNIP1	3,29	4,74	Yes
Q9BY89	K1671	3,46	3,39	No	Q9HB71	CYBP	3,28	1,76	No
Q6NSI4	CX057	3,45	1,92	No	Q14157	UBP2L	3,28	4,43	No
Q8WX93	PALLD	3,44	5,29	Yes	Q8NAV1	PR38A	3,27	2,69	No
P13861	KAP2	3,44	1,91	No	O43353	RIPK2	3,27	3,34	Yes
Q9Y484	WIPI4	3,44	3,35	No	Q9BZH6	WDR11	3,27	4,63	No
Q9BSU1	CP070	3,43	4,40	No	Q6P1R3	MSD2	3,27	3,15	No
O43166	SI1L1	3,43	4,28	No	Q14004	CDK13	3,26	2,92	No
Q9UEY8	ADDG	3,43	3,78	No	Q9NZZ3	CHMP5	3,26	2,88	Yes
Q96JQ2	CLMN	3,42	2,00	Yes	Q8TAT6	NPL4	3,25	3,72	No
Q5T2T1	MPP7	3,41	2,29	No	Q9H6Z4	RANB3	3,25	5,97	No
Q9NP61	ARFG3	3,41	5,59	No	O14976	GAK	3,25	2,04	Yes
Q8TCU4	ALMS1	3,40	4,95	No	P29084	T2EB	3,24	3,02	No
Q9H444	CHM4B	3,40	4,75	No	Q9UHR5	S30BP	3,24	4,84	No
Q9NRL3	STRN4	3,39	2,92	No	Q96CV9	OPTN	3,23	3,99	Yes
Q9BX66	SRBS1	3,38	4,67	No	O00268	TAF4	3,23	1,98	No
Q9BTT0	AN32E	3,38	3,40	No	Q9C037	TRIM4	3,22	0,84	No
Q9H814	PHAX	3,38	2,34	No	O00401	WASL	3,21	2,51	No
Q9NQC3	RTN4	3,38	3,00	No	Q96AY4	TTC28	3,21	4,98	Yes
Q8WW12	PCNP	3,38	5,87	No	O43399	TPD54	3,20	3,45	No
Q9Y2D4	EXC6B	3,37	3,78	No	O15173	PGRC2	3,20	2,88	No
Q9Y266	NUDC	3,37	4,78	No	Q08378	GOGA3	3,20	3,92	No
Q5T481	RBM20	3,36	2,73	No	Q12979	ABR	3,19	2,04	No
Q9UQN3	CHM2B	3,35	2,63	No	Q70E73	RAPH1	3,19	1,64	Yes
Q8N9B5	JMY	3,35	5,69	No	P15170	ERF3A	3,19	4,50	No
P16333	NCK1	3,35	1,96	Yes	Q5T5X7	BEND3	3,17	3,33	No
Q6NXE6	ARMC6	3,34	3,54	No	Q9UKZ1	CNO11	3,17	2,68	No
Q0JRZ9	FCHO2	3,34	5,08	No	Q8WVK7	SKA2	3,17	2,28	No
O00560	SDCB1	3,34	3,33	No	Q99733	NP1L4	3,17	4,15	No
Q9NZM3	ITSN2	3,34	6,12	No	P84098	RL19	3,16	2,11	No
Q504Q3	PAN2	3,33	3,17	No	O15498	YKT6	3,16	3,28	No

Supplementary table 1 continued …

protein IDs	Gene names	Log2FC (NS1+Dox/ NS1-Dox)	-Log(P)	IRG gene	protein IDs	Gene names	Log2FC (NS1+Dox/ NS1-Dox)	-Log(P)	IRG gene
P42025	ACTY	3,16	4,55	No	Q9C026	TRIM9	3,01	2,08	No
Q8N5L8	RP25L	3,15	4,36	No	Q16204	CCDC6	3,00	2,81	No
Q8NHQ8	RASF8	3,15	4,75	No	Q9P2S5	WRP73	3,00	4,39	No
Q2M2I8	AAK1	3,15	2,58	Yes	Q00341	VIGLN	2,99	5,39	No
P30419	NMT1	3,14	6,94	Yes	Q86XL3	ANKL2	2,99	1,62	No
Q15051	IQCB1	3,14	4,92	Yes	Q9Y6A4	CFA20	2,99	2,48	No
Q5VUJ6	LRCH2	3,13	5,69	Yes	Q9H869	YYAP1	2,99	3,48	No
Q9H307	PININ	3,13	4,02	No	Q9P2I0	CPSF2	2,98	4,79	No
Q3MHD2	LSM12	3,13	4,23	No	Q1ED39	KNOP1	2,96	5,02	No
Q08AD1	CAMP2	3,13	4,02	No	O60231	DHX16	2,96	1,51	No
Q8N6N3	CA052	3,13	4,94	No	Q01850	CDR2	2,95	3,44	Yes
Q9NVX0	HAUS2	3,13	3,11	No	P33176	KINH	2,95	6,66	No
Q9UJU6	DBNL	3,11	5,27	Yes	Q8N3X1	FNBP4	2,95	2,08	No
Q9UJX2	CDC23	3,11	3,77	No	P22234	PUR6	2,95	5,30	No
O00151	PDLI1	3,11	1,94	No	Q8IWB9	TEX2	2,95	3,28	Yes
P53367	ARFP1	3,11	3,18	No	Q96KM6	Z512B	2,95	2,19	No
Q86W56	PARG	3,10	3,26	Yes	Q9UMZ2	SYNRG	2,94	3,96	Yes
Q8IYB1	M21D2	3,10	3,67	No	P78316	NOP14	2,93	1,90	No
O00213	APBB1	3,10	4,54	No	Q9BVA0	KTNB1	2,93	2,88	No
P49327	FAS	3,10	8,47	Yes	Q96AC1	FERM2	2,92	3,73	No
P49321	NASP	3,08	4,54	Yes	Q86X83	COMD2	2,92	2,15	No
Q99816	TS101	3,08	3,97	No	P49591	SYSC	2,92	4,00	No
Q9NUG6	PDRG1	3,07	2,64	No	Q14141	SEPT6	2,92	2,25	Yes
Q76FK4	NOL8	3,07	1,95	No	O75663	TIPRL	2,91	4,35	No
Q12872	SFSWA	3,06	6,45	No	Q6QNY1	BL1S2	2,91	1,99	No
Q8WXW3	PIBF1	3,05	3,87	No	P61081	UBC12	2,91	2,76	No
Q8IXH7	NELFD	3,05	2,49	No	P54652	HSP72	2,91	5,01	No
O75817	POP7	3,04	4,39	Yes	O15042	SR140	2,90	5,32	No
P78371	TCPB	3,04	5,72	No	Q13190	STX5	2,90	3,65	No
Q16181	SEPT7	3,04	5,90	No	Q5TH69	BIG3	2,89	3,96	No
P26358	DNMT1	3,04	3,42	No	Q8NFC6	BD1L1	2,88	1,92	No
Q9C0B7	TNG6	3,04	6,23	No	Q9HCN4	GPN1	2,88	1,82	Yes
Q5T5U3	RHG21	3,04	3,37	No	O95757	HS74L	2,88	3,62	No
Q99832	TCPH	3,03	6,23	No	Q5RKV6	EXOS6	2,87	4,56	No
P52739	ZN131	3,03	3,42	No	Q8WYQ5	DGCR8	2,87	2,61	No
Q9NQW6	ANLN	3,03	3,19	Yes	Q13033	STRN3	2,87	3,68	Yes
Q14677	EPN4	3,03	4,76	No	Q9Y3A3	PHOCN	2,87	3,01	No
C4AMC7; Q6VEQ5; A8K0Z3	WASH3; WASH2; WASH1	3,02	4,71	No	P52657	T2AG	2,86	1,41	No
P35249	RFC4	3,02	4,29	No	O00750	P3C2B	2,86	3,89	No
Q8TBA6	GOGA5	3,02	2,27	No	Q9UKF6	CPSF3	2,85	5,41	No
O43809	CPSF5	3,01	5,50	No	Q7KZ85	SPT6H	2,85	2,50	No

Supplementary table 1 continued …

protein IDs	Gene names	Log2FC (NS1+Dox/ NS1-Dox)	-Log(P)	IRG gene	protein IDs	Gene names	Log2FC (NS1+Dox/ NS1-Dox)	-Log(P)	IRG gene
P98174	FGD1	2,84	5,06	No	Q8N6V9	TEX9	2,72	2,18	No
Q9Y490	TLN1	2,84	7,59	No	Q15417	CNN3	2,72	4,09	No
Q15545	TAF7	2,84	2,09	No	Q96RU2	UBP28	2,71	1,88	No
Q9UHY1	NRBP	2,84	3,11	No	Q8WWM7	ATX2L	2,71	4,26	No
Q8NBF2	NHLC2	2,84	2,06	No	Q9UNZ2	NSF1C	2,71	2,50	No
Q01518	CAP1	2,84	2,68	No	A0JNW5	UH1BL	2,70	2,60	No
Q16630	CPSF6	2,83	4,21	No	P42167	LAP2B	2,70	4,25	No
Q9GZR1	SENP6	2,83	3,34	No	Q12888	TP53B	2,69	1,84	No
Q6BDS2	URFB1	2,82	3,92	No	Q9UJW0	DCTN4	2,69	3,53	No
Q9H3R5	CENPH	2,82	3,14	No	Q9HBM6	TAF9B	2,69	2,33	No
Q9UGP4	LIMD1	2,81	6,00	No	Q9H8K7	CJ088	2,69	4,43	No
Q9UHD8	SEPT9	2,81	5,10	Yes	Q15154	PCM1	2,68	3,35	No
Q96RL1	UIMC1	2,81	2,92	No	Q9H425	CA198	2,67	3,22	No
Q93052	LPP	2,81	3,14	No	Q9UBB5	MBD2	2,67	1,46	No
P78345	RPP38	2,81	5,72	No	Q7Z6K5	ARPIN	2,67	2,61	No
Q06546	GABPA	2,81	4,82	No	Q9H6D7	HAUS4	2,67	1,54	No
A3KN83	SBNO1	2,81	1,37	No	O95817	BAG3	2,67	3,24	Yes
Q9UI95	MD2L2	2,80	4,00	No	Q9H792	PEAK1	2,67	4,53	No
P35612	ADDB	2,80	2,20	No	Q9Y2I7	FYV1	2,66	5,19	No
Q9H074	PAIP1	2,79	3,38	No	Q53SF7	COBL1	2,66	4,70	No
Q9H1E3	NUCKS	2,79	5,25	No	O60884	DNJA2	2,66	4,19	No
Q9Y6M7	S4A7	2,79	4,11	No	Q8N0Z3	SPICE	2,65	5,17	No
Q5VUA4	ZN318	2,79	2,00	No	Q9H5Z1	DHX35	2,65	3,06	Yes
P19484	TFEB	2,79	4,00	Yes	Q9BVJ6	UT14A	2,65	2,16	No
O95295	SNAPN	2,78	4,35	No	Q8WU90	ZC3HF	2,65	2,03	No
Q32MZ4	LRRF1	2,78	3,82	No	Q9NYF8	BCLF1	2,65	5,07	No
Q2TBE0	C19L2	2,78	4,80	No	Q8NEL9	DDHD1	2,65	3,66	No
P48643	TCPE	2,77	5,52	No	Q9NWV8	BABA1	2,64	5,48	No
Q04637	IF4G1	2,77	6,11	No	Q9P215	POGK	2,64	5,11	No
Q92620	PRP16	2,77	2,63	No	O43660	PLRG1	2,63	2,41	No
Q9HC35	EMAL4	2,76	2,63	No	P49368	TCPG	2,63	6,15	No
Q92560	BAP1	2,76	3,70	No	P08579	RU2B	2,63	6,02	No
Q9UEE9	CFDP1	2,76	2,40	No	O95292	VAPB	2,63	5,40	No
Q04206	TF65	2,76	3,56	No	Q9BW85	CCD94	2,62	4,80	No
Q8TC07	TBC15	2,76	6,11	No	Q86UK7	ZN598	2,62	3,92	No
P48163	MAOX	2,75	4,85	No	P23193	TCEA1	2,62	1,55	Yes
Q5TKA1	LIN9	2,75	3,48	Yes	Q9NZ09	UBAP1	2,62	4,87	No
Q7L4I2	RSRC2	2,74	4,99	No	O75822	EIF3J	2,62	6,17	No
Q96RU3	FNBP1	2,74	4,53	No	Q15056	IF4H	2,61	1,48	No
Q8N668	COMD1	2,74	3,96	No	Q5VZK9	CARL1	2,61	3,28	No
O95777	LSM8	2,73	3,65	No	Q96BP3	PPWD1	2,61	3,36	No
P22681	CBL	2,73	3,46	Yes	O43432	IF4G3	2,60	5,86	No
Q8TF46	DI3L1	2,73	3,17	No	Q658Y4	F91A1	2,60	3,99	No

Supplementary table 1 continued …

protein IDs	Gene names	Log2FC (NS1+Dox/ NS1-Dox)	-Log(P)	IRG gene	protein IDs	Gene names	Log2FC (NS1+Dox/ NS1-Dox)	-Log(P)	IRG gene
P40818	UBP8	2,59	2,86	No	P17987	TCPA	2,50	5,56	No
Q9Y600	CSAD	2,59	4,92	No	P29083	T2EA	2,50	2,36	No
Q99567	NUP88	2,59	2,26	No	Q9Y2J2	E41L3	2,49	5,62	No
P40227	TCPZ	2,59	5,22	No	Q9UKJ3	GPTC8	2,49	2,61	No
Q96N67	DOCK7	2,59	1,84	No	Q15459	SF3A1	2,49	4,97	No
Q9BR76	COR1B	2,58	2,35	No	Q8WUX9	CHMP7	2,49	4,47	No
Q09161	NCBP1	2,58	2,06	Yes	Q5HYK7	SH319	2,48	3,65	No
Q03001	DYST	2,58	3,31	No	O14974	MYPT1	2,47	1,84	No
Q6UUV7	CRTC3	2,58	3,91	No	Q8IXS6	PALM2	2,46	3,56	Yes
Q96R06	SPAG5	2,58	1,69	No	Q13017	RHG05	2,46	5,64	No
P20290	BTF3	2,58	1,29	No	Q4G0J3	LARP7	2,46	2,51	No
Q9C0C2	TB182	2,57	1,70	No	Q9Y5X1	SNX9	2,45	3,30	No
Q99627	CSN8	2,57	4,01	No	Q92540	SMG7	2,45	2,76	Yes
O75528	TADA3	2,57	2,18	No	P35241	RADI	2,45	1,41	No
Q9UBI1	COMD3	2,56	2,95	No	Q12996	CSTF3	2,44	3,77	Yes
Q99590	SCAFB	2,56	3,18	No	O43172	PRP4	2,44	4,71	No
Q9Y613	FHOD1	2,56	5,38	Yes	O60879	DIAP2	2,43	2,67	No
O76064	RNF8	2,56	2,00	No	Q8IX12	CCAR1	2,43	4,97	No
O75937	DNJC8	2,55	2,23	No	Q9HCE5	MET14	2,42	2,46	No
Q53EL6	PDCD4	2,55	2,51	Yes	O75683	SURF6	2,42	1,94	No
Q96NC0	ZMAT2	2,55	2,18	No	Q8IZE3	PACE1	2,42	4,05	No
Q96M89	CC138	2,55	2,44	No	Q5R372	RBG1L	2,42	2,47	No
Q9Y520	PRC2C	2,55	2,93	No	Q9Y295	DRG1	2,42	5,80	No
O15164	TIF1A	2,55	2,10	No	Q99550	MPP9	2,41	1,97	No
Q14186	TFDP1	2,54	2,83	No	O75449	KTNA1	2,40	6,29	No
Q12768	STRUM	2,54	4,50	No	P36543; Q96A05	VATE1; VATE2	2,40	3,14	No
Q9P0K7	RAI14	2,54	4,14	Yes	Q9Y230	RUVB2	2,40	3,86	No
P42166	LAP2A	2,54	4,19	No	O00299	CLIC1	2,40	4,21	No
Q9Y265	RUVB1	2,53	4,34	No	Q2M389	WASH7	2,39	5,76	No
P27816	MAP4	2,53	6,02	No	O15063	K0355	2,39	2,92	No
P35606	COPB2	2,53	3,79	No	Q969X6	UTP4	2,38	1,22	No
Q68DQ2	CRBG3	2,53	4,05	No	Q7Z2K8	GRIN1	2,38	2,38	Yes
Q96AG4	LRC59	2,53	1,60	No	Q8IZD4	DCP1B	2,38	2,12	No
Q92667	AKAP1	2,52	4,04	No	Q96ES7	SGF29	2,37	1,95	No
Q8N684	CPSF7	2,52	4,84	No	Q14966	ZN638	2,37	1,71	No
O14530	TXND9	2,51	4,98	No	O75420	PERQ1	2,37	3,25	No
Q13596	SNX1	2,51	4,27	Yes	O14737	PDCD5	2,37	2,94	No
Q99459	CDC5L	2,51	2,63	No	Q9BY77	PDIP3	2,37	1,81	No
Q9HB21	PKHA1	2,51	3,09	No	Q9ULU4	PKCB1	2,36	2,07	No
P20810	ICAL	2,51	2,20	No	Q3B7T1	EDRF1	2,36	2,44	Yes
O75348	VATG1	2,51	4,25	No	Q15019	SEPT2	2,35	6,00	Yes
Q9BY44	EIF2A	2,50	2,20	No	Q14651	PLSI	2,35	5,41	No

Supplementary table 1 continued …

protein IDs	Gene names	Log2FC (NS1+Dox/ NS1-Dox)	-Log(P)	IRG gene	protein IDs	Gene names	Log2FC (NS1+Dox/ NS1-Dox)	-Log(P)	IRG gene
Q6P2C8	MED27	2,35	4,80	No	P83436	COG7	2,23	1,30	No
Q96LB3	IFT74	2,34	2,31	Yes	Q86UE4	LYRIC	2,23	4,58	No
Q9Y2D8	ADIP	2,34	1,93	No	Q13586	STIM1	2,22	4,81	Yes
O75586	MED6	2,33	1,34	No	P78332	RBM6	2,22	2,35	No
Q14247	SRC8	2,32	3,24	No	O60502	OGA	2,22	7,02	No
O14777	NDC80	2,31	2,32	Yes	Q7LBC6	KDM3B	2,21	3,75	No
Q8NC51	PAIRB	2,31	4,86	No	Q9BX63	FANCJ	2,21	2,81	No
Q63HK5	TSH3	2,31	3,60	No	Q13042	CDC16	2,21	1,73	No
Q9UJ41	RABX5	2,31	3,75	No	Q92797	SYMPK	2,21	1,99	No
Q86V48	LUZP1	2,30	4,45	Yes	Q9UBK9	UXT	2,21	2,45	No
Q92665	RT31	2,30	2,35	No	P62312	LSM6	2,21	5,55	No
P23588	IF4B	2,30	4,01	No	Q9UHR4	BI2L1	2,20	2,87	No
Q8N201	INT1	2,30	3,71	No	Q06124	PTN11	2,20	2,48	No
Q96QG7	MTMR9	2,29	2,69	No	Q9NXR7	BRE	2,20	1,31	No
O43301	HS12A	2,29	1,35	No	Q9BSJ8	ESYT1	2,20	3,11	No
Q8WYA0	IFT81	2,29	1,54	Yes	P51858	HDGF	2,20	2,33	No
Q9Y3P9	RBGP1	2,29	1,80	No	Q8N1G2	CMTR1	2,19	2,16	Yes
Q96SI9	STRBP	2,29	2,47	No	O15357	SHIP2	2,19	2,72	No
Q9BXF6	RFIP5	2,29	3,98	No	P98170	XIAP	2,19	4,97	Yes
Q9UNS2	CSN3	2,28	5,21	No	P62136	PP1A	2,19	4,55	No
Q9BRJ2	RM45	2,28	3,49	No	Q9Y2F5	ICE1	2,18	4,13	No
O94992	HEXI1	2,27	1,96	No	P78347	GTF2I	2,18	5,38	Yes
Q15061	WDR43	2,27	1,52	No	Q6ZSZ6	TSH1	2,18	3,32	No
Q9Y496	KIF3A	2,27	3,11	No	Q9NQT8	KI13B	2,18	3,20	No
Q6UN15	FIP1	2,27	4,05	No	Q13405	RM49	2,18	2,81	No
Q9BQ61	CS043	2,27	1,30	No	P51003	PAPOA	2,17	4,30	No
P49848	TAF6	2,27	1,30	No	Q13464	ROCK1	2,15	4,11	No
Q6PKG0	LARP1	2,26	6,02	No	P29590	PML	2,15	1,90	Yes
Q96SI1	KCD15	2,26	2,64	No	Q52LJ0	FA98B	2,15	1,90	No
Q9Y217	MTMR6	2,25	3,39	Yes	P48382	RFX5	2,15	3,19	Yes
Q9NVM9	ASUN	2,25	2,28	No	P09661	RU2A	2,15	6,31	No
Q6VMQ6	MCAF1	2,25	2,16	No	Q9BUI4	RPC3	2,14	3,25	No
O76003	GLRX3	2,25	2,85	No	Q9Y4E5	ZN451	2,14	2,12	No
Q7Z401	MYCPP	2,25	3,20	No	P21333	FLNA	2,13	3,49	Yes
Q9NVR5	KTU	2,25	1,87	No	Q96ST2	IWS1	2,13	3,23	No
Q7Z4H3	HDDC2	2,25	2,27	No	Q9UKV8	AGO2	2,13	3,65	No
Q92576	PHF3	2,24	3,60	No	P78344	IF4G2	2,13	4,19	No
O95487	SC24B	2,24	3,98	No	P49643	PRI2	2,12	4,67	No
Q15370	ELOB	2,24	2,07	No	Q8N3F8	MILK1	2,12	2,90	No
O75909	CCNK	2,24	1,75	No	Q8TBC3	SHKB1	2,12	3,46	No
Q8NI36	WDR36	2,24	4,52	No	Q659C4	LAR1B	2,10	4,17	No
P49757	NUMB	2,23	1,54	Yes	Q9UQR0	SCML2	2,10	4,50	No
P35611	ADDA	2,23	4,86	No	P49902	5NTC	2,10	3,14	No

Supplementary table 1 continued …

protein IDs	Gene names	Log2FC (NS1+Dox/ NS1-Dox)	-Log(P)	IRG gene	protein IDs	Gene names	Log2FC (NS1+Dox/ NS1-Dox)	-Log(P)	IRG gene
Q9H2G2	SLK	2,10	5,40	Yes	P34932	HSP74	1,97	3,30	No
Q6P3W7	SCYL2	2,09	5,32	No	Q99707	METH	1,97	2,10	No
O43491	E41L2	2,09	4,98	No	P00491	PNPH	1,97	1,76	No
Q9BTC0	DIDO1	2,09	3,96	Yes	Q8TEQ6	GEMI5	1,96	4,68	No
Q92598	HS105	2,09	4,97	No	P52756	RBM5	1,95	2,52	Yes
O60282	KIF5C	2,08	2,11	No	Q86YS7	C2CD5	1,95	2,44	No
Q8IX15	HOMEZ	2,08	3,23	No	Q6ZSR9	YJ005	1,94	2,27	No
P16949	STMN1	2,08	2,80	Yes	Q96L93	KI16B	1,93	3,09	No
Q9BYW2	SETD2	2,08	2,70	Yes	Q05397	FAK1	1,92	1,89	No
Q96F63	CCD97	2,07	1,59	No	Q9H0H5	RGAP1	1,92	6,32	No
Q9Y5P4	C43BP	2,06	2,26	No	Q9UBW8	CSN7A	1,92	7,54	No
Q9UGU5	HMGX4	2,06	2,48	No	Q14008	CKAP5	1,91	5,32	Yes
P11717	MPRI	2,05	3,36	No	P15311	EZRI	1,91	2,62	No
Q03188	CENPC	2,05	2,44	No	Q9H8H0	NOL11	1,91	3,65	No
P50991	TCPD	2,05	5,02	No	O43447	PPIH	1,91	2,91	No
Q15311	RBP1	2,04	3,12	Yes	Q9Y467	SALL2	1,91	2,89	No
O15031	PLXB2	2,04	2,35	No	Q9NX55	HYPK	1,91	3,25	No
Q9BZF1	OSBPL8	2,04	2,31	No	P14859	PO2F1	1,91	2,89	No
P62380	TBPL1	2,03	2,34	No	Q6UUV9	CRTC1	1,90	4,24	No
Q9Y3B9	RRP15	2,03	5,45	No	P62314	SMD1	1,90	5,04	No
Q96KQ7	EHMT2	2,03	3,26	Yes	Q9NYL2	MLTK	1,90	3,13	Yes
Q9UJC3	HOOK1	2,03	2,73	No	O43169	CYB5B	1,90	2,22	No
Q9HCS7	SYF1	2,03	7,10	No	Q9NPI6	DCP1A	1,90	3,90	Yes
P11171	41	2,03	4,50	No	Q86XN7	PRSR1	1,90	2,75	No
Q969J2	ZKSC4	2,03	1,75	No	Q10570	CPSF1	1,89	4,54	No
P31689	DNJA1	2,03	5,85	No	Q16890	TPD53	1,89	2,96	No
Q7Z3B4	NUP54	2,02	2,92	No	Q9Y3F4	STRAP	1,89	4,63	No
Q8ND24	RN214	2,02	3,20	No	P11274	BCR	1,89	2,53	No
P46736	BRCC3	2,01	4,35	Yes	P51610	HCFC1	1,89	3,61	Yes
Q9Y4Y9	LSM5	2,01	2,90	No	Q96PZ0	PUS7	1,88	2,42	No
Q8TAD4	ZNT5	2,01	3,62	No	Q9H2D6	TARA	1,88	2,19	No
Q9NZ32	ARP10	2,01	2,71	No	Q9H467	CUED2	1,88	3,88	No
Q9UPN6	SCAF8	2,01	3,74	No	Q15428	SF3A2	1,87	4,51	Yes
Q8NI35	INADL	2,00	2,23	No	Q8WXE0	CSKI2	1,87	2,47	No
Q9BT78	CSN4	2,00	4,28	No	Q9UPR3	SMG5	1,87	2,06	No
P82979	SARNP	2,00	3,84	No	Q8NFD5	ARI1B	1,86	2,69	No
Q8N6H7	ARFG2	1,99	2,00	No	O14776	TCRG1	1,86	5,38	No
O43768	ENSA	1,99	2,13	Yes	P55209	NP1L1	1,86	4,27	No
P62316	SMD2	1,99	2,98	No	Q96HR3	MED30	1,85	3,87	No
P78356	PI42B	1,99	3,27	No	Q8WXF1	PSPC1	1,85	3,57	No
Q9BS18	APC13	1,98	3,38	No	Q9UMS4	PRP19	1,85	5,77	No
Q3YEC7	RABL6	1,98	2,20	No	O60563	CCNT1	1,84	3,07	Yes
Q9Y5T5	UBP16	1,98	2,51	No	Q13263	TIF1B	1,84	4,35	No

Supplementary table 1 continued …

protein IDs	Gene names	Log2FC (NS1+Dox/ NS1-Dox)	-Log(P)	IRG gene
P62306	RUXF	1,83	3,50	No
Q8TBX8	PI42C	1,83	2,80	No
O95985	TOP3B	1,82	2,32	No
Q9Y2X7	GIT1	1,82	5,25	No
Q709C8	VP13C	1,79	3,48	No
Q9BRP1	PDD2L	1,79	2,82	No
P52948	NUP98	1,79	3,96	Yes
Q9Y4C8	RBM19	1,78	2,49	Yes
Q13428	TCOF	1,78	4,13	No
Q96QK1	VPS35	1,78	2,84	No
Q13029	PRDM2	1,77	4,35	Yes
O60503	ADCY9	1,77	5,02	No
Q9UBF2	COPG2	1,76	4,13	No
Q96JM7	LMBL3	1,76	3,02	No
Q8ND56	LS14A	1,76	4,35	No
P50750	CDK9	1,75	3,39	No
O94885	SASH1	1,74	3,29	Yes
P49588	SYAC	1,74	3,41	No
Q92733	PRCC	1,73	4,97	No
Q13416	ORC2	1,73	3,77	No
Q9H9A5	CNO10	1,73	4,90	No
Q96HC4	PDLI5	1,72	3,96	No
Q9UJA5	TRM6	1,72	3,46	No
Q7L014	DDX46	1,71	4,71	Yes
P38117	ETFB	1,71	3,53	Yes
Q9H9T3	ELP3	1,71	6,40	No
Q96DN5	TBC31	1,70	5,46	No
Q14444	CAPR1	1,70	3,67	No
P40763	STAT3	1,70	4,51	Yes
Q8N163	CCAR2	1,68	4,25	No
Q96I24	FUBP3	1,68	4,32	No
Q14C86	GAPD1	1,65	4,37	No
Q7L5N1	CSN6	1,64	5,12	No
Q14160	SCRIB	1,59	5,78	No

IRG = Interferon regulated gene

Supplementary table 2: NS2 proxeome identified by BioID

Majority protein IDs	Gene names	Log2FC (NS2+Dox/NS2-Dox)	-Log(P)	IRG gene	Majority protein IDs	Gene names	Log2FC (NS2+Dox/NS2-Dox)	-Log(P)	IRG gene
Q9H6R7	C2orf44	7,46	5,62	No	P48643	CCT5	3,95	7,96	No
P68032; P68133	ACTC1; ACTA1	6,48	1,70	No	Q9Y230	RUVBL2	3,93	7,64	No
Q9BVM2	DPCD	6,05	6,50	No	P50990	CCT8	3,91	8,35	No
O75153	CLUH	5,86	5,45	Yes	P52655	GTF2A1	3,88	3,29	No
Q96RG2	PASK	5,77	5,33	Yes	Q8IZP2; P50502; Q8NFI4	ST13P4; ST13; ST13P5	3,87	3,97	No
O14530	TXNDC9	5,69	7,19	No	P50991	CCT4	3,87	8,30	No
O60925	PFDN1	5,68	4,88	No	P78318	IGBP1	3,84	6,13	No
Q9NRA8	EIF4ENIF1	5,59	5,77	No	Q86W92	PPFIBP1	3,77	4,42	Yes
Q13371	PDCL	5,15	6,33	Yes	Q68CZ6	HAUS3	3,77	1,97	Yes
A8MVW0	FAM171A2	5,13	5,06	No	O75147	OBSL1	3,68	4,38	Yes
P61758	VBP1	4,86	6,44	No	Q96N67	DOCK7	3,67	3,10	No
Q9NZ52	GGA3	4,72	4,26	No	Q92551	IP6K1	3,65	3,17	Yes
Q8IVD9	NUDCD3	4,64	5,48	No	P31689	DNAJA1	3,60	6,98	Yes
O15212	PFDN6	4,57	5,45	No	A0JNW5	UHRF1BP1L	3,59	4,21	No
Q99471	PFDN5	4,57	8,05	Yes	Q6ZWJ1	STXBP4	3,57	3,89	No
P61962	DCAF7	4,56	1,76	No	P28070	PSMB4	3,56	6,42	No
Q9H2J4	PDCL3	4,54	6,37	No	P51648	ALDH3A2	3,55	4,80	Yes
Q5VUB5	FAM171A1	4,54	4,30	Yes	Q9NQC7	CYLD	3,52	3,04	Yes
Q86XP1	DGKH	4,46	6,15	No	Q6PI26	SHQ1	3,48	3,04	No
Q9P2F8	SIPA1L2	4,37	2,31	Yes	A6NKD9	CCDC85C	3,47	3,56	No
P49368	CCT3	4,28	6,68	Yes	A8MXV4	NUDT19	3,47	5,26	No
P17987	TCP1	4,28	7,62	Yes	O60884	DNAJA2	3,47	6,63	No
Q13464	ROCK1	4,27	4,01	No	Q8WVK7	SKA2	3,45	2,51	No
O94927	HAUS5	4,24	3,94	Yes	Q1MSJ5	CSPP1	3,45	3,66	No
Q9ULT8	HECTD1	4,23	2,71	No	Q96BD8	SKA1	3,43	6,57	No
Q9NQP4	PFDN4	4,21	2,03	No	Q9NRL3	STRN4	3,41	2,64	No
Q5XUX1	FBXW9	4,18	4,80	No	Q5EBL8	PDZD11	3,39	4,01	No
Q99832	CCT7	4,14	8,40	No	Q08AD1	CAMSAP2	3,39	5,70	Yes
Q9UPU7	TBC1D2B	4,14	6,20	Yes	Q9Y2Z0	SUGT1	3,36	4,95	No
Q9H3P7	ACBD3	4,12	3,60	No	Q9BZF3	OSBPL6	3,34	2,47	Yes
Q14126	DSG2	4,11	3,44	No	Q8IX90	SKA3	3,31	4,20	No
Q99615	DNAJC7	4,06	1,16	No	Q9Y4E1	FAM21C	3,31	3,73	Yes
Q9H425	C1orf198	4,03	1,88	No	O60566	BUB1B	3,30	4,94	Yes
Q96JH7	VCPIP1	4,02	4,01	Yes	Q8TCU4	ALMS1	3,27	2,25	No
P78371	CCT2	4,01	7,14	No	Q96AG4	LRRC59	3,25	3,29	No
O75665	OFD1	4,00	4,86	No	Q86TX2; P49753	ACOT1; ACOT2	3,25	1,39	No
Q92526	CCT6B	4,00	1,22	No	P49366	DHPS	3,24	3,13	No
Q9Y265	RUVBL1	3,99	7,43	No	P18827	SDC1	3,21	5,41	Yes
P40227	CCT6A	3,97	6,07	No	Q14596	NBR1	3,19	3,42	Yes
Q96MX6	WDR92	3,96	4,72	No	P19484	TFEB	3,18	2,77	Yes

Supplementary table 2 continued …

Majority protein IDs	Gene names	Log2FC (NS2+Dox/ NS2-Dox)	-Log(P)	IRG gene	Majority protein IDs	Gene names	Log2FC (NS2+Dox/ NS2-Dox)	-Log(P)	IRG gene
Q12800	TFCP2	3,17	5,05	No	Q99707	MTR	2,80	4,02	No
O95801	TTC4	3,17	1,21	No	Q9H089	LSG1	2,79	2,21	No
Q9BT25	HAUS8	3,16	4,15	No	Q6AI12	ANKRD40	2,77	3,78	No
P28290	SSFA2	3,15	3,74	Yes	P42694	HELZ	2,77	4,50	No
Q9HAU0	PLEKHA5	3,14	2,15	No	Q9UKD1	GMEB2	2,77	4,14	No
Q9Y6M7	SLC4A7	3,13	5,40	Yes	P49591	SARS	2,76	1,93	Yes
Q5T5Y3	CAMSAP1	3,13	1,13	Yes	Q9ULV0	MYO5B	2,74	1,53	Yes
P62310	LSM3	3,12	2,77	Yes	O43166	SIPA1L1	2,74	4,17	No
Q8IXH7	NELFCD	3,10	3,33	No	P20290	BTF3	2,73	1,55	No
Q9H6T3	RPAP3	3,09	4,68	No	Q9BRZ2	TRIM56	2,73	3,27	Yes
O76041	NEBL	3,09	1,72	Yes	O00459	PIK3R2	2,73	3,03	Yes
Q8IYB1	MB21D2	3,09	2,89	No	O14867	BACH1	2,72	3,35	Yes
P29317	EPHA2	3,08	4,81	Yes	Q8TAA9	VANGL1	2,72	3,99	No
Q9Y484	WDR45	3,05	3,57	Yes	Q96SU4	OSBPL9	2,71	2,26	Yes
Q96SN8	CDK5RAP2	3,05	4,70	No	Q96PY6	NEK1	2,71	1,70	No
P14735	IDE	3,04	1,45	No	Q86UW6	N4BP2	2,71	4,88	No
Q9P2S5	WRAP73	3,03	1,88	No	O15063	KIAA0355	2,70	2,05	No
Q9HB71	CACYBP	3,02	4,29	No	Q5VZ89	DENND4C	2,69	5,22	Yes
Q8N0Z3	SPICE1	3,01	4,37	No	P34741	SDC2	2,69	4,06	Yes
Q6XZF7	DNMBP	3,01	2,70	Yes	O60573	EIF4E2	2,68	3,23	No
Q9Y6U3	SCIN	3,00	1,59	Yes	Q96LT7	C9orf72	2,68	3,19	Yes
O43399	TPD52L2	2,99	3,20	No	O75170	PPP6R2	2,67	3,28	No
O43815	STRN	2,98	3,28	Yes	Q99733	NAP1L4	2,66	1,98	No
P51665	PSMD7	2,98	2,52	No	P16333	NCK1	2,65	1,62	Yes
Q504Q3	PAN2	2,95	1,86	No	P46108	CRK	2,64	5,24	No
Q96JK2	DCAF5	2,94	2,76	No	Q8TC07	TBC1D15	2,64	5,86	No
Q9UGP4	LIMD1	2,94	4,03	No	Q7Z4H7	HAUS6	2,63	6,37	No
Q9NZM3	ITSN2	2,92	1,68	No	O60503	ADCY9	2,59	2,39	No
O94763	URI1	2,92	3,93	No	Q8ND56	LSM14A	2,57	3,55	Yes
Q96K17	BTF3L4	2,90	2,95	No	Q9BXB4	OSBPL11	2,56	4,76	No
O95905	ECD	2,90	4,21	No	O14531	DPYSL4	2,56	2,01	Yes
Q9BQA1	WDR77	2,89	3,07	No	Q8NDI1	EHBP1	2,55	4,34	No
Q5JRA6	MIA3	2,87	3,66	Yes	Q15056	EIF4H	2,55	2,48	No
Q13625	TP53BP2	2,87	4,50	Yes	P62879; P62873; Q9HAV0	GNB2; GNB1; GNB4	2,54	5,08	No
P49023	PXN	2,87	3,08	No	P09936	UCHL1	2,54	1,70	No
Q12979	ABR	2,87	3,35	No	O43303	CCP110	2,54	2,72	No
Q2KHM9	KIAA0753	2,87	2,40	No	Q9ULL1	PLEKHG1	2,52	2,56	No
Q9P2D6	FAM135A	2,86	1,66	Yes	Q8IZ21	PHACTR4	2,52	5,99	Yes
Q9HCM4; Q9H329	EPB41L5; EPB41L4B	2,85	2,58	No	Q53EZ4	CEP55	2,52	2,61	Yes
Q9Y2K5	R3HDM2	2,83	2,72	No	Q92905	COPS5	2,52	1,63	No
P33240	CSTF2	2,81	4,22	No	P31948	STIP1	2,51	2,14	Yes

Supplementary table 2 continued …

Majority protein IDs	Gene names	Log2FC (NS2+Dox/ NS2-Dox)	-Log(P)	IRG gene	Majority protein IDs	Gene names	Log2FC (NS2+Dox/ NS2-Dox)	-Log(P)	IRG gene
Q96C36	PYCR2	2,49	4,53	No	Q6P1R3	MSANTD2	2,18	2,21	No
Q86UP3	ZFHX4	2,49	1,39	No	Q8NG31	CASC5	2,18	3,99	No
Q8NHM5	KDM2B	2,48	3,25	No	Q15276	RABEP1	2,18	3,40	No
Q9H0B6	KLC2	2,46	1,71	Yes	Q13017	ARHGAP5	2,18	1,60	No
Q04206	RELA	2,45	3,31	Yes	Q68DQ2	CRYBG3	2,17	4,01	No
Q8IW35	CEP97	2,44	2,61	No	Q9NVU0	POLR3E	2,17	1,71	No
Q9NZN5	ARHGEF12	2,44	1,65	No	Q96R06	SPAG5	2,16	2,15	No
O00750	PIK3C2B	2,43	2,50	Yes	Q9UKZ1	CNOT11	2,16	3,23	No
Q03164	KMT2A	2,42	1,65	No	O75487	GPC4	2,14	1,28	Yes
Q9NYL9	TMOD3	2,42	1,11	No	Q5T6F2	UBAP2	2,14	4,84	No
Q9NR28	DIABLO	2,41	1,62	No	P61289	PSME3	2,13	5,16	No
O00161	SNAP23	2,40	1,70	Yes	O60216	RAD21	2,13	4,65	No
Q5JSZ5	PRRC2B	2,40	2,04	Yes	Q14186	TFDP1	2,13	1,84	No
O14737	PDCD5	2,39	3,27	No	O75817	POP7	2,11	1,45	Yes
Q6Y7W6	GIGYF2	2,39	6,93	No	Q8NHV4	NEDD1	2,10	1,97	No
Q96BY7	ATG2B	2,38	5,93	No	Q9UNH7	SNX6	2,09	3,54	Yes
O95757	HSPA4L	2,36	2,11	No	Q96LB3	IFT74	2,09	3,09	Yes
Q5VT06	CEP350	2,34	1,62	No	Q9HA65	TBC1D17	2,09	3,36	No
O95817	BAG3	2,33	2,04	Yes	Q06190	PPP2R3A	2,08	2,22	Yes
P07476	IVL	2,33	0,94	No	P61160	ACTR2	2,08	5,10	No
Q9UJX5	ANAPC4	2,32	3,34	No	Q14157	UBAP2L	2,08	5,43	No
Q04721	NOTCH2	2,31	1,96	No	Q9NX08	COMMD8	2,07	3,58	No
Q92572	AP3S1	2,31	3,90	No	O15116	LSM1	2,07	2,16	No
Q8WVJ2	NUDCD2	2,31	4,80	No	O75381	PEX14	2,06	4,31	No
Q8IY67	RAVER1	2,30	1,90	Yes	Q15417	CNN3	2,05	4,73	No
Q96RL7	VPS13A	2,30	2,86	Yes	O75352	MPDU1	2,04	2,01	No
Q9P2D0	IBTK	2,30	3,96	No	Q8TEP8	CEP192	2,03	2,89	Yes
Q9H869	YY1AP1	2,29	2,26	No	Q9NNW5	WDR6	2,03	3,28	Yes
O75461	E2F6	2,29	1,91	No	Q9UNS2	COPS3	2,01	1,74	No
Q9NWS0	PIH1D1	2,28	3,05	No	Q15208	STK38	2,01	1,23	No
O94986	CEP152	2,27	3,16	Yes	Q5T5X7	BEND3	2,01	2,76	No
O75348	ATP6V1G1	2,27	1,33	No	Q9ULE6	PALD1	2,01	3,73	No
Q14318	FKBP8	2,26	2,54	No	Q99550	MPHOSPH9	2,00	2,08	Yes
Q9C0C2	TNKS1BP1	2,26	3,08	No	Q99614	TTC1	2,00	1,36	No
Q9Y266	NUDC	2,23	6,14	No	Q658Y4	FAM91A1	1,99	4,16	No
Q70CQ3	USP30	2,23	2,70	Yes	Q99961	SH3GL1	1,98	2,59	No
Q9NVX0	HAUS2	2,22	3,30	No	Q15370	TCEB2	1,97	1,72	No
P55036	PSMD4	2,22	3,19	No	Q9NWV8	BABAM1	1,97	3,15	No
P48163	ME1	2,21	4,49	Yes	Q01850	CDR2	1,97	2,78	Yes
Q99439	CNN2	2,21	1,62	No	Q8TF46	DIS3L	1,97	3,21	No
Q9UJX2	CDC23	2,21	5,48	No	Q9Y2H2	INPP5F	1,97	3,62	No
O43169	CYB5B	2,21	2,64	No	Q9UNH6	SNX7	1,96	1,96	No
P27986	PIK3R1	2,19	1,52	No	P54578	USP14	1,96	1,72	No

Supplementary table 2 continued …

Majority protein IDs	Gene names	Log2FC (NS2+Dox/ NS2-Dox)	-Log(P)	IRG gene	Majority protein IDs	Gene names	Log2FC (NS2+Dox/ NS2-Dox)	-Log(P)	IRG gene
P26358	DNMT1	1,94	1,61	No	P34932	HSPA4	1,73	3,15	Yes
Q9UPQ9	TNRC6B	1,94	3,52	Yes	Q0JRZ9	FCHO2	1,73	3,39	No
Q9P013	CWC15	1,93	4,04	No	O75534	CSDE1	1,72	5,27	Yes
Q8IWZ3	ANKHD1	1,93	5,31	Yes	P50579	METAP2	1,68	1,90	No
Q9Y3A3	MOB4	1,92	1,67	No	Q9HDC5	JPH1	1,67	2,11	Yes
Q5R372	RABGAP1L	1,91	4,09	Yes	Q9C0C9	UBE2O	1,66	4,88	No
Q96AY4	TTC28	1,91	3,10	Yes	P55196	MLLT4	1,66	6,33	No
Q6P1M3	LLGL2	1,90	2,74	No	Q6W2J9	BCOR	1,66	3,47	No
Q8TBA6	GOLGA5	1,90	2,35	No	P25054	APC	1,66	4,01	Yes
Q96JQ2	CLMN	1,90	1,32	Yes	Q5H9R7	PPP6R3	1,65	4,92	No
Q9NRY5	FAM114A2	1,90	1,60	No	Q9Y6Y8	SEC23IP	1,65	2,55	No
Q6MZP7	LIN54	1,88	3,22	No	Q8N8S7	ENAH	1,65	2,72	No
Q9BUR4	WRAP53	1,88	2,70	No	Q9UBW8	COPS7A	1,64	2,54	No
Q9C0B7	TANGO6	1,88	1,78	No	O14974	PPP1R12A	1,64	4,75	No
P59780	AP3S2	1,88	2,32	Yes	Q9BVA0	KATNB1	1,63	2,46	Yes
Q9UPY3	DICER1	1,88	3,39	Yes	Q14145	KEAP1	1,63	6,66	No
Q96RT1	ERBB2IP	1,88	4,93	No	Q9H6D7	HAUS4	1,63	3,25	No
Q3YEC7	RABL6	1,87	4,13	No	O43776	NARS	1,62	2,55	Yes
O75113	N4BP1	1,87	4,07	Yes	Q92625	ANKS1A	1,62	3,45	Yes
Q9HD26	GOPC	1,86	1,61	No	Q02790	FKBP4	1,61	4,51	No
O43237	DYNC1LI2	1,86	1,43	No	Q15154	PCM1	1,61	7,63	No
Q08378	GOLGA3	1,85	2,91	Yes	O60292	SIPA1L3	1,61	2,48	Yes
P61158	ACTR3	1,85	1,59	No	C4AMC7; Q6VEQ5	WASH3P; WASH2P	1,61	2,49	No
Q8WU90	ZC3H15	1,85	2,39	No	Q5TH69	ARFGEF3	1,60	3,43	No
Q9UHY1	NRBP1	1,83	1,54	No	P55010	EIF5	1,58	3,73	No
O15067	PFAS	1,82	5,02	No	O43684	BUB3	1,57	4,17	No
P49189	ALDH9A1	1,81	1,46	Yes	Q15652	JMJD1C	1,55	3,99	No
Q13501	SQSTM1	1,81	4,49	No	P22234	PAICS	1,54	4,56	No
Q659C4	LARP1B	1,80	4,79	No	Q9NR09	BIRC6	1,54	3,85	No
Q5T5U3	ARHGAP21	1,79	4,68	No	P49915	GMPS	1,54	3,79	No
Q92599	SEPT8	1,78	2,14	No	Q96C92	SDCCAG3	1,53	3,75	No
O75179	ANKRD17	1,77	4,53	No	P62333	PSMC6	1,53	5,31	No
Q12768	KIAA0196	1,77	3,52	No	Q7Z739	YTHDF3	1,53	4,18	No
Q96M89	CCDC138	1,76	2,26	No	Q9H1A4	ANAPC1	1,51	3,93	No
Q92598	HSPH1	1,75	4,11	No	O60502	MGEA5	1,48	4,04	No
Q8N0X7	SPG20	1,74	6,65	Yes	Q9BZH6	WDR11	1,47	4,12	No
Q8IVW6	ARID3B	1,74	3,58	No	Q07157	TJP1	1,44	5,48	No

IRG = Interferon regulated gene

Supplementary table 3: MYLK4 proxeome identified by BioID

Majority protein IDs	Gene names	Log2FC (MYLK4+Dox/ MYLK4-Dox)	-Log(P)	Shared	IRG gene
Q6WKZ4	RAB11FIP1	6,79	6,66		Yes
Q15811	ITSN1	4,90	5,09	NS1, NS2	Yes
Q7Z4S6	KIF21A	4,87	5,36	NS2	No
Q641Q2	FAM21A	4,81	4,56	NS1, NS2	No
Q9BRR8	GPATCH1	4,81	6,15	NS1, NS2	No
Q6ZU35	KIAA1211	4,67	6,28	NS1	No
Q7Z569	BRAP	4,60	2,31	NS1, NS2	No
Q9Y4E8	USP15	4,60	4,47	NS1, NS2	Yes
Q8TE02	ELP5	4,51	4,38	NS1	No
Q96EB1	ELP4	4,49	3,82	NS1, NS2	No
Q9NRY4	ARHGAP35	4,44	6,65	NS1	Yes
Q96CT7	CCDC124	4,36	3,93		No
Q9UPN7	PPP6R1	4,33	5,00	NS1, NS2	No
O15084	ANKRD28	4,33	2,50	NS1, NS2	Yes
P62140	PPP1CB	4,32	4,81	NS1, NS2	Yes
P98175	RBM10	4,30	5,65	NS1	No
Q9Y4P8	WIPI2	4,22	3,36	NS1	Yes
Q8TEV9	SMCR8	4,19	6,36	NS1, NS2	No
Q9UPN4	CEP131	4,18	4,52	NS1, NS2	No
Q9UK76	HN1	4,17	4,88	NS1	Yes
O95425	SVIL	4,16	3,86	NS1, NS2	Yes
Q15691	MAPRE1	4,13	5,69	NS1	No
Q15398	DLGAP5	4,11	3,58	NS1, NS2	Yes
Q8IUD2	ERC1	3,98	3,87	NS1, NS2	No
Q9UHV9	PFDN2	3,97	3,18	NS1, NS2	No
O95721	SNAP29	3,96	5,43	NS1	No
O75935	DCTN3	3,94	4,42		No
P51114	FXR1	3,91	4,66	NS1	No
Q9UPQ0	LIMCH1	3,90	5,28	NS1	Yes
Q96F24	NRBF2	3,88	4,33	NS1, NS2	Yes
Q5JSH3	WDR44	3,88	6,04	NS1	Yes
Q8TDM6	DLG5	3,88	3,50	NS1, NS2	No
P05386	RPLP1	3,87	5,03		Yes
O75717	WDHD1	3,84	4,24	NS1	No
O60664	PLIN3	3,83	4,51	NS1	No
Q9H7E2	TDRD3	3,79	4,92	NS1, NS2	Yes
P55081	MFAP1	3,74	5,15	NS1	No
Q9H0L4	CSTF2T	3,74	3,92	NS1	Yes
C9JLW8	FAM195B	3,66	3,87	NS1, NS2	No
O95372	LYPLA2	3,58	4,26	NS1	No
P20340; Q9NRW1	RAB6A; RAB6B	3,46	4,76		No

Supplementary table 3 continued …

Majority protein IDs	Gene names	Log2FC (MYLK4+Dox/ MYLK4-Dox)	-Log(P)	Shared	IRG gene
Q8IZH2	XRN1	3,42	4,18	NS1, NS2	Yes
Q13573	SNW1	3,32	4,60	NS1	No
P63208	SKP1	3,28	6,29		No
P35269	GTF2F1	3,22	4,94	NS1	No
Q8IWC1	MAP7D3	3,21	4,88	NS1, NS2	Yes
Q9UNE7	STUB1	3,21	4,68	NS1, NS2	No

IRG = Interferon regulated gene

Supplementary table 4: NS1 interactome identified by affinity purification

Protein IDs	Gene names	Log_2 (NS1-Flag/EV)	-LOG (P-value)
P63208	SKP1	2,72	2,50
Q9BZF1	OSBPL8	2,08	2,64

Supplementary table 5: NS2 interactome identified by affinity purification

Protein IDs	Gene names	Log_2 (NS2-Flag/EV)	-LOG (P-value)
P19105;O14950;P24844	MYL12A;MYL12B;MYL9	3,36	2,58
Q03135	CAV1	3,12	5,48
O94832	MYO1D	2,99	1,31
O15511	ARPC5	2,86	3,55
Q9Y4I1	MYO5A	2,85	1,43
P08754	GNAI3	2,69	0,75
Q14573	ITPR3	2,68	1,35
Q92614	MYO18A	2,67	1,61
Q9BPX5	ARPC5L	2,59	1,33
O95425	SVIL	2,57	1,50
Q14254	FLOT2	2,57	2,85
Q96IZ0	PAWR	2,55	1,20
Q9UBQ5	EIF3K	2,48	4,99
P35579	MYH9	2,44	1,81
Q6ZVM7	TOM1L2	2,41	4,88
Q7Z406	MYH14	2,40	1,65
P53985	SLC16A1	2,39	1,31
O96008	TOMM40	2,34	0,97
P63000;P60763;P15153	RAC1;RAC3;RAC2	2,33	1,26
Q96PY5	FMNL2	2,32	1,85
O60716	CTNND1	2,31	4,52
P14649	MYL6B	2,30	1,88
Q5T9A4	ATAD3B	2,30	1,31
Q5VT25	CDC42BPA	2,28	2,78

O43251;Q9NWB1	RBFOX2;RBFOX1	2,27	0,90
Q9P0K7	RAI14	2,23	1,72
O75431	MTX2	2,23	1,88
P61158	ACTR3	2,22	2,26
Q9UPQ0	LIMCH1	2,22	2,70
Q8WWI1	LMO7	2,21	1,66
P60660	MYL6	2,21	1,84
P09497	CLTB	2,19	1,47
Q9UBX3	SLC25A10	2,18	0,76
Q69YQ0	SPECC1L	2,17	1,86
P59998	ARPC4	2,15	2,33
Q9NVH1	DNAJC11	2,14	1,55
P35580	MYH10	2,14	1,67
Q9Y608	LRRFIP2	2,13	1,15
Q9UM54	MYO6	2,12	1,76
P09493	TPM1	2,12	1,49
P07947	YES1	2,11	1,52
Q14677	CLINT1	2,10	1,08
O15145	ARPC3	2,07	2,07
O75955	FLOT1	2,04	2,58
Q14571	ITPR2	2,03	1,73
P61160	ACTR2	2,03	1,91
Q6WCQ1	MPRIP	2,01	1,56
O15144	ARPC2	1,98	1,79
Q96N67	DOCK7	1,97	3,01
Q96SB3	PPP1R9B	1,96	1,39
Q9ULV0	MYO5B	1,93	2,42
O75477	ERLIN1	1,90	1,57
O15143	ARPC1B	1,89	1,90
Q12965	MYO1E	1,88	1,90
Q92747	ARPC1A	1,86	1,81
O43795	MYO1B	1,86	1,43
Q15370	TCEB2	1,84	1,03
Q9HBL7	PLGRKT	1,83	1,03
Q14126	DSG2	1,81	1,10
Q15286	RAB35	1,80	1,67
O00159	MYO1C	1,76	1,25
P80723	BASP1	1,75	1,11
Q13045	FLII	1,73	3,54
Q9Y281	CFL2	1,72	1,47
Q9ULV4	CORO1C	1,70	1,54
Q9NVI7	ATAD3A	1,68	1,60
P62873	GNB1	1,67	1,23
P14923	JUP	1,67	1,30
P28288	ABCD3	1,67	2,61
P63096	GNAI1	1,67	1,43

P01893; …	HLA-H;HLA-B;HLA-A;HLA-C	1,66	1,55
P61421	ATP6V0D1	1,66	1,29
O95782	AP2A1	1,65	3,46
Q96C19	EFHD2	1,65	1,39
Q9NQX4	MYO5C	1,64	1,56
O14974	PPP1R12A	1,64	1,66
Q9Y512	SAMM50	1,63	2,80
Q9Y277	VDAC3	1,61	1,12
Q16891	IMMT	1,61	1,49
Q9NYL9	TMOD3	1,60	1,64
P06753	TPM3	1,60	1,63
P04899	GNAI2	1,56	1,33
Q9UBI6	GNG12	1,54	1,15
P67936	TPM4	1,53	2,00
Q9NX63	CHCHD3	1,51	1,41
O00161	SNAP23	1,50	1,33
P62140	PPP1CB	1,47	3,56
P47756	CAPZB	1,47	2,14
P62879;Q9HAV0	GNB2;GNB4	1,44	1,38
O94905	ERLIN2	1,42	1,90
Q12792	TWF1	1,41	1,79
P11166	SLC2A1	1,41	1,51
P50151	GNG10	1,40	2,01
O60237	PPP1R12B	1,39	1,22
P68133;P68032;P63267;P62736	ACTA1;ACTC1;ACTG2;ACTA2	1,39	1,54
P63092;Q5JWF2	GNAS	1,39	1,41
Q92667	AKAP1	1,39	1,58
O15260	SURF4	1,37	2,42
O75531	BANF1	1,36	2,54
Q9UJZ1	STOML2	1,34	1,46
Q14258	TRIM25	1,34	1,45
O60784	TOM1	1,34	1,56
P35613	BSG	1,33	1,71
P47755	CAPZA2	1,32	1,91
Q9ULJ8	PPP1R9A	1,31	1,94
P23528	CFL1	1,31	2,25
P29992;O95837	GNA11;GNA14	1,28	1,72
O43491	EPB41L2	1,27	2,48
P63261	ACTG1	1,26	1,60
P38606	ATP6V1A	1,25	2,94
Q14160	SCRIB	1,22	2,51
P52907	CAPZA1	1,20	1,93
O75695	RP2	1,20	1,92
P35221	CTNNA1	1,19	2,24

Supplementary table 6: MYLK4 interactome identified by affinity purification

Protein IDs	Gene names	Log_2 (Flag-MYLK4-Myc/EV)	-LOG (P-value)
Q86YV6	MYLK4	10,15	6,44
P42677	RPS27	4,05	4,45
O95816	BAG2	3,11	5,30
P63208	SKP1	2,43	2,51
Q5SSJ5	HP1BP3	2,11	1,75
Q9NTJ3	SMC4	2,03	2,18
Q9NRX1	PNO1	1,70	1,20
Q9UNE7	STUB1	1,60	4,79
Q16543	CDC37	1,40	3,45
P01834	IGKC	1,22	4,34
P11142	HSPA8	1,05	4,57

Part IV:
General conclusions, discussion and future perspectives

RSV is an important human pathogen

RSV is a significant treat for human health and is recognized as the most important cause of acute lower respiratory tract infection (ALRI) in infants worldwide. For 2005, a total of 34 million ALRIs in children below 5 years of age were estimated to be due to RSV globally, which represented about 22% of all ALRIs in this age group [1]. Of these RSV-associated ALRIs, about 66,000-199,000 cases were estimated to have resulted in a fatal outcome, of which 99% occurred in developing countries. In recent years, the elderly have been recognized as a second major risk group for the development of severe RSV disease [2]. Although RSV was discovered more than half a century ago with numerous vaccine candidates being tested since then, there is still no licensed RSV vaccine, except for palivizumab, a recombinant monoclonal antibody directed against the viral fusion protein. Palivizumab (brand name Synagis®) is a humanized mouse monoclonal antibody that can neutralize RSV *in vitro* by binding to the F protein and is approved for prophylactic use in infants at increased risk of developing severe RSV disease [3]. Protection induced by Palivizumab, however, is only partial and its high cost does not allow systemic use.

Moreover, an effective therapeutic drug against RSV is currently lacking. Currently, different promising candidate small compound drugs are in clinical trials, *e.g.* the RSV-F targeting small compounds GS-5806 (phase IIa completed) [4, 5], JNJ-53718678 (phase IIa completed) [6, 7], AK0529 (setting-up phase II) [8] and BTA585 (phase IIa completed) [9] and the RSV-polymerase targeting small compound ALS-008176 (setting-up phase IIb) [10, 11]. Another promising strategy for the development of a therapeutic drug against RSV is the use of the variable domain of heavy-chain only antibodies (VHH) found in *e.g.* camelids, which is also named a nanobody®. A trivalent VHH specific for the pre- and post-fusion conformation of the F protein, ALX-0171, is currently also tested in Phase II clinical trials. Daily inhalation of ALX-0171 was safe, reduced the viral load in the respiratory tract and ameliorated symptoms in infants up to 23 months of age that were hospitalized due to RSV infection (phase IIa) [12, 13]. Our group recently described a highly potent RSV-neutralizing VHH that specifically binds to the pre-fusion conformation of the F protein and looks a very promising candidate for further clinical development [14].

Elucidating host-RSV interactions may identify novel strategies to combat RSV

To date, nearly all approved antiviral drugs to treat 9 human viral diseases have been designed to directly target a viral component [15]. On the downside, use of such drugs can lead to the emergence of drug-resistant viruses. Generally, viral RNA-dependent RNA polymerases lack proofreading activity, leading to relatively high mutation rates in RNA viruses. These high mutation rates combined with massive viral replication are an ideal source for the development of drug-resistant strains, necessitating a labour-intensive continuous search for new antiviral drugs. Targeting a host protein that is important for viral replication may strongly reduce the risk of developing drug-resistant strains. For RSV, for example, a drug called Danirixin that can modulate the activation and migration of neutrophils, a hallmark of RSV-associated disease, was evaluated in a phase I clinical trial [16]. Danirixin is a small compound inhibitor of the chemokine receptor CXCR2 [17]. Results of this trial have not (yet)

been published. Of course, not every host protein is equally druggable. A recent estimate revealed that 4,479 (~22%) of the 20,300 human protein-coding genes would be druggable [18], whereas about 10% of the genes is disease-related [19]. Druggable genes and disease-related genes, however, do not necessarily overlap, suggesting that only a small percentage of human genes would be a candidate drug target for treating human (infectious) diseases. Identifying appropriate host proteins as candidate drug targets to treat viral infections requires a thorough knowledge on the interplay between viruses and their host. For RSV this knowledge is currently rather limited. For example, there is still no consensus on the RSV receptor(s) with several candidate receptors having been proposed such as heparan sulphate [20, 21], surfactant protein A [22, 23], annexin II [24] and CX3CR1 [25] for the RSV-G protein and ICAM-1 [26], nucleolin [27] and the EGFR [28] for the RSV-F protein. Yet, it is unclear which of these host molecules are also used as a receptor *in vivo*. What route RSV uses to enter the cell after receptor binding is also still debated [29-31]. Other unanswered questions amongst many others include what signal triggers the F protein to undergo a conformational change from the pre - to the post-fusion form during entry, how exactly is the matrix layer uncoated following fusion between the viral and host membrane and which mechanism(s) are used by RSV to spread from cell to cell.

Elucidating host-RSV interactions may identify novel strategies to increase RSV yields

RSV replication in cell cultures generally yields rather low amounts of infectious virus, which can be further reduced in the case of attenuated strains. A better understanding of the role of host proteins during RSV infection could aid in the identification of host proteins that counteract RSV infections. Such host proteins could be considered as drug targets to increase the yield of infectious RSV virions in cell culture, *e.g.* for the production of live-attenuated vaccine strains. Four live-attenuated RSV strains are currently in clinical trials to evaluate their safety and immunogenicity as candidate vaccines, *i.e.* MEDI-559 (phase I/IIa completed) [32], RSV MEDI ΔM2-2 (phase I completed) [33], RSV cps2 (phase I completed) [34] and RSV ΔNS2 Δ1313/1314L (setting-up phase I) [35].

Strategies to identify host proteins as drug targets that can reduce RSV replication

Basically, two different strategies can be used to identify host proteins involved in viral infections as candidate drug targets on a systemic scale. A first strategy is to use large libraries of small compounds in cell culture to select hits that either reduce or increase viral infection. Advantages of this strategy are that structurally-related primary hits can serve as a direct starting point for further development of candidate drugs. Many toxic compounds are also eliminated early on during such screens. A disadvantage of this strategy is that identifying the exact target, which can be either a viral or a host protein or even non-protein molecules, may be challenging. Moreover, host proteins involved in a viral infection that are not targeted by the current small compound libraries may be missed, whereas such proteins may become a drug target in the future with the development of novel types of drugs. In recent years, several high-throughput screens with small compound libraries have been reported for RSV. Whereas most screens identified antiviral compounds without evidence of the target [36-41], others could identify compounds that inhibited the viral polymerase, M2-1 and P proteins [42-45]. Two

screens identified antiviral compounds targeting host pathways. Bonavia and colleagues identified two compounds that inhibited the de novo pyrimidine biosynthesis pathway, which reduced RSV replication *in vitro* [46]. One of these two compounds was subsequently tested in cotton rats, an animal model for RSV infection, however, no reduction in viral titer was observed. Laganas and colleagues identified an antiviral compound that induced a cell cycle arrest for which no escape viruses could be isolated [43]. However, safety issues for this compound may arrest further clinical development.

A second strategy is to first identify host proteins involved in viral replication and subsequently examine the druggability of these proteins. Investigating the role of a large number of host proteins in parallel during a viral infection can be achieved by different techniques, *e.g.* siRNA-mediated knockdown, CRISPR/Cas9-mediated knockout and interactome analysis of the viral proteins. For RSV, large-scale gene by gene knockdown or knockout screens have not yet been published. Interactome studies on the other hand have been performed for the NS1 protein [47], the M protein [48] and the polymerase complex [49]. These studies revealed a role for cell-cycle regulators, cofilin-1, caveolin-2, the zinc finger protein ZNF502 and the HSP90 and 70 families during RSV infections.

Study of phosphorylation-dependent signaling pathways activated during RSV infection

In this thesis, we have focused on phosphorylation-dependent signaling pathways that are activated and possibly exploited by RSV infection to try to identify novel host proteins as candidate drug targets for RSV infections and to better understand the complex interplay between RSV and the host. Phosphorylation-dependent signaling is involved in basically every cellular process and the enzymes regulating phosphorylation, kinases and phosphatases, are generally considered to have high druggability properties. This is highlighted by the fact that more than 37 kinase inhibitors are currently approved by the United States food and drug administration, with a large number of these inhibitors being approved in the last decade [50]. To study phosphorylation-dependent signaling pathways we have performed two high-throughput screens in parallel.

A RNA interference screen to identify human kinases involved in RSV replication

First, we knocked down each human kinase one-by-one by using 714 pools of 4 siRNAs in a model lung epithelial cell line, A549 cells. These cells are very permissive for RSV. We evaluated the effect of the knockdown on RSV replication by staining RSV plaques formed by multiple rounds of infection. We opted for such a labour intensive read-out because plaque formation and plaque size is quantifiable and grasps multiple rounds of RSV infection *in vitro*. As controls, we knocked down the expression of three human proteins, nucleolin, PAK1 and CLT B, and the RSV nucleoprotein in parallel. In line with published results, we observed a reduced replication of RSV upon knockdown of PAK1 and CLT B and a near complete abolishment of RSV replication upon knockdown of the nucleoprotein [30, 51]. In contrast to literature, however, we did not observe a reduction in RSV replication upon knockdown of nucleolin [27]. Although we cannot exclude that this striking difference is caused by differences in the used cell lines (A549 vs 1HAEo- cells) and/or RSV strains (RSV-A2 vs a recombinant GFP expressing RSV

strain derived from RSV-A2), our results suggest that nucleolin is not used as a cellular receptor for RSV or is important during RSV infection. This is in agreement with the observation that recombinant RSV-F protein fails to interact with recombinant nucleolin, even at high concentrations (personal communications with Dr. J. Mclellan).

Of the 714 human kinase-directed siRNA pools tested, 104 reduced or increased the RSV plaque size, suggesting that the expression levels of these kinases support or counteract RSV replication, respectively. These 104 kinases were subsequently tested in a RSV replication kinetics experiment. Ten kinases that either reduced or increased both RSV plaque size and - titer were selected for further validation by deconvolution of the siRNA pool in 4 different siRNAs per kinase. For 8 of the 10 kinases, however, we only observed an affected plaque size upon transfection of maximum 1 siRNA. These results highlight that off-target silencing by siRNAs may be a serious treat for the correct interpretation of primary hits in siRNA screens, even when a pool of 4 siRNAs is used to reduce the concentration (and thus the likelihood of off-target effects) of each individual siRNA. Despite some reports of the identification of false positive results in RNAi screens [52, 53], this problem is likely underestimated as the scientific community remains eager to publish positive results and "negative" results are perceived as difficult to publish. For 2 kinases, IRAK3 and MYLK4, however, we observed a reduced plaque size by at least 2 different siRNAs, suggesting that on-target silencing of these kinases caused the reduced plaque size. Endogenous expression at the mRNA level was, however, only detected for MYLK4 and not for IRAK3, which is in line with the restricted expression of IRAK3 in monocytes and macrophages mainly [54]. In addition, issues of reproducibility made us conclude that the initially observed reduction in RSV plaque size upon IRAK3 knockdown was likely not caused by on-target silencing of IRAK3 (compare figure 14A with 19 from chapter V). We also excluded that the IRAK3-targeting siRNAs caused a reduction of the cellular metabolism or induced type I IFNs and as such could have resulted in a reduction in RSV plaque size. Sequence-dependent off-target silencing of host genes in a miRNA-like manner is currently the most plausible explanation for the reduced RSV plaque size that we observed with the IRAK3-targeting siRNA pool from Dharmacon.

For MYLK4, we observed a reduced RSV plaque size and - titer upon knockdown by a pool of 4 siRNAs. Subsequent pool deconvolution showed that RSV plaque size can be reduced by at least 2 different siRNAs in two sources of A549 cells, but not in HeLa or Hep-2 cells. In future experiments, we could investigate by RT-PCR if MYLK4 is expressed in HeLa and Hep-2 cells. Possibly, MYLK4 expression is absent in HeLa and Hep-2 cells, hence explaining why no reduction of RSV plaque size was observed in these cells. In addition to the laboratory strain RSV-A2, we also observed a reduction of plaque size for other RSV strains, both laboratory strains and clinical isolates of both A and B subtypes, by at least 2 different MYLK4-targeting siRNAs. Similar to the IRAK3-targeting siRNAs, we did not observe a reduction in the cellular metabolism or an induction of type I IFNs, which could have contributed to the reduced RSV plaque size upon transfection of MYLK4-targeting siRNAs. At first sight, these results suggest that MYLK4 is important for RSV replication/spreading in A549 cells in a strain-independent manner. RSV was recently shown to induce the formation of filopodia, thin cell protrusions containing actin filaments, as a way to spread progeny virus to uninfected cells in the proximity [55]. Induction of

filopodia appears specific for RSV infections in A549 cells at first glance, as the viruses PIV3 and hMPV and the cell lines Calu-3 and Vero did not induce these filopodia. Currently, we are setting-up experiments with confocal microscopy to detect these filopodia. We are now specifically interested if the length of these filopodia is reduced upon transfection of the MYLK4-targeting siRNAs, which could explain the reduced RSV plaque size. In particular, we wonder if these filopodia are also induced upon RSV infection of confluent A549 cells, which was the starting condition of our siRNA transfection/RSV infection protocol.

A number of observations, however, suggest that the reduced RSV plaque size upon transfection of the MYLK4-targeting siRNAs could be due to off-target effects. First, MYLK4-targeting siRNAs from another source (Qiagen) did not reduce RSV plaque size. Although these siRNAs were (somewhat) less efficient compared to the original siRNAs from Dharmacon to reduce endogenous MYLK4 mRNA, some of these siRNAs more strongly reduced overexpressed MYLK4 at the protein level. Secondly, we were unable to restore normal RSV plaque formation by rescuing MYLK4 expression. Lastly, CRISPR/Cas9 generated A549 cells presumed to carry a full knockout of MYLK4 allowed normal RSV plaque formation. Confirmation of the absence of MYLK4 protein expression in the latter cells, however, has been hampered by the fact that we have not been able to detect endogenous MYLK4 protein by western blotting or immunofluorescence. A targeted mass spectrometry-based detection of MYLK4 may ultimately prove if these cells indeed lack any MYLK4 protein expression. To investigate possible off-target silencing induced by MYLK4-targeting siRNAs, we have recently performed two independently repeated RNA sequencing experiments. Preliminary analysis of these RNAseq results already showed that several hundreds of genes are deregulated, mostly downregulated, upon transfection of MYLK4-targeting siRNAs. Even between two siRNAs designed to reduce complementarity with human mRNAs as much as possible, several hundreds of genes were deregulated. These results suggest that, although possible for some deregulated genes, secondary effects of MYLK4 knockdown do not explain all the deregulated genes upon transfection of MYLK4-targeting siRNAs. Currently, we are looking into the overlap between both RNA sequencing experiments to identify common patterns in this deregulation. Although complementarity between the siRNA seed sequence and human gene 3' UTR regions is a main driver of off-target silencing [56-58], other factors such as the thermostability of the seed-3'UTR match, the melting temperature of the adjacent non-seed region and the GC content of the corresponding sequence in the 3'UTR region have been shown to play a role [59-61]. In the near future, we will investigate if these parameters indeed contribute to the off-target silencing induced by the MYLK4-targeting siRNAs and if possible other parameters also contribute. We plan to publish the results of the kinase knockdown screen, thereby highlighting the risk of false positive results in large scale RNAi experiments. We will reinforce our message by focussing on the RNAseq results that identified widespread off-target silencing by siRNAs. In the past, siRNA-mediated off-target effects have mainly been investigated by microarray experiments. We believe that our RNAseq data will provide deeper insights into the off-target silencing effects of siRNAs.

In conclusion, we obtained evidence that MYLK4 is a kinase that is important for RSV plaque formation and replication. However, the control experiments that we have performed to try to confirm that MYLK4 mRNA downregulation results in impaired RSV replication are not conclusive and thus this "hit" may represent a false-positive result due to off-target silencing induced by the MYLK4-targeting siRNAs.

A phosphoproteomics study of RSV infection

In parallel to the siRNA-mediated knockdown screen of the human kinome, we performed a phosphoproteomics screen at an early time point after RSV infection in A549 cells. To our knowledge, this is the first unbiased screen to identify host protein (de)phosphorylations during RSV infection. We were able to identify and quantify 3,220 different human proteins and 3 viral proteins. Out of 1,933 human proteins, we could identify and quantify 4,996 phosphosites. Label-free quantification of the phosphosites and the corresponding protein revealed 8 RSV-induced phosphorylation events and 13 RSV-induced dephosphorylation events. Some of these (de)phosphorylation events were identified on di- or tri-phosphorylated peptides, which made it hard to correctly assign the exact phosphosite modulated by RSV within those peptides. For these RSV-modulated phosphorylation events it could be considered to generate expression vectors encoding the corresponding protein with single point mutations at the possible phosphosites identified in our screen. Expression of these mutant proteins in cells followed by a RSV infection could unravel which site is exactly (de)phosphorylated upon RSV infection. A major bottleneck to validate the identified phosphorylation events was the lack of commercially available phosphosite-specific antibodies. As a consequence, we tried to validate RSV-induced (de)phosphorylation of a subset of the proteins by electrophoretic mobility shift assays. This technique, however, does not work for every protein and should be tested empirically. Of the 8 proteins tested, we could detect expression of 5 proteins by western blotting of which only 2, CTTN and RPS6, showed a mobility shift upon phosphatase treatment. Of these 2 proteins, we confirmed a RSV-induced phosphorylation of CTTN, in line with previous observations [62]. As phosphosite-specific antibodies are more straightforward to validate stimulus-induced (de)phosphorylation events, we may consider to generate these in-house in the future. Peptides carrying the identified phosphosites could be synthesized and subsequently used for immunizing rabbits. Polyclonal rabbit serum could then be tested on the phosphorylated peptide and a non-phosphorylated peptide counterpart as negative control to determine the phosphosite-specificity of the serum. In case phosphosite-specific antibodies can be isolated, it will be interesting to determine if the RSV-induced (de)phosphorylations occur with other RSV strains, both laboratory and clinical RSV isolates of both subtype A and B. Alternatively, we could also investigate the significance of the RSV-induced (de)phosphorylations by testing inhibitors of the predicted upstream kinases and/or phosphatases. Redundancy in the predicted kinases, however, may complicate such an analysis.

Some interesting overlaps between the siRNA-mediated knockdown screen and the phosphoproteomics screen were identified. For example, knockdown of PRPF4B resulted in an increased RSV plaque size in both knockdown screens, yet, we did not observe an increased RSV titer,

so this kinase was not investigated further. In the phosphoproteomics screen we identified a RSV-induced dephosphorylation of PRPF4B at Ser-387 or Ser-381. PRPF4B is a kinase that is important for the assembly of human spliceosomal B complexes by phosphorylating PRP6 and PRP31 [63]. So our results suggest a possible role for PRPF4B during RSV infection, which may affect splicing of host genes. Another possible interesting link is that MYLK1 kinase interacts with CTTN and NAA10 [64, 65], two proteins that we identified in our phosphoproteomics screen with a RSV-induced phosphorylation and - dephosphorylation, respectively. Moreover, PTK2B phosphorylation is regulated by MYLK1 and the phosphatase PTPN12, which was dephosphorylated at Thr-587 upon RSV infection [66]. Although we did not identify MYLK1 in the kinase knockdown screen, which is clearly expressed in A549 cells according to the RNAseq data, we identified MYLK4 as a possible kinase involved in RSV replication in A549 cells. In future experiments, it could be interesting to test if MYLK4 also interacts with CTTN and/or NAA10. At first glance, interaction between CTTN and MYLK4 is unlikely, as the domains in MYLK1 important for cortactin binding are not present in MYLK4 [64].

In conclusion, we identified 21 RSV-induced (de)phosphorylation events. RSV-induced phosphorylation of CTTN was confirmed by an electrophoretic mobility shift assay. Phosphosite-specific antibodies may help confirming the other identified (de)phosphorylation events.

Interactome analysis of the non-structural proteins of RSV

RSV encodes two non-structural proteins with very potent activities to suppress type I and III IFN responses at different levels. NS1 and NS2 function individually and synergistically to suppress the induction and signaling of type I and III IFNs. Moreover, recent evidence indicates that NS1 expression degrades the ISG OASL, highlighting that the NS proteins may also directly target ISGs [67]. To exert these diverse functions, it is believed that the NS proteins must interact with many host proteins. To better understand the biology of the NS proteins and to identify interacting host proteins that could serve as drug targets, we analyzed the interactomes of the NS proteins. Therefore, we used three complementary PPI mapping techniques, BioID, Virotrap and affinity purification. Candidate interactors of NS1 and NS2 identified by these techniques were analyzed by pathway analysis tools to detect families of proteins or pathways that could be manipulated by the NS proteins. BioID revealed that nearly all members of the cleavage and polyadenylation of precursor mRNA pathway were present in the NS1 proxeome, suggesting that NS1 may manipulate the processing of host mRNAs in the nucleus by interacting with one or more members of this pathway. To validate these candidate NS1 interactors, we performed co-immunoprecipitation experiments with tagged NS1. With this experiment we could not (yet) confirm the interaction of NS1 with one or more proteins of the cleavage and polyadenylation of precursor mRNA pathway. However, a known interactor of NS1, MAVS, could also not be confirmed by coIP, although it was picked up in the BioID screen. Further optimization of lysis, purification and washing conditions and/or overexpression of these candidate NS1 interactors may increase the sensitivity to detect these candidate NS1 interactions. As an alternative to coIP, we may consider to use PPI mapping techniques such as fluorescence life-time imaging microscopy for

validation, which relies on the identification of PPIs in the natural cellular context like BioID. It will also be interesting to quantify polyadenylated mRNAs in the cytoplasm upon expression of NS1, e.g. by RNA sequencing, to see if the possible interaction of NS1 with one or more proteins of the cleavage and polyadenylation of precursor mRNA pathway indeed affects mRNA processing in the nucleus. RNA sequencing may reveal if NS1 affects the amount of processed mRNAs in the cytoplasm generally or gene-specifically.

To further validate the candidate NS1 and NS2 interactors, a number of essential questions require further attention. We investigated candidate NS1 and NS2 interactors upon overexpression of NS1 or NS2 separately. During a RSV infection NS1 and NS2 are coexpressed with NS2 causing a relocalization of NS1 to the mitochondria [68, 69]. Therefore, it is necessary to confirm candidate NS1 and NS2 interactors upon overexpression of both NS1 and NS2 and more importantly during a natural RSV infection. Efficient antibody-based detection of NS1 and/or NS2 may require an epitope-tagged version of NS1 and/or NS2. Therefore, a reverse genetics system of RSV, which has been developed, could be used to generate recombinant viruses with tagged NS1 and/or NS2. As the NS2 protein has a short half-life, addition of proteasome inhibitors may help preserving NS2 expression and host protein interactions. Host protein interactions that can be confirmed in a natural RSV infection may be studied further. A binary PPI mapping technique, *e.g.* Y2H or MAPPIT, may be interesting to investigate if a candidate NS1 and/or NS2 interactor directly interacts with NS1 and/or NS2 or is only co-purified in a complex. Furthermore, we could investigate which domain(s) or residues of NS1/NS2 are important for the interaction and how the interaction affects the cellular function(s) of the host protein. Mapping host protein interaction domains of the NS proteins may particularly be of interest for the generation of live-attenuated strains as vaccine candidates. By selectively deleting or preserving host protein interaction domains in the NS proteins, RSV strains could be designed with a desired degree of attenuation to be safe and immunogenic at the same time.

Pathway analysis of the different candidate interactors identified by BioID and Virotrap revealed a striking overlap of the proteasome complex and the protein ubiquitination pathway for both NS1 and NS2. These results are in line with the hypothesis that NS1 and NS2 form a so called “NS degradasome”, a proteasome-like multiprotein complex of which the exact composition is currently unknown [68]. Our results identified several subunits of the proteasome as candidate subunits of the NS degradasome. We hypothesize that the extensive list of proteins in the NS1 - and NS2 proxeomes may contain substrates of such a NS degradasome. An interesting follow-up experiment on the NS degradasome hypothesis would be to detect cellular peptides by LC-MS after NS1/NS2 overexpression (versus a mock vector) without doing the classical protease digest at LC-MS. If proteins from the proxeome lists are enriched in such cellular peptide lists, than these proteins likely represent degradasome substrates. Possibly, peptidase counter measurements will be required to preserve the cellular peptides from full degradation to single amino acids upon cell lysis. Candidate substrates of the NS degradasome could subsequently be validated during a natural RSV infection, *e.g.* by quantifying these proteins in cells infected with wild type - versus ΔNS1/2 RSV. Alternatively, we could also detect biotinylated peptides after doxycycline-induced expression of NS1-BirA* or NS2-BirA* by

LC-MS without protease digest. It has also been suggested that NS1 and NS2 act as E3 ubiquitin ligases. Detection of ubiquitinated proteins by LC-MS (after immunoprecipitation with a ubiquitin-specific antibody) upon overexpression of NS1 and/or NS2 could reveal which host proteins get ubiquitinated. The addition of a proteasome inhibitor could aid in the preservation of such ubiquitinated proteins. It would be interesting to determine the overlap between such a list of ubiquitinated proteins and the NS1 and NS2 proxeome lists, to identify candidate substrates of NS1 and/or NS2-mediated protein ubiquitination.

In conclusion, we identified several candidate NS1 and/or NS2 interactors, of which the proteasome subunits are of particular interest for further validation. These results may help to understand the biology of the RSV NS proteins and in the development of live-attenuated strains as vaccine candidates.

Reference list

1. Nair, H., et al., *Global burden of acute lower respiratory infections due to respiratory syncytial virus in young children: a systematic review and meta-analysis.* Lancet, 2010. **375**(9725): p. 1545-55.
2. Widmer, K., et al., *Rates of hospitalizations for respiratory syncytial virus, human metapneumovirus, and influenza virus in older adults.* J Infect Dis, 2012. **206**(1): p. 56-62.
3. *Palivizumab, a humanized respiratory syncytial virus monoclonal antibody, reduces hospitalization from respiratory syncytial virus infection in high-risk infants. The IMpact-RSV Study Group.* Pediatrics, 1998. **102**(3 Pt 1): p. 531-7.
4. DeVincenzo, J.P., et al., *Oral GS-5806 activity in a respiratory syncytial virus challenge study.* N Engl J Med, 2014. **371**(8): p. 711-22.
5. Perron, M., et al., *GS-5806 Inhibits a Broad Range of Respiratory Syncytial Virus Clinical Isolates by Blocking the Virus-Cell Fusion Process.* Antimicrob Agents Chemother, 2015. **60**(3): p. 1264-73.
6. Huntjens, D.R., et al., *Population Pharmacokinetic Modeling of JNJ-53718678, a Novel Fusion Inhibitor for the Treatment of Respiratory Syncytial Virus: Results from a Phase I, Double-Blind, Randomized, Placebo-Controlled First-in-Human Study in Healthy Adult Subjects.* Clin Pharmacokinet, 2017.
7. Roymans, D., et al., *Therapeutic efficacy of a respiratory syncytial virus fusion inhibitor.* Nat Commun, 2017. **8**(1): p. 167.
8. ArkBio. *Ark's Anti-RSV AK0529 Successfully Completes Phase 1 Study*. 2015; Available from: http://www.arkbiosciences.com/index.php?g=&m=article&a=index&id=17&cid=8.
9. therapeutics, A., *A Study of the Safety and Pharmacokinetics of Single and Multiple-ascending Doses of BTA585, a Novel Fusion Inhibitor of Respiratory Syncytial Virus, in Healthy Volunteers*. 2014.
10. Wang, G., et al., *Discovery of 4'-chloromethyl-2'-deoxy-3',5'-di-O-isobutyryl-2'-fluorocytidine (ALS-8176), a first-in-class RSV polymerase inhibitor for treatment of human respiratory syncytial virus infection.* J Med Chem, 2015. **58**(4): p. 1862-78.
11. DeVincenzo, J.P., et al., *Activity of Oral ALS-008176 in a Respiratory Syncytial Virus Challenge Study.* N Engl J Med, 2015. **373**(21): p. 2048-58.
12. Detalle, L., et al., *Generation and Characterization of ALX-0171, a Potent Novel Therapeutic Nanobody for the Treatment of Respiratory Syncytial Virus Infection.* Antimicrob Agents Chemother, 2015. **60**(1): p. 6-13.

13. Van Heeke, G., et al., *Nanobodies(R) as inhaled biotherapeutics for lung diseases.* Pharmacol Ther, 2017. **169**: p. 47-56.
14. Rossey, I., et al., *Potent single-domain antibodies that arrest respiratory syncytial virus fusion protein in its prefusion state.* Nat Commun, 2017. **8**: p. 14158.
15. De Clercq, E. and G. Li, *Approved Antiviral Drugs over the Past 50 Years.* Clin Microbiol Rev, 2016. **29**(3): p. 695-747.
16. Medicine, N.U.S.N.l.o. *Evaluation of Danirixin (GSK1325756) inhibition of CD11b cell surface expression*. 2014; Available from: https://clinicaltrials.gov/ct2/show/NCT02201303?term=danirixin&cond=RSV+Infection&rank=1.
17. Miller, B.E., et al., *The pharmacokinetics and pharmacodynamics of danirixin (GSK1325756)--a selective CXCR2 antagonist --in healthy adult subjects.* BMC Pharmacol Toxicol, 2015. **16**: p. 18.
18. Finan, C., et al., *The druggable genome and support for target identification and validation in drug development.* Sci Transl Med, 2017. **9**(383).
19. Hopkins, A.L. and C.R. Groom, *The druggable genome.* Nat Rev Drug Discov, 2002. **1**(9): p. 727-30.
20. Feldman, S.A., R.M. Hendry, and J.A. Beeler, *Identification of a linear heparin binding domain for human respiratory syncytial virus attachment glycoprotein G.* J Virol, 1999. **73**(8): p. 6610-7.
21. Hallak, L.K., et al., *Glycosaminoglycan sulfation requirements for respiratory syncytial virus infection.* J Virol, 2000. **74**(22): p. 10508-13.
22. Barr, F.E., et al., *Surfactant protein-A enhances uptake of respiratory syncytial virus by monocytes and U937 macrophages.* Am J Respir Cell Mol Biol, 2000. **23**(5): p. 586-92.
23. Hickling, T.P., et al., *Lung surfactant protein A provides a route of entry for respiratory syncytial virus into host cells.* Viral Immunol, 2000. **13**(1): p. 125-35.
24. Malhotra, R., et al., *Isolation and characterisation of potential respiratory syncytial virus receptor(s) on epithelial cells.* Microbes Infect, 2003. **5**(2): p. 123-33.
25. Johnson, S.M., et al., *Respiratory Syncytial Virus Uses CX3CR1 as a Receptor on Primary Human Airway Epithelial Cultures.* PLoS Pathog, 2015. **11**(12): p. e1005318.
26. Behera, A.K., et al., *Blocking intercellular adhesion molecule-1 on human epithelial cells decreases respiratory syncytial virus infection.* Biochem Biophys Res Commun, 2001. **280**(1): p. 188-95.
27. Tayyari, F., et al., *Identification of nucleolin as a cellular receptor for human respiratory syncytial virus.* Nat Med, 2011. **17**(9): p. 1132-5.
28. Currier, M.G., et al., *EGFR Interacts with the Fusion Protein of Respiratory Syncytial Virus Strain 2-20 and Mediates Infection and Mucin Expression.* PLoS Pathog, 2016. **12**(5): p. e1005622.
29. Srinivasakumar, N., P.L. Ogra, and T.D. Flanagan, *Characteristics of fusion of respiratory syncytial virus with HEp-2 cells as measured by R18 fluorescence dequenching assay.* J Virol, 1991. **65**(8): p. 4063-9.
30. Kolokoltsov, A.A., et al., *Small interfering RNA profiling reveals key role of clathrin-mediated endocytosis and early endosome formation for infection by respiratory syncytial virus.* J Virol, 2007. **81**(14): p. 7786-800.
31. Krzyzaniak, M.A., et al., *Host cell entry of respiratory syncytial virus involves macropinocytosis followed by proteolytic activation of the F protein.* PLoS Pathog, 2013. **9**(4): p. e1003309.
32. Malkin, E., et al., *Safety and immunogenicity of a live attenuated RSV vaccine in healthy RSV-seronegative children 5 to 24 months of age.* PLoS One, 2013. **8**(10): p. e77104.
33. Karron, R.A., et al., *A gene deletion that up-regulates viral gene expression yields an attenuated RSV vaccine with improved antibody responses in children.* Sci Transl Med, 2015. **7**(312): p. 312ra175.
34. Medicine, N.U.S.N.l.o. *Evaluating the Safety and Immune Response to a Single Dose of a Respiratory Syncytial Virus (RSV) Vaccine in RSV-Seronegative Infants and Children*. 2013; Available from: https://clinicaltrials.gov/ct2/show/NCT01852266.

35. Medicine, N.U.S.N.l.o. *Evaluating the Infectivity, Safety, and Immunogenicity of the Recombinant Live-Attenuated Respiratory Syncytial Virus Vaccines RSV ΔNS2/Δ1313/I1314L or RSV 276 in RSV-Seronegative Infants 6 to 24 Months of Age*. 2017; Available from: https://clinicaltrials.gov/ct2/show/NCT03227029?term=1313%2F1314L&rank=1.
36. Noah, J.W., et al., *A Cell Based HTS Approach for the Discovery of New Inhibitors of RSV*, in *Probe Reports from the NIH Molecular Libraries Program*. 2010: Bethesda (MD).
37. Rasmussen, L., et al., *A high-throughput screening strategy to overcome virus instability.* Assay Drug Dev Technol, 2011. **9**(2): p. 184-90.
38. Chung, D.H., et al., *A cell based high-throughput screening approach for the discovery of new inhibitors of respiratory syncytial virus.* Virol J, 2013. **10**: p. 19.
39. Tiong-Yip, C.L., et al., *Development of a high-throughput replicon assay for the identification of respiratory syncytial virus inhibitors.* Antiviral Res, 2014. **101**: p. 75-81.
40. Gobel, J., et al., *A Phenotypic High-Throughput Screen with RSV-Infected Primary Human Small Airway Epithelial Cells (SAECs).* J Biomol Screen, 2015. **20**(6): p. 729-38.
41. Plant, H., et al., *High-Throughput Hit Screening Cascade to Identify Respiratory Syncytial Virus (RSV) Inhibitors.* J Biomol Screen, 2015. **20**(5): p. 597-605.
42. Sudo, K., et al., *YM-53403, a unique anti-respiratory syncytial virus agent with a novel mechanism of action.* Antiviral Res, 2005. **65**(2): p. 125-31.
43. Laganas, V.A., et al., *Characterization of novel respiratory syncytial virus inhibitors identified by high throughput screen.* Antiviral Res, 2015. **115**: p. 71-4.
44. Bailly, B., et al., *Targeting human respiratory syncytial virus transcription anti-termination factor M2-1 to inhibit in vivo viral replication.* Sci Rep, 2016. **6**: p. 25806.
45. Duvall, J.R., et al., *Novel diversity-oriented synthesis-derived respiratory syncytial virus inhibitors identified via a high throughput replicon-based screen.* Antiviral Res, 2016. **131**: p. 19-25.
46. Bonavia, A., et al., *Identification of broad-spectrum antiviral compounds and assessment of the druggability of their target for efficacy against respiratory syncytial virus (RSV).* Proc Natl Acad Sci U S A, 2011. **108**(17): p. 6739-44.
47. Wu, W., et al., *The interactome of the human respiratory syncytial virus NS1 protein highlights multiple effects on host cell biology.* J Virol, 2012. **86**(15): p. 7777-89.
48. Kipper, S., et al., *New host factors important for respiratory syncytial virus (RSV) replication revealed by a novel microfluidics screen for interactors of matrix (M) protein.* Mol Cell Proteomics, 2015. **14**(3): p. 532-43.
49. Munday, D.C., et al., *Interactome analysis of the human respiratory syncytial virus RNA polymerase complex identifies protein chaperones as important cofactors that promote L-protein stability and RNA synthesis.* J Virol, 2015. **89**(2): p. 917-30.
50. Roskoski, R.J. *FDA-approved protein kinase inhibitors*. 2017; Available from: http://www.brimr.org/PKI/PKIs.htm.
51. Alvarez, R., et al., *RNA interference-mediated silencing of the respiratory syncytial virus nucleocapsid defines a potent antiviral strategy.* Antimicrob Agents Chemother, 2009. **53**(9): p. 3952-62.
52. Schultz, N., et al., *Off-target effects dominate a large-scale RNAi screen for modulators of the TGF-beta pathway and reveal microRNA regulation of TGFBR2.* Silence, 2011. **2**: p. 3.
53. Meier, R., et al., *Genome-wide small interfering RNA screens reveal VAMP3 as a novel host factor required for Uukuniemi virus late penetration.* J Virol, 2014. **88**(15): p. 8565-78.
54. atlas, T.h.p. *IRAK3*. Available from: https://www.proteinatlas.org/ENSG00000090376-IRAK3/cell.
55. Mehedi, M., et al., *Actin-Related Protein 2 (ARP2) and Virus-Induced Filopodia Facilitate Human Respiratory Syncytial Virus Spread.* PLoS Pathog, 2016. **12**(12): p. e1006062.
56. Birmingham, A., et al., *3' UTR seed matches, but not overall identity, are associated with RNAi off-targets.* Nat Methods, 2006. **3**(3): p. 199-204.

57. Jackson, A.L., et al., *Widespread siRNA "off-target" transcript silencing mediated by seed region sequence complementarity.* RNA, 2006. **12**(7): p. 1179-87.
58. Anderson, E.M., et al., *Experimental validation of the importance of seed complement frequency to siRNA specificity.* RNA, 2008. **14**(5): p. 853-61.
59. Ui-Tei, K., et al., *Thermodynamic stability and Watson-Crick base pairing in the seed duplex are major determinants of the efficiency of the siRNA-based off-target effect.* Nucleic Acids Res, 2008. **36**(22): p. 7100-9.
60. Gu, S., et al., *Weak base pairing in both seed and 3' regions reduces RNAi off-targets and enhances si/shRNA designs.* Nucleic Acids Res, 2014. **42**(19): p. 12169-76.
61. Kamola, P.J., et al., *The siRNA Non-seed Region and Its Target Sequences Are Auxiliary Determinants of Off-Target Effects.* PLoS Comput Biol, 2015. **11**(12): p. e1004656.
62. Rezaee, F., et al., *Sustained protein kinase D activation mediates respiratory syncytial virus-induced airway barrier disruption.* J Virol, 2013. **87**(20): p. 11088-95.
63. Schneider, M., et al., *Human PRP4 kinase is required for stable tri-snRNP association during spliceosomal B complex formation.* Nat Struct Mol Biol, 2010. **17**(2): p. 216-21.
64. Dudek, S.M., et al., *Novel interaction of cortactin with endothelial cell myosin light chain kinase.* Biochem Biophys Res Commun, 2002. **298**(4): p. 511-9.
65. Shin, D.H., et al., *Arrest defective-1 controls tumor cell behavior by acetylating myosin light chain kinase.* PLoS One, 2009. **4**(10): p. e7451.
66. Xu, J., et al., *Nonmuscle myosin light-chain kinase mediates neutrophil transmigration in sepsis-induced lung inflammation by activating beta2 integrins.* Nat Immunol, 2008. **9**(8): p. 880-6.
67. Dhar, J., et al., *2'-5'-Oligoadenylate Synthetase-Like Protein Inhibits Respiratory Syncytial Virus Replication and Is Targeted by the Viral Nonstructural Protein 1.* J Virol, 2015. **89**(19): p. 10115-9.
68. Goswami, R., et al., *Viral degradasome hijacks mitochondria to suppress innate immunity.* Cell Res, 2013. **23**(8): p. 1025-42.
69. Swedan, S., et al., *Multiple functional domains and complexes of the two nonstructural proteins of human respiratory syncytial virus contribute to interferon suppression and cellular location.* J Virol, 2011. **85**(19): p. 10090-100.

Part V: Addendum

CURRICULUM VITAE

Personal information

Name	Koen Sedeyn Johan V
Date of birth	11.07.1988
Place of birth	Ghent
Nationality	Belgian
Address	Westremstraat 90 9230 Westrem (Wetteren)
Phone	Home: 09/279.47.44 Mobile: 0495/37.47.77
E-mail	Home: koensedeyn@hotmail.com Work: koen.sedeyn@vib-UGent.be
Family status	Official co-habitation, two daughters (Auke, °24/10/2015 and Jutta, °12/12/2017)

Professional experience

- 2011-currently: **Doctoral researcher, VIB, Center for Medical Biotechnology**

Fundamental research in virology: RNA interference, phosphoproteomics, interactomics, kinases, High throughput screening

Doctoral thesis: Host-RSV interactions: a siRNA and proteomics approach

- 2010-2011: **Internship Master, VIB, Unit Molecular Virology**

Applied research: testing a new RSV vaccine candidate based on the ectodomain of the small hydrophobic protein of RSV in a mouse model by using serology (ELISA) and virus titration.

Master thesis: Study of the respiratory syncytial virus small hydrophobic protein as vaccine antigen

- International publications: https://biblio.ugent.be/person/000060456359

1. Rossey, I., Gilman, M. S., Kabeche, S. C., **Sedeyn, K**., Wrapp, D., Kanekiyo, M., Saelens, X. (2017). Potent single-domain antibodies that arrest respiratory syncytial virus fusion protein in its prefusion state. Nat Commun, 8, 14158. doi:10.1038/ncomms14158
2. Schepens, B., **Sedeyn, K.**, Vande Ginste, L., De Baets, S., Schotsaert, M., Roose, K., Saelens, X. (2014). Protection and mechanism of action of a novel human respiratory syncytial virus vaccine candidate based on the extracellular domain of small hydrophobic protein. EMBO Mol Med, 6(11), 1436-1454. doi:10.15252/emmm.201404005
3. Rossey, I., **Sedeyn, K.**, De Baets, S., Schepens, B., & Saelens, X. (2014). CD8+ T cell immunity against human respiratory syncytial virus. Vaccine, 32(46), 6130-6137. doi:10.1016/j.vaccine.2014.08.063
4. De Baets, S., Schepens, B., **Sedeyn, K**., Schotsaert, M., Roose, K., Bogaert, P., Saelens, X. (2013). Recombinant influenza virus carrying the respiratory syncytial virus (RSV) F85-93 CTL epitope reduces RSV replication in mice. J Virol, 87(6), 3314-3323. doi:10.1128/JVI.03019-12

Education

- 2011-2017: **PhD in Biochemistry and biotechnology**
  Unit Molecular Virology, VIB-Center for Medical Biotechnology
  Faculty of sciences, University Ghent, Belgium
- 2009-2011: **Master biochemistry and biotechnology** Summa cum laude
  Faculty of sciences, University Ghent, Belgium
- 2006-2009: **Bachelor biochemistry and biotechnology** Magna cum laude
  faculty of sciences, University Ghent, Belgium
- 2000-2006: **Science-mathematics**
  Don Bosco College – Zwijnaarde

Courses/training

- 2016: Scientific writing, VIB training: Adrian Liston
- 2014: Training in ingenuity pathway analysis, VIB training: Stéphane Plaisance
- 2012: Training in microscopy, VIB training: BioImaging core
- 2010-2011: Course on laboratory animal science I and II: FELASA C certificate for laboratory animal experiments, Ghent University

Symposia/conferences

- 9th international Respiratory Syncytial Virus symposium, Cape Town, South-Africa, 9-13 November, 2014, Poster
- Early events in virus infection, Ascona, Switzerland, 25-28 August, 2014, Poster
- 15th international Negative strand virus meeting, Granada, Spain, 16-21 June, 2013, Poster
- National meetings: Belvir, BSM, VIB symposia, …

Oral presentations of this work

- 2015: Center for medical biotechnology, Ghent, 20 May 2015
- 2014: 2nd annual meeting of the Belgian society for Virology, Brussels, 8 December 2014
- 2013: Inflammation research Center, VIB, 26 June 2013

Guidance/training of people

- 2016: Soraya Van Cauwenberghe, Master thesis, Master of Science in Industrial Sciences: Biochemistry
- 2015: Kerstin Alt, Master I project, Master Biochemistry and Biotechnology
- 2014: Integrated practical courses Bachelor 2, Bachelor Biochemistry and Biotechnology

- 2013: Sander Hemelsoet, Master I project, Master Biochemistry and Biotechnology

Involvement in organisational tasks

- 2014-2017: Tissue culture responsible room/lab
- 2016, 2014, 2012: Week of Sciences: one day workshop for high school students
- 2014: Biotech day

Personal skills/information

- **Personality**: Organised, GLP complient, accurate, hard-working, motivated, team player, Social
- **Languages**: Dutch: mother tongue
English: writing – proficiant / speaking – proficiant
French: writing – proficiant / speaking – proficiant
- **IT skills**: MS office 2016 (Word, Excel, Powerpoint)
ELN, Graphpad prism, CLC main workbench 7, Fiji, Flowing

Dankwoord

Oooeeef, we zijn er geraakt! De eindmeet is in zicht. Met dit laatste stukje zijn we aan de laatste passage op de Champs-Élysées gekomen tijdens de Tour de France. Net als de Tour de France is ook dit doctoraat een zware beproeving geworden met Alpencols die bedwongen moesten worden en talrijke platte banden die voor de nodige vertraging en tegenslagen hebben gezorgd in de afgelopen 6 jaar. Het heeft soms bloed, zweet en tranen gekost, zowel letterlijk als figuurlijk dan. Zoals die keer dat mijn vingers toch net iets langer bleken dan gedacht en konden ervaren dat de klapdeuren in het VIB toch behoorlijk zwaar zijn. Het zweet dat nodig was om zoveel mogelijk met de fiets naar het werk te komen, goed voor ongeveer 40.000 km of een rondje rond de aarde. Of het pijnlijke afscheid met een ferme krop in de keel die ik nog nooit meemaakte, toen Ruth en Auke voor een weekje naar zee vertrokken deze zomer, waarbij ik mezelf had opgelegd om dit doctoraat verder te schrijven. Voor het eerst sinds Auke haar geboorte zou ik haar langer dan een nacht niet zien. Gelukkig waren er de afgelopen 6 jaar, net als in de Tour de France, ook talrijke supporters aanwezig die mij steeds gesteund hebben en zonder wie dit doctoraat misschien niet gelukt was. Dit stukje is een ideale kans om iedereen nog eens te bedanken. Het fameuze dankwoord waar iedereen, of toch bijna iedereen, direct naar doorbladert ☺. Voor zij die dit werk net gelezen hebben, bedankt voor de inspanning en hopelijk heeft het jullie geboeid.

Eerst en vooral zou ik graag 2 mensen heel hard bedanken die het dichtst betrokken waren bij mijn project, mijn promotoren **Xavier en Bert**. Xavier, het was tijdens de cursus “Host-Virus interactions” dat ik geboeid raakte door de opmerkelijke wereld van virussen. Minuscuul kleine verzamelingen van moleculen die strikt gezien zelfs geen organismen zijn, waarbij dikwijls slechts een handvol genen volstaan om bijvoorbeeld een mens ziek te maken of zelfs plat te leggen. Bedankt dat ik de kans kreeg om in jouw labo een master thesis te kunnen doen, gevolgd door een doctoraat. Voor de blijvende steun en vertrouwen in mij, ondanks dat het project niet echt van een leien dakje liep. Ik heb dikwijls gedacht “dit komt niet goed”, maar bij elk negatief resultaat bleef je de positieve elementen vinden om mij te motiveren toch verder te doen. Ik blijf ervan versteld staan hoe snel ik feedback krijg als ik een tekst doorstuur, ook al is dit ’s avonds laat na het werk, waarbij ik dan denk “dju hoe ben ik daar zelf niet opgekomen”. Bedankt dat ik nu aan een nieuw project mag beginnen in het labo. Bert, toen ik mijn master thesis bij jou begon in 2011 had je nog iets meer haar dan nu, hopelijk komt dit niet door mij ☺. Zowel tijdens mijn master thesis als doctoraat was jij mijn directe begeleider en kon ik steeds bij jou terecht met al mijn vragen. Ook jij bleef steeds geloven in het project en dit heeft echt geholpen om door te zetten. Bij elk gelukt experiment, hoe klein en banaal het soms ook was, had ik steeds de neiging om dit direct aan jou te komen vertellen, waarbij jouw enthousiasme extra energie gaf. Bedankt ook om samen met Xavier mijn volledige thesis na te lezen en suggesties te geven. Xavier en Bert, een dikke merci.

Dan zou ik uiteraard graag mijn ouders bedanken. **Papa** en **mama,** bedankt om 30 jaar geleden toch voor een 3^{e} kind te gaan, ondanks enige twijfel nadat de 2^{e} zoon nogal een huilbaby bleek te zijn ☺. Ik heb een fantastische jeugd gehad met enorm veel mogelijkheden en kansen die mij toch voor een groot deel gevormd hebben zoals ik nu ben. Bedankt om steeds vol enthousiasme en fierheid elke week naar mijn loopwedstrijd te komen kijken en voor de onvergetelijke, talrijke vakanties in Frankrijk. Ook nu nog staan jullie steeds paraat om ons te helpen. Papa, het is soms nodig om je op tijd te boeken voor het weekend ☺, maar de 3 gelijktijdige bouwprojecten van je zonen doe je met volle overgave.

Mama, bedankt om op gelijk welk moment in te springen, nogal dikwijls als één van de ondertussen 7 kleinkinderen plots ziek wordt. RSV kent ondertussen geen geheimen meer voor jou! De kleinkinderen mogen in hun handjes wrijven met jullie als mamie en papie.

Jan en **Linda**, mijn schoonouders. Het begon allemaal met een veel te grote pot stoofvlees bedoeld voor een 4-tal vrienden, niet wetende dat Ruth stiekem enkel mij uitgenodigd had. Hoewel jullie nu na bijna 12 jaar al meermaals hebben gemerkt dat ik redelijk wat kan eten, bleek die pot toch echt wel te groot te zijn om die avond op te eten, waardoor ik mij verplicht voelde om jullie deur nadien regelmatig plat te lopen ☺. Bedankt dat ik mij direct en altijd thuis heb mogen voelen bij jullie. Het is leuk om zien hoe graag jullie jullie kleinkinderen zien.

Mijn 2 broer(tjes), **Bert** en **Dries**. Oké, ik geef het toe, ik ben dan wel de jongste en volgens jullie soms de meest verwende, maar dankzij jullie heb ik toch geleerd moeilijke uitdagingen aan te gaan, lees: ik wou jullie volgen maar was wel diegene die achteraf genaaid moest worden ☺. Bedankt om ons ook nu regelmatig te helpen en voor de leuke familiemomenten samen.

Mijn schoonzussen en schoonbroer, **Linde, Evelyn, Saar** en **Andy,** bedankt voor de leuke familiemomenten samen.

Daarnaast wil ik graag een aantal vrienden bedanken. De **"bende konijnen"**, we zijn grotendeels samen afgestudeerd aan de middelbare school op enkele honderden meters van het VIB. Er is veel veranderd sinds we als gloednieuwe meerderjarigen in de wijde wereld gedropt werden, er zijn al behoorlijk wat kindjes geboren, huisjes zijn gekocht of gebouwd, fietsen zijn gebruikt om de wereld rond te reizen en toch spreken we nog bijna maandelijks af na 12 jaar. Ik amuseer mij nog altijd als we samen afspreken en ook tijdens het schrijven van deze thesis zorgde dit voor de nodige afleiding en ambiance. Ik hoop echt dat we elkaar nog lang blijven zien, wie weet ooit als Benidorm bastards met valse tanden en een rollator ☺. Enkele BCBT'ers in het bijzonder, Lisa, Cedrick, Mieke, Giel en Silvie. We kenden elkaar niet voor we samen begonnen aan onze opleiding. Toch zijn we elkaar vrij snel goed beginnen kennen en nu nog proberen we regelmatig eens af te spreken. Het is soms zoeken om het west-vloamsch van sommige te begrijpen, maar het lukt beter en beter ☺. Naast de vele theoretische lessen hebben we samen ook soms legendarische practica gedaan. Eén van de meest memorabele practica was het practicum radiochemie. Ik zal nooit vergeten hoe we onze roervlo per ongeluk in een afvalvat zagen verdwijnen achter een beschermingsmuurtje voor radioactiviteit, ik en Cedrick elkaar eens aankeken met een "oeps-blik", om net op dat moment van een begeleider te horen: "ahja vergeten zeggen, kunnen jullie voorzichtig zijn met de roervlo want anders moet ik dat er opnieuw gaan uitvissen", waarop we allebei in een luide lachbui schoten. **Lisa**, veel succes nog met je ondertussen niet meer zo nieuwe job en met jullie roadtrip/wereldreis. Hoewel we de laatste brunch hebben moeten overslaan door een "ik wil er bijna uit baby" is het altijd tof om uitgenodigd te worden in jullie unieke woonst, bedankt. **Cedrick**, we zijn ook al meerdere keren gastvrij ontvangen in het verre "bijna Zeveren", hoewel het nu voor sommige weggebruikers niet direct meer duidelijk is waar Zeveren net begint ☺. Veel succes op je nieuwe job en hopelijk blijven we elkaar regelmatig zien. **Mieke**, veel succes met je plan om een marathon te lopen en de rest van je toekomst. **Giel**, mijn bib-buddy ☺. We hebben samen vele uren in de bibliotheek gespendeerd om elk ons doctoraat te schrijven. De moeilijkste momenten voor mezelf waren zeker de weekends, wetende dat veel mensen dan leuke activiteiten doen. Het is echt een grote steun voor mij geweest dat jij toen ook in de bibliotheek was en dat ik af en toe een

babbeltje kon komen doen. Hopelijk heb ik niet te veel gezaagd op die momenten ☺. Toen ik klaar was met schrijven en jij pas later kon indienen voelde ik mij toch een beetje schuldig dat ik je daar in de bibliotheek achterliet, maar ik had het echt wel effe gehad met de bibliotheek. Heel binnenkort ben je er ook vanaf, dus heel veel succes met je verdediging. **Silvie,** hoewel er initieel maar 1 plaats voor een master thesis was in het labo, wouden we er allebei graag starten. We waren allebei te braaf om die ene plaats voor onszelf op te eisen, maar gelukkig konden we er allebei starten na enig lobbywerk. Hoewel jouw project niet bepaald van een leien dakje liep, ben je volledig op stoom gekomen tijdens je doctoraat ☺. Je legendarische rode haar, je welbekende diepvries checks en diepvries dubbel-checks en je hello kitty verzameling zullen me altijd bijblijven ☺. Bedankt voor de vele succes en steun berichten tijdens het schrijven. Veel succes met het bouwavontuur samen met Giel en op je nieuwe job.

Dan een aantal mensen met wie ik het grootste deel van mijn doctoraat heb doorgebracht, de **UXSa collega's,** die eigenlijk meer zijn dan collega's alleen. Eén van de belangrijkste eigenschappen om een doctoraat tot een goed einde te brengen zijn een goede begeleiding en aangename werksfeer. Vanaf de eerste dag heb ik mij goed gevoeld in het labo. De eerlijkheid, oprechte bereidheid om te helpen en het plezier dat we samen beleven, zowel tijdens als buiten het werk, hebben ervoor gezorgd dat ik met plezier ben komen werken. Ik denk dat onze doctoraatsfilmpjes hier de beste getuigen van zijn. Hopelijk blijft dit zo nadat ik mijn filmpje gezien heb ☺. **Iebe**, mijn buurvrouw die af en toe ingesloten wordt door een stapel papieren van mij. Hoewel ik toch af en toe een stress'ke had, bleef je steeds een zen-bron naast mij. Bedankt voor de leuke momenten samen en babbels over onderwerpen die ons beide nauw aan het hart liggen. Als we ooit herbruikbare luiers gebruiken dan zal dit dankzij jou zijn! Veel succes met de verdere ontwikkeling van je nanobody, of correcter VHH ☺, en met David en Siem. **Dorien**, vanaf het begin dat je in het labo kwam viel je enthousiasme meteen op. We hebben dikwijls gelachen samen, ook al had je in het weekend je basketbalwedstrijd verloren ☺. Je bent ondertussen waarschijnlijk de panning-master geworden in het labo, dus als ik ooit met nanobodies werk kom ik zeker bij je langs. Veel succes met het einde van je doctoraat en je schrijven. **Marlies**, hoewel ik ooit primers van je kreeg die ik gebruikt heb in mijn doctoraat kende ik je niet zo goed tot je recent in ons labo kwam werken. Je bent een toffe collega nu die zich heel snel geïntegreerd heeft in ons labo en waar je steeds op kan rekenen als je hulp nodig hebt. **Lien,** hoewel het niet direct duidelijk was in het begin dat je een nieuwe collega was van ons, zijn alle twijfels nu dubbel en dik weg ☺. Ik denk niet dat ik jou ooit al in een minder vrolijke bui heb gezien in het labo. Je neemt bijzonder veel initiatief in het labo en dat is echt leuk voor de groepssfeer. Veel succes met je artikel, doctoraat en het bouwavontuur. Als we ooit een professionele metsersknecht zoeken weet ik wel waar zoeken. Misschien voorzien we wel best een stevig helmpje om je te beschermen tegen de balken ☺. **Eline,** de benjamin van de groep wonende in een ongekend boerengat, ahja nee het was niet ver van de molecule zeker e, dat weet ik liggen ☺. Je lach werkt zo aanstekelijk in het labo dat iedereen instant vrolijk wordt. Ook de manier hoe je regelmatig je verwondering toont met de ondertussen bekende woorden "Ma alléee" vind ik altijd grappig ☺. Je hebt nog even tijd voor je doctoraat dus ga ik je vooral geslaagde experimenten wensen en veel succes met de sloop/bouwwerken. **Jan** of beter gezegd kersvers Dr. Jan. Je bent dikwijls de redding in nood geweest voor al mijn IT problemen. Waarschijnlijk heb je dikwijls gedacht "amai wat voor een pietluttigheid ben ik nu moeten gaan oplossen", IT is nu éénmaal niet echt mijn ding ☺. Bedankt om mij te helpen met de flow cytometrie analyses. Veel succes met de zoektocht naar een job die je op het lijf geschreven is, misschien als Mr. Flow-man. **Jackeline,**

je bent de meest recente aanwinst van het labo en de samenwerking lijkt nu al meer dan geslaagd. Hopelijk gaan we samen nog mooie resultaten bekomen en ik probeer alvast niet te veel te vergeten ☺. **Tine,** als moederkloek van 2 koddige zoontjes ben ik dikwijls bij je langs gegaan om advies te vragen over kakjes, boertjes en flesjes. Bedankt voor de vele tips en de leuke momenten samen. Veel succes met jullie verbouwingen en met je 3 (mini)porties testosteron. **Kenny,** zolang ikzelf nog geen 30 ben, mag ik je toch een semi-oudje blijven noemen e ☺. Sorry dat ik je af en toe geplaagd heb met je weelderige haardos die stilletjes aan verdwijnt, maar wees gerust, je blijft de man met het hoogste knuffel-gehalte van de UXSa's ☺. Bedankt dat ik steeds bij je terecht kon met al mijn vragen waarbij je graag je ervaring deelt. **Anouk,** bedankt dat je steeds klaar stond om bij te springen als het druk was, bijvoorbeeld als de incubatoren alweer eens gekuist moesten worden. De eerste jaren kon ik ook (soms te) gretig naar de voorraad wine gums grijpen om mijn suikerspiegel op peil te houden. Nu draag je bij om te vermijden dat ik type 2 diabetes ontwikkel op mijn oude dag! Je bent deze zomer altijd welkom om het WK voetbal te komen volgen nu de Oranje's thuis mogen blijven ☺. **Emma,** whenever I see a giant panda I have to think about your mobile phone cover, which makes me smile ☺. Good luck with the NA project, Kevin and your new living place. **Annasaheb**, thank you for the nice talks and the great indian kitchen that we could taste. Good luck with the writing of your PhD. **Ioanna,** good luck with the finishing of your PhD and your daughter Thalia.

Ook een aantal ex-UXSa collega's zou ik graag bedanken voor de jaren dat we samen gewerkt hebben. **Judith**, naast een uitstekend wetenschapster was je ook steeds beschikbaar voor een bouwkundig advies tussendoor ☺. **Sarah,** bedankt voor de leuke momenten en veel succes met de laatste weken van je 2^{e} zwangerschap. **Liesbeth,** bedankt dat je steeds beschikbaar was om te helpen en veel succes in jullie nieuwe woonst. **Soraya,** met jouw thesis heb je mij goed vooruit geholpen met het interactomics project. Bedankt en veel succes met de (ondertussen succesvolle?) zoektocht naar een huis voor jou en Jens. **Michael, Itati, Miguel, Farzaneh, Lei, Kijoon, Flor, Ilse, Janina, Joke and Sella,** thank you all for the nice moments together.

Tenslotte zou ik graag een aantal mensen van het VIB in het bijzonder willen bedanken. **Delphi** en **Francis** van het PEC, super hard bedankt voor het werk dat jullie gedaan hebben voor het analyseren van de stalen voor de phosphoproteomics en interactomics data. **Delphine en Sven,** heel hard bedankt voor het uitvoeren en analyseren van de Virotrap experimenten. **Amanda**, **Evelien** en **Eef** van de bioimaging core, bedankt voor de hulp en advies bij het nemen van mooie microscopie foto's. **Liesbet**, bedankt voor de hulp bij het analyseren van de RNA seq data. **Gert,** bedankt om te helpen bij de FACS analyse. De **UNCa's** voor de leuke sfeer in onze gedeelde bureaus en labo.

Als laatste, mijn meest dierbare vrouwtjes... **Ruth,** bijna 12 jaar geleden gingen we samen schaatsen op een maandagnamiddag in de paasvakantie met een aantal vrienden. Onze voltallige vriendengroep en zelfs een Zuid-Afrikaans meisje zagen het al veel langer aankomen, maar geen van ons beide durfde de eerste stap te zetten. Toen je bewust treuzelde totdat alle vrienden weg waren en je alleen bij mij overbleef, nodigde je mij uit om mee te gaan naar je thuis, wetende dat je moeder ondertussen hard labeur verrichte om een grote pot stoofvlees voor 4 extra man te maken. Verzot dat ik op je was, ben ik je gevolgd, jij op je brommertje, ik met de fiets ernaast, goed voor een tocht van 20 km... Nu, 12 jaar later rijden we nog steeds wekelijks naar je thuis. Een aantal zaken zijn nog steeds hetzelfde gebleven: ik ben nog steeds verzot op je en af en toe wordt er nog eens stoofvlees gegeten bij je thuis, goed voor een pot voor 4 extra man. Er zijn echter ook een aantal zaken veranderd. De tocht is niet meer 20 km,

maar 15 km vanuit ons eigen huisje. Ik rij ook niet meer met de fiets naast je brommertje, maar we rijden samen met de auto, waarbij onze achterbank gevuld is met onze 2 grootste schatten, Auke en Jutta, onze moncchichi's. **Auke**, je bent nu 2 jaar en 3 maanden en grote zus geworden. Fier als een gieter wil je al voor je zusje zorgen, hoewel je zusje niet altijd even graag een tuut in haar mondje geduwd krijgt. Ik geniet met volle teugen van je schaterlach als ik je kriebels neem en als je vraagt "nog een beetje" als ik eventjes stop om je op adem te laten komen. Als je lief aan mij komt vragen: "uisje bouwen?" of als je 's avonds in bed vraagt: "papa, kusje". We hebben samen weinig leuke dingen kunnen doen deze zomer, maar ik beloof je dat we dit dubbel en dik gaan goed maken. **Jutta,** het was eventjes spannend of ik mijn doctoraat ging kunnen verdedigen. Mijn verdediging was gepland voor 17 november, jij was uitgerekend voor 6 december en mama bleef lange tijd herhalen "ik denk dat die vroeger gaat komen ze". De 17e november passeerde en papa (en mama en Auke) konden een grote zucht van verluchting slaken. Jij had echter een spannender plannetje in mama's buik. Op 11 december, de dag dat gans Vlaanderen geblokkeerd stond door de felle sneeuwval, besloot jij dat het welletjes was geweest in mama's buik. Mits enige moeite zijn papa en mama toch in het ziekenhuis geraakt en op 12 december konden we je eindelijk na 9 maanden in onze armen sluiten. Je dikke kaakjes, je oefeningen om een lachje te tonen en je weelderig Venetiaans blonde haarkopje maken je nu al onmisbaar in ons gezinnetje na 4 weken. Ruth, ik weet dat ik je deze zomer heel vaak alleen thuis heb achtergelaten. Hoewel ik met tranen in de ogen van onze oprit reed toen ik Auke aan het raam zag zwaaien naar mij op het einde van mijn schrijven, besef ik maar al te goed dat het ook voor jou een zware zomer is geweest. Ook het familiepark Harry Malter heeft zo zijn beperkingen na meerdere bezoeken ☺. 2018 belooft opnieuw een uitdagend jaar te worden, we zouden graag starten met onze nieuwbouw, ik start met een nieuw project en jij start je eigen praktijk als kinesiste. Eén ding is echter zeker, ik wil er 200% voor gaan, samen met jou, samen met ons gezinnetje. XXX

Bedankt iedereen!

Koen

"Save the planet, ride your bicycle"